

Final Report

*Development of MASH Computer Simulated Steel
Bridge Rail and Transition Details*

Prepared for: **Maine Department of Transportation**

State Project No: **023430.18**

Federal Project No: **2343018**

Prepared by: **Chuck A. Plaxico, Ph.D.
Ethan M. Ray**

ROADSAFE LLC
P.O. BOX 312
CANTON, ME 04221



April 28, 2020

DEVELOPMENT OF MASH COMPUTER SIMULATED STEEL BRIDGE RAIL AND TRANSITION DETAILS

Chuck A. Plaxico, Ph.D.
and
Ethan M. Ray

**Prepared for
The New England Transportation Consortium
April 28, 2020**

NETCR18

Project No. 18-1

This report, prepared in cooperation with the New England Transportation Consortium, does not constitute a standard, specification, or regulation. The contents of this report reflect the views of the authors who are responsible for the facts and the accuracy of the data presented herein. The contents do not necessarily reflect the views of the New England Transportation Consortium or the Federal Highway Administration.

ACKNOWLEDGEMENTS

The following are the members of the Technical Committee that developed the scope of work for the project and provided technical oversight throughout the course of the research:

- **Chair** – Jeff Folsom, Maine Department of Transportation
- **Director, Transportation Research** – Dale Peabody, Maine Department of Transportation
- **Project Manager** – Kirsten Seeber, CTC & Associates
- David Kilpatrick, Connecticut Department of Transportation
- Alex Bardow, Massachusetts Department of Transportation
- Robert Landry, New Hampshire Department of Transportation
- Michael Savella, Rhode Island Department of Transportation
- Jim Lacroix, Vermont Agency of Transportation

TECHNICAL REPORT DOCUMENTATION PAGE

1. Report No. NETCR115		2. Government Accession No. N/A		3. Recipient's Catalog No. N/A	
4. Title and Subtitle Development of MASH Computer Simulated Steel Bridge Rail and Transition Details				5. Report Date April 28, 2020	
				6. Performing Organization Code N/A	
7. Author(s) Chuck A. Plaxico and Ethan M. Ray				8. Performing Organization Report No. TR-200323-NETC115	
9. Performing Organization Name and Address Roadsafe LLC 12 Main Street Canton, Maine 04221				10. Work Unit No. N/A	
				11. Contract or Grant No. N/A	
12. Sponsoring Agency Name and Address New England Transportation Consortium C/O Transportation Research MaineDOT 24 Child Street Augusta, ME 04333				13. Type of Report and Period Covered Final Report (Oct 2018 - April 2020)	
				14. Sponsoring Agency Code NETC 18-1: A study conducted in cooperation with the U.S. DOT	
15. Supplementary Notes N/A					
16. Abstract The predominate bridge rail and approach guardrail transition (AGT) systems used among the New England states include details for 2-bar, 3-bar and 4-bar designs which were developed and tested under previous crash test standards (i.e., AASHTO GSBRL PL2 and NCHRP Report 350). These basic designs are currently being implemented among various participating states using slight variations in design details, such as spacing between tube rails and curb height. The objectives of this study were to (1) conduct a detailed review of each State's Standards to identify differences in design details and to recommend dimensional and material specifications to ensure consistency among the States and (2) to evaluate the crash performance of the NETC bridge rail and transition designs using finite element analysis (FEA) to determine if these systems comply with current test standards of <i>MASH</i> .					
17. Key Words NETC, Steel Bridge Rail, 2-Bar, 3-Bar, 4-Bar, Approach Guardrail Transition, AGT, MASH, TL3, TL4, Finite Element Analysis, FEA, Critical Impact Point, CIP, Computer Simulation			18. Distribution Statement No restrictions. This document is available through the National Technical Information Service, Springfield, VA 22161. Enter any other agency mandated distribution statements. Remove NTIS statement if it does not apply.		
19. Security Classif. (of this report) Unclassified		20. Security Classif. Unclassified		21. No. of Pages 838	22. Price

SI* (MODERN METRIC) CONVERSION FACTORS

APPROXIMATE CONVERSIONS TO SI UNITS

APPROXIMATE CONVERSIONS TO SI UNITS

When You Know		Multiply By		When You Know		Multiply By		To Find		Symbol	
LENGTH											
in	inches	25.4	millimetres	mm	mm	mm	millimetres	0.039	inches	in	in
ft	feet	0.305	metres	m	m	m	metres	3.28	feet	ft	ft
yd	yards	0.914	metres	m	m	m	metres	1.09	yards	yd	yd
mi	miles	1.61	kilometres	km	km	km	kilometres	0.621	miles	mi	mi
AREA											
in ²	square inches	645.2	millimetres squared	mm ²	mm ²	mm ²	millimetres squared	0.0016	square inches	in ²	in ²
ft ²	square feet	0.093	metres squared	m ²	m ²	m ²	metres squared	10.764	square feet	ft ²	ft ²
yd ²	square yards	0.836	metres squared	m ²	m ²	ha	hectares	2.47	acres	ac	ac
ac	acres	0.405	hectares	ha	ha	km ²	kilometres squared	0.386	square miles	mi ²	mi ²
mi ²	square miles	2.59	kilometres squared	km ²	km ²						
VOLUME											
fl oz	fluid ounces	29.57	millilitres	mL	mL	mL	millilitres	0.034	fluid ounces	fl oz	fl oz
gal	gallons	3.785	Litres	L	L	L	litres	0.264	gallons	gal	gal
ft ³	cubic feet	0.028	metres cubed	m ³	m ³	m ³	metres cubed	35.315	cubic feet	ft ³	ft ³
yd ³	cubic yards	0.765	metres cubed	m ³	m ³	m ³	metres cubed	1.308	cubic yards	yd ³	yd ³
MASS											
oz	ounces	28.35	grams	g	g	g	grams	0.035	ounces	oz	oz
lb	pounds	0.454	kilograms	kg	kg	kg	kilograms	2.205	pounds	lb	lb
T	short tons (2000 lb)	0.907	megagrams	Mg	Mg	Mg	megagrams	1.102	short tons (2000 lb)	T	T
TEMPERATURE (exact)											
°F	Fahrenheit temperature	5(F-32)/9	Celsius temperature	°C	°C	°C	Celsius temperature	1.8C+32	Fahrenheit temperature	°F	°F

NOTE: Volumes greater than 1000 L shall be shown in m³

* SI is the symbol for the International System of Measurement

TABLE OF CONTENTS

ACKNOWLEDGEMENTS	IV
TECHNICAL REPORT DOCUMENTATION PAGE	III
METRICS CONVERSION PAGE	IV
TABLE OF CONTENTS.....	V
LIST OF FIGURES.....	XII
LIST OF TABLES.....	XXVII
LIST OF APPENDICES.....	XXX
1 INTRODUCTION.....	1
1.1 PROBLEM STATEMENT	1
1.2 OBJECTIVES	1
2 RESEARCH APPROACH AND SCOPE OF THE STUDY	2
3 LITERATURE REVIEW	3
3.1 SUMMARY OF CURRENT NETC BRIDGE RAIL DESIGNS	3
3.2 SUMMARY OF CURRENT NETC TRANSITION DESIGNS.....	4
3.3 PREVIOUS FULL-SCALE TESTING OF NETC HARDWARE	6
3.3.1 <i>NETC 2-Bar Bridge Rail</i>	6
3.3.2 <i>NETC 4-Bar Bridge Rail</i>	7
3.3.3 <i>NHDOT 2-Bar Rail to Thrie-Beam AGT</i>	9
3.3.4 <i>NHDOT 3-Bar Rail to Thrie-Beam AGT</i>	10
3.4 <i>MASH</i> EQUIVALENCY ASSESSMENT	11
3.4.1 <i>Rail Geometric Evaluations</i>	12
3.4.2 <i>Rail Strength Evaluations (Bridge Rails)</i>	14
3.4.3 <i>Summary of Strength Assessments for Baseline NETC Designs</i>	30
3.5 CRITICAL REVIEW OF CURRENT STANDARD DETAILS FOR NETC STYLE BRIDGE RAILS.....	30
3.5.1 <i>Rail Bars</i>	30
3.5.2 <i>Bridge Rail Post</i>	32
3.5.3 <i>Rail-to-Post Attachment</i>	34
3.5.4 <i>Baseplate and Anchor Bolts</i>	37
3.5.5 <i>Field Splice</i>	39
3.5.6 <i>Expansion Splice</i>	40
3.5.7 <i>Concrete Curb</i>	42
3.6 CRITICAL REVIEW OF CURRENT STANDARD DETAILS FOR NETC STYLE BRIDGE RAIL TRANSITIONS.....	43
3.6.1 <i>NHDOT 2-Bar Transition</i>	44
3.6.2 <i>NHDOT 3-Bar Transition</i>	47
3.6.3 <i>MaineDOT 4-Bar Transition</i>	50
3.6.4 <i>Alternate 4-Bar Transition (Sloped Rail Style)</i>	53
4 RECOMMENDATIONS FOR DIMENSIONAL AND MATERIAL SPECIFICATIONS	56
4.1 NETC BRIDGE RAIL DESIGNS	56

4.2	NETC APPROACH GUARDRAIL TRANSITION DESIGNS.....	60
4.3	SUMMARY	65
5	FEA VEHICLE MODELS	65
6	MODEL DEVELOPMENT AND VALIDATION OF THE NETC 4-BAR BRIDGE RAIL	73
6.1	MODEL DEVELOPMENT.....	73
6.1.1	<i>Posts.....</i>	74
6.1.2	<i>Tubular Rails and Mounting Bolts.....</i>	75
6.1.3	<i>Baseplate and Anchor Bolts</i>	76
6.1.4	<i>Concrete Curb, Sidewalk and Deck.....</i>	77
6.1.5	<i>Materials.....</i>	79
6.2	MODEL VALIDATION	79
6.2.1	<i>Model Set-Up and Impact Conditions</i>	79
6.2.2	<i>Issues and Limitations Regarding Test Data for Validation</i>	80
6.2.3	<i>Simulated Impact Summary.....</i>	83
6.2.4	<i>Sequential Views</i>	84
6.2.5	<i>Damage to Bridge Rail.....</i>	84
6.2.6	<i>Occupant Risk Measures.....</i>	94
6.2.7	<i>Time-History Data Comparison.....</i>	96
6.2.8	<i>PIRT – Crash Specific Phenomena</i>	99
6.2.9	<i>Summary and Conclusions on Model Validation.....</i>	103
7	MODEL DEVELOPMENT AND VALIDATION OF THE NETC 2-BAR TRANSITION	105
7.1	MODEL DEVELOPMENT.....	105
7.2	MATERIALS	107
7.3	DEVELOPMENT OF THE TRANSITION MODEL	107
7.3.1	<i>Rail Elements and Terminal Connector</i>	107
7.3.2	<i>Splice Bolts</i>	110
7.3.3	<i>Post Bolts</i>	111
7.3.4	<i>Wood Transition Posts</i>	111
7.3.5	<i>W6x25 Transition Posts</i>	112
7.3.6	<i>Transition Rail Tubes.....</i>	113
7.3.7	<i>Curb.....</i>	114
7.3.8	<i>Soil Model</i>	114
7.4	MODEL VALIDATION	116
7.4.1	<i>Simulated Impact Summary.....</i>	116
7.4.2	<i>Sequential Views.....</i>	118
7.4.3	<i>Damage to Bridge Rail.....</i>	118
7.4.4	<i>Occupant Risk Measures.....</i>	118
7.4.5	<i>Time-History Data Comparison.....</i>	126
7.4.6	<i>Quantitative Validation</i>	129
7.5	SUMMARY AND CONCLUSIONS ON MODEL VALIDATION	136
8	EVALUATION CRITERIA FOR FEA CRASH ANALYSIS	137

9	EVALUATION OF THE NETC 3-BAR BRIDGE RAIL FOR MASH TL4	141
9.1	TEST 4-10	143
9.1.1	<i>Summary of Key Phenomenological Events</i>	143
9.1.2	<i>Time History Data Evaluation</i>	144
9.1.3	<i>Occupant Risk Measures</i>	146
9.1.4	<i>Occupant Compartment Intrusion</i>	147
9.1.5	<i>Damages to the Barrier System</i>	147
9.1.6	<i>Damages to Vehicle</i>	149
9.1.7	<i>Exit Box</i>	150
9.1.8	<i>Results Summary</i>	150
9.2	TEST 4-11	153
9.2.1	<i>Summary of Key Phenomenological Events</i>	153
9.2.2	<i>Time History Data Evaluation</i>	154
9.2.3	<i>Occupant Risk Measures</i>	156
9.2.4	<i>Occupant Compartment Intrusion</i>	157
9.2.5	<i>Damages to the Barrier System</i>	157
9.2.6	<i>Damages to Vehicle</i>	159
9.2.7	<i>Exit Box</i>	160
9.2.8	<i>Results Summary</i>	160
9.3	TEST 4-12	163
9.3.1	<i>Summary of Key Phenomenological Events</i>	164
9.3.2	<i>Time History Data Evaluation</i>	165
9.3.3	<i>Occupant Risk Measures</i>	168
9.3.4	<i>Occupant Compartment Intrusion</i>	169
9.3.5	<i>Damages to the Barrier System</i>	170
9.3.6	<i>Peak Forces on Barrier</i>	172
9.3.7	<i>Damages to Vehicle</i>	173
9.3.8	<i>Exit Box</i>	173
9.3.9	<i>Test 4-12 Results Summary</i>	174
9.4	CONCLUSION FOR TL4 EVALUATION OF NETC 3-BAR BRIDGE RAIL	178
9.4.1	<i>Structural Adequacy: (PASS)</i>	178
9.4.2	<i>Occupant Risk (PASS)</i>	178
9.4.3	<i>Vehicle Trajectory (PASS)</i>	178
9.4.4	<i>Full-Scale Test Results of Similar Bridge Rail Design</i>	178
10	EVALUATION OF THE NETC 3-BAR TRANSITION FOR MASH TL4	180
10.1	DETERMINING CRITICAL IMPACT POINT	181
10.2	TEST 4-20	182
10.2.1	<i>CIP for Test 4-20</i>	182
10.2.2	<i>Summary of Key Phenomenological Events</i>	183
10.2.3	<i>Time History Data Evaluation</i>	184
10.2.4	<i>Occupant Risk Measures</i>	185
10.2.5	<i>Occupant Compartment Intrusion</i>	186

10.2.6 Damages to the Barrier System	187
10.2.7 Damages to Vehicle	188
10.2.8 Exit Box	188
10.2.9 Results Summary.....	189
10.3 TEST 4-21	191
10.3.1 CIP for Test 4-21.....	191
10.3.2 Summary of Key Phenomenological Events	193
10.3.3 Time History Data Evaluation	195
10.3.4 Occupant Risk Measures.....	197
10.3.5 Occupant Compartment Intrusion	198
10.3.6 Damages to the Barrier System	198
10.3.7 Damages to Vehicle	200
10.3.8 Exit Box	201
10.3.9 Results Summary.....	201
10.4 TEST 4-22	203
10.4.1 CIP for Test 4-22.....	203
10.4.2 Summary of Key Phenomenological Events	205
10.4.3 Time History Data Evaluation	206
10.4.4 Occupant Risk Measures.....	209
10.4.5 Occupant Compartment Intrusion	209
10.4.6 Damages to the Barrier System	210
10.4.7 Peak Forces on Barrier	211
10.4.8 Damages to Vehicle	212
10.4.9 Exit Box	213
10.4.10 Test 4-22 Results Summary	213
10.5 CONCLUSIONS FOR MASH TL4 EVALUATION OF THE 3-BAR TRANSITION	216
10.5.1 Structural Adequacy: (PASS)	216
10.5.2 Occupant Risk (PASS)	216
10.5.3 Vehicle Trajectory (PASS)	216
11 EVALUATION OF THE NETC 4-BAR BRIDGE RAIL FOR MASH TL4	216
11.1 TEST 4-10	217
11.1.1 Summary of Key Phenomenological Events.....	218
11.1.2 Time History Data Evaluation	219
11.1.3 Occupant Risk Measures.....	221
11.1.4 Occupant Compartment Intrusion	222
11.1.5 Damages to the Barrier System	223
11.1.6 Damages to Vehicle	224
11.1.7 Exit Box	225
11.1.8 Results Summary.....	225
11.2 TEST 4-11	228
11.2.1 Summary of Key Phenomenological Events.....	229
11.2.2 Time History Data Evaluation	230

11.2.3	Occupant Risk Measures	231
11.2.4	Occupant Compartment Intrusion	232
11.2.5	Damages to the Barrier System	233
11.2.6	Damages to Vehicle	234
11.2.7	Exit Box	235
11.2.8	Results Summary.....	235
11.3	TEST 4-12	238
11.3.1	Summary of Key Phenomenological Events	238
11.3.2	Time History Data Evaluation	239
11.3.3	Occupant Risk Measures.....	242
11.3.4	Occupant Compartment Intrusion	243
11.3.5	Damages to the Barrier System	244
11.3.6	Peak Forces on Barrier	246
11.3.7	Damages to Vehicle	246
11.3.8	Exit Box	247
11.3.9	Test 4-12 Results Summary.....	247
11.4	CONCLUSION FOR TL4 EVALUATION OF NETC 4-BAR BRIDGE RAIL.....	250
11.4.1	Structural Adequacy: (PASS)	250
11.4.2	Occupant Risk (PASS)	250
11.4.3	Vehicle Trajectory (PASS)	250
12	EVALUATION OF THE CONCRETE TRANSITION TO THRIE-BEAM FOR 4-BAR BRIDGE RAILS	250
12.1	MODEL DEVELOPMENT.....	250
12.2	TEST 4-20	255
12.2.1	CIP for Test 4-20.....	255
12.2.2	Summary of Key Phenomenological Events	257
12.2.3	Time History Data Evaluation	258
12.2.4	Occupant Risk Measures.....	260
12.2.5	Occupant Compartment Intrusion	261
12.2.6	Damages to the Barrier System	261
12.2.7	Damages to Vehicle	264
12.2.8	Exit Box	264
12.2.9	Results Summary.....	264
12.2.10	Comparison to MASH Test 4-20 on Similar AGT System.....	267
12.3	TEST 4-21	270
12.3.1	CIP for Test 4-21.....	270
12.3.2	Summary of Key Phenomenological Events	274
12.3.3	Time History Data Evaluation	276
12.3.4	Occupant Risk Measures.....	277
12.3.5	Occupant Compartment Intrusion	278
12.3.6	Damages to the Barrier System	280
12.3.7	Damages to Vehicle	282
12.3.8	Exit Box	282

12.3.9 Results Summary.....	282
12.4 TEST 4-22	285
12.4.1 CIP for Test 4-22.....	285
12.4.2 Summary of Key Phenomenological Events	287
12.4.3 Time History Data Evaluation	289
12.4.4 Occupant Risk Measures.....	292
12.4.5 Occupant Compartment Intrusion	293
12.4.6 Damages to the Barrier System	294
12.4.7 Peak Forces on Barrier	295
12.4.8 Damages to Vehicle	296
12.4.9 Exit Box	297
12.4.10 Test 4-22 Results Summary	297
12.5 CONCLUSIONS FOR MASH TL4 EVALUATION OF THE CONCRETE TRANSITION TO THRIE-BEAM SYSTEM.....	300
12.5.1 Structural Adequacy: (Marginal Pass)	300
12.5.2 Occupant Risk (Fail)	300
12.5.3 Vehicle Trajectory (PASS)	300
13 EVALUATION OF THE NETC 2-BAR BRIDGE RAIL FOR MASH TL3	300
13.1 TEST 3-10	301
13.1.1 Summary of Key Phenomenological Events.....	302
13.1.2 Time History Data Evaluation	303
13.1.3 Occupant Risk Measures.....	305
13.1.4 Occupant Compartment Intrusion	306
13.1.5 Damages to the Barrier System	307
13.1.6 Damages to Vehicle	308
13.1.7 Exit Box	309
13.1.8 Results Summary.....	309
13.2 TEST 3-11	312
13.2.1 Summary of Key Phenomenological Events.....	312
13.2.2 Time History Data Evaluation	313
13.2.3 Occupant Risk Measures.....	315
13.2.4 Occupant Compartment Intrusion	316
13.2.5 Damages to the Barrier System	316
13.2.6 Damages to Vehicle	318
13.2.7 Exit Box	319
13.2.8 Results Summary.....	319
13.3 CONCLUSION FOR TL3 EVALUATION OF NETC 2-BAR BRIDGE RAIL.....	322
13.3.1 Structural Adequacy: (PASS)	322
13.3.2 Occupant Risk (PASS)	322
13.3.3 Vehicle Trajectory (PASS)	322
13.3.4 Barrier Damages	322
14 EVALUATION OF THE NETC 2-BAR TRANSITION FOR MASH TL3	322
14.1 DETERMINING CRITICAL IMPACT POINT.....	323

14.2	TEST 3-20	324
14.2.1	CIP for Test 3-20.....	324
14.2.2	Summary of Key Phenomenological Events.....	325
14.2.3	Time History Data Evaluation	327
14.2.4	Occupant Risk Measures.....	328
14.2.5	Occupant Compartment Intrusion	329
	Damages to the Barrier System.....	330
14.2.6	Damages to Vehicle	331
14.2.7	Exit Box	331
14.2.8	Results Summary.....	332
14.3	TEST 3-21	334
14.3.1	CIP for Test 3-21.....	334
14.3.2	Summary of Key Phenomenological Events.....	337
14.3.3	Time History Data Evaluation	338
14.3.4	Occupant Risk Measures.....	340
14.3.5	Occupant Compartment Intrusion	341
14.3.6	Damages to the Barrier System	341
14.3.7	Damages to Vehicle	343
14.3.8	Exit Box	343
14.3.9	Results Summary.....	343
14.4	CONCLUSIONS FOR MASH TL3 EVALUATION OF THE 2-BAR TRANSITION	346
14.4.1	Structural Adequacy: (PASS)	346
14.4.2	Occupant Risk (PASS).....	346
14.4.3	Vehicle Trajectory (PASS).....	346
15	MODIFIED DESIGNS AND EVALUATIONS	346
15.1	MODIFIED NETC 3-BAR BRIDGE RAIL WITH STIFFER LOWER RAIL.....	346
15.1.1	Analysis Cases.....	347
15.1.2	Test 4-10	348
15.2	3-BAR TRANSITION WITH INCREASED POST SPACING AT FIRST BRIDGE RAIL POST	353
15.2.1	Design Cases Evaluated	354
15.2.2	Test 4-20	356
15.2.3	Test 4-21	365
15.2.4	Test 4-22	370
15.2.5	Conclusions and Recommendations.....	377
15.3	MODIFIED NETC 4-BAR BRIDGE RAIL WITH W8X28 POSTS	377
15.3.1	Test 4-12	378
15.3.2	Conclusions and Recommendations.....	385
16	SUMMARY OF DESIGN EVALUATIONS	385
16.1	SUMMARY OF MASH LRFD STRENGTH AND RAIL-GEOMETRIC CALCULATIONS	386
16.2	COMPARISON OF DESIGN DETAIL SPECIFICATIONS SUMMARY	386
16.3	SUMMARY OF FEA MODEL VALIDATION	387
16.3.1	NETC 4-Bar Bridge Rail Model Validation	387

16.3.2	NETC 2-Bar Transition Model Validation	387
16.3.3	Possible Accuracy Issues	388
16.4	SUMMARY OF THE MASH EVALUATIONS OF NETC BRIDGE RAIL AND TRANSITION DESIGNS	390
16.4.1	NETC 2-Bar Bridge Rail (TL3).....	391
16.4.2	NETC 3-Bar Bridge Rail (TL4).....	391
16.4.3	Modified NETC 3-Bar Bridge Rail with HSS 5x4x5/16 Lower Rail	392
16.4.4	NETC 4-Bar Bridge Rail (TL4).....	393
16.4.5	Modified NETC 4-Bar Bridge Rail with W8x28 Posts.....	394
16.4.6	NETC 2-Bar Transition (TL3).....	394
16.4.7	NETC 3-Bar Transition (TL4).....	395
16.4.8	NETC 3-Bar Transition with 5.5-ft Post Spacing at First Bridge Rail Post (TL4).....	397
16.4.9	Concrete Transition Barrier to Thrie Beam (TL4).....	398
17	CONCLUSIONS AND RECOMMENDATIONS	401
17.1	NETC BRIDGE RAIL DESIGNS	401
17.1.1	Conclusions regarding Critical Design Aspects.....	401
17.1.2	Conclusions and Recommendations on Final Design	404
17.2	NETC TRANSITION DESIGNS.....	406
18	REFERENCES	413

LIST OF FIGURES

FIGURE 1.	NETC BRIDGE RAIL DESIGNS.	3
FIGURE 2.	NETC 4-BAR CURB-MOUNTED BRIDGE RAIL DESIGN.....	4
FIGURE 3.	ELEVATION DRAWING OF THE CURRENT AGTs TO BE EVALUATED IN THIS STUDY.	5
FIGURE 4.	CONCRETE BUTTRESS FOR THE MAINE AGT TO 4-BAR BRIDGE RAIL.....	5
FIGURE 5.	NETC 4-BAR (SBB44B) BRIDGE RAIL. [KIMBALL99]	8
FIGURE 6.	NHDOT 2-BAR RAIL TO THRIE-BEAM AGT. [ALBERSON06]	10
FIGURE 7.	AASHTO SECTION 13 FIGURES A13.1.1-2 AND A13.1.1-3 INCLUDING NETC BRIDGE RAIL. [AASHTO12]	12
FIGURE 8.	RAIL GEOMETRICS SUMMARY FOR NETC STYLE BARRIERS BY STATE (BLUE DENOTES PRIORITY DESIGNS).	13
FIGURE 9.	EXAMPLE CALCULATIONS FOR THE RAIL GEOMETRIC CRITERIA BASED ON A POST SETBACK DISTANCE OF 4 INCHES.....	14
FIGURE 10.	WELD SPECIFICATIONS FOR POST-TO-BASEPLATE IN NETC RAILING DESIGNS.....	18
FIGURE 11.	CONCRETE DAMAGE MODES EXPERIENCED IN NCHRP REPORT 350 TEST 3-11 ON THE TXDOT T77 BRIDGE RAIL.	20
FIGURE 12.	PUNCHING SHEAR DAMAGE MODE EXPERIENCED IN NCHRP REPORT 350 TEST 3-11 ON THE TXDOT T101 BRIDGE RAIL.	20
FIGURE 13.	THEORETICAL FAILURE PLANES FOR PRY-OUT SHEAR CONE FAILURE IN CONCRETE.	21
FIGURE 14.	(A) ASSUMED LOAD/REACTION POINTS FOR THE ANCHOR BOLT PRY-OUT RESISTANCE CALCULATIONS AND (B) DIMENSIONS OF THE NETC BASEPLATE.....	21
FIGURE 15.	APPROXIMATED FAILURE PLANES FOR PUSH-OUT SHEAR FAILURE IN CONCRETE.....	22
FIGURE 16.	CALCULATION FOR SHEAR PLANES A AND B FOR PUSH-OUT SHEAR FAILURE.	23
FIGURE 17.	PUNCHING SHEAR FAILURE MODE (FIGURE A13.4.3.2-1 IN 2012 LRFD).....	24
FIGURE 18.	(A) ASSUMED LOAD/REACTION POINTS FOR THE PUNCHING SHEAR RESISTANCE CALCULATIONS AND (B) DIMENSIONS OF THE NETC BASEPLATE.....	24
FIGURE 19.	EXPANSION SPLICE DETAILS FOR A) NHDOT AND RIDOT, B) MAINE DOT AND C) VTRANS.....	41
FIGURE 20.	DRAWINGS OF THE TWO DESIGN CONCEPTS FOR NETC APPROACH GUARDRAIL TRANSITIONS (AGT).	44

FIGURE 21. NHDOT T2 AGT UPSTREAM W-BEAM SECTION.	44
FIGURE 22. NHDOT T2 AGT SYMMETRICAL W-BEAM TO THRIE-BEAM TRANSITION SECTION.	45
FIGURE 23. NHDOT T2 AGT DOUBLE NESTED THRIE-BEAM SECTION.	45
FIGURE 24. NHDOT T2 AGT SLOPED RAIL SECTION.	46
FIGURE 25. POST RAIL ASSEMBLY NHDOT T2 AGT (T3 SIMILAR)	47
FIGURE 26. TERMINAL AND CONNECTION PLATE DETAIL DRAWINGS FOR NHDOT T2 AGT (T3 SIMILAR).....	47
FIGURE 27. NHDOT T3 AGT UPSTREAM W-BEAM SECTION.....	48
FIGURE 28. NHDOT T3 AGT SYMMETRICAL W-BEAM TO THRIE-BEAM TRANSITION SECTION.	48
FIGURE 29. NHDOT T3 AGT DOUBLE NESTED THRIE-BEAM SECTION.	49
FIGURE 30. NHDOT T3 AGT SLOPED RAIL SECTION.....	49
FIGURE 31. MAINE DOT TYPE IA AGT UPSTREAM W-BEAM SECTION.....	50
FIGURE 32. MAINE DOT TYPE IA AGT ASYMMETRICAL W-BEAM TO THRIE-BEAM TRANSITION SECTION.	51
FIGURE 33. MAINE DOT TYPE IA AGT DOUBLE NESTED THRIE-BEAM SECTION.	51
FIGURE 34. MAINE DOT TYPE IA AGT CONCRETE BUTTRESS SECTION.	52
FIGURE 35. STANDARDIZED BUTTRESS DESIGN. [ROSENBAUGH18]	52
FIGURE 36. PLAN AND PROFILE VIEW OF THE SHAPED BUTTRESS.	53
FIGURE 37. NHDOT T4 AGT UPSTREAM W-BEAM SECTION (VTRANS SIMILAR EXCEPT BOTTOM BAR AND SIDEWALK).	54
FIGURE 38. NHDOT T4 AGT SYMMETRICAL W-BEAM TO THRIE-BEAM TRANSITION SECTION (VTRANS SIMILAR EXCEPT BOTTOM BAR AND HEIGHT).	54
FIGURE 39. NHDOT T4 AGT DOUBLE NESTED THRIE-BEAM SECTION.	55
FIGURE 40. NHDOT T4 AGT SLOPED RAIL SECTION.....	55
FIGURE 41. VTRANS 4-BAR AGT SLOPED RAIL SECTION.	56
FIGURE 42. IMAGES OF THE FEA MODEL FOR THE BASELINE AND DETAILED CARGO-BOX MODELS (REAR DOOR NOT SHOWN TO FACILITATE VIEWING INSIDE OF CARGO BOX).....	67
FIGURE 43. VEHICLE PROPERTY SHEET FOR THE 8000S VEHICLE MODEL COMPARED WITH FULL-SCALE TEST NETC-3 (I.E., VALIDATION CASE).....	68
FIGURE 44. VEHICLE PROPERTY SHEET FOR THE C2500R VEHICLE MODEL COMPARED WITH FULL-SCALE TEST 401181-1 (I.E., VALIDATION CASE).....	69
FIGURE 45. VEHICLE PROPERTY SHEET FOR THE 1100C VEHICLE MODEL COMPARED WITH A RECENT TEST VEHICLE FROM TEST 607451-3	70
FIGURE 46. VEHICLE PROPERTY SHEET FOR THE 2270P VEHICLE MODEL COMPARED WITH A RECENT TEST VEHICLE FROM TEST 607451-2.	71
FIGURE 47. VEHICLE PROPERTY SHEET FOR THE BASELINE 10000S VEHICLE MODEL COMPARED WITH A RECENT TEST VEHICLE FROM TEST 607451-1.	72
FIGURE 48. FINITE ELEMENT ANALYSIS MODEL OF THE NETC 4-BAR BRIDGE RAIL (PLAN VIEW).....	73
FIGURE 49. FINITE ELEMENT ANALYSIS MODEL OF THE NETC 4-BAR BRIDGE RAIL (ISOMETRIC VIEW).	74
FIGURE 50. REPRESENTATIVE SECTION OF THE FEA MODEL OF THE BRIDGE RAIL.	74
FIGURE 51. FEA MODEL OF BRIDGE RAIL POST.	75
FIGURE 52. FE MESH OF THE MIDDLE TUBE-RAIL AND BOLT (ONE BOLT REMOVED TO FACILITATE VIEWING SLOTTED MOUNTING HOLE).	75
FIGURE 53. MODEL OF RAIL SPLICE FOR VALIDATION MODEL WITH RAIL-TUBE SHOWN TRANSPARENT.	76
FIGURE 54. UPDATED MODEL OF RAIL SPLICE USED IN MASH EVALUATIONS WITH RAIL-TUBE SHOWN TRANSPARENT.	76
FIGURE 55. TRANSPARENT VIEW OF CONCRETE SHOWING MODEL OF BASEPLATE AND ANCHOR BOLTS.....	77
FIGURE 56. PROFILE VIEW OF SIDEWALK MODEL.	78
FIGURE 57. PLAN VIEW OF SIDEWALK MODEL (FROM BACK OF BRIDGE RAIL).	78

FIGURE 58. STRESS VS. STRAIN CURVE FOR ASTM A615 GRADE 60 STEEL	78
FIGURE 59. LONGITUDINAL (X-DIRECTION) ACCELERATION MEASURED AT VEHICLE C.G. IN TEST NETC-3. [KIMBALL99]	80
FIGURE 60. LATERAL (Y-DIRECTION) ACCELERATION MEASURED AT VEHICLE C.G. IN TEST NETC-3. [KIMBALL99]	81
FIGURE 61. VERTICAL (Z-DIRECTION) ACCELERATION MEASURED AT VEHICLE C.G. IN TEST NETC-3. [KIMBALL99]	81
FIGURE 62. YAW-RATE MEASURED AT VEHICLE C.G. IN TEST NETC-3. [KIMBALL99]	82
FIGURE 63. FEA VEHICLE AND TEST VEHICLE ILLUSTRATING THE DIFFERENCES IN CARGO-BOX LENGTH AND BUMPER DESIGN.	82
FIGURE 64. SEQUENTIAL VIEWS OF TEST NETC-3 AND FE ANALYSIS FROM UPSTREAM VIEWPOINT.	85
FIGURE 65. SEQUENTIAL VIEWS OF TEST NETC-3 AND FE ANALYSIS FROM DOWNSTREAM VIEWPOINT.	88
FIGURE 66. SEQUENTIAL VIEWS OF TEST NETC-3 AND FE ANALYSIS FROM OVERHEAD VIEWPOINT.	90
FIGURE 67. DAMAGE TO BRIDGE RAIL IN FULL-SCALE TEST NETC-3 FROM (A) POSTS 6 THROUGH 8 AND (B) 8 THROUGH 11.	92
FIGURE 68. CONTOUR PLOT OF EFFECTIVE PLASTIC STRAIN SHOWING DEFORMATIONS OF THE BRIDGE RAIL MODEL (TRAFFIC SIDE).	93
FIGURE 69. CONTOUR PLOT OF EFFECTIVE PLASTIC STRAIN SHOWING DEFORMATIONS OF THE BRIDGE RAIL MODEL (BACK SIDE).	93
FIGURE 70. DEFORMATION OF BASEPLATE FOR TEST (LEFT) AND FEA MODEL (RIGHT).	93
FIGURE 71. LOCATION OF ACCELEROMETER IN FE MODEL.	94
FIGURE 72. GRAPHICAL COMPARISON OF FEA VS. TEST FOR KEY OCCUPANT RISK METRICS	96
FIGURE 73. LONGITUDINAL ACCELERATION-TIME HISTORY PLOT FROM ACCELEROMETER AT C.G. FOR FULL-SCALE TEST NETC-3 AND FEA (180 HZ. FILTER AND 50-MS MOVING AVERAGES)	96
FIGURE 74. LATERAL ACCELERATION-TIME HISTORY PLOT FROM ACCELEROMETER AT C.G. FOR FULL-SCALE TEST NETC-3 AND FEA (180 HZ. FILTER AND 50-MS MOVING AVERAGES).	97
FIGURE 75. VERTICAL ACCELERATION-TIME HISTORY PLOT FROM ACCELEROMETER AT C.G. FOR FULL-SCALE TEST NETC-3 AND FEA (180 HZ. FILTER AND 50-MS MOVING AVERAGES).	97
FIGURE 76. YAW-TIME HISTORY PLOT FROM ACCELEROMETER AT C.G. FOR FEA (ANGULAR RATE AND DISPLACEMENT).	97
FIGURE 77. ROLL-TIME HISTORY PLOT FROM ACCELEROMETER AT C.G. FOR FEA (ANGULAR RATE AND DISPLACEMENT).	98
FIGURE 78. PITCH-TIME HISTORY PLOT FROM ACCELEROMETER AT C.G. FOR FEA (ANGULAR RATE AND DISPLACEMENT).	98
FIGURE 79. POST-TEST PHOTO OF VEHICLE DAMAGES.	98
FIGURE 80. FINITE ELEMENT ANALYSIS MODEL OF THE NETC 2-BAR TRANSITION AND BRIDGE RAIL	106
FIGURE 81. GENERAL MODEL ASSEMBLY FOR THE NETC 2-BAR TRANSITION (RAIL LABELING).	106
FIGURE 82. GENERAL MODEL ASSEMBLY FOR THE NETC 2-BAR TRANSITION (POST LABELING).	106
FIGURE 83: FEA MESH FOR (A) W-BEAM PANEL AND (B) THRIE-BEAM PANEL.	107
FIGURE 84. FEA MESH FOR THE THRIE-BEAM TRANSITION PANEL.	108
FIGURE 85. FEA MESH FOR THE THRIE-BEAM END-SHOE TERMINAL CONNECTOR.	109
FIGURE 86. FEA MESH FOR THE CONNECTION PLATE.	109
FIGURE 87. FEA MESH FOR THE DEFLECTOR PLATE.	110
FIGURE 88. (A) FEA MESH FOR SPLICE BOLT AND (B) PROFILE OF SPLICE BEFORE AND AFTER TIGHTENING SPLICE BOLT TIGHTENING.	111
FIGURE 89. FEA MODEL OF THE POST BOLT (TYP) WITH THE BLOCKOUT, POST, AND RAIL DISPLAYED IN TRANSPARENCY MODE TO FACILITATE VIEWING.	111
FIGURE 90. FEA MODEL OF WOOD AGT POSTS.	112
FIGURE 91. FEA MESH OF THE W6X25 POSTS OF THE TRANSITION.	113
FIGURE 92. FEA MESH OF THE TRANSITION TUBE RAILS.	113
FIGURE 93. FEA MODEL FOR CURB.	114
FIGURE 94. SOIL MODELS USED IN THE TRANSITION MODEL.	115
FIGURE 95. CONTINUUM SOIL MODEL MESH AND DIMENSIONS.	115
FIGURE 96. IMPACT POINT FOR TEST AND SIMULATION FOR REPORT 350 TEST 3-21 ON THE 2-BAR TRANSITION.	116

FIGURE 97. SEQUENTIAL VIEWS OF FE ANALYSIS AND TEST 401181-1 FROM AN OVERHEAD VIEWPOINT.	119
FIGURE 98. SEQUENTIAL VIEWS OF FE ANALYSIS AND TEST 401181-1 FROM A DOWNSTREAM VIEWPOINT.	122
FIGURE 99. COMPARING OVERALL DEFORMATION OF SYSTEM FOR FEA AND TEST 401181-1.	124
FIGURE 100. LOCATION OF ACCELEROMETER IN THE FE MODEL.	125
FIGURE 101. GRAPHICAL COMPARISON OF FEA VS. TEST FOR KEY OCCUPANT RISK METRICS.	126
FIGURE 102. LONGITUDINAL ACCELERATION-TIME HISTORY PLOT FROM ACCELEROMETER AT C.G. FOR FULL-SCALE TEST 401181-1 AND FEA (10-MS AND 50-MS MOVING AVERAGES).	127
FIGURE 103. LATERAL ACCELERATION-TIME HISTORY PLOT FROM ACCELEROMETER AT C.G. FOR FULL-SCALE TEST 401181-1 AND FEA (10-MS AND 50-MS MOVING AVERAGES).	127
FIGURE 104. VERTICAL ACCELERATION-TIME HISTORY PLOT FROM ACCELEROMETER AT C.G. FOR FULL-SCALE TEST 401181-1 AND FEA (10-MS AND 50-MS MOVING AVERAGES).	127
FIGURE 105. YAW-TIME HISTORY PLOT FROM ACCELEROMETER INSIDE CABIN FOR FULL-SCALE TEST 401181-1 AND FEA (ANGULAR RATE AND DISPLACEMENT).....	128
FIGURE 106. ROLL-TIME HISTORY PLOT FROM ACCELEROMETER INSIDE CABIN FOR FULL-SCALE TEST 401181-1 AND FEA (ANGULAR RATE AND DISPLACEMENT).....	128
FIGURE 107. PITCH-TIME HISTORY PLOT FROM ACCELEROMETER INSIDE CABIN FOR FULL-SCALE TEST 401181-1 AND FEA (ANGULAR RATE AND DISPLACEMENT).....	128
FIGURE 108. PLOT OF GLOBAL ENERGY-TIME HISTORIES FROM THE ANALYSIS.	130
FIGURE 109. LOCATION OF C.G. IN FEA MODEL OF 1100C VEHICLE.	139
FIGURE 110. LOCATION OF C.G. IN FEA MODEL OF 2270P VEHICLE.	139
FIGURE 111. LOCATION OF ACCELEROMETERS AND C.G. IN FEA MODEL OF 10000S VEHICLE.	139
FIGURE 112. <i>MASH</i> EXIT BOX. [AASHTO16].....	141
FIGURE 113. FEA MODEL OF CURB-MOUNTED NETC 3-BAR COMPARED WITH BASELINE SIDEWALK-MOUNTED 4-BAR MODEL.	142
FIGURE 114. IMPACT POINT FOR TEST 4-10 ON THE NETC 3-BAR BRIDGE RAIL.	143
FIGURE 115. 10- AND 50-MILLISECOND AVERAGE X-ACCELERATION FROM FEA OF TEST 4-10 ON THE NETC 3-BAR BRIDGE RAIL.....	144
FIGURE 116. 10- AND 50-MILLISECOND AVERAGE Y-ACCELERATION FROM FEA OF TEST 4-10 ON THE NETC 3-BAR BRIDGE RAIL.....	145
FIGURE 117. 10- AND 50-MILLISECOND AVERAGE Z-ACCELERATION FROM FEA OF TEST 4-10 ON THE NETC 3-BAR BRIDGE RAIL.....	145
FIGURE 118. YAW RATE AND YAW ANGLE TIME-HISTORY FROM FEA OF TEST 4-10 ON THE NETC 3-BAR BRIDGE RAIL.	145
FIGURE 119. ROLL RATE AND ROLL ANGLE TIME-HISTORY FROM FEA OF TEST 4-10 ON THE NETC 3-BAR BRIDGE RAIL.....	146
FIGURE 120. PITCH RATE AND PITCH ANGLE TIME-HISTORY FROM FEA OF TEST 4-10 ON THE NETC 3-BAR BRIDGE RAIL.	146
FIGURE 121. OCCUPANT COMPARTMENT DEFORMATION RESULTING FROM TEST 4-10 ON THE NETC 3-BAR BRIDGE RAIL.	147
FIGURE 122. OVERHEAD VIEW OF NETC 3-BAR BRIDGE RAIL AFTER TEST 4-10 SHOWING EXTENT OF DAMAGE.	148
FIGURE 123. CONTOUR PLOT OF LATERAL DISPLACEMENT FOR THE BRIDGE RAIL FOR TEST 4-10 AT THE TIME OF MAXIMUM DYNAMIC DEFLECTION.	148
FIGURE 124. CONTOUR PLOT OF MAXIMUM PERMANENT DEFLECTION OF THE BRIDGE RAIL FOR TEST 4-10.	148
FIGURE 125. CONTOURS OF EFFECTIVE PLASTIC STRAINS FOR TEST 4-10 ON THE NETC 3-BAR BRIDGE RAIL.	149
FIGURE 126. CONTOURS OF 1 ST PRINCIPAL STRAINS FOR CONCRETE AT THE CRITICAL POST FOR TEST 4-10 ON THE NETC 3-BAR BRIDGE RAIL.....	149
FIGURE 127. DAMAGES TO VEHICLE IN TEST 4-10 ANALYSIS OF THE NETC 3-BAR BRIDGE RAIL.	150
FIGURE 128. EXIT BOX FOR TEST 4-10 ANALYSIS OF THE NETC 3-BAR BRIDGE RAIL.	150
FIGURE 129. SUMMARY RESULTS FOR <i>MASH</i> TEST 4-10 ON THE NETC 3-BAR BRIDGE RAIL.....	152
FIGURE 130. IMPACT POINT FOR TEST 4-11 ON THE NETC 3-BAR BRIDGE RAIL.	153
FIGURE 131. 10- AND 50-MILLISECOND AVERAGE X-ACCELERATION FROM FEA OF TEST 4-11 ON THE NETC 3-BAR BRIDGE RAIL.....	154
FIGURE 132. 10- AND 50-MILLISECOND AVERAGE Y-ACCELERATION FROM FEA OF TEST 4-11 ON THE NETC 3-BAR BRIDGE RAIL.....	155

FIGURE 133. 10- AND 50-MILLISECOND AVERAGE Z-ACCELERATION FROM FEA OF TEST 4-11 ON THE NETC 3-BAR BRIDGE RAIL.	155
FIGURE 134. YAW RATE AND YAW ANGLE TIME-HISTORY FROM FEA OF TEST 4-11 ON THE NETC 3-BAR BRIDGE RAIL.	155
FIGURE 135. ROLL RATE AND ROLL ANGLE TIME-HISTORY FROM FEA OF TEST 4-11 ON THE NETC 3-BAR BRIDGE RAIL.	156
FIGURE 136. PITCH RATE AND PITCH ANGLE TIME-HISTORY FROM FEA OF TEST 4-11 ON THE NETC 3-BAR BRIDGE RAIL.	156
FIGURE 137. OCCUPANT COMPARTMENT DEFORMATION RESULTING FROM TEST 4-11 ON THE NETC 3-BAR BRIDGE RAIL.	157
FIGURE 138. OVERHEAD VIEW OF NETC 3-BAR BRIDGE RAIL AFTER TEST 4-11 SHOWING EXTENT OF DAMAGE.	158
FIGURE 139. CONTOUR PLOT OF LATERAL DISPLACEMENT FOR THE BRIDGE RAIL FOR TEST 4-11 AT THE TIME OF MAXIMUM DYNAMIC DEFLECTION.	158
FIGURE 140. CONTOUR PLOT OF MAXIMUM PERMANENT DEFLECTION OF THE BRIDGE RAIL FOR TEST 4-11.	158
FIGURE 141. CONTOURS OF EFFECTIVE PLASTIC STRAINS FOR TEST 4-11 ON THE NETC 3-BAR BRIDGE RAIL.	159
FIGURE 142. CONTOURS OF 1 ST PRINCIPAL STRAINS FOR CONCRETE AT THE CRITICAL POST FOR TEST 4-11 ON THE NETC 3-BAR BRIDGE RAIL.	159
FIGURE 143. DAMAGES TO VEHICLE IN TEST 4-11 ANALYSIS OF THE NETC 3-BAR BRIDGE RAIL.	159
FIGURE 144. EXIT BOX FOR TEST 4-11 ANALYSIS OF THE NETC 3-BAR BRIDGE RAIL.	160
FIGURE 145. SUMMARY RESULTS FOR <i>MASH</i> TEST 4-11 ON THE NETC 3-BAR BRIDGE RAIL.	162
FIGURE 146. IMPACT POINT FOR TEST 4-12 ON THE NETC 3-BAR BRIDGE RAIL.	163
FIGURE 147. 10- AND 50-MILLISECOND AVERAGE X-ACCELERATION FROM FEA OF TEST 4-12 ON THE NETC 3-BAR BRIDGE RAIL (C.G. ACCELEROMETER).....	166
FIGURE 148. 10- AND 50-MILLISECOND AVERAGE Y-ACCELERATION FROM FEA OF TEST 4-12 ON THE NETC 3-BAR BRIDGE RAIL (C.G. ACCELEROMETER).....	166
FIGURE 149. 10- AND 50-MILLISECOND AVERAGE Z-ACCELERATION FROM FEA OF TEST 4-12 ON THE NETC 3-BAR BRIDGE RAIL (C.G. ACCELEROMETER).....	166
FIGURE 150. 10- AND 50-MILLISECOND AVERAGE X-ACCELERATION FROM FEA OF TEST 4-12 ON THE NETC 3-BAR BRIDGE RAIL (CABIN ACCELEROMETER).....	167
FIGURE 151. 10- AND 50-MILLISECOND AVERAGE Y-ACCELERATION FROM FEA OF TEST 4-12 ON THE NETC 3-BAR BRIDGE RAIL (CABIN ACCELEROMETER).....	167
FIGURE 152. 10- AND 50-MILLISECOND AVERAGE Z-ACCELERATION FROM FEA OF TEST 4-12 ON THE NETC 3-BAR BRIDGE RAIL (CABIN ACCELEROMETER).....	167
FIGURE 153. YAW RATE AND YAW ANGLE TIME-HISTORY FROM FEA OF TEST 4-12 ON THE NETC 3-BAR BRIDGE RAIL (CABIN ACCELEROMETER).....	168
FIGURE 154. ROLL RATE AND ROLL ANGLE TIME-HISTORY FROM FEA OF TEST 4-12 ON THE NETC 3-BAR BRIDGE RAIL (CABIN ACCELEROMETER).....	168
FIGURE 155. PITCH RATE AND PITCH ANGLE TIME-HISTORY FROM FEA OF TEST 4-12 ON THE NETC 3-BAR BRIDGE RAIL (CABIN ACCELEROMETER).....	168
FIGURE 156. OCCUPANT COMPARTMENT DEFORMATION RESULTING FROM TEST 4-12 ON THE NETC 3-BAR BRIDGE RAIL SYSTEM.	170
FIGURE 157. CONTOUR PLOT OF LATERAL DISPLACEMENT FOR THE BRIDGE RAIL FROM TEST 4-12 AT THE TIME OF MAXIMUM DYNAMIC DEFLECTION FOR THE NETC 3-BAR BRIDGE RAIL.	170
FIGURE 158. CONTOUR PLOT OF PERMANENT DEFLECTION FOR THE BRIDGE RAIL FROM TEST 4-12 FOR THE NETC 3-BAR BRIDGE RAIL.	171
FIGURE 159. CONTOURS OF EFFECTIVE PLASTIC STRAINS ON THE CRITICAL POST FOR TEST 4-12 ON THE NETC 3-BAR BRIDGE RAIL.	171
FIGURE 160. PLOT OF MATERIAL STRESS-STRAIN CURVE FOR POST WITH NECKING STRAIN IDENTIFIED.	172
FIGURE 161. CONTOURS OF 1 ST PRINCIPAL STRAINS FOR CONCRETE AT THE CRITICAL POST FOR TEST 4-12 ON THE NETC 3-BAR BRIDGE RAIL.	172
FIGURE 162. LATERAL FORCE-TIME HISTORY BETWEEN VEHICLE AND BARRIER FOR TEST 4-12 ON NETC 3-BAR BRIDGE RAIL.....	173
FIGURE 163. DAMAGES TO VEHICLE IN TEST 4-12 ANALYSIS OF NETC 3-BAR BRIDGE RAIL FOR CASES 1 AND 2.....	173
FIGURE 164. EXIT BOX FOR TEST 4-12 FOR CASE 1 ON THE NETC 3-BAR BRIDGE RAIL.	174

FIGURE 165. EXIT BOX FOR TEST 4-12 FOR CASE 2 ON THE NETC 3-BAR BRIDGE RAIL.	174
FIGURE 166. SUMMARY RESULTS FOR <i>MASH</i> TEST 4-12 ON THE NETC 3-BAR BRIDGE RAIL (CASE 1).	176
FIGURE 167. SUMMARY RESULTS FOR <i>MASH</i> TEST 4-12 ON THE NETC 3-BAR BRIDGE RAIL (CASE 2).	177
FIGURE 168. PHOTO AND CROSS-SECTION DRAWING OF THE <i>MASH</i> TL4 TXDOT C2P BRIDGE RAIL.	179
FIGURE 169. FEA MODEL OF THE 3-BAR TRANSITION (OBLIQUE VIEWPOINT).	181
FIGURE 170. ILLUSTRATION OF POTENTIAL SNAG POINTS ON THE 3-BAR TRANSITION FOR PASSENGER VEHICLES.	181
FIGURE 171. ILLUSTRATION OF POTENTIAL SNAG POINT ON THE 3-BAR TRANSITION FOR THE SINGLE UNIT TRUCK.	182
FIGURE 172. RESULTS OF TEST 4-20 CIP EVALUATIONS FOR THE 3-BAR TRANSITION.	182
FIGURE 173. IMPACT POINT FOR TEST 4-20 ON THE 3-BAR TRANSITION.	183
FIGURE 174. 10- AND 50-MILLISECOND AVERAGE X-ACCELERATION FROM FEA OF TEST 4-20 ON THE 3-BAR TRANSITION.	184
FIGURE 175. 10- AND 50-MILLISECOND AVERAGE Y-ACCELERATION FROM FEA OF TEST 4-20 ON THE 3-BAR TRANSITION.	184
FIGURE 176. 10- AND 50-MILLISECOND AVERAGE Z-ACCELERATION FROM FEA OF TEST 4-20 ON THE 3-BAR TRANSITION.	184
FIGURE 177. YAW RATE AND YAW ANGLE TIME-HISTORY FROM FEA OF TEST 4-20 ON THE 3-BAR TRANSITION.	185
FIGURE 178. ROLL RATE AND ROLL ANGLE TIME-HISTORY FROM FEA OF TEST 4-20 ON THE 3-BAR TRANSITION.	185
FIGURE 179. PITCH RATE AND PITCH ANGLE TIME-HISTORY FROM FEA OF TEST 4-20 ON THE 3-BAR TRANSITION.	185
FIGURE 180. OCCUPANT COMPARTMENT DEFORMATION RESULTING FROM TEST 4-20 ON THE 3-BAR TRANSITION.	186
FIGURE 181. OVERHEAD VIEW OF 3-BAR TRANSITION AFTER TEST 4-20 SHOWING EXTENT OF DAMAGE.	187
FIGURE 182. CONTOUR PLOT OF LATERAL DISPLACEMENT FOR THE TRANSITION AT THE TIME OF MAXIMUM DYNAMIC DEFLECTION.	187
FIGURE 183. CONTOUR PLOT OF MAXIMUM PERMANENT DEFLECTION FOR THE TRANSITION.	187
FIGURE 184. CONTOURS OF EFFECTIVE PLASTIC STRAINS ON THE STEEL RAILS AND POSTS FOR 3-BAR TRANSITION.	188
FIGURE 185. DAMAGES TO VEHICLE IN TEST 4-20 ANALYSIS OF THE 3-BAR TRANSITION.	188
FIGURE 186. EXIT BOX FOR TEST 4-20 ANALYSIS OF THE 3-BAR TRANSITION.	189
FIGURE 187. SUMMARY RESULTS FOR <i>MASH</i> TEST 4-20 ON THE 3-BAR TRANSITION.	190
FIGURE 188. MEASUREMENT POINTS FOR DETERMINING CIP FOR POCKETING FOR TEST 4-21.	191
FIGURE 189. RELATIVE DISPLACEMENTS OF RAIL FOR TEST 4-21 SIMULATIONS IN CIP EVALUATIONS.	191
FIGURE 190. PLOTS OF RELATIVE DISPLACEMENTS FOR TEST 4-21 SIMULATIONS IN CIP EVALUATIONS.	192
FIGURE 191. TOTAL DEFLECTION OF THE RAIL AT THE CRITICAL SNAG POINT ON THE TRANSITION FOR TEST 4-21.	192
FIGURE 192. PLOTS OF (A) VEHICLE ACCELERATIONS AND (B) IMPACT SEVERITY AT TIME WHEN VEHICLE IS POSITIONED AT CRITICAL SNAG POINT.	193
FIGURE 193. IMPACT POINT FOR TEST 4-21 ON THE 3-BAR TRANSITION.	195
FIGURE 194. 10- AND 50-MILLISECOND AVERAGE X-ACCELERATION FROM FEA OF TEST 4-21 ON THE 3-BAR TRANSITION.	195
FIGURE 195. 10- AND 50-MILLISECOND AVERAGE Y-ACCELERATION FROM FEA OF TEST 4-21 ON THE 3-BAR TRANSITION.	196
FIGURE 196. 10- AND 50-MILLISECOND AVERAGE Z-ACCELERATION FROM FEA OF TEST 4-21 ON THE 3-BAR.	196
FIGURE 197. YAW RATE AND YAW ANGLE TIME-HISTORY FROM FEA OF TEST 4-21 ON THE 3-BAR TRANSITION.	196
FIGURE 198. ROLL RATE AND PITCH ANGLE TIME-HISTORY FROM FEA OF TEST 4-21 ON THE 3-BAR TRANSITION.	197
FIGURE 199. PITCH RATE AND PITCH ANGLE TIME-HISTORY FROM FEA OF TEST 4-21 ON THE 3-BAR TRANSITION.	197
FIGURE 200. OCCUPANT COMPARTMENT DEFORMATION RESULTING FROM TEST 4-21 ON THE 3-BAR TRANSITION.	198
FIGURE 201. OVERHEAD VIEW OF 3-BAR TRANSITION AFTER TEST 4-21 SHOWING EXTENT OF DAMAGE.	199
FIGURE 202. CONTOUR PLOT OF LATERAL DISPLACEMENT FOR TEST 4-21 ON THE 3-BAR TRANSITION AT THE TIME OF MAXIMUM DYNAMIC DEFLECTION.	199
FIGURE 203. CONTOUR PLOT OF MAXIMUM PERMANENT DEFLECTION FOR TEST 4-21 ON THE 3-BAR TRANSITION.	199
FIGURE 204. CONTOURS OF EFFECTIVE PLASTIC STRAINS ON THE STEEL RAILS AND POSTS FOR TEST 4-21 ON 3-BAR TRANSITION.	200
FIGURE 205. DAMAGES TO VEHICLE IN TEST 4-21 ANALYSIS OF THE 3-BAR TRANSITION.	200

FIGURE 206. EXIT BOX FOR TEST 4-21 ANALYSIS OF THE 3-BAR TRANSITION.....	201
FIGURE 207. SUMMARY RESULTS FOR <i>MASH</i> TEST 4-21 ON THE 3-BAR TRANSITION SYSTEM	202
FIGURE 208. ILLUSTRATION OF POTENTIAL SNAG POINT FOR TEST 4-22 ON THE 3-BAR TRANSITION AND IMPACT POINTS EVALUATED. ...	203
FIGURE 209. LONGITUDINAL, LATERAL AND RESULTANT FORCES ON BARRIER FOR EACH ANALYSIS CASE.	204
FIGURE 210. OVERLAY OF FORCE-TIME HISTORY FOR ALL CASES.	204
FIGURE 211. CARGO-BOX BED RAILS SNAG ON TOP OF BRIDGE RAIL POSTS.	204
FIGURE 212. 10- AND 50-MILLISECOND AVERAGE X-ACCELERATION FROM FEA OF TEST 4-22 ON THE 3-BAR TRANSITION (C.G. ACCELEROMETER).....	206
FIGURE 213. 10- AND 50-MILLISECOND AVERAGE Y-ACCELERATION FROM FEA OF TEST 4-22 ON THE 3-BAR TRANSITION (C.G. ACCELEROMETER).....	206
FIGURE 214. 10- AND 50-MILLISECOND AVERAGE Z-ACCELERATION FROM FEA OF TEST 4-22 ON THE 3-BAR TRANSITION (C.G. ACCELEROMETER).....	207
FIGURE 215. 10- AND 50-MILLISECOND AVERAGE X-ACCELERATION FROM FEA OF TEST 4-22 ON THE 3-BAR TRANSITION (CABIN ACCELEROMETER).....	207
FIGURE 216. 10- AND 50-MILLISECOND AVERAGE Y-ACCELERATION FROM FEA OF TEST 4-22 ON THE 3-BAR TRANSITION (CABIN ACCELEROMETER).....	207
FIGURE 217. 10- AND 50-MILLISECOND AVERAGE Z-ACCELERATION FROM FEA OF TEST 4-22 ON THE 3-BAR TRANSITION (CABIN ACCELEROMETER).....	208
FIGURE 218. YAW RATE AND YAW ANGLE TIME-HISTORY FROM FEA OF TEST 4-22 ON THE 3-BAR TRANSITION (CABIN ACCELEROMETER).	208
FIGURE 219. ROLL RATE AND ROLL ANGLE TIME-HISTORY FROM FEA OF TEST 4-22 ON THE 3-BAR TRANSITION (CABIN ACCELEROMETER).	208
FIGURE 220. PITCH RATE AND PITCH ANGLE TIME-HISTORY FROM FEA OF TEST 4-22 ON THE 3-BAR TRANSITION (CABIN ACCELEROMETER).	209
FIGURE 221. OCCUPANT COMPARTMENT DEFORMATION RESULTING FROM TEST 4-12 ON THE NETC 3-BAR BRIDGE RAIL SYSTEM.	210
FIGURE 222. CONTOUR PLOT OF LATERAL DISPLACEMENT FOR THE 3-BAR TRANSITION FOR TEST 4-22 AT THE TIME OF MAXIMUM DYNAMIC DEFLECTION.	210
FIGURE 223. CONTOUR PLOT OF PERMANENT DEFLECTION FOR THE 3-BAR TRANSITION FOR TEST 4-22.....	211
FIGURE 224. CONTOURS OF EFFECTIVE PLASTIC STRAINS ON THE TRANSITION AND BRIDGE RAIL FOR TEST 4-22 ON THE 3-BAR TRANSITION.	211
FIGURE 225. WORKING WIDTH FOR TEST 4-22 ON 3-BAR TRANSITION.	212
FIGURE 226. LONGITUDINAL, LATERAL AND RESULTANT FORCE-TIME HISTORY BETWEEN VEHICLE AND BARRIER FOR TEST 4-22 ON THE 3-BAR TRANSITION.	212
FIGURE 227. DAMAGES TO VEHICLE IN TEST 4-22 ANALYSIS OF THE 3-BAR TRANSITION.	212
FIGURE 228. EXIT BOX FOR TEST 4-22 FOR THE 3-BAR TRANSITION.	213
FIGURE 229. SUMMARY RESULTS FOR <i>MASH</i> TEST 4-22 ON THE 3-BAR TRANSITION.	215
FIGURE 230. FEA MODEL OF SIDEWALK-MOUNTED NETC 4-BAR BRIDGE RAIL.	217
FIGURE 231. INITIAL STARTING POINT AND TARGET IMPACT POINT FOR TEST 4-10 ON THE NETC 4-BAR BRIDGE RAIL.	218
FIGURE 232. ACTUAL IMPACT POINT ON BARRIER FOR TEST 4-10 ON THE NETC 4-BAR BRIDGE RAIL.	218
FIGURE 233. 10- AND 50-MILLISECOND AVERAGE X-ACCELERATION FROM FEA OF TEST 4-10 ON THE NETC 4-BAR BRIDGE RAIL.....	220
FIGURE 234. 10- AND 50-MILLISECOND AVERAGE Y-ACCELERATION FROM FEA OF TEST 4-10 ON THE NETC 4-BAR BRIDGE RAIL.....	220
FIGURE 235. 10- AND 50-MILLISECOND AVERAGE Z-ACCELERATION FROM FEA OF TEST 4-10 ON THE NETC 4-BAR BRIDGE RAIL.....	220
FIGURE 236. YAW RATE AND YAW ANGLE TIME-HISTORY FROM FEA OF TEST 4-10 ON THE NETC 4-BAR BRIDGE RAIL.	221
FIGURE 237. ROLL RATE AND ROLL ANGLE TIME-HISTORY FROM FEA OF TEST 4-10 ON THE NETC 4-BAR BRIDGE RAIL.....	221
FIGURE 238. PITCH RATE AND PITCH ANGLE TIME-HISTORY FROM FEA OF TEST 4-10 ON THE NETC 4-BAR BRIDGE RAIL.	221

FIGURE 239. OCCUPANT COMPARTMENT DEFORMATION RESULTING FROM TEST 4-10 ON THE NETC 4-BAR BRIDGE RAIL	222
FIGURE 240. CONTOUR PLOT OF LATERAL DISPLACEMENT FOR THE BRIDGE RAIL FOR TEST 4-10 AT THE TIME OF MAXIMUM DYNAMIC DEFLECTION.	223
FIGURE 241. CONTOUR PLOT OF MAXIMUM PERMANENT DEFLECTION OF THE BRIDGE RAIL FOR TEST 4-10.	223
FIGURE 242. CONTOURS OF EFFECTIVE PLASTIC STRAINS FOR TEST 4-10 ON THE NETC 4-BAR BRIDGE RAIL.	224
FIGURE 243. CONTOURS OF 1 ST PRINCIPAL STRAINS FOR CONCRETE AT THE CRITICAL POST FOR TEST 4-10 ON THE NETC 4-BAR BRIDGE RAIL.....	224
FIGURE 244. DAMAGES TO VEHICLE IN TEST 4-10 ANALYSIS OF THE NETC 4-BAR BRIDGE RAIL.	225
FIGURE 245. EXIT BOX FOR TEST 4-10 ANALYSIS OF THE NETC 4-BAR BRIDGE RAIL.	225
FIGURE 246. SUMMARY RESULTS FOR <i>MASH</i> TEST 4-10 ON THE NETC 4-BAR BRIDGE RAIL.....	227
FIGURE 247. INITIAL STARTING POINT AND TARGET IMPACT POINT FOR TEST 4-11 ON THE NETC 4-BAR BRIDGE RAIL.	228
FIGURE 248. ACTUAL IMPACT POINT ON BARRIER FOR TEST 4-11 ON THE NETC 4-BAR BRIDGE RAIL.	228
FIGURE 249. 10- AND 50-MILLISECOND AVERAGE X-ACCELERATION FROM FEA OF TEST 4-11 ON THE NETC 4-BAR BRIDGE RAIL.....	230
FIGURE 250. 10- AND 50-MILLISECOND AVERAGE Y-ACCELERATION FROM FEA OF TEST 4-11 ON THE NETC 4-BAR BRIDGE RAIL.....	230
FIGURE 251. 10- AND 50-MILLISECOND AVERAGE Z-ACCELERATION FROM FEA OF TEST 4-11 ON THE NETC 4-BAR BRIDGE RAIL.	230
FIGURE 252. YAW RATE AND YAW ANGLE TIME-HISTORY FROM FEA OF TEST 4-11 ON THE NETC 4-BAR BRIDGE RAIL.	231
FIGURE 253. ROLL RATE AND ROLL ANGLE TIME-HISTORY FROM FEA OF TEST 4-11 ON THE NETC 4-BAR BRIDGE RAIL.....	231
FIGURE 254. PITCH RATE AND PITCH ANGLE TIME-HISTORY FROM FEA OF TEST 4-11 ON THE NETC 4-BAR BRIDGE RAIL.	231
FIGURE 255. OCCUPANT COMPARTMENT DEFORMATION RESULTING FROM TEST 4-11 ON THE NETC 4-BAR BRIDGE RAIL.	232
FIGURE 256. CONTOUR PLOT OF LATERAL DISPLACEMENT FOR THE BRIDGE RAIL FOR TEST 4-11 AT THE TIME OF MAXIMUM DYNAMIC DEFLECTION.	233
FIGURE 257. CONTOUR PLOT OF MAXIMUM PERMANENT DEFLECTION OF THE BRIDGE RAIL FOR TEST 4-11.	233
FIGURE 258. CONTOURS OF EFFECTIVE PLASTIC STRAINS FOR TEST 4-11 ON THE NETC 4-BAR BRIDGE RAIL.	234
FIGURE 259. CONTOURS OF 1 ST PRINCIPAL STRAINS FOR CONCRETE AT THE CRITICAL POST FOR TEST 4-11 ON THE NETC 4-BAR BRIDGE RAIL.....	234
FIGURE 260. DAMAGES TO VEHICLE IN TEST 4-11 ANALYSIS OF THE NETC 4-BAR BRIDGE RAIL.	235
FIGURE 261. EXIT BOX FOR TEST 4-11 ANALYSIS OF THE NETC 4-BAR BRIDGE RAIL.	235
FIGURE 262. SUMMARY RESULTS FOR <i>MASH</i> TEST 4-11 ON THE NETC 4-BAR BRIDGE RAIL.....	237
FIGURE 263. (A) TARGET AND (B) ACTUAL IMPACT POINT FOR TEST 4-12 ON THE NETC 4-BAR BRIDGE RAIL.....	238
FIGURE 264. 10- AND 50-MILLISECOND AVERAGE X-ACCELERATION FROM FEA OF TEST 4-12 ON THE NETC 4-BAR BRIDGE RAIL (C.G. ACCELEROMETER).....	240
FIGURE 265. 10- AND 50-MILLISECOND AVERAGE Y-ACCELERATION FROM FEA OF TEST 4-12 ON THE NETC 4-BAR BRIDGE RAIL (C.G. ACCELEROMETER).....	240
FIGURE 266. 10- AND 50-MILLISECOND AVERAGE Z-ACCELERATION FROM FEA OF TEST 4-12 ON THE NETC 4-BAR BRIDGE RAIL (C.G. ACCELEROMETER).....	240
FIGURE 267. 10- AND 50-MILLISECOND AVERAGE X-ACCELERATION FROM FEA OF TEST 4-12 ON THE NETC 4-BAR BRIDGE RAIL (CABIN ACCELEROMETER).....	241
FIGURE 268. 10- AND 50-MILLISECOND AVERAGE Y-ACCELERATION FROM FEA OF TEST 4-12 ON THE NETC 4-BAR BRIDGE RAIL (CABIN ACCELEROMETER).....	241
FIGURE 269. 10- AND 50-MILLISECOND AVERAGE Z-ACCELERATION FROM FEA OF TEST 4-12 ON THE NETC 4-BAR BRIDGE RAIL (CABIN ACCELEROMETER).....	241
FIGURE 270. YAW RATE AND YAW ANGLE TIME-HISTORY FROM FEA OF TEST 4-12 ON THE NETC 4-BAR BRIDGE RAIL (CABIN ACCELEROMETER).....	242
FIGURE 271. ROLL RATE AND ROLL ANGLE TIME-HISTORY FROM FEA OF TEST 4-12 ON THE NETC 4-BAR BRIDGE RAIL (CABIN ACCELEROMETER).....	242

FIGURE 272. PITCH RATE AND PITCH ANGLE TIME-HISTORY FROM FEA OF TEST 4-12 ON THE NETC 4-BAR BRIDGE RAIL (CABIN ACCELEROMETER).....	242
FIGURE 273. OCCUPANT COMPARTMENT DEFORMATION RESULTING FROM TEST 4-12 ON THE NETC 4-BAR BRIDGE RAIL SYSTEM.	243
FIGURE 274. EXTENT OF DAMAGE TO THE BRIDGE RAIL FOR TEST 4-12 ON THE NETC 4-BAR BRIDGE RAIL SYSTEM.	244
FIGURE 275. CONTOUR PLOT OF LATERAL DISPLACEMENT FOR THE BRIDGE RAIL FROM TEST 4-12 AT THE TIME OF MAXIMUM DYNAMIC DEFLECTION FOR THE NETC 4-BAR BRIDGE RAIL.	244
FIGURE 276. CONTOUR PLOT OF PERMANENT DEFLECTION FOR THE BRIDGE RAIL FROM TEST 4-12 FOR THE NETC 4-BAR BRIDGE RAIL.	244
FIGURE 277. CONTOURS OF EFFECTIVE PLASTIC STRAINS ON THE CRITICAL POST FOR TEST 4-12 ON THE NETC 4-BAR BRIDGE RAIL.	245
FIGURE 278. CONTOURS OF 1 ST PRINCIPAL STRAINS FOR CONCRETE AT THE CRITICAL POST FOR TEST 4-12 ON THE NETC 4-BAR BRIDGE RAIL.....	245
FIGURE 279. LONGITUDINAL AND LATERAL FORCE-TIME HISTORY BETWEEN VEHICLE AND BARRIER FOR TEST 4-12 ON NETC 4-BAR BRIDGE RAIL.....	246
FIGURE 280. DAMAGES TO VEHICLE IN TEST 4-12 ANALYSIS OF NETC 4-BAR BRIDGE RAIL.....	246
FIGURE 281. EXIT BOX FOR TEST 4-12 FOR CASE 1 ON THE NETC 4-BAR BRIDGE RAIL.	247
FIGURE 282. SUMMARY RESULTS FOR <i>MASH</i> TEST 4-12 ON THE NETC 4-BAR BRIDGE RAIL.....	249
FIGURE 283. ELEVATION VIEW OF THE CONCRETE TRANSITION BARRIER FOR THE NETC 4-BAR BRIDGE RAIL.....	251
FIGURE 284. MAINE DOT BRIDGE TRANSITION TYPE 1.	251
FIGURE 285. FEA MODEL ILLUSTRATING THE VARIOUS COMPONENTS OF THE SYSTEM.	252
FIGURE 286. FEA MODEL ILLUSTRATING THE POST TYPES AND POST SPACING.	252
FIGURE 287. COMPLETE FEA MODEL OF THE MAINE DOT TRANSITION AND BRIDGE RAIL.....	252
FIGURE 288. SOIL CONTINUUM MODEL FROM AN OBLIQUE AND SECTION VIEW.....	253
FIGURE 289. FEA MODEL OF TRANSITION BUTTRESS WITH DIMENSIONS AND STEEL REINFORCEMENT DETAILS.	253
FIGURE 290. FEA MODEL OF BUTTRESS ILLUSTRATING ATTACHMENT DETAILS TO THRIE-BEAM AND BRIDGE DECK.....	254
FIGURE 291. TEST SET-UP FOR MEASURING FORCE-DEFLECTION RESPONSE OF A STANDARD TWO-POST GUARDRAIL END-TERMINAL ANCHOR.	254
FIGURE 292. MEASURED AND APPROXIMATED FORCE-DEFLECTION RESPONSE FOR THE END-ANCHOR.....	255
FIGURE 293. RESULTS OF THE TEST 4-20 SIMULATIONS SHOWING THE DEFORMATION AND POSITION OF THE VEHICLE JUST BEFORE THE TIRE IMPACTED AGAINST THE BUTTRESS FOR EACH CASE.....	256
FIGURE 294. ACCELERATION DATA COLLECTED AT THE C.G. OF THE VEHICLE FOR EACH CASE.	256
FIGURE 295. PLOTS OF OIV AND MAXIMUM ORA FOR EACH CASE.	257
FIGURE 296. IMPACT POINT FOR TEST 4-20 ON THE MAINE DOT TRANSITION FOR 4-BAR BRIDGE RAIL.....	258
FIGURE 297. 10- AND 50-MILLISECOND AVERAGE X-ACCELERATION FROM FEA OF TEST 4-20 ON THE MAINE DOT TRANSITION.	258
FIGURE 298. 10- AND 50-MILLISECOND AVERAGE Y-ACCELERATION FROM FEA OF TEST 4-20 ON THE MAINE DOT TRANSITION.	259
FIGURE 299. 10- AND 50-MILLISECOND AVERAGE Z-ACCELERATION FROM FEA OF TEST 4-20 ON THE MAINE DOT TRANSITION.	259
FIGURE 300. YAW RATE AND YAW ANGLE TIME-HISTORY FROM FEA OF TEST 4-20 ON THE MAINE DOT TRANSITION.....	259
FIGURE 301. ROLL RATE AND ROLL ANGLE TIME-HISTORY FROM FEA OF TEST 4-20 ON THE MAINE DOT TRANSITION.	260
FIGURE 302. PITCH RATE AND PITCH ANGLE TIME-HISTORY FROM FEA OF TEST 4-20 ON THE MAINE DOT TRANSITION.....	260
FIGURE 303. OCCUPANT COMPARTMENT DEFORMATION RESULTING FROM TEST 4-20 ON THE MAINE DOT TRANSITION.....	261
FIGURE 304. OVERHEAD VIEW OF MAINE DOT TRANSITION AFTER TEST 4-20 SHOWING EXTENT OF DAMAGE.	262
FIGURE 305. CONTOURS OF EFFECTIVE PLASTIC STRAINS ON THE STEEL RAILS AND POSTS FOR TEST 4-20 ON THE MAINE DOT TRANSITION.	262
FIGURE 306. CONTOUR PLOT OF LATERAL DISPLACEMENT FOR THE MAINE DOT TRANSITION AT THE TIME OF MAXIMUM DYNAMIC DEFLECTION.	263
FIGURE 307. CONTOUR PLOT OF MAXIMUM PERMANENT DEFLECTION FOR THE MAINE DOT TRANSITION.	263

FIGURE 308. CONTOUR PLOT OF 1 ST PRINCIPLE STRAIN ON CONCRETE BUTTRESS.....	263
FIGURE 309. DAMAGES TO VEHICLE IN TEST 4-20 ANALYSIS OF THE MAINE DOT TRANSITION.	264
FIGURE 310. EXIT BOX FOR TEST 4-20 ANALYSIS OF THE 3-BAR TRANSITION.....	264
FIGURE 311. SUMMARY RESULTS FOR <i>MASH</i> TEST 4-20 ON THE 3-BAR TRANSITION.	266
FIGURE 312. CONCRETE AGT TESTED BY MWRSF (TEST 34AGT-2). [<i>ROENBAUGH19</i>]	267
FIGURE 313. TIRE SNAG ON THE BUTTRESS FOR TEST 34AGT-2 AND THE FEA ANALYSIS.	268
FIGURE 314. OVERLAY OF THE ACCELERATIONS FROM SLICE 1 AND SLICE 2 FROM FULL-SCALE TEST 34AGT-2. [<i>ROSENBAUGH19</i>].....	268
FIGURE 315. OVERLAY OF ACCELERATION-TIME HISTORIES FOR FEA AND TESTS.	269
FIGURE 316. COMPARISON OF VEHICLE DAMAGE FOR FEA (MAINE DOT TRANSITION) AND FULL-SCALE TEST (MWRSF TRANSITION)...	270
FIGURE 317. MEASUREMENT POINTS FOR DETERMINING CIP FOR POCKETING FOR TEST 4-21.....	271
FIGURE 318. (A) RELATIVE DISPLACEMENTS OF RAIL AND (B) IMPACT SEVERITY AND KINETIC ENERGY AT TIME OF IMPACT WITH BUTTRESS FOR TEST 4-21 CIP EVALUATIONS.	271
FIGURE 319. PLOTS OF LONGITUDINAL AND LATERAL ACCELERATIONS INDICATING THE TIME OF VEHICLE CONTACT WITH THE BUTTRESS.	272
FIGURE 320. COMPARISON OF OCCUPANT RISK METRICS COMPUTED IN TRAP FOR TEST 4-21.	272
FIGURE 321. CONTOUR PLOTS OF 1 ST PRINCIPLE STRAIN FOR THE BUTTRESS.....	273
FIGURE 322. CONTOUR PLOTS OF 1 ST PRINCIPLE STRAIN FOR THE DECK.	274
FIGURE 323. STARTING POINT AND TARGET IMPACT POINT FOR TEST 4-21 ON THE MAINE DOT TRANSITION FOR 4-BAR BRIDGE RAIL.	275
FIGURE 324. ACTUAL IMPACT POINT FOR TEST 4-21 ON THE MAINE DOT TRANSITION FOR 4-BAR BRIDGE RAIL.	275
FIGURE 325. 10- AND 50-MILLISECOND AVERAGE X-ACCELERATION FROM FEA OF TEST 4-21 ON THE MAINE DOT TRANSITION.	276
FIGURE 326. 10- AND 50-MILLISECOND AVERAGE Y-ACCELERATION FROM FEA OF TEST 4-21 ON THE MAINE DOT TRANSITION.	276
FIGURE 327. 10- AND 50-MILLISECOND AVERAGE Z-ACCELERATION FROM FEA OF TEST 4-21 ON THE MAINE DOT TRANSITION.	277
FIGURE 328. YAW RATE AND ROLL ANGLE TIME-HISTORY FROM FEA OF TEST 4-21 ON THE MAINE DOT TRANSITION.	277
FIGURE 329. ROLL RATE AND PITCH ANGLE TIME-HISTORY FROM FEA OF TEST 4-21 ON THE MAINE DOT TRANSITION.	277
FIGURE 330. PITCH RATE AND YAW ANGLE TIME-HISTORY FROM FEA OF TEST 4-21 ON THE MAINE DOT TRANSITION.	277
FIGURE 331. OCCUPANT COMPARTMENT DEFORMATION RESULTING FROM TEST 4-21 ON THE MAINE DOT TRANSITION.....	279
FIGURE 332. OVERHEAD VIEW OF MAINE DOT TRANSITION AFTER TEST 4-21 SHOWING EXTENT OF DAMAGE.	280
FIGURE 333. CONTOUR PLOT OF LATERAL DISPLACEMENT FOR TEST 4-21 ON THE MAINE DOT TRANSITION AT THE 1 ST PEAK DEFLECTION.	280
FIGURE 334. CONTOUR PLOT OF LATERAL DISPLACEMENT FOR TEST 4-21 ON THE MAINE DOT TRANSITION AT MAXIMUM DYNAMIC DEFLECTION.	281
FIGURE 335. CONTOUR PLOT OF MAXIMUM PERMANENT DEFLECTION FOR TEST 4-21 ON THE MAINE DOT TRANSITION.	281
FIGURE 336. CONTOURS OF EFFECTIVE PLASTIC STRAINS ON THE STEEL RAILS AND POSTS FOR TEST 4-21 ON MAINE DOT TRANSITION.	281
FIGURE 337. DAMAGES TO VEHICLE IN TEST 4-21 ANALYSIS OF THE MAINE DOT TRANSITION.	282
FIGURE 338. EXIT BOX FOR TEST 4-21 ANALYSIS OF THE MAINE DOT TRANSITION.	282
FIGURE 339. SUMMARY RESULTS FOR <i>MASH</i> TEST 4-21 ON THE MAINE DOT TRANSITION SYSTEM	284
FIGURE 340. ILLUSTRATION OF POTENTIAL SNAG POINT FOR TEST 4-22 ON THE MAINE DOT TRANSITION AND IMPACT POINTS EVALUATED.	285
FIGURE 341. LONGITUDINAL, LATERAL AND RESULTANT FORCES ON BARRIER FOR EACH ANALYSIS CASE.	286
FIGURE 342. OVERHEAD IMAGES WITH TRANSPARENT CARGO-BOX SHOWING THE INTERACTION OF THE REAR WHEEL SET AND THE CONCRETE BUTTRESS.....	286
FIGURE 343. CARGO-BOX BED RAILS SNAG ON TOP OF BRIDGE RAIL POSTS.	287
FIGURE 344. INITIAL IMPACT POINT ON THE CURB-FACE FOR TEST 4-22 ON THE SIDEWALK-MOUNTED MAINE DOT TRANSITION.	287
FIGURE 345. IMPACT POINT ON THE BARRIER FOR TEST 4-22 ON THE SIDEWALK-MOUNTED MAINE DOT TRANSITION.	288

FIGURE 346. 10- AND 50-MILLISECOND AVERAGE X-ACCELERATION FROM FEA OF TEST 4-22 ON THE MAINE DOT TRANSITION (C.G. ACCELEROMETER).....	290
FIGURE 347. 10- AND 50-MILLISECOND AVERAGE Y-ACCELERATION FROM FEA OF TEST 4-22 ON THE MAINE DOT TRANSITION (C.G. ACCELEROMETER).....	290
FIGURE 348. 10- AND 50-MILLISECOND AVERAGE Z-ACCELERATION FROM FEA OF TEST 4-22 ON THE MAINE DOT TRANSITION (C.G. ACCELEROMETER).....	290
FIGURE 349. 10- AND 50-MILLISECOND AVERAGE X-ACCELERATION FROM FEA OF TEST 4-22 ON THE MAINE DOT TRANSITION (CABIN ACCELEROMETER).....	291
FIGURE 350. 10- AND 50-MILLISECOND AVERAGE Y-ACCELERATION FROM FEA OF TEST 4-22 ON THE MAINE DOT TRANSITION (CABIN ACCELEROMETER).....	291
FIGURE 351. 10- AND 50-MILLISECOND AVERAGE Z-ACCELERATION FROM FEA OF TEST 4-22 ON THE MAINE DOT TRANSITION (CABIN ACCELEROMETER).....	291
FIGURE 352. YAW RATE AND YAW ANGLE TIME-HISTORY FROM FEA OF TEST 4-22 ON THE MAINE DOT TRANSITION (CABIN ACCELEROMETER).....	292
FIGURE 353. ROLL RATE AND ROLL ANGLE TIME-HISTORY FROM FEA OF TEST 4-22 ON THE MAINE DOT TRANSITION (CABIN ACCELEROMETER).....	292
FIGURE 354. PITCH RATE AND PITCH ANGLE TIME-HISTORY FROM FEA OF TEST 4-22 ON THE MAINE DOT TRANSITION (CABIN ACCELEROMETER).....	292
FIGURE 355. OCCUPANT COMPARTMENT DEFORMATION RESULTING FROM TEST 4-22 ON THE MAINE DOT TRANSITION.....	293
FIGURE 356. CONTOUR PLOT OF LATERAL DISPLACEMENT FOR THE MAINE DOT TRANSITION FOR TEST 4-22 AT THE TIME OF MAXIMUM DYNAMIC DEFLECTION.	294
FIGURE 357. CONTOURS OF EFFECTIVE PLASTIC STRAINS ON THE TRANSITION AND BRIDGE RAIL FOR TEST 4-22 ON THE MAINE DOT TRANSITION.....	294
FIGURE 358. CLOSE-UP VIEW OF END-POST ON BRIDGE RAIL AND THE HIGH DEFORMATION AREA OF THE THREE-BEAM AT THE BUTTRESS.	295
FIGURE 359. WORKING WIDTH FOR TEST 4-22 ON MAINE DOT TRANSITION.	295
FIGURE 360. LONGITUDINAL, LATERAL AND RESULTANT FORCE-TIME HISTORY BETWEEN VEHICLE AND BARRIER FOR TEST 4-22 ON THE MAINE DOT TRANSITION.	296
FIGURE 361. DAMAGES TO VEHICLE IN TEST 4-22 ANALYSIS OF THE MAINE DOT TRANSITION.	296
FIGURE 362. EXIT BOX FOR TEST 4-22 FOR THE MAINE DOT TRANSITION.....	297
FIGURE 363. SUMMARY RESULTS FOR MASH TEST 4-22 ON THE MAINE DOT TRANSITION.	299
FIGURE 364. SECTION VIEW DRAWING AND THE FEA MODEL OF THE NETC 2-BAR BRIDGE RAIL.	301
FIGURE 365. IMPACT POINT FOR TEST 3-10 ON THE NETC 2-BAR BRIDGE RAIL.	302
FIGURE 366. 10- AND 50-MILLISECOND AVERAGE X-ACCELERATION FROM FEA OF TEST 3-10 ON THE NETC 2-BAR BRIDGE RAIL.....	303
FIGURE 367. 10- AND 50-MILLISECOND AVERAGE Y-ACCELERATION FROM FEA OF TEST 3-10 ON THE NETC 2-BAR BRIDGE RAIL.....	303
FIGURE 368. 10- AND 50-MILLISECOND AVERAGE Z-ACCELERATION FROM FEA OF TEST 3-10 ON THE NETC 2-BAR BRIDGE RAIL.....	304
FIGURE 369. YAW RATE AND YAW ANGLE TIME-HISTORY FROM FEA OF TEST 3-10 ON THE NETC 2-BAR BRIDGE RAIL.	304
FIGURE 370. ROLL RATE AND ROLL ANGLE TIME-HISTORY FROM FEA OF TEST 3-10 ON THE NETC 2-BAR BRIDGE RAIL.....	304
FIGURE 371. PITCH RATE AND PITCH ANGLE TIME-HISTORY FROM FEA OF TEST 3-10 ON THE NETC 2-BAR BRIDGE RAIL.	305
FIGURE 372. OCCUPANT COMPARTMENT DEFORMATION RESULTING FROM TEST 3-10 ON THE NETC 2-BAR BRIDGE RAIL.	306
FIGURE 373. OVERHEAD VIEW OF NETC 3-BAR BRIDGE RAIL AFTER TEST 3-10 SHOWING EXTENT OF DAMAGE.	307
FIGURE 374. CONTOUR PLOT OF LATERAL DISPLACEMENT FOR THE BRIDGE RAIL FOR TEST 3-10 AT THE TIME OF MAXIMUM DYNAMIC DEFLECTION.	307
FIGURE 375. CONTOUR PLOT OF MAXIMUM PERMANENT DEFLECTION OF THE NETC 2-BAR BRIDGE RAIL FOR TEST 3-10.	307

FIGURE 376. CONTOURS OF (A) VERTICAL DISPLACEMENT ON BASEPLATE AND (B) EFFECTIVE PLASTIC STRAINS ON BARRIER FOR TEST 3-10 ON THE NETC 2-BAR BRIDGE RAIL.	308
FIGURE 377. CONTOURS OF 1 ST PRINCIPAL STRAINS FOR CONCRETE AT THE CRITICAL POST FOR TEST 3-10 ON THE NETC 2-BAR BRIDGE RAIL.	308
FIGURE 378. DAMAGES TO VEHICLE IN TEST 3-10 ANALYSIS OF THE NETC 2-BAR BRIDGE RAIL.	309
FIGURE 379. EXIT BOX FOR TEST 3-10 ANALYSIS OF THE NETC 2-BAR BRIDGE RAIL.	309
FIGURE 380. SUMMARY RESULTS FOR <i>MASH</i> TEST 3-10 ON THE NETC 2-BAR BRIDGE RAIL.	311
FIGURE 381. IMPACT POINT FOR TEST 3-11 ON THE NETC 2-BAR BRIDGE RAIL.	312
FIGURE 382. 10- AND 50-MILLISECOND AVERAGE X-ACCELERATION FROM FEA OF TEST 3-11 ON THE NETC 2-BAR BRIDGE RAIL.	313
FIGURE 383. 10- AND 50-MILLISECOND AVERAGE Y-ACCELERATION FROM FEA OF TEST 3-11 ON THE NETC 2-BAR BRIDGE RAIL.	313
FIGURE 384. 10- AND 50-MILLISECOND AVERAGE Z-ACCELERATION FROM FEA OF TEST 3-11 ON THE NETC 2-BAR BRIDGE RAIL.	314
FIGURE 385. YAW RATE AND YAW ANGLE TIME-HISTORY FROM FEA OF TEST 3-11 ON THE NETC 2-BAR BRIDGE RAIL.	314
FIGURE 386. ROLL RATE AND ROLL ANGLE TIME-HISTORY FROM FEA OF TEST 3-11 ON THE NETC 2-BAR BRIDGE RAIL.	314
FIGURE 387. PITCH RATE AND PITCH ANGLE TIME-HISTORY FROM FEA OF TEST 3-11 ON THE NETC 2-BAR BRIDGE RAIL.	315
FIGURE 388. OCCUPANT COMPARTMENT DEFORMATION RESULTING FROM TEST 3-11 ON THE NETC 2-BAR BRIDGE RAIL.	316
FIGURE 389. OVERHEAD VIEW OF NETC 3-BAR BRIDGE RAIL AFTER TEST 3-11.	316
FIGURE 390. CONTOUR PLOT OF LATERAL DISPLACEMENT FOR THE BRIDGE RAIL FOR TEST 3-11 ON NETC 2-BAR BRIDGE RAIL AT THE TIME OF MAXIMUM DYNAMIC DEFLECTION.	317
FIGURE 391. CONTOUR PLOT OF MAXIMUM PERMANENT DEFLECTION OF THE NETC 2-BAR BRIDGE RAIL FOR TEST 3-11.	317
FIGURE 392. CONTOURS OF EFFECTIVE PLASTIC STRAINS FOR TEST 3-11 ON THE NETC 2-BAR BRIDGE RAIL.	318
FIGURE 393. CONTOURS OF 1 ST PRINCIPAL STRAINS FOR CONCRETE AT THE CRITICAL POST FOR TEST 3-11 ON THE NETC 2-BAR BRIDGE RAIL.	318
FIGURE 394. DAMAGES TO VEHICLE IN TEST 3-11 ANALYSIS OF THE NETC 2-BAR BRIDGE RAIL.	319
FIGURE 395. EXIT BOX FOR TEST 3-11 ANALYSIS OF THE NETC 2-BAR BRIDGE RAIL.	319
FIGURE 396. SUMMARY RESULTS FOR <i>MASH</i> TEST 3-11 ON THE NETC 2-BAR BRIDGE RAIL.	321
FIGURE 397. FEA MODEL OF THE 2-BAR TRANSITION (OBLIQUE VIEWPOINT).	323
FIGURE 398. ILLUSTRATION OF POTENTIAL SNAG POINTS ON THE 2-BAR TRANSITION FOR PASSENGER VEHICLES.	323
FIGURE 399. RESULTS OF TEST 3-20 CIP EVALUATIONS FOR THE 2-BAR TRANSITION.	324
FIGURE 400. PLOTS OF X-ACCELERATION AND Y-ACCELERATION MEASURED AT THE C.G. OF THE VEHICLE.	325
FIGURE 401. OIV AND ORA METRICS CALCULATED FOR THE FIVE TEST 3-20 ANALYSIS CASES ON THE 2-BAR TRANSITION.	325
FIGURE 402. IMPACT POINT FOR TEST 3-20 ON THE 2-BAR TRANSITION.	326
FIGURE 403. 10- AND 50-MILLISECOND AVERAGE X-ACCELERATION FROM FEA OF TEST 3-20 ON THE 2-BAR TRANSITION.	327
FIGURE 404. 10- AND 50-MILLISECOND AVERAGE Y-ACCELERATION FROM FEA OF TEST 3-20 ON THE 2-BAR TRANSITION.	327
FIGURE 405. 10- AND 50-MILLISECOND AVERAGE Z-ACCELERATION FROM FEA OF TEST 3-20 ON THE 2-BAR TRANSITION.	327
FIGURE 406. YAW RATE AND YAW ANGLE TIME-HISTORY FROM FEA OF TEST 3-20 ON THE 2-BAR TRANSITION.	328
FIGURE 407. ROLL RATE AND ROLL ANGLE TIME-HISTORY FROM FEA OF TEST 3-20 ON THE 2-BAR TRANSITION.	328
FIGURE 408. PITCH RATE AND PITCH ANGLE TIME-HISTORY FROM FEA OF TEST 3-20 ON THE 2-BAR TRANSITION.	328
FIGURE 409. OCCUPANT COMPARTMENT DEFORMATION RESULTING FROM TEST 3-20 ON THE 2-BAR TRANSITION.	329
FIGURE 410. OVERHEAD VIEW OF 2-BAR TRANSITION AFTER TEST 3-20 SHOWING EXTENT OF DAMAGE.	330
FIGURE 411. CONTOUR PLOT OF LATERAL DISPLACEMENT FOR THE TRANSITION AT THE TIME OF MAXIMUM DYNAMIC DEFLECTION.	330
FIGURE 412. CONTOUR PLOT OF MAXIMUM PERMANENT DEFLECTION FOR THE TRANSITION.	330
FIGURE 413. CONTOURS OF EFFECTIVE PLASTIC STRAINS ON THE STEEL RAILS AND POSTS FOR 2-BAR TRANSITION.	331
FIGURE 414. DAMAGES TO VEHICLE IN TEST 3-20 ANALYSIS OF THE 2-BAR TRANSITION.	331

FIGURE 415. EXIT BOX FOR TEST 3-20 ANALYSIS OF THE 2-BAR TRANSITION.....	332
FIGURE 416. SUMMARY RESULTS FOR <i>MASH</i> TEST 3-20 ON THE 2-BAR TRANSITION.	333
FIGURE 417. MEASUREMENT POINTS FOR DETERMINING CIP FOR POCKETING FOR TEST 3-21.....	334
FIGURE 418. RELATIVE DISPLACEMENTS OF RAIL FOR TEST 3-21 SIMULATIONS IN CIP EVALUATIONS.	335
FIGURE 419. TOTAL DEFLECTION OF THE RAIL AT THE CRITICAL SNAG POINT ON THE TRANSITION FOR TEST 3-21.	335
FIGURE 420. PLOTS OF VEHICLE LONGITUDINAL AND LATERAL ACCELERATIONS MEASURED AT THE C.G. OF THE VEHICLE.	336
FIGURE 421. IMPACT SEVERITY AND KINETIC ENERGY OF THE VEHICLE AT THE TIME WHEN THE VEHICLE IS POSITIONED AT THE CRITICAL SNAG POINT.	336
FIGURE 422. MAXIMUM OIV AND ORA VALUES FOR THE TEST 4-21 CASES.	336
FIGURE 423. IMPACT POINT FOR TEST 3-21 ON THE 2-BAR TRANSITION.	338
FIGURE 424. 10- AND 50-MILLISECOND AVERAGE X-ACCELERATION FROM FEA OF TEST 3-21 ON THE 3-BAR TRANSITION.	338
FIGURE 425. 10- AND 50-MILLISECOND AVERAGE Y-ACCELERATION FROM FEA OF TEST 3-21 ON THE 2-BAR TRANSITION.	339
FIGURE 426. 10- AND 50-MILLISECOND AVERAGE Z-ACCELERATION FROM FEA OF TEST 3-21 ON THE 2-BAR	339
FIGURE 427. YAW RATE AND YAW ANGLE TIME-HISTORY FROM FEA OF TEST 3-21 ON THE 2-BAR TRANSITION.....	339
FIGURE 428. ROLL RATE AND PITCH ANGLE TIME-HISTORY FROM FEA OF TEST 3-21 ON THE 2-BAR TRANSITION.	340
FIGURE 429. PITCH RATE AND PITCH ANGLE TIME-HISTORY FROM FEA OF TEST 3-21 ON THE 2-BAR TRANSITION.	340
FIGURE 430. OCCUPANT COMPARTMENT DEFORMATION RESULTING FROM TEST 3-21 ON THE 2-BAR TRANSITION.....	341
FIGURE 431. OVERHEAD VIEW OF 2-BAR TRANSITION AFTER TEST 3-21 SHOWING EXTENT OF DAMAGE.....	342
FIGURE 432. CONTOUR PLOT OF LATERAL DISPLACEMENT FOR TEST 3-21 ON THE 3-BAR TRANSITION AT THE TIME OF MAXIMUM DYNAMIC DEFLECTION AND MAXIMUM PERMANENT DEFLECTION.....	342
FIGURE 433. CONTOURS OF EFFECTIVE PLASTIC STRAINS ON THE STEEL RAILS AND POSTS FOR TEST 3-21 ON 2-BAR TRANSITION.....	342
FIGURE 434. DAMAGES TO VEHICLE IN TEST 3-21 ANALYSIS OF THE 2-BAR TRANSITION.	343
FIGURE 435. EXIT BOX FOR TEST 3-21 ANALYSIS OF THE 2-BAR TRANSITION.....	343
FIGURE 436. SUMMARY RESULTS FOR <i>MASH</i> TEST 3-21 ON THE 2-BAR TRANSITION SYSTEM	345
FIGURE 437. ANALYSIS CASES EVALUATED FOR THE MODIFIED NETC 3-BAR WITH STIFFER LOWER RAIL.	348
FIGURE 438. CROSS-SECTION VIEW OF SPLICE FOR EACH CASE IDENTIFYING TUBE SIZE AND INTERNAL GAP SIZE.	348
FIGURE 439. IMPACT POINT FOR TEST 4-10 ON THE MODIFIED NETC 3-BAR BRIDGE RAIL.....	349
FIGURE 440. OVERHEAD TRANSPARENT VIEW SHOWING MAXIMUM DEFLECTIONS OF THE LOWER RAIL FOR EACH ANALYSIS CASE COMPARED TO BASELINE.....	349
FIGURE 441. OBLIQUE VIEW SHOWING MAXIMUM DYNAMIC DEFLECTIONS OF THE BARRIER FOR EACH ANALYSIS CASE COMPARED TO BASELINE.	350
FIGURE 442. 10- AND 50-MILLISECOND AVERAGE X-ACCELERATION FROM FEA OF TEST 4-10 ON THE MODIFIED NETC 3-BAR BRIDGE RAIL.....	350
FIGURE 443. 10- AND 50-MILLISECOND AVERAGE Y-ACCELERATION FROM FEA OF TEST 4-10 ON THE MODIFIED NETC 3-BAR BRIDGE RAIL DESIGN CASES.	351
FIGURE 444. 10- AND 50-MILLISECOND AVERAGE Z-ACCELERATION FROM FEA OF TEST 4-10 ON THE MODIFIED NETC 3-BAR BRIDGE RAIL DESIGN CASES.	351
FIGURE 445. YAW RATE AND YAW ANGLE TIME-HISTORY FROM FEA OF TEST 4-10 ON THE MODIFIED NETC 3-BAR BRIDGE RAIL DESIGN CASES.	351
FIGURE 446. ROLL RATE AND ROLL ANGLE TIME-HISTORY FROM FEA OF TEST 4-10 ON THE MODIFIED NETC 3-BAR BRIDGE RAIL DESIGN CASES.	352
FIGURE 447. PITCH RATE AND PITCH ANGLE TIME-HISTORY FROM FEA OF TEST 4-10 ON THE MODIFIED NETC 3-BAR BRIDGE RAIL DESIGN CASES.	352
FIGURE 448. OI32.5V AND ORA VALUES FOR TEST 4-10 ON THE MODIFIED NETC 3-BAR DESIGN CASE.	352

FIGURE 449. SKEW JOINT	354
FIGURE 450. POST AND SPLICE SPACING FOR (A) ORIGINAL AND (B) MODIFIED DESIGNS.	355
FIGURE 451. EXPANSION SPLICE CASES EVALUATED.	355
FIGURE 452. TAPERED POST BASED ON MASSDOT S3-TL4 BRIDGE RAIL DESIGN.	356
FIGURE 453. CRITICAL IMPACT POINT LOCATIONS.....	356
FIGURE 454. BRIDGE RAIL AND SPLICE DESIGNS USED FOR THE TEST 4-20 EVALUATIONS.....	357
FIGURE 455. IMPACT POINT LOCATIONS FOR TEST 4-20 ON THE 3-BAR TRANSITION WITH INCREASED POST SPACING.	357
FIGURE 456. TEST 4-20 RESULTS AT TIME OF POTENTIAL IMPACT WITH CRITICAL POST.	358
FIGURE 457. TEST 4-20 RESULTS AT TIME OF POTENTIAL SNAG ON CRITICAL SPLICE.	358
FIGURE 458. PEAK 10-MS MOVING AVERAGE ACCELERATION DATA FOR TEST 4-20 IMPACT CASES.	359
FIGURE 459. GRAPHICAL REPRESENTATION OF OIV, THIV, ORA AND PHD METRICS FOR TEST 4-20.	360
FIGURE 460. IMPACT POINT FOR TEST 4-20 ON DESIGN CASE 2.	361
FIGURE 461. 10- AND 50-MILLISECOND AVERAGE X-ACCELERATION FROM FEA OF TEST 4-20 ON THE 3-BAR TRANSITION WITH 5.5-FT POST SPACING.	361
FIGURE 462. 10- AND 50-MILLISECOND AVERAGE Y-ACCELERATION FROM FEA OF TEST 4-20 ON THE 3-BAR TRANSITION WITH 5.5-FT POST SPACING.	361
FIGURE 463. 10- AND 50-MILLISECOND AVERAGE Z-ACCELERATION FROM FEA OF TEST 4-20 ON THE 3-BAR TRANSITION WITH 5.5-FT POST SPACING.	362
FIGURE 464. YAW RATE AND YAW ANGLE TIME-HISTORY FROM FEA OF TEST 4-20 ON THE 3-BAR TRANSITION WITH 5.5-FT POST SPACING.	362
FIGURE 465. ROLL RATE AND ROLL ANGLE TIME-HISTORY FROM FEA OF TEST 4-20 ON THE 3-BAR TRANSITION WITH 5.5-FT POST SPACING.	362
FIGURE 466. PITCH RATE AND PITCH ANGLE TIME-HISTORY FROM FEA OF TEST 4-20 ON THE 3-BAR TRANSITION WITH 5.5-FT POST SPACING.	362
FIGURE 467. CONTOUR PLOT OF LATERAL DISPLACEMENT FOR THE SYSTEM AT THE TIME OF MAXIMUM DYNAMIC DEFLECTION.	364
FIGURE 468. TEST 4-20 RESULTS AT TIME OF POTENTIAL IMPACT WITH CRITICAL POST.	364
FIGURE 469. DAMAGES TO VEHICLE IN TEST 4-20 ANALYSIS OF THE 3-BAR TRANSITION.	364
FIGURE 470. EXIT BOX FOR TEST 4-20 ANALYSIS OF THE 3-BAR TRANSITION.....	365
FIGURE 471. IMPACT POINT LOCATIONS FOR TEST 4-21 ON THE 3-BAR TRANSITION WITH INCREASED POST SPACING.	366
FIGURE 472. TEST 4-21 RESULTS AT TIME OF IMPACT WITH EXPANSION SPLICE (OBLIQUE VIEW).	366
FIGURE 473. TEST 4-21 RESULTS AT TIME OF IMPACT WITH EXPANSION SPLICE (UNDERNEATH VIEW).	367
FIGURE 474. TEST 4-21 RESULTS AT TIME OF IMPACT WITH EXPANSION SPLICE (TIRE-ONLY VIEW).	367
FIGURE 475. CLOSEUP VIEW OF SPLICE FOR TEST 4-21 IMPACT CASE IP 6.0 FT.....	368
FIGURE 476. PEAK 10-MS MOVING AVERAGE ACCELERATION DATA FOR TEST 4-21 IMPACT CASES.	368
FIGURE 477. GRAPHICAL REPRESENTATION OF OIV, THIV, ORA AND PHD METRICS FOR TEST 4-21.	369
FIGURE 478. CRITICAL IMPACT POINT AND 10000S VEHICLE SELECTED FOR THE TEST 4-22 SIMULATIONS.	370
FIGURE 479. IMAGES OF THE ANALYSIS RESULTS FOR CASES 1 – 3 COMPARED TO THE BASELINE CASE AT 0.4 SECONDS OF THE IMPACT (CARGO BOX TRANSPARENT).....	371
FIGURE 480. PEAK IMPACT FORCES ON THE BARRIER FOR CASE 1 – 3 COMPARED WITH BASELINE CASE.....	371
FIGURE 481. 10- AND 50-MILLISECOND AVERAGE X-ACCELERATION FROM FEA OF TEST 4-22 FOR CASE 1-3 ON THE 3-BAR TRANSITION WITH 5.5-FT POST SPACING COMPARED WITH BASELINE (C.G. ACCELEROMETER).....	372
FIGURE 482. 10- AND 50-MILLISECOND AVERAGE Y-ACCELERATION FROM FEA OF TEST 4-22 FOR CASE 1-3 ON THE 3-BAR TRANSITION WITH 5.5-FT POST SPACING COMPARED WITH BASELINE (C.G. ACCELEROMETER).....	372

FIGURE 483. 10- AND 50-MILLISECOND AVERAGE Z-ACCELERATION FROM FEA OF TEST 4-22 FOR CASE 1-3 ON THE 3-BAR TRANSITION WITH 5.5-FT POST SPACING COMPARED WITH BASELINE (C.G. ACCELEROMETER).....	372
FIGURE 484. 10- AND 50-MILLISECOND AVERAGE X-ACCELERATION FROM FEA OF TEST 4-22 FOR CASE 1-3 ON THE 3-BAR TRANSITION WITH 5.5-FT POST SPACING COMPARED WITH BASELINE (CABIN ACCELEROMETER).	373
FIGURE 485. 10- AND 50-MILLISECOND AVERAGE Y-ACCELERATION FROM FEA OF TEST 4-22 FOR CASE 1-3 ON THE 3-BAR TRANSITION WITH 5.5-FT POST SPACING COMPARED WITH BASELINE (CABIN ACCELEROMETER).	373
FIGURE 486. 10- AND 50-MILLISECOND AVERAGE Z-ACCELERATION FROM FEA OF TEST 4-22 FOR CASE 1-3 ON THE 3-BAR TRANSITION WITH 5.5-FT POST SPACING COMPARED WITH BASELINE (CABIN ACCELEROMETER).	373
FIGURE 487. YAW RATE AND YAW ANGLE TIME-HISTORY FROM FEA OF TEST 4-22 FOR CASE 1-3 ON THE 3-BAR TRANSITION WITH 5.5-FT POST SPACING COMPARED WITH BASELINE (C.G. ACCELEROMETER).....	374
FIGURE 488. ROLL RATE AND ROLL ANGLE TIME-HISTORY FROM FEA OF TEST 4-22 FOR CASE 1-3 ON THE 3-BAR TRANSITION WITH 5.5-FT POST SPACING COMPARED WITH BASELINE (C.G. ACCELEROMETER).....	374
FIGURE 489. PITCH RATE AND PITCH ANGLE TIME-HISTORY FROM FEA OF TEST 4-22 FOR CASE 1-3 ON THE 3-BAR TRANSITION WITH 5.5-FT POST SPACING COMPARED WITH BASELINE (C.G. ACCELEROMETER).....	374
FIGURE 490. DEFLECTION-TIME HISTORY AT EXPANSION SPLICE FOR CASES 1-3 COMPARED WITH BASELINE CASE.	375
FIGURE 491. PEAK LATERAL DEFLECTIONS OF THE BARRIER FOR CASES 1-3 COMPARED WITH BASELINE CASE.....	375
FIGURE 492. CONTOUR PLOT OF EFFECTIVE PLASTIC STRAIN FOR CASES 1-3 COMPARED WITH BASELINE CASE.	376
FIGURE 493. TYPICAL DAMAGE TO POST 1 OF THE BRIDGE RAIL FOR ORIGINAL (NON-TAPERED) AND MODIFIED (TAPERED) POST DESIGNS.	376
FIGURE 494. DESIGN MODIFICATIONS FOR THE 4-BAR BRIDGE RAIL.....	378
FIGURE 495. (A) TARGET AND (B) ACTUAL IMPACT POINT FOR TEST 4-12 ON THE MODIFIED NETC 4-BAR BRIDGE RAIL.	379
FIGURE 496. SEQUENTIAL VIEWS FOR ANALYSES OF (A) BASELINE DESIGN AND (B) MODIFIED DESIGN.	379
FIGURE 497. 10- AND 50-MILLISECOND AVERAGE X-ACCELERATION FROM FEA OF TEST 4-12 ON THE BASELINE AND MODIFIED NETC 4-BAR BRIDGE RAIL (CABIN ACCELEROMETER).....	380
FIGURE 498. 10- AND 50-MILLISECOND AVERAGE Y-ACCELERATION FROM FEA OF TEST 4-12 ON THE BASELINE AND MODIFIED NETC 4-BAR BRIDGE RAIL (CABIN ACCELEROMETER).....	380
FIGURE 499. 10- AND 50-MILLISECOND AVERAGE Z-ACCELERATION FROM FEA OF TEST 4-12 ON THE BASELINE AND MODIFIED NETC 4-BAR BRIDGE RAIL (CABIN ACCELEROMETER).....	380
FIGURE 500. 10- AND 50-MILLISECOND AVERAGE X-ACCELERATION FROM FEA OF TEST 4-12 ON THE BASELINE AND MODIFIED NETC 4-BAR BRIDGE RAIL (C.G. ACCELEROMETER).	381
FIGURE 501. 10- AND 50-MILLISECOND AVERAGE Y-ACCELERATION FROM FEA OF TEST 4-12 ON THE BASELINE AND MODIFIED NETC 4-BAR BRIDGE RAIL (C.G. ACCELEROMETER).	381
FIGURE 502. 10- AND 50-MILLISECOND AVERAGE Z-ACCELERATION FROM FEA OF TEST 4-12 ON THE BASELINE AND MODIFIED NETC 4-BAR BRIDGE RAIL (C.G. ACCELEROMETER).	381
FIGURE 503. YAW RATE AND YAW ANGLE TIME-HISTORY FROM FEA OF TEST 4-12 ON THE BASELINE AND MODIFIED NETC 4-BAR BRIDGE RAIL (C.G. ACCELEROMETER).....	382
FIGURE 504. ROLL RATE AND ROLL ANGLE TIME-HISTORY FROM FEA OF TEST 4-12 ON THE BASELINE AND MODIFIED NETC 4-BAR BRIDGE RAIL (C.G. ACCELEROMETER).....	382
FIGURE 505. PITCH RATE AND PITCH ANGLE TIME-HISTORY FROM FEA OF TEST 4-12 ON THE BASELINE AND MODIFIED NETC 4-BAR BRIDGE RAIL (C.G. ACCELEROMETER).	382
FIGURE 506. (A) LONGITUDINAL AND (B) LATERAL IMPACT FORCE-TIME HISTORY FOR THE BASELINE AND MODIFIED DESIGN CASES.	383
FIGURE 507. CONTOUR PLOT OF LATERAL DISPLACEMENT FOR THE BRIDGE RAIL FROM TEST 4-12 AT THE TIME OF MAXIMUM DEFLECTION FOR THE ORIGINAL AND MODIFIED DESIGN CASES.	383
FIGURE 508. CONTOURS OF EFFECTIVE PLASTIC STRAIN ON THE BRIDGE RAIL POSTS AND BASEPLATES FOR THE ORIGINAL AND MODIFIED DESIGN CASES.	384

FIGURE 509. CONTOURS OF 1 ST PRINCIPAL STRAINS FOR CONCRETE AT THE CRITICAL POST FOR THE ORIGINAL AND MODIFIED DESIGN CASES AT TIME OF PEAK DYNAMIC STRAIN.....	384
FIGURE 510. CONTOURS OF 1 ST PRINCIPAL STRAINS FOR CONCRETE AT THE CRITICAL POST FOR THE ORIGINAL AND MODIFIED DESIGN CASES (PERMANENT STRAINS).....	385
FIGURE 511. POSSIBLE SNAG POINT IN REVERSE-DIRECTION IMPACTS.....	395
FIGURE 512. COMPARISON OF LONGITUDINAL STEEL FOR A) THE NETC AND B) MASSDOT’S S3-TL4 BRIDGE RAIL DESIGNS.....	401

LIST OF TABLES

TABLE 1. SUMMARY OF TEST RESULTS FOR NETC 2-BAR BRIDGE RAIL DESIGN. [MAK98].....	7
TABLE 2. SPLICE TUBE DIMENSIONS FOR THE NETC 4-BAR BRIDGE RAIL IN TEST NETC 1 – NETC 3.....	8
TABLE 3. SUMMARY OF TEST RESULTS FOR NETC 4-BAR BRIDGE RAIL DESIGN. [KIMBALL99].....	9
TABLE 4. SUMMARY OF TEST RESULTS FOR NHDOT 2-BAR RAIL TO THRIE-BEAM AGT. [ALBERSON06].....	11
TABLE 5. CRITICAL RAIL HEIGHT AND DESIGN LATERAL IMPACT LOADS FOR MASH BRIDGE RAILING. [DOLOBROVOLNY17].....	12
TABLE 6. RAIL GEOMETRICS CALCULATIONS FOR NETC BRIDGE RAILS.....	13
TABLE 7. DESIGN FORCES FOR NCHRP REPORT 350 TRAFFIC RAILINGS [AASHTO12].....	14
TABLE 8: DESIGN FORCES AND LOAD HEIGHT FOR MASH TL3 WITH COMPARISON TO NCHRP REPORT 350. [DOLBROVOLNY17].....	15
TABLE 9. DESIGN LOADS FOR MASH BARRIERS USED IN NCHRP 20-07(395) PROJECT. [DOLBROVOLNY17].....	15
TABLE 10. MATERIALS FOR NETC BRIDGE RAIL DESIGNS.....	16
TABLE 11. STRENGTH CALCULATIONS FOR 2-BAR BRIDGE RAIL BASED ON MASH TL3 LOAD CONDITIONS.....	26
TABLE 12. STRENGTH CALCULATIONS FOR 3-BAR BRIDGE RAIL BASED ON MASH TL4 LOAD CONDITIONS.....	27
TABLE 13. STRENGTH CALCULATIONS FOR SIDEWALK-MOUNTED 4-BAR BRIDGE RAIL BASED ON MASH TL4 LOAD CONDITIONS.....	28
TABLE 14. STRENGTH CALCULATIONS FOR CURB-MOUNTED 4-BAR BRIDGE RAIL BASED ON MASH TL4 LOAD CONDITIONS.....	29
TABLE 15. SUMMARY OF MASH EQUIVALENCY ASSESSMENT FOR THE NETC BRIDGE RAIL DESIGNS.....	30
TABLE 16. COMPARISON OF BRIDGE RAIL FEATURES FOR NETC 2-BAR BRIDGE RAILS.....	31
TABLE 17. COMPARISON OF BRIDGE RAIL FEATURES FOR NETC 3-BAR BRIDGE RAILS.....	32
TABLE 18. COMPARISON OF BRIDGE RAIL FEATURES FOR NETC 4-BAR SIDEWALK MOUNTED BRIDGE RAILS.....	32
TABLE 19. COMPARISON OF BRIDGE RAIL FEATURES FOR NETC 4-BAR CURB MOUNTED BRIDGE RAILS.....	32
TABLE 20. MATERIAL STRENGTH PROPERTIES FOR POST MATERIALS.....	33
TABLE 21. COMPARISON OF BRIDGE RAIL POST FEATURES FOR NETC2-BAR BRIDGE RAILS.....	33
TABLE 22. COMPARISON OF BRIDGE RAIL POST FEATURES FOR NETC 3-BAR BRIDGE RAILS.....	33
TABLE 23. COMPARISON OF BRIDGE RAIL POST FEATURES FOR NETC 4-BAR SIDEWALK MOUNTED BRIDGE RAILS.....	34
TABLE 24. COMPARISON OF POST FEATURES FOR NETC 4-BAR CURB MOUNTED BRIDGE RAILS.....	34
TABLE 25. STRENGTH VALUES FOR DIFFERENT BOLTS SPECIFICATIONS FOR RAIL-TO-POST ATTACHMENT.....	35
TABLE 26. COMPARISON OF RAIL-TO-POST ATTACHMENT FEATURES FOR NETC 2-BAR BRIDGE RAILS.....	35
TABLE 27. COMPARISON OF RAIL-TO-POST ATTACHMENT FEATURES FOR NETC 3-BAR BRIDGE RAILS.....	36
TABLE 28. COMPARISON OF RAIL-TO-POST ATTACHMENT FEATURES FOR NETC 4-BAR SIDEWALK MOUNTED BRIDGE RAILS.....	36
TABLE 29. COMPARISON OF RAIL-TO-POST ATTACHMENT FEATURES FOR NETC 4-BAR CURB MOUNTED BRIDGE RAILS.....	36
TABLE 30. STRENGTH VALUES FOR DIFFERENT BOLTS SPECIFICATIONS FOR ANCHOR BOLTS.....	37
TABLE 31. COMPARISON OF BASEPLATE AND ANCHOR BOLT FEATURES FOR NETC 2-BAR BRIDGE RAILS.....	38
TABLE 32. COMPARISON OF BASEPLATE AND ANCHOR BOLT FEATURES FOR NETC 3-BAR BRIDGE RAILS.....	38
TABLE 33. COMPARISON OF BASEPLATE AND ANCHOR BOLT FEATURES FOR NETC 4-BAR SIDEWALK MOUNTED BRIDGE RAILS.....	38

TABLE 34. COMPARISON OF BASEPLATE AND ANCHOR BOLT FEATURES FOR NETC 4-BAR CURB MOUNTED BRIDGE RAILS.	38
TABLE 35. COMPARISON OF FIELD SPLICE FEATURES FOR NETC 2-BAR BRIDGE RAILS.	39
TABLE 36. COMPARISON OF FIELD SPLICE FEATURES FOR NETC 3-BAR BRIDGE RAILS.	39
TABLE 37. COMPARISON OF FIELD SPLICE FEATURES FOR NETC 4-BAR SIDEWALK MOUNTED BRIDGE RAILS.	39
TABLE 38. COMPARISON OF FIELD SPLICE FEATURES FOR NETC 4-BAR CURB MOUNTED BRIDGE RAILS.	40
TABLE 39. COMPARISON OF EXPANSION SPLICE FEATURES FOR NETC 2-BAR BRIDGE RAILS.	40
TABLE 40. COMPARISON OF EXPANSION SPLICE FEATURES FOR NETC 3-BAR BRIDGE RAILS.	40
TABLE 41. COMPARISON OF EXPANSION SPLICE FEATURES FOR NETC 4-BAR SIDEWALK MOUNTED BRIDGE RAILS.	40
TABLE 42. COMPARISON OF EXPANSION SPLICE FEATURES FOR NETC 4-BAR CURB MOUNTED BRIDGE RAILS.	41
TABLE 43. COMPARISON OF EXPANSION SPLICE DETAILS FOR DIFFERENT AMOUNTS OF BRIDGE MOVEMENT.	41
TABLE 44. COMPARISON OF CONCRETE CURB FEATURES FOR NETC 2-BAR BRIDGE RAILS.	42
TABLE 45. COMPARISON OF CONCRETE CURB FEATURES FOR NETC 3-BAR BRIDGE RAILS.	42
TABLE 46. COMPARISON OF CONCRETE CURB FEATURES FOR NETC 4-BAR SIDEWALK MOUNTED BRIDGE RAILS.	43
TABLE 47. COMPARISON OF CONCRETE CURB FEATURES FOR NETC 4-BAR CURB MOUNTED BRIDGE RAILS.	43
TABLE 48. NHDOT T2 AGT SLOPE OF RAIL BAR TRANSITION SECTION.	46
TABLE 49. NHDOT T3 AGT SLOPE OF RAIL BAR TRANSITION SECTION.	49
TABLE 50. NHDOT T4 AND VTRANS 4-BAR AGT SLOPE OF RAIL BAR TRANSITION SECTION.	56
TABLE 51. SUMMARY OF RECOMMENDED SPECIFICATIONS FOR NETC STYLE BRIDGE RAILS.	57
TABLE 52. SUMMARY OF RECOMMENDED SPECIFICATIONS FOR NETC STYLE BRIDGE RAIL TRANSITIONS.	60
TABLE 53. OCCUPANT RISK MEASURED COMPUTED USING TRAP SOFTWARE FOR THE FEA AND TEST NETC-3.	95
TABLE 54. REPORT 350 CRASH TEST CRITERIA WITH THE APPLICABLE TEST NUMBERS.	99
TABLE 55. ROADSIDE SAFETY PHENOMENA IMPORTANCE RANKING TABLE (STRUCTURAL ADEQUACY).	101
TABLE 56. ROADSIDE SAFETY PHENOMENA IMPORTANCE RANKING TABLE (OCCUPANT RISK).	102
TABLE 57. ROADSIDE SAFETY PHENOMENA IMPORTANCE RANKING TABLE (VEHICLE TRAJECTORY).	103
TABLE 58. SUMMARY OF VALIDATION METRICS FOR THE MODEL IN SIMULATION OF TEST NETC-3.	104
TABLE 59. SUMMARY OF PHENOMENOLOGICAL EVENTS FOR FULL-SCALE TEST 401181-1 AND FEA SIMULATION.	117
TABLE 60. OCCUPANT RISK MEASURED COMPUTED USING TRAP SOFTWARE FOR THE FEA AND TEST DATA FOR R350 TEST 4-12.	125
TABLE 61. ANALYSIS SOLUTION VERIFICATION TABLE.	129
TABLE 62. ROADSIDE SAFETY VALIDATION METRICS RATING TABLE – TIME HISTORY COMPARISON (SINGLE-CHANNEL OPTION).	131
TABLE 63. ROADSIDE SAFETY VALIDATION METRICS RATING TABLE – (MULTI-CHANNEL OPTION).	132
TABLE 64. REPORT 350 CRASH TEST CRITERIA WITH THE APPLICABLE TEST NUMBERS.	133
TABLE 65. ROADSIDE SAFETY PHENOMENA IMPORTANCE RANKING TABLE (STRUCTURAL ADEQUACY).	134
TABLE 66. ROADSIDE SAFETY PHENOMENA IMPORTANCE RANKING TABLE (OCCUPANT RISK).	135
TABLE 67. ROADSIDE SAFETY PHENOMENA IMPORTANCE RANKING TABLE (VEHICLE TRAJECTORY).	136
TABLE 68. SAFETY EVALUATION GUIDELINES FOR STRUCTURAL ADEQUACY AND OCCUPANT RISK FOR <i>MASH</i> TL4 FOR LONGITUDINAL BARRIERS AND TRANSITIONS. [AASHTO16].	138
TABLE 69. EXIT BOX DIMENSIONS FOR <i>MASH</i> TESTS SMALL CAR, PICKUP, AND SUT.	141
TABLE 70. SUMMARY OF <i>MASH</i> OCCUPANT RISK METRICS FOR TEST 4-10 ON THE NETC 3-BAR BRIDGE RAIL.	147
TABLE 71. SUMMARY OF <i>MASH</i> TEST 4-10 RESULTS ON THE NETC 3-BAR BRIDGE RAIL.	151
TABLE 72. SUMMARY OF <i>MASH</i> OCCUPANT RISK METRICS FOR TEST 4-11 ON THE NETC 3-BAR BRIDGE RAIL.	157
TABLE 73. SUMMARY OF <i>MASH</i> TEST 4-11 RESULTS ON THE NETC 3-BAR BRIDGE RAIL.	161
TABLE 74. SUMMARY OF OCCUPANT RISK METRICS FOR TEST 4-12 ON THE NETC 3-BAR BRIDGE RAIL.	169

TABLE 75. SUMMARY OF <i>MASH</i> TEST 4-12 RESULTS ON THE CURB-MOUNTED BRIDGE RAIL.	175
TABLE 76. COMPARISON OF NETC 3-BAR DESIGN TO TxDOT C2P.	179
TABLE 77. SUMMARY OF <i>MASH</i> OCCUPANT RISK METRICS FOR TEST 4-20 ON THE 3-BAR TRANSITION.	186
TABLE 78. SUMMARY OF <i>MASH</i> TEST 4-20 RESULTS ON THE 3-BAR TRANSITION.	189
TABLE 79. SUMMARY OF OCCUPANT RISK METRICS FOR TEST 4-11 ON THE 3-BAR TRANSITION.	198
TABLE 80. SUMMARY OF <i>MASH</i> TEST 4-21 RESULTS ON THE NETC 3-BAR TRANSITION.	201
TABLE 81. SUMMARY OF OCCUPANT RISK METRICS FOR TEST 4-22 ON THE 3-BAR TRANSITION.	209
TABLE 82. SUMMARY OF <i>MASH</i> TEST 4-12 RESULTS ON THE CURB-MOUNTED BRIDGE RAIL.	214
TABLE 83. SUMMARY OF <i>MASH</i> OCCUPANT RISK METRICS FOR TEST 4-10 ON THE NETC 4-BAR BRIDGE RAIL.	222
TABLE 84. SUMMARY OF <i>MASH</i> TEST 4-10 RESULTS ON THE NETC 4-BAR BRIDGE RAIL.	226
TABLE 85. SUMMARY OF <i>MASH</i> OCCUPANT RISK METRICS FOR TEST 4-11 ON THE NETC 4-BAR BRIDGE RAIL.	232
TABLE 86. SUMMARY OF <i>MASH</i> TEST 4-11 RESULTS ON THE NETC 4-BAR BRIDGE RAIL.	236
TABLE 87. SUMMARY OF OCCUPANT RISK METRICS FOR TEST 4-12 ON THE NETC 4-BAR BRIDGE RAIL.	243
TABLE 88. SUMMARY OF <i>MASH</i> TEST 4-12 RESULTS ON THE SIDEWALK-MOUNTED NETC 4-BAR BRIDGE RAIL.	248
TABLE 89. SUMMARY OF <i>MASH</i> OCCUPANT RISK METRICS FOR TEST 4-20 ON THE MAINE DOT TRANSITION.	261
TABLE 90. SUMMARY OF <i>MASH</i> TEST 4-20 RESULTS ON THE MAINE DOT TRANSITION FOR 4-BAR BRIDGE RAIL.	265
TABLE 91. OCCUPANT RISK METRICS FROM TEST 34AGT-2 AND THE FEA ANALYSIS.	268
TABLE 92. SUMMARY OF OCCUPANT RISK METRICS FOR TEST 4-21 ON THE MAINE DOT TRANSITION.	278
TABLE 93. SUMMARY OF <i>MASH</i> TEST 4-11 RESULTS ON THE MAINE DOT TRANSITION.	283
TABLE 94. SUMMARY OF OCCUPANT RISK METRICS FOR TEST 4-22 ON THE MAINE DOT TRANSITION.	293
TABLE 95. SUMMARY OF <i>MASH</i> TEST 4-12 RESULTS ON THE CONCRETE TRANSITION TO THREE-BEAM.	298
TABLE 96. SUMMARY OF <i>MASH</i> OCCUPANT RISK METRICS FOR TEST 3-10 ON THE NETC 2-BAR BRIDGE RAIL.	306
TABLE 97. SUMMARY OF <i>MASH</i> TEST 3-10 RESULTS ON THE NETC 2-BAR BRIDGE RAIL.	310
TABLE 98. SUMMARY OF <i>MASH</i> OCCUPANT RISK METRICS FOR TEST 3-11 ON THE NETC 2-BAR BRIDGE RAIL.	315
TABLE 99. SUMMARY OF <i>MASH</i> TEST 3-11 RESULTS ON THE NETC 2-BAR BRIDGE RAIL.	320
TABLE 100. SUMMARY OF <i>MASH</i> OCCUPANT RISK METRICS FOR TEST 3-20 ON THE 2-BAR TRANSITION.	329
TABLE 101. SUMMARY OF <i>MASH</i> TEST 3-20 RESULTS ON THE 2-BAR TRANSITION.	332
TABLE 102. SUMMARY OF OCCUPANT RISK METRICS FOR TEST 3-21 ON THE 2-BAR TRANSITION.	341
TABLE 103. SUMMARY OF <i>MASH</i> TEST 3-21 RESULTS ON THE NETC 2-BAR TRANSITION.	344
TABLE 104. BAR SIZE OPTIONS FOR THE LOWER RAIL OF THE MODIFIED NETC 3-BAR BRIDGE RAIL.	347
TABLE 105. PEAK ACCELERATIONS FOR TEST 4-10 ON THE MODIFIED NETC 3-BAR BRIDGE RAIL DESIGN CASES.	352
TABLE 106. SUMMARY OF RESULTS FOR TEST 4-10 ON THE MODIFIED NETC 3-BAR BRIDGE RAIL WITH LARGER LOWER RAIL.	353
TABLE 107. OCCUPANT RISK METRICS FOR TEST 4-20 IMPACT CASES ON THE 3-BAR TRANSITION WITH INCREASED POST SPACING.	360
TABLE 108. SUMMARY OF <i>MASH</i> OCCUPANT RISK METRICS FOR TEST 4-20 ON THE 3-BAR TRANSITION WITH 5.5-FT POST SPACING.	363
TABLE 109. OCCUPANT RISK METRICS FOR TEST 4-21 IMPACT CASES ON THE 3-BAR TRANSITION WITH INCREASED POST SPACING.	369
TABLE 110. PROPERTIES EXTRACTED FROM MATERIAL CERTIFICATION REPORTS FOR BRIDGE RAIL POSTS IN THREE MAINE DOT PROJECTS.	388
TABLE 111. PROPERTIES EXTRACTED FROM MATERIAL CERTIFICATION REPORTS FOR A500 GRADE B&C TUBULAR RAIL SECTIONS IN THREE MAINE DOT PROJECTS.	389
TABLE 112. SUMMARY OF ANALYSIS CASES CONDUCTED AND THE RESULTS OF THE EVALUATIONS.	400
TABLE 113. COMPARISON OF STRENGTH AND WEIGHT FOR TUBULAR RAIL OPTIONS FOR THE NEW HAMPSHIRE 4-BAR SYSTEM (ALL OTHER DESIGN ASPECTS REMAINING THE SAME).	403
TABLE 114. SUMMARY OF CONCLUSIONS AND RECOMMENDATIONS FOR THE NETC 2-BAR BRIDGE RAIL.	407

TABLE 115. SUMMARY OF CONCLUSIONS AND RECOMMENDATIONS FOR THE NETC 3-BAR BRIDGE RAIL	408
TABLE 116. SUMMARY OF CONCLUSIONS AND RECOMMENDATIONS FOR THE NETC 4-BAR SIDEWALK-MOUNTED BRIDGE RAIL.....	409
TABLE 117. SUMMARY OF CONCLUSIONS AND RECOMMENDATIONS FOR THE NETC 2-BAR TRANSITION.....	410
TABLE 118. SUMMARY OF CONCLUSIONS AND RECOMMENDATIONS FOR THE NETC 3-BAR TRANSITION.	411
TABLE 119. SUMMARY OF CONCLUSIONS AND RECOMMENDATIONS FOR THE <i>CONCRETE-TO-THREE-BEAM</i> TRANSITION	412

LIST OF APPENDICES

- Appendix A:** Maine DOT Standard Bridge Rail and AGT Drawings
- Appendix B:** New Hampshire DOT Standard Bridge Rail and AGT Drawings
- Appendix C:** Vermont DOT Standard Bridge Rail and AGT Drawings
- Appendix D:** Rhode Island DOT Standard Bridge Rail Drawings
- Appendix E:** Validation PIRTs for the finite element model used for the 1100C vehicle
- Appendix F:** Validation Forms for Silverado (2270P) Vehicle Model
- Appendix G:** Validation Forms for the NETC 4-Bar Bridge Rail Model
- Appendix H:** Soil Model Calibration/Validation with Full-Scale Bogie Testing
- Appendix I:** Validation Forms for the NETC 2-Bar Transition Model
- Appendix J:** Sequential Views for Test 4-10 on NETC 3-Bar Bridge Rail
- Appendix K:** Sequential Views for Test 4-11 on NETC 3-Bar Bridge Rail
- Appendix L:** Sequential Views for Test 4-12 on NETC 3-Bar Bridge Rail (Case 1)
- Appendix M:** Sequential Views for Test 4-12 on NETC 3-Bar Bridge Rail (Case 2)
- Appendix N:** Sequential Views for Test 4-20 on NHDOT 3-Bar Transition
- Appendix O:** Sequential Views for Test 4-21 on NHDOT 3-Bar Transition
- Appendix P:** Sequential Views for Test 4-22 on NHDOT 3-Bar Transition
- Appendix Q:** Sequential Views for Test 4-10 on Sidewalk-Mounted NETC 4-Bar Bridge Rail
- Appendix R:** Sequential Views for Test 4-11 on Sidewalk-Mounted NETC 4-Bar Bridge Rail
- Appendix S:** Sequential Views for Test 4-12 on Sidewalk-Mounted NETC 4-Bar Bridge Rail
- Appendix T:** Sequential Views for Test 4-20 on Sidewalk-Mounted MaineDOT Transition
- Appendix U:** Sequential Views for Test 4-21 on Sidewalk-Mounted MaineDOT Transition
- Appendix V:** Sequential Views for Test 4-22 on Sidewalk-Mounted MaineDOT Transition Rail
- Appendix W:** Sequential Views for Test 3-10 on NETC 2-Bar Bridge Rail
- Appendix X:** Sequential Views for Test 3-11 on NETC 2-Bar Bridge Rail
- Appendix Y:** Sequential Views for Test 3-20 on NHDOT 2-Bar Transition
- Appendix Z:** Sequential Views for Test 3-21 on NETC 2-Bar Transition

1 INTRODUCTION

1.1 Problem Statement

The current policy for roadside hardware installed on federal aid projects requires upgrading non-conforming systems to *MASH* acceptance level for full system replacements, certain structural rehabilitations such as deck replacements, or repairing a critically damaged bridge rail system.[*AASHTO16*] The Maine Department of Transportation (MaineDOT) and other New England DOTs have a need to evaluate and, if necessary, improve their existing steel post-and-beam bridge rail designs and corresponding approach guardrail transition (AGT) designs to meet the new crash testing standards of *MASH*.

The predominate bridge rail and approach guardrail transition (AGT) systems used in Maine, as well as the other New England states, include details for 2-bar, 3-bar and 4-bar designs which were developed and tested under the auspices of the New England Transportation Consortium (NETC) under AASHTO Guide Selection for Bridge Rails Performance Level 2 (GSBR PL2) and/or NCHRP Report 350 (R350) test procedures. Per the joint agreement of AASHTO and FHWA, each state will need to specify *MASH* compliant bridge rails for new and full replacements on the National Highway System (NHS) with contract lettings after December 31, 2019. As such, it is of interest to the New England DOT's to determine if these existing NETC bridge rail systems meet the strength and safety criteria of *MASH*, which involve higher impact severities for each test case.

1.2 Objectives

The objectives of this project were to: (1) review existing NETC bridge rail and AGT designs and assess performance aspects to determine preliminary *MASH* compliance/equivalency, (2) review current standard details and specifications for NETC style bridge rails and transitions used by MaineDOT, NHDOT, RIDOT and VTrans to identify differences in material specifications and dimensional details, and (3) evaluate the crash performance of the NETC bridge rail and approach guardrail transition (AGT) designs using finite element analysis (FEA) computer simulation. The impact conditions and assessment procedures for the FEA conforms to the specifications in *MASH* for TL3 or TL4 (as appropriate) and included evaluations of structural capacity of the railing, risk of occupant injury, and vehicle stability during impact and redirection. The systems included in the evaluation are listed below along with the target test level for each system:

- Bridge Rail Systems:
 - NETC curb-mounted 2-bar Rail (TL3)
 - NETC curb-mounted 3-bar Rail (TL4) (4-bar curb mounted NETC rail would be considered equivalent to this type)
 - NETC sidewalk-mounted 4-bar Rail (TL4)

- Bridge Rail Transitions:
 - NETC Style 2-bar Rail to Thrie Beam (TL3) (NHDOT steel rail transition)
 - NETC Style 3-bar Rail to Thrie Beam (TL4) (NHDOT steel rail transition)
 - Concrete Transition Barrier to Thrie Beam (TL4) (MaineDOT standard detail)

These basic designs are used by several New England states with slight variations in design details, such as spacing between tube rails and curb height. The standard bridge rail drawings for Maine, New Hampshire, Vermont and Rhode Island are provided in Appendices A, B, C, and D, respectively.

2 RESEARCH APPROACH AND SCOPE OF THE STUDY

A critical review of current standard details and specifications for NETC style bridge rails and transitions used by MaineDOT, NHDOT, RIDOT and VTrans was conducted to identify differences in material specifications and dimensional details. An initial performance assessment was made for each bridge rail design based on strength calculations and rail geometrics calculations for *MASH* loading conditions according to procedures in Section 13 of the AASHTO LRFD Bridge Design Specifications with updated *MASH* criteria as presented in NCHRP 20-07 Task 395.[*AASHTO12; Dobrovolny17*] Preliminary recommendations were made for NETC bridge rail and AGT design details for further crash performance evaluations in this study. The recommendations were based on the least conservative design details that have an acceptable crash testing record. In this way the more conservative designs would be assumed to have adequate strength.

The crash evaluations were conducted using finite element analysis (FEA) to assess crashworthiness under *MASH* conditions. Detailed FEA models of select bridge rails and transition systems were developed, and the FEA software LS-DYNA was used to simulate existing full-scale crash tests to assess the validity of the models. [*LSDYNA15*] Model validity was assessed through comparison of simulated results with the full-scale test results using the procedures outlined in NCHRP [Web-Document 179](#). [*Ray11*] The validated models were then used as a baseline for the *MASH* evaluations of the systems. Revisions to the baseline system designs were incorporated into the baseline model according to the approved recommendations by the project technical oversight committee (TAC) prior to the *MASH* evaluations.

The evaluations used critical impact points that lead to the greatest potential for structural failure or occupant harm and were determined based on FEA results as well as previous testing. The section of the AGT which transitions from the w-beam guardrail to the thrie-beam system has been evaluated via full-scale testing in previous studies and was therefore not included in this study (e.g., see *Winkelbauer14*).

The results of the analyses in this project cannot guarantee *MASH* compliance – only full-scale testing can do that; but the simulations results should provide reliable predictions for the outcome of such tests.

3 LITERATURE REVIEW

A review of published literature and ongoing research was conducted to investigate performance aspects of select bridge rail systems used among the New England States, as well as, other designs that have demonstrated *MASH* compliance/equivalency. A critical review of current standard details and specifications for NETC style bridge rails and transitions used by MaineDOT, NHDOT, RIDOT and VTrans was also performed to identify differences in material and dimensional details compared to each other as well as to the tested designs. Strength calculations, per Section 13 of the *AASHTO LRFD Bridge Design Specifications*, were performed to determine the strength and capacity of the current bridge railing designs. [AASHTO12]

Preliminary recommendations for dimensional and material specifications are provided based on the review to better ensure consistency for NETC style designs, considering constructability and performance.

3.1 Summary of Current NETC Bridge Rail Designs

The current NETC bridge designs are shown in Figures 1 and 2. In general, these designs include a W6x25 steel post that is welded to a 10x14x1-inch steel baseplate and mounted onto the top of a concrete curb or sidewalk using four (4) 1-inch diameter threaded rods 12 inches long. The posts are spaced at 8 feet on centers. The longitudinal rails are composed of HSS 8x4x5/16-inch and HSS 4x4x1/4-inch sections, as shown in Figure 1. The rails are fastened to the post using 3/4-inch diameter round-head bolts inserted through the face of the rail bar.

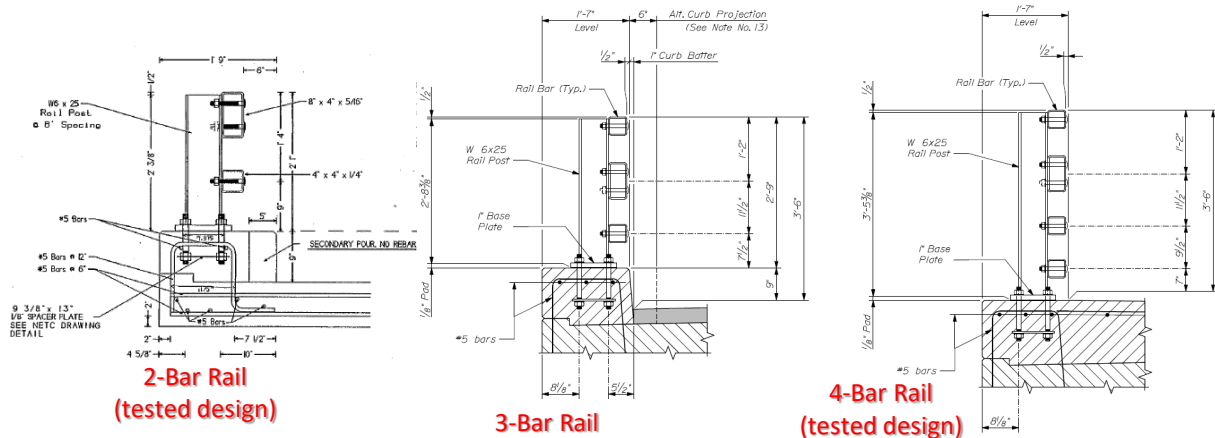


Figure 1. NETC bridge rail designs.

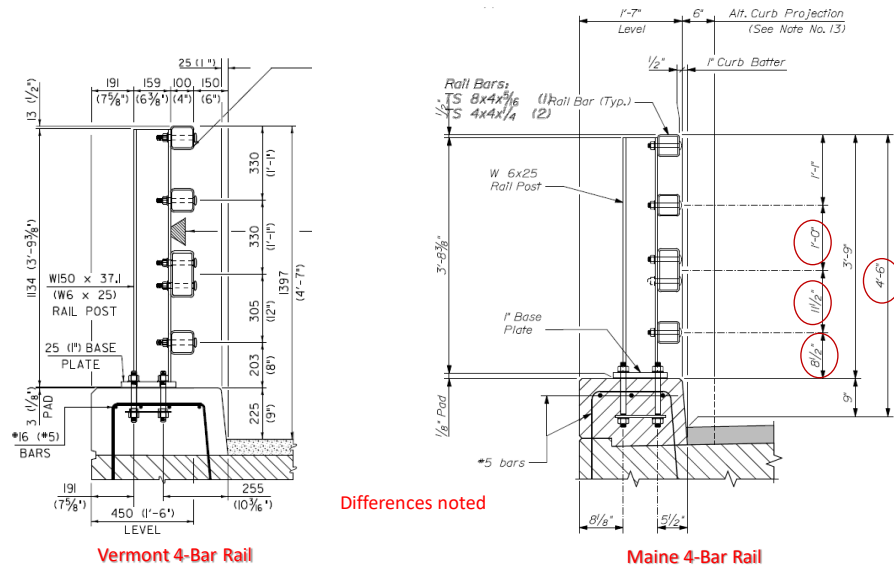


Figure 2. NETC 4-bar curb-mounted bridge rail design.

The 2-bar and 4-bar NETC bridge rail designs shown in Figure 1 were successfully tested under GSBRL2 and R350 TL4 guidelines. [Mak98; Kimball99] The eligibility letter for these two systems is [B-50](#) which can be obtained from the FHWA website¹. The NETC curb-mounted 3-bar design has not been full-scale crash tested but was deemed NCHRP Report 350 TL4 compliant based on the NETC 4-bar test results, acknowledging that the 9-inch reinforced curb serves as a replacement for the lower rail of the system. The eligibility letter for the 3-bar design is [B-242](#) which can also be obtained from the FHWA website.² To our knowledge, there is no eligibility letter for the curb-mounted 4-bar design, as this system has not been full-scale tested. Additional drawing details are provided in the Appendices and in the crash test reports. [Mak98; Kimball99]

3.2 Summary of Current NETC Transition Designs

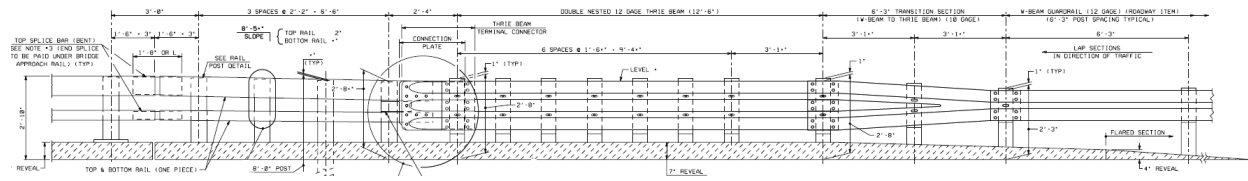
When two barrier systems of different stiffness are connected, such as connecting a semi-rigid guardrail to a rigid bridge rail, it is necessary to ensure a gradual transition across the connection points. Any abrupt change in stiffness of the barrier can lead to pocketing, snagging and/or penetration of the barrier during impact. Thus, a transition guardrail section is necessary to develop a gradual stiffness transition between the two barrier systems.

The approach guardrail transitions (AGT) that were evaluated in this study are shown in Figures 3 and 4. In general, these designs include a w-beam rail attached to a symmetrical thrie-beam transition rail, which is attached to a nested thrie-beam rail, which is then attached to either a tube rail section (e.g., for the 2-bar and 3-bar bridge rail designs) or to a concrete buttress (e.g., for the 4-bar bridge rail design). These guardrails are supported by W6x8.5 steel posts and blockouts. The posts are typically 7', 8' or 8'-8" long and are mounted at decreasing post spacing

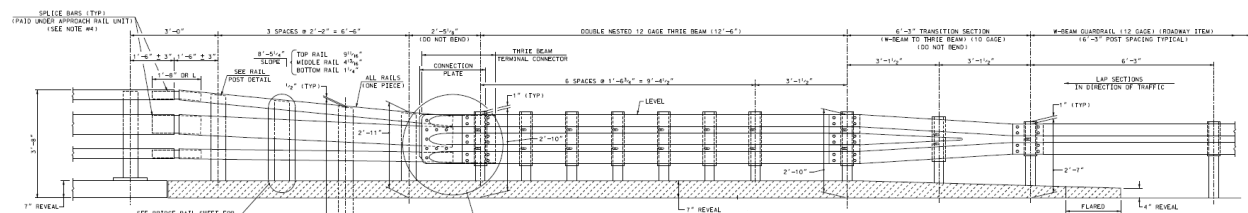
¹ https://safety.fhwa.dot.gov/roadway_dept/countermeasures/reduce_crash_severity/barriers/pdf/b-50.pdf

² https://safety.fhwa.dot.gov/roadway_dept/countermeasures/reduce_crash_severity/barriers/pdf/b242.pdf

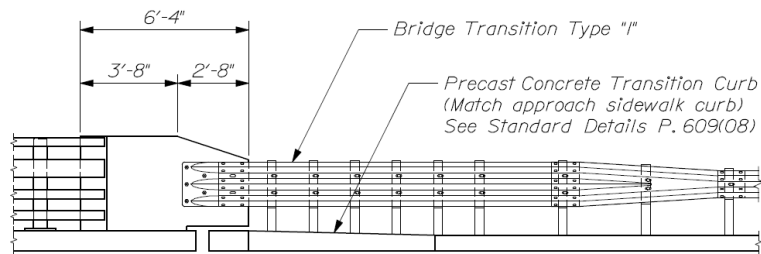
as the system starts at the w-beam guardrail (e.g., 6'-3" spacing) and approaches the rigid bridge rail (e.g., 18.75-inch spacing). Additional drawing details are provided in the Appendices.



(a) NETC Style 2-Bar Rail to Thrie Beam (TL3)



(b) NETC Style 3-Bar Rail to Thrie Beam (TL3)



(c) Maine Concrete to Thrie Beam (TL3)

Figure 3. Elevation drawing of the current AGTs to be evaluated in this study.

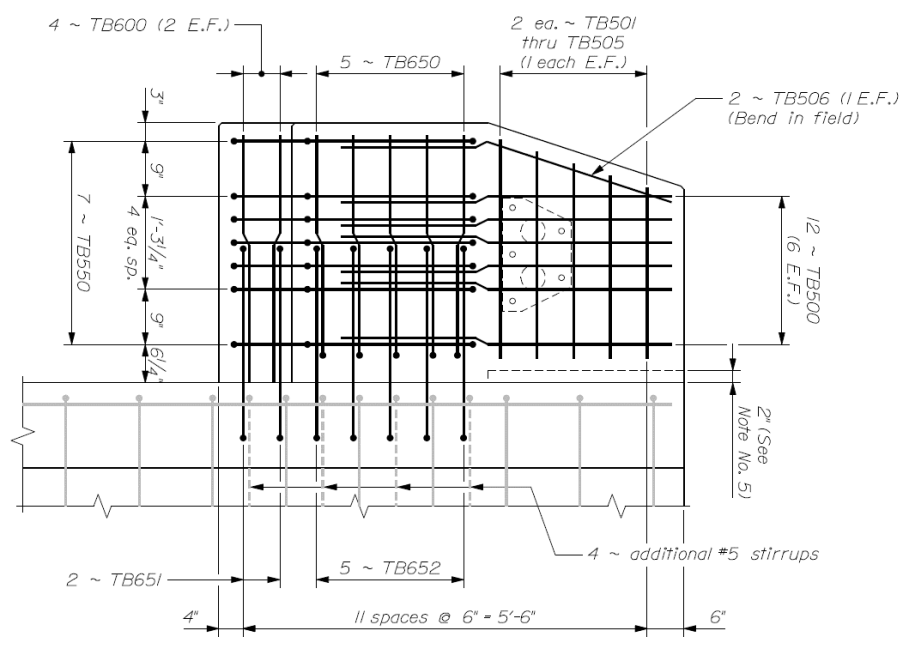


Figure 4. Concrete buttress for the Maine AGT to 4-bar bridge rail.

The NETC 2-bar to three-beam AGT was successfully full-scale crash tested to R350 TL3 by the Texas Transportation Institute (TTI) in 2005. [Alberson06] The NETC 3-bar AGT and NETC 4-bar AGT with transition from three-beam to tube rail have not been crash tested but received R350 TL3 approval from the FHWA based on the NETC 2-bar test (see problem statement of [Mak98] and [Eligibility Letter 146](#)). To our knowledge, the MaineDOT concrete-to-three-beam AGT has not been tested; however, based on results of similar systems, it was expected that the system would require some geometrical changes to the concrete buttress design to prevent vehicle impacting and snagging on the end of the buttress. Additional discussion is provided later in the critical review.

3.3 Previous Full-Scale Testing of NETC Hardware

The following is a summary of the NETC hardware designs that have been successfully crash tested under previous test procedures (e.g., GSBR PL2, R350). These include the curb-mounted NETC 2-bar bridge rail, the sidewalk-mounted NETC 4-bar bridge rail, and the NHDOT AGT for the 2-bar bridge rail. To our knowledge, neither the 3-bar bridge rail nor the AGTs for the 3-bar and 4-bar bridge rail systems have been full-scale crash tested. The test for the NHDOT transition to the 3-bar system was “waived” by the FHWA based on the full-scale test results for the AGT 2-bar system.

3.3.1 NETC 2-Bar Bridge Rail

The NETC 2-bar bridge rail system was tested according to the crash test specifications of 1989 AASHTO *Guide Specifications for Bridge Railings* (GSBR) for performance level 2 (PL2) and R350 TL4. [Mak98] The tests were conducted at the Texas Transportation Institute (TTI). The NETC 2-bar bridge rail, shown in Figure 1, is a R350 TL4 34-inch tall curb-mounted bridge rail composed of two longitudinal tubular rails. The test article included a 100-foot long section of the bridge rail mounted on a simulated bridge deck. The top rail was fabricated from TS 8x4x5/16-inch structural tubing; the lower rail was fabricated from TS 4x4x0.25-inch structural tubing. Each rail was fastened to a W6x25 steel post using two (2) 3/4-inch diameter round-head bolts. The posts were spaced at 8-ft center-to-center. The posts were welded to a 10x14x1-inch baseplate. The baseplate was mounted to the top of a 9-inch tall steel reinforced concrete curb using four 1-inch diameter double-threaded studs. The threaded rods were 9 inches long and were fastened to a 9-3/8 x 13 x 1/8-inch anchor plate embedded in the curb. The curb section was 9 inches tall and 21 inches wide, including a 5-inch wide facing cast in a separate pour on the front of the curb to simulate a granite curb extension. The distance from the face of the curb to the face of the bridge rail was 6 inches.

Test 471470-18 corresponded to the impact conditions of PL2 and involved a 1986 Yugo GV with gross static mass of 1,970 lb, including a 170-lb dummy impacting the bridge rail at 62.7 mph and 20.6 degrees. Test 471470-19 corresponded to the impact conditions of PL2 and involved a 1984 Ford F250 with gross static mass of 5,568 lb impacting the bridge rail at 57.3 mph and 20.6 degrees. Test 471470-29 corresponded to the impact conditions of Report 350 Test 4-12 and involved a 1980 GMC 6000 single unit truck ballasted to 17,621-lb, impacting the bridge rail system at 50.7 mph and angle of 15.5 degrees.

The bridge rail system successfully passed all required structural adequacy and occupant safety criteria for AASHTO PL2 and R350 Test 4-12. Table 1 shows a summary of test results for the NETC 2-bar bridge rail system. Additional details of the tests and results can be found in

the test report. [Mak98] The eligibility letter for this system is [B-50](#) which can be found on the FHWA website.

Table 1. Summary of test results for NETC 2-bar bridge rail design. [Mak98]

	471470-18	NETC-2	NETC-3
Test Designation	PL2-car	PL2-Pickup	R350 Test 4-12
Test Vehicle	1986 Yugo GV	1984 Ford F25	198 GMC 6000
Gross Vehicle Weight (lb)	1,970	5,568	17,621
Impact Speed (mph)	62.7	57.3	50.8
Impact Angle (deg)	20.6	20.6	15.5
Exit Speed (mph)	55.1	48.6	-
Exit Angle (deg)	2.2	2.2	2
Occupant Impact Velocity			
Longitudinal (ft/s)	16.9	12.2	7.5
Lateral (ft/s)	27.5	21.5	12
Ridedown Accel			
Longitudinal (g's)	1.6	2.5	4
Lateral (g's)	6.8	12.2	3.2
Maximum 50 msec Avg Accel			
Longitudinal (g's)	6.1	3.4	1.8
Lateral (g's)	15.2	10.3	2.6
Max Deflection (in)	0.25	0.25	-
Vehicle Trajectory			
Maximum YawAngle (deg)	15	25	16
Maximum Roll Angle (deg)	15	26	19
Maximum Pitch Angle (deg)	32	5	6
NCHRP Report 350 Evaluation			
Structural Adequacy	Pass	Pass	Pass
Occupant Risk	Pass	Pass	Pass
Vehicle Trajectory	Pass	Pass	Pass

3.3.2 NETC 4-Bar Bridge Rail

The NETC 4-bar bridge rail, shown in Figure 1, is an R350 TL4 42-inch tall bridge rail (not including the height of the 9-inch sidewalk) with four longitudinal tubular rails. The top rail, the third rail from the top, and the bottom rail are fabricated from TSS 4 x 4 x 1/4-inch structural tubing; the second rail from the top is fabricated from TS 8 x 4 x 5/16-inch structural tubing. The rails are attached to W6x25 steel posts using 3/4-inch diameter studs with steel washers and locknuts. The posts are spaced at 8-ft center-to-center. The posts are welded to a 10x14x1-inch steel baseplate. The baseplate is fastened to the top of a 9-inch tall steel reinforced concrete sidewalk using four 1-inch diameter anchor bolts.

Each tubular rail section is 23.9 feet long and spans three posts. The rail tubes are joined to the neighboring rails using a 20-inch long tubular sleeve inserted 9-5/8 inches into the ends of the adjoining rails. The adjoining main rails are separated by a 3/4-inch gap and the sleeve is fastened to each main rail tube using two 5/8-inch diameter cap screws. The sleeve tube is fabricated from 3/8-inch steel plate welded along the edges as indicated in Table 2. The clearance of the splice tube inside the main rail tube is 1/16-inch on all sides. Refer to the drawings in the crash test report for additional construction details. [Kimbal99]



Figure 5. NETC 4-bar (SBB44b) Bridge Rail. [Kimball99]

Table 2. Splice tube dimensions for the NETC 4-bar bridge rail in Test NETC 1 – NETC 3.

	TS 8 x 4	TS 4 x 4
Top & Bottom Plates	2½" x 3/8" x 20"	2-5/8" x 3/8" x 20"
Side Plates	6¾" x 3/8" x 20"	2-7/8" x 3/8" x 20"

The material for the rail bars is ASTM A500 Grade B or ASTM A501 steel. The material for the rail posts is ASTM A709 Grade 50. The material for all other shapes and plates are ASTM A709 Grade 36. Anchor studs, washers and exposed nuts conform to ASTM A449, which has a minimum yield of 92 ksi, ultimate strength of 120 ksi, and 14 percent elongation. All other bolts and nuts conform to ASTM A307 with minimum yield of 36 ksi, minimum tensile strength of 60 ksi and 18 percent elongation.

The NETC 4-bar bridge rail system was tested according to the crash test specifications of NCHRP Report 350 for Test Level 4. The test article was a 108-foot long section of the bridge rail mounted on a concrete sidewalk. The sidewalk was 8 inches tall at the traffic face and sloped up to 9 inches tall at the point where the bridge rail was mounted. The distance from the face of the curb to the face of the bridge rail was 5 feet.

The tests were conducted at the Southwest Research Institute (SwRI). Test NETC-1 corresponded to the impact conditions of Report 350 Test 4-10 and involved a 1991 Ford Festiva with gross static mass of 1,989 lb, including a 165-lb dummy impacting the bridge rail at 62.14 mph and 20 degrees. Test NETC-2 corresponded to the impact conditions of Report 350 Test 4-11 and involved a 1991 Ford F-250 with gross static mass of 4,484 lb impacting the bridge rail at 62.14 mph and 25 degrees. Test NETC-3 corresponded to the impact conditions of Report 350 Test 4-12 and involved a 1993 International 4600 LP single unit truck ballasted to 17,875-lb, impacting the bridge rail system at 49.8 mph and angle of 15 degrees.

The bridge rail system successfully passed all required structural adequacy and occupant safety criteria of NCHRP Report 350. Test NETC-3 (i.e., Test 4-12) resulted in an exit trajectory of the vehicle that would indicate intrusion into adjacent lanes; however, this was a preferred, not

required, criterion. Table 3 shows a summary of test results for the NETC 4-bar bridge rail system. The maximum dynamic deflection of the bridge rail was zero inches for NETC-1 and was 1.0 inch for both test NETC-2 and NETC-3. Additional details of the tests and results can be found in the test report. [Kimball99] The eligibility letter for this system is also [B-50](#) which can be obtained from the FHWA website.

Table 3. Summary of test results for NETC 4-bar bridge rail design. [Kimball99]

	NETC-1	NETC-2	NETC-3
Report 350 Test No.	Test 4-10	Test 4-11	Test 4-12
Test Vehicle	1991 Ford Destiva	1991 Ford F-250	1993 International 4600 LP
Gross Vehicle Weight (lb)	1823	4484	17,875
Impact Speed (mph)	62.1	62.1	49.7
Impact Angle (deg)	20	25	15
Exit Speed (mph)	11.4	10.6	35.8
Exit Angle (deg)	6.6	8.2	4.1
Occupant Impact Velocity			
Longitudinal (ft/s)	*	13.1	5.41
Lateral (ft/s)	*	*	9.48
Ridedown Accel			
Longitudinal (g's)	*	2.55	8.95
Lateral (g's)	*	*	14.3
Maximum 50 msec Avg Accel			
Longitudinal (g's)	-	-	2.7
Lateral (g's)	-	-	5.8
Max Deflection (in)	0	1	1
Vehicle Trajectory			
Maximum YawAngle (deg)	34	*	*
Maximum Roll Angle (deg)	10	20	20
Maximum Pitch Angle (deg)	5	15	5
NCHRP Report 350 Evaluation			
Structural Adequacy	Pass	Pass	Pass
Occupant Risk	*	Pass	Pass
Vehicle Trajectory	Pass	Pass	Pass

* No occupant risk data - lateral accelerometer malfunctioned during test.

3.3.3 NHDOT 2-Bar Rail to Thrie-Beam AGT

The NHDOT 2-bar rail to thrie-beam AGT, shown in Figure 6, is an R350 TL3 system. The total length of the transition section was 29 feet from the end of the standard w-beam guardrail to the beginning of the bridge rail. The upstream end of the transition system consisted of a 12-gauge w-beam rail connected to a 10-gauge symmetric w-beam-to-thrie-beam transition rail supported by three 6x8 wood posts that were 7 feet long and spaced 37.5 inches on centers (e.g., half post-spacing). The symmetric transition rail was then connected to two nested 12-gauge thrie-beam rails supported by four 6x8 inch wood posts that were 7 feet long. The first post was spaced at 37.5 inches and the next six (6) posts were spaced at 18.5 inches on centers (quarter post-spacing). The height of the thrie-beam section was 32 inches. The downstream end of the nested thrie-beams was connected to the two-tube transition rail by means of a 10-gauge thrie-beam terminal connector. The two tube transition rails used in the transition section

are the same tubular elements used in the bridge rail. The top rail was a TS 8x4x5/16 and the lower rail was a TS 4x4x1/4. The tube rails were supported on four (4) W6x25 steel posts 8 feet long and spaced at 26 inches on centers. The ends of the rail tubes were connected to the bridge rail through a splice connection. The height of the top rail tube at the connection point to the thrie-beam was 32 inches. The rail element slanted upward slightly such that the downstream end was at the same height of the bridge rail (i.e., 34 inches). The tube rails were connected to the W6x25 steel posts with two 6-inch long, 3/4-inch diameter round-headed bolts. A 7-inch tall simulated granite curb was installed throughout the transition and extend 6 inches in front of the rail tubes and 2-1/4 inches in front of the thrie-beam.



Figure 6. NHDOT 2-Bar rail to thrie-beam AGT. [Alberson06]

The NHDOT 2-bar rail to thrie-beam AGT was tested according to the crash test specifications of NCHRP Report 350 Test 3-21. The test was conducted at the Texas Transportation Institute (TTI). Test 401181-1 involved a 4,706-lb Chevrolet 2500 impacting the system at 64.37 inches downstream of the first bridge rail post at 63.6 mph (102.3 km/hr) and 24.9 degrees. The bridge rail system successfully passed all required structural adequacy and occupant safety criteria for R350 TL3. Table 4 shows a summary of test results for the AGT to 2-bar bridge rail system. Additional details of the tests and results can be found in the test report. [Alberson06]

3.3.4 NHDOT 3-Bar Rail to Thrie-Beam AGT

A photo of this system was not available for this report; however, the drawings can be found in Appendix B. The upstream section of the NHDOT 3-bar AGT design from the w-beam guardrail to the end of the thrie-beam terminal connector is identical to the 2-bar AGT design described in the preceding section. The primary difference in these two systems is the number of rails in the tube-rail section. For the 3-bar AGT, the three tube transition rails used in the transition section are the same tubular elements used in the bridge rail. The top and lower rails are a TS 4x4x1/4 and the middle rail is a TS 8x4x5/16. The tube rails were supported on four (4) W6x25 steel posts 8'-8" long and spaced at 26 inches on centers. The ends of the rail tubes are connected to the bridge rail through a splice connection. The height of the top rail tube at the connection point to the thrie-beam was 34 inches. The top and middle rail elements slanted

upward such that the downstream end was at the same height of the bridge rail (i.e., 44 inches for the top rail). The tube rails were connected to the W6x25 steel posts with two 6-inch long, 3/4-inch diameter round-headed bolts. A 7-inch tall simulated granite curb was installed throughout the transition and extend in front of the rail tubes by 6 inches and the thrie-beam by 2-1/4 inches.

Table 4. Summary of test results for NHDOT 2-Bar Rail to Thrie-Beam AGT. [Albers06]

	401181-1
Test Designation	Test 3-21
Test Vehicle	2000 Chevrolet 2500
Gross Vehicle Weight (lb)	4,706
Impact Speed (mph)	63.6
Impact Angle (deg)	24.9
Exit Speed (mph)	52.9
Exit Angle (deg)	11.7
Occupant Impact Velocity	
Longitudinal (ft/s)	17.1
Lateral (ft/s)	24.6
Ridedown Accel	
Longitudinal (g's)	8.3
Lateral (g's)	10
Maximum 50 msec Avg Accel	
Longitudinal (g's)	8.1
Lateral (g's)	13.5
Max Deflection (in)	7.87
Vehicle Trajectory	
Maximum YawAngle (deg)	56
Maximum Roll Angle (deg)	14
Maximum Pitch Angle (deg)	19
NCHRP Report 350 Evaluation	
Structural Adequacy	Pass
Occupant Risk	Pass
Vehicle Trajectory	Pass

This system is considered R350 TL3 compliant, although it has not been full-scale tested. Full-scale testing of this system was not required by FHWA based on review of the drawings and results of the NETC 2-bar rail to thrie-beam tests. [Albers06]

3.4 MASH Equivalency Assessment

In a recent study performed by the Texas Transportation Institute (TTI) under NCHRP Project 20-07 (Task 395) an assessment of several types and styles of existing bridge rails was conducted to determine if they met suggested *MASH* performance criteria. [Dolobrovolny17] If a system was deemed equivalent to a specific *MASH* test level then it could be ‘grandfathered’ to *MASH* without further testing. The equivalency assessments considered vehicle stability, strength of the railing, and geometry of the railing. According to the assessment, a design was deemed *MASH* equivalent:

- If rail height is sufficient for the *MASH* test level (see Table 5);
- If the system has sufficient strength capacity to withstand *MASH* loads based on strength calculations from Section 13 of the AASHTO LRFD Bridge Design Specifications (see Table 5);

- If potential for vehicle snag on the bridge rail posts is less than critical values based on: (1) “ratio of rail contact width to height” vs “post setback distance” and (2) “vertical clear opening” vs “post setback distance” also contained in the AASHTO LRFD Bridge Design Specifications (see Figure 7).

Table 5. Critical rail height and design lateral impact loads for MASH bridge railing.
[Dolbrovolny17]

MASH Test Level	Rail Height (in)	Design Impact Force (kip)	Height of Design Impact Force (in)
TL-3	≥ 29	71	19
TL-4	36	68	25
	> 36	80	30
TL-5	42	160	35
	> 42	262	43

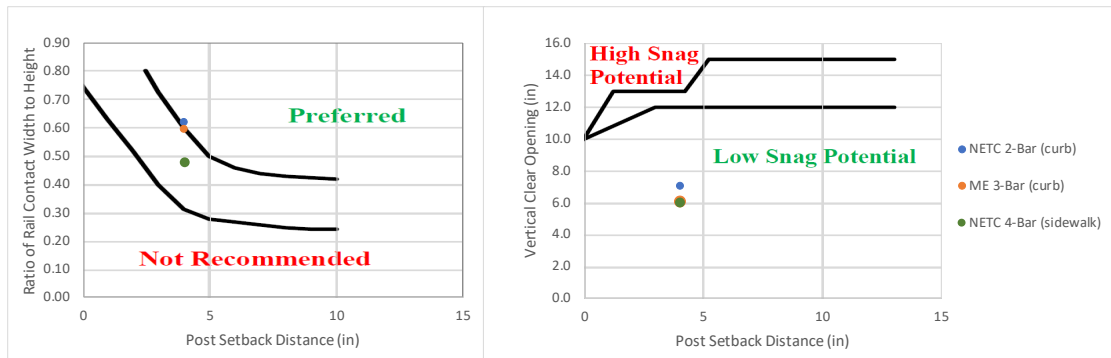


Figure 7. AASHTO Section 13 Figures A13.1.1-2 and A13.1.1-3 including NETC bridge rail.
[AASHTO12]

The MASH minimum rail height requirement for stability were determined from a combination of full-scale testing and FEA. For MASH TL3, the minimum height was determined using finite element analysis (FEA). The FEA model was validated by comparing the analysis results to a full-scale crash test conducted on a 32-inch tall vertical concrete barrier under MASH Test 3-11 conditions (i.e., 5000-lb pickup impacting at 62 mph and 25 degrees). The validated model was then used to assess vehicle stability for MASH Test 3-11 on 27-inch, 28-inch, and 29-inch tall vertical concrete barriers. The pickup was determined to be unstable for the 27- and 28-inch barriers but was stable for the 29-inch tall barrier case. [Dolbrovolny17]

For MASH TL4, the minimum height was determined to be 36 inches using FEA and was then verified via full-scale testing on a 36-inch tall single-slope barrier. [Sheikh11] Previous full-scale testing showed that the 22,000-lb single unit truck rolled over the top of the 32-inch tall barrier under MASH Test 4-12 conditions (i.e., 55 mph and 15 degrees) [Bullard08; Polivka06].

3.4.1 Rail Geometric Evaluations

The geometric relationships for bridge railings are contained in Figures A13.1.1-2 and A13.1.1-3 of Section 13 of the AASHTO LRFD Bridge Design Specifications, and reproduced here in Figure 7 above. [AASHTO12] These relationships were developed based on a review of NCHRP Report 230 crash test data to relate impact performance to the geometric characteristics

of bridge railing systems. The rail geometric criteria correlate the potential for the wheel, bumper or hood snagging against a bridge rail post to high vehicle decelerations and occupant compartment intrusions. These relationships have not yet been confirmed for NCHRP Report 350 or *MASH* test cases but are still commonly applied to bridge rail design.

Table 6 and Figure 8 show a summary of the rail-geometric calculations for the NETC and New England bridge rail designs with the highest priority systems highlighted. Example calculations are shown in Figure 9. For a *post setback distance* of 4 inches, the 2-bar system meets the recommended geometric criteria when the curb height is 9 inches (e.g., NETC and ME); however, there is not sufficient contact width relative to the height of the rail when a 7-inch curb is used (e.g., VT and RI). The 3-bar system also meets the recommended criteria when a 9-inch curb is used (e.g., ME) but not for the 7-inch curb (e.g., NH). The 4-bar systems, however, do not meet recommended criteria for *contact width / barrier height*.

Table 6. Rail geometrics calculations for NETC bridge rails.

Bridge Rail Design (Mount)	State	Post Setback (in)	Rail Height (in)	Max. Vertical Opening (in)	Contact Width (in)	Ratio Contact/Height	Result
2-Bar (curb)	NETC	4	34	7.0	21	0.62	S
	ME	4	34	7.0	21	0.62	S
	*VT	4	34	9.0	19	0.56	M
	*RI	4	34	9.0	19	0.56	M
3-Bar (curb)	ME	4	42	6.0	25	0.60	S
	*NH	4	44	9.0	23	0.52	M
4-Bar (sidewalk)	NETC	4	42	6.0	20	0.48	M
	ME	4	42	6.0	20	0.48	M
	NH	4	42	5.5	20	0.48	M
	RI	4	42	5.5	20	0.48	M
4-Bar (curb)	ME	4	54	7.0	29	0.54	M
	VT	4	55	7.0	29	0.53	M

* VT, NH, and RI use 7-inch curbs for the 2-Bar and 3-Bar systems. The max opening is between the lower rail and top of curb.

S: Satisfactory

M: Marginal

N.S.: Not Satisfactory

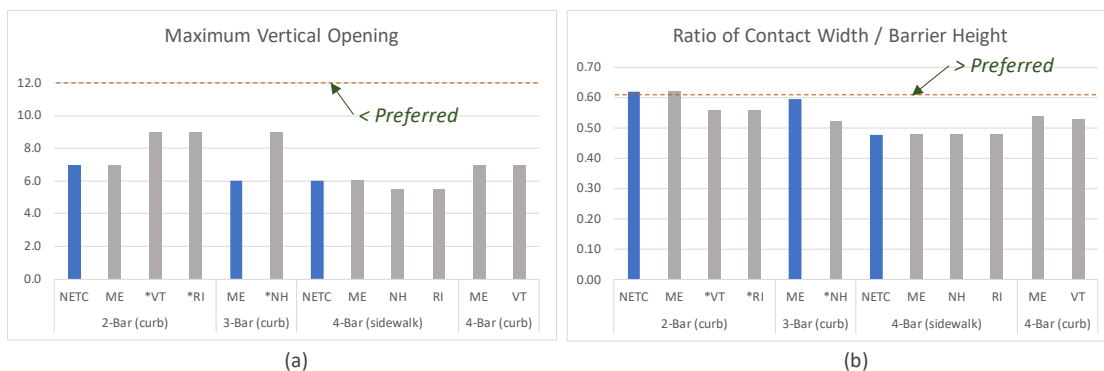


Figure 8. Rail geometrics summary for NETC style barriers by State (blue denotes priority designs).

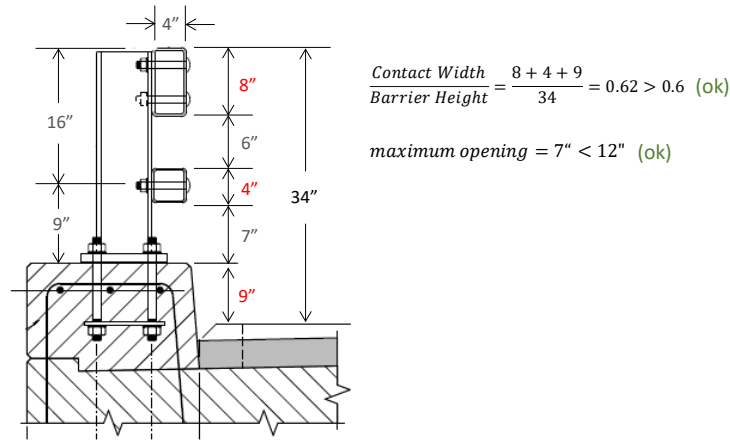


Figure 9. Example calculations for the rail geometric criteria based on a *post setback distance* of 4 inches.

3.4.2 Rail Strength Evaluations (Bridge Rails)

The design forces for bridge railing is provided in Table A13.2-1 of the AASHTO LRFD Bridge Design Specifications, which is shown here in Table 7. Under *MASH* impact conditions, the impact severity increased significantly compared to its predecessors for Test Level 3 (e.g., 13.6 percent) and Test Level 4 (e.g., 56.8 percent). Accordingly, the design forces for bridge railing have also been increased for *MASH* designs. In a research project sponsored by TxDOT, TTI used finite element analysis to calculate lateral impact force characteristics, including magnitude and loading height, for *MASH* TL4 impact conditions for rigid single slope barriers with various heights. [Sheikh11] As part of the NCHRP 20-07(395) project, FEA was used in a similar manner to calculate lateral impact load characteristics for NCHRP Report 350 and *MASH* TL3 impact conditions for a rigid vertical parapet. [Dolobrolyony17] The resulting TL3 and TL4 design loads are shown in Table 8.

Table 7. Design forces for NCHRP Report 350 traffic railings [AASHTO12]

Design Forces and Designations	Railing Test Levels					
	TL-1	TL-2	TL-3	TL-4	TL-5	TL-6
F_t Transverse (kips)	13.5	27.0	54.0	54.0	124.0	175.0
F_L Longitudinal (kips)	4.5	9.0	18.0	18.0	41.0	58.0
F_v Vertical (kips) Down	4.5	4.5	4.5	18.0	80.0	80.0
L_r and L_L (ft)	4.0	4.0	4.0	3.5	8.0	8.0
L_v (ft)	18.0	18.0	18.0	18.0	40.0	40.0
H_e (min) (in.)	18.0	20.0	24.0	32.0	42.0	56.0
Minimum H Height of Rail (in.)	27.0	27.0	27.0	32.0	42.0	90.0

Table 8: Design forces and load height for *MASH* TL3 with comparison to NCHRP Report 350. [Dolbrovolny17]

Design Forces and Designations	Test Level 3			Test Level 4				
	Report 350 ⁽¹⁾	Report 350 ⁽²⁾	MASH ⁽³⁾	Report 350 ⁽¹⁾	MASH ⁽³⁾			
	Barrier Height (in)			Barrier Height (in)				
	all	all	all	all	36	39	42	Tall
F _t Transverse (kip)	54	61	71	54	67.2	72.3	79.1	93.3
F _L Longitudinal (kip)	18			18	21.6	23.6	26.8	27.5
F _v Vertical (kip)	4.5			18	37.8	32.7	22	N/A
L _t and L _L (ft)	4			3.5	4	5	5	14
H _e (in)	24	18	19.5	32	25.1	28.7	30.2	45.5

⁽¹⁾ [AASHTO12]

⁽²⁾ [Dolbrovolny17]

⁽³⁾ [Sheikh11]

N/A Not applicable

The design load for *MASH* TL3 increased to 71 kips applied at 19.5 inches above the reference surface (e.g., top of pavement for curb- and deck-mounted systems, or top of sidewalk for sidewalk-mounted systems). The design loads for *MASH* TL4 also increased and are now a function of rail height, since taller barriers engage more of the cargo bed and reduce roll angle of the vehicle, both of which increase the lateral forces on the barrier.

The design loads used in the 20-07(395) project are shown in Table 9, which were based on those presented in Table 8; the values in Table 9 were adopted for this study. The NETC 2-bar design is being evaluated as a *MASH* TL3 barrier with a design load of 71 kips applied at 19 inches, since it does not meet minimum height requirement for *MASH* TL4. The NETC 3-bar and 4-bar designs are 42 inches tall and are being assessed as *MASH* TL4 barriers, so the lateral design load is 80 kips applied at 30 inches above the reference surface for those cases.

Table 9. Design loads for *MASH* barriers used in NCHRP 20-07(395) project. [Dolbrovolny17]

MASH Test Level	Rail Height (in)	Design Impact Force (kip)	H _e (in)
TL-3	≥ 29	71	19
TL-4	36	68	25
	> 36	80	30
TL-5	42	160	35
	> 42	262	43

3.4.2.1 Materials

The material types and strengths for the primary components of the NETC bridge rail designs used in the New England states are listed in Table 10. In all cases the railing material was AASHTO A500 Grade B with minimum yield strength of 46 ksi. Based on discussions between Maine DOT and HSS suppliers, A500 is supplied under dual specification for Grade B and C. Grade C has minimum yield strength of 50 ksi and this value was used in the strength calculations for each of the systems except for the NETC baseline design, since that system was tested using Grade B. The post and baseplate material were generally ASTM Grade 50 or AASHTO M270 Grade 50 with minimum yield strength of 50 ksi, except for the baseplate in the

tested NETC system which was Grade 36. The concrete strength was 4 ksi or 5 ksi depending on State, and the anchor bolts were either ASTM A449 or AASHTO M314 Grade 105, with minimum tensile strengths of 120 ksi and 125 ksi, respectively.

Table 10. Materials for NETC bridge rail designs.

Description		Variable	Units	NETC	NHDOT	MaineDOT	RIDOT
Rail	Material Type			A500 GrB	A500 Gr B/C	A500 Gr B/C	A500 Gr B/C
	Yield Strength	F_{ytube}	ksi	46	50	50	50
Post	Material Type			A709 Gr50	A572 Gr50	M270 Gr 50	M270 Gr 50
	Yield Strength	F_{ypost}	ksi	50	50	50	50
Base Plate	Material Type			A709 Gr36	A572 Gr50	M270 Gr 50	M270 Gr 50
	Yield Strength	$F_{ybaseplate}$	ksi	36	50	50	50
Anchor Bolts	Material Type			A449	A449	M314 Gr105	A449
	Tensile Strength	F_{ybolt}	ksi	120	120	125	120
Concrete	UCS	f'_c	psi	4000.00	4000.00	5000.00	5000.00

3.4.2.2 Strength Calculations Equations

A strength analysis for the 2-bar, 3-bar and 4-bar NETC designs was performed according to the procedures contained in Section 13 of the AASHTO LRFD Bridge Design Specifications based on plastic strength analysis methods. [AASHTO12] For post-and-beam railings, the critical rail nominal resistance, R' , is taken as the lowest value determined from the following equation (e.g., A13.3.2-3 in [AASHTO12]):

$$R' = \frac{16M_p + (N - 1)(N + 1)P_p L}{2NL - L_t} \quad (\text{failure modes involving even number of spans})$$

$$R' = \frac{16M_p + N^2 P_p L}{2NL - L_t} \quad (\text{failure modes involving odd number of spans})$$

Where,

M_p = Inelastic resistance of all rails contributing to plastic hinge (kip-ft) (i.e., $\sum F_{yi} Z_i$)

F_{yi} = Yield strength of each rail element (ksf)

Z_i = Plastic section modulus for each rail element (ft³)

P_p = Lateral resistance of a single post (kip)

L = Post spacing (ft)

N = Number of spans included in failure hinge evaluations

L_t = length of distributed load on rail

It is assumed that the critical resistive force, R' , corresponds to a resultant resistive force of the rail elements applied a height, Y , above the bridge deck, where Y is computed as:

$$Y = (\sum_{i=1}^N (M_{Pi} h_i)) / M_P$$

Where

M_{Pi} = Inelastic resistance of each rail element

h_i = height to center of each rail element relative to reference base

The lateral resistance of the post is a function of the post material and geometry, as well as the mounting connections of the post to the curb/deck. Thus, the critical value for post strength, P_p , is defined as the minimum of:

- P_{p1} : Plastic strength of the post.
- P_{p2} : Anchor bolt strength (tension and shear).
- P_{p3} : Weld strength.
- P_{p4} : Pry-out of front anchor bolts from concrete (concrete shear cone).
- P_{p5} : Push-out block shear of concrete (lateral shear).
- P_{p6} : Vertical punching shear of concrete from post baseplate.

Calculations for each of these cases are presented in the following sections.

P_{p1} – Plastic Strength of Post

The plastic strength of the post is calculated as:

$$P_{p1} = \frac{Z_{post} * F_y}{Y - h_{curb} - t_{bp}} = \frac{Z_{post} * F_y}{h_p}$$

Where

Z_{post} = plastic section modulus for post

F_y = yield strength of post

Y = equivalent load height above reference surface (e.g., deck or sidewalk)

h_{curb} = curb height

t_{bp} = thickness of baseplate

h_p = height from top of baseplate to Y

P_{p2} – Based on Anchor Bolt Strength

The peak tensile forces of the anchor bolts arise from the bending moment at the base on the post from the lateral impact force on the railing. It is assumed that as the post is pushed back it will tend to rotate about the back edge of the baseplate, which will result in a combination of tensile and shear forces in all mounting bolts. The nominal tensile strength of an anchor bolt, ϕF_{ut} , is computed as:

$$\phi F_{ut} = \phi_t F_u A_{bolt}$$

Where

ϕ_t = strength reduction factor for tension load (1.0)

F_u = ultimate strength of bolt (ksi)

A_{bolt} = stress area of bolt in the thread region (in²)

The stress area is calculated as:

$$A_{bolt} = 0.785(D - 0.9743/n)^2$$

Where

D = bolt diameter (in)

n = number of threads per inch (e.g., n = 8 for 1" diameter UNC bolt)

The resultant plastic moment resistance for the anchor bolt system is:

$$M_{P2} = \phi F_{ut} w_{bolts} N_{bolts}$$

Where

w_{bolts} = resultant moment arm for bolt group from back edge of baseplate

N_{bolts} = number of anchor bolts in the bolt group

The effective strength of the post relative to the anchor bolts is then:

$$P_{P2} = \frac{M_{P2}}{h_p}$$

P_{P3} – Based on Weld Strength:

For all NETC designs, the post is welded to the baseplate using a *seal weld* or an *all-around* weld at the post flanges and web, as illustrated in Figure 10. The weld strength calculations are based elastic strength of the weld and only consider the welds on the tension flange of the post. In this respect, the calculations are considered to be conservative.

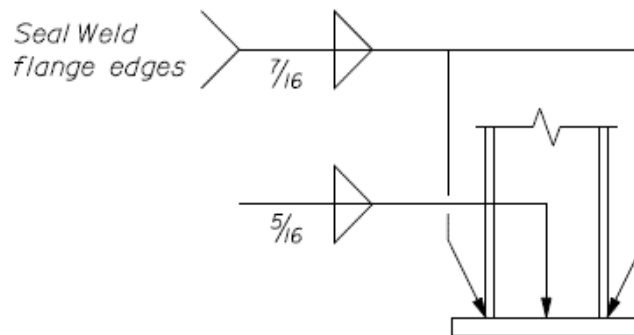


Figure 10. Weld specifications for post-to-baseplate in NETC railing designs.

The design strength, ϕR_n , of the weld is computed as:

$$\phi R_n = \phi_{weld} (0.6 F_{EXX}) (1 + 0.5 \sin(\theta)^{1.5}) A_{eff}$$

Where

ϕ_{weld} = strength reduction factor for the weld (0.75)

F_{EXX} = nominal weld strength (70 ksi)

θ = angle of loading with respect to the longitudinal axis of the weld (90 degrees)

A_{eff} = effective area of the weld

The effective area of the weld is computed as:

$$A_{eff} = t_w b_{post} N_w$$

Where

t_w = weld throat size = 0.707*weld size

b_{post} = width of post flange

N_w = number of welds = 2 (one on each side of flange)

The effective moment strength at the base of the post due to tensile loading on the welds is calculated as:

$$M_{weld} = \frac{\phi R_n}{d_w} = \frac{\phi R_n}{d_{post} - t_f}$$

Where

d_w = distance from center of weld group on flange to back flange of post

d_{post} = depth of post (flange to flange)

t_f = thickness of flange

The effective strength of the post relative to the welds at the baseplate is then:

$$P_{P3} = \frac{M_{weld}}{h_p}$$

P_{P4}, P_{P5}, and P_{P6} – Based on Concrete Failure

There are basically three concrete failure modes for bridge rails mounted to concrete curbs and decks: (1) pry-out shear cone failure due to tensile load on front anchors, (2) push-out shear failure due to shear load from the anchor bolts, and (3) punching shear failure due to the baseplate rotating and punching through the concrete deck at the backside of the deck. The later failure mode is typically only common for thinner decks where the post is mounted very close to the back edge of the deck. Examples of these failure modes are shown in Figures 11 and 12. Figure 11 includes two post-test photos from NCHRP Report 350 Test 3-11 on the TxDOT T77 bridge rail. [Bullard02] The primary failure mode of the concrete for that test was pry-out shear failure; however, the concrete curb showed notable cracks from all three damage modes, as annotated on the photos. Figure 12 shows post-test photos from NCHRP Report 350 Test 3-11 on the TxDOT T101 bridge rail, which clearly illustrates the results from punching shear when the post is set at the edge of a thin bridge deck. [Bligh11]

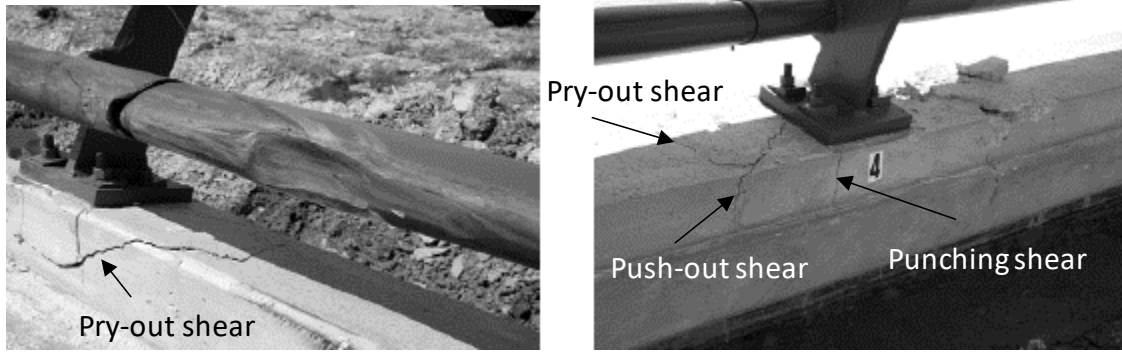


Figure 11. Concrete damage modes experienced in NCHRP Report 350 Test 3-11 on the TxDOT T77 bridge rail.



Figure 12. Punching shear damage mode experienced in NCHRP Report 350 Test 3-11 on the TxDOT T101 bridge rail.

Pry-Out Failure Calculations

The theoretical shear cone failure area, A_p , for tensile loading, T_c , on anchor bolts in concrete is shown in Figure 13, where L_c is the depth of the anchor bolt, m is the distance from the center of the anchor bolt to the curb edge, d_b is the longitudinal spacing between front anchor bolts, and θ is the shear angle taken as 45 degrees. Since there is an anchor plate at the bottom of the anchor bolts, the shear surface extending between the anchor bolts was approximated by a rectangular plane starting at the bolt positions on the anchor plate and extending upward at angle θ of 45 degrees toward the concrete surfaces (i.e., toward both the front and back of the curb).

The pull-out shear cone strength, T_c , of the anchor is computed as:

$$T_c = \phi_t \sqrt{f'_c} * A_p$$

where

ϕ_t = Tensile stress reduction factor (0.85 when anchor head is beyond far face reinforcement)

f'_c = Unconfined compressive strength of concrete.

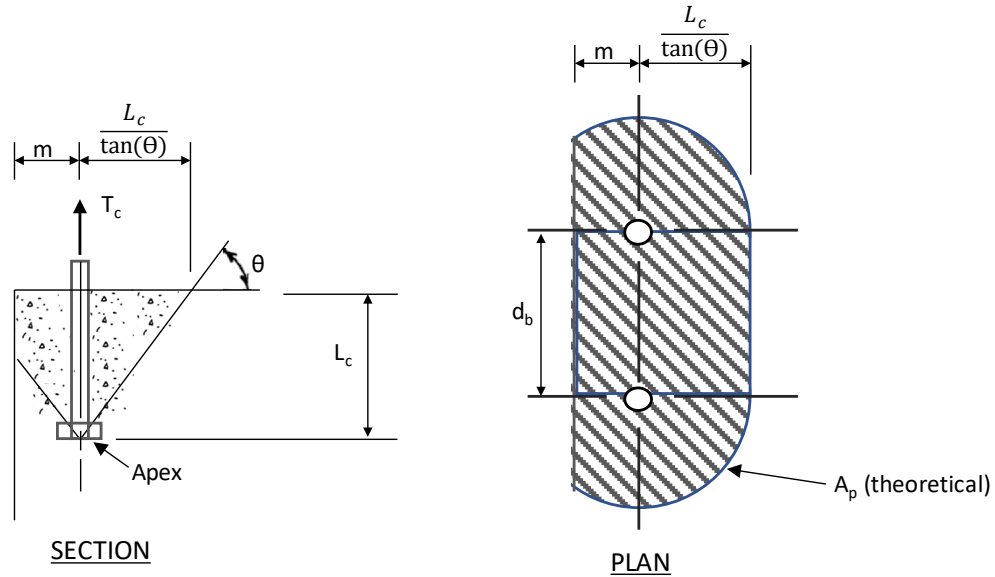


Figure 13. Theoretical failure planes for pry-out shear cone failure in concrete.

The effective moment resistance, M_{Tc} , at the base of the post due to pry-out force of the concrete anchor, as illustrated in Figure 14, is calculated as:

$$M_{Tc} = T_c * d_{Tc}$$

Where d_{Tc} is the distance from the tensile anchor to the point of compression on the baseplate, which is taken here as the lateral distance between anchor bolts, as shown in Figure 14a. This distance is often set as the distance from the front bolt to the back flange of the post but may extend to the back edge of the baseplate, if the baseplate has sufficiently greater stiffness than the post. Note, however, that for the NETC designs the anchor bolts are essentially aligned with the post flanges, as shown in Figure 14b.

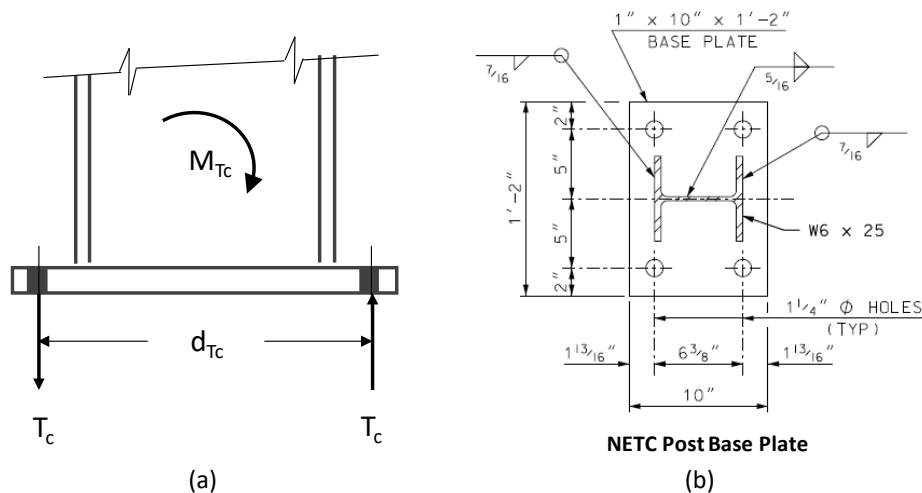


Figure 14. (a) Assumed load/reaction points for the anchor bolt pry-out resistance calculations and (b) dimensions of the NETC baseplate.

The effective strength of the post relative to the pry-out resistance of the anchor bolts is then:

$$P_{P4} = \frac{M_{Tc}}{h_p}$$

Push-Out Shear Failure Calculations

The theoretical failure area, A_p , for push-out shear, R_c , of the concrete due to shear loading on the anchor bolts is illustrated in Figure 15. It is assumed that the shear failure cracks start at the top of the concrete surface at each of the the front anchor bolts. These cracks extend at a 45 degree angle, θ , laterally across the top of the curb and downward toward the bottom of the curb/deck forming three failure plannes. The two failure surface extending outward from the baseplate are denoted in Figure 15 as Failure Plane A. The shear planes between the two anchors under the baseplate will overlap and, for simplitiy, a rectangular shear plane is approximated as a rectangular surface starting at the line between the two bolts at the surface and extending at 45 degrees downward and toward the back of the curb/deck surface. This shear plane is denoted in Figure 15 as Failure Plane B. Plane A in is shown as a trapazoid in Figure 15, since the failure plane reached the “cold joint” between the curb and deck in this example. However, if the curb were deep enough the failure plane would eventually reach the back face of the curb and form a triangular shape (refer to edge d_2 in the bottom-left image in Figure 15).

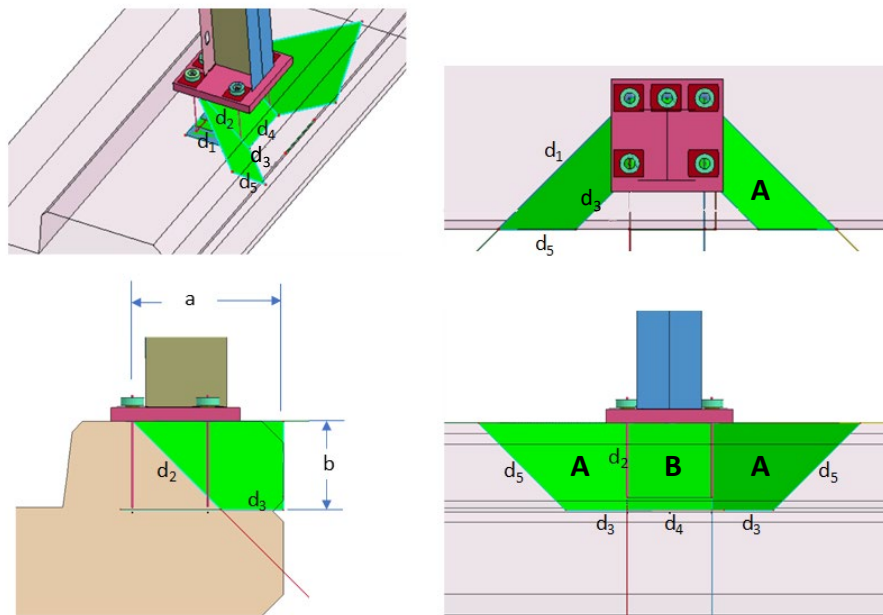


Figure 15. Approximated failure planes for push-out shear failure in concrete.

To compute the shear areas for Planes A and B, the only information required is the horizontal distance, a , from the front anchor bolts to the backedge of the curb, the vertical distance, b , from the top of the curb to either the cold joint or the bottom of the deck (which ever comes first), and the longitudinal distance, d_4 , between anchor bolts.

The push-out block shear resistance of the concrete due to shear on the anchor bolts is computed as:

$$P_{P5} = 2\sqrt{f_c'} * (2A + B)$$

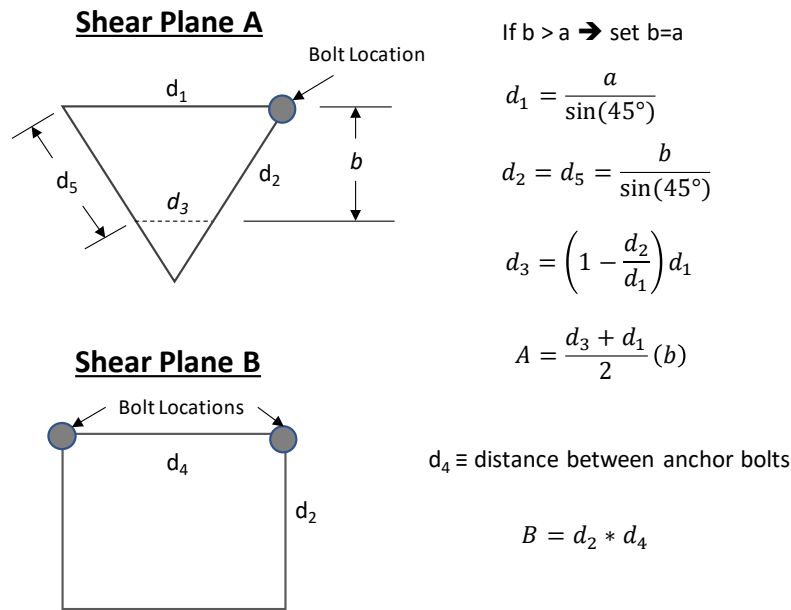


Figure 16. Calculation for Shear Planes A and B for Push-Out Shear Failure.

Punching Shear Failure Calculations

The punching shear is calculated by first calculating the nominal shear resistance provided by tensile stresses in the concrete in ksi (v_c).

$$v_c = \left(0.0633 + \frac{0.1265}{\beta_c}\right) \sqrt{f_c'}$$

Where:

$$\beta_c = W_b/d_b$$

W_b = Width of baseplate (in.)

d_b = Distance from the outer edge of the baseplate to the innermost row of bolts (in.)

f_c' = 28-day compressive strength of concrete.

Next, the nominal shear resistance of the section being considered in kips (V_n) is calculated.

$$V_n = v_c \left[W_b + h + 2 \left(E + \frac{B}{2} + \frac{h}{2} \right) \right] h$$

Where:

h = Depth of slab (in.)

E = Distance from edge of slab to centroid of compressive stress resultant in post (in.)

B = Distance between centroids of tensile and compressive stress resultants in post (in.)

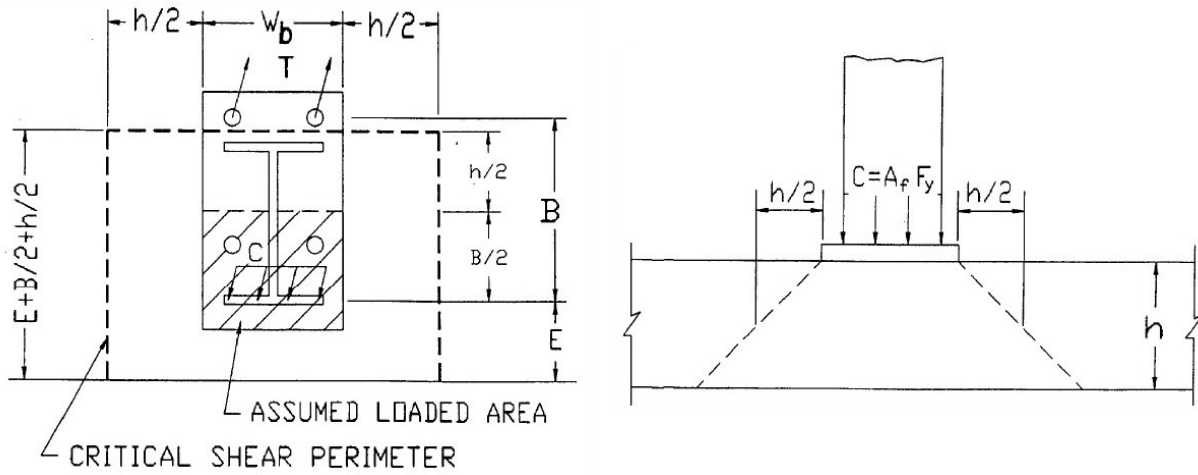


Figure 17. Punching shear failure mode (Figure A13.4.3.2-1 in 2012 LRFD)

The factored shear resistance in kips (V_r) is then calculated as:

$$V_r = \phi V_n$$

Where:

$$\phi = \text{Resistance factor} = 1.0$$

The effective moment resistance, M_{PC} , at the base of the post due to punching shear of the concrete deck, as illustrated in Figure 18, is calculated as:

$$M_{PC} = V_r * B$$

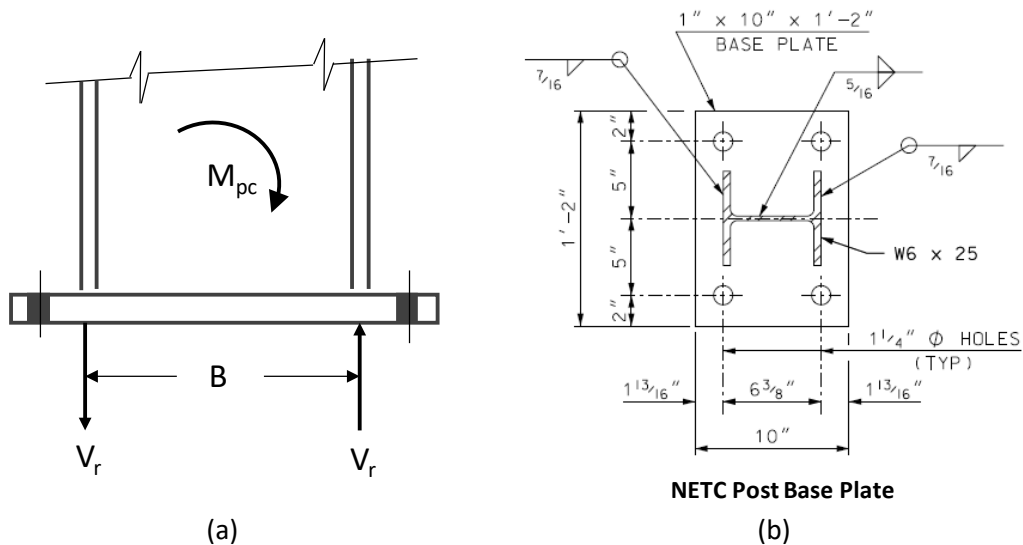


Figure 18. (a) Assumed load/reaction points for the punching shear resistance calculations and (b) dimensions of the NETC baseplate.

The effective strength of the post relative to the punching resistance of the concrete deck is then:

$$P_{P6} = \frac{M_{PC}}{h_p}$$

3.4.2.3 Effective Strength of Bridge Railing for MASH Conditions

The critical resistive force, R , of the bridge railing system for *MASH* design loads is computed from the following equation. The value of R should be greater than or equal to the *MASH* design load applied at H_e as provided in Table 9.

$$R = \frac{R' * Y}{H_e} \geq \text{Design Load}$$

A summary of rail strength calculations based on each State's design details for the 2-bar, 3-bar, and 4-bar NETC designs are shown in Tables 11 - Table 14. The strength calculations for the 2-bar designs were based on *MASH* TL3 loading conditions, as shown in Table 11. In all cases, the post strength was governed by the pry-out resistance of the concrete due to tensile load on the anchor bolts. The calculated strength for *MASH* TL3 conditions was 109 kips, which was well above the minimum criterion of 71 kips.

The strength calculations for the 3-bar designs were based on *MASH* TL4 loading conditions, as shown in Table 12. Only New Hampshire and Maine standards include drawing specifications for the NETC 3-bar design. In both cases, the calculated strengths met *MASH* TL4 criterion of 80 kips. The critical post strength for both designs was governed by concrete pry-out resistance due to anchor bolt tensile force, followed by plastic strength of the post. The primary differences in these two systems were, for New Hampshire and Maine, respectively, system height (44" vs. 42"), curb height (7" vs. 9"), and curb projection (integral vs. alternate). The MaineDOT drawing standards specify that the alternate curb projection detail is intended for use with granite bridge curb. If the MaineDOT design included an integral curb projection, the resulting strength of the system would increase approximately 9 percent (i.e., 83 kips to 90 kips).

The strength calculations for the sidewalk-mounted 4-bar bridge railing were based on *MASH* TL4 loading conditions, as shown in Table 13. New Hampshire, Maine and Rhode Island include this system in their standards. The Maine and Rhode Island designs just met the *MASH* TL4 criterion of 80 kips, while the baseline NETC and Hew Hampshire designs did not meet TL4 criteria. The critical post strength for the New Hampshire design was governed by concrete pry-out resistance, followed closely by the plastic strength of the post. For the Maine and Rhode Island designs, the critical post strength was governed by the plastic strength of the post, followed closely by anchor pryout strength. The primary difference in these designs is that New Hampshire specifies 4000 psi concrete, while Maine and Rhode Island specify 5000 psi concrete. For the 4-bar design to meet *MASH* TL4 conditions, the minimum strength for the post would need to be 40 kips. This could be achieved by using a W8x24 post, a minimum concrete strength of 5000 psi, and an embedment of 10.2 inches for the anchor plate (e.g., \approx 2 inches deeper than current designs).

The strength calculations for the curb-mounted 4-bar bridge railing were based on *MASH* TL4 loading conditions, as shown in Table 14. Only Maine and Vermont include this system in their standards. In both cases the strength calculations meet *MASH* TL4 criterion of 80 kips, with system strengths of 96 kips. The critical post strength for both designs was governed by concrete pry-out resistance. The primary differences in these designs are, for Maine and Vermont, respectively, concrete strength (minimum 5000 psi vs. 4000 psi) and curb projection (0

inches vs. 5 inches). The curb projection in the VTrans design counters the lower concrete strength, resulting in essentially equivalent pry-out strength as the MaineDOT design.

It is also worth noting that these calculations were based on a design load height, H_e , of 30 inches according to Table 9. In the 4-bar curb-mounted cases, the rail height is 54 and 55 inches for Maine and Vermont designs, respectively, which would classify the system as “tall” in Table 8. Table 8 suggests a design load height of 45.5 inches for tall bridge railing, in which case both curb-mounted 4-bar designs would fail *MASH* strength requirements, with a calculated strength of approximately 91 kips vs. 93 kips design strength.

Table 11. Strength calculations for 2-Bar bridge rail based on *MASH* TL3 load conditions.

Description		Variable	Units	2-Bar Bridge Rail				
				NETC	NHDOT and Vtrans	Maine DOT	RIDOT	
Materials	Rail	Material Type		A500 GrB	A500 Gr B/C	A500 Gr B/C	A500 Gr B/C	
		Yield Strength	F_{ytube} ksi	46	50	50	50	
	Post	Material Type		A572 Gr50	A572 Gr50	M270 Gr 50	A572 Gr50	
		Yield Strength	F_{ypost} ksi	50	50	50	50	
	Base Plate	Material Type		M270 Gr36	A572 Gr50	M270 Gr 50	M270 Gr36	
		Yield Strength	$F_{ybaseplate}$ ksi	36	50	50	50	
Anchor Bolts	Material Type		A449	A449	M314 Gr105	A449		
Concrete	Tensile Strength	F_{ybolt} ksi	120	120	125	120		
	Unconfined Compressive Strength	F_c psi	4000.00	4000.00	5000.00	5000.00		
Components	Rail 1 (top)	Shape		4x8x5/16	4x8x5/16	4x8x5/16	4x8x5/16	
		Height	in	30.00	30.00	30.00	30.00	
		Plastic Section Modulus	Z_1 in ³	10.50	10.50	10.50	10.50	
		Plastic Moment	M_{p1} kip-ft	40.25	43.75	43.75	43.75	
	Rail 2 (bottom)	Shape		4x4x1/4	4x4x1/4	4x4x1/4	4x4x1/4	
		Height	in	18.00	18.00	18.00	18.00	
		Plastic Section Modulus	Z_2 in ³	4.97	4.97	4.97	4.97	
		Plastic Moment	M_{p2} kip-ft	19.05	20.71	20.71	20.71	
	Post	Shape		W6x25	W6x25	W6x25	W6x25	
		Plastic Section Modulus	Z_{post} in ³	18.90	18.90	18.90	18.90	
		Plastic Moment	M_{ppost} kip-ft	78.75	78.75	78.75	78.75	
		Post Spacing	ft	8	8	8	8	
	Base Plate	Thickness of Baseplate	in	1.00	1.00	1.00	1.00	
	Weld	Weld Size	t_{weld} in	0.44	0.44	0.44	0.44	
		Number of Weld Sides per Flange	N_w	2.00	2.00	2.00	2.00	
		Weld Strength	F_{7exx} ksi	70.00	70.00	70.00	70.00	
		Diameter of Bolts	d_{bolts} in	1.00	1.00	1.00	1.00	
	Anchor Bolts	Number of Bolts	N_{bolts}	4	4	4	4	
Center of Bolts to Back Edge of Baseplate		W_{bolts} in	4.69	5.00	5.00	5.00		
Curb		Curb Height	in	9.00	7.00	9.00	7.00	
Design Parameters	Test Level		TL3	TL3	TL3	TL3		
	Transverse Design Force	F_T kips	71.00	71.00	71.00	71.00		
	Longitudinal Design Force	F_L kips	18.00	18.00	18.00	18.00		
	Vertical Design Force	F_v kips	4.50	4.50	4.50	4.50		
	Length of Equivalent Distributed Transverse Load	L_i ft	4.00	4.00	4.00	4.00		
	Height of Equivalent Distributed Transverse Load	H_e in	19.00	19.00	19.00	19.00		
	Vehicle Type		2270P	2270P	2270P	2270P		
Vehicle	Weight	W kips	5.00	5.00	5.00	5.00		
	Wheel Base	B ft	6.50	6.50	6.50	6.50		
	Center of Gravity	G in	27.00	27.00	27.00	27.00		
	Component Strength	Summary of Strength by Component	Critical Plastic Moment of Rail	M_p kip-ft	59.30	64.46	64.46	64.46
Height of Resilant Force			Y_{bar} in	26.14	26.14	26.14	26.14	
Summary				Summary	Summary	Summary		
Post Strength Based on Plastic Strength of Post			P_{p1} kips	58.53	52.08	58.53	52.08	
Post Strength Based on Anchor Bolt Tension			P_{p2} kips	63.32	60.06	70.31	60.06	
Post Strength based on Weld Strength			P_{p3} kips	65.22	58.20	65.22	58.03	
Post Strength based on Pryout Shear Cone			P_{p4} kips	47.68	46.21	44.36	38.18	
Post Strength based on Pushout Shear			P_{p5} kips	46.69	50.09	52.20	56.00	
Post Strength based on Punching Shear			P_{p6} kips	131.52	117.87	137.04	131.92	
Critical Plastic Strength of Post			P_p kips	46.69	46.21	44.36	38.18	
Bridge Railing Strength	Assumed Multi-Span Failure Modes	Rail Strength based on failure of 1 rail span	R'_{1-span} kips	79.07	85.94	85.94	85.94	
		Rail Strength based on failure of 2 rail spans	R'_{2-span} kips	87.25	89.65	87.53	80.47	
		Rail Strength based on failure of 3 rail spans	R'_{3-span} kips	89.48	90.65	87.96	78.98	
		Rail Strength based on failure of 4 rail spans	R'_{4-span} kips	115.42	115.77	111.82	98.64	
		Rail Strength based on failure of 5 rail spans	R'_{5-span} kips	130.44	130.31	125.64	110.03	
		Rail Strength based on failure of 6 rail spans	R'_{6-span} kips	156.47	155.87	150.08	130.74	
	Critical Bridge Rail Strength at H_e	R' kips	79.07	85.94	85.94	78.98		
	Critical Bridge Rail Strength at H_e	R kips	108.80	118.26	118.26	108.68		
	Strength Assessment for MASH TL-3				OK	OK	OK	OK

Critical strength values highlighted in red font

Table 12. Strength calculations for 3-bar bridge rail based on MASH TL4 load conditions.

Description		Variable	Units	3-Bar Bridge Rail			
				NHDOT 3 Bar Curb Mounted	MaineDOT 3 Bar Curb Mounted		
Materials	Rail	Material Type		A500 Gr B/C	A500 Gr B/C		
		Yield Strength	F_{yube}	ksi	46	46	
	Post	Material Type		A572 Gr50	M270 Gr 50		
		Yield Strength	F_{ypost}	ksi	50	50	
	Base Plate	Material Type		A572 Gr50	M270 Gr 50		
		Yield Strength	$F_{ybaseplate}$	ksi	50	50	
Anchor Bolts	Material Type		A449	M314 Gr105			
Concrete	Tensile Strength	F_{ybolt}	ksi	120	125		
	Unconfined Compressive Strength	f'_c	psi	4000.00	5000.00		
Component Parameters	Rail 1 (top)	Shape		4x4x1/4	4x4x1/4		
		Height		in	42.00	40.00	
		Plastic Section Modulus	Z_1	in ³	4.97	4.97	
		Plastic Moment	M_{p1}	kip-ft	19.05	19.05	
	Rail 2	Shape		4x8x5/16	4x8x5/16		
		Height		in	30.00	28.00	
		Plastic Section Modulus	Z_2	in ³	10.50	10.50	
		Plastic Moment	M_{p2}	kip-ft	40.25	40.25	
	Rail 3 (bottom)	Shape		4x4x1/4	4x4x1/4		
		Height		in	18.00	16.50	
		Plastic Section Modulus	Z_3	in ³	4.97	4.97	
		Plastic Moment	M_{p3}	kip-ft	19.05	19.05	
	Post	Shape		W6x25	W6x25		
		Plastic Section Modulus	Z_{post}	in ³	18.90	18.90	
		Plastic Moment	M_{ppost}	kip-ft	78.75	78.75	
		Post Spacing		ft	8	8	
	Base Plate	Thickness of Baseplate	t_{BP}	in	1.00	1.00	
	Weld	Weld Size	t_{weld}	in	0.44	0.44	
		Number of Weld Sides per Flange	N_w		2.00	2.00	
		Weld Strength	F_{wexx}	ksi	70.00	70.00	
Anchor Bolts	Diameter of Bolts	d_{bolts}	in	1.00	1.00		
	Number of Bolts	N_{bolts}		4	4		
	Center of Bolts to Back Edge of Baseplate	w_{bolts}	in	5.00	5.00		
Curb	Curb Height		in	7.00	9.00		
Design Parameters	Test Level			TL4	TL4		
	Transverse Design Force	F_T	kips	80.00	80.00		
	Longitudinal Design Force	F_L	kips	27.00	27.00		
	Vertical Design Force	F_v	kips	22.00	22.00		
	Length of Equivalent Distributed Transverse Load	L_L	ft	5.00	5.00		
	Height of Equivalent Distributed Transverse Load	H_e	in	30.00	30.00		
Vehicle	Vehicle Type			SUT	SUT		
	Weight	W	kips	22.00	22.00		
	Wheel Base	B	ft	7.50	7.50		
	Center of Gravity	G	in	63.00	63.00		
Component Strength				Plastic Strength of Rail	Plastic Strength of Rail		
		Critical Plastic Moment of Rail	M_p	kip-ft	78.35	78.35	
		Height of Resultant Force	Y_{bar}	in	30.00	28.12	
	Summary of Strength by Component		Post Strength Based on Plastic Strength of Post	P_{p1}	kips	42.95	52.15
			Post Strength Based on Anchor Bolt Tension	P_{p2}	kips	49.54	62.64
			Post Strength based on Weld Strength	P_{p3}	kips	47.86	58.11
			Post Strength based on Pryout Shear Cone	P_{p4}	kips	38.46	39.77
			Post Strength based on Pushout Shear	P_{p5}	kips	50.09	52.20
		Post Strength based on Punching Shear	P_{p6}	kips	98.11	122.87	
	Critical Plastic Strength of Post	P_p	kips	38.46	39.77		
Bridge Railing Strength	Assumed Multi-Span Failure Modes	Rail Strength based on failure of 1 rail span	R'_{1-span}	kips	113.97	113.97	
		Rail Strength based on failure of 2 rail spans	R'_{2-span}	kips	92.02	93.57	
		Rail Strength based on failure of 3 rail spans	R'_{3-span}	kips	86.40	88.35	
		Rail Strength based on failure of 4 rail spans	R'_{4-span}	kips	104.70	107.54	
		Rail Strength based on failure of 5 rail spans	R'_{5-span}	kips	115.18	118.54	
		Rail Strength based on failure of 6 rail spans	R'_{6-span}	kips	135.51	139.65	
		Critical Bridge Rail Strength at y_{bar}	R'	kips	86.40	88.35	
	Critical Bridge Rail Strength at H_e	R	kips	86.40	82.82		
	Strength Assessment for MASH TL-4			OK	OK		

Table 13. Strength calculations for sidewalk-mounted 4-bar bridge rail based on MASH TL4 load conditions

				4-Bar Bridge Rail				
				Sidewalk-Mounted				
Description		Variable	Units	NETC	NHDOT	MaineDOT	RIDOT	
Materials	Rail	Material Type		A500 GrB	A500 Gr B/C	A500 Gr B/C	A500 Gr B/C	
		Yield Strength	F_{ytube}	ksi	46	50	50	50
	Post	Material Type		A709 Gr50	A572 Gr50	M270 Gr 50	M270 Gr 50	
		Yield Strength	F_{ypost}	ksi	50	50	50	50
	Base Plate	Material Type		A709 Gr36	A572 Gr50	M270 Gr 50	M270 Gr 50	
		Yield Strength	$F_{ybaseplate}$	ksi	36	50	50	50
Anchor Bolts	Material Type		A449	A449	M314 Gr105	A449		
	Tensile Strength	F_{ybolt}	ksi	120	120	125	120	
Concrete	UCS	f'_c	psi	4000.00	4000.00	5000.00	5000.00	
Component Parameters	Rail 1 (top)	Shape		4x4x1/4	4x4x1/4	4x4x1/4	4x4x1/4	
		Height		39.50	40.00	40.00	40.00	
		Plastic Section Modulus	Z_1	in ³	4.97	4.97	4.97	4.97
		Plastic Moment	M_{p1}	kip-ft	19.05	20.71	20.71	20.71
	Rail 2	Shape		4x8x5/16	4x8x5/16	4x8x5/16	4x8x5/16	
		Height		27.50	28.50	28.50	28.50	
		Plastic Section Modulus	Z_2	in ³	10.50	10.50	10.50	10.50
		Plastic Moment	M_{p2}	kip-ft	40.25	43.75	43.75	43.75
	Rail 3	Shape		4x4x1/4	4x4x1/4	4x4x1/4	4x4x1/4	
		Height		16.50	17.00	16.50	17.00	
		Plastic Section Modulus	Z_3	in ³	4.97	4.97	4.97	4.97
		Plastic Moment	M_{p3}	kip-ft	19.05	20.71	20.71	20.71
	Rail 4 (bottom)	Shape		4x4x1/4	4x4x1/4	4x4x1/4	4x4x1/4	
		Height		7.00	7.50	7.00	7.50	
		Plastic Section Modulus	Z_4	in ³	4.97	4.97	4.97	4.97
		Plastic Moment	M_{p4}	kip-ft	19.05	20.71	20.71	20.71
	Post	Shape		W6x25	W6x25	W6x25	W6x25	
		Plastic Section Modulus	Z_{post}	in ³	18.90	18.90	18.90	18.90
		Plastic Moment	M_{ppost}	kip-ft	78.75	78.75	78.75	78.75
		Post Spacing		ft	8	8	8	8
	Base Plate	Thickness of Baseplate	t_{bp}	in	1.00	1.00	1.00	1.00
		Weld Size	t_{weld}	in	0.44	0.44	0.44	0.44
	Weld	Number of Weld Sides per Flange	N_w		2.00	2.00	2.00	2.00
		Weld Strength	F_{Tmax}	ksi	70.00	70.00	70.00	70.00
Anchor Bolts	Diameter of Bolts	d_{bolts}	in	1.00	1.00	1.00	1.00	
	Number of Bolts	N_{bolts}		4.00	4.00	4.00	5.00	
	Center of Bolts to Back Edge of Baseplate	W_{bolts}	in	5.00	5.00	5.00	6.00	
Curb	Curb Height		in	0.00	0.00	0.00	0.00	
Design Parameters	Test Level			TL4	TL4	TL4	TL4	
	Transverse Design Force	F_T	kips	80.00	80.00	80.00	80.00	
	Longitudinal Design Force	F_L	kips	27.00	27.00	27.00	27.00	
	Vertical Design Force	F_V	kips	22.00	22.00	22.00	22.00	
	Length of Equivalent Distributed Transverse Load	L_L	ft	5.00	5.00	5.00	5.00	
	Height of Equivalent Distributed Transverse Load	H_e	in	30.00	30.00	30.00	30.00	
	Vehicle Type			SUT	SUT	SUT	SUT	
Vehicle	Weight	W	kips	22.00	22.00	22.00	22.00	
	Wheel Base	B	ft	7.50	7.50	7.50	7.50	
	Center of Gravity	G	in	63.00	63.00	63.00	63.00	
	Height of Reslant Force	Y_{bar}	in	23.69	24.39	23.99	24.39	
Component Strength	Critical Plastic Moment of Rail			97.41	105.88	105.88	105.88	
	Height of Reslant Force			23.69	24.39	23.99	24.39	
	Summary of Strength by Component				Summary	Summary	Summary	Summary
		Post Strength Based on Plastic Strength of Post	P_{p1}	kips	41.66	40.40	41.10	40.40
		Post Strength Based on Anchor Bolt Tension	P_{p2}	kips	48.04	46.59	49.38	69.88
		Post Strength based on Weld Strength	P_{p3}	kips	46.42	45.01	45.76	44.98
		Post Strength based on Pryout Shear Cone	P_{p4}	kips	37.35	36.28	41.24	40.55
		Post Strength based on Pushout Shear	P_{p5}	kips	42.93	50.09	52.20	56.00
Post Strength based on Punching Shear	P_{p6}	kips	79.96	92.51	97.94	156.96		
Critical Plastic Strength of Post			37.35	36.28	41.10	40.40		
Bridge Railing Strength	Assumed Multi-Span Failure Modes	Rail Strength based on failure of 1 rail span	R'_{1-Span}	kips	141.68	154.00	154.00	154.00
		Rail Strength based on failure of 2 rail spans	R'_{2-Span}	kips	101.99	105.74	111.46	110.62
		Rail Strength based on failure of 3 rail spans	R'_{3-Span}	kips	91.84	93.39	100.57	99.52
		Rail Strength based on failure of 4 rail spans	R'_{4-Span}	kips	107.45	107.42	117.89	116.35
		Rail Strength based on failure of 5 rail spans	R'_{5-Span}	kips	116.40	115.46	127.81	126.00
		Rail Strength based on failure of 6 rail spans	R'_{6-Span}	kips	135.34	133.43	148.70	146.47
	Critical Bridge Rail Strength at Y_{bar} :		R'	kips	91.84	93.39	100.57	99.52
Critical Bridge Rail Strength at H_e :		R	kips	72.51	75.93	80.43	80.92	
Strength Assessment for MASH TL-4				FAIL	FAIL	OK	OK	

Critical strength values highlighted in red font

Table 14. Strength calculations for curb-mounted 4-bar bridge rail based on MASH TL4 load conditions

Description		Variable	Units	4-Bar Bridge Rail		
				Curb-Mounted		
				MaineDOT	Vtrans	
Materials	Rail	Material Type		A500 Gr B/C	A500 Gr B/C	
		Yield Strength	F_{ytube}	ksi	50	50
	Post	Material Type		M270 Gr 50	A572 Gr50	
		Yield Strength	F_{ypost}	ksi	50	50
	Base Plate	Material Type		M270 Gr 50	A572 Gr50	
		Yield Strength	$F_{ybaseplate}$	ksi	50	50
Anchor Bolts	Material Type		M314 Gr105	A449		
Concrete	Tensile Strength	F_{ybolt}	ksi	125	120	
	UCS	f'_c	psi	5000.00	4000.00	
Component Parameters	Rail 1 (top)	Shape		4x4x1/4	4x4x1/4	
		Height		in	52.00	53.00
		Plastic Section Modulus	Z_1	in ³	4.97	4.97
		Plastic Moment	M_{p1}	kip-ft	20.71	20.71
	Rail 2	Shape		4x4x1/4	4x4x1/4	
		Height		in	41.00	42.00
		Plastic Section Modulus	Z_2	in ³	4.97	4.97
		Plastic Moment	M_{p2}	kip-ft	20.71	20.71
	Rail 3	Shape		4x8x5/16	4x8x5/16	
		Height		in	29.00	29.00
		Plastic Section Modulus	Z_3	in ³	10.50	10.50
		Plastic Moment	M_{p3}	kip-ft	43.75	43.75
	Rail 4 (bottom)	Shape		4x4x1/4	4x4x1/4	
		Height		in	17.50	17.00
		Plastic Section Modulus	Z_4	in ³	4.97	4.97
		Plastic Moment	M_{p4}	kip-ft	20.71	20.71
	Post	Shape		W6x25	W6x25	
		Plastic Section Modulus	Z_{post}	in ³	18.90	18.90
		Plastic Moment	M_{ppost}	kip-ft	78.75	78.75
		Post Spacing		ft	8	8
	Base Plate	Thickness of Baseplate	t_{BP}	in	1.00	1.00
	Weld	Weld Size	t_{weld}	in	0.44	0.44
		Number of Weld Sides per Flange	N_w		2.00	2.00
		Weld Strength	F_{wexx}	ksi	70.00	70.00
Anchor Bolts	Diameter of Bolts	d_{bolts}	in	1.00	1.00	
	Number of Bolts	N_{bolts}		4.00	4.00	
	Center of Bolts to Back Edge of Baseplate	W_{bolts}	in	5.00	5.00	
Curb	Curb Height		in	9.00	9.00	
Design Parameters	Test Level			TL4	TL4	
	Transverse Design Force	F_T	kips	80.00	80.00	
	Longitudinal Design Force	F_L	kips	27.00	27.00	
	Vertical Design Force	F_V	kips	22.00	22.00	
	Length of Equivalent Distributed Transverse Load	L_L	ft	5.00	5.00	
	Height of Equivalent Distributed Transverse Load	H_e	in	30.00	30.00	
Vehicle	Vehicle Type			SUT	SUT	
	Weight	W	kips	22.00	22.00	
	Wheel Base	B	ft	7.50	7.50	
	Center of Gravity	G	in	63.00	63.00	
Component Strength	Summary of Strength by Component	Critical Plastic Moment of Rail	M_p	kip-ft	105.88	105.88
		Height of Resilant Force	Y_{bar}	in	33.60	33.89
					Summary	Summary
		Post Strength Based on Plastic Strength of Post	P_{p1}	kips	40.05	39.56
		Post Strength Based on Anchor Bolt Tension	P_{p2}	kips	48.11	45.62
		Post Strength based on Weld Strength	P_{p3}	kips	44.62	44.21
		Post Strength based on Pryout Shear Cone	P_{p4}	kips	30.94	30.90
Post Strength based on Pushout Shear	P_{p5}	kips	59.40	50.09		
Post Strength based on Punching Shear	P_{p6}	kips	112.81	90.66		
		Critical Plastic Strength of Post	P_p	kips	30.94	30.90
Bridge Railing Strength	Assumed Multi-Span Failure Modes	Rail Strength based on failure of 1 rail span	R'_{1-Span}	kips	154.00	154.00
		Rail Strength based on failure of 2 rail spans	R'_{2-Span}	kips	99.41	99.36
		Rail Strength based on failure of 3 rail spans	R'_{3-Span}	kips	85.45	85.38
		Rail Strength based on failure of 4 rail spans	R'_{4-Span}	kips	95.84	95.74
		Rail Strength based on failure of 5 rail spans	R'_{5-Span}	kips	101.80	101.68
		Rail Strength based on failure of 6 rail spans	R'_{6-Span}	kips	116.55	116.40
		Critical Bridge Rail Strength at y_{bar} :	R'	kips	85.45	85.38
		Critical Bridge Rail Strength at H_e :	R	kips	95.69	96.45
	Strength Assessment for MASH TL-4			OK	OK	

Critical strength values highlighted in red font

3.4.3 Summary of Strength Assessments for Baseline NETC Designs

Table 15 shows a summary of the overall assessment results for the baseline NETC systems (i.e., lowest strength design). Based on the assessment, it was determined that both the NETC 2-bar and the Maine 3-bar systems would likely meet *MASH* TL3. The NETC 3-bar system will likely meet *MASH* TL4 requirements; however, only the Maine Design with the 9-inch curb meets the rail geometrics requirements. The sidewalk-mounted 4-bar system designs showed mixed results. All sidewalk-mounted 4-bar designs were considered marginal regarding rail-geometrics criteria; however, the Maine and Rhode Island designs (with 5,000 psi concrete) met strength requirements, while the New Hampshire design (with 4,000 psi concrete) did not. The curb-mounted 4-bar design was considered “marginal” based on potential for vehicle snagging on posts (e.g., the 4-inch setback distance is too low); however, the system was shown to have adequate strength, when considering a design load height of 30 inches. Note that previous study by TTI researchers [*Sheikh11*] indicated that a design load of 93 kips and load height of 45.5 inches should be used for tall systems, as indicated in Table 8, in which case the system would not meet strength requirements.

Table 15. Summary of *MASH* equivalency assessment for the NETC bridge rail designs.

	NETC 2-Bar (TL3)			NETC 3-Bar (TL4)			NETC 4-Bar (TL4)			Curb-Mounted 4-Bar (TL4)		
	Rail Height	Rail Geometrics	Strength	Rail Height	Rail Geometrics	Strength	Rail Height	Rail Geometrics	Strength	Rail Height	Rail Geometrics	Strength
Required	29	(see Table 5)	71 k	36 in	(see Table 5)	80 k	36 in	(see Table 5)	80 k	36 in	(see Table 5)	80 k
Actual	34		109 k	42 in		83-86 k	42 in		76-81 k*	54 in		96 k*
Assessment	S	S	S ⁽¹⁾	S	S ⁽²⁾	S	S	M	NS / S	S	M	S

NS - Not Satisfactory

M - Marginal

S - Satisfactory

S⁽¹⁾ - Satisfactory Rating for TL-3 Only

S⁽²⁾ - Satisfactory when 9" curb is used

* - Differs from 20-07(395) report

3.5 Critical Review of Current Standard Details for NETC Style Bridge Rails

The following sections provide a comparison of system details based on each State’s specifications, along with the research team’s recommendations. Overall, the systems are quite similar. When selecting recommended values for further evaluation using FEA crash simulation of *MASH* testing, the least conservative value that has an acceptable crash testing record was selected. If the crash simulations show that the least conservative designs meet *MASH* criteria, then the more conservative designs could be assumed to meet those criteria as well.

3.5.1 Rail Bars

Most of the features of the bridge rail bars and positions are consistent between designs as can be seen from Table 16 through Table 19, for the 2-bar, 3-bar, 4-bar and 4-bar curb mounted designs, respectively. Although A500 is commonly specified as dual grade B/C and has minimum yield strength of 50 ksi, the material specification for the rail bars in all designs is ASTM A500 Gr. B which has a minimum yield strength of 46 ksi. The shape and size of all small rail bars is HSS 4"x4"x1/4" while it is HSS 8"x4"x5/16" for all large bars.

3.5.1.1 2-Bar System

There are five NETC Style 2-bar bridge rail designs in use in New England states. The five designs come from the NETC, MaineDOT, NHDOT, RIDOT and VTrans. The size of all bars and their order is the same between designs. The top rail height and bottom rail height (from the vehicle running surface) is the same between designs at 2'-10" and 18" respectively. The only difference between designs is the curb height; the MaineDOT and NETC designs use a curb height of 9" while a curb height of 7" is used for all other designs, as shown in Table 16.

3.5.1.2 3-Bar System

There are two NETC Style 3-bar bridge rail designs in use in New England states. The two designs come from MaineDOT and NHDOT. The size of all bars and their order is the same for both designs. The height of each rail bar and the curb height vary slightly between the two designs as can be seen in Table 17.

3.5.1.3 4-Bar System

There are four NETC Style 4-bar sidewalk mounted bridge rail designs in use in New England states. The four designs come from the NETC, MaineDOT, NHDOT and RIDOT. As with the 3-bar system, the size of all bars and their order is the same for each design, while the height of each rail bar and the curb height vary slightly between designs as shown in Table 18.

3.5.1.4 4-Bar Curb Mounted System

There are two NETC Style 4-bar curb mounted bridge rail designs in use in New England states. The two designs come from MaineDOT and VTrans. The size of all bars, their order and the large rail height is the same between both designs. The top rail height varies slightly between the designs as can be seen in Table 19. While the drawings for both 4-bar curb mounted designs call for 9-inch tall curbs, a curb height of 7 inches is recommended for the crash evaluations to be consistent with the other systems (2-bar and 3-bar curb mounted).

Table 16. Comparison of bridge rail features for NETC 2-bar bridge rails.

Design	Material	Size	Order of Bars (from top)	Top Rail Height	Bottom Rail Height	Curb Height
Recommendations	ASTM A500 Grade B (46 ksi)	HSS 4" x 4" x $\frac{1}{4}$ " HSS 8" x 4" x $\frac{5}{16}$ "	8x4, 4x4	2'-10"	18"	7"
NETC	*	*	*	*	*	9"
MaineDOT	*	*	*	*	*	9"
NHDOT	*	*	*	*	*	*
RIDOT	*	*	*	*	*	*
VTrans	*	*	*	*	*	*

* Same as recommended
N.S.: Not Specified

Table 17. Comparison of bridge rail features for NETC 3-bar bridge rails.

Design	Material	Size	Order of Bars (from top)	Top Rail Height (to top)	Middle Rail Height (to center)	Bottom Rail Height (to center)	Curb Height
Recommendations	ASTM A500 Grade B (46 ksi)	HSS 4" x 4" x $\frac{1}{4}$ " HSS 8" x 4" x $\frac{5}{16}$ "	4x4, 8x4, 4x4	3'-8"	30"	18"	7"
MaineDOT	*	*	*	3'-6"	28"	16 $\frac{1}{2}$ "	9"
NHDOT	*	*	*	*	*	*	*

* Same as recommended
N.S.: Not Specified

Table 18. Comparison of bridge rail features for NETC 4-bar sidewalk mounted bridge rails.

Design	Material	Size	Order of Bars (from top)	Top Rail Height (to top)	Large Rail Height (to center)	Mid-Btm Rail Height (to center)	Bottom Rail Height (to center)
Recommendations	ASTM A500 Grade B (46 ksi)	HSS 4" x 4" x $\frac{1}{4}$ " HSS 8" x 4" x $\frac{5}{16}$ "	4x4, 8x4, 4x4, 4x4	3'-6"	28"	16 $\frac{1}{2}$ "	7"
NETC	*	*	*	*	*	*	*
MaineDOT	*	*	*	*	*	*	*
NHDOT	*	*	*	*	28 $\frac{1}{2}$ "	17"	7 $\frac{1}{2}$ "
RIDOT	*	*	*	*	28 $\frac{1}{2}$ "	17"	7 $\frac{1}{2}$ "

* Same as recommended
N.S.: Not Specified

Table 19. Comparison of bridge rail features for NETC 4-bar curb mounted bridge rails.

Design	Material	Size	Order of Bars (from top)	Top Rail Height (to top)	Top-Mid Height (to center)	Large Rail Height (to center)	Bottom Rail Height (to center)	Curb Height
Recommendations	ASTM A500 Grade B (46 ksi)	HSS 4" x 4" x $\frac{1}{4}$ " HSS 8" x 4" x $\frac{5}{16}$ "	4x4, 4x4, 8x4, 4x4	Curb: 3'-9" Pavement: 4'-6"	Curb: 32" Pavement: 41"	Curb: 20" Pavement: 29"	Curb: 8" Pavement: 17"	7"
MaineDOT	*	*	*	*	*	*	Curb: 8 $\frac{1}{2}$ " Pavement: 17 $\frac{1}{2}$ "	9"
VTrans	*	*	*	Curb: 3'-8" Pavement: 4'-7"	Curb: 33" Pavement: 42"	*	*	9"

* Same as recommended
N.S.: Not Specified

3.5.2 Bridge Rail Post

Three different material types are specified in the designs for posts. All specified materials have the same yield strength of 50 ksi. NETC specifies ASTM A709 Gr. 50, MaineDOT specifies AASHTO M270 Gr. 50 while NHDOT, VTrans and RIDOT spec ASTM 572 Gr. 50. The material specifications for all post materials are shown in Table 20. The specific detail for the 2-bar, 3-bar and 4-bar designs are shown in Table 21 through Table 24, respectively. All designs specify W6x25 for the post shape, 8'-0" maximum spacing, $\frac{7}{16}$ -inch flange fillet welds, and $\frac{5}{16}$ -inch web fillet welds. When evaluating the designs, the posts will be aligned normal to grade, thus "normal to grade" will be the recommended practice for vertical alignment. However, it is understood that for some applications (e.g., mountainous regions) there may be limits to when posts should be set vertically, rather than normal to the grade. As in the NHDOT and RIDOT designs, a minimum of 3 posts per rail bar length is recommended. The MaineDOT and VTrans designs both specify that a minimum of two, but preferably four posts, be used per rail bar. The minimum offset to an expansion joint varies slightly between designs but these values are similar.

Table 20. Material strength properties for post materials

Material	Yield (ksi)	Ultimate (ksi)	Elongation at Break
ASTM A709 Gr. 50	50	65.4	18%
AASHTO M270 Gr. 50	50	65.4	18%
ASTM 572 Gr. 50	50	65.3	18%

Table 21. Comparison of bridge rail post features for NETC2-bar bridge rails.

Design	Material	Size	Vert Alignment	Max Spacing	# of Posts per Rail Bar	Min. Offset to Expansion Splice	Flange to Base Plate Weld	Web to Base Plate Weld
Recommendations	AASHTO M270 Grade 50	W6x25	Normal to Grade	8'-0"	3	2'-0"	$\frac{7}{16}$ " All Around Fillet Weld	$\frac{5}{16}$ " All Around Fillet Weld
NETC	N.S.	*	N.S.	*	N.S.	*	N.S.	N.S.
MaineDOT	*	*	*	*	Min. 2 - 4	*	*	*
NHDOT	ASTM 572 Grade 50	*	Normal to Grade except on 5% grade set vertical	*	*	1'-6" (\pm 3")	*	*
RIDOT	*	*	Normal to Grade except on 1.5% grade set vertical	*	*	2'-0" (\pm 3")	*	*
VTrans	ASTM 572 Grade 50	*	*	*	Min. 2 - 4	1'-6" (\pm 3")	*	*

* Same as recommended
N.S.: Not Specified

Table 22. Comparison of bridge rail post features for NETC 3-bar bridge rails.

Design	Material	Size	Vert Alignment	Max Spacing	# of Posts per Rail Bar	Min. Offset to Expansion Splice	Flange to Base Plate Weld	Web to Base Plate Weld
Recommendations	AASHTO M270 Grade 50	W6x25	Normal to Grade	8'-0"	3	2'-0"	$\frac{7}{16}$ " All Around Fillet Weld	$\frac{5}{16}$ " All Around Fillet Weld
MaineDOT	*	*	*	*	Min. 2 - 4	*	*	*
NHDOT	ASTM A572 Grade 50	*	* except on 5% grade set vertical	*	*	1'-6" (\pm 3")	*	*

* Same as recommended
N.S.: Not Specified

Table 23. Comparison of bridge rail post features for NETC 4-bar sidewalk mounted bridge rails.

Design	Material	Size	Vert Alignment	Max Spacing	# of Posts per Rail Bar	Min. Offset to Expansion Splice	Flange to Base Plate Weld	Web to Base Plate Weld
Recommendations	AASHTO M270 Grade 50	W6x25	Normal to Grade	8'-0"	3	2'-0"	$\frac{7}{16}$ " All Around Fillet Weld	$\frac{5}{16}$ " All Around Fillet Weld
NETC	ASTM A709 Grade 50	*	*	*	Min. 2	*	*	*
MaineDOT	*	*	*	*	Min. 2-4	*	*	*
NHDOT	ASTM A572 Grade 50	*	* except on 5% grade, set vertical	*	*	1'-6" (\pm 3")	*	*
RIDOT	ASTM A572 Grade 50	*	* except on 1.5% grade, set vertical	*	*	N.S.	*	*

* Same as recommended
N.S.: Not Specified

Table 24. Comparison of post features for NETC 4-bar curb mounted bridge rails.

Design	Material	Size	Vert Alignment	Max Spacing	# of Posts per Rail Bar	Min. Offset to Expansion Splice	Flange to Base Plate Weld	Web to Base Plate Weld
Recommendations	AASHTO M270 Grade 50	W6x25	Normal to Grade	8'-0"	3	2'-0"	$\frac{7}{16}$ " All Around Fillet Weld	$\frac{5}{16}$ " All Around Fillet Weld
MaineDOT	*	*	*	*	Min. 2-4	*	*	*
VTrans	ASTM A572 Grade 50	*	*	*	Min. 2-4	*	*	*

* Same as recommended
N.S.: Not Specified

3.5.3 Rail-to-Post Attachment

Two methods of rail-to-post attachment exist among the NETC style bridge rail designs, the welded stud design and the bolted connection. Based on discussions with personnel from the New England states it is believed that the most common (i.e. only) method used in the field is the bolted connection method. NHDOT and RIDOT provide details for using threaded studs welded to the bar. Based on feedback from the project technical advisory committee, the welded stud method will not be pursued in the crash evaluation study of this project. The bolt specifications vary between designs. Table 25 displays the minimum strength values for each bolt material specified, as well as the effective strength, calculated from the tensile stress area for each diameter bolt. There are differences between the designs for the size of the holes in both the rail member and the post; however, these differences are consistent for each state across all its designs. For the crash evaluations, the largest hole diameter (or slot) was selected. If the slotted design passes the evaluation, then it will be assumed that the tighter hole tolerances will also pass evaluation. Specific details for each design are shown in Table 26 through Table 29.

Table 25. Strength values for different bolts specifications for rail-to-post attachment.

Bolt Spec	Minimum Strength Requirement		Effective Strength for Ø	
	Tensile (ksi)	Yield (ksi)	Tensile (kips)	Yield (kips)
$\frac{3}{4}$ " Ø A325	120	92	40.080	30.728
$\frac{3}{4}$ " Ø A307 [†]	58	36	19.372	12.024
$\frac{5}{8}$ " Ø A325	120	92	27.120	20.792
$\frac{3}{4}$ " Ø A449 [‡]	120	92	40.080	30.728
$\frac{3}{4}$ " Ø AASHTO M164 (Type1) [§]	120	92	40.080	30.728

[†] As of August 2007, replaced by F1554 Gr. 36
[‡] Virtually identical in chemistry and strength to ASTM A325
[§] This standard is identical to ASTM A325

Table 26. Comparison of rail-to-post attachment features for NETC 2-bar bridge rails.

Design	Specified Method	Number of Bolts	Welded Stud (Detail A)		Bolted (Detail B)		
			Hole in Post	Stud Dimension	Hole in Rail	Hole in Post	Bolt Specifications
Recommendations	Bolted	2/Rail	--	--	$\frac{7}{8}$ "	$1\frac{1}{8}$ " x $1\frac{3}{8}$ " slotted hole	6" x $\frac{3}{4}$ " A325
NETC	*	*	--	--	N.S.	N.S.	*
MaineDOT	*	*	--	--	Bolt Ø + $\frac{1}{16}$ "	Bolt Ø + $\frac{1}{16}$ "	6" x $\frac{3}{4}$ " A307 6" x $\frac{5}{8}$ " A325
NHDOT	Bolted or Welded Stud	*	$1\frac{1}{8}$ " x $1\frac{3}{8}$ " slotted hole	$\frac{3}{4}$ " x $1\frac{3}{4}$ "	*	*	*
RIDOT	Bolted or Welded Stud	*	$1\frac{1}{8}$ " x $1\frac{3}{8}$ " slotted hole	$\frac{3}{4}$ " x $1\frac{3}{4}$ "	*	*	* or A449
VTrans	*	*	--	--	Bolt Ø + $\frac{1}{16}$ "	Bolt Ø + $\frac{1}{16}$ "	6" x $\frac{3}{4}$ " A449

* Same as recommended

N.S.: Not Specified

-- Not applicable

Table 27. Comparison of rail-to-post attachment features for NETC 3-bar bridge rails.

Design	Specified Method	Number of Bolts	Welded Stud (Detail A)		Bolted (Detail B)		
			Hole in Post	Stud Dimension	Hole in Rail	Hole in Post	Bolt Specifications
Recommendations	Bolted	2/Rail	--	--	$\frac{7}{8}$ "	$1\frac{1}{8}$ " x $1\frac{3}{8}$ " slotted hole	6" x $\frac{3}{4}$ " A325
MaineDOT	*	*	--	--	Bolt $\varnothing + \frac{1}{16}$ "	Bolt $\varnothing + \frac{1}{16}$ "	6" x $\frac{3}{4}$ " A307 6" x $\frac{5}{8}$ " A325
NHDOT	Bolted or Welded Stud	*	$1\frac{1}{8}$ " x $1\frac{3}{8}$ " slotted hole	$\frac{3}{4}$ " x $1\frac{3}{4}$ "	*	*	*

* Same as recommended

N.S.: Not Specified

-- Not applicable

Table 28. Comparison of rail-to-post attachment features for NETC 4-bar sidewalk mounted bridge rails.

Design	Specified Method	Number of Bolts	Welded Stud (Detail A)		Bolted (Detail B)		
			Hole in Post	Stud Dimension	Hole in Rail	Hole in Post	Bolt Specifications
Recommendations	Bolted	2/Rail	--	--	$\frac{7}{8}$ "	$1\frac{1}{8}$ " x $1\frac{3}{8}$ " slotted hole	6" x $\frac{3}{4}$ " A325
NETC	Welded	*	1" \varnothing	$\frac{3}{4}$ " x 2" A307	--	--	--
MaineDOT	*	*	--	--	Bolt $\varnothing + \frac{1}{16}$ "	Bolt $\varnothing + \frac{1}{16}$ "	6" x $\frac{3}{4}$ " A307 6" x $\frac{5}{8}$ " A325
NHDOT	Bolted or Welded Stud	*	$1\frac{1}{8}$ " x $1\frac{3}{8}$ " slotted hole	$\frac{3}{4}$ " x $1\frac{3}{4}$ " A304	*	*	*
RIDOT	Bolted or Welded Stud	*	$1\frac{1}{8}$ " x $1\frac{3}{8}$ " slotted hole	$\frac{3}{4}$ " x $1\frac{3}{4}$ " A304	*	*	*

* Same as recommended

N.S.: Not Specified

-- Not applicable

Table 29. Comparison of rail-to-post attachment features for NETC 4-bar curb mounted bridge rails.

Design	Specified Method	Number of Bolts	Welded Stud (Detail A)		Bolted (Detail B)		
			Hole in Post	Stud Dimension	Hole in Rail	Hole in Post	Bolt Specifications
Recommendations	Bolted	2/Rail	--	--	Bolt $\varnothing + \frac{1}{8}$ "	Bolt $\varnothing + \frac{1}{16}$ "	6" x 3/4" A325
MaineDOT	*	*	--	--	Bolt $\varnothing + \frac{1}{16}$ "	*	6" x $\frac{3}{4}$ " A307 6" x $\frac{5}{8}$ " A325
VTrans	*	*	--	--	*	*	6" x $\frac{3}{4}$ " AASHTO M164M (Type I)

* Same as recommended

N.S.: Not Specified

-- Not applicable

3.5.4 Baseplate and Anchor Bolts

Material selection for the baseplate matches the material selections for the post for each design. Baseplate dimensions are consistent across all designs with the exception of RIDOT 4-bar Sidewalk mounted design, described below. While most of the designs, including the recommended design, specify ASTM A449 anchor bolts, MaineDOT specifies AASHTO M314 Gr. 105 bolts. The strength features of these materials are displayed in Table 30. Embedment of the anchor plate also varies between designs. This value also likely varies to some degree in the field. All designs called for 3” of exposed rod above the concrete. Since all designs specify 12” bolts and 3” of exposed rod above the concrete, that leaves 9” of bolt below the concrete. With a maximum of 2.5” of threaded rod below the deck the anchor plate would logically be installed at an embedment depth of between 7” and approximately 8” (accounting for a jamb nut above and standard 1” nut below the anchor plate). The only State drawing that specifies the actual anchor plate embedment depth is the VTrans 2-bar design which specifies 7.5”. During evaluation the more critical 7.5” embedment depth will be used, and greater embedment depths will be assumed to pass if the 7.5” embedment depth design passes. The amount of thread varied between the designs. The 2.5” thread was selected for crash performance evaluation because this offers the greatest chance that some diameter reduction will be in the baseplate shear zone. Like the embedment depth issue, if the 2.5” threaded design passes evaluation, then the 2.25” thread will be assumed to pass as well. Specific details for each design are shown in Table 31 through Table 34.

The baseplate dimensions are consistent across all 4-bar system designs except RIDOT. The RIDOT design has a 5-anchor bolt pattern with an offset post. The 5-bolt design and the post offset yields higher strength for the anchor bolts and the concrete pry-out resistance; however, the plastic strength of the post governed the critical post strength based on the LRFD strength calculations for this system. The 4-bolt design will be evaluated and if it meets *MASH* test criteria then the 5-bolt design will be assumed to pass.

Table 30. Strength values for different bolts specifications for anchor bolts.

Bolt Spec	Minimum Strength Requirement		Effective Strength for Ø	
	Tensile (ksi)	Yield (ksi)	Tensile (kips)	Yield (kips)
1" Ø A449	120	92	72.720	55.752
1" Ø AASHTO M314 Gr. 105	125	105	75.750	63.630

Table 31. Comparison of baseplate and anchor bolt features for NETC 2-bar bridge rails.

Design	Material	Size	Number of Bolts	Bolt Pattern	Size of Holes	Anchor Bolts					
						Size	Material	Embedment	Exposed Rod	Exposed Nut	Nut Torque
Recommendations	ASHTO M270 Grade 50 (50 ksi)	1" x 10" x 1'-2"	4	See drawing	1.25"	1" Ø x 12" L	ASTM A449	7 $\frac{1}{2}$ "	3" 2 $\frac{1}{2}$ " threaded	Heavy hex nut & washer	Snug + 1/8 turn
NETC	*	*	*	*	N.S.	1" Ø x 9" L	N.S.	N.S.	N.S.	N.S.	N.S.
MaineDOT	*	*	*	*	*	*	AASHTO M314, Grade 105	8 $\frac{1}{2}$ "	3" 2 $\frac{1}{4}$ " threaded	*	*
NHDOT	*	*	*	*	*	*	*	9"	*	1"Ø-8 steel nut & 1"Ø washer	*
RIDOT	*	*	*	*	*	*	*	9" (min)	*	*	*
VTrans	*	*	*	*	*	*	*	*	3" 2 $\frac{1}{4}$ " threaded	*	*

* Same as recommended
N.S.: Not Specified

Table 32. Comparison of baseplate and anchor bolt features for NETC 3-bar bridge rails.

Design	Material	Size	Number of Bolts	Bolt Pattern	Size of Holes	Anchor Bolts					
						Size	Material	Embedment	Exposed Rod	Exposed Nut	Nut Torque
Recommendations	AASHTO M270 Grade 50	1" x 10" x 1'-2"	4	See Below	1.25"	1" Ø x 12" L	ASTM A449	7 $\frac{1}{2}$ "	3" 2 $\frac{1}{2}$ " threaded	Heavy hex nut & washer	Snug + 1/8 turn
MaineDOT	*	*	*	*	*	*	AASHTO M314 Grade 105	8 $\frac{1}{2}$ "	3" 2 $\frac{1}{4}$ " threaded	*	*
NHDOT	ASTM A572 Grade 50	*	*	*	*	*	*	9" (min)	*	Steel hex nut & washer	*

* Same as recommended
N.S.: Not Specified

Table 33. Comparison of baseplate and anchor bolt features for NETC 4-bar sidewalk mounted bridge rails.

Design	Material	Size	Number of Bolts	Bolt Pattern	Size of Holes	Anchor Bolts					
						Size	Material	Embedment	Exposed Rod	Exposed Nut	Nut Torque
Recommendations	ASHTO M270 Grade 50	1" x 10" x 1'-2"	4	See NHDOT on Next Slide	1 $\frac{1}{4}$ "	1" Ø x 12" L	ASTM A449	7 $\frac{1}{2}$ "	3" 2 $\frac{1}{2}$ " threaded	Heavy hex nut & washer	Snug + 1/8 turn
NETC	ASHTO M270 Grade 36	*	*	*	*	*	*	8 $\frac{1}{2}$ "	3" 2 $\frac{1}{4}$ " threaded	*	*
MaineDOT	*	*	*	*	*	*	ASHTO M314 Grade 105	8 $\frac{1}{2}$ "	3" 2 $\frac{1}{4}$ " threaded	*	*
NHDOT	ASTM A572 Grade 50	*	*	*	*	*	*	9" (min)	*	Steel nut & washer	*
RIDOT	ASTM A572 Grade 50	1" x 11" x 1'-2"	5	See RIDOT on Next Slide	1 $\frac{1}{16}$ "	*	*	9" (min)	*	Steel nut & washer	*

* Same as recommended
N.S.: Not Specified

Table 34. Comparison of baseplate and anchor bolt features for NETC 4-bar curb mounted bridge rails.

Design	Material	Size	Number of Bolts	Bolt Pattern	Size of Holes	Anchor Bolts					
						Size	Material	Embedment	Exposed Rod	Exposed Nut	Nut Torque
Recommendations	ASHTO M270 Grade 50	1" x 10" x 1'-2"	4	See drawing	1 $\frac{1}{4}$ "	1" Ø x 12" L	ASTM A449	7 $\frac{1}{2}$ "	3" 2 $\frac{1}{2}$ " threaded	Heavy hex nut & washer	Snug + 1/8 turn
MaineDOT	*	*	*	*	*	*	ASHTO M314 Grade 105	8 $\frac{1}{2}$ "	3" 2 $\frac{1}{4}$ " threaded	*	*
VTrans	ASTM A572 Grade 50	*	*	*	*	*	*	8 $\frac{1}{2}$ "	3" 2 $\frac{1}{4}$ " threaded	*	*

* Same as recommended
N.S.: Not Specified

3.5.5 Field Splice

Most field splice features are the same between designs, the biggest differences being the size of the hole in the rail member and the gap between rail bars. It is recommended that the least conservative option be selected for the crash evaluations, which entails the slotted design used by NHDOT and RIDOT for the rail hole feature and a 3/4-inch longitudinal gap between adjacent rail bars. If the design passes the evaluation with these details, then the smaller holes and smaller gap can be assumed to pass as well. Specific details for each design are shown in Table 35 through Table 38.

Table 35. Comparison of field splice features for NETC 2-bar bridge rails.

Design	Splice Tube Dimensions	Connection Details	Number of Bolts	Size of Hole in Rail	Hole in Splice Tube	Bolt	Nut?	Pipe Spacer	Space Between Rail Bars	Splice Tube L	Drain Hole?
Recommendations	HSS 3" x 3" x $\frac{5}{16}$ " HSS 7" x 3" x $\frac{3}{8}$ "	See Figure Below	4	$1\frac{1}{8}$ " x $2\frac{1}{2}$ " slot	$\frac{5}{8}$ " \emptyset tapped hole	$\frac{5}{8}$ " \emptyset x $1\frac{3}{4}$ " Cap Screw	Tack weld on outer holes only	$\frac{3}{4}$ " \emptyset x $\frac{1}{2}$ " Schd. 40 [†]	$\frac{3}{4}$ "	1'-8"	Yes, $\frac{1}{2}$ " \emptyset
NETC	Welded Plates [‡]	*	*	N.S.	N.S.	*	N.S.	N.S.	*	*	N.S.
MaineDOT	*	*	*	$\frac{13}{16}$ " \emptyset hole	*	*	*	No	*	*	N.S.
NHDOT	*	*	*	*	*	* A307	*	*	$\frac{1}{2}$ "	*	*
RIDOT	*	*	*	*	*	* A307	*	*	$\frac{1}{2}$ "	*	*
VTrans	*	*	*	$\frac{3}{4}$ " \emptyset hole	*	$\frac{5}{8}$ " \emptyset x $1\frac{3}{4}$ " Bolt	*	*	$\frac{1}{2}$ "	*	*

* Same as recommended
N.S.: Not Specified
† only 1 side each splice, both rails
‡ TS 4x4: 2-5/8" x 3/8" x 20" and 2-7/8" x 3/8" x 20"
‡ TS 8x4: 2-1/2" x 3/8" x 20" and 6-3/4" x 3/8" x 20"

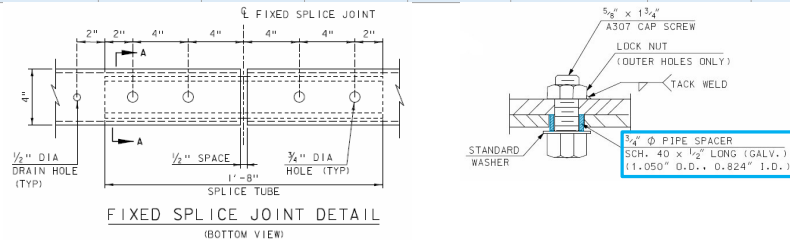


Table 36. Comparison of field splice features for NETC 3-bar bridge rails.

Design	Splice Tube Dimensions	Connection Details	Number of Bolts	Size of Hole in Rail	Hole in Splice Tube	Bolt	Nut?	Pipe Spacer	Space Between Rail Bars	Splice Tube L	Drain Hole?
Recommendations	HSS 3" x 3" x $\frac{5}{16}$ " HSS 7" x 3" x $\frac{3}{8}$ "	See Figure Above	4	$1\frac{1}{8}$ " x $2\frac{1}{2}$ " slot	$\frac{5}{8}$ " \emptyset tapped hole	$\frac{5}{8}$ " \emptyset x $1\frac{3}{4}$ " Cap Screw	Tack weld on outer holes only	$\frac{3}{4}$ " \emptyset x $\frac{1}{2}$ " Schd. 40 [†]	$\frac{3}{4}$ "	1'-8"	Yes, $\frac{1}{2}$ " \emptyset
MaineDOT	*	*	*	$\frac{13}{16}$ " \emptyset hole	*	*	*	No	*	*	N.S.
NHDOT	*	*	*	*	*	*	*	*	*	*	*

* Same as recommended
N.S.: Not Specified
† only 1 side each splice, both rails

Table 37. Comparison of field splice features for NETC 4-bar sidewalk mounted bridge rails.

Design	Splice Tube Dimensions	Connection Details	Number of Bolts	Size of Hole in Rail	Hole in Splice Tube	Bolt	Nut?	Pipe Spacer	Space Between Rail Bars	Splice Tube L	Drain Hole?
Recommendations	HSS 3" x 3" x $\frac{5}{16}$ " HSS 7" x 3" x $\frac{3}{8}$ "	See Figure Above	4	$1\frac{1}{8}$ " x $2\frac{1}{2}$ " slot	$\frac{5}{8}$ " \emptyset tapped hole	$\frac{5}{8}$ " \emptyset x $1\frac{3}{4}$ " Cap Screw	Tack weld on outer holes only	$\frac{3}{4}$ " \emptyset x $\frac{1}{2}$ " Schd. 40 [†]	$\frac{3}{4}$ "	1'-8"	Yes, $\frac{1}{2}$ " \emptyset
NETC	*	*	*	N.S.	N.S.	*	N.S.	N.S.	*	*	N.S.
MaineDOT	*	*	*	$\frac{13}{16}$ " \emptyset hole	*	$\frac{5}{8}$ " \emptyset x $1\frac{3}{4}$ " Bolt & plain hardened washer	*	No	*	*	N.S.
NHDOT	*	*	*	*	*	* A307	*	*	*	*	*
RIDOT	*	*	*	*	*	* A307	*	*	*	*	*

* Same as recommended
N.S.: Not Specified
† only 1 side each splice, both rails

Table 38. Comparison of field splice features for NETC 4-bar curb mounted bridge rails.

Design	Splice Tube Dimensions	Connection Details	Number of Bolts	Size of Hole in Rail	Hole in Splice Tube	Bolt	Nut?	Pipe Spacer	Space Between Rail Bars	Splice Tube L	Drain Hole?
Recommendations	HSS 3" x 3" x $\frac{5}{16}$ " HSS 7" x 3" x $\frac{3}{8}$ "	See Figure Above	4	$1\frac{1}{8}$ " x $2\frac{1}{2}$ " slot	$\frac{5}{8}$ " \emptyset tapped hole	$\frac{5}{8}$ " \emptyset x $1\frac{3}{4}$ " Cap Screw	Tack weld on outer holes only	$\frac{3}{4}$ " \emptyset x $\frac{1}{2}$ " Schd. 40	$\frac{3}{4}$ "	1'-8"	Yes, $\frac{1}{2}$ " \emptyset
MaineDOT	*	*	*	$\frac{13}{16}$ " \emptyset hole	*	$\frac{5}{8}$ " \emptyset x $1\frac{3}{4}$ " Bolt & plain hardened washer	*	No	*	*	N.S.
VTrans	*	*	*	$\frac{3}{4}$ " \emptyset hole	*	$\frac{5}{8}$ " \emptyset x $1\frac{3}{4}$ " Bolt & plain hardened washer	*	No	*	*	N.S.

* Same as recommended
N.S.: Not Specified

3.5.6 Expansion Splice

A comparison of the expansion joint details for the NETC style bridge rail designs is displayed in Table 39 through Table 42 and Figure 19. The NETC designs do not specify any dimensional requirements for expansion joints. There are many differences in the expansion joint details, one main difference being the range of “bridge movements” that the details cover. A supplemental summary of details for each design for each range of bridge movements is provided in Table 43. The expansion splice detail was not evaluated for crash performance in this study; however, the MaineDOT detail would allow the greatest amount of bridge movements.

Table 39. Comparison of expansion splice features for NETC 2-bar bridge rails.

Design	Splice Tube Dimensions	Connection Details	Number of Bolts	Size of Hole in Rail	Hole in Splice Tube	Bolt	Nut?	Pipe Spacer	Space Between Rail Bars	Splice Tube L	Drain Hole?
Recommendations	HSS 3" x 3" x $\frac{5}{16}$ " HSS 7" x 3" x $\frac{3}{8}$ "	See Figure below	4	See MEDOT in Fig. below	$\frac{5}{8}$ " \emptyset tapped hole	$\frac{5}{8}$ " \emptyset x $1\frac{3}{4}$ " Cap Screw	Tack weld on outer holes only	$\frac{3}{4}$ " \emptyset x $\frac{1}{2}$ " Schd. 40	See MEDOT in Fig. below	See MEDOT in Fig. below	Yes, $\frac{1}{2}$ " \emptyset
NETC	N.S.	N.S.	N.S.	N.S.	N.S.	*	N.S.	N.S.	N.S.	N.S.	N.S.
MaineDOT	*	*	*	*	*	*	*	N.S.	*	*	N.S.
NHDOT	*	*	*	See NHDOT in Fig. below	*	* A307	*	*	See NHDOT in Fig. below	See NHDOT in Fig. below	*
RIDOT	*	*	*	See RIDOT in Fig. below	*	* A307	*	*	See RIDOT in Fig. below	See RIDOT in Fig. below	*
VTrans	*	*	*	$1\frac{1}{8}$ " x $3\frac{1}{2}$ " slot	*	$\frac{5}{8}$ " \emptyset x $1\frac{3}{4}$ " Bolt	*	*	4" @68°F	1'-11 $\frac{3}{4}$ "	*

* Same as recommended
N.S.: Not Specified

Table 40. Comparison of expansion splice features for NETC 3-bar bridge rails.

Design	Splice Tube Dimension	Connection Details	Number of Bolts	Size of Hole in Rail	Hole in Splice Tube	Bolt	Nut?	Pipe Spacer	Space Between Rail Bars	Splice Tube L	Drain Hole?
Recommendations	HSS 3" x 3" x $\frac{5}{16}$ " HSS 7" x 3" x $\frac{3}{8}$ "	See Figure below	4	See MaineDOT Next Slide	$\frac{5}{8}$ " \emptyset tapped hole	$\frac{5}{8}$ " \emptyset x $1\frac{3}{4}$ " Cap Screw	Tack weld on outer holes only	$\frac{3}{4}$ " \emptyset x $\frac{1}{2}$ " Schd. 40	See MEDOT in Fig. below	See MEDOT in Fig. below	Yes, $\frac{1}{2}$ " \emptyset
MaineDOT	*	*	*	*	*	*	*	*	*	*	N.S.
NHDOT	*	*	*	See NHDOT Next Slide	*	*	*	*	See NHDOT in Fig. below	See NHDOT in Fig. below	*

* Same as recommended
N.S.: Not Specified

Table 41. Comparison of expansion splice features for NETC 4-bar sidewalk mounted bridge rails.

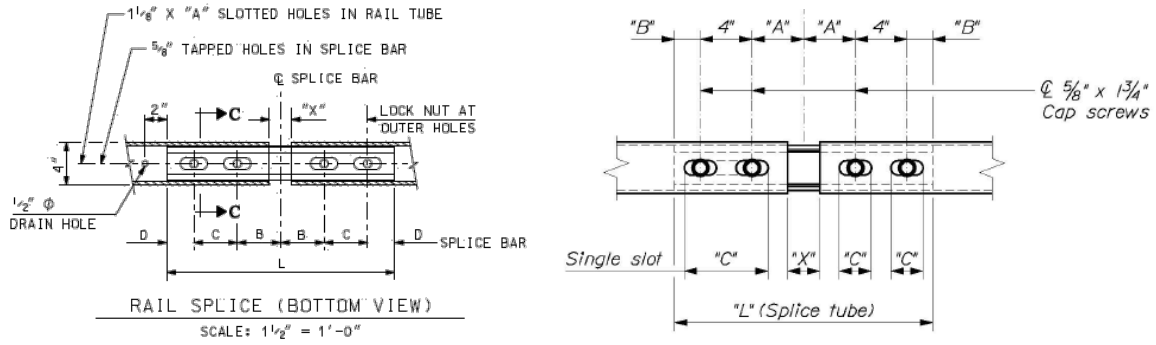
Design	Splice Tube Dimensions	Connection Details	Number of Bolts	Size of Hole in Rail	Hole in Splice Tube	Bolt	Nut?	Pipe Spacer	Space Between Rail Bars	Splice Tube L	Drain Hole?
Recommendations	HSS 3" x 3" x $\frac{5}{16}$ " HSS 7" x 3" x $\frac{3}{8}$ "	See Figure below	4	See MEDOT in Fig. below	$\frac{5}{8}$ " \emptyset tapped hole	$\frac{5}{8}$ " \emptyset x $1\frac{3}{4}$ " A307 Cap Screw	Tack weld on outer holes only	$\frac{3}{4}$ " \emptyset x $\frac{1}{2}$ " Schd. 40	See MaineDOT next slide	See MaineDOT next slide	Yes, $\frac{1}{2}$ " \emptyset
NETC	*	N.S.	N.S.	N.S.	N.S.	N.S.	N.S.	N.S.	N.S.	N.S.	N.S.
MaineDOT	*	*	*	*	*	$\frac{5}{8}$ " \emptyset x $1\frac{3}{4}$ " Bolt & plain hardened washer	*	*	*	*	N.S.
NHDOT	*	*	*	See NHDOT in Fig. below	*	*	*	*	See NHDOT in Fig. below	See NHDOT in Fig. below	*
RIDOT	*	*	*	See RIDOT in Fig. below	*	*	*	*	See RIDOT in Fig. below	See RIDOT in Fig. below	*

* Same as recommended
N.S.: Not Specified

Table 42. Comparison of expansion splice features for NETC 4-bar curb mounted bridge rails.

Design	Splice Tube Dimensions	Connection Details	Number of Bolts	Size of Hole in Rail	Hole in Splice Tube	Bolt	Nut?	Pipe Spacer	Space Between Rail Bars	Splice Tube L	Drain Hole?
Recommendations	HSS 3" x 3" x $\frac{5}{16}$ " HSS 7" x 3" x $\frac{3}{8}$ "	See Figure below	4	See MEDOT in Fig. below	$\frac{5}{8}$ " \emptyset tapped hole	$\frac{5}{8}$ " \emptyset x $1\frac{3}{4}$ " Cap Screw	Tack weld on outer holes only	$\frac{3}{4}$ " \emptyset x $\frac{1}{2}$ " Schd. 40	See MEDOT in Fig. below	See MEDOT in Fig. below	Yes, $\frac{1}{2}$ " \emptyset
MaineDOT	*	*	*	*	*	$\frac{5}{8}$ " \emptyset x $1\frac{3}{4}$ " Bolt & plain hardened washer	*	*	*	*	N.S.
VTrans	*	*	*	See VTrans in Fig. below	*	$\frac{5}{8}$ " \emptyset x $1\frac{3}{4}$ " Bolt & plain hardened washer	*	*	See VTrans in Fig. below	See VTrans in Fig. below	N.S.

* Same as recommended
N.S.: Not Specified



T	A	B	C	D	X	L
INTERIOR	2 1/2"	4"	4"	2"	3/4"	1'-8"
$\leq 3\frac{1}{4}$ "	2 1/2"	4"	4"	2"	2"	1'-8"
$3\frac{1}{4}$ " < T $\leq 5\frac{1}{4}$ "	3 1/2"	5"	5"	2 1/2"	3"	2'-1"

T = TOTAL MOVEMENT OF BRIDGE
* = END SPLICE BAR

T	A	B	C	L	X
Splice	4"	2"	--	1'-8"	3/4"
≤ 4 "	4"	2"	2 1/2"	1'-8"	2 1/2"
$> 4 \leq 6\frac{1}{2}$ "	5 1/2"	2 1/2"	3 1/2"	2'-0"	3 3/4"
$> 6\frac{1}{2} \leq 9$ "	6 1/2"	3 1/2"	5"	2'-4"	5"
$> 9 \leq 13$ "	8 1/2"	4 1/2"	11"	2'-10"	7"

T = Total Movement * = Single Slot

T	A	B	C	L	X
N/A	100 (4")	50 (2")	--	508 (20")	19 (3/4")

T	A	B	C	L	X
< 100 (4")	100 (4")	50 (2")	64 (2 1/2")	508 (20")	64 (2 1/2")
> 100 (4") < 165 (6 1/2")	140 (5 1/2")	60 (2 3/8")	89 (3 1/2")	603 (23 3/4")	100 (4")
> 165 (6 1/2") < 229 (9")	163 (6 1/2")	86 (3 3/8")	229 (9")	705 (27 3/4")	127 (5")
> 229 (9") < 330 (13")	216 (8 1/2")	111 (4 3/8")	279 (11")	857 (33 3/4")	179 (7")

T = TOTAL MOVEMENT AT RAIL EXPANSION JOINT AS SHOWN ON THE CONTRACT PLANS. SEE NOTE 6.
* = SINGLE SLOT

a) NHDOT and RIDOT

b) MEDOT

c) VTrans

Figure 19. Expansion splice details for a) NHDOT and RIDOT, b) MaineDOT and c) VTrans.

Table 43. Comparison of expansion splice details for different amounts of bridge movement.

Design	Bridge Movement	Gap Between Rails	Rail Hole Slot	Distance Between Bolts	Inside Bolt to Splice Bar CL	Outside Bolt to Splice Bar End	Splice Tube L
MaineDOT	≤ 4 "	2.50"	2.50"	4.00"	4.00"	2.00"	1'-8"
	$4" < T \leq 6.5$ "	3.75"	3.50"	4.00"	5.50"	2.50"	2'-0"
	$6.5" < T \leq 9$ "	5.00"	9.00"	4.00"	6.50"	3.50"	2'-4"
	$9" < T \leq 13$ "	7.00"	11.00"	4.00"	8.50"	4.50"	2'-10"
RIDOT & NHDOT	≤ 3.25 "	2.00"	2.50"	4.00"	4.00"	2.00"	1'-8"
	$3.25" < T \leq 5.25$ "	3.00"	3.50"	5.00"	5.00"	2.50"	2'-1"
VTrans 2-Bar	N/A	4.00"	3.50"	4.00"	5.50"	2.375"	1'-11.75"
VTrans 4-bar Curb Mounted	≤ 4 "	2.50"	2.50"	4.00"	4.00"	2.00"	20"
	$4" < T \leq 6.5$ "	4.00"	3.50"	4.00"	5.50"	2.375"	23.75"
	$6.5" < T \leq 9$ "	5.00"	9.00"	4.00"	6.50"	3.375"	27.75"
	$9" < T \leq 13$ "	7.00"	11.00"	4.00"	8.50"	4.375"	33.75"

3.5.7 Concrete Curb

A comparison of the concrete curb details are provided in Table 44 through Table 47. There are many small dimensional differences between the designs. For the crash evaluations it is recommended that the smallest values that are anticipated to pass evaluation be used. For back bolts to deck edge that is 7-5/8" and for front bolts to curb edge it is 4". Concrete strength of 4000 psi is used in the strength evaluations; therefore, designs that specify 5000 psi concrete strength would also be considered to pass if the 4000 psi design passes. There are some differences in the reinforcement bars, particularly the longitudinal bar length. Some only require 5' length while others require full length of the curb and NHDOT doesn't specify a required length. Secondary pours and granite curbs are not included in the strength evaluations since they are not reinforced. Although the curb projections were not used for the strength calculations, they may affect vehicle dynamics during the simulations.

Table 44. Comparison of concrete curb features for NETC 2-bar bridge rails.

Design	Strength Requirement	Curb Dimensions				Reinforcing Steel	
		Curb Height	Curb Width	Back Bolts to Deck Edge	Front Bolts to Curb Edge	Longitudinal Reinforcement Near Post Anchor	Reinforcement Hoop Bars Near Post Anchor
Recommendations	4000 psi	7"	1'-6"	7 $\frac{5}{8}$ "	4"	3 - #5 Bars 5' L minimum	7 - #5 Bars at 6" spacing, engagement required from some deck rebars
NETC	N.S.	9"	1'-4"	4 $\frac{5}{8}$ "	5"	2 - #5 Bars length not specified	*
MaineDOT	5000 psi	9"	1'-8"	8 $\frac{1}{8}$ "	5 $\frac{1}{2}$ "	3 - #5 Bars full length of curb	*
NHDOT	*	*	2'-0"	*	10"	3 - #5 Bars	*
RIDOT	5000 psi	*	*	*	*	*	7 - #5 Bars at 6" spacing. Must engage min. two deck rebars
VTrans	*	*	2'-0"	*	10"	3 - #5 Bars, middle 5' L min, outsides full length of curb	*

* Same as recommended
N.S.: Not Specified

Table 45. Comparison of concrete curb features for NETC 3-bar bridge rails.

Design	Strength Requirement	Curb Dimensions				Reinforcing Steel	
		Curb Height	Curb Width	Back Bolts to Deck Edge	Front Bolts to Curb Edge	Longitudinal Reinforcement Near Post Anchor	Reinforcement Hoop Bars Near Post Anchor
Recommendations	4000 psi	7"	1'-6"	7 $\frac{5}{8}$ "	4"	3 - #5 Bars 5' L minimum	7 - #5 Bars at 6" spacing
MaineDOT	5000 psi	9"	1'-8"	8 $\frac{1}{8}$ "	5 $\frac{1}{2}$ "	3 - #5 Bars full length of curb	*
NHDOT	*	*	2'-0"	*	10"	3 - #5 Bars	*

* Same as recommended
N.S.: Not Specified
--: Not Applicable

Table 46. Comparison of concrete curb features for NETC 4-bar sidewalk mounted bridge rails.

Design	Strength Requirement	Sidewalk Dimensions				Reinforcing Steel	
		Sidewalk Height	Sidewalk Width	Back Bolts to Deck Edge	Front Bolts to Sidewalk Edge	Longitudinal Reinforcement Near Post Anchor	Reinforcement Hoop Bars Near Post Anchor
Recommendations	4000 psi	9"	5' (Min.)	7 $\frac{5}{8}$ "	5'-2"	3 - #5 Bars minimum 5' L	7 - #5 Bars at 6" spacing, engagement required from some deck rebars
NETC	N.S.	N.S.	N.S.	*	N.S.	3 - #5 Bars, middle 5' L min, outsides full length of sidewalk	*
MaineDOT	5000 psi	*	N.S.	8 $\frac{1}{8}$ "	N.S.	3 - #5 Bars full length of curb	*
NHDOT	*	7"	*	*	Min. 5'-4"	3 - #5 Bars, length requirement N.S.	*
RIDOT	5000 psi	7"	*	*	Min. 5'-2"	*	*

* Same as recommended
N.S.: Not Specified

Table 47. Comparison of concrete curb features for NETC 4-bar curb mounted bridge rails.

Design	Strength Requirement	Curb Dimensions				Reinforcing Steel	
		Curb Height	Curb Width	Back Bolts to Deck Edge	Front Bolts to Curb Edge	Longitudinal Reinforcement Near Post Anchor	Reinforcement Hoop Bars Near Post Anchor
Recommendations	4000 psi	7"	1'-8"	7 $\frac{5}{8}$ "	4"	3 - #5 Bars minimum 5' L	7 - #5 Bars at 6" spacing, engagement required from some deck rebars
MaineDOT	5000 psi	9"	*	8 $\frac{1}{8}$ "	5 $\frac{1}{2}$ "	3 - #5 Bars full length of curb	*
VTrans	5000 psi	9"	2'-1"	*	10 $\frac{3}{16}$ "	3 - #5 Bars, middle 5' L min, outsides full length of curb	*

* Same as recommended
N.S.: Not Specified

3.6 Critical Review of Current Standard Details for NETC Style Bridge Rail Transitions

Categorically speaking there are two design concepts for approach guardrail transitions (AGT) on New England bridges (i.e., a sloped rail bar design and a concrete buttress design). Both designs connect a typical highway w-beam to a thrie-beam section using a w-beam to thrie-beam transition. In the “sloped bridge rail” design the thrie-beam section is connected to the sloped rails using a thrie-beam terminal connector element. The downstream end of the sloped rail section is connected to the bridge rail using an angled expansion joint. The sloped rails are composed of HSS steel tubular sections of the same size and material as the bridge rail bars. The “concrete buttress” design replaces the sloped bridge rail with a concrete buttress. The sloped rail design and concrete buttress design are shown in Figure 20. These designs were described in [Previous Full-Scale Testing of NETC Hardware](#) section of this report and are further detailed in the following paragraphs.

For the 2 bar AGT system detail are provided by NHDOT and Vtrans are dimensionally the same and only differ in the material specifications (same materials used in the bridge rail designs). NHDOT is the only state with 3 bar AGT drawings. The MaineDOT concrete buttress design is the only concrete buttress design. Design drawings for the 4-bar sloped rail bar AGT designs are available from NHDOT and VTrans; these two designs vary significantly both in concept and dimensions.

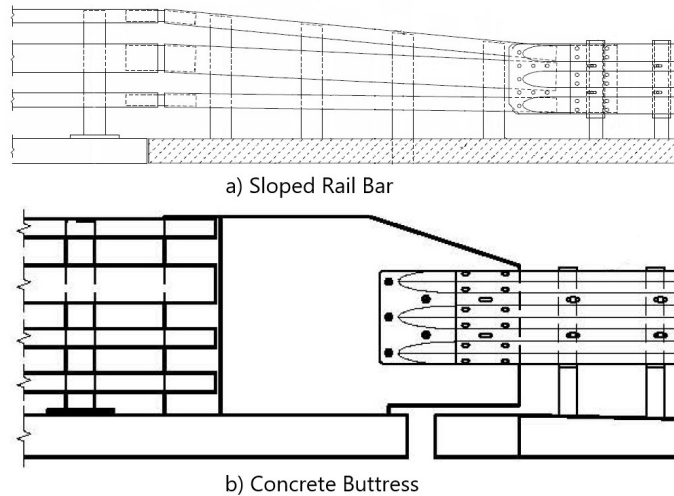


Figure 20. Drawings of the two design concepts for NETC approach guardrail transitions (AGT).

3.6.1 NHDOT 2-Bar Transition

The NHDOT T2 Steel Bridge Approach Rail was successfully crash tested in April 2005 by NETC and accepted as NCHRP 350 TL3. An FHWA acceptance letter was provided for the design, HSSD/B-146. See Section 3.3.4 of this report for more details.

A standard 12-gauge w-beam roadway guardrail is used upstream of the AGT as shown in Figure 21. A 25'-0" section of guardrail is flared at 80:1 to restore the rail-to-rail width. Post spacing in this section is 6'3" (e.g., standard post spacing) and the guardrails are lapped in the direction of traffic. The curb is flared away from the roadway at a 10:1 rate and has a 4" reveal. The curb increases in height from 4" to 7" over the next approximately 9 feet.

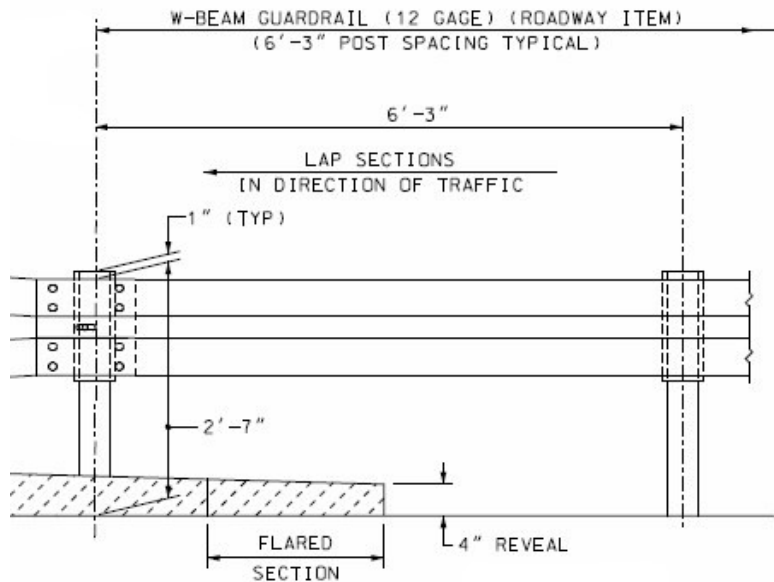


Figure 21. NHDOT T2 AGT upstream w-beam section.

A symmetrical 10-gauge w-beam to thrie-beam transition rail is attached to the standard w-beam on the upstream end as seen in Figure 22. The transition rail is 6'-3" long and post spacing in this section is 3'-1.5" (half post spacing). The height of the rail at the upstream end of the thrie-beam transition rail is 31 inches high and is 34 inches at the downstream end.

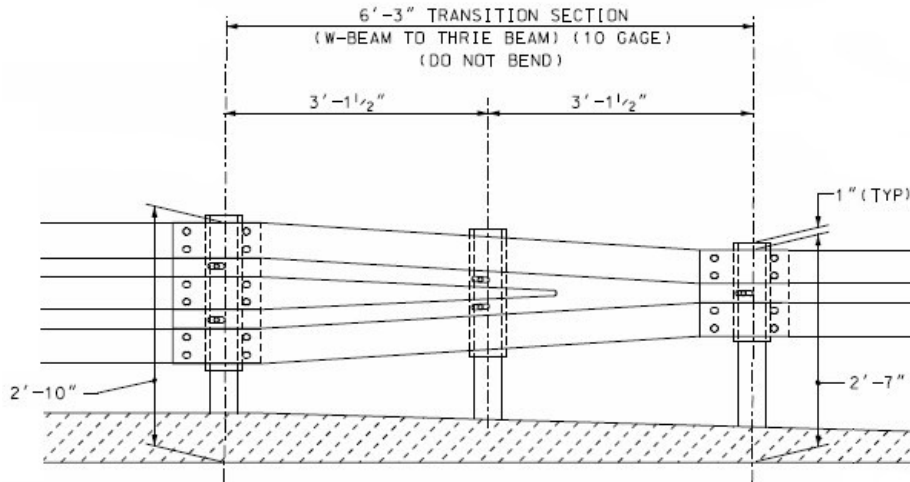


Figure 22. NHDOT T2 AGT symmetrical w-beam to thrie-beam transition section.

The next section is a 12'-6" long double nested 12-gauge thrie-beam section as seen in Figure 23. The first upstream post is spaced at 3'-1.5" (e.g., half post spacing), while the next six posts are spaced 1'-6.75" (quarter-post spacing). A connection plate and thrie-beam terminal connector are used to connect the thrie-beam to the top and bottom sloped bridge rails. An important component of the downstream end of the thrie-beam section where the connection plate fastens to the sloped rail bars is the use of a deflector plate between the top and bottom rail. This deflector plate helps to minimize the risk of the bumper or fender of the vehicle snagging on the post at the end of connector plate; it also reduces the risk of the vehicle snagging on the end of the connector plate in reverse-direction impacts.

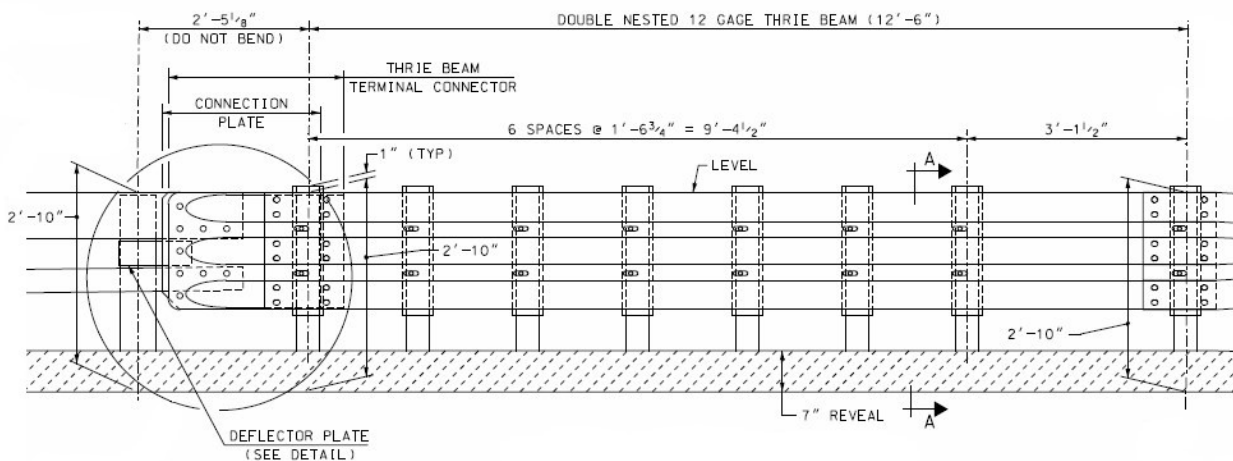


Figure 23. NHDOT T2 AGT double nested thrie-beam section.

The 6'-6" sloped rail section is shown in Figure 24. This section uses rail bars of the same material type and shape as used for the bridge rail. The slope for each rail bar in the transition

section is provided in Table 48. The splice bars that connect the sloped section to the bridge rail are adjusted for slope and bend using complete joint penetration butt welds. The splice bar length and other details should match the details discussed in the bridge rail sections. The posts are set at 2'-2" spacing in this section. The top rail height of 34 inches is maintained throughout this section and onto the bridge rail section.

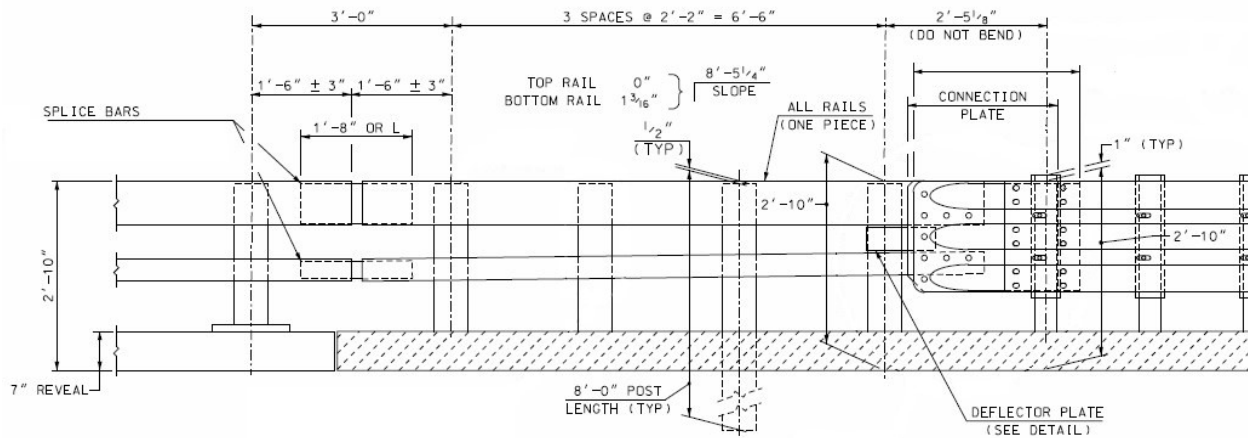


Figure 24. NHDOT T2 AGT sloped rail section.

Table 48. NHDOT T2 AGT slope of rail bar transition section.

	Top Bar	Bottom Bar
Y Displacement	0"	$-1\frac{3}{16}$ "
X Displacement	$8'-5\frac{1}{4}$ "	$8'-5\frac{1}{4}$ "
Slope (Y/X)	0	-0.012

3.6.1.1 Discrepancies in Drawing

When reviewing the drawings, discrepancies were identified for the NHDOT T2 (and NHDOT T3) Bridge Approach Rail. The first discrepancy is the detail for the post bolts in the thrie-beam and transition section. The discrepancies are highlighted in Figure 25. The thrie-beam-to-post bolts are called out as both 5/8" Ø A307 B.H Post Bolt (green highlight) and 5/8" x 1 1/2" Ø Hex Head Bolt (blue highlight). Additionally, the post bolts are indicated to go through both the front and back flange of the post (orange highlight). It is suspected these bolts are actually bolted to the front flange of the W6x8.5 posts.

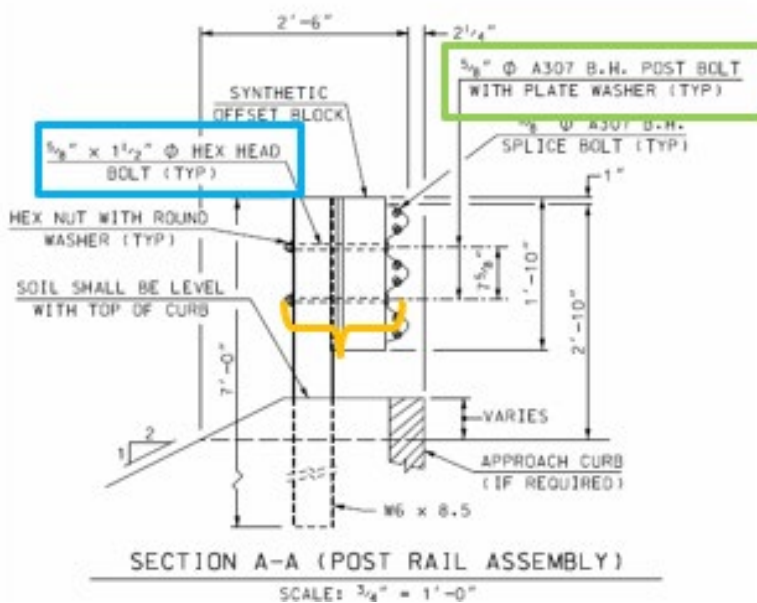


Figure 25. Post rail assembly NHDOT T2 AGT (T3 similar)

The second discrepancy found in the NHDOT T2 (and T3) drawings is also an inconsistency between bolt details. This discrepancy is highlighted in Figure 26. The clamping bolts are called out as 3/4" Ø Button Head Bolts (purple highlight) and 3/4" Carriage Bolt (red highlight).

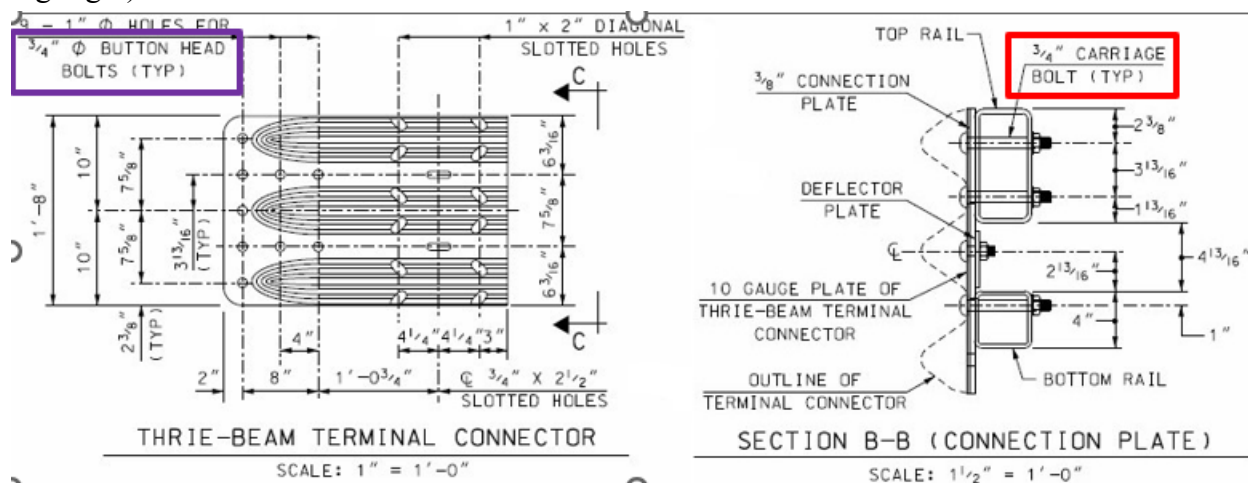


Figure 26. Terminal and connection plate detail drawings for NHDOT T2 AGT (T3 similar)

3.6.2 NHDOT 3-Bar Transition

The NHDOT T3 Steel Bridge Approach Rail was successfully crash tested in April 2005 by NETC and accepted as NCHRP 350 TL3. An FHWA acceptance letter was provided for the design, HSSD/B-146³. See Section 3.3.4 of this report for more details.

³ https://safety.fhwa.dot.gov/roadway_dept/countermeasures/reduce_crash_severity/barriers/pdf/b146.pdf

A standard 12-gauge w-beam roadway guardrail is used upstream of the AGT as seen in Figure 27. A 25'-0" section of guardrail flared at 80:1 to restore the rail-to-rail width. Post spacing in this section is 6'3" (e.g., standard post spacing) and the guardrails are lapped in the direction of traffic. The curb is flared away from the roadway at a 10:1 rate and has a 4" reveal. The curb increases in height from 4" to 7" over the next approximately 9'.

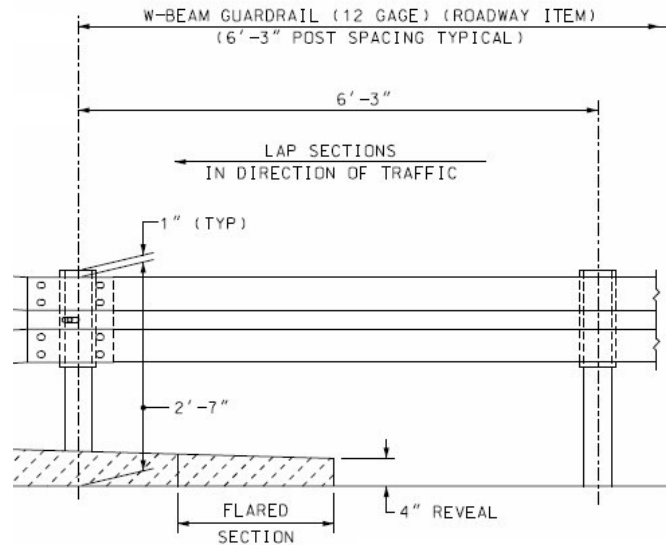


Figure 27. NHDOT T3 AGT upstream w-beam section.

A symmetrical 10-gauge w-beam to thrie-beam transition rail is attached to the standard w-beam on the upstream end as seen in Figure 28. The transition rail is 6'-3" long and post spacing in this section is 3'-1.5" (e.g., half post spacing). The height of the rail at the upstream end of the thrie-beam transition rail is 31 inches high and is 34 inches at the downstream end.

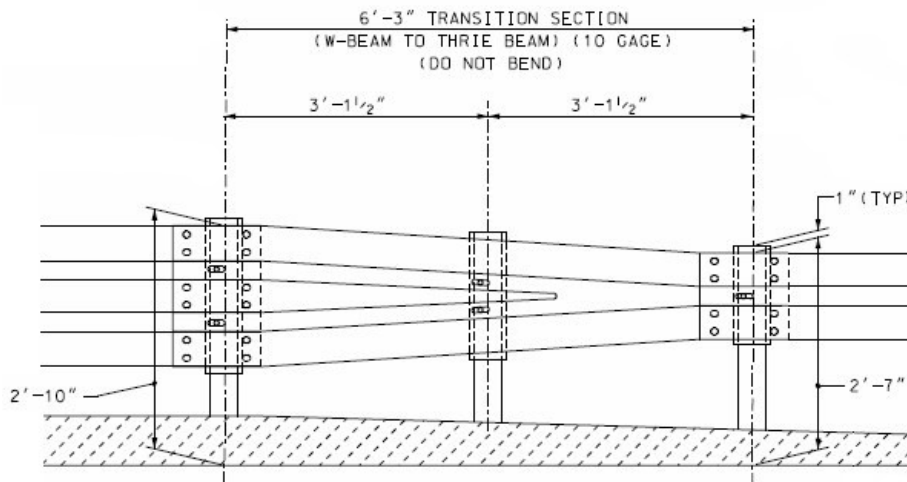


Figure 28. NHDOT T3 AGT symmetrical w-beam to thrie-beam transition section.

The next section is a 12'-6" long double nested 12-gauge thrie-beam section as seen in Figure 29. The first upstream post is spaced at 3'-1.5" (e.g., half-post spacing), while the other posts are spaced 1'-6.75" (e.g., quarter post spacing). A connection plate and thrie-beam

terminal connector are used to connect the thrie-beam to the top and bottom sloped bridge rails. The deflector plate, which is specified in the 2-bar design (see Figure 24), is not present in the 3-bar design.

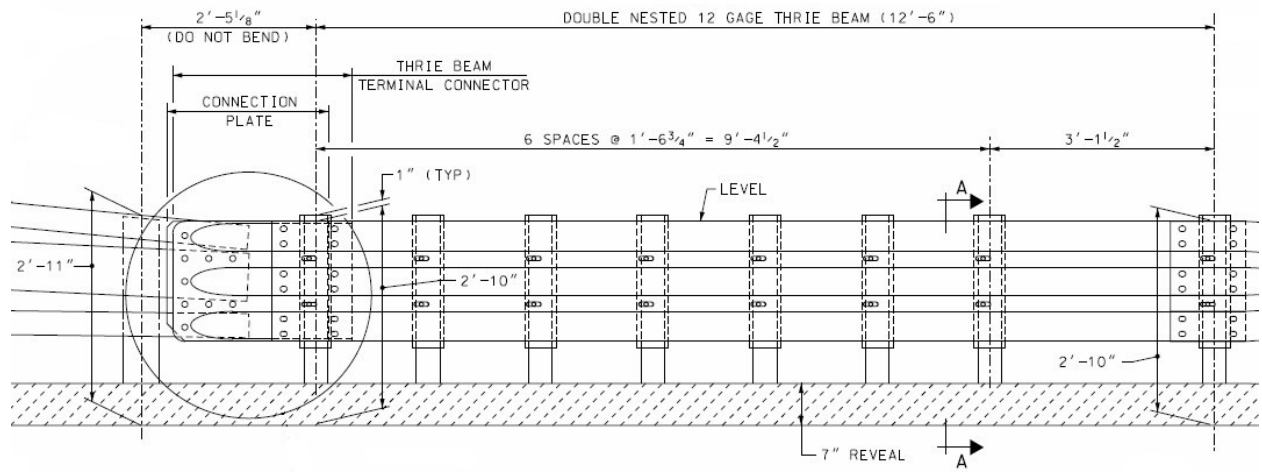


Figure 29. NHDOT T3 AGT double nested thrie-beam section.

The 6'-6" sloped rail section is shown in Figure 30. This section uses rail bars of the same material type and shape as used for the bridge rail. The slope for each rail bar in the transition section is provided in Table 49. The splice bars that connect the sloped section to the bridge rail are adjusted for slope and bend using complete joint penetration butt welds. The splice bar length and other details should match the details discussed in the bridge rail sections. The posts are set at 2'-2" spacing in this section. The sloped-rail section transitions the height of the system from 34 inches at the thrie-beam section to 44 inches at the bridge rail section.

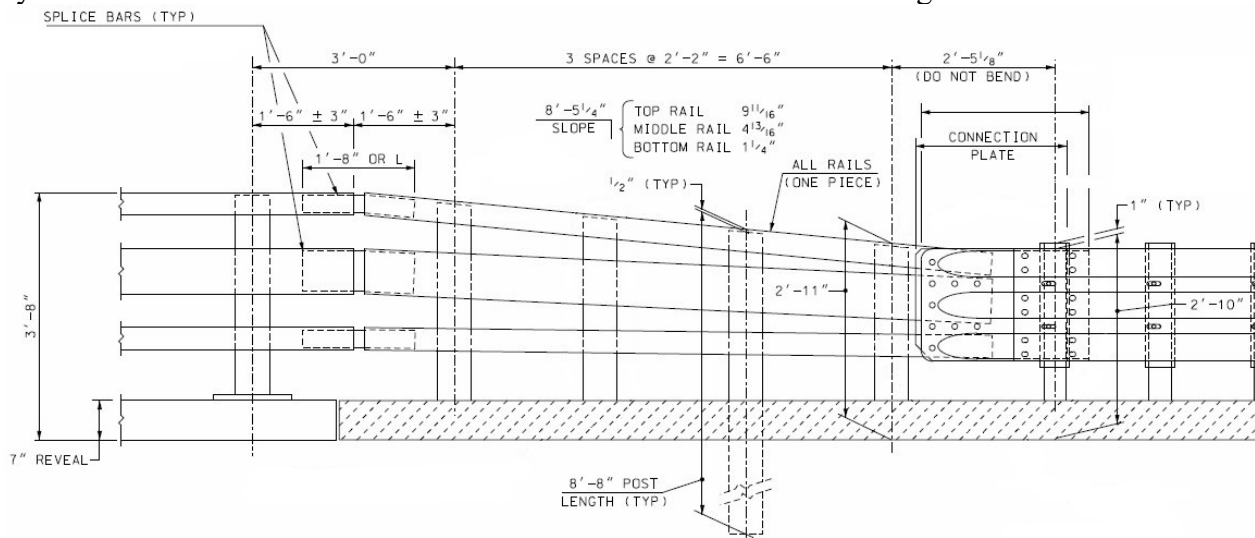


Figure 30. NHDOT T3 AGT sloped rail section.

Table 49. NHDOT T3 AGT slope of rail bar transition section.

	Top Bar	Middle Bar	Bottom Bar
Y Displacement	$9\frac{11}{16}$ "	$4\frac{13}{16}$ "	$1\frac{1}{4}$ "

X Displacement	$8'-5\frac{1}{4}''$	$8'-5\frac{1}{4}''$	$8'-5\frac{1}{4}''$
Slope (Y/X)	0.096	0.048	0.012

3.6.2.1 *Discrepancies in Drawing*

The same discrepancies that were discussed at the end of the NHDOT 2-bar transition section also apply to the NHDOT 3-bar transition drawings.

3.6.3 *MaineDOT 4-Bar Transition*

The detail drawing package provided to the research team contained designs for Type I and Type IA bridge rail transitions. The Type IA is discussed here since the upstream guardrail is specified to be a *MASH* compliant guardrail while the Type I only calls for a Type 3 guardrail. It is believed that the Type IA is required for *MASH* height requirements. A *MASH* compliant w-beam guardrail is used upstream of the AGT as seen in Figure 31. A 25'-0" section of guardrail is provided to match rail heights. Post spacing in this section is 6'-3" (e.g., standard post spacing). For the sidewalk mounted 4-bar bridge rail design there should be a sidewalk in this section, not shown in Figure 31.

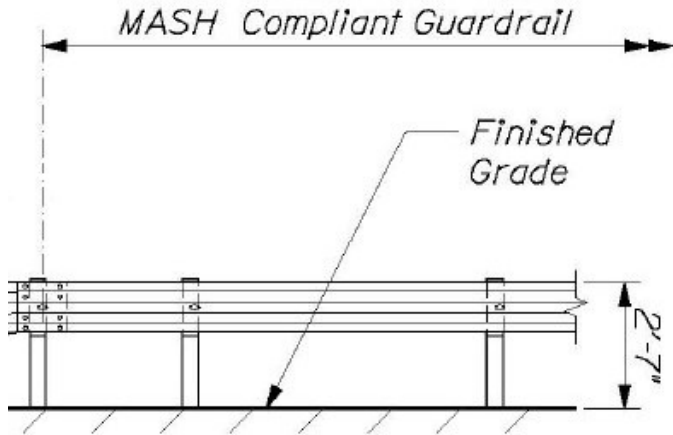


Figure 31. MaineDOT Type IA AGT upstream w-beam section.

An asymmetrical w-beam to thrie-beam transition rail is attached to the standard w-beam on the upstream end as seen in Figure 32. The transition rail is 6'-3" long and post spacing in this section is 3'-1.5" (e.g., half-post spacing). The height of the rail at the upstream end of the transition rail is 31 inches high.

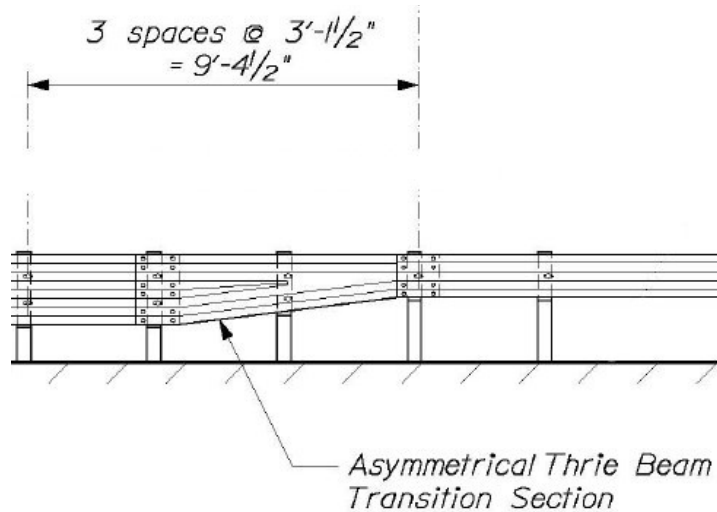


Figure 32. MainedOT Type IA AGT asymmetrical w-beam to thrie-beam transition section.

The next section is a 12'-6" long double nested 12-gauge thrie-beam section as seen in Figure 33. The first upstream post is spaced at 3'-1.5" (e.g., half-post spacing), while the other posts are spaced 1'-6.75" (quarter post spacing). A connection plate is used to connect the thrie-beam to the concrete buttress. In this section a precast concrete transition curb is used for the sidewalk, further details are found in the MainedOT Standard Specifications 609(08).

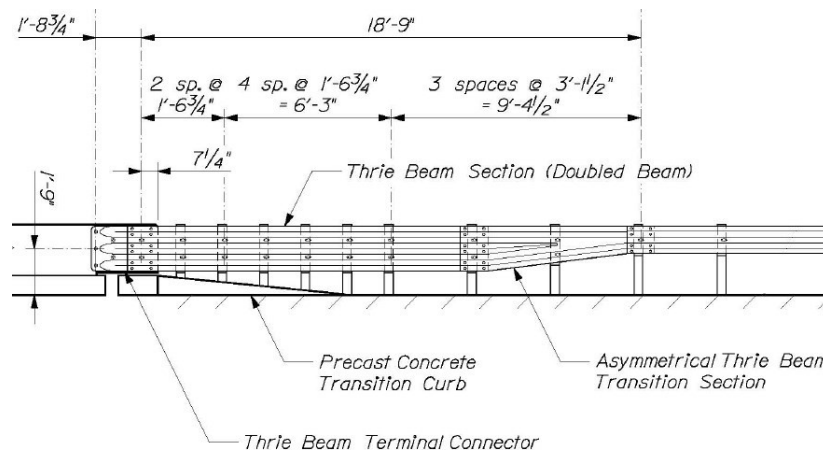


Figure 33. MainedOT Type IA AGT double nested thrie-beam section.

The 6'-4" concrete buttress section is shown in Figure 34. This section uses a concrete buttress constructed of 5000 psi Class LP concrete. Additional details for rebar placement are provided in the MainedOT Standard Specification 526(34-37). The guardrail anchorage bolts that connect to the connection plate are cast inside the buttress using a 1/4" thick guardrail anchor plate. The rail bars are placed into the concrete buttress recess. No hardware is specified to secure the rail bars to the concrete buttress. Other similar designs, such as the MassDOT concrete buttress AGT use studs that are adhesively attached to the buttress to secure the rails in place on the concrete end wall.

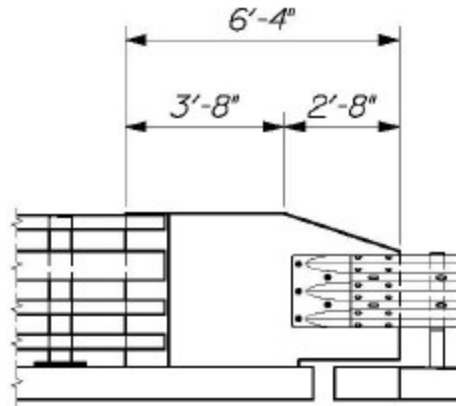


Figure 34. MaineDOT Type IA AGT concrete buttress section.

It is unlikely that the current design will meet *MASH TL4*, due to the potential for snagging on the end of the concrete buttress, which generally involves the tire of the vehicle pushing underneath the rail and impacting the buttress. Other crashworthy buttress designs have been evaluated and/or tested which may be adopted without further analysis. For example, the Midwest Roadside Safety Facility (MwRSF) recently designed and successfully tested a buttress design to *MASH TL3* in which the lower section of the buttress was beveled at the connection to the thrie-beam to prevent tire snag as the vehicle wheel pushes underneath the rail at the thrie-beam-to-buttress juncture. [Rosenbaugh18] As part of the MwRSF study, thirty-nine crash tests, involving 20 different transition systems, were reviewed. The majority of observed failures were the result of excessive vehicle contact with the rigid parapet, especially for AGTs that did not utilize a curb beneath the guardrail.

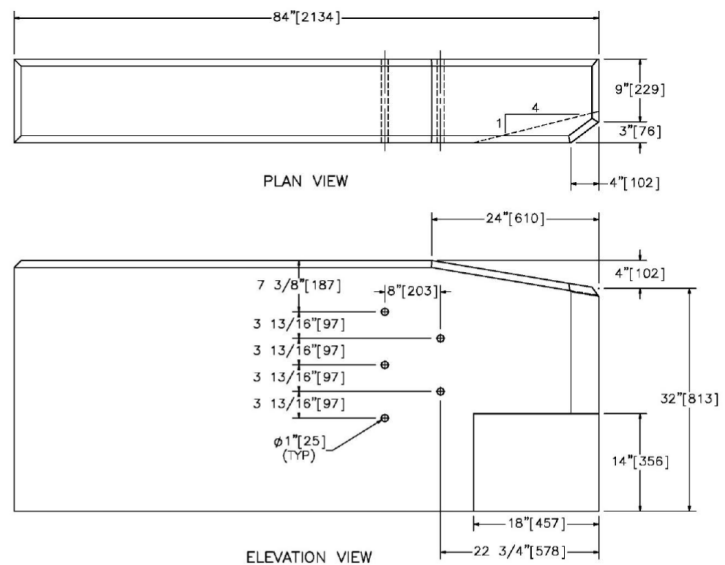
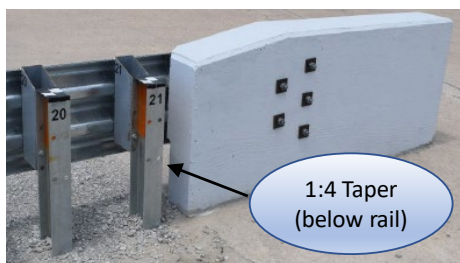


Figure 35. Standardized buttress design. [Rosenbaugh18]

In a recent study performed by Roadsafe LLC for the Massachusetts DOT, a transition system involving a flared face on the nose of the buttress, as illustrated in Figure 36, was evaluated. The results of that evaluation indicated that there was minimal risk for the vehicle to snag on the end of the buttress and that system would successfully meet *MASH TL3* conditions.

However, *MASH* TL4 compliance was uncertain due to difficulty identifying the CIP for Test 4-22. [Plaxico19] This system was also successfully evaluated in full-scale crash tests at the Texas Transportation Institute (TTI) under R350 Test Level 4 conditions. [Ross93; Alberson06]

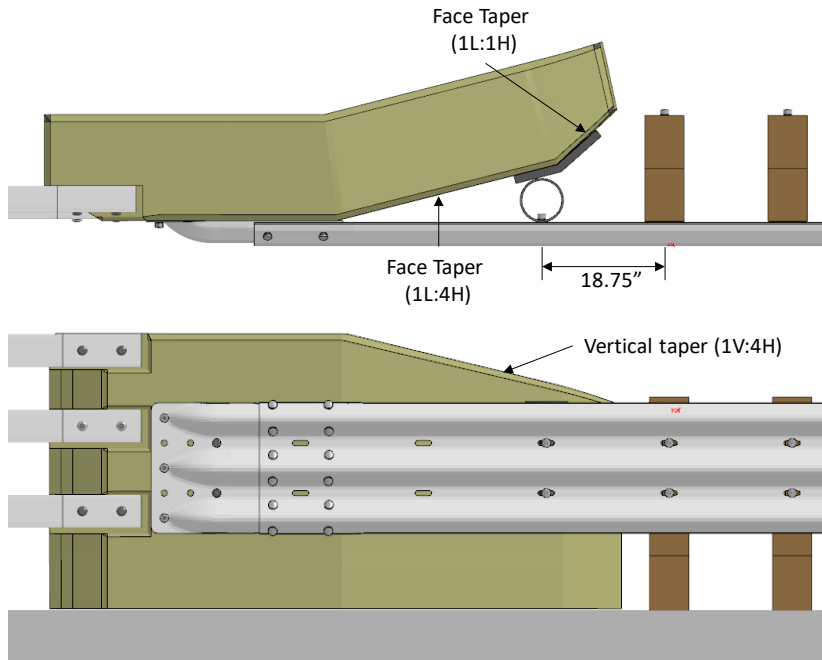


Figure 36. Plan and profile view of the shaped buttress.

3.6.4 Alternate 4-Bar Transition (Sloped Rail Style)

NHDOT and VTrans states provided engineering drawings for an alternate 4-bar AGT system that uses the sloped rail style, rather than the concrete buttress. The NHDOT T4 Steel Bridge Approach Rail was successfully crash tested in April 2005 by NETC and accepted as NCHRP 350 TL3. An FHWA acceptance letter was provided for the design, HSSD/B-146³.

Both designs utilize a standard 12-gauge w-beam roadway guardrail upstream of the AGT as seen in Figure 37. A 25'-0" section of guardrail flared at 80:1 to restore the rail-to-rail width. Post spacing in this section is 6'3" (e.g., standard post spacing) and the guardrails are lapped in the direction of traffic. The VTrans design includes a curb that is flared away from the roadway at a 10:1 rate and has a 4" reveal. The curb increases in height from 4" to 9" over approximately 6'. The NHDOT design is mounted on a sidewalk. The bottom bar on the NHDOT design continues from the bridge railing, through all transition sections and terminates behind the first upstream post in the guardrail section.

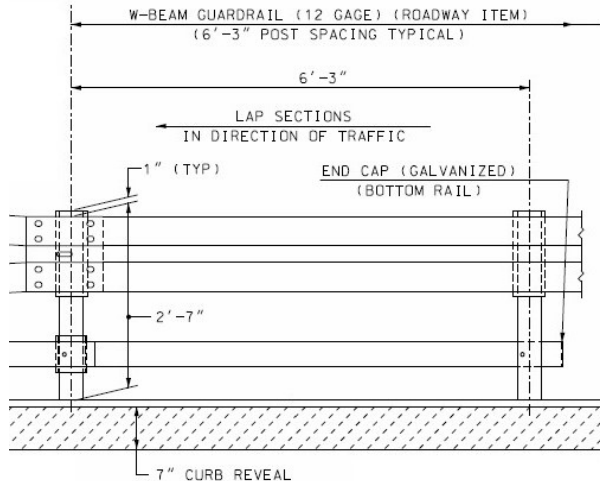


Figure 37. NHDOT T4 AGT upstream w-beam section (VTrans similar except bottom bar and sidewalk).

A symmetrical w-beam to thrie-beam transition rail is attached to the standard w-beam on the upstream end as seen in Figure 38. NHDOT specifies a 10-gauge transition rail and VTrans specifies a 12-gauge transition rail. The transition rails are 6'-3" long and post spacing in this section is 3'-1.5" (e.g., half post spacing). For the NHDOT design the height of the rail at the upstream end of the thrie-beam transition rail is 31 inches high and is 34 inches at the downstream end. For the VTrans design the height of the rail at the upstream end of the thrie-beam transition rail is 27 inches high and is 33-5/16 inches high at the downstream end.

The next section of the NHDOT design is a 12'-6" long double nested 12-gauge thrie-beam section as seen in Figure 39. The first upstream post is spaced at 3'-1.5" (e.g., half-post spacing), while the other posts are spaced 1'-6.75" (e.g., quarter post spacing). A connection plate is used to connect the thrie-beam to the top and bottom sloped bridge rails. The deflector plate, which is specified in the 2-bar design (see Figure 24), is not present in the 4-bar design. The VTrans design does not include a thrie-beam section.

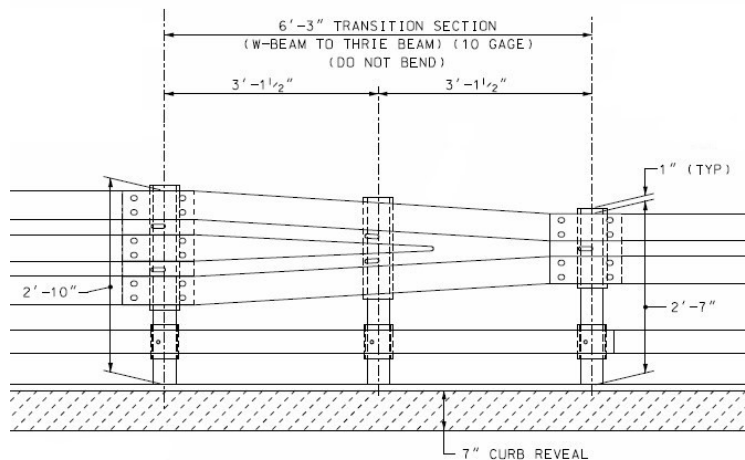


Figure 38. NHDOT T4 AGT symmetrical w-beam to thrie-beam transition section (VTrans similar except bottom bar and height).

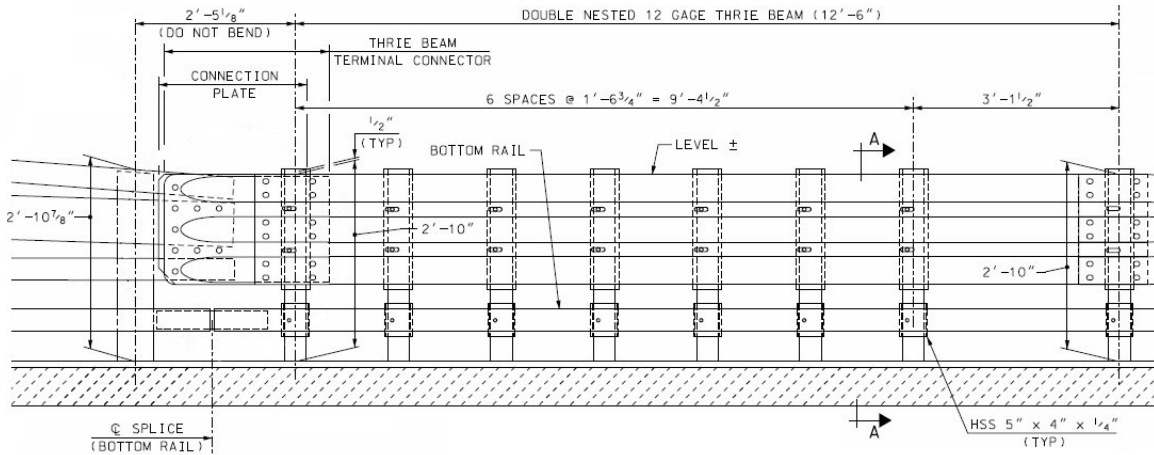


Figure 39. NHDOT T4 AGT double nested thrie-beam section.

The sloped rail sections differ greatly between NHDOT (Figure 40) and VTrans (Figure 41). The distance of the sloped section is approximately 8' for NHDOT and 22'8" for VTrans. The designs use rail bars of the same material type and shape as used for the bridge rail. The splice bars that connect the sloped section to the bridge rail are adjusted for slope and bend using complete joint penetration butt welds. The splice bar length and other details match the details discussed in the bridge rail sections. The NHDOT design uses 2'-2" post spacing, while the VTrans design uses decreasing spacing in the following order:

- 1 space at 4'-8"
- 3 spaces at 3'-2"
- 3 spaces at 2'-2"

The bottom rail on the VTrans design terminates at the bottom rail in the post web section (i.e. between the post flanges) of Post #8. As mentioned earlier the NHDOT design carries the bottom rail all the way through the AGT and terminates it at the guardrail. The slope for each rail bar in the both transition sections is provided in Table 50

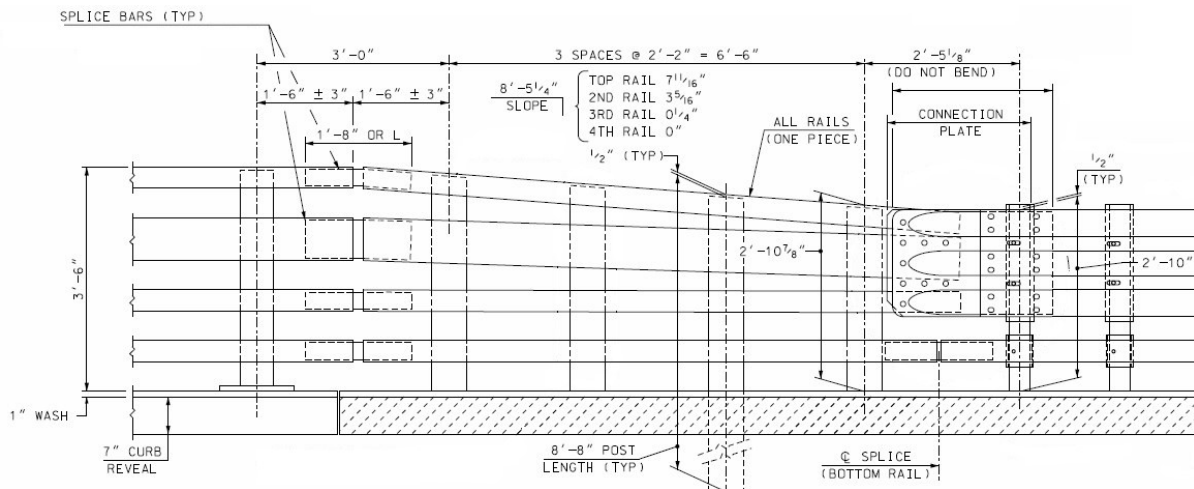


Figure 40. NHDOT T4 AGT sloped rail section.

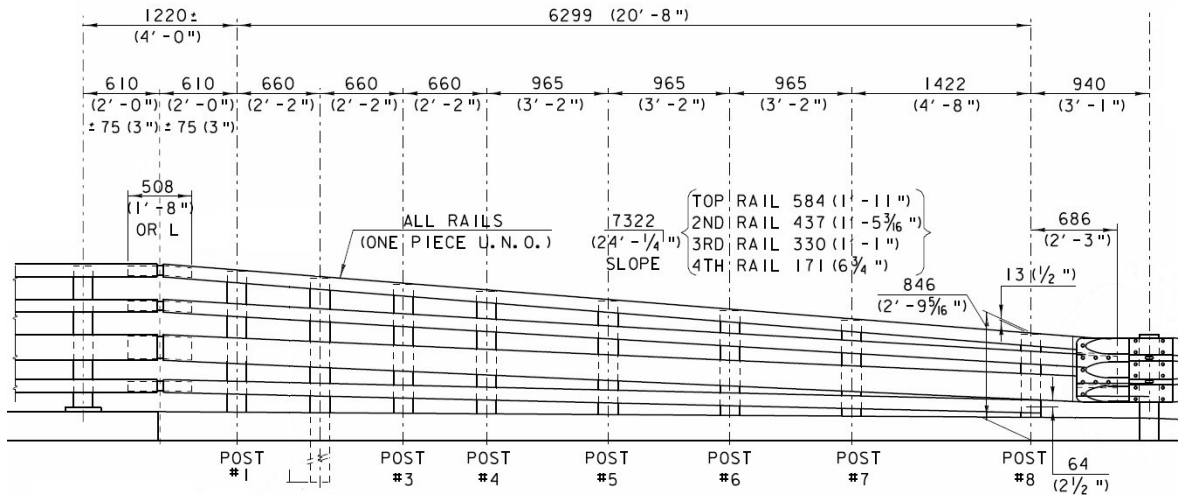


Figure 41. VTrans 4-bar AGT sloped rail section.

Table 50. NHDOT T4 and VTrans 4-bar AGT slope of rail bar transition section.

	Top Bar		Mid-Top Bar		Mid-Btm Bar		Bottom Bar	
	NH	VT	NH	VT	NH	VT	NH	VT
Y Displacement	7 ¹¹ / ₁₆ "	1'-11"	3 ⁵ / ₁₆ "	1'-5 ³ / ₁₆ "	1 ¹ / ₄ "	1'-1"	0"	6 ³ / ₄ "
X Displacement	8'-5 ¹ / ₄ "	24'-1 ¹ / ₄ "	8'-5 ¹ / ₄ "	24'-1 ¹ / ₄ "	8'-5 ¹ / ₄ "	24'-1 ¹ / ₄ "	8'-5 ¹ / ₄ "	24'-1 ¹ / ₄ "
Slope (Y/X)	0.076	0.080	0.033	0.060	0.002	0.045	0.00	0.023

4 RECOMMENDATIONS FOR DIMENSIONAL AND MATERIAL SPECIFICATIONS

4.1 NETC Bridge Rail Designs

The following recommendations are based on using the least conservative value for each design detail which has shown acceptable NCHRP Report 350 crash testing performance and/or met the LRFD strength criteria for *MASH* loading. Table 51 summarizes the research team's recommendations for specific details for the NETC style bridge rails. The sidewalk-mounted 4-bar bridge railing was shown to be borderline regarding strength requirements for *MASH* TL4 but was, however, expected to meet *MASH* TL3 performance criteria based on LRFD strength calculations for those cases (not shown herein). It was therefore recommended that it be included for further evaluation with FEA crash simulation for both TL3 and TL4 conditions.

Table 51. Summary of recommended specifications for NETC style bridge rails.

Feature	2-Bar Bridge Rail	3-Bar Bridge Rail	4-Bar Bridge Rail
Rail Bars			
Material	ASTM A500 Gr. B	ASTM A500 Gr. B	ASTM A500 Gr. B
Sizes	HSS 4" x 4" x $\frac{1}{4}$ " HSS 8" x 4" x $\frac{5}{16}$ "	HSS 4" x 4" x $\frac{1}{4}$ " HSS 8" x 4" x $\frac{5}{16}$ "	HSS 4" x 4" x $\frac{1}{4}$ " HSS 8" x 4" x $\frac{5}{16}$ "
Order of Bars (from top)	Lg – Sm	Sm – Lg – Sm	Sm – Lg – Sm – Sm
1 st Bar Height (to top)	34"	44"	42"
2 nd Bar Height (center)	18"	30"	28"
3 rd Bar Height (center)	N/A	18"	16.5"
4 th Bar Height (center)	N/A	N/A	7"
Post			
Material	AASHTO M270 Gr 50	AASHTO M270 Gr 50	AASHTO M270 Gr 50
Size	W6x25	W6x25	W6x25
Vertical Alignment	Normal to grade	Normal to grade	Normal to grade
Max Spacing	8'-0"	8'-0"	8'-0"
Number of Posts/Rail	3	3	3
Min Offset from Post to Expansion Splice	2'-0"	2'-0"	2'-0"
Post Flange to Baseplate Weld	$\frac{7}{16}$ " all around fillet weld	$\frac{7}{16}$ " all around fillet weld	$\frac{7}{16}$ " all around fillet weld
Post Web to Baseplate Weld	$\frac{5}{16}$ " all around fillet weld	$\frac{5}{16}$ " all around fillet weld	$\frac{5}{16}$ " all around fillet weld
Rail Bar-Post Attachment			
Method	Bolted	Bolted	Bolted
Number of Bolts/Rail	2	2	2
Hole Size in Rail	$\frac{7}{8}$ "	$\frac{7}{8}$ "	$\frac{7}{8}$ "
Hole Size in Post	1 $\frac{1}{8}$ " x 1 $\frac{3}{8}$ " slotted hole	1 $\frac{1}{8}$ " x 1 $\frac{3}{8}$ " slotted hole	1 $\frac{1}{8}$ " x 1 $\frac{3}{8}$ " slotted hole

Bolt Specification	6" x $\frac{3}{4}$ " A325	6" x $\frac{3}{4}$ " A325	6" x $\frac{3}{4}$ " A325
--------------------	---------------------------	---------------------------	---------------------------

Baseplate

Material	ASHTO M270 Gr. 50	ASHTO M270 Gr. 50	ASHTO M270 Gr. 50
Size	1" x 10" x 1'-2"	1" x 10" x 1'-2"	1" x 10" x 1'-2"
Number of Bolts	4	4	4
Bolt Pattern	See MaineDOT details	See MaineDOT details	See MaineDOT details
Size of Holes	1.25"	1.25"	1.25"

Anchor Bolts

Material	ASTM A449	ASTM A449	ASTM A449
Size	1" Ø x 12" L	1" Ø x 12" L	1" Ø x 12" L
Embedment	7.5"	7.5"	7.5"
Exposed Rod	3"	3"	3"
Threaded Length	2.5	2.5	2.5
Exposed Nut Type	Heavy hex nut	Heavy hex nut	Heavy hex nut
Nut Torque	Snug + $\frac{1}{8}$ turn	Snug + $\frac{1}{8}$ turn	Snug + $\frac{1}{8}$ turn

Field Splice

Tube Dimensions	HSS 3" x 3" x $\frac{5}{16}$ " HSS 7" x 3" x $\frac{3}{8}$ "	HSS 3" x 3" x $\frac{5}{16}$ " HSS 7" x 3" x $\frac{3}{8}$ "	HSS 3" x 3" x $\frac{5}{16}$ " HSS 7" x 3" x $\frac{3}{8}$ "
Details	See MaineDOT details	See MaineDOT details	See MaineDOT details
Number of Bolts	4	4	4
Size of Hole in Rail	1 $\frac{1}{8}$ " x 2 $\frac{1}{2}$ " slot	1 $\frac{1}{8}$ " x 2 $\frac{1}{2}$ " slot	1 $\frac{1}{8}$ " x 2 $\frac{1}{2}$ " slot
Hole in Splice Tube	$\frac{5}{8}$ " Ø tapped hole	$\frac{5}{8}$ " Ø tapped hole	$\frac{5}{8}$ " Ø tapped hole
Bolt	$\frac{5}{8}$ " Ø x 1 $\frac{3}{4}$ " Cap Screw	$\frac{5}{8}$ " Ø x 1 $\frac{3}{4}$ " Cap Screw	$\frac{5}{8}$ " Ø x 1 $\frac{3}{4}$ " Cap Screw
Tack Weld Nut Required?	On outer holes only	On outer holes only	On outer holes only
Pipe Spacer	$\frac{3}{4}$ " Ø x $\frac{1}{2}$ " Schd. 40 (Only 1 side ea splice)	$\frac{3}{4}$ " Ø x $\frac{1}{2}$ " Schd. 40 (Only 1 side ea splice)	$\frac{3}{4}$ " Ø x $\frac{1}{2}$ " Schd. 40 (Only 1 side ea splice)
Space Between Bars	$\frac{3}{4}$ "	$\frac{3}{4}$ "	$\frac{3}{4}$ "
Splice Tube Length	1'-8"	1'-8"	1'-8"

Drain Hole Required?	Yes, $\frac{1}{2}$ " \varnothing	Yes, $\frac{1}{2}$ " \varnothing	Yes, $\frac{1}{2}$ " \varnothing
----------------------	------------------------------------	------------------------------------	------------------------------------

Expansion Splice

Tube Dimensions	HSS 3" x 3" x $\frac{5}{16}$ " HSS 7" x 3" x $\frac{3}{8}$ "	HSS 3" x 3" x $\frac{5}{16}$ " HSS 7" x 3" x $\frac{3}{8}$ "	HSS 3" x 3" x $\frac{5}{16}$ " HSS 7" x 3" x $\frac{3}{8}$ "
Details	See MaineDOT details	See MaineDOT details	See MaineDOT details
Number of Bolts	4	4	4
Size of Hole in Rail	See MaineDOT details	See MaineDOT details	See MaineDOT details
Hole in Splice Tube	$\frac{5}{8}$ " \varnothing tapped hole	$\frac{5}{8}$ " \varnothing tapped hole	$\frac{5}{8}$ " \varnothing tapped hole
Bolt	$\frac{5}{8}$ " \varnothing x $1\frac{3}{4}$ " Cap Screw	$\frac{5}{8}$ " \varnothing x $1\frac{3}{4}$ " Cap Screw	$\frac{5}{8}$ " \varnothing x $1\frac{3}{4}$ " Cap Screw
Tack Weld Nut Required?	On outer holes only	On outer holes only	On outer holes only
Pipe Spacer	$\frac{3}{4}$ " \varnothing x $\frac{1}{2}$ " Schd. 40	$\frac{3}{4}$ " \varnothing x $\frac{1}{2}$ " Schd. 40	$\frac{3}{4}$ " \varnothing x $\frac{1}{2}$ " Schd. 40
Space Between Bars	See MaineDOT details	See MaineDOT details	See MaineDOT details
Splice Tube Length	See MaineDOT details	See MaineDOT details	See MaineDOT details
Drain Hole Required?	Yes, $\frac{1}{2}$ " \varnothing	Yes, $\frac{1}{2}$ " \varnothing	Yes, $\frac{1}{2}$ " \varnothing

Concrete Curb/Sidewalk

Strength Required	4000 psi	4000 psi	4000 psi
Height	7"	7"	9"
Width	1'-6"	1'-6"	5' min.
Back Baseplate Bolts to Deck Edge	7 $\frac{5}{8}$ "	7 $\frac{5}{8}$ "	7 $\frac{5}{8}$ "
Front Baseplate Bolts to Concrete Edge	4"	4"	5'-2"
Longitudinal Rebar	3 - #5 bars 5' L min	3 - #5 bars 5' L min	3 - #5 bars 5' L min
Hoop Bar Rebar	7 - #5 bars at 6"	7 - #5 bars at 6"	7 - #5 bars at 6"
Hoop Bar Engagement w/ Deck Rebar?	Yes	Yes	Yes

4.2 NETC Approach Guardrail Transition Designs

Table 52 outlines the features, materials and dimensional specifications for the selected AGTs.

Table 52. Summary of recommended specifications for NETC style bridge rail transitions.

Feature	NH T2 AGT	NH T3 AGT	MaineDOT AGT
Approach Curb			
Upstream Reveal	4"	4"	
Flare Rate	10:1 away from road	10:1 away from road	
Curb Full Height	7"	7"	
Curb Face to Thrie Beam	2 $\frac{1}{4}$ "	2 $\frac{1}{4}$ "	N.S.
Curb Face to Face of Rail	6"	6"	N.S.
Height from Top of Curb to Bottom of Thrie Beam	3"	3"	N.S.
Strength	4000 psi	4000 psi	5000 psi
Roadway Guardrail Section			
Guardrail Type	12-gauge w-beam	12-gauge w-beam	<i>MASH</i> Compliant
Guardrail Specification	AASHTO M180 Type II, Class A	AASHTO M180 Type II, Class A	N.S.
Flare Back	80:1 for 25'-0" to restore rail-to-rail W	80:1 for 25'-0" to restore rail-to-rail W	25' - As required to match rail heights
Post Type	W6x8.5	W6x8.5	N.S.
Post Material	ASTM A36	ASTM A36	N.S.
Post Spacing	6'-3"	6'-3"	6'-3"
Block-out Type	Synthetic	Synthetic	Composite or wood
Post Length	7'-0"	7'-0"	N.S.
Rail Height	2'-7"	2'-7"	2'-7"
W-Beam to Thrie Beam Transition Section			
Transition Type	10-gauge symmetrical	10-gauge symmetrical	10-ga asymmetrical
Transition Specification	AASHTO M180 Type II, Class A	AASHTO M180 Type II, Class A	N.S.
Total Transition Length	7'-3 $\frac{1}{4}$ "	7'-3 $\frac{1}{4}$ "	N.S.

Post Attachment Hole Size	$\frac{3}{4}$ " x $2\frac{1}{2}$ " slot	$\frac{3}{4}$ " x $2\frac{1}{2}$ " slot	N.S.
Post Attachment Hardware	$\frac{5}{8}$ " \emptyset A307 button head post bolts with washer	$\frac{5}{8}$ " \emptyset A307 button head post bolts with washer	N.S.
W-Beam Hole Size	$\frac{29}{32}$ " x $1\frac{1}{8}$ " slot	$\frac{29}{32}$ " x $1\frac{1}{8}$ " slot	N.S.
W-Beam Hardware	$\frac{5}{8}$ " \emptyset A307 button head splice bolts	$\frac{5}{8}$ " \emptyset A307 button head splice bolts	N.S.
Thrie Beam Attachment Hole Size	$\frac{29}{32}$ " x $1\frac{1}{8}$ " slot	$\frac{29}{32}$ " x $1\frac{1}{8}$ " slot	N.S.
Thrie Beam Attachment Hardware	$\frac{5}{8}$ " \emptyset A307 button head splice bolts	$\frac{5}{8}$ " \emptyset A307 button head splice bolts	N.S.
Post Type	W6x8.5	W6x8.5	N.S.
Post Material	ASTM A36	ASTM A36	N.S.
Post Spacing	3'- $1\frac{1}{2}$ "	3'- $1\frac{1}{2}$ "	3'- $1\frac{1}{2}$ "
Block-Out Type	Synthetic	Synthetic	N.S.
Block-Out Size	8" deep x 1'-6" long	8" deep x 1'-6" long	N.S.
Post Length	7'-0"	7'-0"	N.S.
Upstream Rail Height	2'-7"	2'-7"	2'-7"
Downstream Rail Height	2'-10"	2'-10"	2'-7"

Thrie Beam Section

Thrie Beam Configuration	Double nested 12-gauge	Double nested 12-gauge	Double beam
Thrie Beam Specification	AASHTO M180 Type II, Class A	AASHTO M180 Type II, Class A	N.S.
Total Thrie Beam Section Length	12'-6"	12'-6"	12'-0"
Post Attachment Hole Size	$\frac{3}{4}$ " x $2\frac{1}{2}$ " slot	$\frac{3}{4}$ " x $2\frac{1}{2}$ " slot	N.S.
Post Attachment Hardware	$\frac{5}{8}$ " \emptyset A307 button head post bolts	$\frac{5}{8}$ " \emptyset A307 button head post bolts	N.S.
Thrie Beam Attachment Hole Size	$\frac{29}{32}$ " x $1\frac{1}{8}$ " slot	$\frac{29}{32}$ " x $1\frac{1}{8}$ " slot	N.S.
Thrie Beam Attachment Hardware	$\frac{5}{8}$ " \emptyset A307 button head splice bolts	$\frac{5}{8}$ " \emptyset A307 button head splice bolts	N.S.

Post Type	W6x8.5	W6x8.5	N.S.
Post Material	ASTM A36	ASTM A36	N.S.
Post Spacing	One @ 3'-1 $\frac{1}{2}$ " Six @ 1'-6 $\frac{3}{4}$ "	One @ 3'-1 $\frac{1}{2}$ " Six @ 1'-6 $\frac{3}{4}$ "	One @ 3'-1 $\frac{1}{2}$ " Six @ 1'-6 $\frac{3}{4}$ "
Block-Out Type	Synthetic	Synthetic	N.S.
Block-Out Size	8" deep x 1'-10" long	8" deep x 1'-10" long	N.S.
Post Length	7'-0"	7'-0"	N.S.
Rail Height	2'-10"	2'-10"	2'-7"

Connection Plate

Connection Plate Size	$\frac{3}{8}$ " thick x 27" x 20"	$\frac{3}{8}$ " thick x 27" x 20"	$\frac{1}{4}$ " thick x 11 $\frac{1}{4}$ " x 1'-6 $\frac{1}{2}$ ", cast 6 $\frac{1}{2}$ " deep in buttress
Connection Plate Material	Grade 36	Grade 36	N.S.
Thrie Beam Terminal Connector Size	3 $\frac{3}{8}$ " deep x 30" x 20"	3 $\frac{3}{8}$ " deep x 30" x 20"	N.S.
Order of Components (from Traffic Side)	Thrie beam terminal connector – connection plate – sloped bridge rails	Thrie beam terminal connector – connection plate – sloped bridge rails	Thrie beam terminal connector – concrete buttress – anchor plate
Thrie Beam to Terminal Connector Hole	1" x 2" diagonal slots	1" x 2" diagonal slots	N.S.
Thrie Beam to Terminal Connector Bolt	$\frac{5}{8}$ " Ø A307 button head splice bolts	$\frac{5}{8}$ " Ø A307 button head splice bolts	N.S.
Clamping Hardware Hole Size	1" Ø hole	1" Ø hole	N.S.
Clamping Bolt Type	$\frac{3}{4}$ " Ø button head, various lengths (or carriage bolt)	$\frac{3}{4}$ " Ø button head, various lengths (or carriage bolt)	$\frac{7}{8}$ " Ø x 8" L A325 bolts cast in buttress
Deflector Plate	$\frac{3}{8}$ " bent @ $\frac{3}{4}$ " radius	--	--
Upstream Post Type	W6x8.5	W6x8.5	N.S.
Upstream Post Material	ASTM A36	ASTM A36	N.S.
Upstream Post Block-Out Material	Synthetic	Synthetic	N.S.
Upstream Post Block-Out Size	8" deep x 1'-10" long	8" deep x 1'-10" long	N.S.

Upstream Post Length	7'-0"	7'-0"	N.S.
Upstream Rail Height	2'-10"	2'-10"	2'-7"
Downstream Post Type	W6x25	W6x25	--
Downstream Post Material	ASTM A572 Gr 50	ASTM A572 Gr 50	--
Downstream Block-Out	None	None	--
Downstream Post Length	8'-0"	8'-8"	--
Downstream Rail Height	2'-10"	2'-11"	3'-6 $\frac{1}{2}$ "
Post Spacing	2'-5 $\frac{1}{8}$ "	2'-5 $\frac{1}{8}$ "	--

Sloped Rail/Concrete Buttress Section

Bar Material	ASTM A500 Gr B	ASTM A500 Gr B	--
Bar Size	HSS 4 x 4" x $\frac{1}{4}$ " HSS 8" x 4" x $\frac{5}{16}$ "	HSS 4" x 4" x $\frac{1}{4}$ " HSS 8" x 4" x $\frac{5}{16}$ "	--
Sloped Bar Length	8'-5 $\frac{1}{4}$ "	8'-5 $\frac{1}{4}$ "	--
Top Bar Vertical Displacement	0"	9 $\frac{11}{16}$ "	--
Top Bar Slope	0.000	0.096	--
Mid Bar Vertical Displacement	--	4 $\frac{13}{16}$ "	--
Mid Bar Slope	--	0.048	--
Bottom Bar Vertical Displacement	-1 $\frac{3}{16}$ "	1 $\frac{1}{4}$ "	--
Bottom Bar Slope	-0.012	0.012	--
Rail-to-Post Attachment Preferred Method	Bolted	Bolted	--
Rail-to-Post Attachment Hole in Rail	$\frac{7}{8}$ "	$\frac{7}{8}$ "	--
Rail-to-Post Attachment Hole in Post	1 $\frac{1}{8}$ " x 1 $\frac{3}{8}$ " slotted hole	1 $\frac{1}{8}$ " x 1 $\frac{3}{8}$ " slotted hole	--
Rail-to-Post Attachment Bolt Specification	6" x $\frac{3}{4}$ " A325	6" x $\frac{3}{4}$ " A325	--
Post Type	W6x25	W6x25	--
Post Material	ASTM A572 Gr 50	ASTM A572 Gr 50	--
Block-Out	None	None	--
Post Length	8'-0"	8'-8"	--

Upstream Rail Height	2'-10"	2'-11"	--
Downstream Rail Height	2'-10"	3'-8"	--
Post Spacing	2'-2"	2'-2"	--
Buttress Width	--	--	1'-7"
Buttress Length	--	--	6'-4"
Upstream Buttress Height	--	--	2'-8"
Downstream Buttress Height	--	--	3'-6"
Slope	--	--	~0.303
Recess Depth	--	--	5"
Recess Height	--	--	3'-6" (full height)
Rail Bar Attachment to Buttress	--	--	None
Rebar Detail	--	--	Shown in 526(34-37)

Bridge Rail Splice Bar Section

Splice Bar Size	HSS 3" x 3" x $\frac{5}{16}$ " HSS 7" x 3" x $\frac{3}{8}$ "	HSS 3" x 3" x $\frac{5}{16}$ " HSS 7" x 3" x $\frac{3}{8}$ "	--
Splice Bar Material	ASTM A500 Gr B	ASTM A500 Gr B	--
Splice Bar Length	1'-8" or L	1'-8" or L	--
Splice Bar Configuration	Adjusted for slope using complete joint penetration butt welds	Adjusted for slope using complete joint penetration butt welds	--
Upstream Post Type	W6x25	W6x25	--
Upstream Post Material	ASTM A572 Gr 50	ASTM A572 Gr 50	--
Upstream Post Length	8'-0"	8'-8"	--
Upstream Rail Height	2'-10"	Less than 3'-8"	--
Downstream Post Type	W6x25	W6x25	--
Downstream Post Material	ASTM A572 Gr 50	ASTM A572 Gr 50	--
Downstream Post Length	2'-1 $\frac{3}{8}$ " welded to baseplate bolted to bridge	2'-11 $\frac{3}{8}$ " welded to baseplate bolted to bridge	--
Downstream Rail Height	2'-10"	3'-8"	--
Post Spacing	3'-0"	3'-0"	--

4.3 Summary

A critical review of current standard details and specifications for NETC style bridge rails and transitions used by MaineDOT, NHDOT, RIDOT and VTrans was performed to (1) determine *MASH* equivalency for each State's design per Section 13 of the AASHTO *LRFD Bridge Design Specifications [AASHTO12]*, and (2) identify differences in material and dimensional details for each state's design. Preliminary recommendations for standardized designs were then provided based on the review to better ensure consistency for NETC style designs, considering constructability and performance. The crash performance of the recommended designs will be further evaluated based on *MASH* crash testing conditions and criteria using finite element analysis in subsequent tasks of this study.

In most cases, the recommendations included the least conservative value for each design detail, which has either shown acceptable R350 crash testing performance or met the LRFD strength criteria for *MASH* loading. The one exception was the sidewalk-mounted 4-bar design, in which the least conservative design (i.e., 4,000 psi concrete) did not meet the current recommended strength requirements based on LRFD calculations, but was selected for further evaluation using finite element analysis to determine crash performance (e.g., *MASH* TL3 or TL4). If the FEA results indicate that these designs meet *MASH* requirements, then it would follow that the more conservative design details would meet those requirements as well.

Redesign of the bridge rail systems was not a primary focus of this study; however, in some cases general recommendations for design improvements were provided that the research team believes would further improve crash performance.

5 FEA VEHICLE MODELS

The vehicle models used in the crash performance evaluations include:

- NCHRP Report 350 crash simulation cases:
 - C2500D version 5b (Revision 160309)
 - F800 version 181114 ballasted to 8,000 kg (i.e., 8000S vehicle with modified bed-height)
- *MASH* crash simulation cases:
 - YarisC version 1L (i.e., 1100C vehicle)
 - SilveradoC_v3a (i.e., 2270P vehicle)
 - F800 version 170809 ballasted to 10,000 kg (i.e., 10,000S vehicle).

The model for the 2000P vehicle used for NCHRP Report 350 analysis cases was the NCAC C2500D version 5B. This model has been used extensively over the past decade in simulating R350 TL3 impact scenarios with great success. [*Plaxico06; Plaxico07; Marzougui08; Marzougui10; Plaxico15; Plaxico16*] It has also been validated against NHTSA end-cap tests [*Zaouk96*].

The models for the 1100C and 2270P vehicles used for the *MASH* analysis cases were the YarisC_v1L model (based on a 2010 Toyota Yaris) and the SilveradoC_v3a model (based on a 2007 quad-cab Chevy Silverado). These vehicles closely represent the two test vehicles specified in *MASH*. [*AASHTO16*] The vehicle models were developed through the process of

reverse engineering by the members of George Mason University (GMU) and were initially validated based on NCAP frontal wall impact tests through comparison with NHTSA test data.[*Marzougui08*] The models also include validated suspension and steering subsystems.[*Marzougui10*] The Silverado model has been continually improved by GMU as well as the user community since its development and has been used successfully in several studies involving crash analysis with roadside safety hardware. The Silverado model, however, tends to over-predict lateral acceleration magnitude during the backslap of the vehicle when impacting rigid barriers compared to full-scale crash tests. It is not clearly understood why this occurs, but it is assumed that cause is in part because the rear suspension of the test vehicles (i.e., Dodge Ram) is fundamentally different from that of the Silverado model.

Additional modifications were made to the 2270P model for this study, which included changing the material characterization for some of the parts that were previously modeled as “rigid” (e.g., wheel rims and various suspension components) to an appropriate steel material (characterized as *Mat_24 in LS-DYNA) corresponding to the specific part. Based on preliminary results of the vehicle traversing the 8-inch tall curb and sidewalk, further modifications were incorporated for the tire model based on the work by Orengo et al. and Reid et al. [*Orengo03; Reid06*] The Yaris model has not been used as much as the Silverado but is expected to provide reasonable results. Validation PIRTs for these models were provided by George Mason University and are included with this report as Appendix E and Appendix F.

The baseline model for the 8000S and the 10000S single unit truck vehicle was developed at the National Crash Analysis Center (NCAC) in Ashburn, Virginia. This model was further modified by various researchers over the years to improve its fidelity in analysis of impact conditions corresponding to NCHRP Report 350 Test 4-12. [*Miele05; Mohan07; Plaxico13*] Additional modifications to the baseline model made in this study included remeshing of several parts in the crush zone of the vehicle and changing the element type to the fully integrated shell element (i.e., type 16 in LS-DYNA). The model of the ballast was calibrated to the mass inertial properties of the test vehicle specifications (e.g., 8000S and 10000S as appropriate). In particular, the ballast type was modeled based on a recent test vehicle used by the Texas Transportation Institute (TTI) in full-scale test number 607451-1 [*Williams17b*]. The ballast included two rigid blocks with dimensions 60 inches wide x 30 inches long x 30 inches tall, positioned one behind the other, and the ballasts were fastened to the truck frame rail using a series of cables. The positioning of the ballast model inside the cargo box for the 8000S and the 10000S vehicle models was determined based on the reported centers of gravity of the vehicles used in the R350 test series which are being used for model validation (i.e., Test 404251-3 (8000S) and Test 404251-6 (8000S)), and a recent *MASH* Test 4-12 test performed at TTI using a 10000S vehicle.[*Buth99a; Williams17b*]

Additional modifications to the SUT model included replacing the cargo box on the baseline model with a more detailed model with better geometric and material fidelity, as shown in Figure 42. Based on visual inspection of several single unit truck boxes, it was decided that the basic structure for the cargo box model would be adopted from an existing semitrailer model and subsequently modified to match the external dimensions of the existing baseline model. An overview of the various components that were included in the model, as well as their corresponding dimensions and material assignments can be found in [*Plaxico19*]. Further details regarding the development of this box structure can be found in the literature. [*Plaxico09; Miele10*]

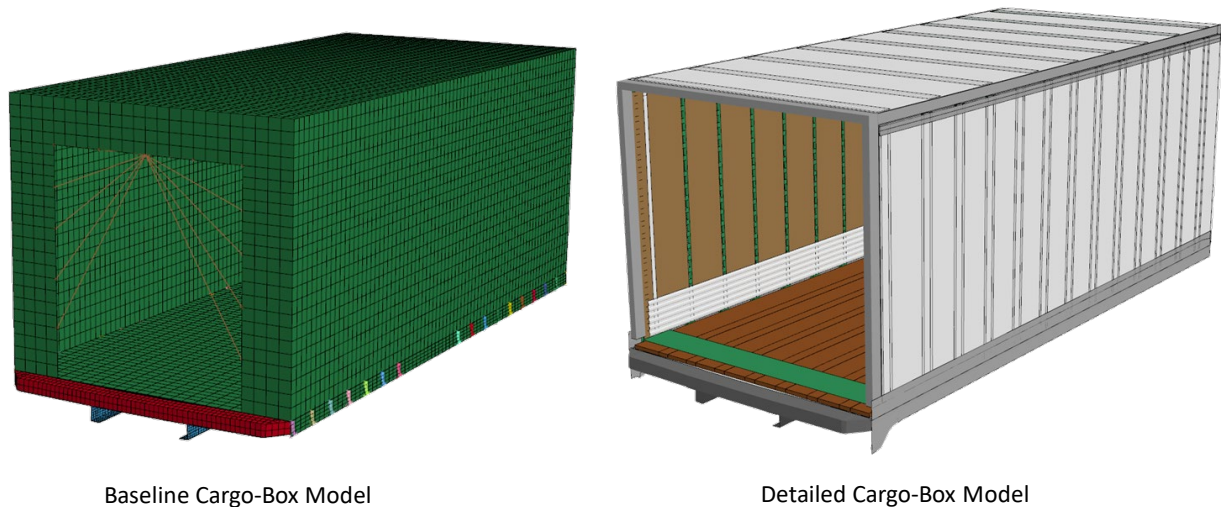


Figure 42. Images of the FEA model for the baseline and detailed cargo-box models (rear door not shown to facilitate viewing inside of cargo box).

Comparisons of the physical and inertial properties of the 8000S vehicle models with those of the test vehicle in full-scale test NETC-3 is provided in Figure 43. The physical dimensions of the test vehicle were not reported; however, the height of the cargo bed of the FEA model was raised from 46.75 inches to 50 inches to match that of another International 4700 used in full-scale test 490026-4-3.[*Williams17a*] It was determined that results of this test case was sensitive to the height of the cargo-bed which was very close to the height of the bridge rail. Slight differences in this metric will affect whether the cargo-box impacts directly against the rail or passes over the top of the rail.

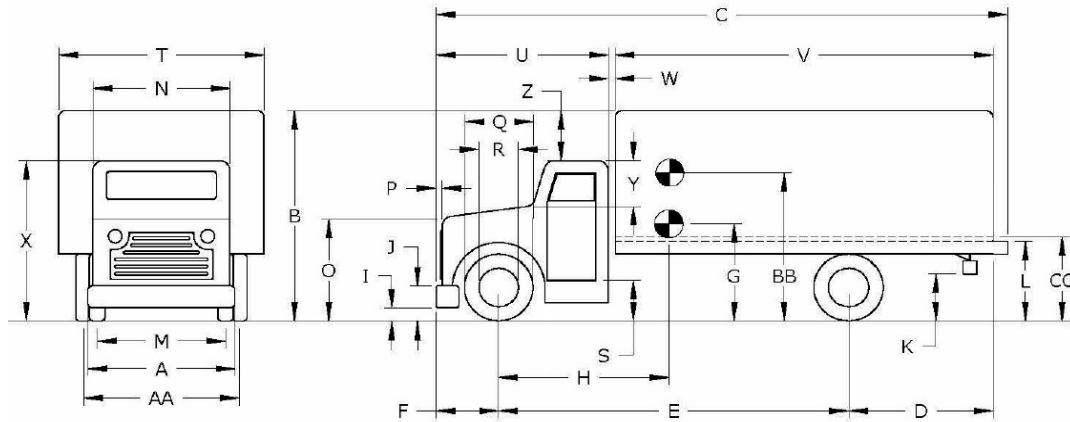
Comparison of the physical and inertial properties of the C2500D vehicle model with those of the test vehicle in full-scale test 401181-1 is provided in Figure 44. Except for the front bumper extension (e.g., items B and L in Figure 44), all other vehicle geometry properties were within 10 percent of the test vehicle, and most were within 3 percent. The gross static weight of the model was 2.8 percent lighter than the test vehicle. The center of gravity of the model was 2.17 inches (3.8 percent) forward compared with the test vehicle.

A comparison of the physical and inertial properties of the *MASH* vehicle models with those of recent full-scale test vehicles (i.e., Test 607451-3, Test 607451-2 and Test 607451-1) is provided in Figure 45, Figure 46 and Figure 47, respectively.[*Williams17a*] The most notable difference for the 1100C vehicle was that the center of gravity (c.g.) was set approximately 7 inches farther back in the model compared to the test vehicle, which resulted in a 19 percent difference. For the 2270P vehicle model, except for the *bumper extension* and the *wheel-well clearance*, all other measurements were within 4 percent of those measured on the test vehicle. The longitudinal and vertical c.g. of the 2270P model was within 1.5 percent and 4 percent, respectively, compared to the test vehicle. The accelerometer for both the 1100C and the 2270P models were positioned at the c.g. of the vehicle. For the 10000S vehicle model, the differences in several of the dimensions were greater than 10 percent compared to the test vehicle; however, those particular properties were considered to have minimal effect on the applied loading to the barrier or to the resulting dynamic response of the vehicle during impact.

VEHICLE PROPERTIES AND INFORMATION

Date: 7/22/1999
 Year: 1987
 Odometer: 142826

Test No.: 404251-6 Vin No.: 1GDJ7D1B5HV514329
 Make: GMC Model: 7000
 Tire Size Front: 11R22.5 Tire Size Rear: 11R22.5



Vehicle Geometry (in)

	<u>Test</u>	<u>Model</u>	<u>% Error</u>		<u>Test</u>	<u>Model</u>	<u>% Error</u>
A Front Bumper Width:	-	93.11	-	P Bumper Extension:	-	-	-
B Overall Height:	-	132.60	-	Q Front Tire Width:	-	37.40	-
C Overall Length:	-	337.60	-	R Front Wheel Width:	-	23.54	-
D Rear Overhang:	-	89.96	-	S Bottom Door Height:	-	36.93	-
E Wheel Base:	-	208.15	-	T Overall Width:	-	96.10	-
F Front Overhang:	-	33.07	-	U Cab Length:	-	108.66	-
G C.G. Height:	-	50.46	-	V Box Length:	-	226.34	-
H C.G. Horz. Dist.	-	136.40	-	W Gap Width:	-	3.19	-
I Front Bumper Bottom:	-	22.46	-	X Overall front Height:	-	87.95	-
J Front Bumper Top:	-	34.61	-	Y Roof-Hood Dist.	-	18.82	-
K Rear Bumper Bottom:	-	19.84	-	Z Roof-Box Height Diff.	-	43.39	-
L Rear frame Top:	-	-	-	AA Rear Track Width	-	72.72	-
M Front Track Width:	-	80.51	-	BB Ballast Center of Mass	-	63.78	-
N Roof width:	-	57.80	-	CC Cargo Bed Height:	-	48.70	-
O Hood Height:	-	64.22	-		X	Y	Z

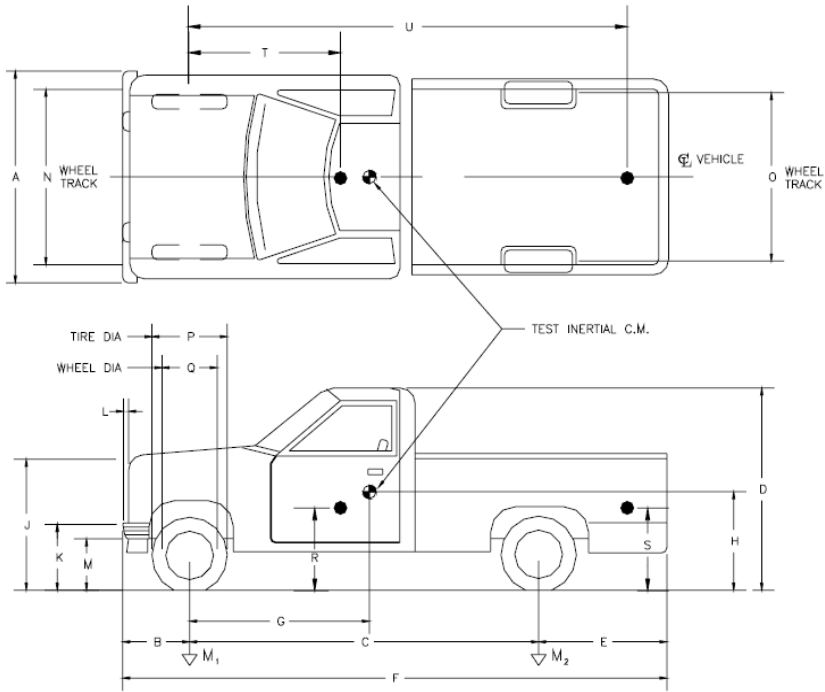
Weights (lb)

	<u>Curb</u>			<u>Test Inertial</u>			
	<u>Test</u>	<u>Model</u>	<u>% Error</u>	<u>Test</u>	<u>Model</u>	<u>% Error</u>	
W_{front axle}	-	5,529	-	W_{front axle}	-	6,174	-
W_{rear axle}	-	6,825	-	W_{rear axle}	-	11,737	-
W_{total}	-	12,355	-	W_{total}	17,875	17,911	0.2
Ballast	-	-	-	Ballast	-	5,556	-

Figure 43. Vehicle property sheet for the 8000S vehicle model compared with full-scale Test NETC-3 (i.e., validation case).

VEHICLE PROPERTIES AND INFORMATION

Date: 4/14/2005 Test No.: 401181-1 Vin No.: 1GCGC24R7Y171118
 Year: 2000 Make: Chevrolet Model: 2500
 Odometer: 218443 Tire Size Front: 245 75 R16 Tire Size Rear: 245 75 R16



Vehicle Geomerty (inches)

	Test Vehicle	FE Model	Error %
A	74.0	73.3	-0.9
B	31.9	35.6	11.5
C	131.9	132.6	0.6
D	71.7	73.0	1.8
E	51.6	52.8	2.4
F	215.4	221.3	2.8
G	57.0	54.8	-3.8
H	-	27.6	-
J	40.9	40.5	-0.9
K	25.0	26.0	3.9
L	2.8	3.5	25.7
M	16.3	18.0	9.9
N	62.6	65.1	4.0
O	63.4	65.0	2.6
P	28.5	28.4	-0.4
Q	17.3	16.4	-5.2
R	29.5	28.7	-2.8
S	35.4	-	-
T	57.5	57.3	-0.3
U	132.3	-	-

Mass -Properties

		Curb			Test Inertial			Gross Static		
		Test Vehicle	FE Model	Error %	Test Vehicle	FE Model	Error %	Test Vehicle	FE Model	Error %
M ₁	(lb)	2,639	-	-	2,672	-	-	2,672	2,683	0.4
M ₂	(lb)	2,114	-	-	2,035	-	-	2,035	1,892	-7.0
M _{Total}	(lb)	4,753	3,995	-16.0	4,707	-	-	4,707	4,575	-2.8
I ₁₁	(lb - ft ²)	-	-	-	-	-	-	-	17,997	-
I ₂₂	(lb - ft ²)	-	-	-	-	-	-	-	104,080	-
I ₃₃	(lb - ft ²)	-	-	-	-	-	-	-	111,341	-

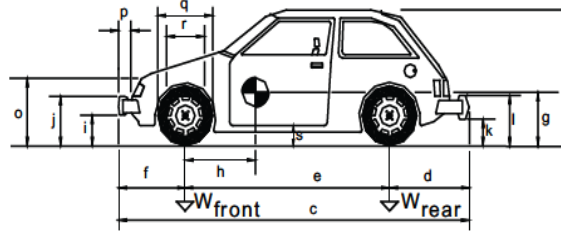
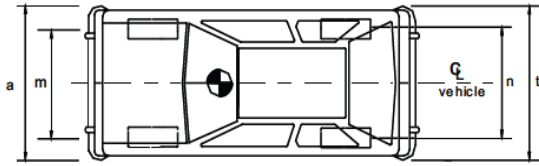
Figure 44. Vehicle property sheet for the C2500R vehicle model compared with full-scale Test 401181-1 (i.e., validation case).

VEHICLE PROPERTIES AND INFORMATION

Date: 12/21/2016
 Year: 2010
 Odometer: 140035

Test No.: 607451-3
 Make: Kia
 Tire Size: 35/65R14

Vin No.: KNADHA33A6692034
 Model: Rio
 Tire Inflation Pressure: 32 psi



Vehicle Geometry (inches)

	<u>Test</u>	<u>Model</u>	<u>% Error</u>
a Front Bumper Width:	66.38	64.528	-2.79
b Overall Height:	58	57.717	-0.49
c Overall Length:	165.75	169.13	2.04
d Rear Overhang:	34	37.087	9.08
e Wheel Base:	98.75	99.961	1.23
f Front Overhang:	33	32.126	-2.65
g C.G. Height:		21.732	
h C.G. Horz. Dist.	35.28	42.008	19.07
i Front Bumper Bottom:	8	7.9134	-1.08
j Front Bumper Top:	21	21.417	1.99
k Rear Bumper Bottom:	11.5	13.74	19.48
l Rear Bumper Top:	25	25.197	0.79
m Front Track Width:	57.75	58.622	1.51
n Rear Track Width:	57.7	57.638	-0.11
o Hood Height:	28.25	31.732	12.33

	<u>Test</u>	<u>Model</u>	<u>% Error</u>
p Bumper Extension:	4.12	3.661417	-11.13
q Front Tire Width:	22.5	23.50394	4.46
r Front Wheel Width:	15.8	16.14173	2.16
s Bottom Door Height:	8	11.88976	48.62
t Rear Bumper Width:	66.2	63.70079	-3.78
Wheel Center Height:	11	11.92913	8.45
Engine Type:	4 cylinder		
Engine Size:	1.6 liter		

	X	Y	Z
Accelerometer Location (inches) - measured from front axle and ground	35.25		15.62

Weights (lbs)

	<u>Curb</u>		
	<u>Test</u>	<u>Model</u>	<u>% Error</u>
$W_{front\ axle}$	1597	-	-
$W_{rear\ axle}$	921	-	-
W_{total}	2518	-	-

	<u>Test Inertial</u>		
	<u>Test</u>	<u>Model</u>	<u>% Error</u>
$W_{front\ axle}$	1561	1504.542	-3.62
$W_{rear\ axle}$	868	1090.59	25.64
W_{total}	2429	2595.132	6.84

GVWR Ratings (lbs)

	<u>Test</u>	<u>Model</u>	<u>% Error</u>
Front	1718	-	-
Rear	1874	-	-

Dummy Data

Type	_____
Mass (lbs)	_____
Seat Position	_____

Other Notes:

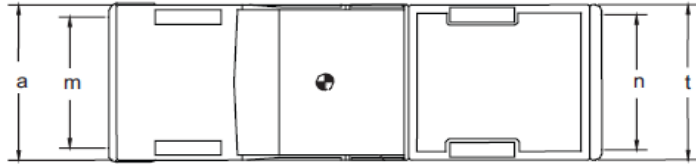
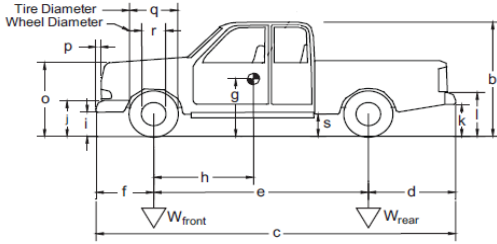
Figure 45. Vehicle property sheet for the 1100C vehicle model compared with a recent test vehicle from Test 607451-3

VEHICLE PROPERTIES AND INFORMATION

Date: 12/20/2016
 Year: 2011
 Odometer: 262075

Test No.: 607451-2
 Make: Dodge
 Tire Size Front: 265/70R17

Vin No.: 1D7RB1GP9BS673991
 Model: 1500
 Tire Size Rear: 265/70R17



Vehicle Geometry (inches)

	<u>Test</u>	<u>Model</u>	<u>% Error</u>
a Front Bumper Width:	78.5	79.843	1.71
b Overall Height:	75	75.354	0.47
c Overall Length:	227.5	229.8	1.01
d Rear Overhang:	47	46.929	-0.15
e Wheel Base:	140.5	143.5	2.14
f Front Overhang:	40	39.567	-1.08
g C.G. Height:	29.25	28.819	-1.47
h C.G. Horz. Dist.	62.39	60.039	-3.77
i Front Bumper Bottom:	12	12.402	3.35
j Front Bumper Top:	27	26.614	-1.43
k Rear Bumper Bottom:	20.25	20.748	2.46
l Rear frame Top:	29.5	30.236	2.50
m Front Track Width:	68.5	69.488	1.44
n Rear Track Width:	68	66.142	-2.73
o Hood Height:	46.5	47.087	1.26

	<u>Test</u>	<u>Model</u>	<u>% Error</u>
p Bumper Extension:	3	2.4015748	-19.95
q Front Tire Width:	30.5	30.393701	-0.35
r Front Wheel Width:	18	18.425197	2.36
s Bottom of Body Height:	13	12.874016	-0.97
t Overall Width:	77	79.488189	3.23
Wheel Center Height Front:	14.75	15.275591	3.56
Wheel Center Height Back:	14.75	15.275591	3.56
Wheel Well Clearance (F):	6	7.7952756	29.92
Wheel Well Clearance (R):	9.25	9.6456693	4.28
Frame Height (F):	17	17.562992	3.31
Frame Height (R):	25.5	25.984252	1.90
Engine Type:			
Engine Size:			

	<u>X</u>	<u>Y</u>	<u>Z</u>
Accelerometer Location (inches) - measured from front axle and ground			

Weights (lbs)

	<u>Curb</u>		
	<u>Test</u>	<u>Model</u>	<u>% Error</u>
$W_{front\ axle}$	2828	0	-100.00
$W_{rear\ axle}$	2108	0	-100.00
W_{total}	4936	0	-100.00

	<u>Test Inertial</u>		
	<u>Test</u>	<u>Model</u>	<u>% Error</u>
$W_{front\ axle}$	2800	3051.4978	8.98
$W_{rear\ axle}$	2237	1949.7269	-12.84
W_{total}	5037	5001.2115	-0.71

GVWR Ratings (lbs)

	<u>Test</u>	<u>Model</u>	<u>% Error</u>
Front	3700	0	-100.00
Rear	3900	0	-100.00

Dummy Data

Type	50th Percentile Male		
Mass (lbs)	165	0	-100.00
Seat Position	Driver		

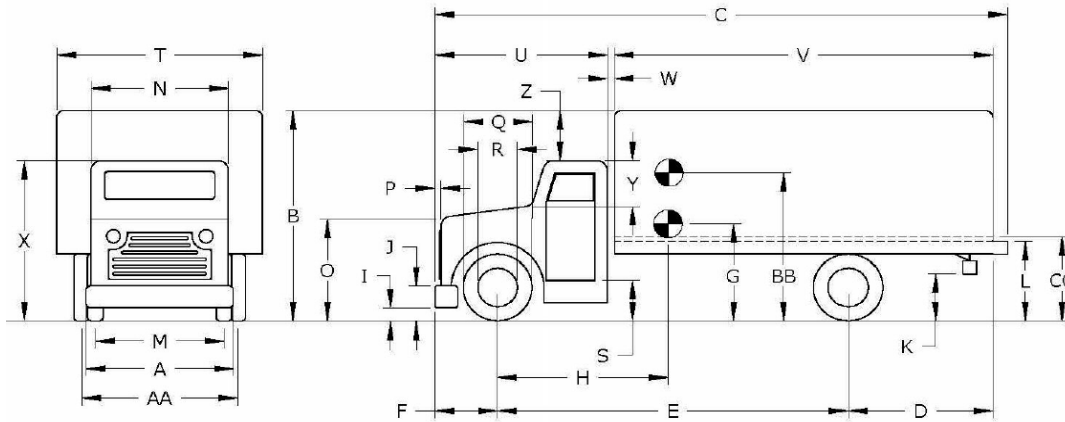
Other Notes:

Figure 46. Vehicle property sheet for the 2270P vehicle model compared with a recent test vehicle from Test 607451-2.

VEHICLE PROPERTIES AND INFORMATION

Date: 12/16/2016
 Year: 2006
 Odometer: 275640

Test No.: 607451-1 Vin No.: 1HMPAFN86h206312
 Make: International Model: 4200
 Tire Size Front: _____ Tire Size Rear: _____



Vehicle Geometry (in)

	<u>Test</u>	<u>Model</u>	<u>% Error</u>		<u>Test</u>	<u>Model</u>	<u>% Error</u>
A Front Bumper Width:	95.00	93.11	-2.0	P Bumper Extension:	1.00	0	-100.00
B Overall Height:	132.00	131.46	-0.4	Q Front Tire Width:	39.00	37.40	-4.1
C Overall Length:	329.75	337.60	2.4	R Front Wheel Width:	23.50	23.54	0.2
D Rear Overhang:	89.00	89.96	1.1	S Bottom Door Height:	37.00	38.50	4.1
E Wheel Base:	204.75	208.15	1.7	T Overall Width:	96.00	96.10	0.1
F Front Overhang:	36.00	33.07	-8.1	U Cab Length:	106.00	101.65	-4.1
G C.G. Height:	-	50.44	-	V Box Length:	227.00	226.34	-0.3
H C.G. Horz. Dist.	133.28	133.47	0.1	W Gap Width:	1.00	3.19	218.9
I Front Bumper Bottom:	19.00	20.94	10.2	X Overall front Height:	98.50	87.95	-10.7
J Front Bumper Top:	34.00	32.64	-4.0	Y Roof-Hood Dist.	30.00	18.82	-37.3
K Rear Bumper Bottom:	-	18.66	-	Z Roof-Box Height Diff.	36.00	43.39	20.5
L Rear frame Top:	37.00	41.65	12.6	AA Rear Track Width	73.00	72.72	-0.4
M Front Track Width:	80.00	80.51	0.6	BB Ballast Center of Mass	61.90	62.52	1.0
N Roof width:	71.00	57.80	-18.6	CC Cargo Bed Height:	49.25	48.70	-1.1
O Hood Height:	59.00	62.87	6.6		X	Y	Z

Weights (lb)

	<u>Curb</u>			<u>Test Inertial</u>		
	<u>Test</u>	<u>Model</u>	<u>% Error</u>	<u>Test</u>	<u>Model</u>	<u>% Error</u>
W_{front axle}	6,090	6,811	11.8	7,690	7,915	2.9
W_{rear axle}	6,090	5,521	-9.4	14,340	14,146	-1.4
W_{total}	12,180	12,332	1.2	22,030	22,061	0.1
				+165lb for dummy not included in TIM		
Ballast				10,282	9,729	-5.4

Figure 47. Vehicle property sheet for the baseline 1000S vehicle model compared with a recent test vehicle from Test 607451-1.

6 MODEL DEVELOPMENT AND VALIDATION OF THE NETC 4-BAR BRIDGE RAIL

6.1 Model Development

A detailed finite element model of the NETC 4-bar bridge rail was developed, as shown in Figures 49 and 49, based on construction drawings provided in the full-scale test report for this system and the standard drawings for NHDOT, which are provided in Appendix B of this report. [Kimball99] Refer to Section 3 for more detailed description of the design. The FEA model includes 120 feet of the bridge rail. Details of the model, regarding material characterization and element formulations used for the various components, are presented here. The basic components of the bridge rail model include:

- Fifteen (15) W6x25 posts,
- One (1) 12"x10"x1" post-baseplate at each post,
- Four (4) anchor bolts at each baseplate connecting the baseplate to the sidewalk/deck,
- Fifteen (15) HSS 4 x 4 x 1/4-inch tube rails that are 23.94 feet long (each) and hardware,
- Five (5) HSS 8 x 4 x 3/16-inch tube rails that are 23.94 feet long (each) and hardware,
- Twenty (20) splice tubes 20 inches long (each) made from 3/8-inch thick steel plate and bolt hardware,
- Concrete sidewalk and short length of bridge deck based on NHDOT drawings,
- Sidewalk steel reinforcement based on NHDOT drawings.

The model includes fifteen posts spaced at 8 feet (typical) on centers; and five sections of tube railing at 23.94" each, including splice connections with a 3/4-inch splice gap between adjoining rails. The geometry of these components was modeled according to the drawings in the test report.[Kimball99] A representative section of the FEA model for the bridge rail is shown in Figure 50. The profile view in Figure 50 provides specific height dimensions of the railing elements. Additional details of the FEA model for each of the bridge rail components is provided in the following sections.

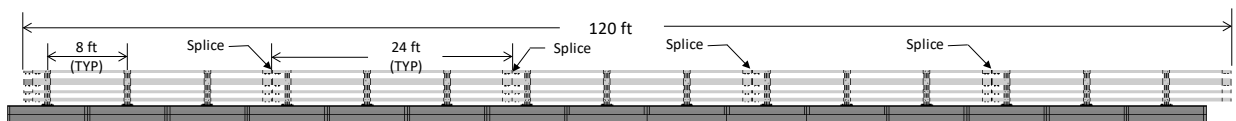


Figure 48. Finite element analysis model of the NETC 4-bar bridge rail (plan view)

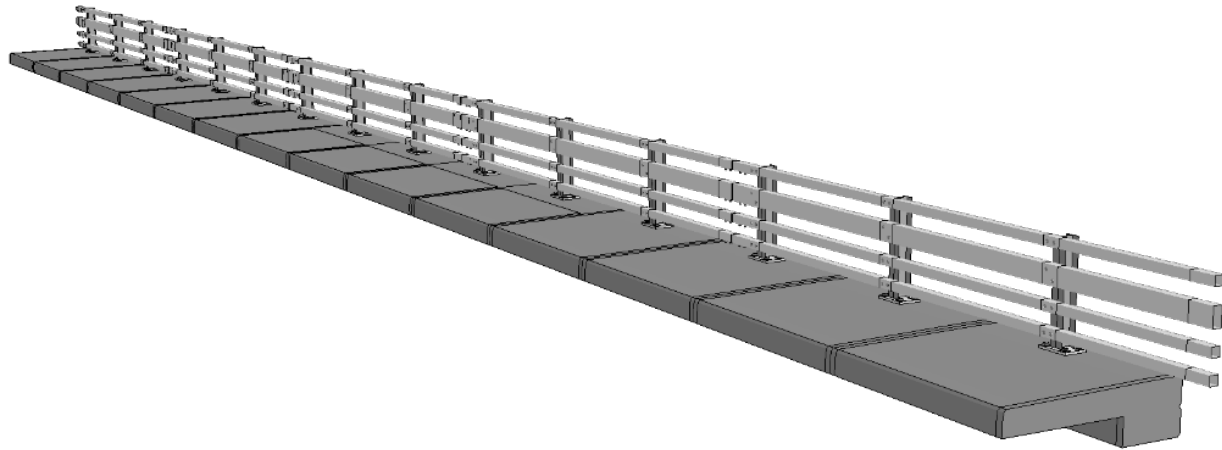


Figure 49. Finite element analysis model of the NETC 4-bar bridge rail (isometric view).

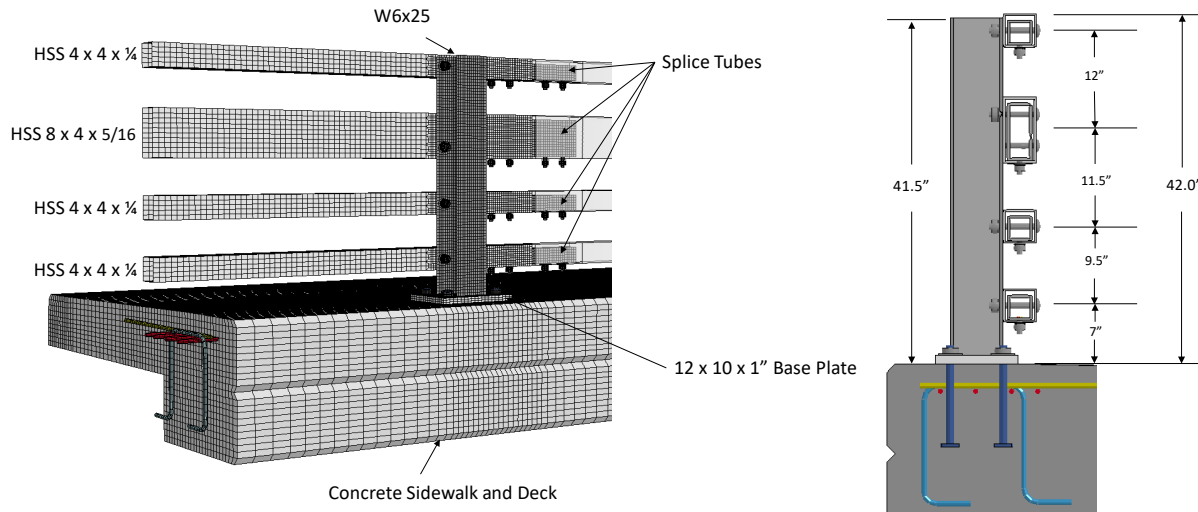


Figure 50. Representative section of the FEA model of the bridge rail.

6.1.1 Posts

The geometry of the posts was modeled according to the detailed drawings in the test report and included six (6) horizontally slotted mounting holes in the flanges with dimensions 1-1/8" x 1-3/8". The FEA model of the post is shown in Figure 51. The material for the post model conformed to ASTM A709 Grade 50 steel. The post was modeled with thin-shell Belytschko-Tsay elements (Type 2 in LS-DYNA) with five (5) integration points through the thickness. The flange and web were meshed with a nominal element size of 0.43 x 0.5 inches. The elements around the edge of the mounting holes were meshed with nominal element size of 0.32 inches.

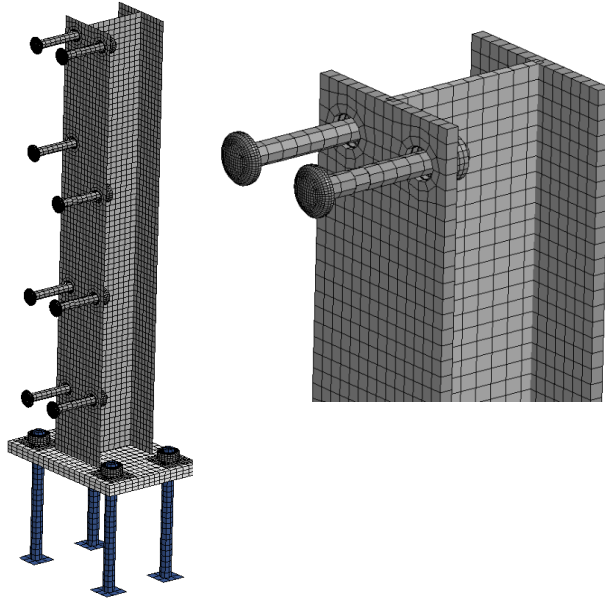


Figure 51. FEA Model of bridge rail post.

6.1.2 Tubular Rails and Mounting Bolts

The tubular rail sections were modeled according to the dimensional specifications for HSS 4"x4"x 1/4" (top and lower two rails) and HSS 8"x4"x5/16" (third rail from bottom). The material for all tube railing conformed to ASTM A500 Grade C. The tube rails were modeled with Type 2 element with five (5) integration points through the thickness. The nominal element size for the mesh is 0.75 x 1 inches for the span of rail between the posts and 0.4 x 0.4 inches for the section of rail in contact with the posts. The mounting holes in the rail were 7/8" diameter. The mesh around the slotted holes were meshed with a nominal element length of 0.25 inches.

The 3/4-inch diameter button head mounting bolts were modeled with Hughes-Liu beam elements (Type 1 in LS-DYNA) with properties corresponding to ASTM A325. The head of the bolts, as well as the nuts and washers were modeled with rigid material properties, since the effects of deformation of these components were expected to be negligible compared to the effects of bolt deformations. The bolts were given a pre-strain condition to tighten the railing onto the post.

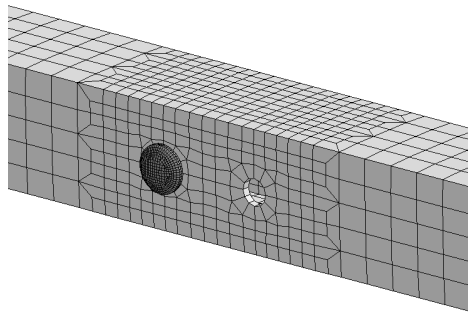


Figure 52. FE mesh of the middle tube-rail and bolt (one bolt removed to facilitate viewing slotted mounting hole).

Two models of the tube-rail splice connection were developed. The model used in the validation is shown in Figure 53, which included stud-and-nut hardware and did not include the spacer/bushings for the cap screws (refer to drawings in Appendix B). The model was later updated, as shown in Figure 54, to include (1) correct cap-screw dimensions, (2) bushing-spacers for the cap screws on one side of the splice, and (3) proper clamping force for the cap screws on the opposite side of the splice. The updated model was used for all subsequent *MASH* evaluations of the NETC bridge rails.

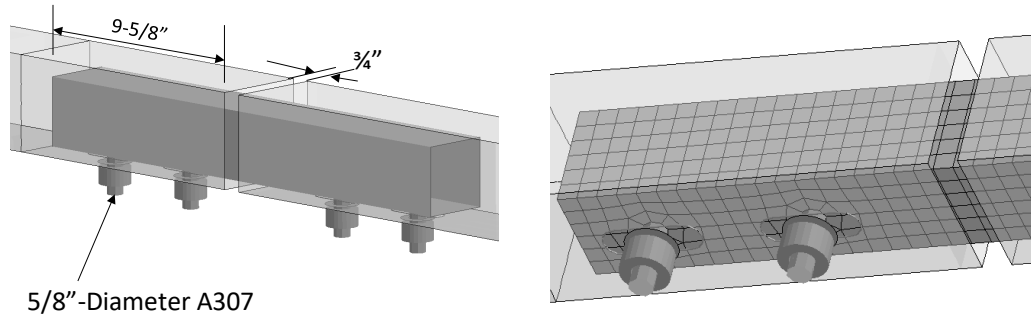


Figure 53. Model of rail splice for validation model with rail-tube shown transparent.

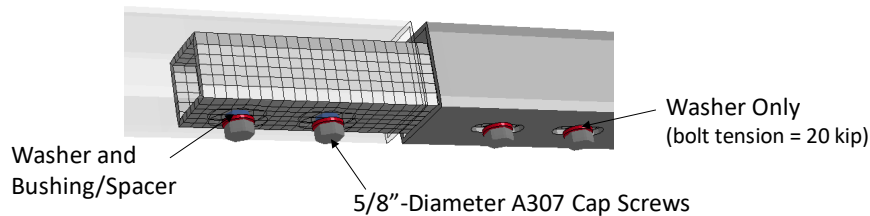


Figure 54. Updated model of rail splice used in *MASH* evaluations with rail-tube shown transparent.

The splice tubes were modeled with the same material properties and mesh details as the main rail tubes. The splice connection of the adjoining tube rails included a 20-inch long tubular sleeve inserted 9.625 inches into the upstream and downstream ends of the main rails (see Appendix B for dimension details). The cap-screw connections of the splice to the rail bars was modeled with Hughes-Liu beam elements (Type 1 in LS-DYNA) with 5/8" diameter cross-section. The cap screws were rigidly fastened to the splice tube using constrained-nodal-rigid-bodies in ls-dyna and were fastened to the rail bars with nuts and washers. The properties for the cap screws were modeled as ASTM A307. The slotted openings in the rail bars for the cap screws were 1-1/8" x 2-1/2". The splice hole dimensions were not provided in the test report, so the model was developed using the recommended dimensions as provided in Table 35. A 3/4-inch gap between the adjoining main-rail sections was included at the splice according to design. The splice tubes were modeled with the same material properties and mesh details as the main rail tubes.

6.1.3 Baseplate and Anchor Bolts

The baseplate was modeled with dimensions 12" x 10" x 1" and with material properties conforming to ASTM A709 Grade 50. The part was meshed with Type 2 (selective reduced 2x2 in-plane integration) thick shell elements. The welded connection of the post to the baseplate

was modeled using continuous **Constrained_spotwelds* around the perimeter of the base of the post. The 1" diameter anchor rods were modeled with Type 1 beam elements in LS-DYNA. The length of the anchor rods was 12 inches. The material for the anchor bolts conformed to ASTM A449, which has a minimum yield of 92 ksi, ultimate strength of 120 ksi, and 14 percent elongation. The nuts and washers were modeled as rigid. The anchor bolts extended into the rigid deck and connected to a 3/8-inch thick plate, as illustrated in Figure 55. The bolts were anchored inside the deck using the **Constrained_Beam_in_Solid* option in LS-DYNA.

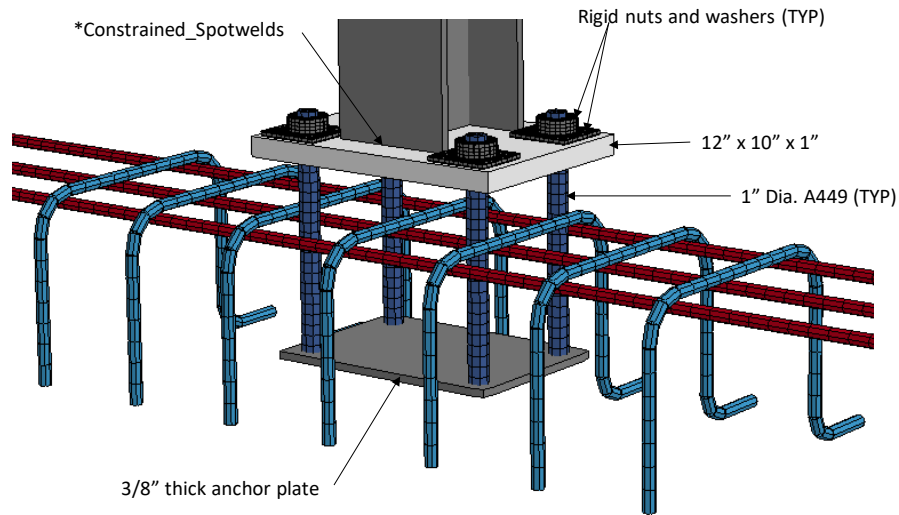


Figure 55. Transparent view of concrete showing model of baseplate and anchor bolts.

6.1.4 Concrete Curb, Sidewalk and Deck

The materials for the sidewalk and deck components were modeled using **Mat_RHT* in LS-DYNA, with default material properties based on an unconfined compressive strength of 4,000 psi. The concrete was modeled with Type 1 brick elements in LS-DYNA with nominal element size of 1" x 1" x 1" at the post locations and with the element side length then gradually increasing to approximately 3 inches at maximum distance from the post, as illustrated in Figure 56 and Figure 57.

The longitudinal reinforcement (relative to the bridge rail) at the top of the sidewalk near the anchor bolts was modeled with four #5 bars. The reinforcement steel running lateral to the bridge rail was modeled with #5 bars at the top of the sidewalk at 12" spacing on centers. The stirrups were also modeled with #5 bars with 6-inch spacing. Refer to Appendix B for additional details regarding location of the reinforcing steel.

All reinforcing bars were modeled with Type 1 beam elements with a nominal element length of 1 inch. The material properties for the reinforcing steel conformed to ASTM A615 Grade 60 steel with properties measured at Turner Fairbanks Highway Research Center.[*TFHRC15*] The stress-strain characterization is shown in Figure 58.

The interaction of the reinforcing steel within the concrete curb/deck was modeled using the **Constrained_Beam_in_Solid* option in LS-DYNA. Unfortunately, slip of the anchor bolts in the concrete cannot be simulated with this method unless the concrete fails around the rebar; however, it is apparent from the drawings that the anchor bolts cannot physically "slip" unless they break from the anchor plate which is buried deep inside the sidewalk/deck.

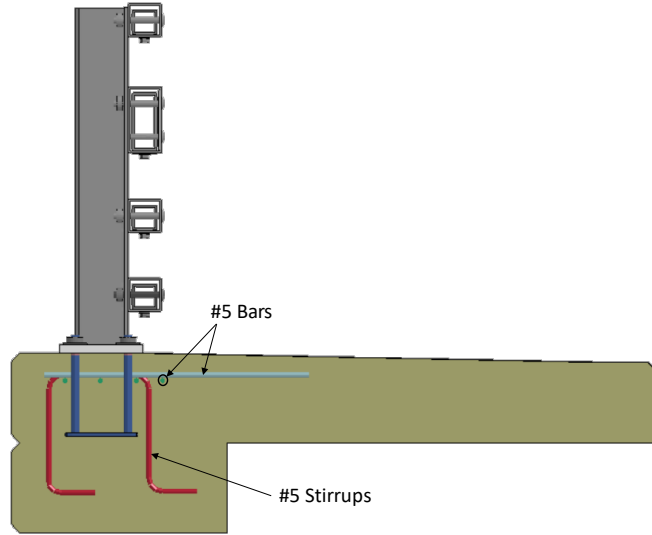


Figure 56. Profile view of sidewalk model.

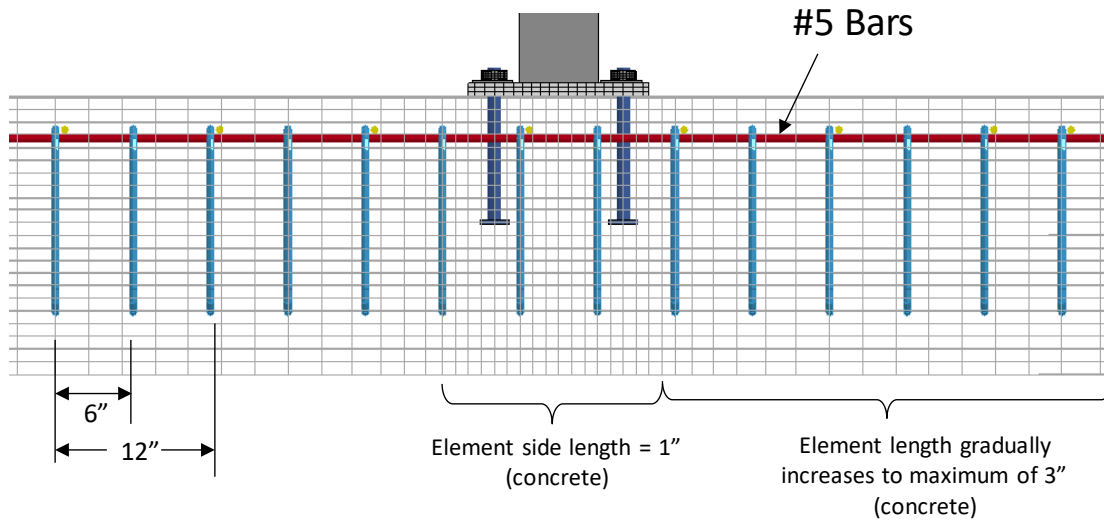


Figure 57. Plan view of sidewalk model (from back of bridge rail).

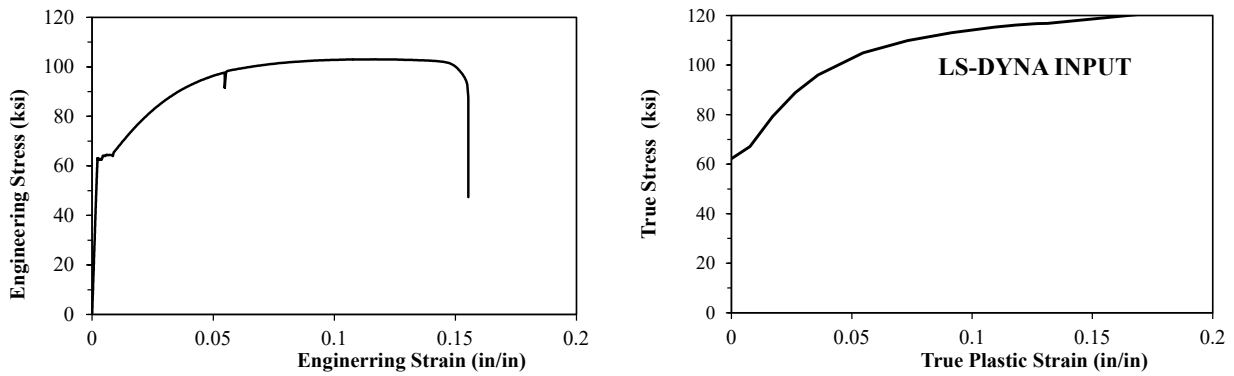


Figure 58. Stress vs. strain curve for ASTM A615 Grade 60 steel.

6.1.5 Materials

All steel materials were modeled in LS-DYNA using material model *Mat_Piecewise_Linear_Plasticity. The Young's modulus was set to 29,000 ksi and Poisson's ratio was set to 0.33. The piecewise-linear stress-strain characterization for each component varied depending on steel type and grade.

The tubular rail sections were modeled with material conforming to ASTM A500 Grade B. The minimum yield and tensile strength for the structural tube material is 46 ksi and 58 ksi, respectively. All steel posts and baseplates were modeled as ASTM A572 Grade 50 steel (e.g., same as AASHTO M270 Grade 50); the material characterization was based on stress-strain curves from tensile tests conducted at the Turner-Fairbank Highway Research Center (TFHRC) in McLean, Virginia in an earlier study performed by Roadsafe. The material for all tube rails were modeled as ASTM A500 Grade C, with minimum yield and tensile strength of 50.6 ksi and 70 ksi, respectively.

All 3/4-inch diameter round head bolts were modeled as ASTM A325 with yield strength of 92 ksi and ultimate strength of 120 ksi (nominal stress). The 1-inch diameter anchor rods were modeled as ASTM A449 with yield strength of 92 ksi and ultimate strength of 120 ksi (engineering stress).

The material model for the sidewalk, curb and deck was dependent on the location. Outside the impact region, the materials for the sidewalk, curb and deck components were modeled with rigid properties. Inside the impact region, the constitutive properties for the sidewalk, curb and bridge deck were modeled using *Mat_RHT in LS-DYNA with default material properties based on an unconfined compressive strength of 4,000 psi. This material model in LS-DYNA was selected based on the results of a recent study performed by the research team in which the material model was validated against pendulum impact tests on reinforced concrete columns where the columns were subjected to lateral impact forces.[Ray18]

6.2 Model Validation

6.2.1 Model Set-Up and Impact Conditions

The FEA model of the NETC 4-bar bridge rail was used to simulate Test NETC-3. The details of the NETC-3 test were provided in Section 3.3.2; a summary of the test article and impact conditions are repeated here for convenience. The NETC 4-bar bridge rail system was tested according to the crash test specifications of NCHRP Report 350 for Test Level 4. The test article was a 108-foot long section of the bridge rail mounted on a concrete sidewalk. The sidewalk was 8 inches tall at the traffic face and sloped up to 9 inches tall at the point where the bridge rail was mounted. The distance from the face of the curb to the face of the bridge rail was 5 feet.

The tests were conducted at the Southwest Research Institute (SwRI). Test NETC-3 corresponded to the impact conditions of Report 350 Test 4-12 and involved a 1993 International 4600 LP single unit truck ballasted to 17,875-lb, impacting the bridge rail system at 49.8 mph and angle of 15 degrees. The initial point of contact was 2.0 feet upstream of Post 6. The vehicle struck the test article on the left side of the vehicle (e.g., reverse-direction impact).

The vehicle model used in analysis was the 8000S single unit truck model with modified cargo-bed height described in Section 5. A comparison of the vehicle properties for the model and the test vehicle is shown in Figure 43.

There were a few differences between the tested design and the FEA model as described in Section 3.3.2 and Section 6.1 regarding the concrete material and the rail-to-post connection:

- Concrete material: Modeled with unconfined compressive strength of 4,000 psi. The concrete strength for the test article was not reported.
- Rail-to-post connection: Modeled with 3/4-inch diameter button-head bolts with properties consistent with ASTM A325. The tested system used 3/4" stud-bolts made from ASTM A307.

6.2.2 Issues and Limitations Regarding Test Data for Validation

The validation effort was limited by the amount of data available from the full-scale test. The test was conducted in December 1997 and, unfortunately, the retention time for test data at SwRI was only three years. Copies of the test videos were obtained from NETC and the FHWA; however, the electronic time-history data from the vehicle-mounted accelerometers, which are needed for the quantitative validation process, were no longer available. Figure 59 through Figure 62 shows images of the acceleration-time histories and the yaw-rate-time history plots from the test report and correspond to the data collected at the c.g. of the vehicle. [Kimball99]

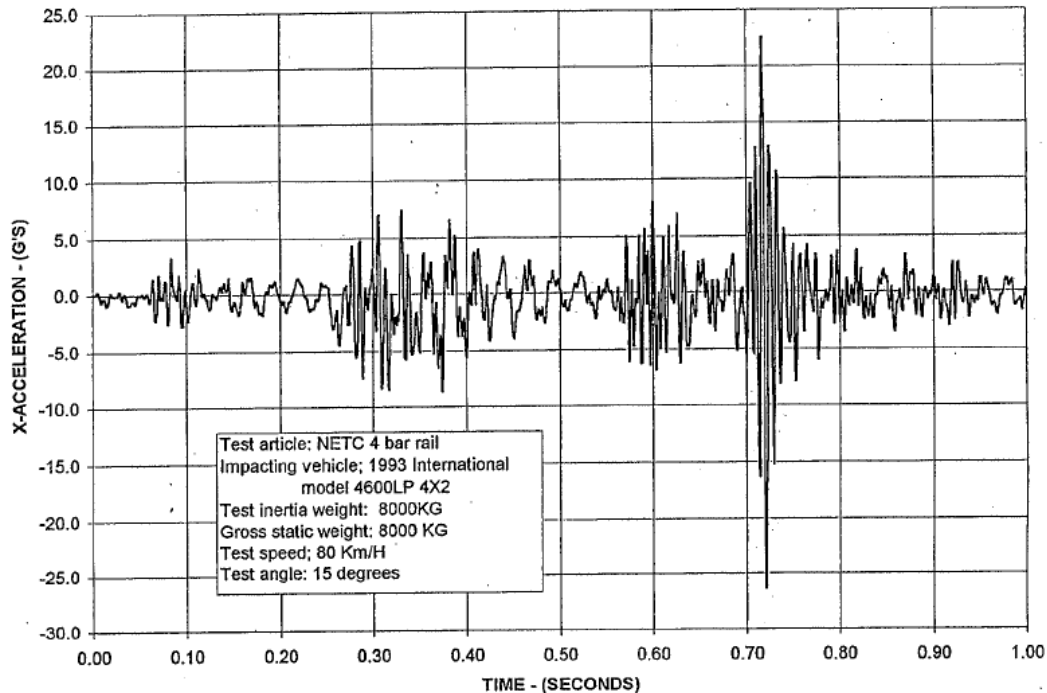


Figure 59. Longitudinal (x-direction) acceleration measured at vehicle c.g. in Test NETC-3. [Kimball99]

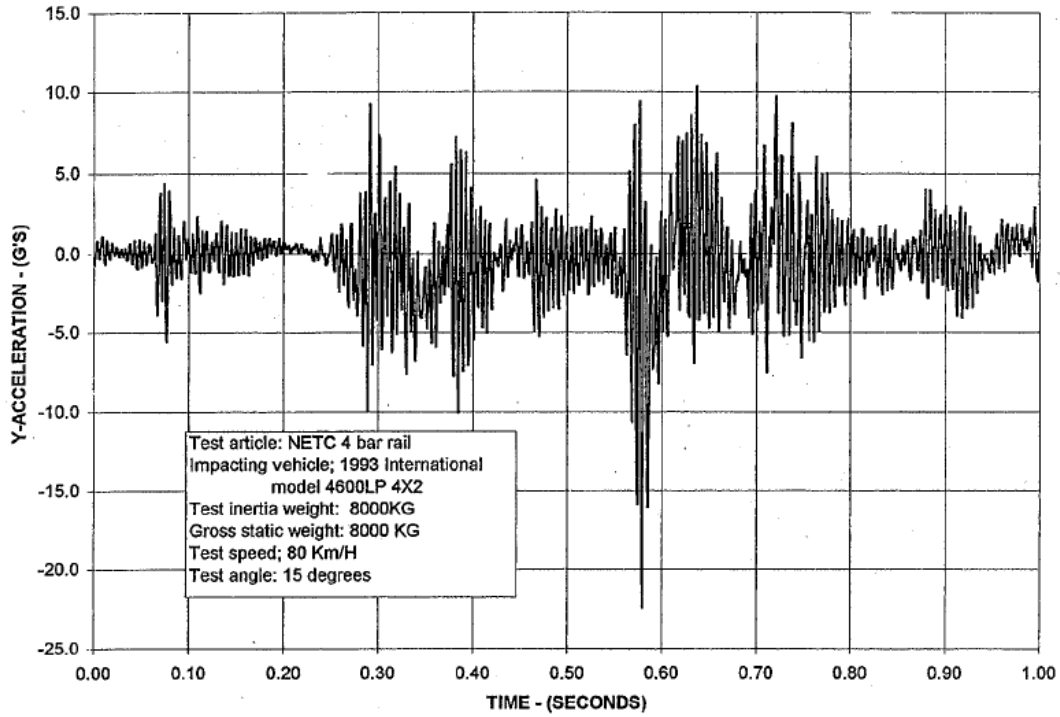


Figure 60. Lateral (y-direction) acceleration measured at vehicle c.g. in Test NETC-3. [Kimball99]

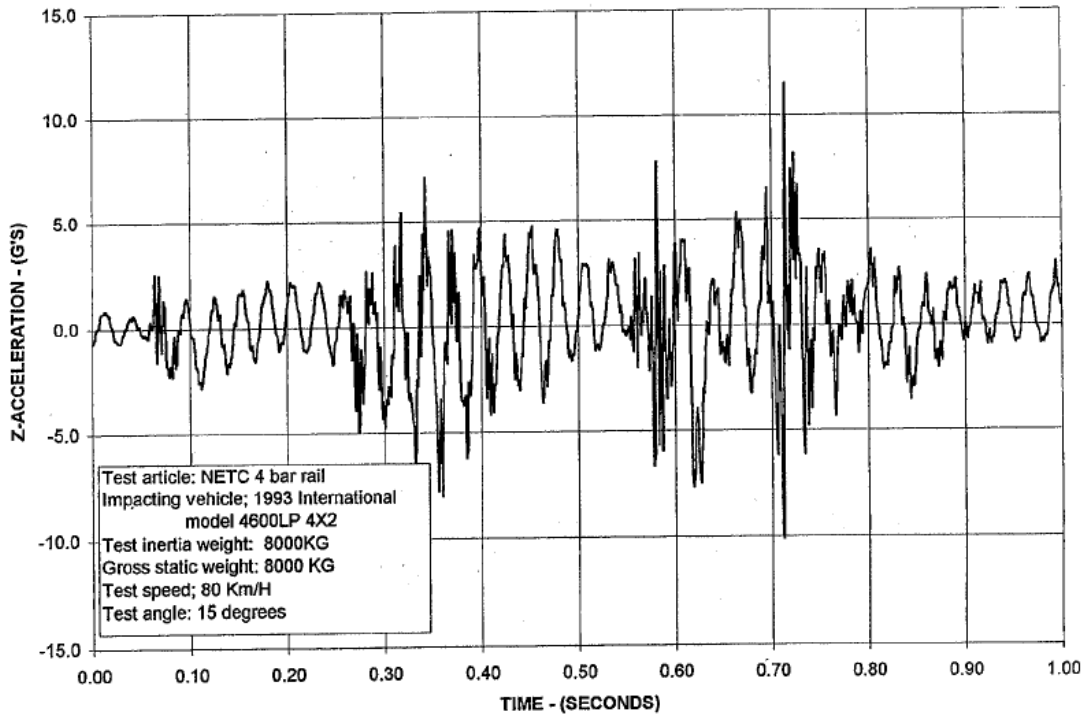


Figure 61. Vertical (z-direction) acceleration measured at vehicle c.g. in Test NETC-3. [Kimball99]

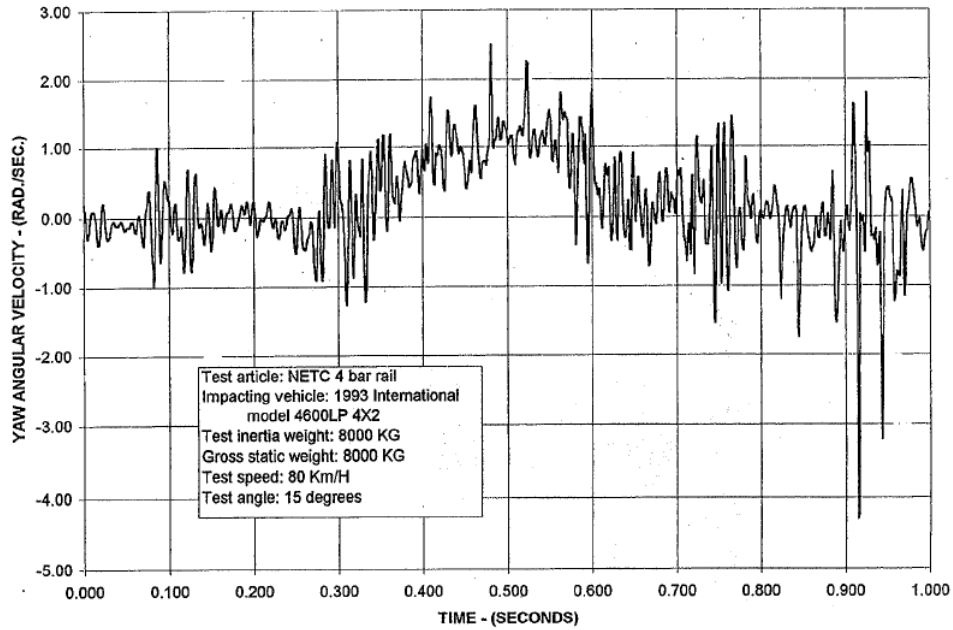


Figure 62. Yaw-rate measured at vehicle c.g. in Test NETC-3.[Kimball99]

Also, the test-vehicle properties measurements were not reported, so it was not possible to calibrate the vehicle model’s dimensions with the test vehicle. The cargo-box for the test vehicle was visibly longer than the FEA model, as illustrated in Figure 63. The rear bumper on the test vehicle extended the full width of the cargo box, as shown in Figure 63. The ballast for the test vehicle was not reported, but the pre-test photos show that the primary ballast consists hay. The ballast was modeled with approximate overall dimensions of the visible ballast and the ballast’s density was set to achieve the overall ballasted mass of the test vehicle (e.g., 17,875 lb.).



Figure 63. FEA vehicle and test vehicle illustrating the differences in cargo-box length and bumper design.

6.2.3 *Simulated Impact Summary*

The analysis was performed using LS-DYNA version mpp_s_R8.0.0 revision number 95309. The analysis was conducted with a time-step of 1.0 microsecond for a time period of 1.5 seconds. The vehicle model was traveling in the opposite direction of the test vehicle; thus, the vehicle model struck the barrier on the right-side of the vehicle (i.e., primary direction impact). This impact direction was used in the analysis so that the fuel tank would be positioned opposite of the impact side, which was consistent with the full-scale test. The sequential views for the FEA were mirrored to facilitate comparison with the test views in Figures 64 through 66.

The front impact side tire of the vehicle model contacted the 9-inch curb within a few milliseconds of the start of the analysis. At 0.045 seconds the front tire had fully mounted the curb, and at 0.055 seconds the front impact side suspension was fully compressed. At 0.8 seconds the front of the cargo box began to pitch upward. The rear impact side tires impacted the curb at 0.24 seconds; also, at this time the vehicle started to roll slightly away from the barrier. At 0.255 seconds the front bumper and fender of the vehicle impacted the two top rails (Rail 3 and Rail 4) of the bridge rail at 15 inches upstream of Post 7. At 0.265 seconds the front-impact side tire contacted the lower two rails. At 0.28 seconds the rear impact side tire was fully mounted onto the sidewalk. At 0.3 seconds the front tire on the non-impact side began to lift off the ground and at 0.36 seconds the cargo-box began to roll toward the barrier. The u-bolts connecting the front axle to the suspension on the impact side failed at 0.405 seconds; also, at this time the rear tandem wheel set on the non-impact side began to lift off the ground. At 0.415 seconds the lower edge of the cargo box impacted against the top edge of the top bridge rail element and then began to slide along the top of the rail. At 0.45 seconds the side-step on the cabin contacted the second rail from the top. At 0.545 seconds the rear tandem wheel set on the impact side impacted against the three lower bridge rail elements. At 0.575 seconds the rear of the cargo box passed over the top of the top rail. At 0.595 seconds the maximum deflection of the bridge rail occurred with magnitude 1.77 inches; whereas, the test resulted in 1-inch dynamic deflection. At 0.61 seconds the truck box was parallel to the rail. At 0.675 seconds the lower edge of the cargo box extended over the rail and contacted the top of Posts 8 and 9 simultaneously. At 0.68 seconds the rear of the cargo box began to pitch upward. At 0.72 seconds the truck box reached peak roll angle of 7.1 degrees toward the barrier. At 0.76 seconds the front lower corner of the cargo box snagged on the top of post 10. At 0.86 seconds the front tire on the non-impact side recontacted the ground, and the vehicle steered back toward the bridge rail. At approximately 1 second the truck box began to roll aggressively away from the barrier; at this time the vehicle reached a peak pitch angle of 5.4 degrees (rear pitching upward). At 1.14 seconds the vehicle lost contact with the barrier. At 1.22 seconds the rear tandem wheel set on the impact side recontacted the top of the sidewalk, and 1.275 seconds the rear tandem wheel set on the non-impact side recontacted the ground. The analysis was terminated at 1.5 seconds, at which time:

- The roll angle of the vehicle was 14.7 degrees away from the barrier and increasing,
- The pitch angle of the vehicle was 1.26 degrees and decreasing,
- The yaw angle of the vehicle was 7.2 degrees toward the barrier) and constant,
- The forward velocity of the vehicle was 38.8 mph.

6.2.4 Sequential Views

A qualitative assessment was made by comparing sequential snapshots of the full-scale crash test with the results of the simulation to verify vehicle kinematic response as well as sequence and timing of key phenomenological events. The results from the FE analysis compare reasonably well with the results from full-scale crash test NETC-3. Figure 64 shows sequential snapshots of the impact event from an upstream viewpoint. Figure 65 shows the sequential views from an oblique (downstream and behind the barrier) viewpoint. Figure 66 shows sequential views from an overhead viewpoint. Based on visual inspection the model appears to simulate the basic kinematic behavior of the truck and adequately captures the basic phenomenological events that occur during impact. The differences in the vehicle kinematics appear to result from the effects of the rear bumper impact against the bridge rail in the full-scale test. Recall that the bumper on the FEA model does not extend the width of the truck and therefore does not contact rail. As a result, the bed of the cargo box passed over the top of the rail in the FEA. This also allowed for slightly higher pitch of the cargo box as the impact event continued.

6.2.5 Damage to Bridge Rail

The crash test installation received minor damage as shown in Figure 67. The test resulted in only minor scuffing of the rail and tire marks. The maximum dynamic deflection of the bridge rail was 1.0 inch (25 mm) occurring near the critical post (Post 7). The resulting permanent deflection at these locations was reported as 0.51 inches (13 mm). Posts 6 and 7 were tilted back and the baseplates of both posts were raised upward at the center approximately 0.14 inches (3.5 mm).

The damage to the bridge rail in the finite element analysis was similar to that of the full-scale test. The vehicle was in contact with the barrier for 42 feet from post 6 through post 11. The vehicle then remained near to, and parallel to, the rail until the vehicle exited the system at the end of the sidewalk. The maximum dynamic deflection of Post 6 and Post 7 was 1.77 inches and 1.70 inches, respectively; the resulting permanent deflections were 0.7 inches for both posts. Figures 68 and 69 shows contour plots of effective plastic strain on the railing from a traffic-side and back-side viewpoint, respectively. As post 7 was tilted back, the baseplate was deflected upward at the front-center of the plate 0.11 inches, compared to 0.14 inches in the full-scale test, as illustrated in Figure 70. Overall, the simulated barrier response was very similar to that observed in the full-scale test.

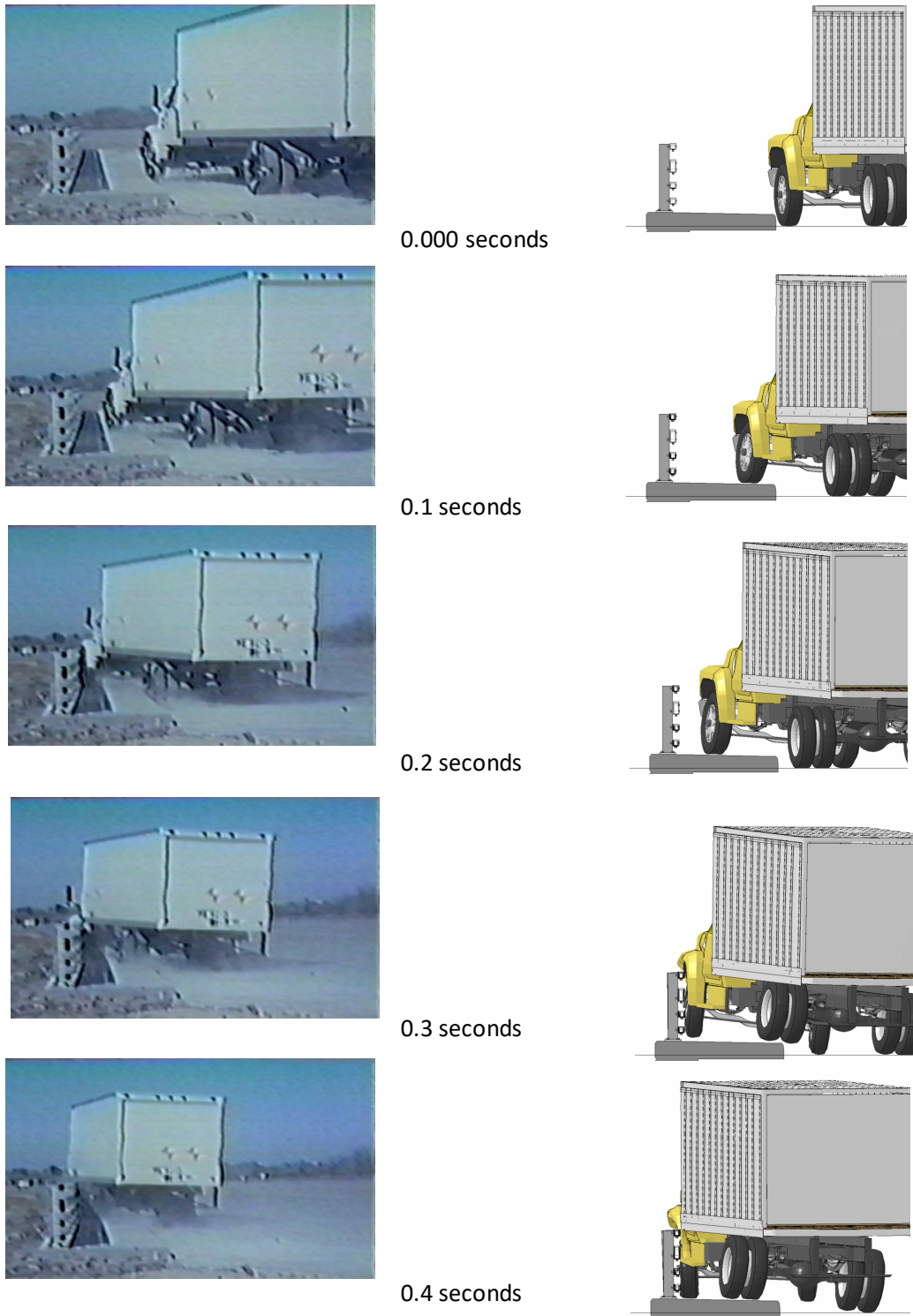
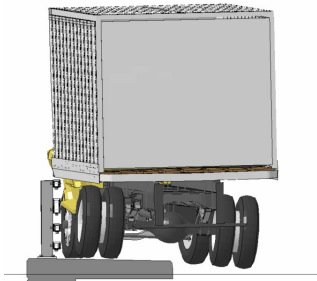


Figure 64. Sequential views of Test NETC-3 and FE analysis from upstream viewpoint.



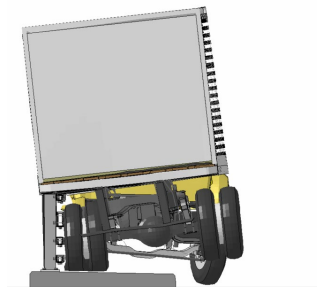
0.5 seconds



0.6 seconds



0.7 seconds



0.8 seconds



0.9 seconds

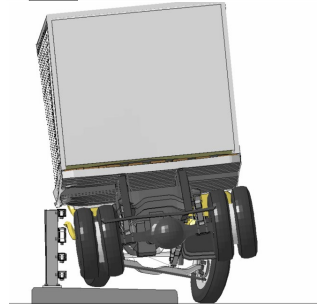


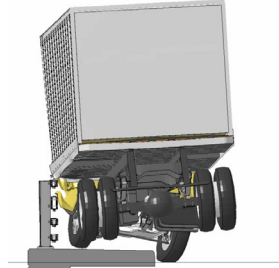
Figure 64. [CONTINUED] Sequential views of Test NETC-3 and FE analysis from upstream viewpoint.



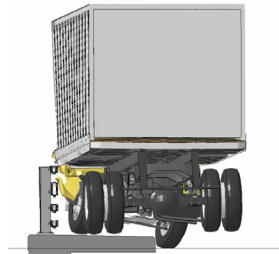
1.0 seconds



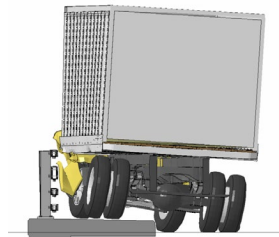
1.1 seconds



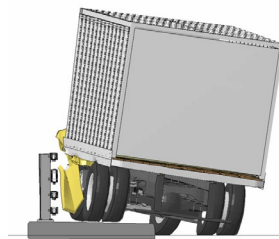
1.2 seconds



1.3 seconds



1.4 seconds



1.5 seconds

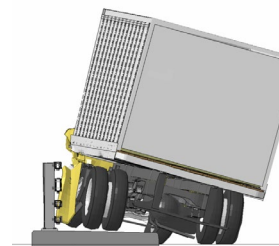
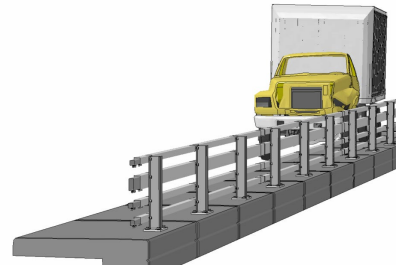


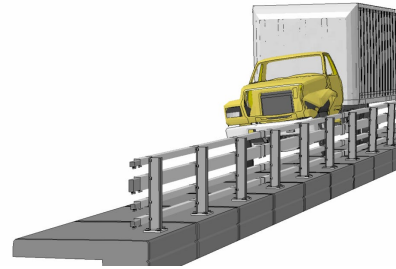
Figure 64. [CONTINUED] Sequential views of Test NETC-3 and FE analysis from upstream viewpoint.



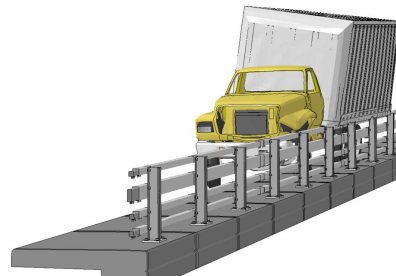
0.5 seconds



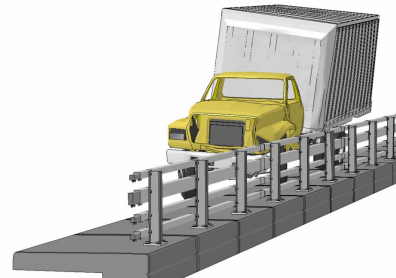
0.6 seconds



0.7 seconds



0.8 seconds



0.9 seconds

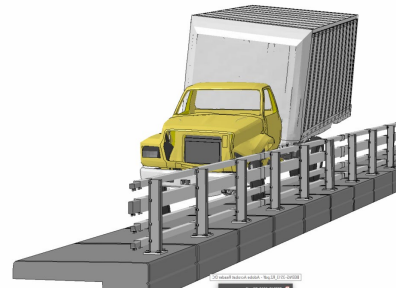
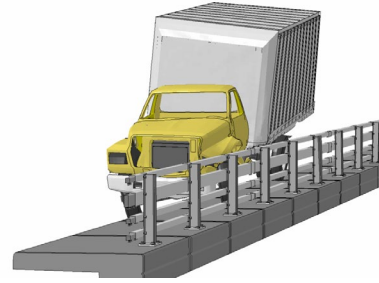


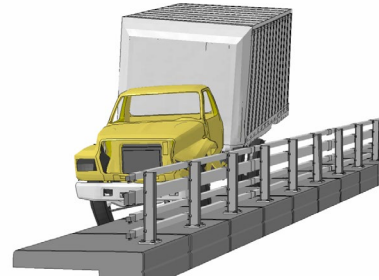
Figure 65. Sequential views of Test NETC-3 and FE analysis from downstream viewpoint.



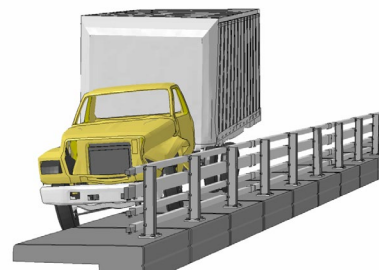
1.0 seconds



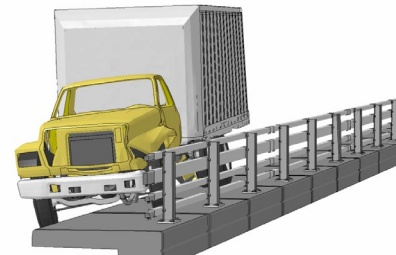
1.1 seconds



1.2 seconds



1.3 seconds



1.4 seconds

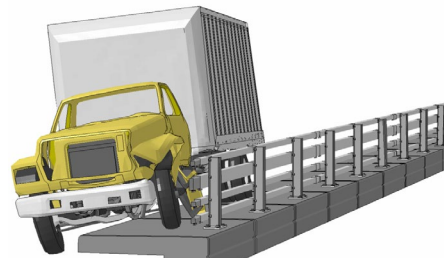


Figure 65. [CONTINUED] Sequential views of Test NETC-3 and FE analysis from downstream viewpoint.

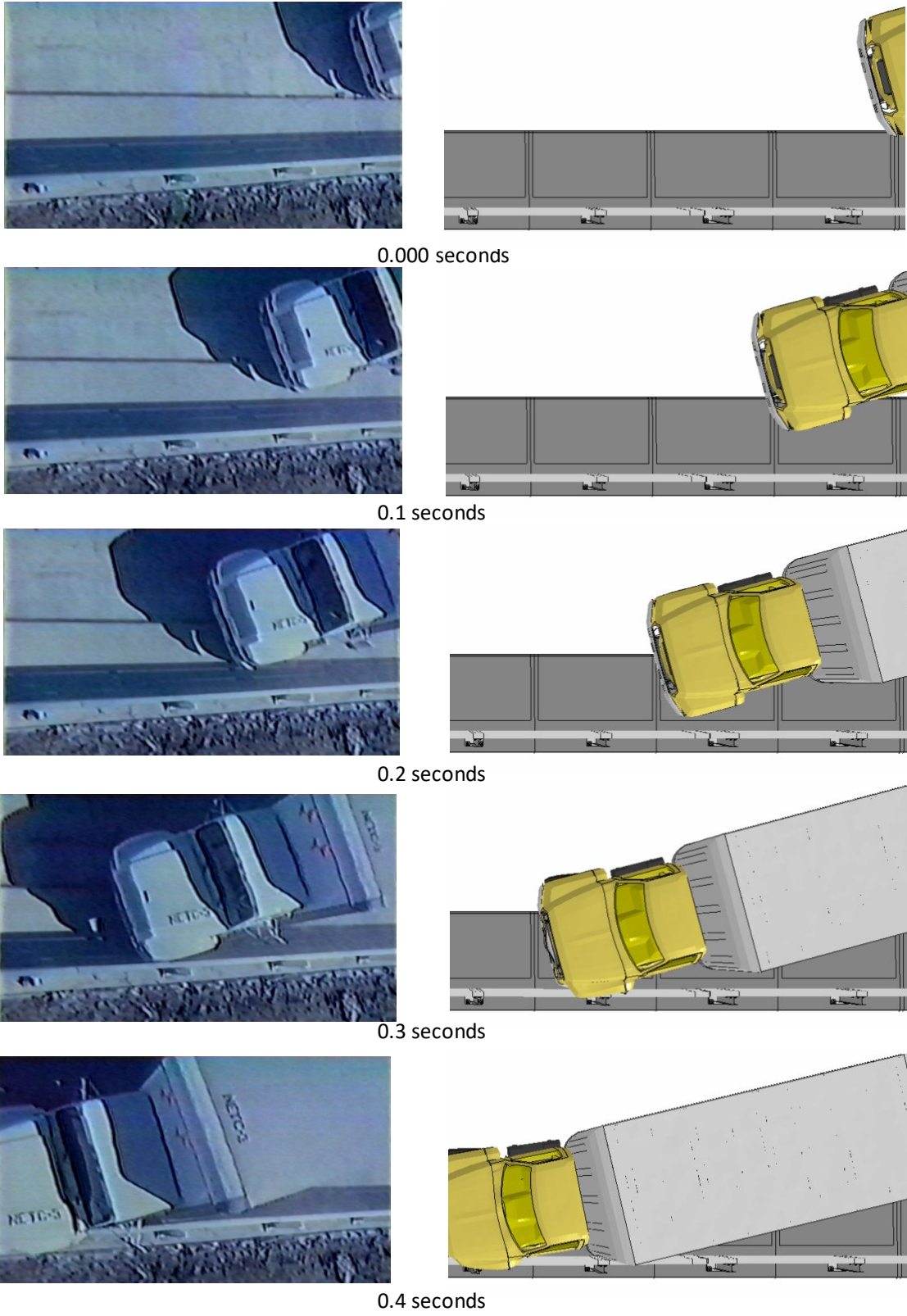
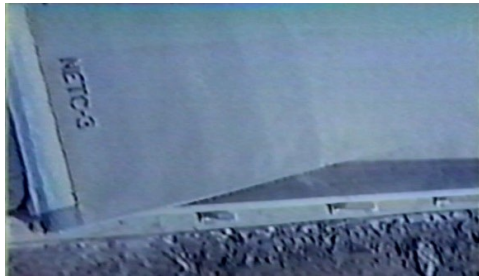
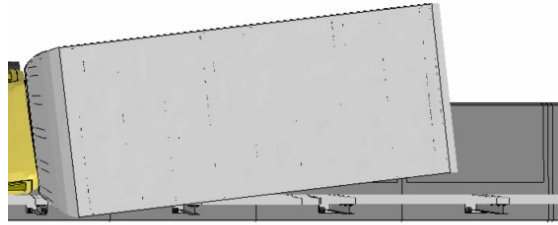


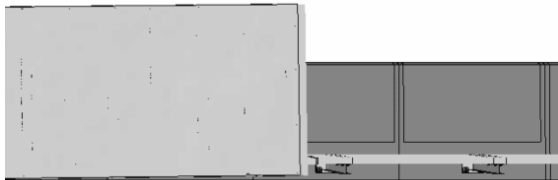
Figure 66. Sequential views of Test NETC-3 and FE analysis from overhead viewpoint.



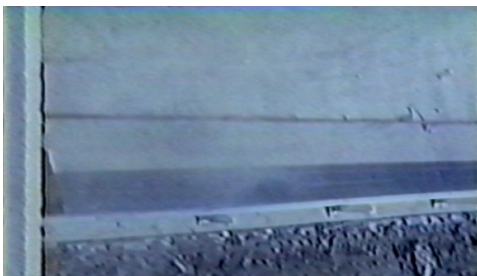
0.5 seconds



0.6 seconds



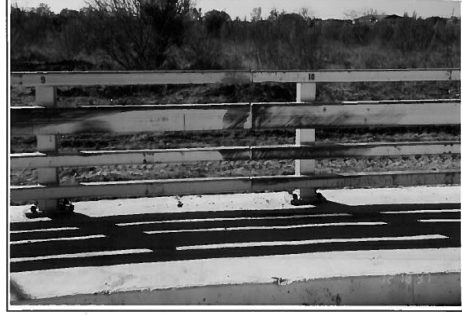
0.7 seconds



0.8 seconds



Figure 66. [CONTINUED] Sequential views of Test NETC-3 and FE analysis from overhead viewpoint.



(a)

(b)

Figure 67. Damage to bridge rail in full-scale test NETC-3 from (a) posts 6 through 8 and (b) 8 through 11.

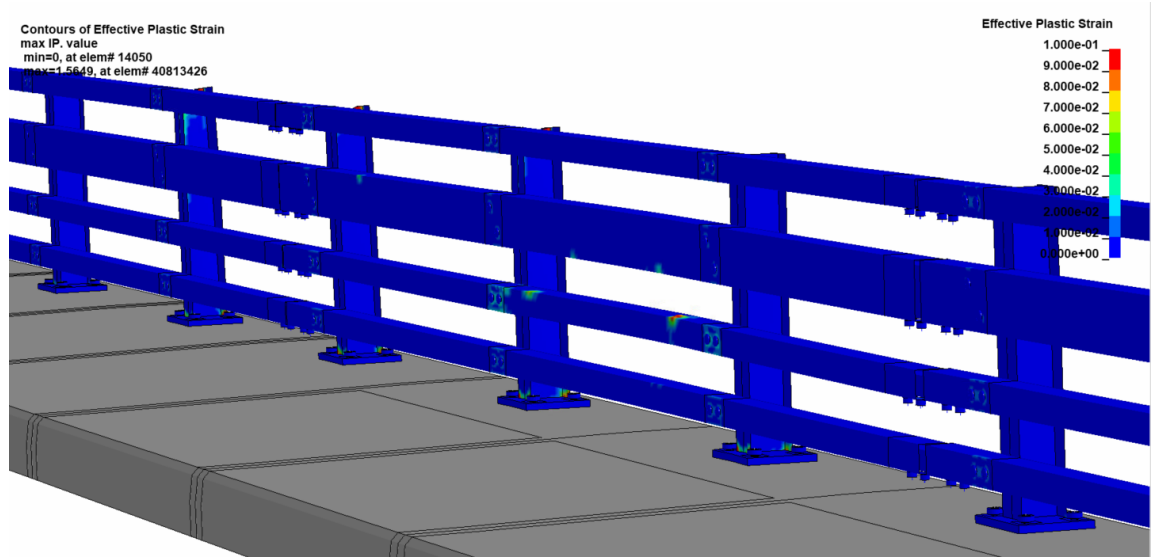


Figure 68. Contour plot of effective plastic strain showing deformations of the bridge rail model (traffic side).

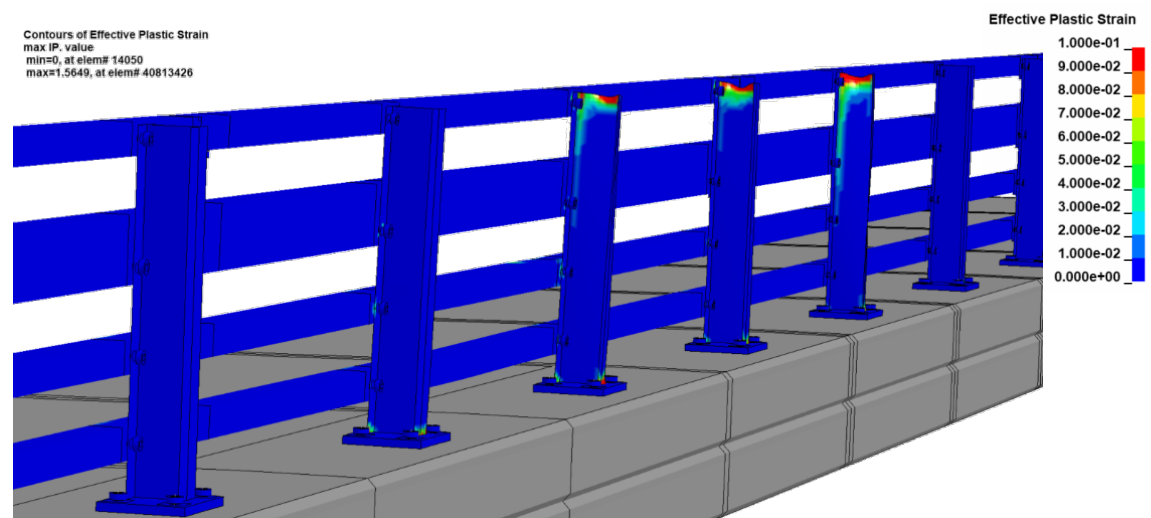


Figure 69. Contour plot of effective plastic strain showing deformations of the bridge rail model (back side).

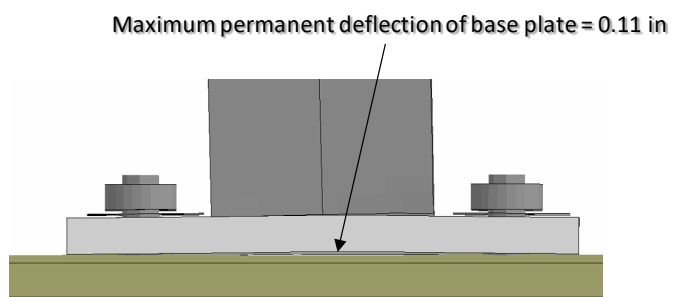


Figure 70. Deformation of baseplate for test (left) and FEA model (right).

6.2.6 Occupant Risk Measures

Acceleration-time histories and angular rate-time histories were collected inside the cargo box near the center of gravity of the vehicle, as illustrated in Figure 71 (compare to G and H in Figure 43). The time-history data was collected from the accelerometers in a local reference coordinate system that was fixed to the vehicle with the x-direction coincident with the forward direction of the vehicle, the local y-direction was oriented toward the right side of the vehicle and the local z-direction was oriented downward. The data was collected at a frequency of 50 kHz. Since the vehicle model struck the bridge rail from the opposite direction than the test vehicle, the “sign” for the data values collected for several of the channels was reversed for direct comparison with the test data (e.g., y-acceleration, roll-rate, and yaw-rate channels).

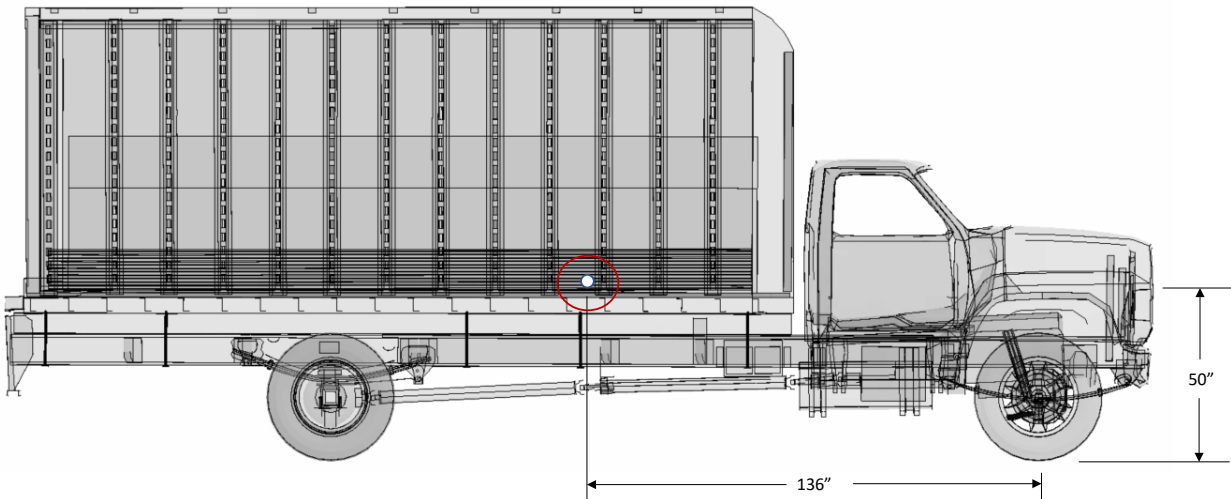


Figure 71. Location of accelerometer in FE model.

The analysis results from TRAP for the full-scale test and the FE analysis are shown in Table 53 and Figure 72. The acceleration data used in the TRAP program was pre-filtered using the BW Class 180 filter. The table shows the two occupant risk factors recommended by R350: 1) the lateral and longitudinal components of Occupant Impact Velocity (OIV), and 2) the maximum lateral and longitudinal component of resultant vehicle acceleration averaged over a 10-millisecond interval after occupant impact, called the Occupant Ridedown Acceleration (ORA). Also provided in the table are the CEN risk factors including the Theoretical Head Impact Velocity (THIV), the Post Impact Head Deceleration (PHD) and the Acceleration Severity Index (ASI). The table also includes comparison of the 50-millisecond moving average of the accelerations.

The occupant risk metrics for both the full-scale test and the simulation are in good agreement. The occupant impact velocity in the longitudinal direction was predicted from the simulation to be 5.9 ft/s (0.5 ft/s higher than the test OIV of 5.4 ft/s) at 0.4455 seconds. In the transverse direction, the occupant impact velocity predicted in the simulation was 12.1 ft/s (2.65 ft/s higher than the test OIV of 9.5 ft/s). The highest 0.010-second occupant ridedown acceleration in the longitudinal direction was 4.95 g (4 g lower than test ORA of 8.95 g) between 0.5490 and 0.5590 seconds. In the transverse direction, the highest 0.010-second occupant ridedown acceleration was 12.1 g (15.4 percent or 2.2 g lower than test ORA of 14.3) between 0.6883 and 0.6983 seconds. The THIV, PHD and ASI predicted from the simulation were 13.8 ft/s, 12.8 g's, and 0.42, respectively. These values were not reported in the test report. The

maximum 50-millisecond moving average accelerations in the x-, y-, and z-directions were 2.2 g (0.52 g lower than test), 3.8 g (2.1 g lower than test), and 1.2 g (not reported in test), respectively. The maximum yaw, roll and pitch angles were 16.2 degrees (1.43 degrees higher), 14.7 degrees (5.3 degrees lower) and 5.4 degrees (0.4 degrees higher), respectively. The roll and pitch angles reported in the test were approximated from the test videos, since these data were not collected using on-board instrumentation.

Except for the roll angle, the results of the FEA were well within the recommended limits of NCHRP Web Report 179 for each of the comparison metrics. That is, the difference in OIV was less than 20 percent or 6.6 ft/s; the difference in maximum ORA was less than 20 percent or 4 g; and the difference in angular displacement was less than 20 percent or 5 degrees. As mentioned previously, the reported roll angle was approximated from the test video as 20 degrees, which was higher than the FEA. However, the sequential views in Figure 64 show the roll angle of the FEA model to be very similar to the test during interaction with the barrier, and somewhat greater than the test during post-impact trajectory.

Table 53. Occupant risk measured computed using TRAP software for the FEA and Test NETC-3.

Occupant Risk Factors		MASH Test 3-11		Error		W179 Criteria	
		NETC-3	FEA				
		(0 - 1.0 seconds)	(0 - 1.0 seconds)	%	Absolute	Criteria	Pass
Occupant Impact Velocity (ft/s)	x-direction	5.4	5.9	9.1%	0.49212	<20% or < 6.6 f/s	Y
	y-direction	-9.5	-12.1	28.0%	2.657448	<20% or < 6.6 f/s	Y
	at time		at 0.4455 seconds on left side of interior				
THIV (m/s)			13.8 at 0.4411 seconds on left side of interior	-	13.77936	<20% or < 6.6 f/s	-
Ridedown Acceleration (g's)	x-direction	8.95	4.95 (0.5490 - 0.5590 seconds)	44.7%	4	<20% or < 4G	Y
	y-direction	-14.3	-12.1 (0.6883 - 0.6983 seconds)	15.4%	2.2	<20% or < 4G	Y
PHD (g's)			12.8 (0.6882 - 0.6982 seconds)	-	12.8	<20% or < 4G	-
ASI			0.42 (0.5880 - 0.6380 seconds)	-	0.42	<20% or < 0.2	-
Max 50-ms moving avg. acc. (g's)	x-direction	-2.72	-2.2 (0.6603 - 0.7103 seconds)	19.1%	0.52	<20% or < 4G	Y
	y-direction	5.9	3.8 (0.6073 - 0.6573 seconds)	35.6%	2.1	<20% or < 4G	Y
	z-direction		-1.2 (0.2700 - 0.3200 seconds)	-	1.2	<20% or < 4G	-
Maximum Angular Disp. (deg)	Yaw	14.77	16.2 (0.6784 seconds)	9.7%	1.43	<20% or < 5 deg	Y
	Roll	20	14.7 (1.4987 seconds)	26.5%	5.3	<20% or < 5 deg	N
	Pitch	-5.0	-5.4 (1.0139 seconds)	8.0%	0.4	<20% or < 5 deg	Y

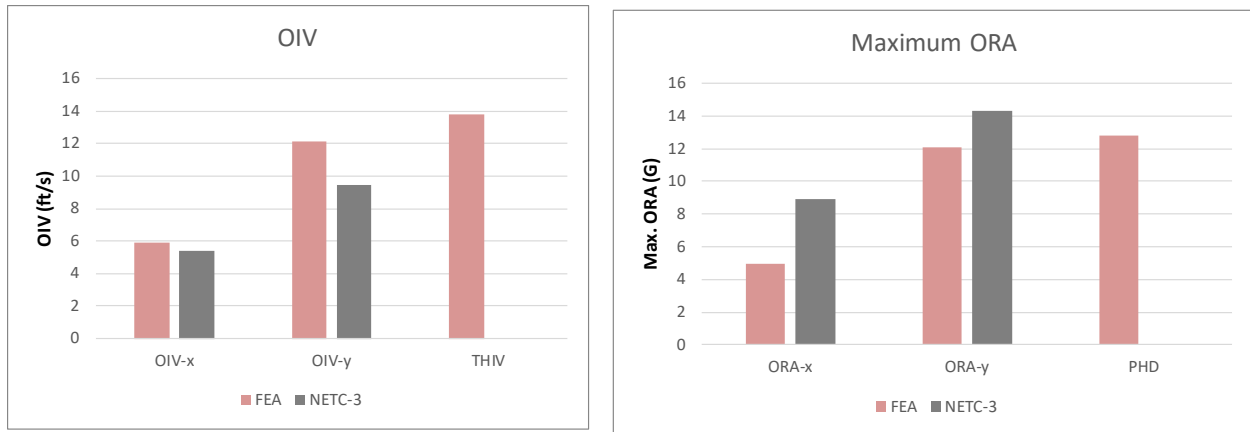


Figure 72. Graphical comparison of FEA vs. Test for key occupant risk metrics

6.2.7 Time-History Data Comparison

Figure 73, Figure 74, and Figure 75 show a comparison of the acceleration-time histories (i.e., filtered at 180 Hz. and running 50-ms average) at the c.g. of the vehicle (i.e., on the cargo box) for the longitudinal, transverse and vertical channels, respectively. Figure 76, Figure 77 and Figure 78 show comparisons of the angular rates and angular displacements (i.e., yaw, roll, and pitch) measured from the c.g. in the test and FE analysis. The test data was taken directly from images in the test report; thus, the comparison was made only cases where data was reported.

There was a very significant spike in y-acceleration at approximately 0.57 seconds, corresponding to the time of impact of the rear tandem wheel set against the rail. The higher accelerations in the test are assumed to be due to the rear bumper impacting against the railing; which was not applicable in the FEA. Without the rear bumper interaction in the FEA, the rear of the cargo box passed over the top of the railing, resulting in lower forces against the vehicle. There was also a significant spike in the x-acceleration at approximately 0.70 – 0.75 seconds. In the FEA, this corresponded to the lower edge of the cargo box snagging on the top of the bridge rail posts. The cause for the spikes in the test was not reported, but from the high-speed video it was assumed that the spike in acceleration was due to a combination of the cargo box snagging on the tops of the posts and the rear bumper snagging on the railing (see Figure 79).

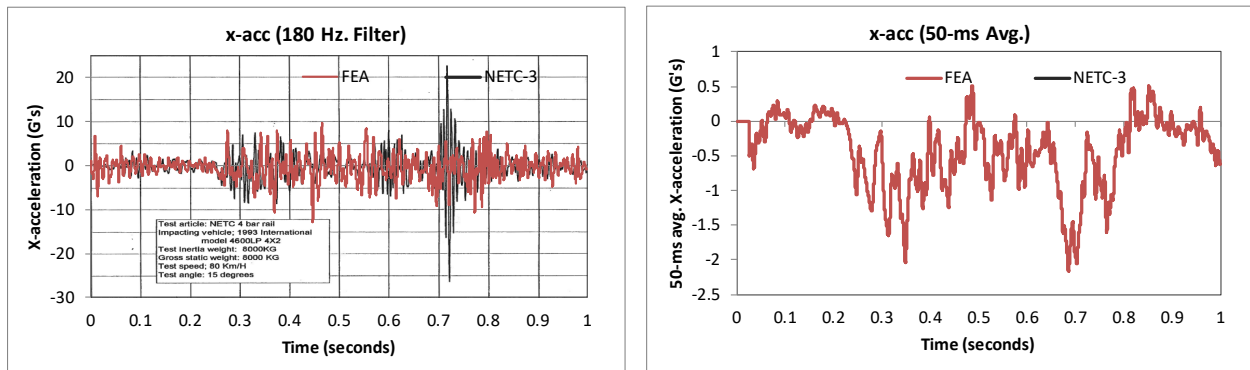


Figure 73. Longitudinal acceleration-time history plot from accelerometer at c.g. for full-scale Test NTC-3 and FEA (180 Hz. filter and 50-ms moving averages).

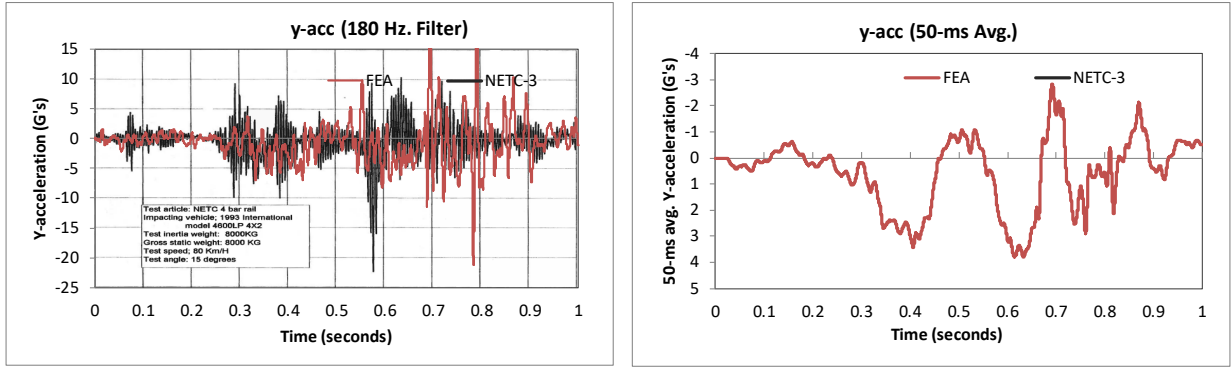


Figure 74. Lateral acceleration-time history plot from accelerometer at c.g. for full-scale Test NETC-3 and FEA (180 Hz. filter and 50-ms moving averages).

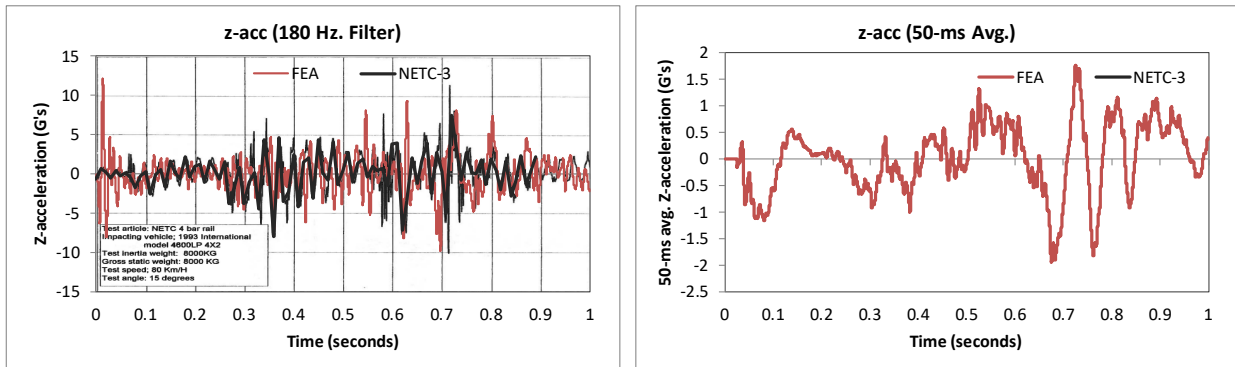


Figure 75. Vertical acceleration-time history plot from accelerometer at c.g. for full-scale Test NETC-3 and FEA (180 Hz. filter and 50-ms moving averages).

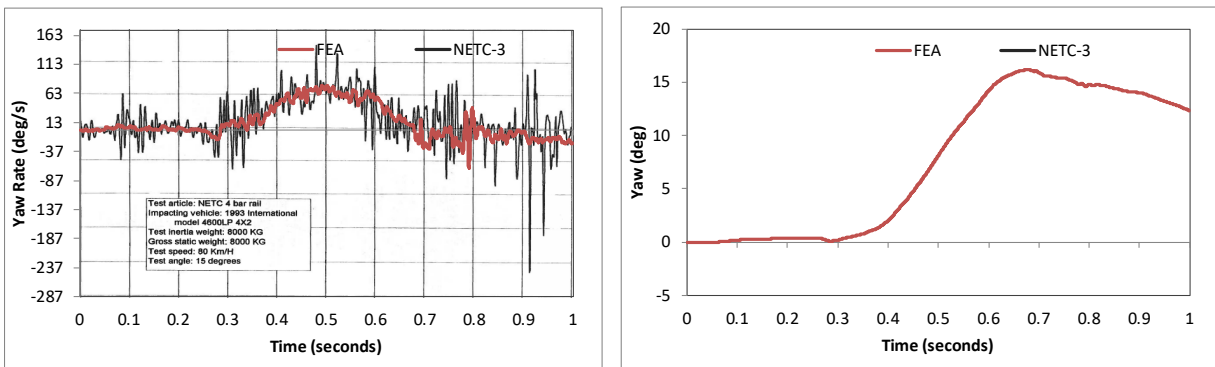


Figure 76. Yaw-time history plot from accelerometer at c.g. for FEA (angular rate and displacement).

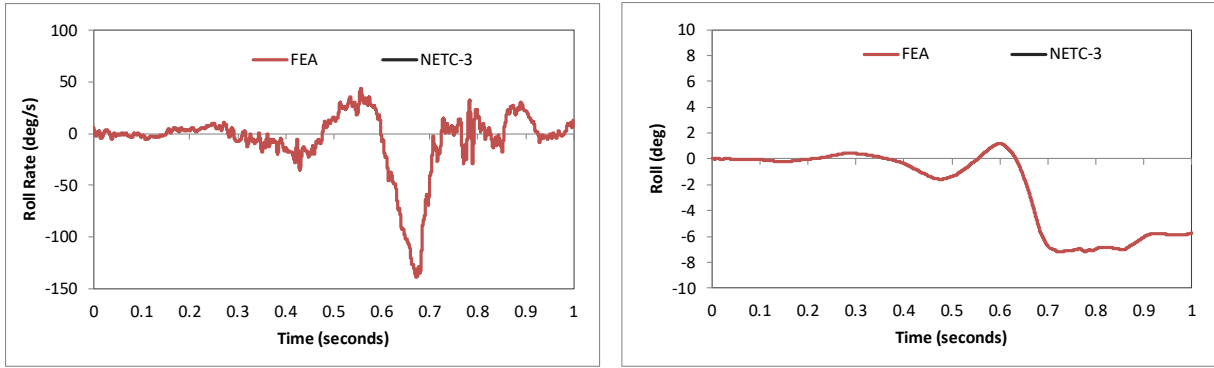


Figure 77. Roll-time history plot from accelerometer at c.g. for FEA (angular rate and displacement).

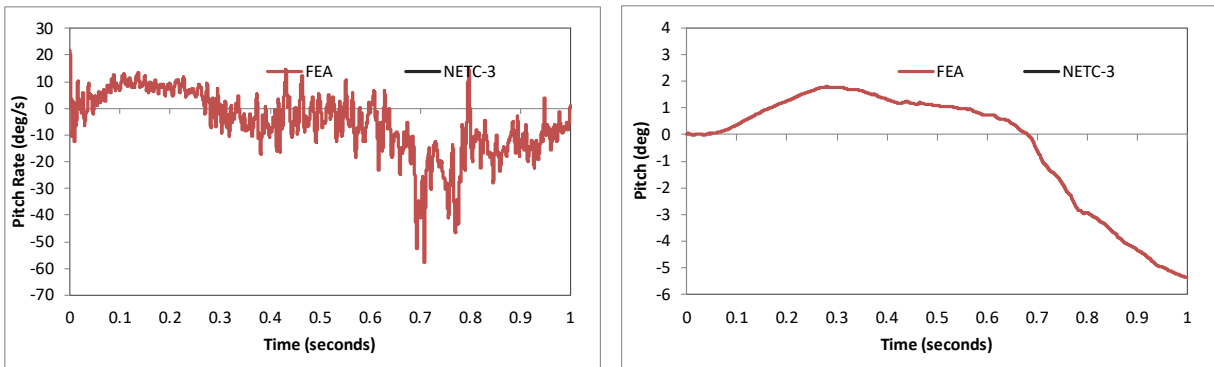


Figure 78. Pitch-time history plot from accelerometer at c.g. for FEA (angular rate and displacement).



Figure 79. Post-test photo of vehicle damages.

6.2.8 PIRT – Crash Specific Phenomena

Table 54 contains the Report 350 crash test criteria. Those that apply to Test 4-12 are marked in red. These include criteria A, D, G, K and M. Table 55 through Table 57 contain an expanded list of these same criteria including additional specific phenomena that were measured in the test and that could be directly compared to the numerical solution. Table 55 contains a comparison of phenomena related to structural adequacy, Table 56 contains a comparison of phenomena related to occupant risk, and Table 57 contains a comparison of phenomena related to vehicle trajectory. Some of this information has already been presented but is repeated here for completeness of the recommended validation forms. Comparisons for all the applicable crash specific phenomena between the FEA and test were within the allowable limits of Report W179, except for the roll angle which was explained in the Occupant Risk Measures section.

Table 54. Report 350 crash test criteria with the applicable test numbers.

Evaluation Factors	Evaluation Criteria			Applicable Tests
Structural Adequacy	A	Test article should contain and redirect the vehicle; the vehicle should not penetrate, under-ride, or override the installation although controlled lateral deflection of the test article is acceptable.		10, 11, 12, 20, 21, 22, 35, 36, 37, 38
	B	The test article should readily activate in a predictable manner by breaking away, fracturing or yielding.		60, 61, 70, 71, 80, 81
	C	Acceptable test article performance may be by redirection, controlled penetration or controlled stopping of the vehicle.		30, 31, 32, 33, 34, 39, 40, 41, 42, 43, 44, 50, 51, 52, 53
Occupant Risk	D	Detached elements, fragments or other debris from the test article should not penetrate or show potential for penetrating the occupant compartment, or present an undue hazard to other traffic, pedestrians or personnel in a work zone.		All
	E	Detached elements, fragments or other debris from the test article, or vehicular damage should not block the driver's vision or otherwise cause the driver to lose control of the vehicle. (Answer Yes or No)		70, 71
	F	The vehicle should remain upright during and after the collision although moderate roll, pitching and yawing are acceptable.		All except those listed in criterion G
	G	It is preferable, although not essential, that the vehicle remain upright during and after collision.		12, 22 (for test level 1 – 30, 31, 32, 33, 34, 35, 36, 37, 38, 39, 40, 41, 42, 43, 44)
	H	Occupant impact velocities should satisfy the following:		
Occupant Impact Velocity Limits (m/s)				
Component		Preferred	Maximum	
	Longitudinal and Lateral	9	12	

		Longitudinal	3	5		60, 61, 70, 71
	I	Occupant ridedown accelerations should satisfy the following:				10, 20, 30,31, 32, 33, 34, 36, 40, 41, 42, 43, 50, 51, 52, 53, 60, 61, 70, 71, 80, 81
		Occupant Ridedown Acceleration Limits (g's)				
		Component	Preferred	Maximum		
		Longitudinal and Lateral	15	20		
Vehicle Trajectory	K	After collision it is preferable that the vehicle's trajectory not intrude into adjacent traffic lanes.				All
	L	The occupant impact velocity in the longitudinal direction should not exceed 40 ft/sec and the occupant ride-down acceleration in the longitudinal direction should not exceed 20 G's.				11,21, 35, 37, 38, 39
	M	The exit angle from the test article preferable should be less than 60 percent of test impact angle, measured at the time of vehicle loss of contact with test device.				10, 11, 12, 20, 21, 22, 35, 36, 37, 38, 39
	N	Vehicle trajectory behind the test article is acceptable.				30, 31, 32, 33, 34, 39, 42, 43, 44, 60, 61, 70, 71, 80, 81

Table 55. Roadside safety phenomena importance ranking table (structural adequacy).

		Evaluation Criteria	Known Result	Analysis Result	Difference Relative/Absolute	Agree ?	
Structural Adequacy	A	A1	Test article should contain and redirect the vehicle; the vehicle should not penetrate, under-ride, or override the installation although controlled lateral deflection of the test article is acceptable. (Answer Yes or No)	Y	Y	X	Y
		A2	Maximum dynamic deflection: - Relative difference is less than 20 percent or - Absolute difference is less than 6 inches	1.0 in	1.77 in	0.77 in	Y
		33	Maximum permanent deflection: - Relative difference is less than 20 percent or - Absolute difference is less than 6 inches	0.51 in	0.7 in	0.19 in	Y
		A4	Length of vehicle-barrier contact (at initial separation): - Relative difference is less than 20 percent or - Absolute difference is less than 6.6 ft	N.R. Posts 6-11	42 ft Posts 6-11		Y
		A5	Number of broken or significantly bent posts is less than 20 percent.	0	0		Y
		A6	Did the rail element rupture or tear (Answer Yes or No)	No	No	X	Y
		A7	Concrete curb/deck failure	No	No	X	Y
		8	Was there significant snagging between the vehicle wheels and barrier elements (Answer Yes or No).	N	N	X	Y
		A9	Was there significant snagging between vehicle body components and barrier elements (Answer Yes or No).	N*	N	X	Y

* There was additional snagging between the bumper and the rail in the test that could not be captured in the FE model due to differences in bumper width.

N.R. – Not Reported

Table 56. Roadside safety phenomena importance ranking table (occupant risk).

Evaluation Criteria			Known Result	Analysis Result	Difference Relative/ Absolute	Agree ?	
Occupant Risk	D	Detached elements, fragments or other debris from the test article should not penetrate or show potential for penetrating the occupant compartment, or present an undue hazard to other traffic, pedestrians or personnel in a work zone. (Answer Yes or No)	N	N		Y	
	F	F1	The vehicle should remain upright during and after the collision although moderate roll, pitching and yawing are acceptable. (Answer Yes or No)	Y	Y		Y
		F2	Maximum roll of the vehicle through 1.0 seconds: - Relative difference is less than 20 percent or - Absolute difference is less than 5 degrees.	*20.0 Deg	14.7 deg	26.5 % 5.3 deg	N
		F3	Maximum pitch of the vehicle through 1.0 seconds: - Relative difference is less than 20 percent or - Absolute difference is less than 5 degrees.	*5.0 deg	5.4 deg	8.0 % 0.4 deg	Y
		F4	Maximum yaw of the vehicle through 0.446 seconds: - Relative difference is less than 20 percent or - Absolute difference is less than 5 degrees.	14.8 deg	16.2 deg	9.7 % 1.4 deg	Y
	G	1	Did the vehicle remain upright during and after collision	Y	Y		Y
	L	L1	Occupant impact velocities: - Relative difference is less than 20 percent or - Absolute difference is less than 6.6 ft/s.				
			• Longitudinal OIV (ft/s)	5.4	5.9	9.1% 0.5 ft/s	Y
			• Lateral OIV (ft/s)	-9.5	-12.1	28% 2.7 ft/s	Y
		• THIV (ft/s)	N.R.	13.8			
		L2	Occupant accelerations: - Relative difference is less than 20 percent or - Absolute difference is less than 4 g's.				
			• Longitudinal ORA	8.95	4.95	44.7 % 4 g	Y
			• Lateral ORA	14.3	12.1	15.4 % 2.2 g	Y
	• PHD		N.R.	12.8			
• ASI	N.R.	0.42					

N.R. – Not Reported

* Reported as “approximate”

The reported roll angle was approximated from the test video as 20 degrees, which was higher than the FEA. However, the sequential views Figure 64 show the roll angle of the FEA model to be very similar to the test during interaction with the barrier, and somewhat greater than the test during post-impact trajectory.

Table 57. Roadside safety phenomena importance ranking table (vehicle trajectory).

Evaluation Criteria				Known Result	Analysis Result	Difference Relative/ Absolute	Agree ?
Vehicle Trajectory	K	M1	The exit angle from the test article preferable should be less than 60 percent of test impact angle, measured at the time of vehicle loss of contact with test device.	1.3%	8.0%	X	Y
		M2	Exit angle at loss of contact: - Relative difference is less than 20 percent or - Absolute difference is less than 5 degrees.	4.1 deg	1.2 deg	2.9 deg	Y
	M	M3	Exit velocity at loss of contact: - Relative difference is less than 20 percent or - Absolute difference is less than 6.2 mph.	35.8 mph	40.3 mph	12.8 % 4.6 mph	Y
		4	Front axle disconnected from suspension	Y	Y		Y

6.2.9 Summary and Conclusions on Model Validation

The baseline finite element model of the NETC 4-bar bridge rail was used to simulate full-scale crash NETC-3. The test corresponded to R350 Test 4-12 on the sidewalk-mounted bridge rail system. The results of the analysis were compared to the full-scale tests to validate the fidelity of the model. The validation included qualitative assessments involving: (1) comparing sequential snapshots of the test and simulation to verify vehicle kinematic response, as well as, the sequence and timing of key phenomenological events, (2) comparing acceleration and angular-rate time-history data from the FEA and test, and (3) comparison of crash-specific phenomena from the event related to structural adequacy, occupant risk and vehicle trajectory.

There were issues regarding missing information from the test data that were noted. In particular, the physical properties of the test vehicle were not included in the test report but were visibly different than that of the FEA model. Also, quantitative comparison of the time-history data could not be performed, since the test data was not available.

In general, the results of the analyses demonstrated that the finite element model replicated the basic phenomenological behavior of the system under Report 350 Test 4-12 impact conditions. There was good agreement between the tests and the simulations with respect to event timing, overall kinematics of the vehicle, barrier damage, and deflections. One exception involved the rear bumper snagging on the bridge rail resulting in higher longitudinal deceleration of the vehicle than occurred in the FEA. The model is, however, considered adequately “valid” and will be used as a baseline model for developing and evaluating *MASH* impact conditions for the NETC bridge rails. Table 58 provides a summary of key validation metrics for the evaluation of the model for the curb-mounted system.

Table 58. Summary of validation metrics for the model in simulation of Test NETC-3.

Summary of FEA vs. Test Validation Metrics																	
System Type: Bridge Rail				Comparison: Crash tested original design to FEA of original design													
Device Name:/Variant: NETC 4-Bar sidewalk-mounted				Submissions Type:		Non-Significant -- Effect is Uncertain											
Testing Criterion: Report 350						Non-Significant -- Effect is Positive											
Test Level: TL4						Non-Significant -- Effect is Inconsequential											
FHWA Letter:				X		Baseline Validation of Crash Test to FEA Analysis.											
Crash Test																	
	Time = 0.0 sec		0.2 sec		0.4 sec		0.6 sec		0.9 sec		1.2 sec						
FEA Analysis																	
	Baseline Crash Test						W-179 Table E-5: Roadside PIRTS										
Test Number:		SwRI NETC-3				<u>Structural Adequacy</u>		<u>Test</u>		<u>FEA</u>		<u>Occupant Risk (cont.)</u>		<u>Test</u>		<u>FEA</u>	
Vehicle:		1993 International 4600 LP				A1 - Acceptable perf.?		yes		yes		H2 – Long. OIV		5.4 ft/s		5.9 ft/s	
Vehicle Mass:		17,875 lbs				A2 – Permanent Deflection:		0.51 in		0.7 in		H3 – Lat. OIV		9.5 ft/s		12.1 ft/s	
Impact Speed:		49.8 mph				A3 – Contact Length		-		42 ft		I2 – Long. ORA		8.95 g		4.95 g	
Impact Location:		2 ft upstream of Post 6				A4 - Component Failure		no		no		I3 – Lat. ORA		14.3 g		12.1 g	
Tested Hardware:		Original Design				A5 – Barrier Rupture?		no		no		<u>Vehicle Trajectory</u>					
FEA Hardware:		Original Design				A7 – Wheel Snagging?		no		no		K – Intruded into travel lanes?		no		no	
W-179 Table E-1: Verification Evaluation Summary						A8 – Vehicle Snagging?		no		no		N – Travel behind barrier?		no		no	
Total Energy:		0%		Pass		<u>Occupant Risk</u>		<u>Test</u>		<u>FEA</u>		W-179 Table E-3 (Multi-Channel Method)					
Hourglass Energy:		0%		Pass		D – Detached elements?		no		no		Sprague-Geer Magnitude < 40		-		-	
Mass Added:		0%		Pass		F2 – Max. Vehicle Roll		20		14.7		Sprague-Geer Phase < 40		-		-	
Shooting Nodes:		no		Pass		F3 – Max. Vehicle Pitch		5		5.4		ANOVA Mean		-		-	
Negative Volumes:		no		Pass		F4 – Max. Vehicle Yaw		14.8		1602		ANOVA Standard Deviation		-		-	

7 MODEL DEVELOPMENT AND VALIDATION OF THE NETC 2-BAR TRANSITION

7.1 Model Development

A detailed finite element model of the NETC 2-bar approach guardrail transition was developed as shown in Figure 80. The general assembly of the transition model is shown in Figures 81 and 82. Refer to Section 3 for more detailed description of the design. The FEA model includes 42 feet of the transition system and 23.8 feet of the NETC 2-bar bridge rail. Details of the transition model are presented in the following sections regarding material characterization and element formulations used for the various components. The bridge rail model was developed using the validated NETC 4-bar bridge rail as a baseline. Although the model of the NETC 2-bar bridge rail was included as part of the transition model analysis, it was not a major influence in the results since the vehicle did not contact the bridge rail during impact or redirection. Refer to Sections 6 and 7 for further details of the bridge rail model development.

The basic components of the transition model included:

- Twelve (12) 6"x8" wood posts at decreasing post spacing approaching the bridge rail,
- Five (5) discrete element soil model assemblies, one at each post of the w-beam rail and the w-beam-to-thrie-beam transition rail,
- One soil continuum model 7.1' (vertical depth) x 8.34 (lateral width) x 21.27' (long).
- One (1) standard 12-gauge w-beam panel and hardware,
- One (1) 10-gauge w-beam to thrie-beam transition panel and hardware,
- Two (2) thrie-beam panels (nested) and hardware,
- One (1) thrie-beam end shoe and hardware,
- One (1) connection plate and hardware,
- One (1) deflector plate and hardware,
- One (1) 9.44 feet long HSS 8" x 4" x 5/16" tubular section and post mounting bolt hardware,
- One (1) 9.44 feet long HSS 4" x 4" x 1/4" tubular section and post mounting bolt hardware,
- Four (4) 8.0 feet long W6x25 posts

The basic components of the bridge rail model include:

- Three (3) W6x25 posts,
- Three (3) post-baseplates that are 12"x10"x1",
- Twelve (12) anchor bolts (4 at each baseplate) connecting the baseplates to the curb,
- One (1) 9.44 feet long HSS 8" x 4" x 5/16" tubular section and post mounting bolt hardware,
- One (1) 9.44 feet long HSS 4" x 4" x 1/4" tubular section and post mounting bolt hardware,

- One (1) HSS 7" x 3" x 3/8" splice tube 20 inches long,
- One (1) HSS 3" x 3" x 5/16" splice tube 20 inches long
- Concrete curb and bridge deck model 21.5 feet long with steel reinforcement.

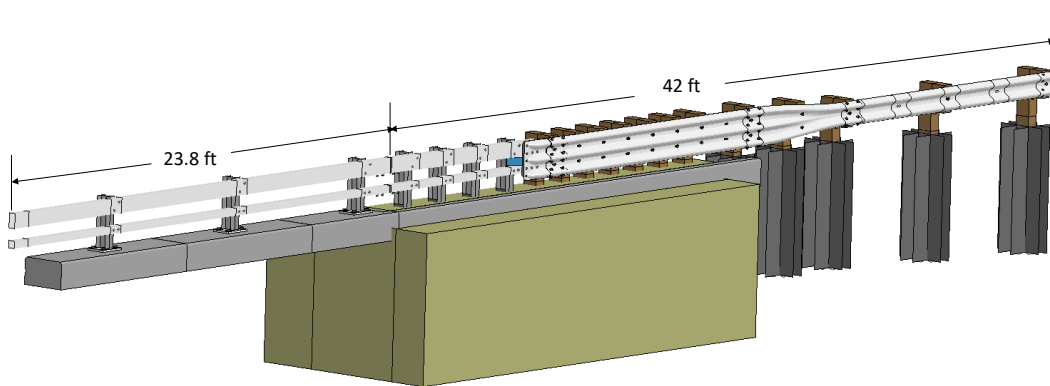


Figure 80. Finite element analysis model of the NETC 2-bar transition and bridge rail.

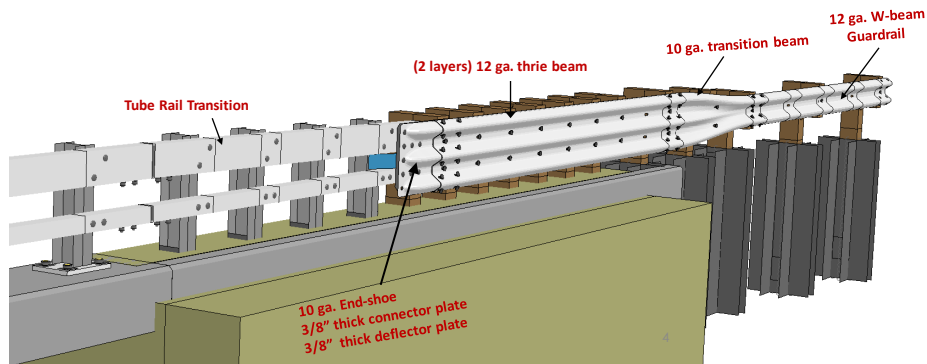


Figure 81. General model assembly for the NETC 2-bar transition (rail labeling).

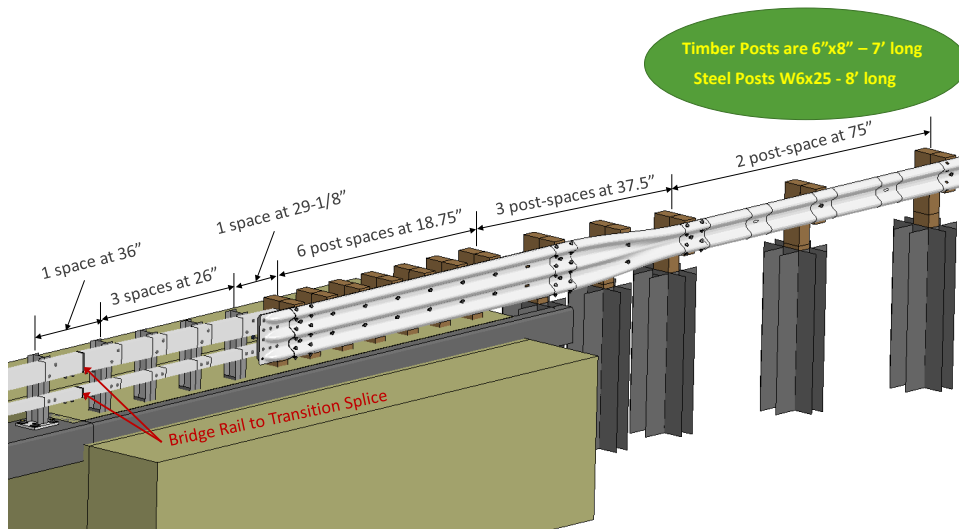


Figure 82. General model assembly for the NETC 2-bar transition (post labeling).

7.2 Materials

All steel posts, tube rails, baseplates, concrete and rebar were modeled as described for the NETC bridge rail model in Section 10. All wood material was modeled in LS-DYNA using material model *Mat_Wood_Pine with properties corresponding to Grade 1 Pine. The material for all thrie-beam and w-beam rails were modeled as AASHTO M180 Class A Type II, with minimum yield and tensile strength of 60 ksi and 72 ksi, respectively. The material for all plate material in the transition was modeled as AASHTO M180 Class A Type II steel with properties developed by Wright et. al. [Wright97]. All the post-bolts in the transition were modeled as ASTM A307 Grade A with yield strength of 46 ksi and ultimate strength of 62 ksi (engineering stress) or 72.8 ksi (true stress).

7.3 Development of the Transition model

7.3.1 Rail Elements and Terminal Connector

The material for w-beam, thrie-beam and thrie-beam transition components were modeled as AASHTO M180 Class A Type II steel. [Wright97]. The guardrail end of the transition model consists of a standard 13.55 feet long 12-ga w-beam panel. The finite element mesh for the w-beam is shown in Figure 83(a). The rail was modeled with thin-shell Belytschko-Tsay elements (Type 2 in LS-DYNA) with three integration points through the thickness. The sections of rail between post connection points were meshed with a nominal element size of 0.79 x 0.83 inches. The sections at the post connection points and splice connections were meshed with a nominal element size of 0.39" x 0.39". The elements around the edge of the splice-bolt holes were meshed with nominal element size of 0.12 inches.

The thrie-beam panel was modeled as 13.55 ft long with 12-ga thickness. The finite element mesh for the thrie-beam is shown in Figure 83(b). Slotted post-bolt holes were located at nine (9) locations on the panel at 18.75-inch spacing. The rail was modeled with Type 2 elements in LS-DYNA with five (5) integration points through the thickness. The panel was meshed with a nominal element size of 0.55 x 0.55 inches. The elements around the edge of the splice-bolt holes were meshed with nominal element size of 0.25 inches.

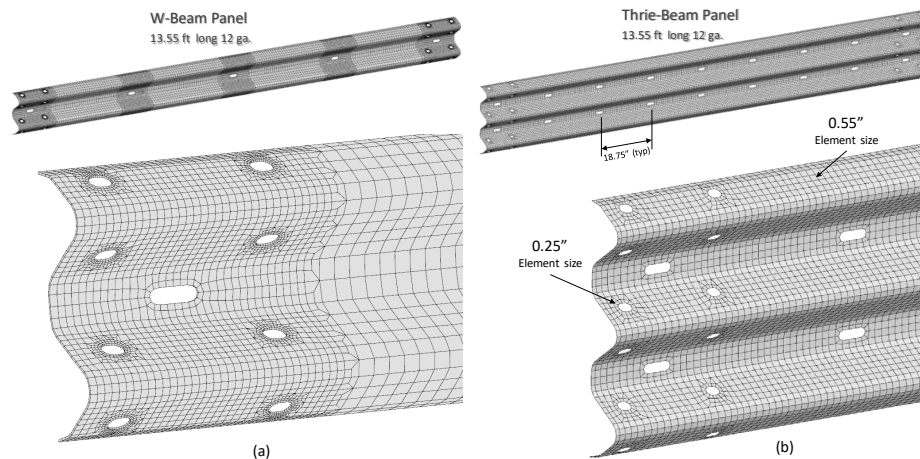


Figure 83: FEA mesh for (a) w-beam panel and (b) thrie-beam panel.

The geometry and mesh for the transition panel was created based on the drawings provided in Appendix B. The material was modeled as AASHTO M180 Class A Type II steel. The rail was modeled with Type 2 thin-shell elements in LS-DYNA with five (5) integration points through the thickness. The w-beam end of the panel was meshed identical to the standard w-beam model. The remainder of the panel was meshed with a nominal element size of 0.55 x 0.55 inches. The smallest elements were located around the edge of the splice-bolt holes with nominal element size of 0.25 inches.

The geometry for the thrie-beam terminal connector was developed in a previous project and conforms to the dimensions in Appendix B. The part was modeled with Type 2 thin-shell elements in LS-DYNA with five (5) integration points through the thickness. The part was meshed with a nominal element size of 0.51 x 0.55 inches. The elements around the edge of the bolt holes were meshed with nominal element size of 0.38 inches, with the smallest element size being 0.25.

The 3/8-inch thick connector plate and deflector plate were modeled with dimensions consistent with the detailed drawings in Appendix B. The material was modeled as ASTM A36 steel with material characterization adopted from Wright et. al. [Wright97]. The finite element models for the connection plate and the deflector plate are shown in Figure 86 and Figure 87, respectively. The parts were modeled with Type 2 thin-shell elements in LS-DYNA with five (5) integration points through the thickness. The connection plate was meshed with a nominal element size of 0.72 x 0.72 inches. The elements around the edge of the bolt holes were meshed with nominal element size of 0.25 inches. The deflector plate was meshed with a nominal element size of 0.5 x 0.5 inches. The elements around the edge of the bolt holes were meshed with nominal element size of 0.35 inches.

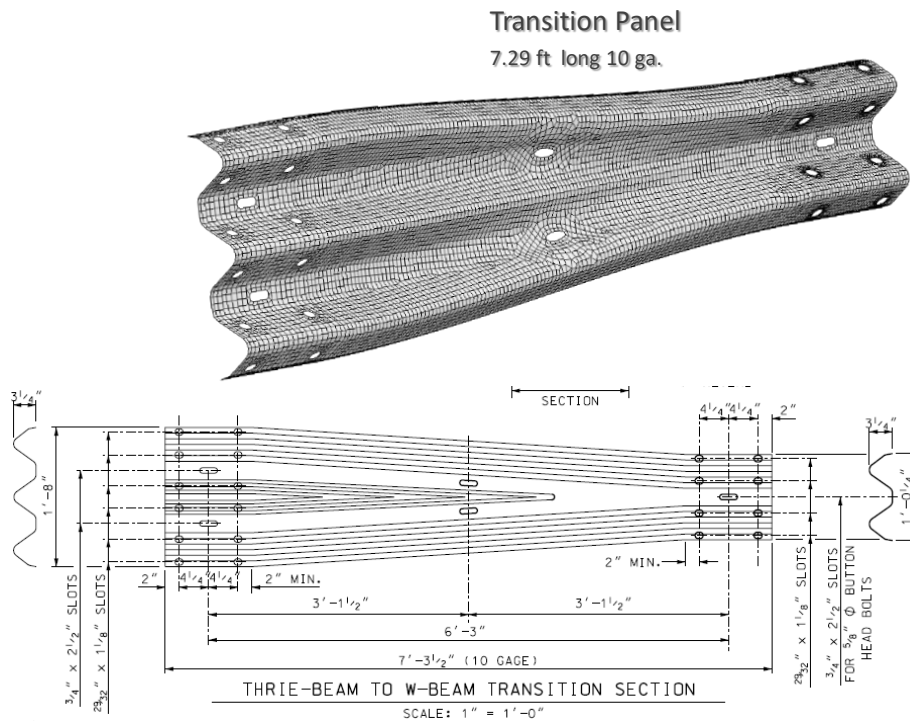


Figure 84. FEA mesh for the thrie-beam transition panel.

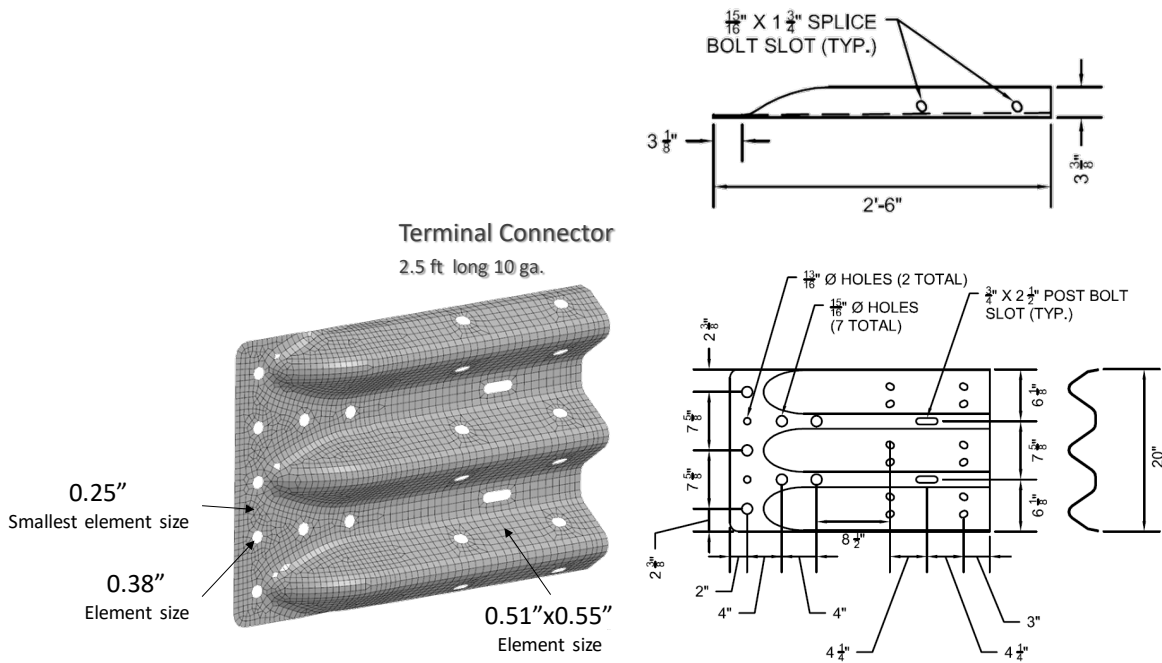


Figure 85. FEA mesh for the thrie-beam end-shoe terminal connector.

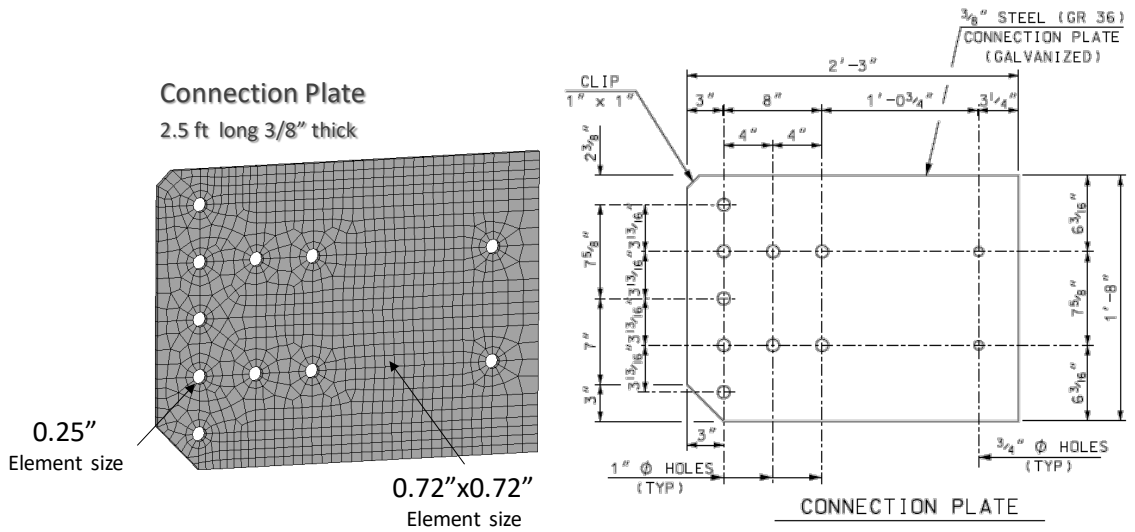


Figure 86. FEA mesh for the connection plate.

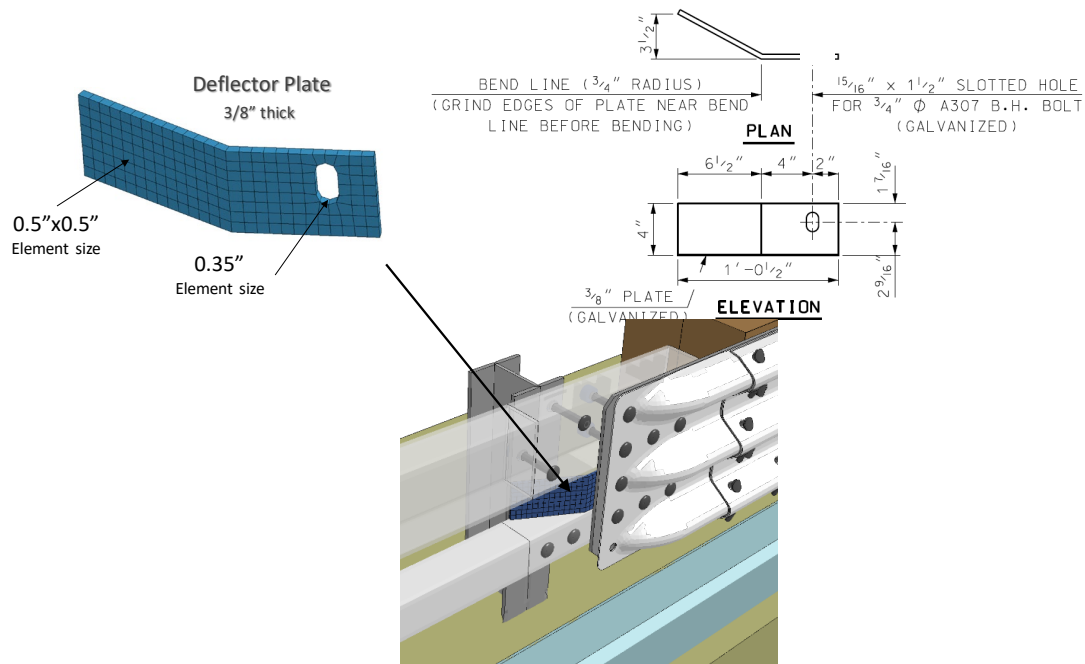


Figure 87. FEA mesh for the deflector plate.

7.3.2 Splice Bolts

Splice-bolt hardware seldom fails during impact, thus the material properties for the bolts and nuts were modeled with rigid material characterization. Failure of the splice connection is generally due to the “rigid” bolts rotating and tearing through the relatively thin w-beam material. Therefore, the bolts were modeled with geometric fidelity to obtain accurate force distribution and stress concentrations in the w-beam splice holes. The dimensions of the bolt hardware were modeled according to the standard drawing FBB01 for guardrail bolt and recessed nut (designation from AASHTO’s *A Standardized Guide to Highway Barrier Hardware*). [AASHTO04] The model of the splice bolts do not include the bolt-threads. Compression springs and dampers were attached between the end of the bolt and the nut to push the nut onto the bolt and clamp the rail panels together. The dampers are modeled as one-way dampers that “lock” the nut onto the bolt by preventing the nut from reversing direction. The FEA mesh of the splice bolts is shown in Figure 88(a). The images in Figure 88(b) show the bolt and rail at time equal zero (prior to bolt tightening) and at time equal 0.005 seconds (after bolts are tightened).

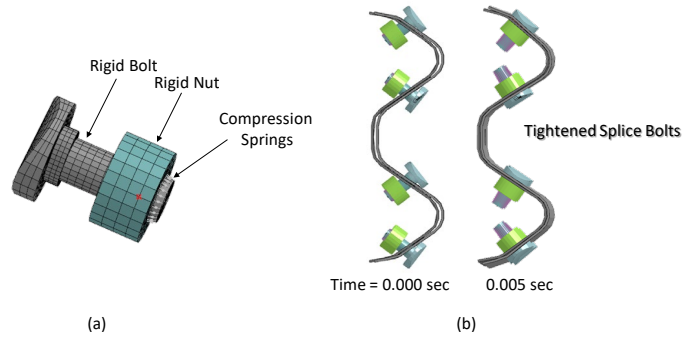


Figure 88. (a) FEA mesh for splice bolt and (b) profile of splice before and after tightening splice bolt tightening.

7.3.3 Post Bolts

The 5/8-inch diameter button-head post bolts were modeled with Hughes-Liu beam elements (Type 1 in LS-DYNA) with properties corresponding to ASTM A307. The FEA model of the post bolt is shown in Figure 89. The bolt-head, nut and the washer were modeled with rigid material properties, since the effects of deformation of these components are typically negligible compared to the effects of bolt deformations. To tighten the bolt and clamp the rail to the post, the nut was rigidly constrained to the end of the bolt, and a gradual pre-strain condition was then applied to 3-inch long section of the bolt (blue shading in Figure 89) in order to shrink the bolt approximately 3/8 inch in approximately 0.01 seconds.

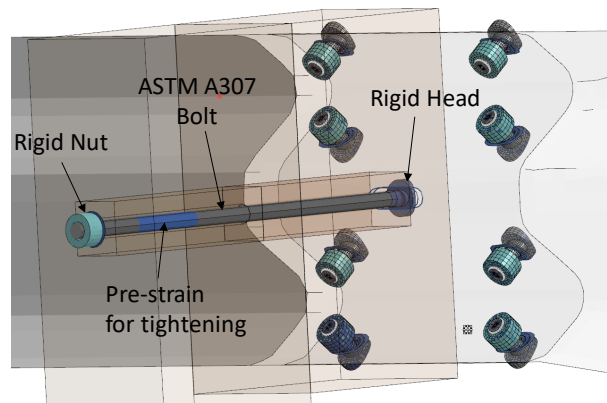


Figure 89. FEA model of the post bolt (typ) with the blockout, post, and rail displayed in transparency mode to facilitate viewing.

7.3.4 Wood Transition Posts

The cross-section dimensions of the wood posts and blockouts of the transition were 6 x 8 inches, and the length of the posts was 7 feet, as shown in the detailed drawing in Appendix B. The FEA mesh for a typical post is shown in Figure 90. The post was modeled with solid elements with single integration point. The post and blockout parts were meshed with a nominal element size of 1"x 1". The mesh in the post-bolt region was meshed with a nominal element size of 0.33"x0.33". The mesh of the post-bolt region was "tied" to the elements of the post using the *Contact_Tied option in LS-DYNA.

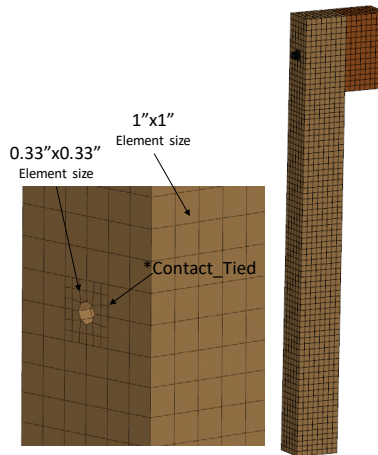


Figure 90. FEA model of wood AGT posts.

The wood material was modeled with mechanical properties consistent with Southern Yellow Pine. The LS-DYNA material model *Mat_Wood_Pine (material type 143) was used for the wood posts. The material model *Mat_Wood was developed by APTEK through a study sponsored by the Federal Highway Administration. [Murray07] This material model was developed specifically for finite element analyses of vehicle collisions into wooden guardrail posts. The constitutive model in *MAT_WOOD is characterized as a transversely isotropic material with yield surfaces. The model effectively simulates the stiffness, strength and post-peak softening behavior in the two primary directions of wood (i.e., parallel and perpendicular to wood grain). The model also includes rate effects which effectively increase the strength properties of the material as a function of strain rate. The default properties for Grade 1 Southern Yellow Pine were used in the FEA model. Additional information regarding validation of the wood material calibration for modeling wooden guardrail posts can be found in Plaxico, et al. [Plaxico15]

7.3.5 W6x25 Transition Posts

The posts in the tube-rail section of the transition (refer to Figures 80-82) are W6x25 and 8 feet long. The material for the post model conformed to ASTM A572 Grade 50 steel. The post was modeled with thin-shell Belytschko-Tsay elements (Type 2 in LS-DYNA) with five (5) integration points through the thickness. The flange and web were meshed with a nominal element size of 0.43 x 0.5 inches. The elements around the edge of the mounting holes were meshed with nominal element size of 0.32 inches.

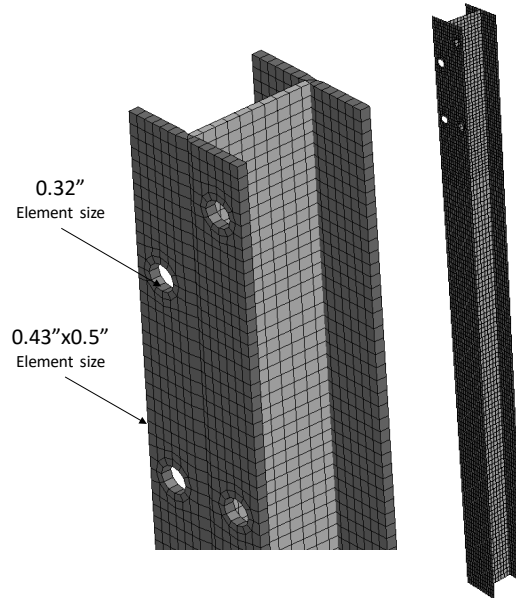


Figure 91. FEA mesh of the W6x25 posts of the transition.

7.3.6 Transition Rail Tubes

The tubular rail sections were modeled according to the dimensional specifications for HSS 4"x4"x 1/4" and HSS 8"x4"x 5/16". The material for all tube railing conformed to ASTM A500 Grade B. The tube rails were modeled with Type 2 thin-shell elements with five (5) integration points through the thickness. The finite element mesh for these components are shown in Figure 92. The nominal element size for the mesh was 0.75 x 1 inches for the span of rail between the posts, and 0.4 x 0.4 inches for the section of rail in contact with the posts. The mounting holes in the rail were 7/8" diameter and were meshed with a nominal element length of 0.25 inches around the hole opening.

The 3/4-inch diameter button head mounting bolts were modeled with Hughes-Liu beam elements (Type 1 in LS-DYNA) with properties corresponding to ASTM A325. The head of the bolts, as well as the nuts and washers were modeled with rigid material properties, since the effects of deformation of these components were expected to be negligible compared to the effects of bolt deformations. The bolts were given a pre-strain condition to tighten the railing onto the post.

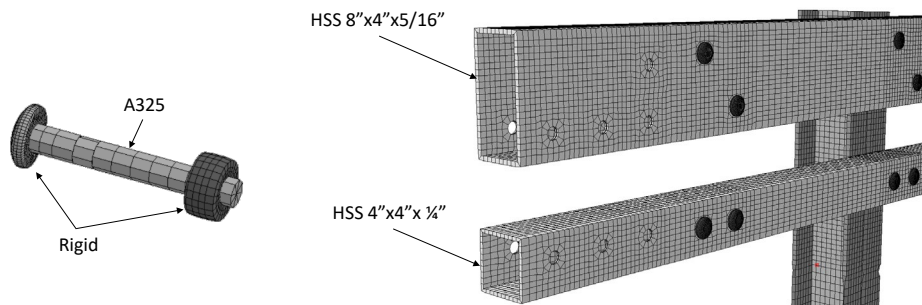


Figure 92. FEA mesh of the transition tube rails.

7.3.7 Curb

The transition includes a 7-inch tall granite curb with a 6-inch offset from the face of the tubular rails. The FEA model of the curb was modeled as a rigid material, thus damage to the curb (e.g., cracking and spalling) was not accounted for in the model. The soil grade for the posts in the transition is at the top of the curb.

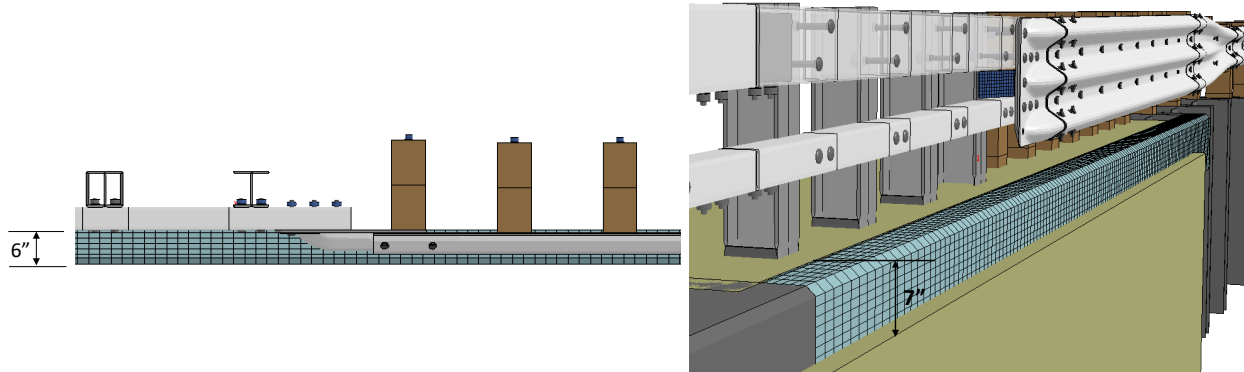


Figure 93. FEA model for curb.

7.3.8 Soil Model

There are several approaches that may be used for modeling the soil in analyses of guardrail posts embedded in soil. Some common approaches include: 1) posts embedded in a soil continuum of solid finite elements, 2) posts embedded in a continuum of meshless finite elements, and 3) subgrade reaction approach in which the post is supported by an array of uncoupled springs.

Each of these methods have been used by the research team with reasonable success. Some advantages of the discrete element approach are that the soil model can undergo large deformations without affecting numerical accuracy and stability, and fewer calculations are required making the solution much more efficient.[Plaxico98; Patzner99; Plaxico15; Plaxico19] The continuum method is reasonably accurate for low to moderate soil displacement but has the advantage of modeling soil interaction between neighboring posts.

For the current study, two methods were used, as illustrated in Figures 94 and 95. The discrete elements method (i.e., springs and dampers) was used to model the soil in the w-beam section; and the soil continuum method (solid elements) was used in the impact region on the transition where the posts were closely spaced (i.e., thrie-beam and tube-rail sections). Both soil models were qualitatively validated based on comparison with impact tests on wood and steel guardrail posts performed at the Midwest Roadside Safety Facility (MwRSF) [Rosenbaugh11]. A summary of the validation effort is presented in Appendix H.

A representative model for the discrete element soil method is shown in Figure 94. Rather than connecting the springs directly to the post, a shell element interface was included to separate the soil springs from the post. The shell elements were meshed such that the element size was consistent with the element size of the posts and each line of nodes of the mesh was spaced at 1.97 inches (50 mm). A single discrete spring element was attached to each row of nodes at the center of the shell section. The shell elements were modeled with null material properties so that the resistance to the elements movement/deformation was due solely to the

discrete springs. Each row of nodes was constrained to move as a rigid body with its corresponding spring element. That is, for the elements representing y-direction displacement of the soil, each individual row of nodes was constrained in the x- and z-directions using the *Constrained_Nodal_Rigidbody_SPC option in LS-DYNA.

The continuum soil model included a 2:1 slope starting just behind the three-beam posts, as illustrated in Figure 95. The overall dimensions of the soil model were 21.7 feet long, 8.34 feet lateral width, and 7.1 feet vertical depth. The material was modeled using the Drucker-Prager material model and was calibrated based on comparison to full-scale tests (see Appendix H). The soil in the immediate post region was meshed with element side lengths of approximately 1.3 – 1.6 inches. The soil away from the posts was meshed with element side lengths of 2.5 – 3 inches. The refined-mesh region was tied to the elements of the coarse-mesh region using the *Contact_Tied option in LS-DYNA.

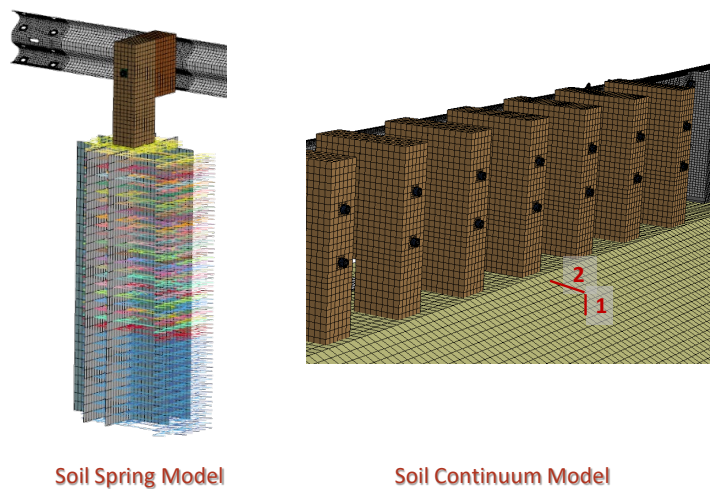


Figure 94. Soil models used in the transition model.

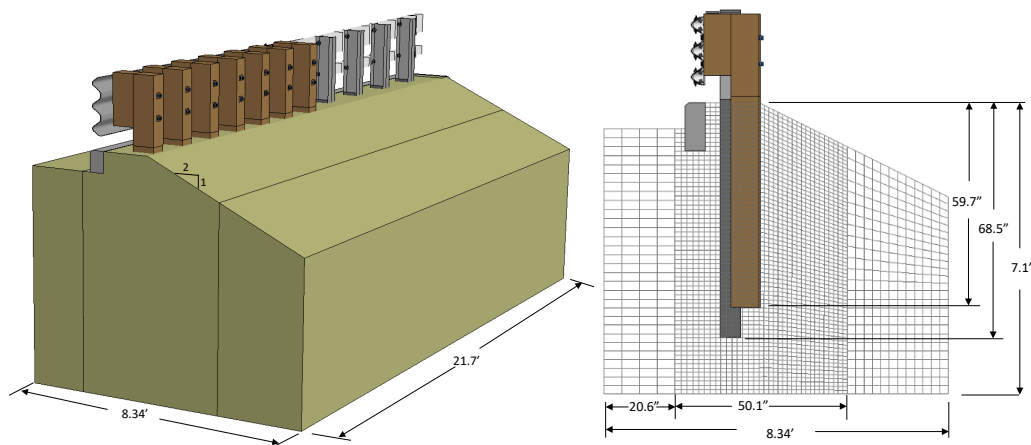


Figure 95. Continuum soil model mesh and dimensions.

7.4 Model Validation

The FEA model of the 2-bar transition was used to simulate TTI Test No. 401181-1 which involved a 4,706-lb Chevrolet 2500 impacting the system at 5.36 feet upstream of the first post of the tube-rail section of the transition at an impact speed of 63.6 mph and angle of 24.9 degrees. The FEA simulation included the C2500D-V5b-R160309 vehicle model, as described in Section 5, with impact conditions consistent with the full-scale test, as illustrated in Figure 96. The analysis was performed using LS-DYNA version mpp_s_R8.0.0 revision number 95309. The analysis was conducted with a time-step of 1.0 microsecond for a time period of 1.0 seconds. A comparison of the vehicle properties for the model and the test vehicle is shown in Figure 44.

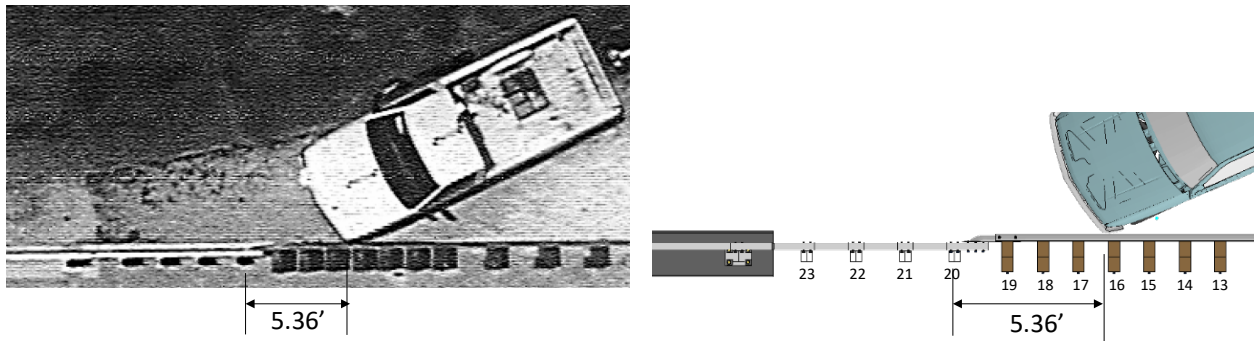


Figure 96. Impact point for test and simulation for Report 350 Test 3-21 on the 2-bar transition.

7.4.1 Simulated Impact Summary

The following is a commentary describing the timing and occurrence of various events during the simulated impact with comparison to the full-scale test. The information for the test here is slightly different than that in the test report. The event timing was determined here from provided test videos; while vehicle speed and angular information was obtained from the TRAP output (consistent with the way the FEA data was reported). This comparison is also tabulated in Table 59.

The vehicle struck the center corrugation of the nested thrie-beam at the downstream edge of Post 16, and the post began to deflect. At 0.01 seconds the front-right tire contacted the granite curb. At 0.03 seconds the front-right tire and rim was significantly deformed. Tire deflection was not included in the model; however, the magnitude of deformations would indicate tire debanding and/or rupture (the tire deflated at 0.032 seconds in the test). At 0.035 seconds Post 20 began to deflect (same in test). At 0.05 seconds the front bumper was at Post 19; at 0.061 seconds the vehicle began to redirect (same as test). At 0.075 seconds the front bumper was at Post 20 (0.076 seconds in test). At 0.1 seconds Post 19 reached maximum deflection of 5.3 inches (8.03 inches at 0.94 seconds in test). At 0.105 seconds the front bumper was at Post 21 (0.098 in test). At 0.11 seconds Post 20 reached maximum deflection of 4.53 inches (0.1 seconds in test). At 0.125 seconds the front bumper was at Post 22 (0.12 seconds in test). At 0.155 seconds the front bumper was at the last post in the transition (0.147 seconds in test). At 0.185 seconds the front bumper was at the splice connection to the bridge rail (≈ 0.174 seconds in test); also, at this time the rear-right tire contacted the curb (0.174 seconds in test). At 0.215 seconds the rear bumper contacted the top corrugation of the nested thrie-beam at Post 17

(0.208 seconds in test). At 0.226 seconds the vehicle was parallel to the barrier traveling at 44.9 mph (0.222 seconds and 48 mph in test). At 0.375 seconds the rear-right tire separated from the barrier as the vehicle exited the transition (\approx same time in test) traveling at 44.6 mph (47 mph in test) and exit angle of 8.95 degrees (8.21 degrees in test). At 0.47 seconds the vehicle reached maximum roll angle of 17 degrees with the vehicle rolling toward barrier (0.59 seconds and 19.4 degrees in test). At 0.57 seconds the vehicle reached maximum pitch angle of 16.5 degrees with the rear of the vehicle pitching upward (0.66 seconds and 13.7 degrees in test). The analysis was terminated at 1.0 seconds, at which time:

- The roll angle of the vehicle was 0.2 degrees and stable (4.3 degrees in test),
- The pitch angle was 0.2 degrees and stable (1.2 degrees in test),
- The yaw angle was 22.9 degrees relative to the barrier (30.7 degrees in test), and
- The forward velocity of the vehicle was 42.2 mph (41.7 mph).

Table 59. Summary of phenomenological events for full-scale Test 401181-1 and FEA simulation.

Event	Test 401181-1	FE Analysis
Front-right tire deflated	0.032 sec	N.A.
Post 20 began to deflect	0.035 sec	0.035 sec
Front bumper at Post 19	0.05 sec	0.05 sec
Vehicle began to redirect	0.061sec	0.061sec
Front bumper was at Post 20	0.076 sec	0.075 sec
Post 19 reached maximum deflection	0.94 sec / 8.0 in	0.1 sec / 5.3 in
Front bumper was at Post 21	0.098 sec	0.105 sec
Post 20 reached maximum deflection	\approx 0.1 sec	0.11 sec / 4.53 in
Front bumper was at Post 22	0.12 sec	0.125 sec
Front bumper was at Post 23	0.147 sec	0.155 sec
Rear tire contacted curb	0.174 sec	0.185 sec
Front bumper was as bridge rail splice	0.174 sec	0.185 sec
Rear bumper contacted rail	0.208 sec	0.215 sec
Vehicle parallel with rail	0.222 sec	0.226 sec
Speed at parallel	48 mph	44.9 mph
Vehicle exits rail	0.375 sec	0.375 sec
Speed at exit	47 mph	44.6 mph
Exit angle	8.21 deg	8.95 deg
Maximum Roll	0.59 sec / 19.4 deg	0.47 sec / 17 deg
Maximum Pitch	0.66 sec / 13.7 deg	0.57 sec / 16.5 deg

7.4.2 Sequential Views

A qualitative assessment was made by comparing sequential snapshots of the simulation with the full-scale crash test to verify vehicle kinematic response as well as sequence and timing of key phenomenological events. The results from the FE analysis compare well with the test. Figure 97 shows sequential snapshots of the impact event from an overhead viewpoint. Figure 98 shows the sequential views from a downstream viewpoint. Additional views are included in Appendix I. Based on visual inspection the model appears to simulate the basic kinematic behavior of the truck and adequately captures the basic phenomenological events that occur during impact.

7.4.3 Damage to Bridge Rail

Damage to the bridge rail is shown in Figure 99. The damage to the system was moderate. The thrie-beam sustained some deformation from the point of impact to the attachment to the thrie-beam terminal connector. Maximum dynamic deflection during the impact simulation was 5.3 inches at Post 19, compared to 8.03 inches at Post 18 in the test. The maximum permanent deflection for the simulation was 4.13 inches, compared to 5.8 inches in the test. The total length of contact of the vehicle with the transition was 14.7 feet in the simulation, compared to 14.4 feet in the test.

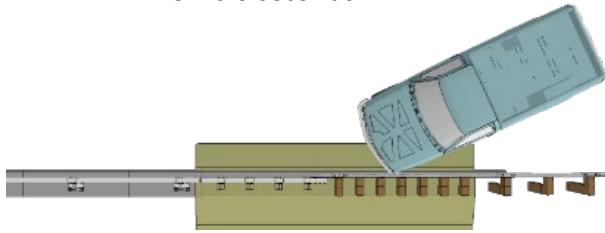
7.4.4 Occupant Risk Measures

Acceleration-time histories and angular rate-time histories were collected at the center of gravity of the vehicle model using the *Element-Seatbelt-Accelerometer option in LS-DYNA. The time-history data was collected from the accelerometer in a local reference coordinate system that was fixed to the vehicle with the x-direction coincident with the forward direction of the vehicle, the local y-direction is fixed toward the right side of the vehicle and the local z-direction is fixed downward; which was consistent with the way the test data was collected from physical accelerometers. The data was collected at a frequency of 50 kHz which was sufficient to avoid aliasing of the data. The model included eight accelerometers with one positioned near the center of gravity of the vehicle on the cabin floor, as identified in Figure 100.

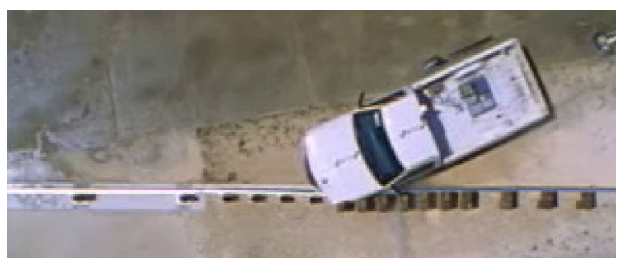
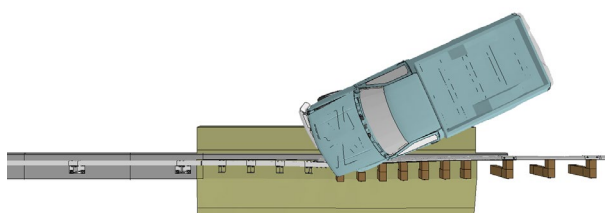
The occupant risk assessment measures were computed using the acceleration time-histories and angular-rate time histories collected at the center of gravity of the vehicle. The Test Risk Assessment Program (TRAP) calculates standardized occupant risk factors from vehicle crash data in accordance with the National Cooperative Highway Research Program (NCHRP) guidelines and the European Committee for Standardization (CEN). [TTI98]

The analysis results obtained from TRAP for the full-scale test and the FE analysis are shown in Table 60 and Figure 101. The acceleration data used in the TRAP program was pre-filtered using the SAE Class 180 filter. The table shows the two occupant risk factors recommended by R350: 1) the lateral and longitudinal components of Occupant Impact Velocity (OIV) and 2) the maximum lateral and longitudinal component of resultant vehicle acceleration averaged over 10-millisecond interval after occupant impact called the Occupant Ridedown Acceleration (ORA). Also provided in the table are the CEN risk factors including the Theoretical Head Impact Velocity (THIV), the Post Impact Head Deceleration (PHD) and the Acceleration Severity Index (ASI). The table also includes comparison of the 50-millisecond moving average of the accelerations.

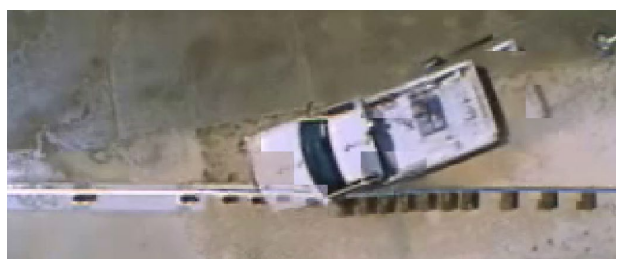
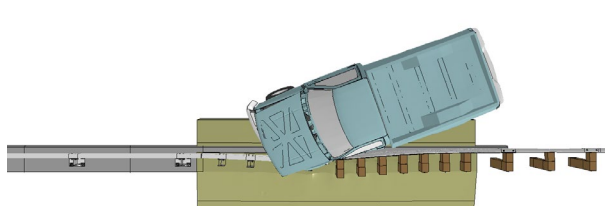
Time = 0.0 seconds



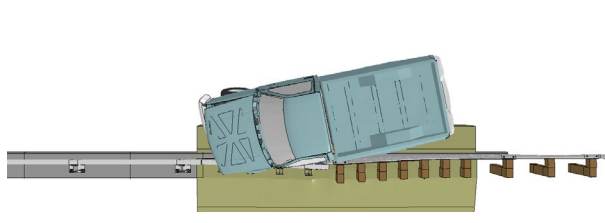
Time = 0.05 seconds



Time = 0.1 seconds



Time = 0.15 seconds



Time = 0.20 seconds

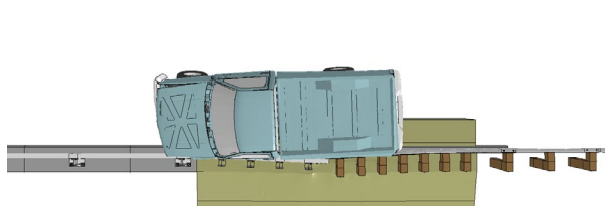
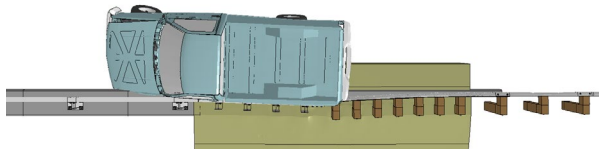
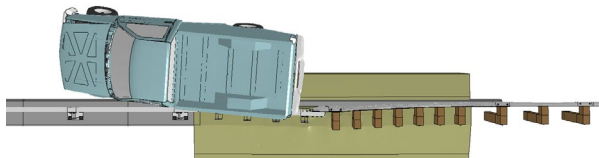


Figure 97. Sequential views of FE analysis and Test 401181-1 from an overhead viewpoint.

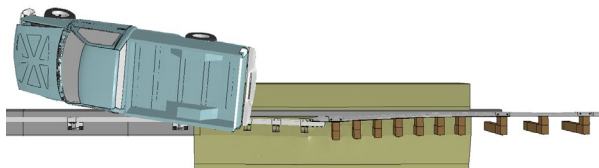
Time = 0.25 seconds



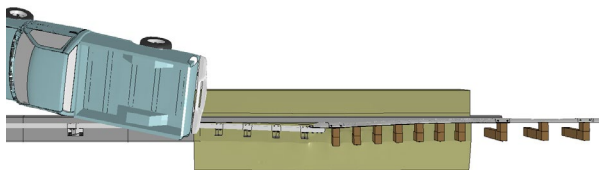
Time = 0.3 seconds



Time = 0.35 seconds



Time = 0.4 seconds



Time = 0.45 seconds

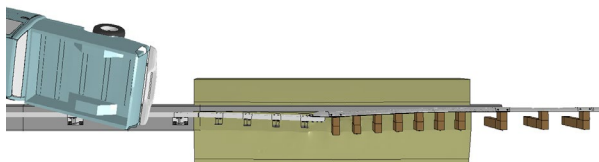


Figure 97. [Continued] Sequential views of FE analysis and Test 401181-1 from an overhead viewpoint.

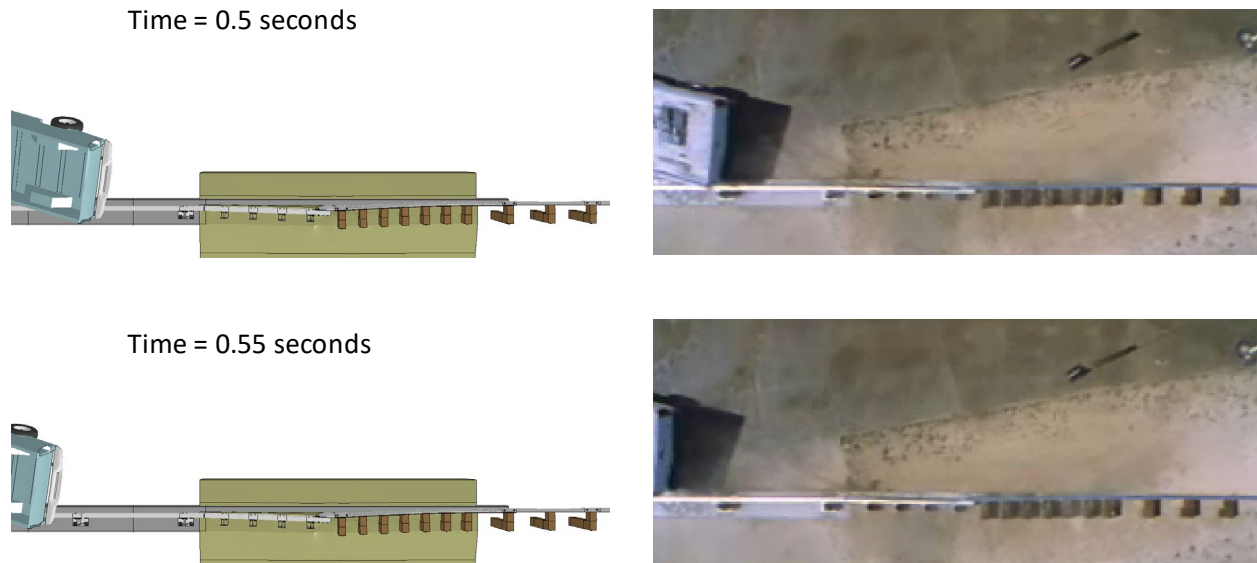


Figure 97. [Continued] Sequential views of FE analysis and Test 401181-1 from an overhead viewpoint.

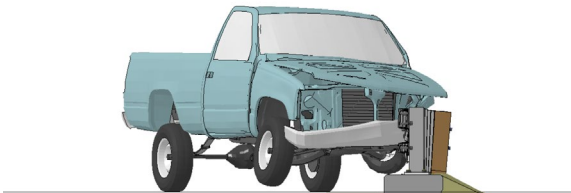
The results indicate that the occupant risk factors for both the full-scale test and the simulation are similar. The occupant impact velocity in the longitudinal direction was predicted from the simulation to be 19.7 ft/s (15.4 percent higher than the test OIV of 17.1 ft/s) at 0.1005 seconds. In the transverse direction, the occupant impact velocity predicted in the simulation was 24.9 ft/s (1.3 percent higher than the test OIV of 24.6 ft/s). The highest 0.010-second occupant ridedown acceleration in the longitudinal direction was 8.3 g (same as test) between 0.1018 and 0.1118 seconds. In the transverse direction, the highest 0.010-second occupant ridedown acceleration was 7.5 g (2.5 g lower than test ORA of 10 g) between 0.1388 and 0.1488 seconds. The THIV, PHD and ASI predicted from the simulation were 31.5 ft/s (5.5 percent higher), 9.1 g's (2.8 g higher), and 1.48 (14.9 percent lower), respectively. The maximum 50-millisecond moving average accelerations in the x-, y-, and z-directions were 9.6 g (18.5 percent higher), 11 g (18.5 percent lower), and 3.8 g (50 percent or 3.8 g lower), respectively.

The criteria from Report W179 recommends that the differences between the analysis and test for each of the occupant risk measures be less than 20 percent, unless the magnitude is relatively small; in which case the absolute difference between the FEA and test values should be used. For example, the criteria for maximum absolute difference for the occupant impact velocity (OIV) is 6.6 ft/s and for the occupant ridedown accelerations (ORA) it is 4 g. There are no recommended limits for the remaining metrics, but the values were provided here for further comparisons. The results of the FEA were well within the recommended limits of Report W179 for each of the comparison metrics.

Time = 0.0 seconds



Time = 0.1 seconds



Time = 0.2 seconds



Time = 0.3 seconds

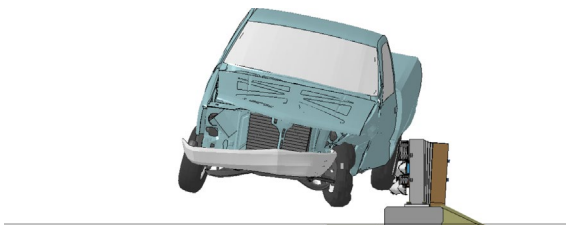
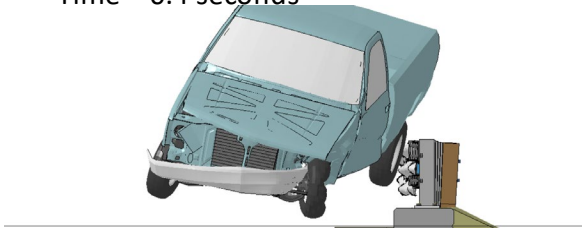
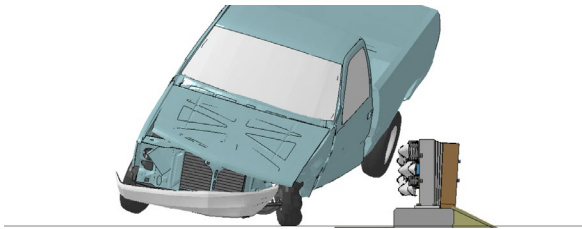


Figure 98. Sequential views of FE analysis and Test 401181-1 from a downstream viewpoint.

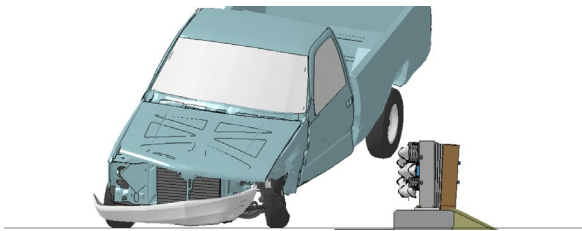
Time = 0.4 seconds



Time = 0.5 seconds



Time = 0.6 seconds



Time = 0.7 seconds

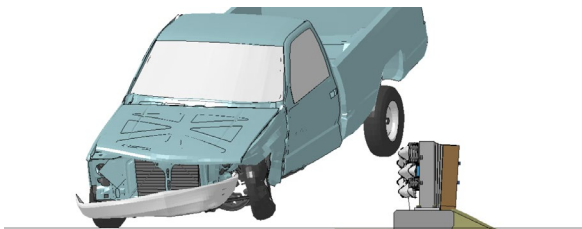


Figure 98. [Continued] Sequential views of FE analysis and Test 401181-1 from a downstream viewpoint.

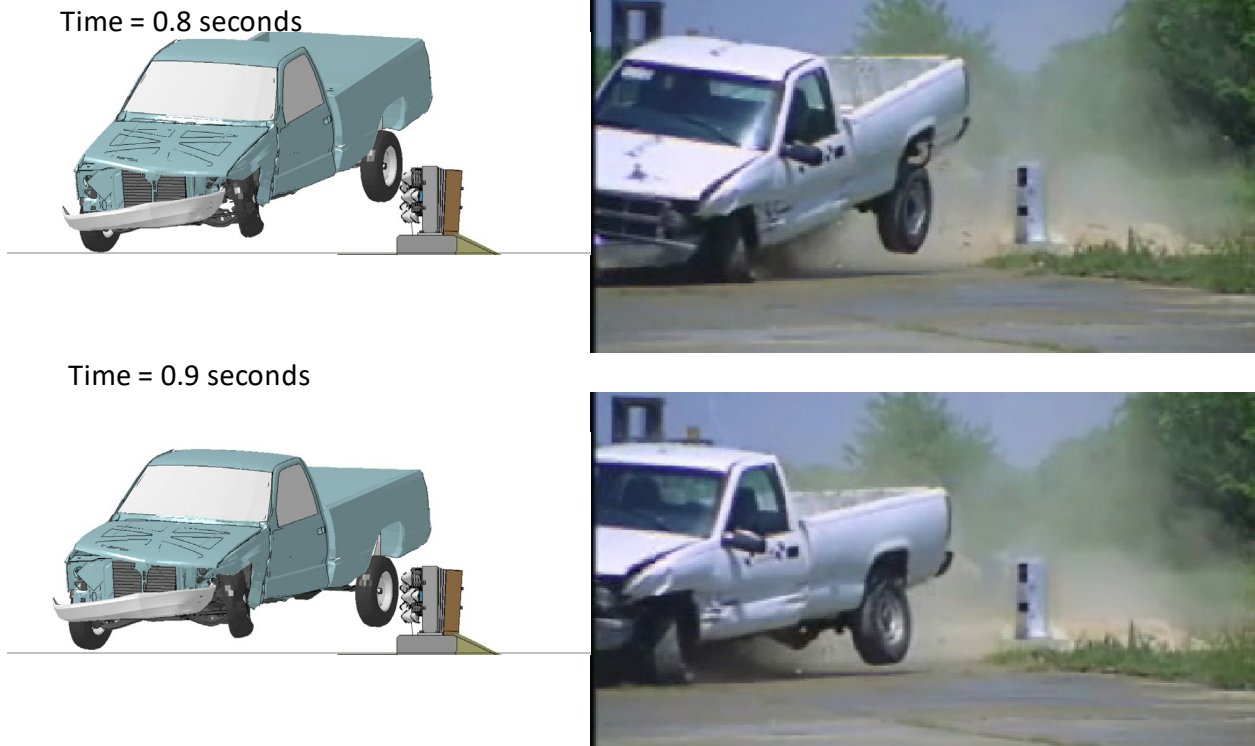


Figure 98. [Continued] Sequential views of FE analysis and Test 401181-1 from a downstream viewpoint.

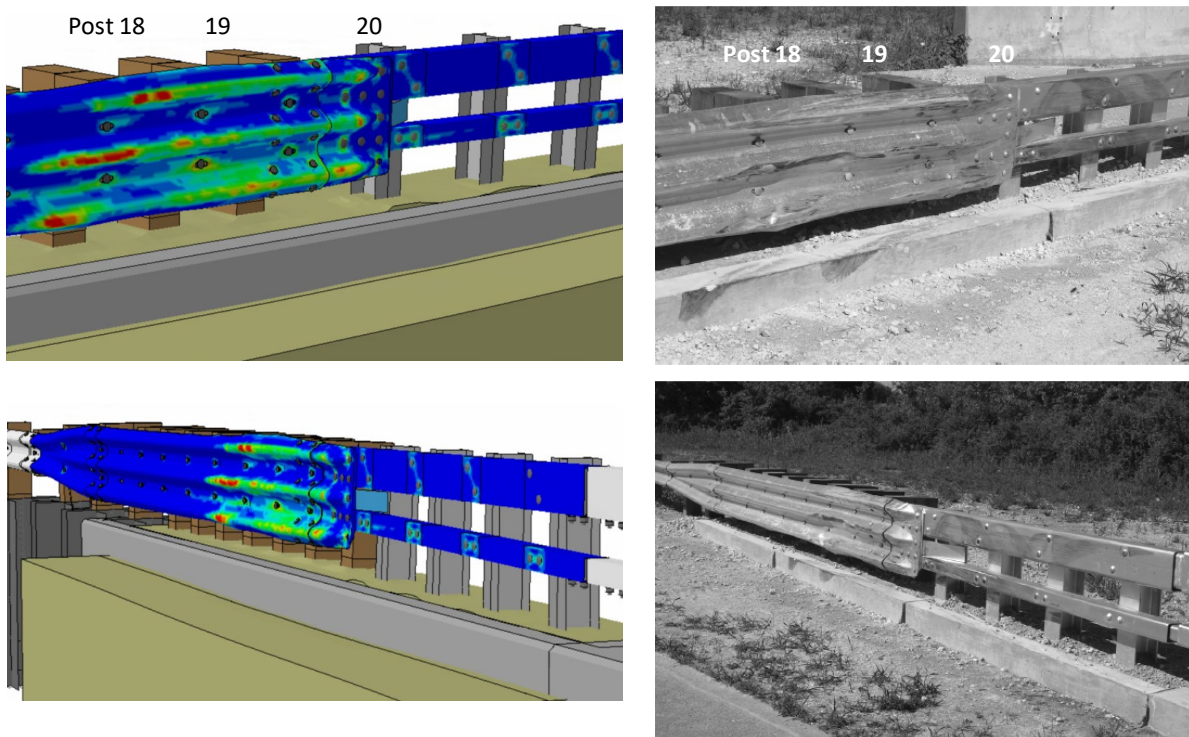


Figure 99. Comparing overall deformation of system for FEA and Test 401181-1.

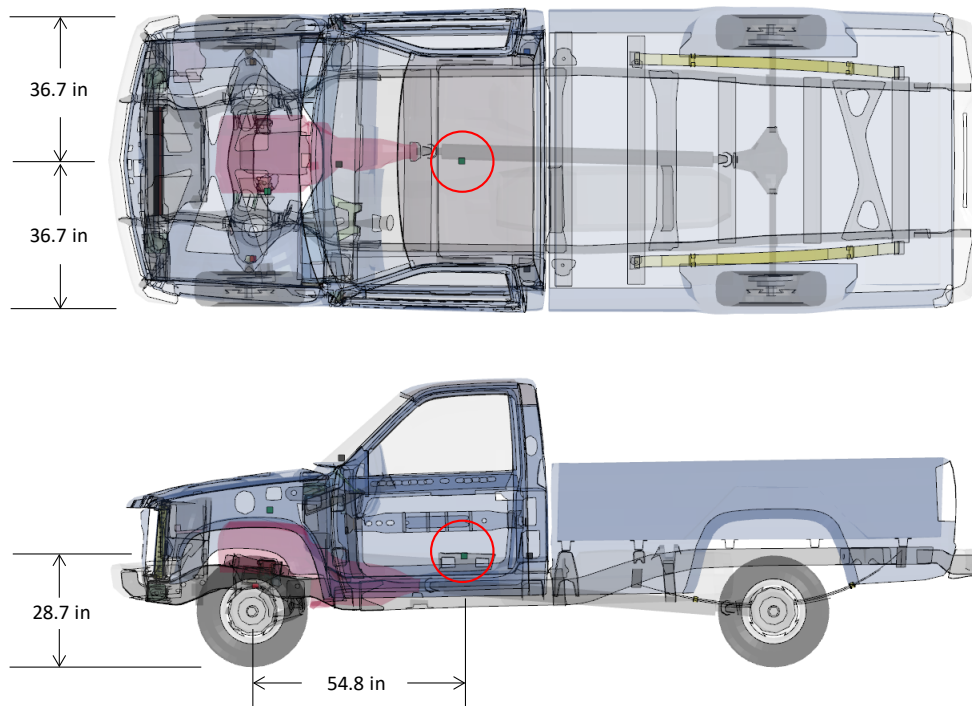


Figure 100. Location of accelerometer in the FE model.

Table 60. Occupant risk measured computed using TRAP software for the FEA and test data for R350 Test 4-12.

Occupant Risk Factors		MASH Test 3-11		Error		W179 Criteria	
		Test 401181-1 (0 - 1.0 seconds)	FEA (0 - 1.0 seconds)	%	Absolute	Criteria	Pass
Occupant Impact Velocity (ft/s)	x-direction	17.06	19.68	15.4%	2.62	<20% or < 6.6 f/s	Y
	y-direction	-24.61	-24.93	1.3%	-0.33	<20% or < 6.6 f/s	Y
	at time	at 0.0948 seconds on left side of interior	at 0.1005 seconds on left side of interior				
THIV (m/s)		29.9 at 0.0948 seconds on left side of interior	31.5 at 0.0986 seconds on left side of interior	5.5%	1.64	<20% or < 6.6 f/s	Y
Ridedown Acceleration (g's)	x-direction	-8.3 (0.1153 - 0.1253 seconds)	-8.3 (0.1018 - 0.1118 seconds)	0.0%	0.00	<20% or < 4G	Y
	y-direction	10 (0.1182 - 0.1282 seconds)	7.5 (0.1388 - 0.1488 seconds)	25.0%	-2.50	<20% or < 4G	Y
PHD (g's)		11.9 (0.1180 - 0.1280 seconds)	9.1 (0.1344 - 0.1444 seconds)	23.5%	-2.80	<20% or < 4G	Y
ASI		1.74 (0.0216 - 0.0716 seconds)	1.48 (0.0355 - 0.0855 seconds)	14.9%	-0.26	<20% or < 0.2	Y
Max 50-ms moving avg. acc. (g's)	x-direction	-8.1 (0.0334 - 0.0834 seconds)	-9.6 (0.0342 - 0.0842 seconds)	18.5%	-1.50	<20% or < 4G	Y
	y-direction	13.5 (0.0216 - 0.0716 seconds)	11 (0.0448 - 0.0948 seconds)	18.5%	-2.50	<20% or < 4G	Y
	z-direction	-7.6 (0.0209 - 0.0709 seconds)	-3.8 (0.0359 - 0.0859 seconds)	50.0%	3.80	<20% or < 4G	Y
Maximum Angular Disp. (deg)	Yaw	55.6 (1.0000 seconds)	48.2 (0.9426 seconds)	13.3%	-7.40	<20% or < 5 deg	Y
	Roll	-19.4 (0.5914 seconds)	-17 (0.4713 seconds)	12.4%	2.40	<20% or < 5 deg	Y
	Pitch	-13.7 (0.6647 seconds)	-16.5 (0.5674 seconds)	20.4%	-2.80	<20% or < 5 deg	Y

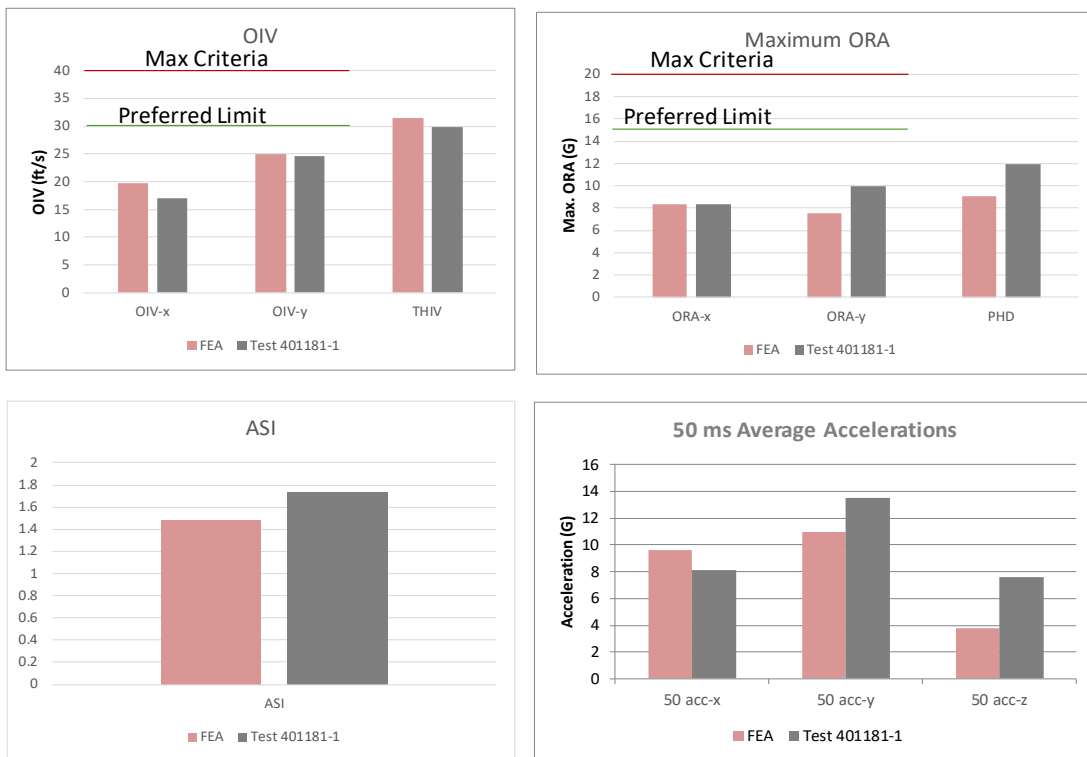


Figure 101. Graphical comparison of FEA vs. Test for key occupant risk metrics.

7.4.5 Time-History Data Comparison

Figures 102 - 104 show a comparison of the 10-millisecond moving average and the 50-millisecond moving average acceleration-time history at the c.g. of the pickup for the longitudinal, transverse and vertical channels, respectively. Figures 105 - 107 show comparisons of the angular rates and angular displacements (i.e., yaw, roll, and pitch) at the c.g. of the pickup for the test and FE analysis. Values for the quantitative evaluation metrics are also shown on the time-history plots. These quantities were computed from the raw acceleration data and are shown with these plots only for reference. The values in red font indicate poor correlation between test and analysis results, while the values in black font indicate good correlation. The quantitative metrics are discussed in more detail in Section 0 below.

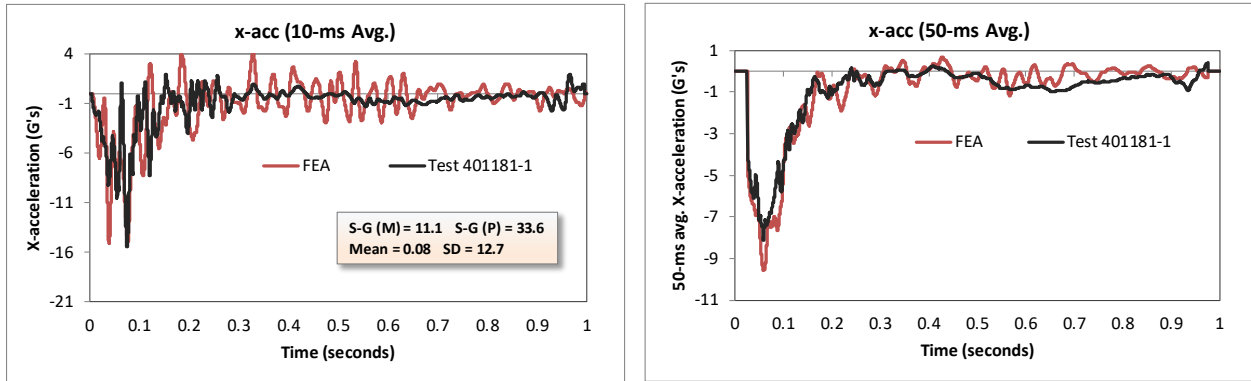


Figure 102. Longitudinal acceleration-time history plot from accelerometer at c.g. for full-scale Test 401181-1 and FEA (10-ms and 50-ms moving averages).

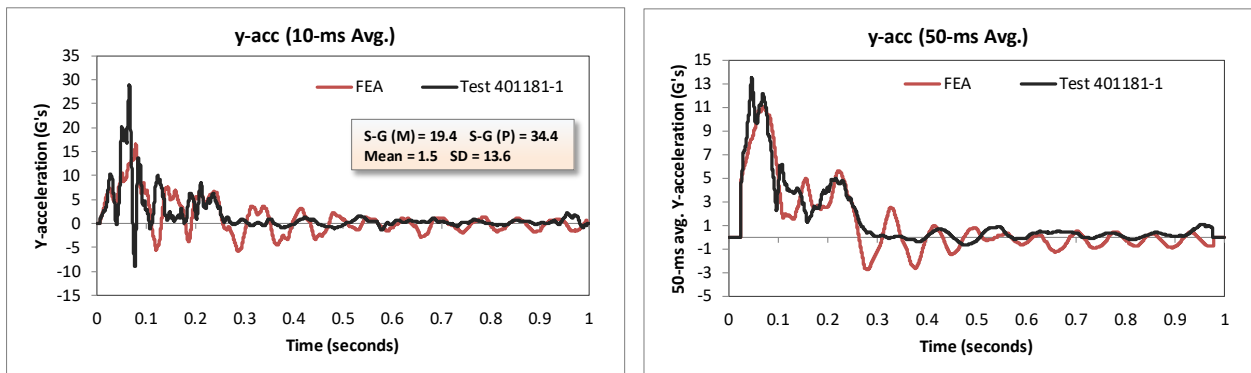


Figure 103. Lateral acceleration-time history plot from accelerometer at c.g. for full-scale Test 401181-1 and FEA (10-ms and 50-ms moving averages).

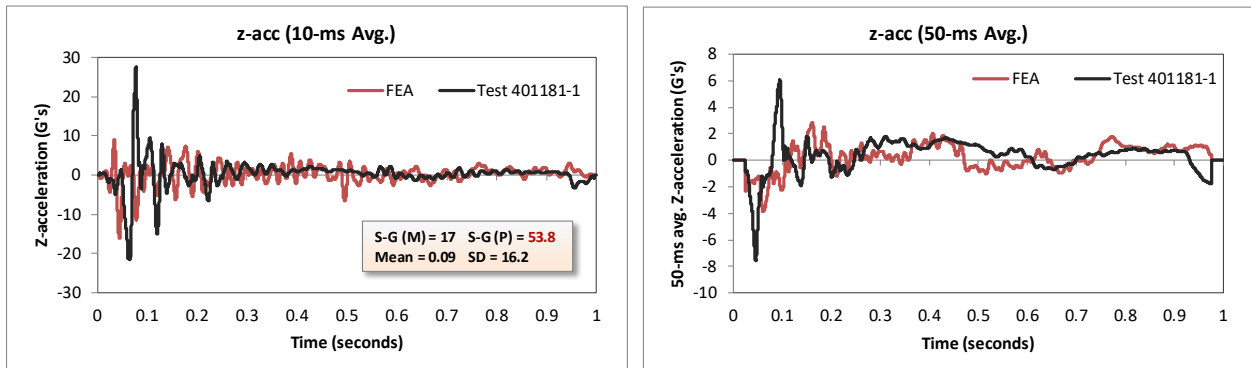


Figure 104. Vertical acceleration-time history plot from accelerometer at c.g. for full-scale Test 401181-1 and FEA (10-ms and 50-ms moving averages).

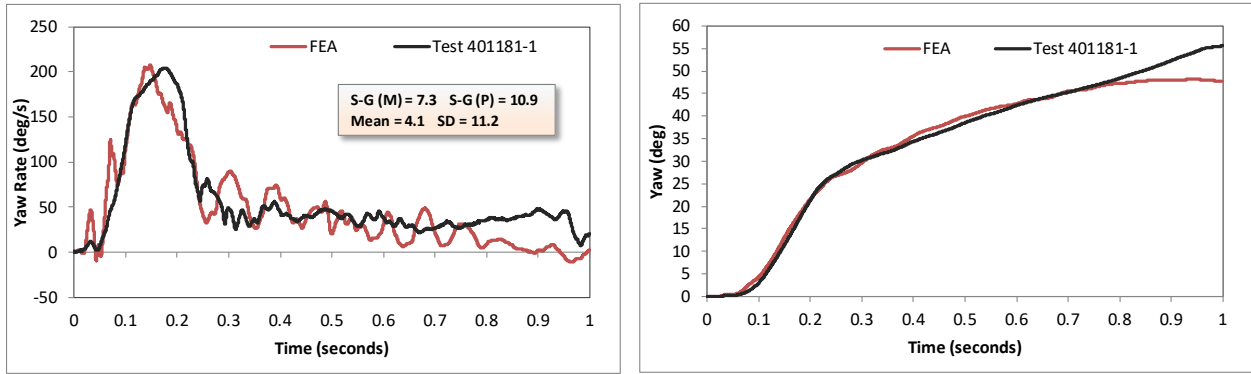


Figure 105. Yaw-time history plot from accelerometer inside cabin for full-scale test 401181-1 and FEA (angular rate and displacement).

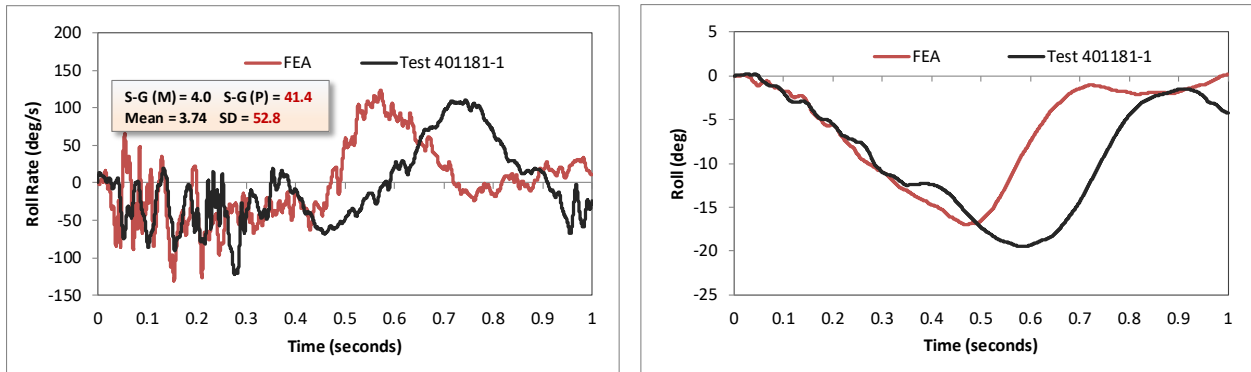


Figure 106. Roll-time history plot from accelerometer inside cabin for full-scale test 401181-1 and FEA (angular rate and displacement).

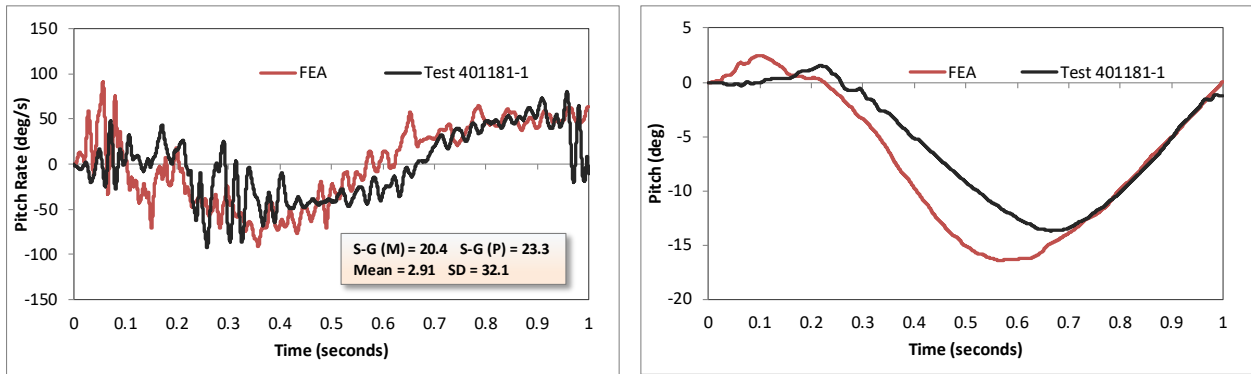


Figure 107. Pitch-time history plot from accelerometer inside cabin for full-scale test 401181-1 and FEA (angular rate and displacement).

7.4.6 Quantitative Validation

The quantitative evaluation was based on comparison of acceleration-time histories and angular rate-time histories computed in the analysis to those measured in full-scale crash test 401181-1 using the procedures specified in Report W179.[Ray10] A summary of the quantitative comparison results are provided here. Additional comparison data can be found in Appendix I.

7.4.6.1 Solution Verification

Table 61 shows a summary of the global verification assessment based on criteria recommended in Report W179. Figure 108 shows a plot of the global energy-time histories from the analysis. All the solution verification parameters were satisfied.

Table 61. Analysis solution verification table.

Verification Evaluation Criteria	Change	Pass?
<i>Total energy</i> of the analysis solution (i.e., kinetic, potential, contact, etc.) must not vary more than 10 percent from the beginning of the run to the end of the run.	8.6%	Y
<i>Hourglass Energy</i> of the analysis solution at the end of the run is less than <i>five percent</i> of the total <i>initial energy</i> at the <i>beginning</i> of the run.	0%	Y
<i>Hourglass Energy</i> of the analysis solution at the end of the run is less than <i>ten percent</i> of the total <i>internal energy</i> at the <i>end</i> of the run.	0%	Y
The part/material with the highest amount of hourglass energy at the end of the run is less than twenty percent of the total internal energy of the part/material at the end of the run.	0%	Y
Mass added to the total model is less than five percent of the total model mass at the beginning of the run.	0%	Y
The part/material with the most mass added had less than 10 percent of its initial mass added.	0%	Y
The moving parts/materials in the model have less than five percent of mass added to the initial moving mass of the model.	0%	Y
There are no shooting nodes in the solution?	Y	Y
There are no solid elements with negative volumes?	Y	Y

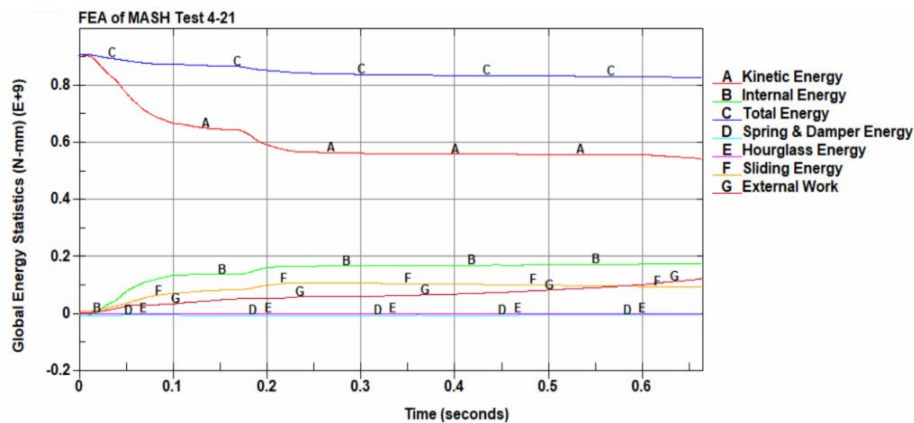


Figure 108. Plot of global energy-time histories from the analysis.

7.4.6.2 Time-History Validation

The data from the three acceleration channels located at the center of gravity of the vehicle and the angular rate data (i.e., roll, pitch and yaw) which were collected from inside the cabin were input into the RSVVP software to calculate quantitative differences between the FEA and test results. The data was filtered in RSVVP using a CFC Class 60 filter. The synchronization options in RSVVP were not used for the physical test data since both the test and analysis data started at the time of impact with the barrier. The default metrics evaluation options in RSVVP were used, which included the Sprague & Geers and the ANOVA metrics. The curves were evaluated over 1.0 second of the impact event, corresponding to the limits of the test data.

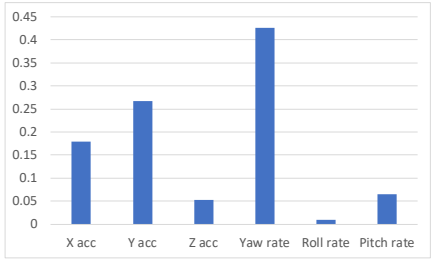
The results from RSVVP are shown in Table 62. Based on the validation metrics, a comparison of the individual components of acceleration indicated that the simulation was in good agreement for the x-acceleration, y-acceleration, yaw-rate and pitch-rate. The z-acceleration and the roll-rate was in good agreement regarding the Sprague-Geers magnitude but was slightly out of phase. The standard deviation of residual errors for the roll-rate also indicated that that channel was not in agreement with the test. Since the metrics computed for the individual data channels did not all satisfy the acceptance criteria, the multi-channel option in RSVVP was used to calculate the weighted Sprague-Geer and ANOVA metrics for the six channels of data.

Table 63 shows the results from RSVVP for the multi-channel option. The resulting weights computed for each channel are shown in both tabular form and graphical form in the tables. The results indicate that the x- and y-acceleration and the yaw rate have significant influence over the kinematics of the impact event; while the z-acceleration, roll-rate and pitch rate had minimal influence on the vehicle's impulse response. The weighted metrics computed in RSVVP in the multi-channel mode all satisfy the acceptance criteria; therefore, the time history comparison can be considered acceptable.

Table 62. Roadside safety validation metrics rating table – time history comparison (single-channel option).

Evaluation Criteria							Time interval [0.00 – 1.0 sec]		
Sprague-Geers Metrics List all the data channels being compared. Calculate the M and P metrics using RSVVP and enter the results. Values less than or equal to 40 are acceptable.							M	P	Pass?
RSVVP Curve Preprocessing Options									
	Filter Option	Sync. Option	Shift		Drift				
			True Curve	Test Curve	True Curve	Test Curve			
X acceleration	CFC 60	none	none	none	none	none	11.1	33.6	Y
Y acceleration	CFC 60	none	none	none	none	none	19.4	34.4	Y
Z acceleration	CFC 60	none	none	none	none	none	17	53.8	N
Yaw rate	CFC 60	none	none	none	none	none	7.3	10.9	Y
Roll rate	CFC 60	none	none	none	none	none	4.0	41.4	≈Y
Pitch rate	CFC 60	none	none	none	none	none	20.4	23.3	Y
ANOVA Metrics List all the data channels being compared. Calculate the ANOVA metrics using RSVVP and enter the results. Both of the following criteria must be met: <ul style="list-style-type: none"> • The mean residual error must be less than five percent of the peak acceleration ($\bar{e} \leq 0.05 \cdot a_{peak}$) and • The standard deviation of the residuals must be less than 35 percent of the peak acceleration ($\sigma \leq 0.35 \cdot a_{peak}$) 							Mean Residual (%)	Standard Deviation of Residuals	Pass?
X acceleration/Peak							0.08	12.7	Y
Y acceleration/Peak							1.5	13.6	Y
Z acceleration/Peak							0.09	16.8	Y
Yaw rate							4.1	11.2	Y
Roll rate							3.74	52.8	N
Pitch rate							2.91	32.1	Y

Table 63. Roadside safety validation metrics rating table – (multi-channel option).

Evaluation Criteria (time interval [0.0 – 1.0 seconds])				
Channels (Select which were used)				
<input checked="" type="checkbox"/> X Acceleration	<input checked="" type="checkbox"/> Y Acceleration	<input checked="" type="checkbox"/> Z Acceleration		
<input checked="" type="checkbox"/> Roll rate	<input checked="" type="checkbox"/> Pitch rate	<input checked="" type="checkbox"/> Yaw rate		
Multi-Channel Weights - Area II method -	X Channel: 0.180 Y Channel: 0.268 Z Channel: 0.053 Yaw Channel: 0.426 Roll Channel: 0.009 Pitch Channel: 0.065			
O	Sprague-Geer Metrics Values less or equal to 40 are acceptable.	M	P	Pass?
		24.6	27.9	Y
P	ANOVA Metrics Both of the following criteria must be met: <ul style="list-style-type: none"> The mean residual error must be less than five percent of the peak acceleration ($\bar{e} \leq 0.05 \cdot a_{Peak}$) The standard deviation of the residuals must be less than 35 percent of the peak acceleration ($\sigma \leq 0.35 \cdot a_{Peak}$) 	Mean Residual	Standard Deviation of Residuals	Pass?
		1.9	14.1	Y

7.4.6.3 PIRT – Crash Specific Phenomena

Table 64 contains the Report 350 crash test criteria. Those that apply to Test 4-21 are marked in red. These include criteria A, D, F, K, L and M. Table 65 through Table 67 contain an expanded list of these same criteria including additional specific phenomena that were measured in the test and that could be directly compared to the numerical solution. Table 65 contains a comparison of phenomena related to structural adequacy, Table 66 contains a comparison of phenomena related to occupant risk, and Table 67 contains a comparison of phenomena related to vehicle trajectory. Some of this information has already been presented but is repeated here for convenience. Comparisons for all the applicable crash specific phenomena between the FEA and test were within the allowable limits of Report W179.

Table 64. Report 350 crash test criteria with the applicable test numbers.

Evaluation Factors	Evaluation Criteria		Applicable Tests	
Structural Adequacy	A	Test article should contain and redirect the vehicle; the vehicle should not penetrate, under-ride, or override the installation although controlled lateral deflection of the test article is acceptable.	10, 11, 12, 20, 21 , 22, 35, 36, 37, 38	
	B	The test article should readily activate in a predictable manner by breaking away, fracturing or yielding.	60, 61, 70, 71, 80, 81	
	C	Acceptable test article performance may be by redirection, controlled penetration or controlled stopping of the vehicle.	30, 31, 32, 33, 34, 39, 40, 41, 42, 43, 44, 50, 51, 52, 53	
Occupant Risk	D	Detached elements, fragments or other debris from the test article should not penetrate or show potential for penetrating the occupant compartment, or present an undue hazard to other traffic, pedestrians or personnel in a work zone.	All	
	E	Detached elements, fragments or other debris from the test article, or vehicular damage should not block the driver's vision or otherwise cause the driver to lose control of the vehicle. (Answer Yes or No)	70, 71	
	F	The vehicle should remain upright during and after the collision although moderate roll, pitching and yawing are acceptable.	All except those listed in criterion G	
	G	It is preferable, although not essential, that the vehicle remain upright during and after collision.	12, 22	
	H	Occupant impact velocities should satisfy the following:		10, 20, 30,31, 32, 33, 34, 36, 40, 41, 42, 43, 50, 51, 52, 53, 80, 81
		Occupant Impact Velocity Limits (m/s)		
Component		Preferred	Maximum	
	Longitudinal and Lateral	9	12	
	Longitudinal	3	5	60, 61, 70, 71
I	Occupant ridedown accelerations should satisfy the following:		10, 20, 30,31, 32, 33, 34, 36, 40, 41, 42, 43, 50, 51, 52, 53, 60, 61, 70, 71, 80, 81	
	Occupant Ridedown Acceleration Limits (g's)			
	Component	Preferred		Maximum
	Longitudinal and Lateral	15	20	
Vehicle Trajectory	K	After collision it is preferable that the vehicle's trajectory not intrude into adjacent traffic lanes.	All	
	L	The occupant impact velocity in the longitudinal direction should not exceed 40 ft/sec and the occupant ride-down acceleration in the longitudinal direction should not exceed 20 G's.	11, 21 , 35, 37, 38, 39	
	M	The exit angle from the test article preferable should be less than 60 percent of test impact angle, measured at the time of vehicle loss of contact with test device.	10, 11, 12, 20, 21 , 22, 35, 36, 37, 38, 39	
	N	Vehicle trajectory behind the test article is acceptable.	30, 31, 32, 33, 34, 39, 42, 43, 44, 60, 61, 70, 71, 80, 81	

Table 65. Roadside safety phenomena importance ranking table (structural adequacy).

		Evaluation Criteria		Known Result	Analysis Result	Difference Relative/ Absolute	Agree?
Structural Adequacy	A	A1	Test article should contain and redirect the vehicle; the vehicle should not penetrate, under-ride, or override the installation although controlled lateral deflection of the test article is acceptable. (Answer Yes or No)	Y	Y	X	Y
		A2	Maximum dynamic deflection: - Relative difference is less than 20 percent or - Absolute difference is less than 6 inches	8.0 in	5.8 in (0.1 sec)	27.5% 2.2 in	Y
		A3	Maximum permanent deflection: - Relative difference is less than 20 percent or - Absolute difference is less than 6 inches	5.8 in	4.3 in	25.9% 1.5 in	Y
		A4	Length of vehicle-barrier contact (at initial separation): - Relative difference is less than 20 percent or - Absolute difference is less than 6.6 ft	14.4 ft	14.7 ft	1.5 % 0.22 ft	Y
		A5	Number of broken or significantly bent posts is less than 20 percent.	0	0	X	Y
		A6	Did the rail element rupture or tear (Answer Yes or No)	No	No	X	Y
		A7	Was there significant snagging between the vehicle wheels and barrier elements (Answer Yes or No).	N	N	X	Y
		A8	Was there significant snagging between vehicle body components and barrier elements (Answer Yes or No).	N	N	X	Y

Table 66. Roadside safety phenomena importance ranking table (occupant risk).

Evaluation Criteria		Known Result	Analysis Result	Difference Relative/ Absolute	Agree?		
Occupant Risk	D	Detached elements, fragments or other debris from the test article should not penetrate or show potential for penetrating the occupant compartment, or present an undue hazard to other traffic, pedestrians or personnel in a work zone. (Answer Yes or No)	N	N		Y	
	F	F1	The vehicle should remain upright during and after the collision although moderate roll, pitching and yawing are acceptable. (Answer Yes or No)	Y	Y		Y
		F2	Maximum roll of the vehicle through 1.0 seconds: - Relative difference is less than 20 percent or - Absolute difference is less than 5 degrees.	-19.4 deg	-17 deg	12.4% 2.4 deg	Y
		F3	Maximum pitch of the vehicle through 1.0 seconds: - Relative difference is less than 20 percent or - Absolute difference is less than 5 degrees.	-13.7 deg	-16.5 deg	20.0 % 2.8 deg	Y
		F4	Maximum yaw of the vehicle through 1.0 seconds: - Relative difference is less than 20 percent or - Absolute difference is less than 5 degrees.	55.6 deg	48.2 deg	13.3 % 7.4 deg	Y
		5	Did the vehicle remain upright during and after collision	Y	Y		Y
	L	L1	Occupant impact velocities: - Relative difference is less than 20 percent or - Absolute difference is less than 6.6 ft/s.				
			•Longitudinal OIV (ft/s)	17.1	19.7	15.2% 2.6 ft/s	Y
			•Lateral OIV (ft/s)	-24.6	-24.9	1.2% 0.3 ft/s	Y
			•THIV (ft/s)	29.9	31.5	5.4% 1.6 ft/s	Y
		L2	Occupant accelerations: - Relative difference is less than 20 percent or - Absolute difference is less than 4 g's.				
			•Longitudinal ORA	-8.3	-8.3	0% 0 g	Y
			•Lateral ORA	10.0	7.5	25 % 2.5 g	Y
			•PHD	11.9	9.1	23.5 % 2.8 g	Y
			•ASI	1.74	1.48	14.9 % 0.26	Y

Table 67. Roadside safety phenomena importance ranking table (vehicle trajectory).

Evaluation Criteria			Known Result	Analysis Result	Difference Relative/ Absolute	Agree?	
Vehicle Trajectory	K	M1	The exit angle from the test article preferable should be less than 60 percent of test impact angle, measured at the time of vehicle loss of contact with test device.	*33%	36%		Y
		M2	Exit angle at loss of contact: - Relative difference is less than 20 percent or - Absolute difference is less than 5 degrees.	*8.21 deg (0.375 sec)	8.95 deg (0.375 sec)	9.0% 0.74 deg	Y
	M	M3	Exit velocity at loss of contact: - Relative difference is less than 20 percent or - Absolute difference is less than 6.2 mph.	*47.0 mph	44.6 mph	5.1 % 2.4 mph	Y

*Reported as 11.7 degrees. Test data showed the 8.21 degrees at 0.375 seconds in TRAP report.

** Reported as 52.9 mph. Test data showed 47 mph at 0.375 seconds in TRAP report.

7.5 Summary and Conclusions on Model Validation

The baseline finite element model of the 2-bar transition was used to simulate the full-scale crash tests on the system. The test corresponded to R350 Test 3-21 on the curb-mounted AGT system. The results of the analysis were compared to the full-scale tests to validate the fidelity of the model. The validation included both qualitative and quantitative elements. Qualitative assessments included comparing sequential snapshots of the test and simulation to verify vehicle kinematic response, as well as, the sequence and timing of key phenomenological events. The quantitative assessment was performed according to the procedures specified in NCHRP Web Report 179. These procedures included: (1) verifying that the analysis solution was stable and obeying basic laws of physics, (2) point-by-point comparison of the acceleration and angular-rate time-history data from the FEA and test (collected from accelerometers and rate gyros placed on-board the vehicle) using the RSVVP software, and (3) comparison of crash-specific phenomena from the event related to structural adequacy, occupant risk and vehicle trajectory.

In general, the results of the analyses demonstrated that the finite element model replicated the basic phenomenological behavior of the system for Report 350 Test 3-21 impact conditions. There was good agreement between the tests and the simulations with respect to event timing, overall kinematics of the vehicle, barrier damage, and deflections. Quantitative comparison of the time-history data indicated that the finite element model sufficiently replicated the results of the baseline crash tests. Thus, the model is considered valid and will be used in subsequent tasks for assessing *MASH* impact performance on this and similar NETC AGT systems.

8 EVALUATION CRITERIA FOR FEA CRASH ANALYSIS

Detailed finite element analysis models were developed for the NETC bridge rail and transition designs based on the validated models presented in Sections 6 and 7, and LS-DYNA was used to simulate the required impact conditions for *MASH* TL3 or *MASH* TL4, as appropriate. The crash performance evaluations were based on structural capacity, occupant risk measures, and vehicle stability during impact and redirection according to the recommended procedures and criteria contained in *MASH*. The required test conditions specified in *MASH* for test level 4 evaluation of longitudinal barrier and transition elements include:

- Test 4-10/Test 4-20 – the 1100C vehicle (2,225-lb sedan) impacting the transition barrier at the critical impact point at a nominal speed and angle of 62.0 mph and 25 degrees, respectively.
- Test 4-11/ Test 4-21 – the 2270P vehicle (5,000-lb ½-ton quad-cab pickup) impacting the barrier at the critical impact point at a nominal speed and angle of 62.0 mph and 25 degrees, respectively.
- Test 4-12/ Test 4-22 – the 10000S vehicle (22,046-lb single unit truck) impacting the barrier at the critical impact point at a nominal speed and angle of 56.0 mph and 15 degrees, respectively.

Table 68 shows the evaluation criteria required for *MASH* TL4 for longitudinal barrier and transitions denoting the specific conditions for each criterion and identifying the applicable tests. Accelerometers were included at the center of gravity for each of the vehicle models. For the 1100C vehicle (e.g., passenger car) and the 2270P vehicle (e.g., pickup), the center of gravity was located between the front seat occupants. For the 10000S vehicle (e.g., single unit truck) the center of gravity was located inside the cargo box, typically just in front of the ballast. Thus, for the single unit truck (SUT) an additional accelerometer was included inside the cabin of the truck model for use in computing occupant risk metrics. The location of the accelerometers and center of gravity for the FEA vehicle models for the 1100C, 2270P and 10000S vehicle model are shown in Figures 109, 110 and 111, respectively. Refer to Section 5 for additional vehicle property information.

Table 68. Safety evaluation guidelines for structural adequacy and occupant risk for *MASH* TL4 for longitudinal barriers and transitions. [AASHTO16]

Evaluation Factors	Evaluation Criteria	Test 4-10	Test 4-11	Test 4-12
Structural Adequacy	A. Test article should contain and redirect the vehicle or bring the vehicle to a controlled stop; the vehicle should not penetrate, underide, or override the installation although controlled lateral deflection of the test article is acceptable.	Y	Y	Y
Occupant Risk	D. Detached elements, fragments or other debris from the test article should not penetrate or show potential for penetrating the occupant compartment, or present an undue hazard to other traffic, pedestrians or personnel in a work zone. Deformations of, or intrusions into, occupant compartment should not exceed limits set forth in Section 5.2.2 and Appendix E.	Y	Y	Y
	F. The vehicle should remain upright during and after the collision. The maximum roll and pitch angles are not to exceed 75 degrees.	Y	Y	N
	G. It is preferable, although not essential, that the vehicle remain upright during and after collision.	N	N	Y
	H. The longitudinal and lateral occupant impact velocity (OIV) shall not exceed 40 ft/s (12.2 m/s), with a preferred limit of 30 ft/s (9.1 m/s)	Y	Y	N
	I. The longitudinal and lateral occupant ridedown acceleration (ORA) shall not exceed 20.49 G, with a preferred limit of 15.0 G.	Y	Y	N

The acceleration-time histories and angular rate-time histories were collected from the cabin accelerometers during the impact event and were used to evaluate occupant risk metrics according to the procedures outlined in *MASH*. The acceleration data from the analyses were collected at a frequency of 50,000 Hz and were filtered using the SAE Class 180 filter prior to input into the Test Risk Assessment Program (TRAP).[TTI98] The TRAP program calculates standardized occupant risk factors from vehicle crash data in accordance with *MASH* guidelines and the European Committee for Standardization (EN1317). TRAP computes important evaluation parameters including the occupant impact velocities (OIV), ridedown accelerations (ORA), 50 millisecond running average acceleration, and maximum roll, pitch and yaw. Also computed in TRAP are the EN1317 occupant risk metrics which include the Theoretical Head Impact Velocity (THIV), the Post Impact Head Deceleration (PHD) and the Acceleration Severity Index (ASI). The details of these calculations are provided in *MASH*. [AASHTO16] The evaluation of occupant risk metrics is not required for Test 4-22; however, they are included herein for completeness. In all cases, the time-history data was collected from the accelerometers in a local reference coordinate system that was fixed to the vehicle with the x-direction coincident with the forward direction of the vehicle, the local y-direction was oriented toward the right side of the vehicle and the local z-direction was oriented downward.

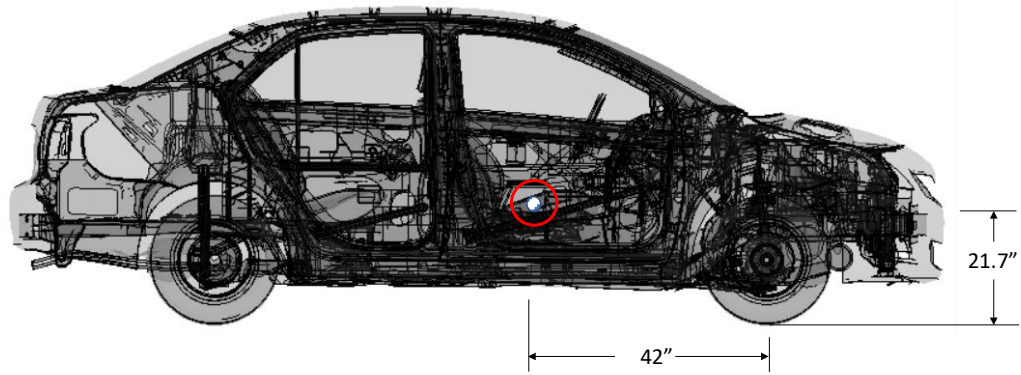


Figure 109. Location of c.g. in FEA model of 1100C vehicle.

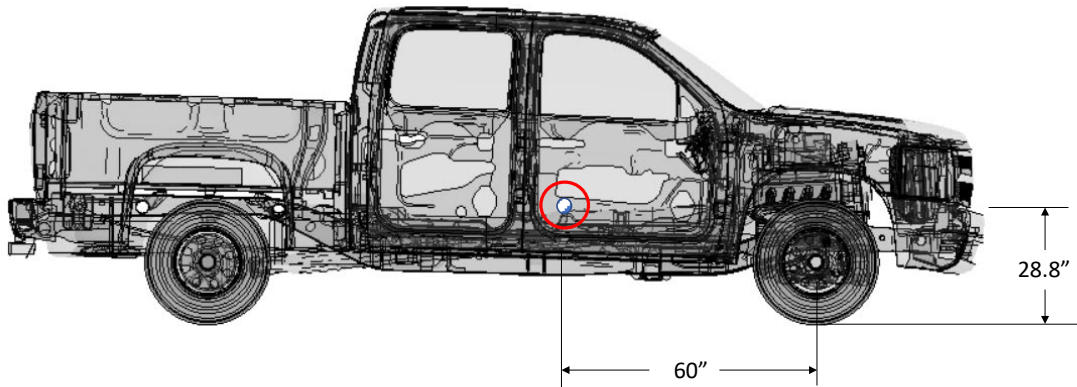


Figure 110. Location of c.g. in FEA model of 2270P vehicle.

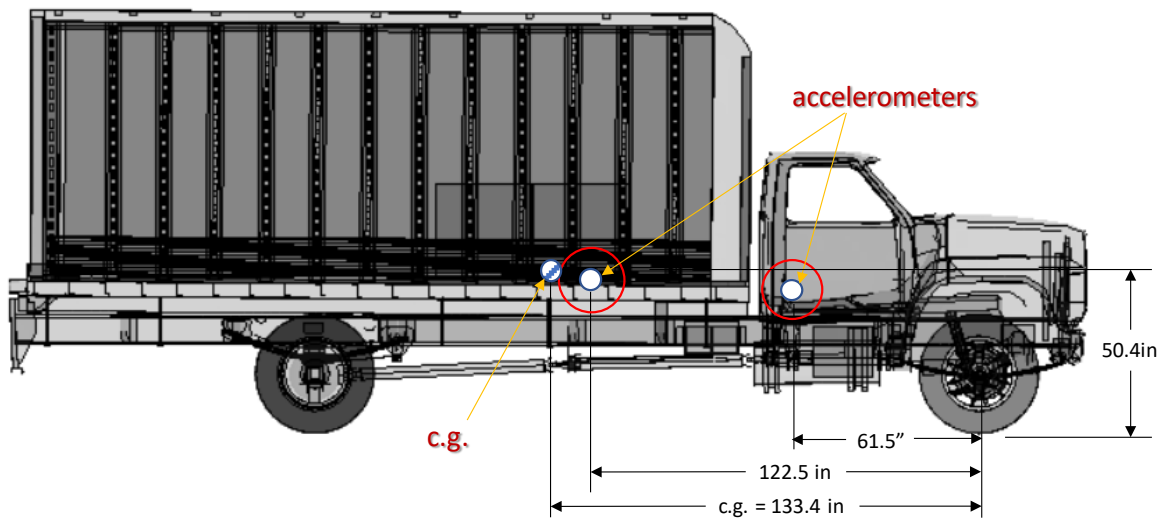


Figure 111. Location of accelerometers and c.g. in FEA model of 10000S vehicle.

With regards to evaluation criteria “D”, *MASH* lists certain limitations for passenger compartment intrusion. Specifically, it states:

“A clear distinction should be made between: (a) penetration, in which a component of the test article actually penetrates into the occupant compartment; and (b) intrusion or deformation, in which the occupant compartment is deformed and reduced in size, but no actual penetration is observed. No penetration by any element of the test article into the occupant compartment is allowed. As for deformation or intrusion, the extent of deformation varies by area of the vehicle damaged and should be limited as follows:”

- “Roof \leq 4.0 in. (102 mm).
- Windshield – no tear of plastic liner and maximum deformation of 3 in. (76 mm).
- Window – no shattering of a side window resulting from direct contact with a structural member of the test article, except for special considerations pertaining to tall, continuous barrier elements discussed below (Note: evaluation of this criteria requires the side windows to be in the up position for testing). In cases where side windows are laminated, the guidelines for windshields will apply.
- A- and B- pillars – no complete severing of support member and maximum resultant deformation of 5 in. (127 mm). Lateral deformation should be limited to 3 in. (76 mm).
- Wheel/foot well and toe pan areas \leq 9 in. (229 mm).
- Side front panel (forward of A-pillar) \leq 12 in. (305 mm).
- Front side door area (above seat) \leq 9 in. (229 mm).
- Front side door area (below seat) \leq 12 in. (305 mm).
- Floor pan and transmission tunnel areas \leq 12 in. (305 mm).” [*AASHTO16*]

Post-impact vehicle behavior, although not required by *MASH*, was examined for completeness of the evaluations. *MASH* uses the concept of the “exit box” which was adopted directly from CEN standards. It is defined by the initial traffic face of the barrier and a line parallel to the initial traffic face of the barrier at a lateral distance “A” plus the width of the vehicle plus 16 percent of the length of the vehicle, starting at the final intersection (break) of the wheel track with the initial traffic face of the barrier for a longitudinal distance of “B”. All wheel tracks of the vehicle should not cross the parallel line within the distance B. [*AASHTO16*]
A graphical representation of the exit box is shown in Figure 112.

Distance for Exit Box Criterion

Vehicle Type	A ft (m)	B ft (m)
Car/Pickup	$7.2 + V_W + 0.16V_L$ ($2.2 + V_W + 0.16V_L$)	32.8 (10.0)
Other Vehicles	$14.4 + V_W + 0.16V_L$ ($4.4 + V_W + 0.16V_L$)	65.6 (20.0)

V_W = Vehicle Width
 V_L = Vehicle Length

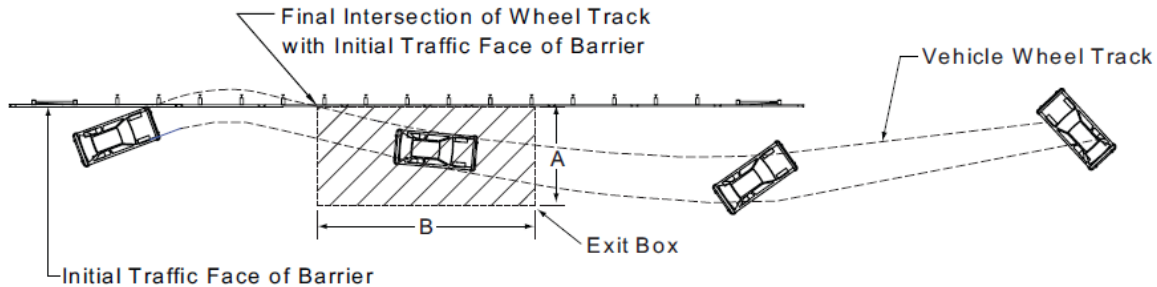


Figure 112. MASH exit box. [AASHTO16]

The exit box values were calculated based on the dimensions of the finite element analysis vehicle models. Table 69 shows the vehicle widths and lengths and resulting exit box dimensions for the small car, pickup truck, and SUT.

Table 69. Exit box dimensions for MASH Tests small car, pickup, and SUT

Test	V_w (ft)	V_L (ft)	A (ft)	B (ft)
4-20	5.5	14.1	15	32.8
4-21	6.02	16.8	15.86	32.8
4-22	8.01	28.15	26.95	65.6

9 EVALUATION OF THE NETC 3-BAR BRIDGE RAIL FOR MASH TL4

The FEA model of the curb-mounted NETC 3-bar bridge rail was developed based on the baseline NETC 4-bar model that was validated in Section 6. The modifications to the baseline model included:

- Reducing the length of the post,
- Removing one of the rails,
- Repositioning rails,
- Incorporating the updated splice model (refer to Figure 54),
- Moving splice to opposite side of post (for convenience of analysis),
- Removing the sidewalk, and
- Development of the curb and deck model.

The FEA model for the NETC 3-bar bridge rail is shown in Figure 113. The dimensions of the curb and reinforcing were modeled based on the RIDOT design for the 2-bar system (refer to Appendix D) which includes a granite curb extending 6 inches from the face of the rail. The adjacent surfaces between the granite curb and the concrete curb were not connected (i.e., nodes of the FEA model of the curb were not merged at the interface). By design, the splice for the tubular rails are placed on the downstream side of the posts to minimize potential for vehicles snagging at the joint in primary-direction impacts. The critical impact condition for the splice is therefore a reverse-direction impact where the vehicle impacts from the opposite direction. The FEA models for the vehicles, however, are meshed for evaluating primary-direction impacts (i.e., right side of vehicle has improved mesh refinement). To simulate reverse-direction impact cases, the splice was moved to the opposite side of the post, as illustrated in Figure 114.

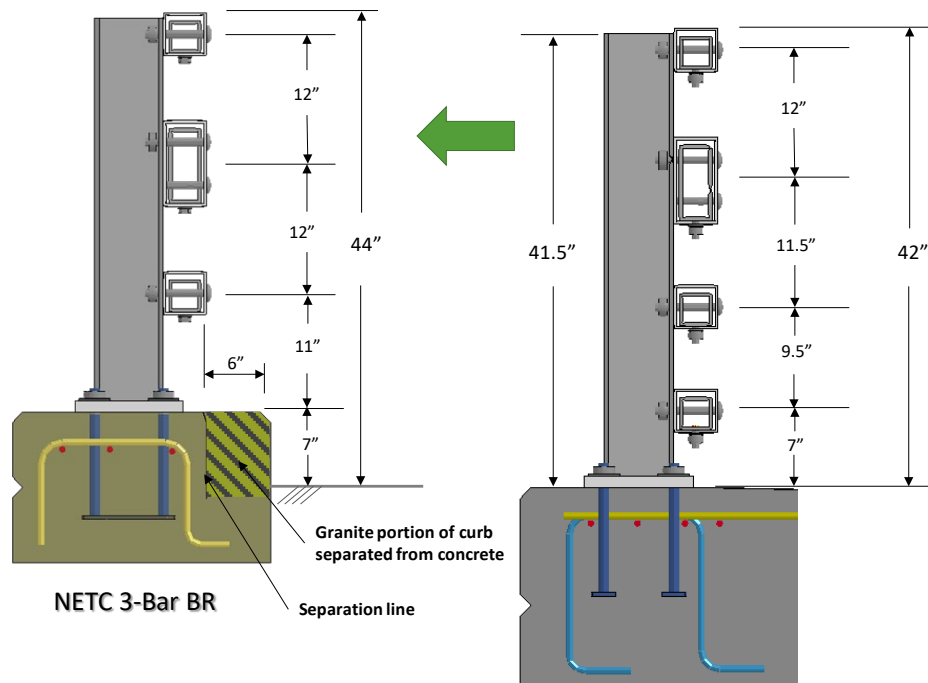


Figure 113. FEA model of curb-mounted NETC 3-bar compared with Baseline sidewalk-mounted 4-bar model.

FEA was used to evaluate the crash performance of the NETC 3-bar bridge rail based on structural adequacy, vehicle stability during and after redirection, and occupant risk factors using criteria specified in *MASH* for Test Level 4. Four impact cases were evaluated:

- Simulation of Test 4-10 included the 1100C Yaris model ballasted to 2,595 lb (1177 kg) impacting the barrier at 62.2 mph and 25 degrees. The critical impact point was selected as 3.6 feet (1.1 m) upstream of a bridge rail post.
- Simulation of Test 4-11 included the 2270P Chevrolet Silverado model ballasted to 5,001lb (2,269 kg) impacting the railing at 62.2 mph and 25 degrees. The critical impact point was selected as 4.3 feet (1.3 m) upstream of a bridge rail post.
- Simulation of Test 4-12 (Case 1) included the 10000S model ballasted to 22,198 lb (10,068 kg) impacting at 56 mph and 15 degrees. Cargo-bed height = 47.5 inches. The impact point was set to 5.0 feet (1.52 m) upstream of a bridge rail post.

- Simulation of Test 4-12 (Case 2) included the 10000S model ballasted to 22,198 lb (10,068 kg) impacting at 56 mph and 15 degrees. Cargo-bed height = 50 inches. The impact point was set to 5.0 feet (1.52 m) upstream of a bridge rail post.

The analysis in all cases was performed using LS-DYNA version mpp_s_R8.0.0 revision number 95309. The analysis was conducted with a time-step of 1.0 microsecond for a time period of 0.7 seconds for Test 4-10, 0.8 seconds for test 4-11, and 1.5 seconds for Test 4-12.

9.1 Test 4-10

The critical impact condition for Test 4-10 was selected based the *MASH* recommended CIP for rigid barrier tests (see Table 2-7 of *MASH*).[*AASHTO16*] The target impact point was 3.6 feet upstream of Post 7 and was selected to maximize potential for snagging at the post, while also providing adequate opportunity for snag at the splice connection for the tubular rails. The splice is located 1.5 feet upstream of the post. The following sections provide a summary of the results and include a commentary describing the timing and occurrence of various events during the simulated impact, time-history data evaluation, occupant risk assessments, and damages sustained by both the barrier and vehicle.

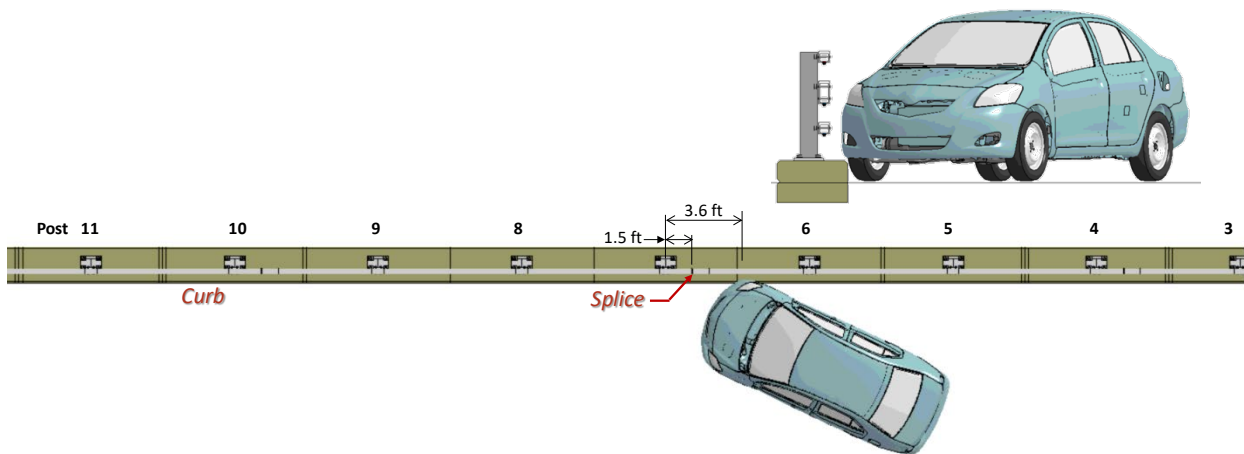


Figure 114. Impact point for Test 4-10 on the NETC 3-bar bridge rail.

9.1.1 Summary of Key Phenomenological Events

The sequential views of the impact event are shown in Appendix J in Figures J-1 through J-3 from an overhead viewpoint, downstream and upstream viewpoint, and oblique viewpoint, respectively. At time equal zero seconds the front-right tire contacted the curb, and at 0.01 seconds the front bumper contacted the lower railing. At 0.015 seconds the front fender contacted the middle railing. Also, at this time, the front-right tire was deformed enough to indicate debanding and deflation; however, that attribute was not included in the FEA model. At 0.02 seconds the middle and lower railings began to deflect. At 0.025 seconds the front bumper contacted the splice but did not snag; also, at this time, Post 7 began to deflect. At 0.035 seconds the front bumper was aligned with Post 7, and the front-right tire was fully mounted onto the curb. At 0.04 seconds the front bumper contacted Post 7 but did not snag on the post. At 0.045 seconds the front-right tire contacted the splice. At 0.06 seconds the lower railing reached maximum dynamic deflection of 3.35 inches at the splice, and Post 7 reached maximum dynamic deflection of 2.23 inches. At 0.065 seconds the front-right tire contacted Post 7 but did not snag

on the post. Also, at this time, the deformation at the lower edge of the A-Pillar caused the windshield to crack. At 0.0792 seconds the vehicle occupant contacted the right side of the interior at longitudinal velocity of 25.6 ft/s and lateral velocity of 32.5 ft/s. At 0.086 seconds the maximum ORA in the longitudinal direction occurred with magnitude 6.7 G. At 0.125 seconds the front of the vehicle separated from the barrier. At 0.15 seconds the rear-right tire contacted the curb. At 0.165 seconds the rear-right tire rim began to bend. At 0.167 seconds the vehicle was parallel to the barrier. At 0.19 seconds the rear quarter panel and rear bumper contacted the middle and lower railings, respectively, at Post 7. Also, at this time the tire damage indicated that tire deflation was likely. At 0.2 seconds the rear-left tire lifted off the ground. At 0.205 seconds the rear-right tire was fully mounted onto the curb. At 0.236 seconds the maximum ORA in the lateral direction occurred with magnitude 6 G. At 0.285 seconds the vehicle separated from the barrier traveling at 42.3 mph with exit angle of 11.1 degrees (44.4 percent of impact angle). At 0.489 seconds the vehicle reached a maximum pitch of 5.2 degrees (rear pitching upward). At 0.536 seconds the vehicle reached a maximum roll angle of 7.3 degrees (toward barrier). The vehicle remained stable throughout post-impact trajectory. The analysis ended at 0.7 seconds, at which time:

- The roll, pitch, and yaw of the vehicle were, respectively, 4.3 degrees (toward barrier), 3.6 degrees (rear pitching up), and 36 degrees (11 degrees relative to and away from barrier).
- The forward velocity of the vehicle was 39.8 mph (64.1 km/h).

9.1.2 Time History Data Evaluation

Figures 115 through 117 show the longitudinal, transverse, and vertical acceleration-time histories, respectively, computed from the center of gravity of the vehicle; Figures 118 through 120 show the comparison of the angular rates and angular displacements (i.e., yaw, roll and pitch) at the center of gravity of the vehicle.

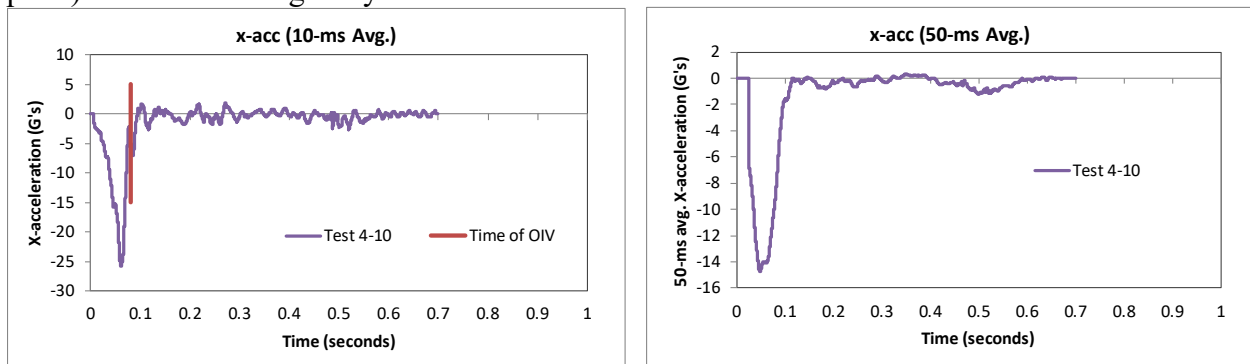


Figure 115. 10- and 50-millisecond average X-acceleration from FEA of Test 4-10 on the NETC 3-bar bridge rail.

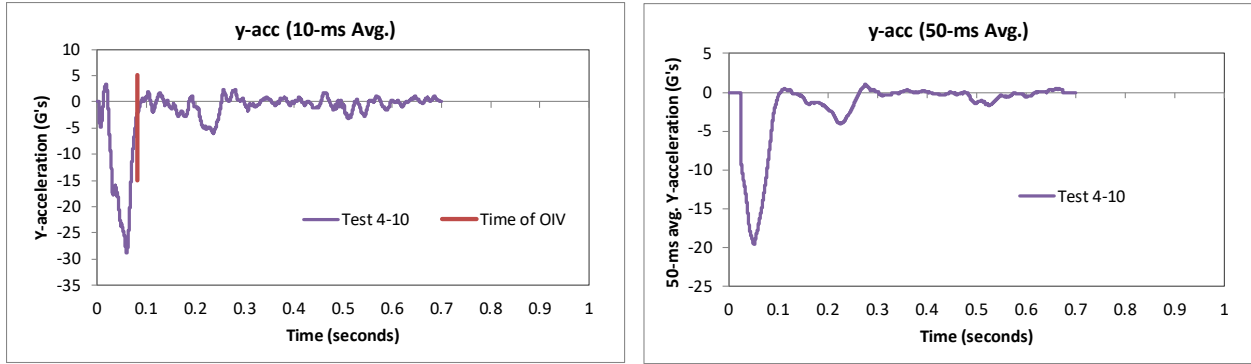


Figure 116. 10- and 50-millisecond average Y-acceleration from FEA of Test 4-10 on the NETC 3-bar bridge rail.

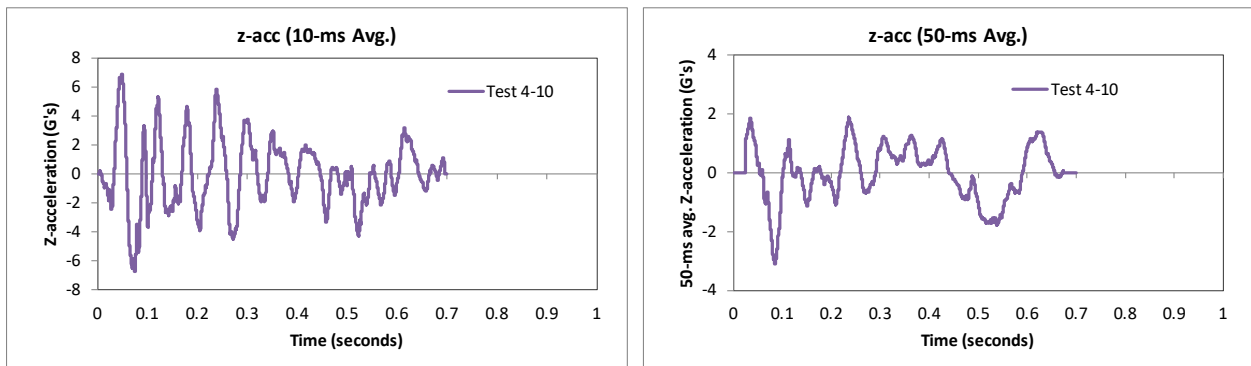


Figure 117. 10- and 50-millisecond average Z-acceleration from FEA of Test 4-10 on the NETC 3-bar bridge rail.

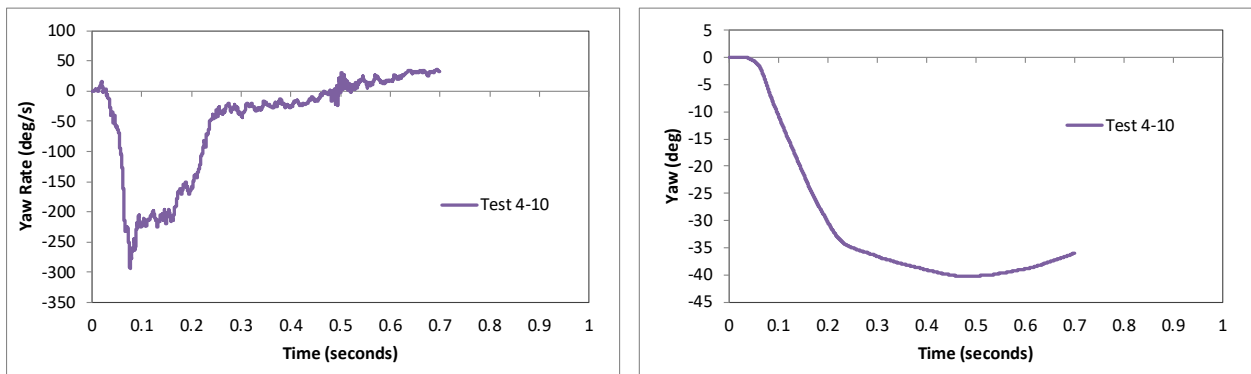


Figure 118. Yaw rate and yaw angle time-history from FEA of Test 4-10 on the NETC 3-bar bridge rail.

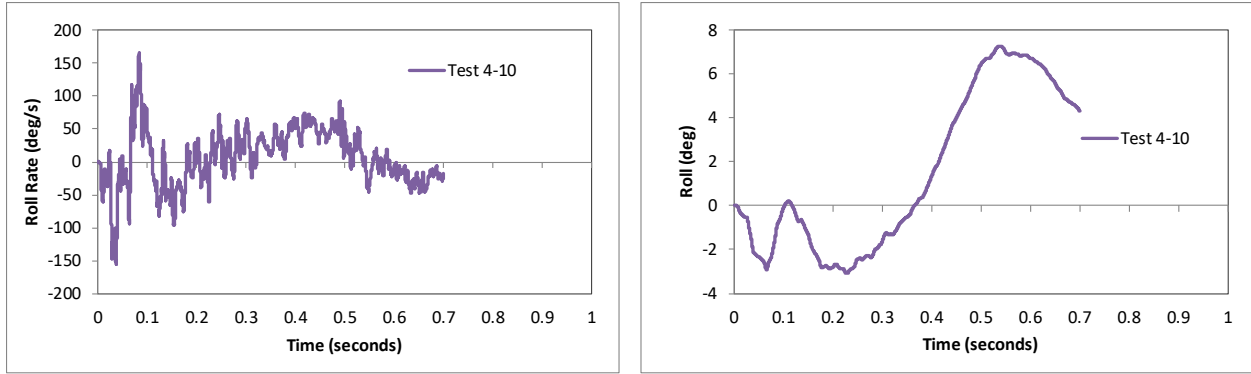


Figure 119. Roll rate and roll angle time-history from FEA of Test 4-10 on the NETC 3-bar bridge rail.

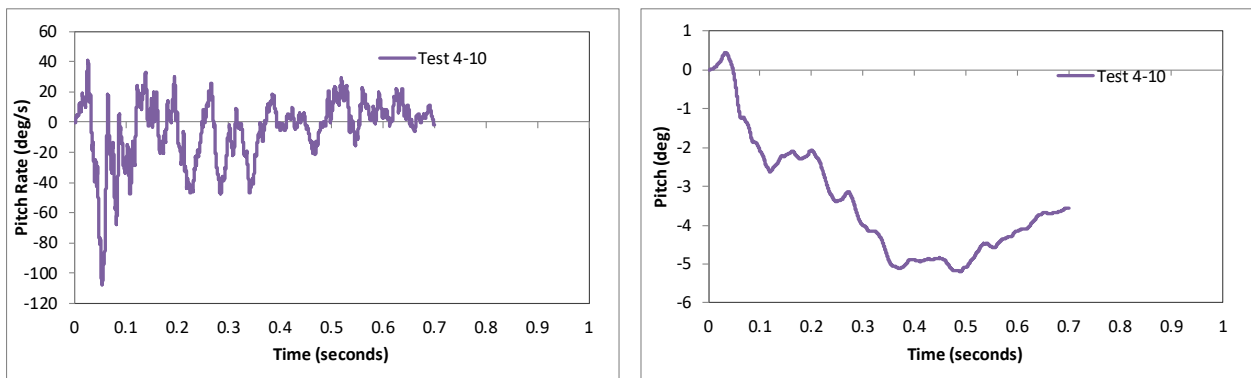


Figure 120. Pitch rate and pitch angle time-history from FEA of Test 4-10 on the NETC 3-bar bridge rail.

9.1.3 Occupant Risk Measures

The acceleration-time histories and angular rate-time histories collected at the center of gravity of the vehicle were used to evaluate occupant risk metrics according to the procedures outlined in *MASH*. Table 70 shows the results for the occupant risk calculations. The results indicate that the occupant risk factors meet safety criteria specified in *MASH*.

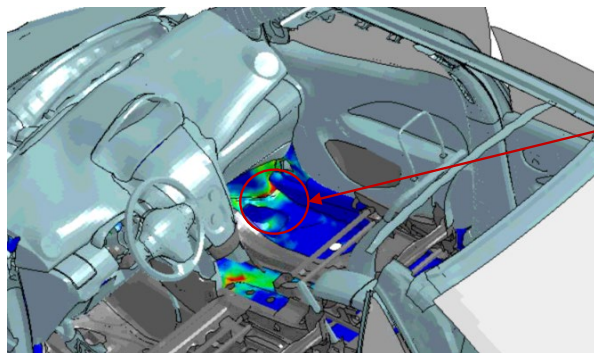
The occupant impact velocities in the longitudinal and transverse directions were 25.6 ft/s and 32.5 ft/s, respectively, which were within critical limits specified in *MASH*. The highest 0.010-second occupant ridedown acceleration in the longitudinal and transverse directions were 6.7 g and 6 g, respectively, which were well within preferred limits specified in *MASH*. However, these values are highly dependent on time of occupant impact with the interior, as shown in Figures 115 and 116. The maximum 50-ms moving average acceleration values in the longitudinal and transverse directions were 14.8 g and 19.6 g, respectively, which are considered relatively high. The maximum roll and pitch angles of the vehicle were 7.3 degrees and 5.2 degrees, respectively, which were well below critical limits in *MASH*.

Table 70. Summary of *MASH* occupant risk metrics for Test 4-10 on the NETC 3-bar bridge rail.

Occupant Risk Factors		MASH T4-10	MASH Criteria
		Test 4-10	
Occupant Impact Velocity (ft/s)	x-direction	25.6	} > 30 ft/s (preferred) < 40 ft/s (limit) ✓
	y-direction	32.5	
	at time	at 0.0792 seconds on right side of interior	
THIV (ft/s)		41.3	}
		at 0.0792 seconds on right side of interior	
Ridedown Acceleration (g's)	x-direction	-6.7 (0.0811 - 0.0911 seconds)	} < 15 G (preferred) ✓ < 20.49 G (limit)
	y-direction	-6 (0.2306 - 0.2406 seconds)	
PHD (g's)		7.1 (0.0800 - 0.0900 seconds)	
ASI		2.49 (0.0253 - 0.0753 seconds)	
Max 50-ms moving avg. acc. (g's)	x-direction	-14.8 (0.0241 - 0.0741 seconds)	}
	y-direction	-19.6 (0.0262 - 0.0762 seconds)	
	z-direction	-3.1 (0.0602 - 0.1102 seconds)	
Maximum Angular Disp. (deg)		7.3	} < 75 deg ✓
	Roll	(0.5359 seconds)	
	Pitch	-5.2 (0.4892 seconds)	
	Yaw	-40.3 (0.4954 seconds)	

9.1.4 Occupant Compartment Intrusion

The maximum deformation of the occupant compartment was approximately 2.76 inches at the lower right-front corner of the toe-pan at the wheel well. Figure 121 shows a view of the vehicle interior after the impact, with several components removed to facilitate viewing. The deformation was less than the critical limit of 9 inches specified in *MASH* for this area of the occupant compartment.



Maximum OCI of the floor, doors, and side panels was ≈**2.76 inches** (70 mm) and occurred at the right-front toe-pan at the wheel well.
Maximum allowable is 9".

Figure 121. Occupant compartment deformation resulting from Test 4-10 on the NETC 3-bar bridge rail.

9.1.5 Damages to the Barrier System

The damages to the barrier were minimal. Figure 122 shows an overhead view of the post impact deformation of the bridge rail indicating the extent of damage. The vehicle was in contact with the barrier for 10.5 feet. The barrier was deformed over 9.7 feet of the system with deformation extending from Post 6 (first post upstream of impact) to 1.7 feet downstream of Post

7. Figure 123 and Figure 124 show images of the maximum dynamic deflection and permanent deflection of the barrier, respectively, with a contour plot of lateral displacement on the rail elements. The maximum dynamic and permanent deflections were 3.35 inches and 1.85 inches, respectively, and occurred at the lower tube rail at the splice, as illustrated in Figures 182 - 184.

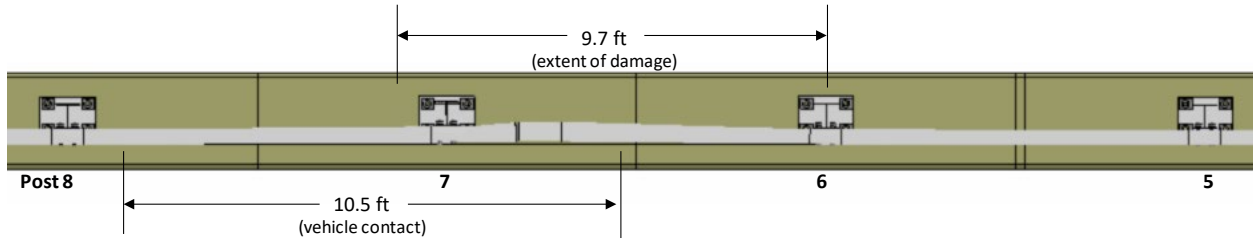


Figure 122. Overhead view of NETC 3-bar bridge rail after Test 4-10 showing extent of damage.

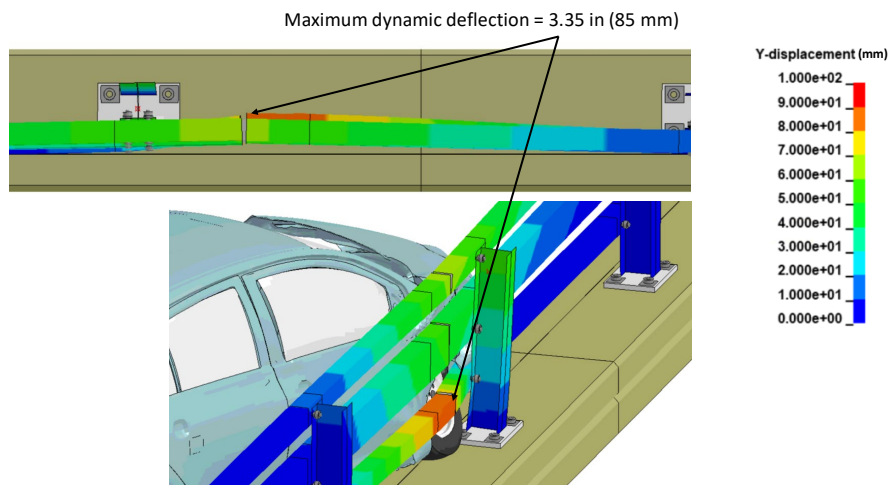


Figure 123. Contour plot of lateral displacement for the bridge rail for Test 4-10 at the time of maximum dynamic deflection.

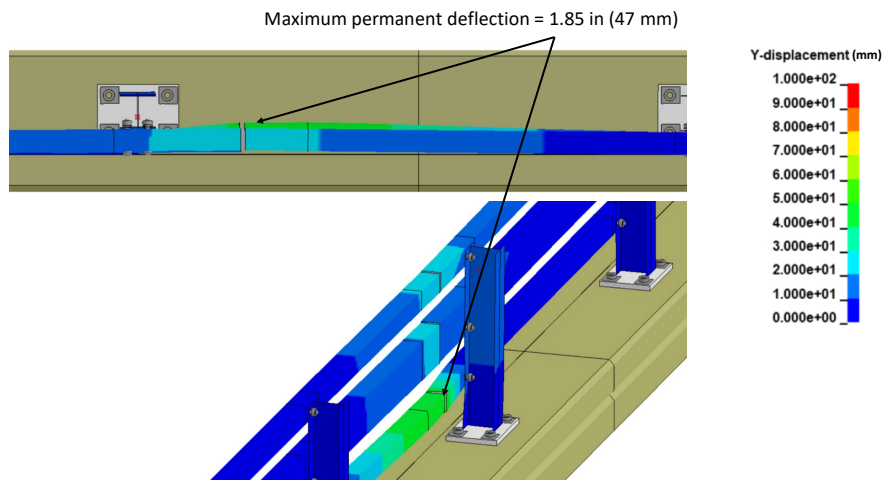


Figure 124. Contour plot of maximum permanent deflection of the bridge rail for test 4-10.

Figure 125 shows contours of true effective plastic strains on the bridge rail. The damage was limited to deformations of the lower rail at the splice connection, as well as, the post and the

baseplate at the critical post location. The maximum vertical dynamic deflection of the baseplate was 0.43 inches (10.9 mm) and the maximum permanent deflection of the baseplate was 0.14 inches (3.7 mm).

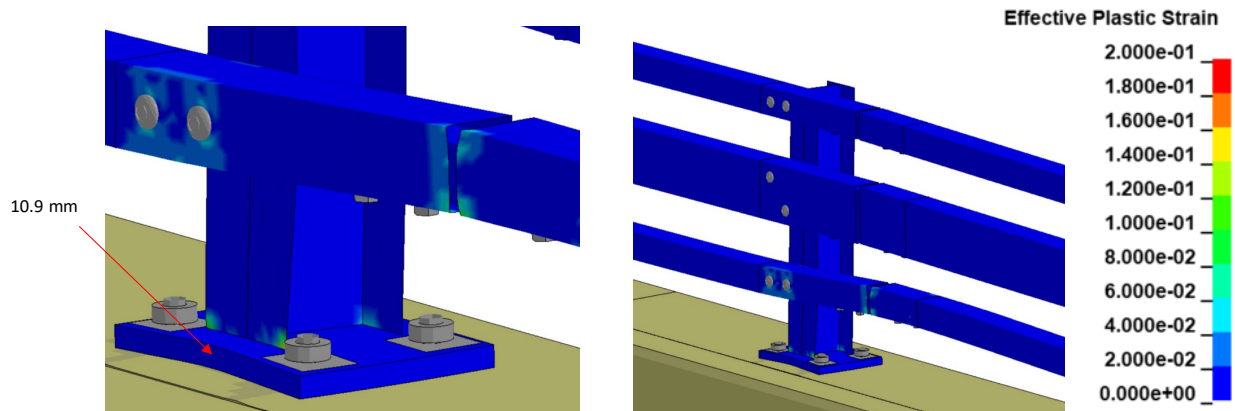


Figure 125. Contours of effective plastic strains for Test 4-10 on the NETC 3-bar bridge rail.

Figure 126 shows contours of 1st principal strain with contours cut off at strains of 0.1. In an earlier project conducted by the research team, the concrete material model used in the current study was validated against full-scale tests involving a rigid pendulum impacting into fixed-fixed steel reinforced concrete columns.[*Ray18a; Ray18b*] The results of that study indicated that values of 1st Principle strain of 0.07 to 0.08 (yellow contours) indicated initial crack openings in the concrete, when correlated to the column impact tests, and that strains values of 0.08 to 0.1 (orange/red contours) corresponded to significant crack openings. The 1st Principal strain values for the concrete in these cases was 0.06 dynamic strain and was 0.017 permanent strain, which indicated a very low probability for concrete failure.

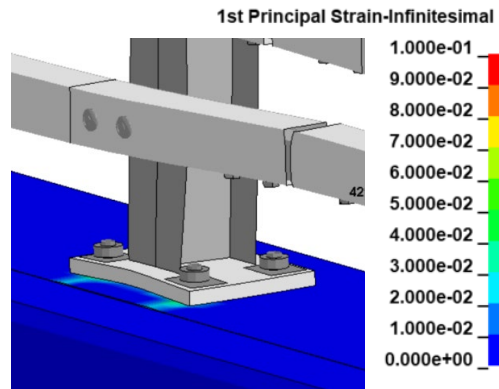


Figure 126. Contours of 1st principal strains for concrete at the critical post for Test 4-10 on the NETC 3-bar bridge rail.

9.1.6 Damages to Vehicle

Figure 127 shows contour plots of effective plastic strain for the vehicle, which were used to identify areas of the vehicle that suffered damage during the simulated impact event. The most severe damages were to the front fender, the upper and lower control arm of front suspension, front wheel, lower edge of windshield on the impact side, the rear wheel, and the rear quarter panel of the vehicle on the impact side.

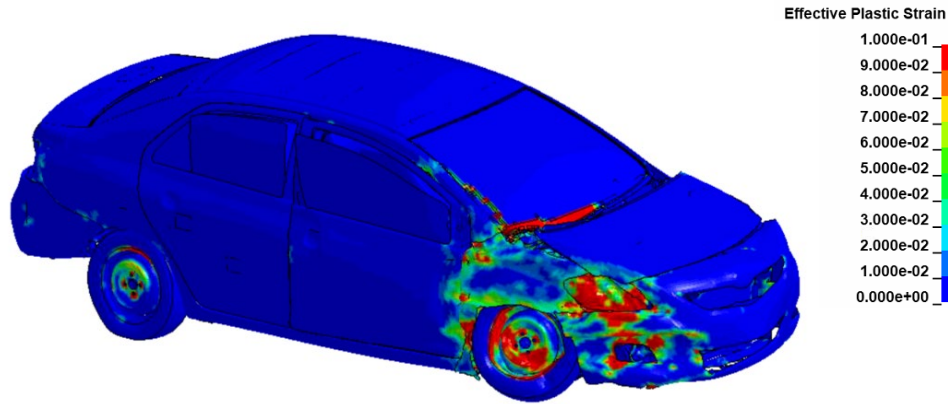


Figure 127. Damages to vehicle in Test 4-10 analysis of the NETC 3-bar bridge rail.

9.1.7 Exit Box

Figure 128 shows the exit box for Test 4-10 on the bridge rail, where the vehicle was smoothly redirected and its path was well within the exit box criteria of *MASH*.

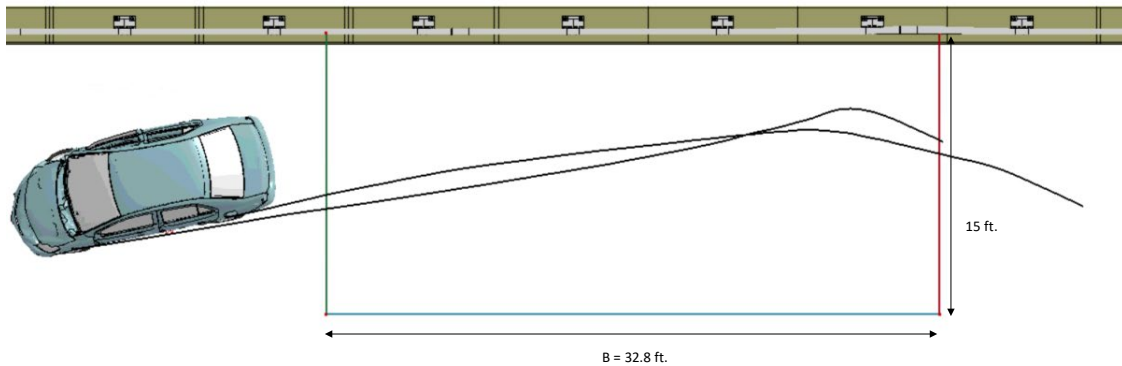


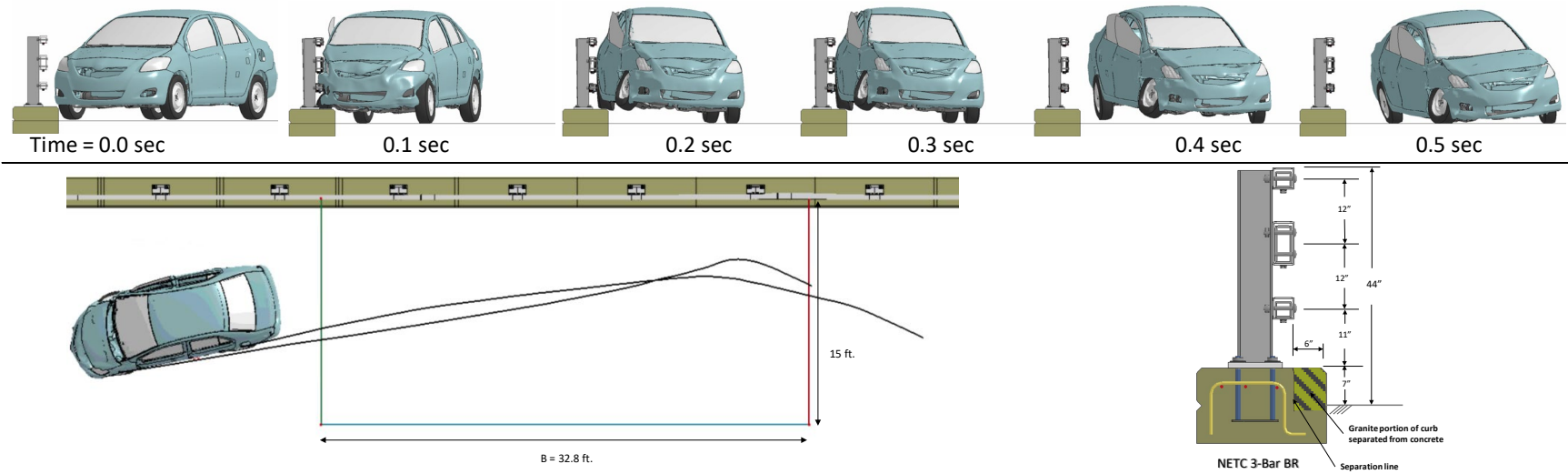
Figure 128. Exit box for Test 4-10 analysis of the NETC 3-bar bridge rail.

9.1.8 Results Summary

A summary of the *MASH* Test 4-10 results on the NETC 3-bar bridge rail is shown in Table 71 and Figure 129. The barrier successfully contained and redirected the small car with minimal damage to the system. There were no detached elements from the barrier that showed potential for penetrating the occupant compartment or presenting undue hazard to other traffic. The windshield cracked during contact between the A-Pillar and top railing, and the side windows on the passenger side failed, but the failure was not due to direct impact from the railing on the glass. Therefore, the head-slap criteria passed. The vehicle remained upright and very stable throughout impact and redirection. The OIV and maximum ORA values were within recommended limits specified in *MASH*. Based on the results of this analysis, the barrier is expected to meet all structural and occupant risk criteria in *MASH* for Test 4-10 impact conditions.

Table 71. Summary of MASH Test 4-10 results on the NETC 3-bar bridge rail.

Evaluation Factors	Evaluation Criteria	Results
Structural Adequacy	A Test article should contain and redirect the vehicle or bring the vehicle to a controlled stop; the vehicle should not penetrate, underride, or override the installation although controlled lateral deflection of the test article is acceptable.	Pass
Occupant Risk	D Detached elements, fragments, or other debris from the test article should not penetrate or show potential for penetrating the occupant compartment, or present undue hazard to other traffic, pedestrians, or personnel in a work zone. Deformations of, or intrusions into, to occupant compartment should not exceed limits set forth in Section 5.2.2 and Appendix E.	Pass
	F The vehicle should remain upright during and after collision. The maximum roll and pitch angles are not to exceed 75 degrees.	Pass
	H The longitudinal and lateral occupant impact velocity (OIV) shall not exceed 40 ft/s (12.2 m/s), with a preferred limit of 30 ft/s (9.1 m/s)	Pass
	I The longitudinal and lateral occupant ridedown acceleration (ORA) shall not exceed 20.49 G, with a preferred limit of 15.0 G	Pass



General Information		Impact Conditions		Max50-millisecond Avg. (G)	
Analysis Agency	Roadsafe LLC	Speed	62 mph	Longitudinal	14.8 g
Test Standard Test No.	MASH Test 4-10	Angle	25 degrees	Lateral	19.6 g
Analysis No.	NETC18_3BarBR_T410_M2	Location	3.6 ft upstream of Post 7	Vertical	3.1 g
Analysis Date	4/15/2019				
Test Article		Impact Severity		Test Article Deflections (in)	
Type	Bridge Rail	59.5 kip-ft		Dynamic	3.4 inches
Name	NETC 3-Bar	Exit Conditions		Permanent	1.9 inches
Installation Length	120 feet	Speed	42.3 mph	Working Width	
Material or Key Elements		Angle	11 degrees		
		Time	0.28 seconds	Max. OCI	
				2.76 inch	
Soil Type and Condition		Occupant Risk Values		Vehicle Stability	
N.A.		Longitudinal OIV	25.6 ft/s	Roll	7.3 degees
Analysis Vehicle		Lateral OIV	32.5 ft/s	Pitch	5.2 degrees
Type / Designation	1100C	Longitudinal ORA	6.7 g	Yaw	40.3 degrees
FEA Model name	510_YarisC_V1I_R180228	Lateral ORA	6.0 g		
Mass	2,595 lb	THIV	41.3 ft/s		
		PHD	7.1 g		
		ASI	2.49		

Figure 129. Summary results for MASH Test 4-10 on the NETC 3-bar bridge rail.

9.2 Test 4-11

The critical impact condition for *MASH* Test 4-11 was selected based the *MASH* recommended CIP for rigid barrier tests. The target impact point was 4.3 feet upstream of Post 7, as shown in Figure 130, and was selected to maximize potential for snagging at the post, while also providing adequate opportunity for snag at the splice connection of the tubular rails. [AASHTO16] The following sections provide a summary of the results and include a commentary describing the timing and occurrence of various events during the simulated impact, time-history data evaluation, occupant risk assessments, and damages sustained by both the barrier and vehicle.

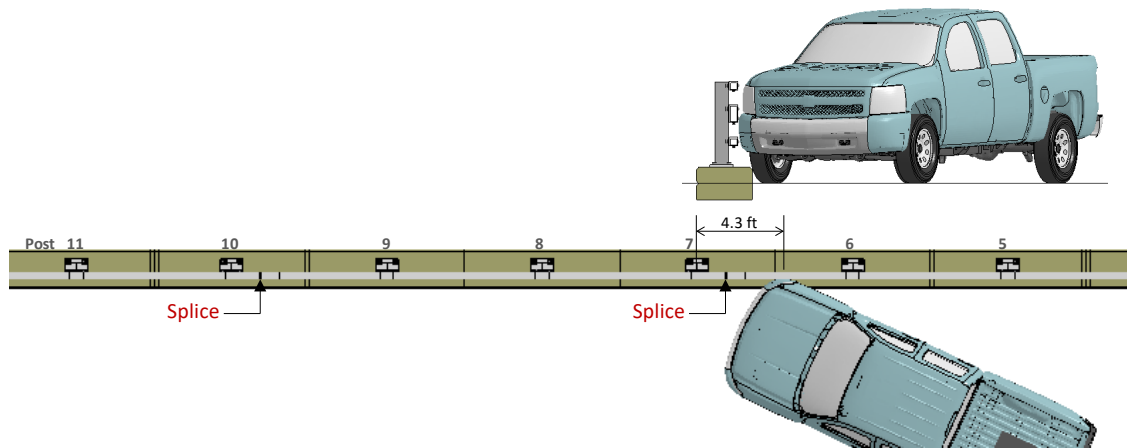


Figure 130. Impact point for Test 4-11 on the NETC 3-bar bridge rail.

9.2.1 Summary of Key Phenomenological Events

The sequential views of the impact event are shown in Appendix K in Figures K-1 through K-3 from an overhead viewpoint, downstream and upstream viewpoint, and oblique viewpoint, respectively. At time equal zero seconds the front-right tire contacted the curb, and the front bumper contacted the middle and lower railing. At 0.005 seconds the front fender contacted the top railing. At 0.01 seconds the front-right tire contacted the lower railing, and Post 7 began to deflect. At 0.015 seconds the tire front-right tire contacted the middle railing. Also, at this time, the tire was deformed enough to indicate debanding and deflation; however, that attribute was not included in the FEA model. At 0.03 seconds the front-right tire was fully mounted onto the curb. At 0.035 seconds the front-right tire was steered parallel to the barrier. At 0.04 seconds the front bumper was aligned with Post 7. At 0.05 seconds the rim of the front-right tire snagged on the end of the lower rail at the splice connection. Also, at this time, the lower control arm joint failed. At 0.055 seconds the rail reached maximum dynamic deflection of 4.2 inches at the splice connection on the top rail. At 0.065 seconds Post 7 reached a peak lateral deformation of 3.4 inches. At 0.085 seconds the front-right tire was aligned with Post 7 but did not contact the post. At 0.0912 seconds the vehicle occupant contacted the right side of the interior at longitudinal velocity of 22 ft/s and lateral velocity of 26.6 ft/s; and immediately after, the maximum ORA in the longitudinal direction occurred with magnitude 4.79.4 G at 0.0995 seconds. At 0.13 seconds the front bumper was aligned with Post 8. At 0.16 seconds the front of the vehicle separated from the barrier. At 0.17 seconds the rear-right tire contacted the curb. At 0.176 seconds the front-right tire was aligned with Post 8. At 0.18 seconds the rear

quarter panel of the vehicle impacted the upper and middle rails. At 0.181 the vehicle was parallel to the barrier traveling at 46 mph. At 0.185 seconds the rear bumper impacted against the middle rail, and the rear-left tire lifted off the ground. At 0.19 seconds the rear-right tire was deformed enough to indicate deflation (not included in model). At 0.195 seconds the rear-right tire contacted the middle and lower rails. At 0.2069 seconds the maximum ORA in the lateral direction occurred with magnitude 15.4 G. At 0.21 seconds the rear-right tire was fully mounted onto the curb; also, at this time, Post 6 and Post 8 reached a peak lateral dynamic deflection of 1.1 inches for both posts. At 0.22 seconds post 7 reached a second peak deformation of 3 inches. At 0.27 seconds the vehicle separated from the rail traveling at 45.2 mph and at an exit angle of 4.5 degrees. At 0.455 seconds the vehicle reached a maximum pitch angle of 7.5 degrees (rear pitching up), and at 0.649 seconds the vehicle reached maximum roll angle of 9.9 degrees (rolling toward barrier). The vehicle remained stable throughout post-impact trajectory. The analysis ended at 0.8 seconds, at which time:

- The roll, pitch, and yaw of the vehicle were, respectively, 4.1 degrees (toward barrier), 1.5 degrees (rear pitching up), and 17.9 degrees (7.1 degrees relative to and toward barrier).
- The forward velocity of the vehicle was 39.3 mph (63.3 km/h).

9.2.2 Time History Data Evaluation

Figures 131 through 133 show the longitudinal, transverse, and vertical acceleration-time histories, respectively, computed from the center of gravity of the vehicle; Figures 134 through 136 show the comparison of the angular rates and angular displacements (i.e., yaw, roll and pitch) at the center of gravity of the vehicle.

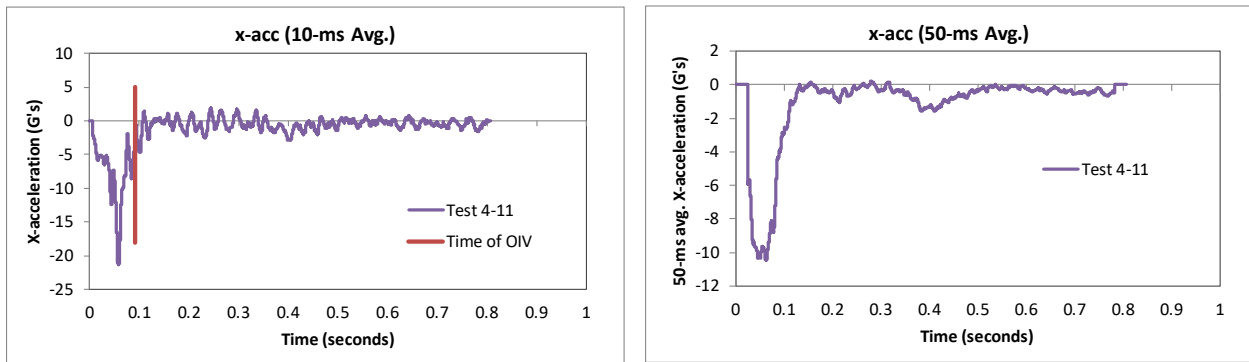


Figure 131. 10- and 50-millisecond average X-acceleration from FEA of Test 4-11 on the NETC 3-bar bridge rail.

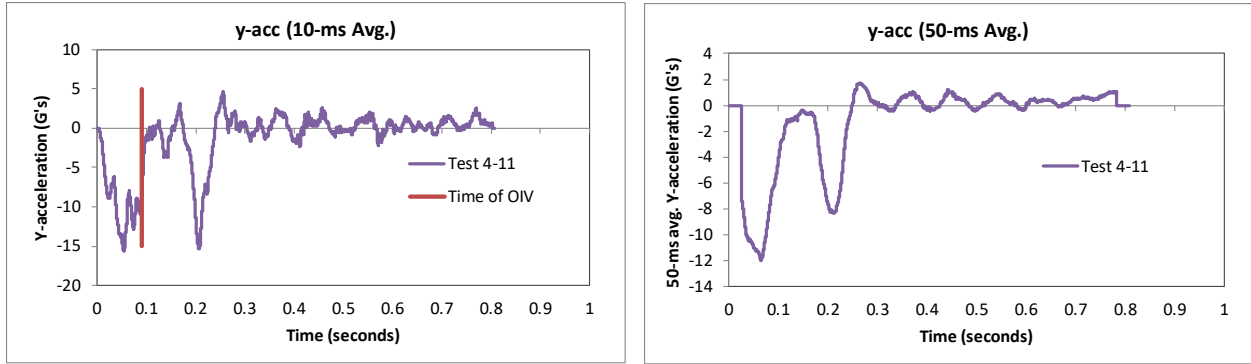


Figure 132. 10- and 50-millisecond average Y-acceleration from FEA of Test 4-11 on the NETC 3-bar bridge rail.

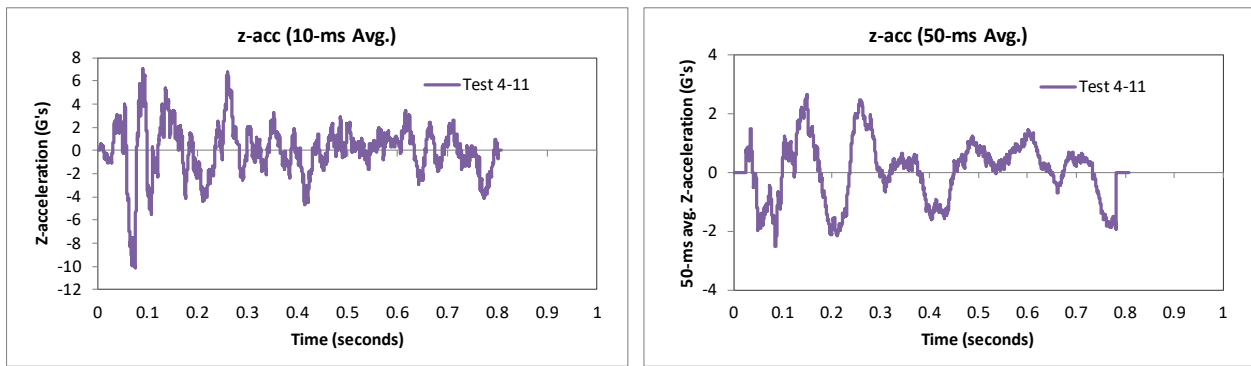


Figure 133. 10- and 50-millisecond average Z-acceleration from FEA of Test 4-11 on the NETC 3-bar bridge rail.

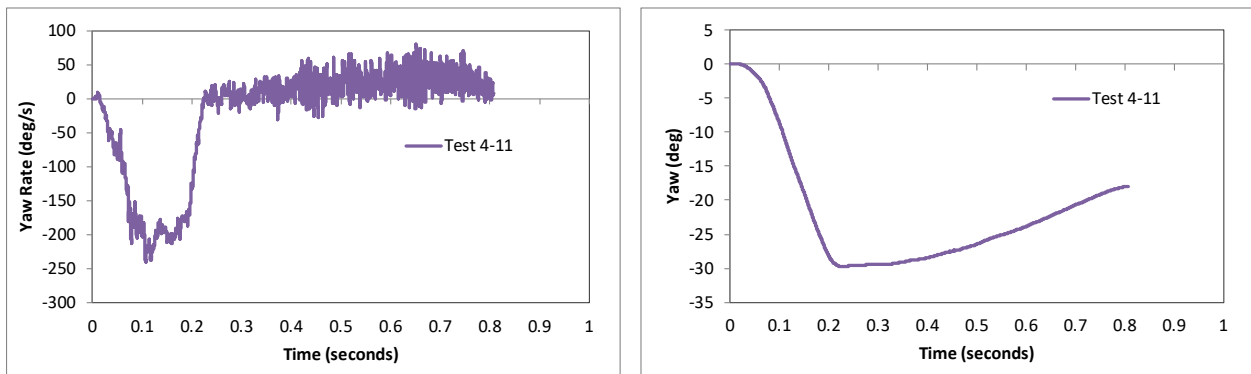


Figure 134. Yaw rate and yaw angle time-history from FEA of Test 4-11 on the NETC 3-bar bridge rail.

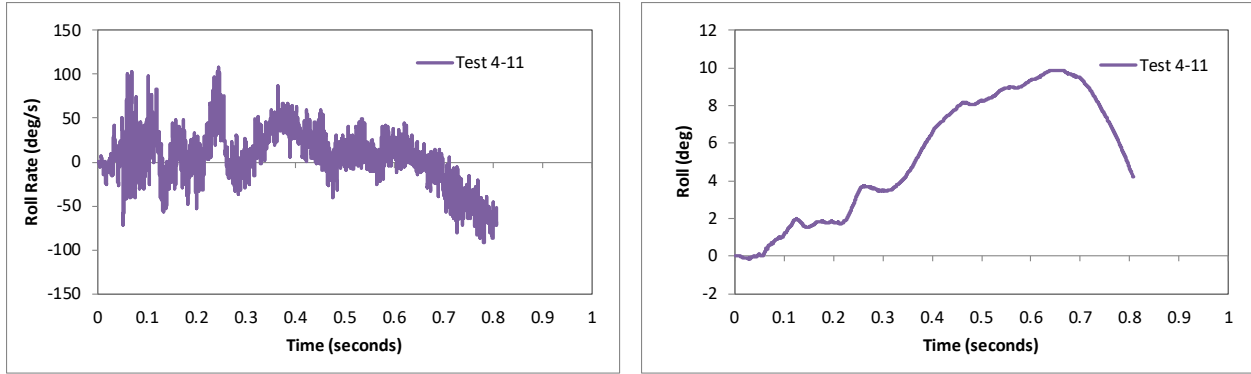


Figure 135. Roll rate and roll angle time-history from FEA of Test 4-11 on the NETC 3-bar bridge rail.

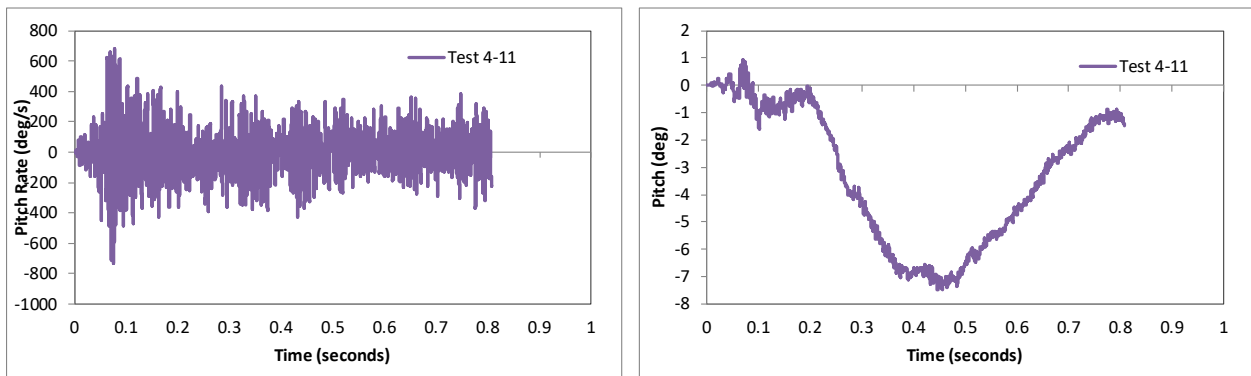


Figure 136. Pitch rate and pitch angle time-history from FEA of Test 4-11 on the NETC 3-bar bridge rail.

9.2.3 Occupant Risk Measures

The acceleration-time histories and angular rate-time histories collected at the center of gravity of the vehicle were used to evaluate occupant risk metrics according to the procedures outlined in *MASH*. Table 72 shows the results for the occupant risk calculations. The results indicate that the occupant risk factors meet safety criteria specified in *MASH*.

The occupant impact velocities in the longitudinal and transverse directions were 22.0 ft/s and 26.6 ft/s, respectively, which were within critical limits specified in *MASH*. The highest 0.010-second occupant ridedown acceleration in the longitudinal and transverse directions were 4.7 g and 15.4 g, respectively, which were within preferred limits specified in *MASH*. The maximum 50-ms moving average acceleration values in the longitudinal and transverse directions were 10.5 g and 12 g, respectively. The maximum roll and pitch angles of the vehicle were 9.9 degrees and 7.5 degrees, respectively, which were well below critical limits in *MASH*.

Table 72. Summary of *MASH* occupant risk metrics for Test 4-11 on the NETC 3-bar bridge rail.

Occupant Risk Factors		MASH	MASH Criteria
		Test 4-11	
Occupant Impact Velocity (ft/s)	x-direction	22.0	} < 30 ft/s (preferred) ✓ < 40 ft/s (limit)
	y-direction	26.6	
	at time	at 0.0912 seconds on right side of interior	
THIV (ft/s)		34.1 at 0.0884 seconds on right side of interior	
Ridedown Acceleration (g's)	x-direction	-4.7 (0.0945 - 0.1045 seconds)	} < 15 G (preferred) ✓ < 20.49 G (limit)
	y-direction	-15.4 (0.2019 - 0.2119 seconds)	
PHD (g's)		15.4 (0.2018 - 0.2118 seconds)	
ASI		1.6 (0.0389 - 0.0889 seconds)	
Max 50-ms moving avg. acc. (g's)	x-direction	-10.5 (0.0381 - 0.0881 seconds)	} < 75 deg ✓
	y-direction	-12 (0.0392 - 0.0892 seconds)	
	z-direction	2.6 (0.1245 - 0.1745 seconds)	
Maximum Angular Disp. (deg)	Roll	9.9 (0.6491 seconds)	} < 75 deg ✓
	Pitch	-7.5 (0.4551 seconds)	
	Yaw	-29.7 (0.2255 seconds)	

9.2.4 Occupant Compartment Intrusion

The maximum deformation of the occupant compartment was approximately 3.3 inches at the right-front corner of the toe-pan at the wheel well. Figure 137 shows a view of the vehicle interior after the impact, with several components removed to facilitate viewing. The deformation was less than the critical limit of 9 inches specified in *MASH* for this area of the occupant compartment.

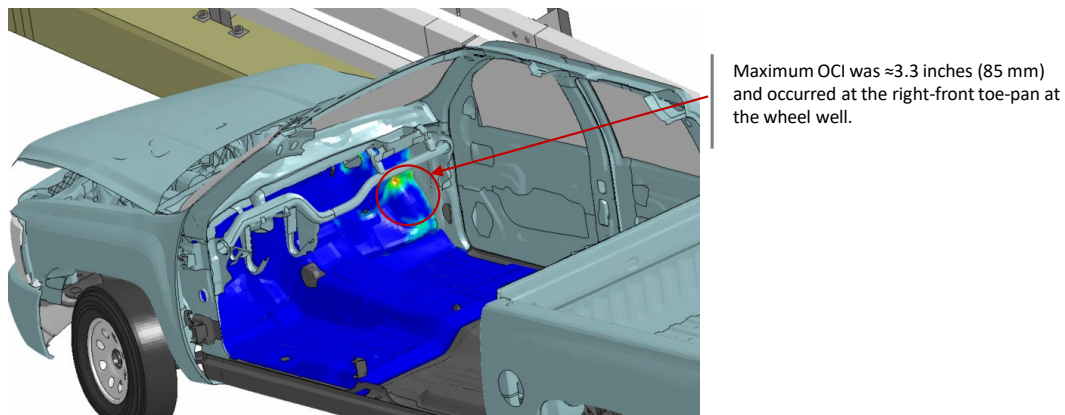


Figure 137. Occupant compartment deformation resulting from Test 4-11 on the NETC 3-bar bridge rail.

9.2.5 Damages to the Barrier System

The damages to the barrier were moderate. Figure 138 shows an overhead view of the post impact deformation of the bridge rail indicating the extent of damage. The vehicle was in

contact with the barrier for 12.1 feet. The barrier was deformed over 31 feet of the system with deformation extending from just downstream of Post 5 to just upstream of Post 9. Figure 139 and Figure 140 show images of the maximum dynamic deflection and permanent deflection of the barrier, respectively, with a contour plot of lateral displacement on the rail elements. The maximum dynamic and permanent deflections were 4.2 inches and 1.9 inches, respectively, and occurred at the top rail tube at the splice, as indicated in Figures 139 and 140.

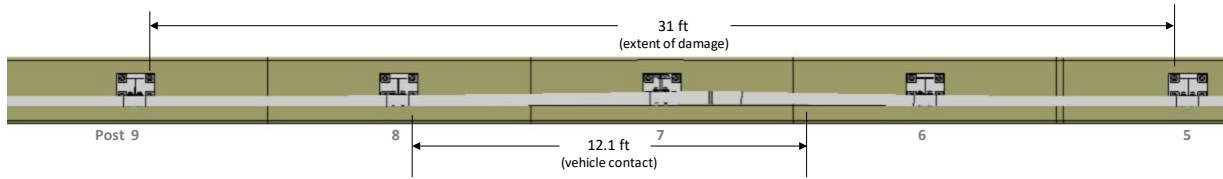


Figure 138. Overhead view of NETC 3-bar bridge rail after Test 4-11 showing extent of damage.

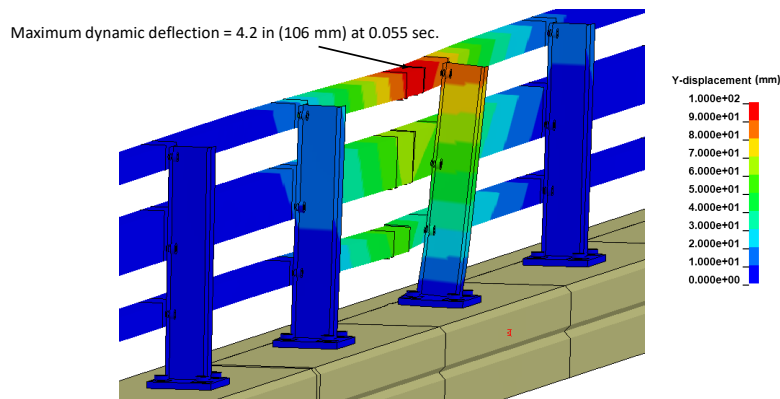


Figure 139. Contour plot of lateral displacement for the bridge rail for Test 4-11 at the time of maximum dynamic deflection.

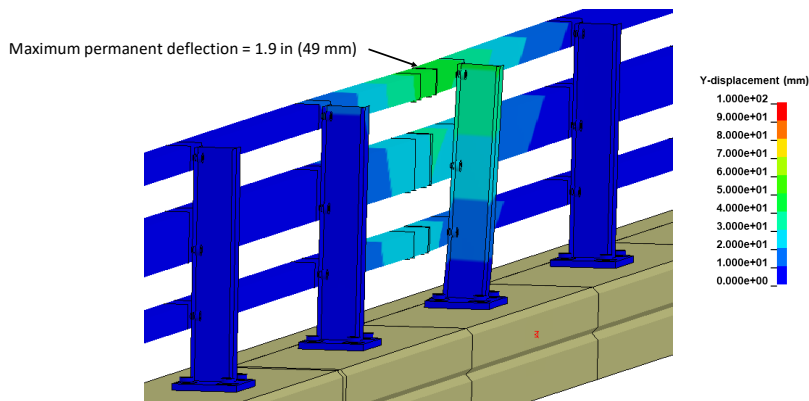


Figure 140. Contour plot of maximum permanent deflection of the bridge rail for test 4-11.

Figure 141 shows contours of true effective plastic strains on the bridge rail. The damage was primarily limited to the rail section between Post 6 and Post 7 and included plastic deformation of those posts, baseplates and all three rails. There was also slight plastic deformation at the base of Posts 6 and 7. The maximum vertical dynamic deflection of the baseplate at Post 7 was 0.63 inches (16 mm) and the maximum permanent deflection of the baseplate was 0.29 inches (7.4 mm).

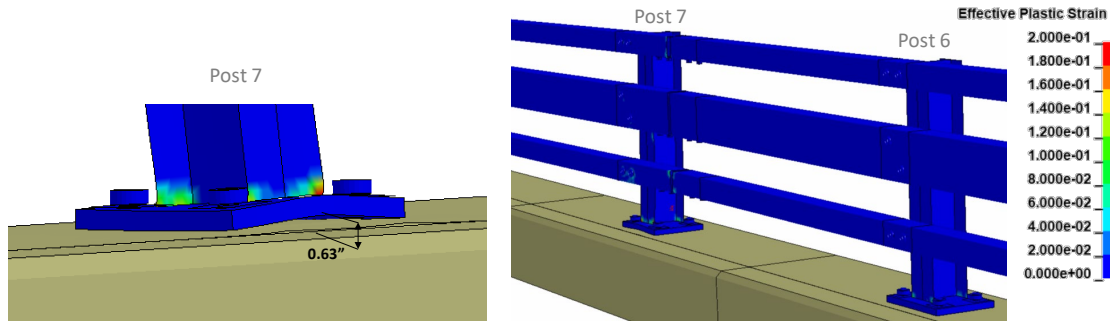


Figure 141. Contours of effective plastic strains for Test 4-11 on the NETC 3-bar bridge rail.

Figure 142 shows contours of 1st principal strain with contours cut off at strains of 0.1. The 1st Principal strain values for the concrete in these cases was 0.07 dynamic strain and was 0.0 permanent, which indicates a relatively low probability for concrete failure.

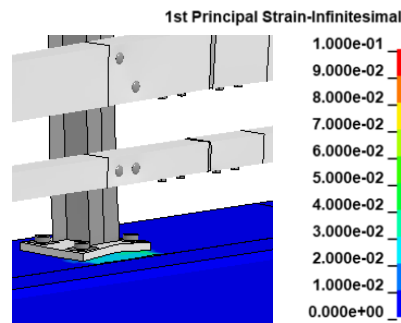


Figure 142. Contours of 1st principal strains for concrete at the critical post for Test 4-11 on the NETC 3-bar bridge rail.

9.2.6 Damages to Vehicle

Figure 143 shows contour plots of effective plastic strain for the vehicle, which were used to identify areas of the vehicle that suffered damage during the simulated impact event. The most severe damages were to the front bumper, front fender, front edge of the passenger front door, the upper and lower control arm of front suspension, front wheel, the rear wheel, and the rear quarter panel of the vehicle on the impact side.

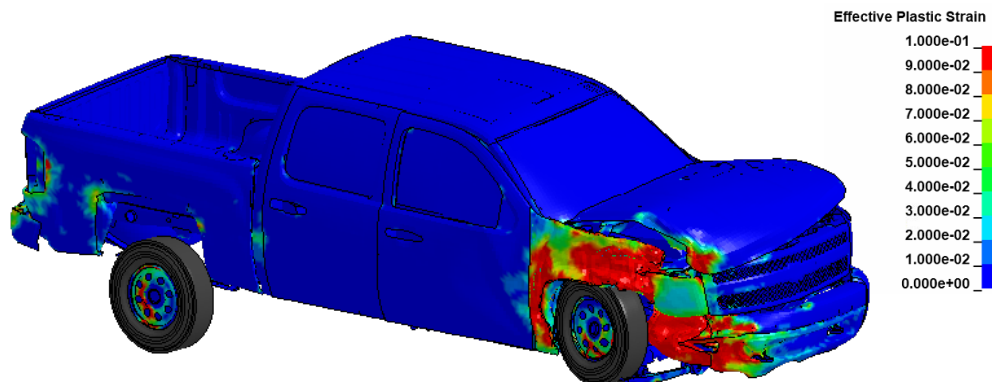


Figure 143. Damages to vehicle in Test 4-11 analysis of the NETC 3-bar bridge rail.

9.2.7 Exit Box

Figure 144 shows the exit box for Test 4-11 on the bridge rail, where the vehicle was smoothly redirected and its path was well within the exit box criteria of *MASH*.

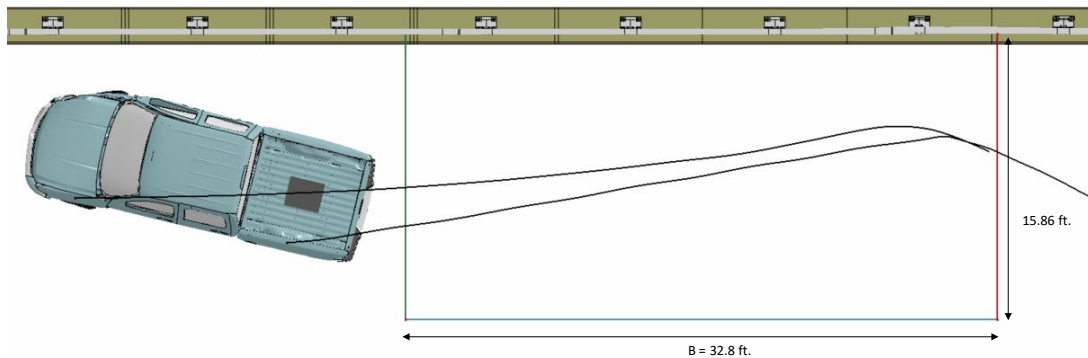


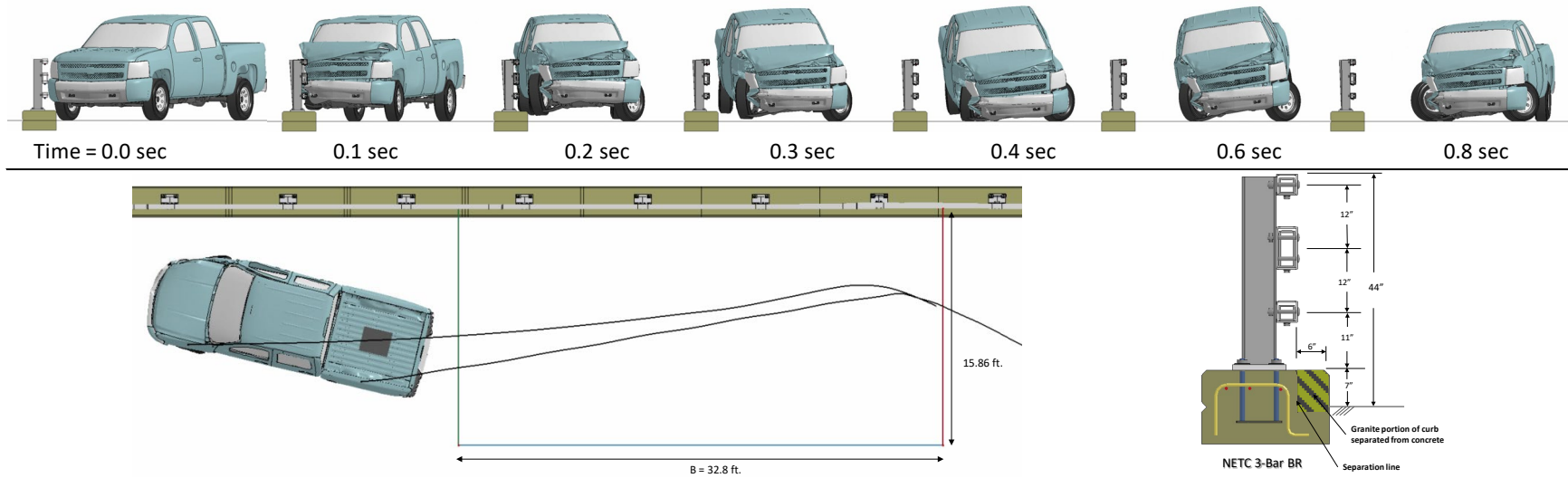
Figure 144. Exit box for Test 4-11 analysis of the NETC 3-bar bridge rail.

9.2.8 Results Summary

A summary of the *MASH* Test 4-11 results on the NETC 3-bar bridge rail is shown in Table 73 and Figure 145. The barrier successfully contained and redirected the pickup with moderate damage to the system. There were no detached elements from the barrier that showed potential for penetrating the occupant compartment or presenting undue hazard to other traffic. The vehicle remained upright and very stable throughout impact and redirection. The OIV and ORA were within recommended limits as specified in *MASH*. Based on the results of this analysis, the barrier meets all structural and occupant risk criteria in *MASH* for Test 4-11 impact conditions.

Table 73. Summary of MASH Test 4-11 results on the NETC 3-bar bridge rail.

Evaluation Factors	Evaluation Criteria	Results
Structural Adequacy	A Test article should contain and redirect the vehicle or bring the vehicle to a controlled stop; the vehicle should not penetrate, underide, or override the installation although controlled lateral deflection of the test article is acceptable.	Pass
Occupant Risk	D Detached elements, fragments, or other debris from the test article should not penetrate or show potential for penetrating the occupant compartment, or present undue hazard to other traffic, pedestrians, or personnel in a work zone. Deformations of, or intrusions into, to occupant compartment should not exceed limits set forth in Section 5.2.2 and Appendix E.	Pass
	F The vehicle should remain upright during and after collision. The maximum roll and pitch angles are not to exceed 75 degrees.	Pass
	H The longitudinal and lateral occupant impact velocity (OIV) shall not exceed 40 ft/s (12.2 m/s), with a preferred limit of 30 ft/s (9.1 m/s)	Pass
	I The longitudinal and lateral occupant ridedown acceleration (ORA) shall not exceed 20.49 G, with a preferred limit of 15.0 G	Pass



General Information		Impact Conditions		Max50-millisecond Avg. (G)	
Analysis Agency	Roadsafe LLC	Speed	62 mph	Longitudinal	10.5 g
Test Standard Test No.	MASH Test 4-11	Angle	25 degrees	Lateral	12.0 g
Analysis No.	NETC18_3BarBR_T411_M2	Location	4.3 ft upstream of Post 7	Vertical	2.6 g
Analysis Date	4/14/2019				
Test Article		Impact Severity		Test Article Deflections (in)	
Type	Bridge Rail	114.7 kip-ft		Dynamic	4.2 inches
Name	NETC 3-Bar	Exit Conditions		Permanent	1.9 inches
Installation Length	120 feet	Speed	45.3 mph	Working Width	1.12 feet
Material or Key Elements		Angle	4.5 degrees		
		Time	0.27 seconds	Max. OCI	
				3.3 inch	
Soil Type and Condition		Occupant Risk Values		Vehicle Stability	
N.A.		Longitudinal OIV	22.0 ft/s	Roll	9.9 degees
Analysis Vehicle		Lateral OIV	26.6 ft/s	Pitch	7.5 degrees
Type / Designation	2270P	Longitudinal ORA	4.7 g	Yaw	29.7 degrees
FEA Model name	SilveradoC_V3a_V180201_TireRS_35psi	Lateral ORA	15.4 g		
Mass	5,001 lb	THIV	34.1 ft/s		
		PHD	15.4 g		
		ASI	1.6		

Figure 145. Summary results for MASH Test 4-11 on the NETC 3-bar bridge rail.

9.3 Test 4-12

The critical impact point for *MASH* Test 4-12 was selected based the *MASH* recommended CIP for rigid barrier tests. The target impact point was 5.0 feet upstream of a bridge rail post, as illustrated in Figure 146, which was consistent with the recommended CIP in *MASH* and was selected to maximize loading on a post.[*AASHTO16*] Two analysis cases were evaluated for Test 4-12:

- Case 1: Vehicle bed height = 47.5 inches.
- Case 2: Vehicle bed height = 50 inches

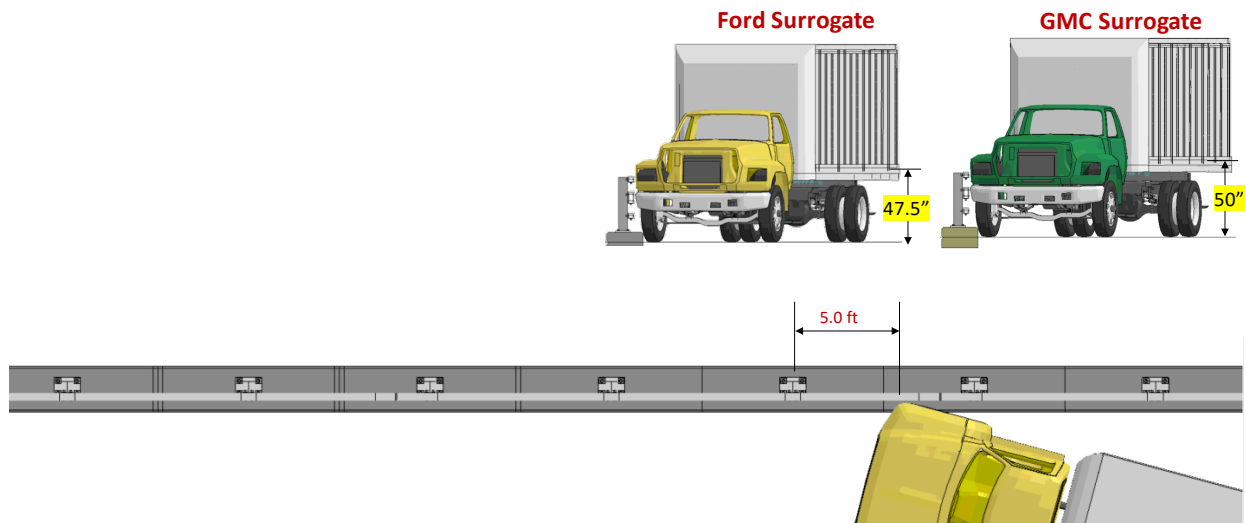


Figure 146. Impact point for Test 4-12 on the NETC 3-bar bridge rail.

The cargo-bed height for the FEA model was 47.5 inches measured from the ground to the top of the cargo-bed floor. This height was consistent with Ford 800 test vehicles (which was the basis for the model) but was lower than most other test vehicles. For example, test 420020-9b involved a 1991 International 4700 with 48-inch bed height [*Sheikh11*]; Test 404251-6 involved a Chevrolet C 70 with 50-inch cargo bed height [*Buth99a*]; Test 490026-4-3 involved an International 4200 with 50-inch cargo-bed height [*Williams17b*]; Test 607451-1 involved an International 4200 with 49.25-inch cargo-bed height [*Williams17a*]. When the top of the bridge rail is at approximately the same height as the bed of the cargo-box, then slight differences in the bed height will determine if the cargo-box impacts directly against the rail or passes over the top of the rail. Two different versions of the SUT vehicle model were used for evaluation of Test 4-12: one with cargo-bed height of 47.5 inches (lower bound) and another with cargo-bed height of 50 inches (upper bound), as illustrated in Figure 146.

The following sections provide a summary of the results and include a commentary describing the timing and occurrence of various events during the simulated impact, time-history data evaluation, occupant risk assessments, and damages sustained by both the barrier and vehicle.

9.3.1 Summary of Key Phenomenological Events

9.3.1.1 Case 1

The 22,198-lb single unit truck struck the barrier at 5.0 feet upstream of Post 5 at a speed of 56 mph and at an angle of 15 degrees, as illustrated in Figure 146. The sequential views of the Case 1 impact event are shown in Appendix L in Figures L-1 through L-3 from an overhead viewpoint, downstream and upstream viewpoint, and an oblique viewpoint, respectively. At time equal zero seconds the front-right tire contacted the curb. At 0.005 seconds the front bumper contacted the middle railing of the barrier and the front-right fender contacted the upper railing. At 0.01 seconds the railing began to deflect. At 0.02 seconds the front-right tire contacted the lower and middle rails and began to steer away from the barrier. At 0.04 seconds the tire was fully mounted onto the curb, and at 0.06 seconds the tire was parallel to the barrier. At 0.08 seconds one of the u-bolts connecting the front axle to the front-right suspension failed, but the second u-bolt did not fail, and the axle remained attached. At 0.09 seconds the front-right tire was centered at Post 7 (target critical post). At 0.14 seconds the lower front-right corner of the cargo-box contacted the top railing at approximately 29 inches upstream of Post 7. Also, at this time the front-left tire lifted off the ground. At 0.215 seconds the rear tandems of the vehicle contacted the curb. At 0.24 seconds the rear-right tandem wheels contacted the middle and lower railings; also, at this time the deflection of the railing began to increase. At 0.25 seconds the rear of the cargo-box impacted against the top railing. At 0.273 seconds the maximum loading on the barrier occurred with magnitude of 109 kips (25 millisecond moving average) and 100 kip (50 millisecond moving average). At 0.29 seconds the maximum dynamic deflection of the barrier was 7.64 inches and occurred approximately mid-span between Posts 7 and 8. also, at this time the rear-left tandem wheel set lifted off the ground as the vehicle continued to roll toward the barrier. At 0.304 seconds the vehicle was parallel to the barrier. At 0.47 seconds the vehicle lost contact with the barrier traveling at an exit speed and angle of 50.5 mph and 2.3 degrees. At 0.63 seconds the front-left tire recontacted the ground. At 0.703 seconds the cargo-box reached maximum pitch angle of 6.0 degrees (rear pitching upward); at 0.713 seconds the cabin reached maximum pitch angle of 7.8 degrees (rear pitching up). At 0.77 seconds the rear-right tire recontacted the ground. At 0.783 seconds the cargo-box experienced maximum roll angle of 22.4 degrees (cargo-box rolling toward the barrier); at 0.960 seconds the cabin of the vehicle reached a maximum roll angle of 20.8 degrees (toward the barrier). At 0.98 seconds the rear-left tires recontacted the ground. The vehicle remained upright and relatively stable throughout post-impact trajectory. The analysis ended at 1.5 seconds, at which time:

- The roll, pitch, and yaw of the truck cabin were, respectively, 8.4 degrees (toward barrier), 0.8 degrees (rear pitching up), and 17.8 degrees (2.8 degrees relative to and away from barrier).
- The roll, pitch, and yaw of the cargo-box were, respectively, 5.4 degrees (toward barrier), 2.0 degrees (rear pitching up), and 20 degrees (5 degrees relative to and away from barrier).
- The forward velocity of the vehicle was 49.6 mph (79.8 km/h).

9.3.1.2 Case 2

The 22,198-lb single unit truck struck the barrier at 5.0 feet upstream of Post 5 at a speed of 56 mph and at an angle of 15 degrees, as illustrated in Figure 146. The sequential views of the

Case 2 impact event are shown in Appendix M in Figures M-1 through M-3 from an overhead viewpoint, downstream and upstream viewpoint, and an oblique viewpoint, respectively.

At time equal zero seconds the front-right tire contacted the curb. At 0.005 seconds the front bumper contacted the middle railing of the barrier and the front-right fender contacted the upper railing. At 0.01 seconds the railing began to deflect. At 0.02 seconds the front-right tire contacted the lower and middle rails and began to steer away from the barrier. At 0.04 seconds the tire was fully mounted onto the curb, and at 0.06 seconds the tire was parallel to the barrier. At 0.08 seconds one of the u-bolts connecting the front axle to the front-right suspension failed, but the second u-bolt did not fail, and the axle remained attached. At 0.09 seconds the front-right tire was centered at Post 7 (target critical post). At 0.115 seconds the front-left tire lifted off the ground. At 0.125 seconds the lower front-right corner of the cargo-box contacted the top-edge of the top railing at approximately 32 inches upstream of Post 7. At 0.21 seconds the rear tandems of the vehicle contacted the curb. At 0.235 seconds the rear-right tandem wheels contacted the middle and lower railings; also, at this time the deflection of the railing began to increase. At 0.25 seconds the rear of the cargo-box impacted against the top railing. At 0.275 seconds the rear-left tires lifted off the ground as the vehicle continued to roll toward the barrier. At 0.29 seconds the maximum dynamic deflection of the barrier was 8.1 inches and occurred approximately mid-span between Posts 7 and 8. At 0.317 seconds the vehicle was parallel to the barrier. At 0.385 seconds the rear-right tires recontacted the ground. At 0.41 seconds the vehicle lost contact with the barrier traveling at an exit speed and angle of 49.4 mph and parallel to barrier. At 0.43 seconds the rear-right tires again lifted off the ground. At 0.705 seconds the rear-right tires again recontacted the ground.

At 0.63 seconds the cabin reached maximum pitch angle of 6.9 degrees (rear pitching up); at 0.64 seconds the cargo-box reached maximum pitch angle of 6.8 degrees (rear pitching upward). At 1.5 seconds the roll angle of the cabin was 70.8 degrees (rolling toward the barrier), and the roll angle of the cargo-box was of 66.8 degrees (cargo-box rolling toward the barrier). The analysis ended at 1.5 seconds, at which time:

- The roll, pitch, and yaw of the truck cabin were, respectively, 70.8 degrees (toward barrier) and increasing, 4.44 degrees (rear pitching up), and 38 degrees (23 degrees relative to and away from barrier).
- The roll, pitch, and yaw of the cargo-box were, respectively, 66.8 degrees (toward barrier) and increasing, 2.7 degrees (rear pitching up), and 39 degrees (24 degrees relative to and away from barrier).
- The forward velocity of the vehicle was 44.4 mph (71.4 km/h).
- The vehicle was expected to continue to roll onto its side.

9.3.2 Time History Data Evaluation

Acceleration-time histories and angular rate-time histories were collected at two locations on the vehicle: (1) on the cargo box at the center of gravity of the vehicle, and (2) a point inside the cabin of the truck, as shown in Figure 111. The acceleration and angular rate data used for the occupant risk measures came from the cabin location. Figures 147 through 149 show the longitudinal, transverse, and vertical acceleration-time histories, respectively, computed from near the center of gravity of the vehicle which falls inside the cargo-box near the front of the ballast.

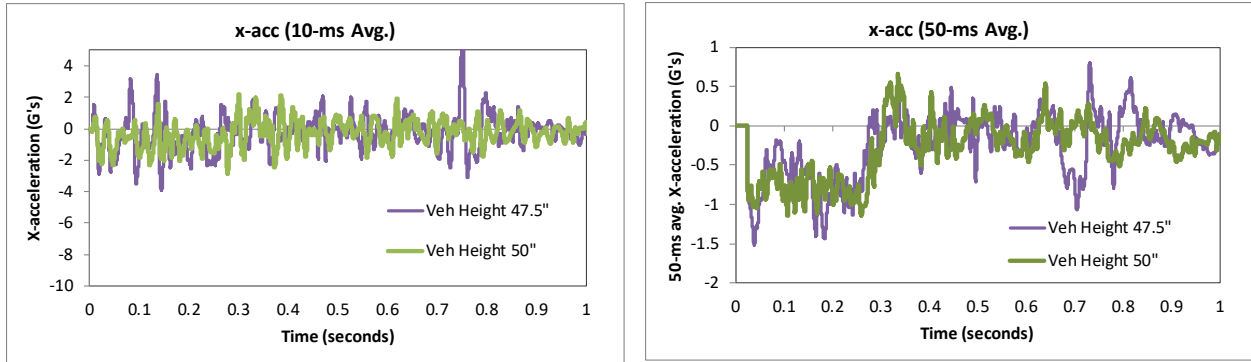


Figure 147. 10- and 50-millisecond average X-acceleration from FEA of Test 4-12 on the NETC 3-bar bridge rail (c.g. accelerometer).

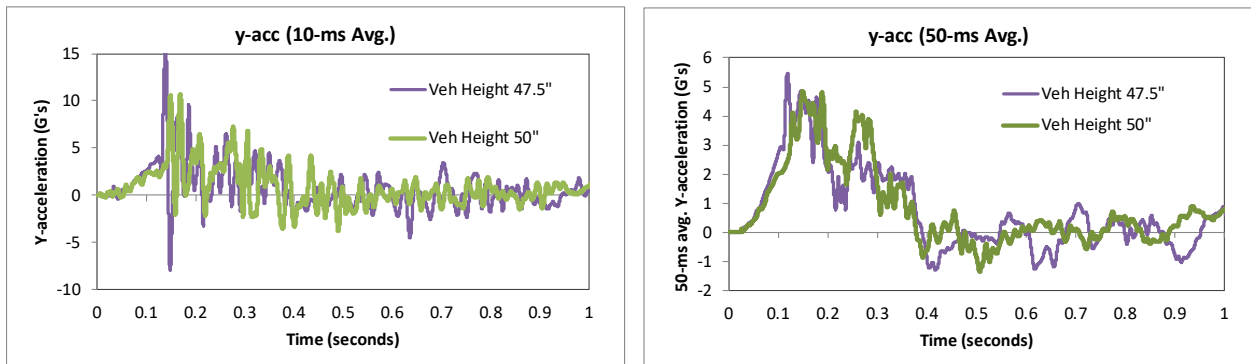


Figure 148. 10- and 50-millisecond average Y-acceleration from FEA of Test 4-12 on the NETC 3-bar bridge rail (c.g. accelerometer).

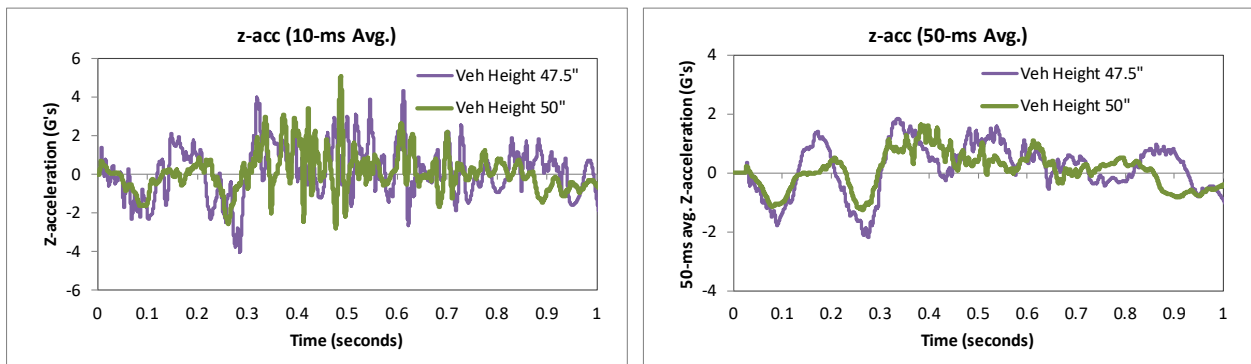


Figure 149. 10- and 50-millisecond average Z-acceleration from FEA of Test 4-12 on the NETC 3-bar bridge rail (c.g. accelerometer).

Figures 150 through Figure 152 show the longitudinal, transverse, and vertical acceleration-time histories, respectively, computed from the inside the cabin of the vehicle; Figures 153 through 155 show the comparison of the angular rates and angular displacements about the x-, y-, and z-axis from the cabin location. These data are used for calculating the occupant risk metrics. *MASH* does not require that occupant risk be evaluated; however, they are reported herein for completeness (see following section).

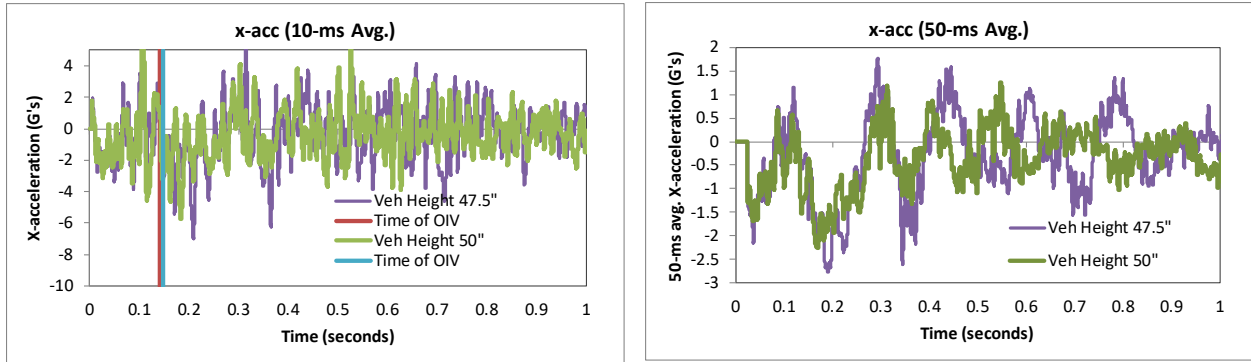


Figure 150. 10- and 50-millisecond average X-acceleration from FEA of Test 4-12 on the NETC 3-bar bridge rail (cabin accelerometer).

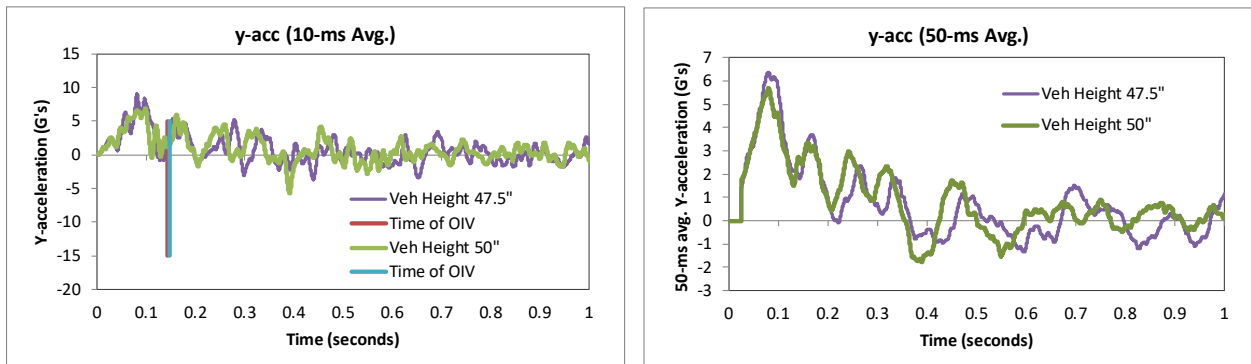


Figure 151. 10- and 50-millisecond average Y-acceleration from FEA of Test 4-12 on the NETC 3-bar bridge rail (cabin accelerometer).

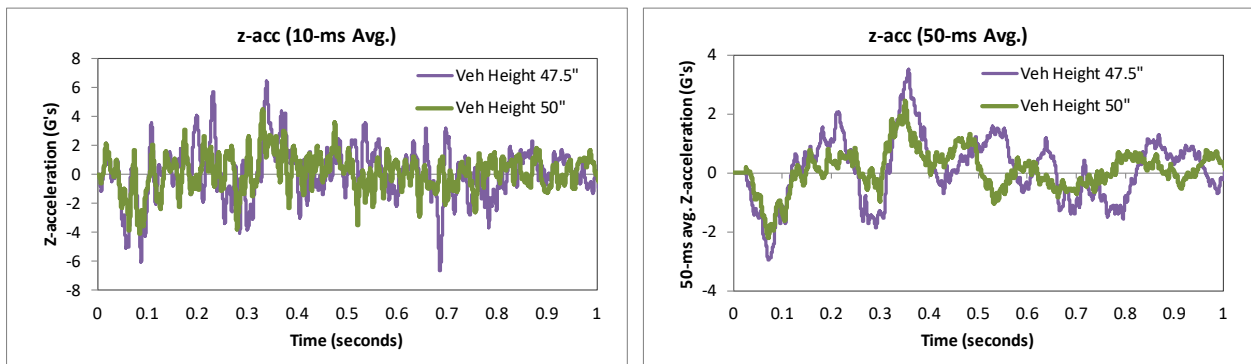


Figure 152. 10- and 50-millisecond average Z-acceleration from FEA of Test 4-12 on the NETC 3-bar bridge rail (cabin accelerometer).

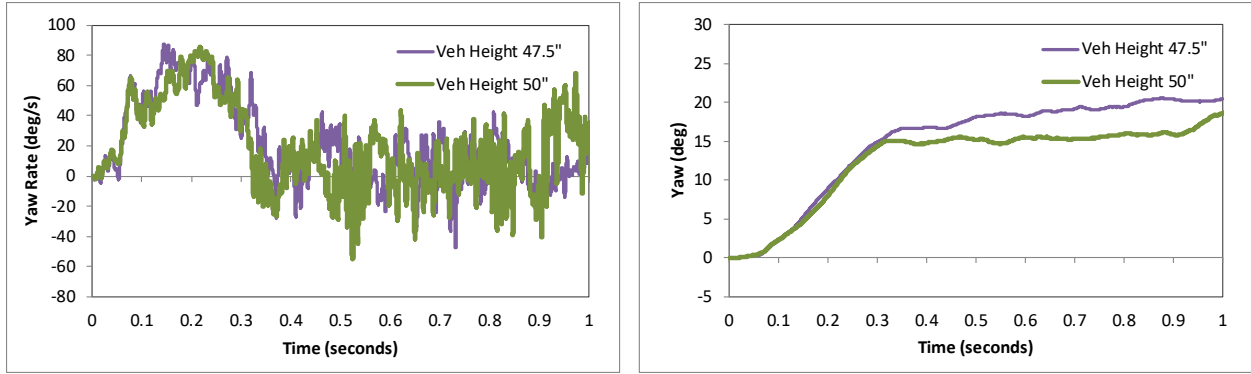


Figure 153. Yaw rate and yaw angle time-history from FEA of Test 4-12 on the NETC 3-bar bridge rail (cabin accelerometer).

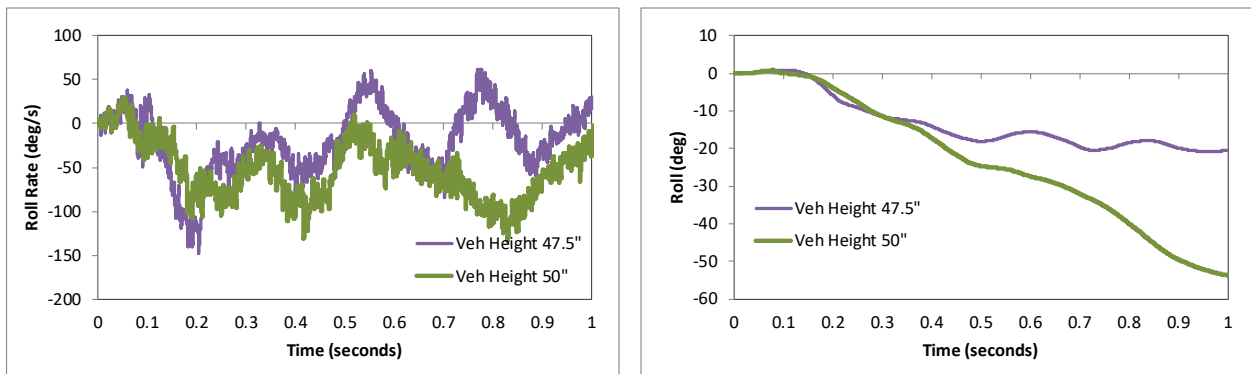


Figure 154. Roll rate and roll angle time-history from FEA of Test 4-12 on the NETC 3-bar bridge rail (cabin accelerometer).

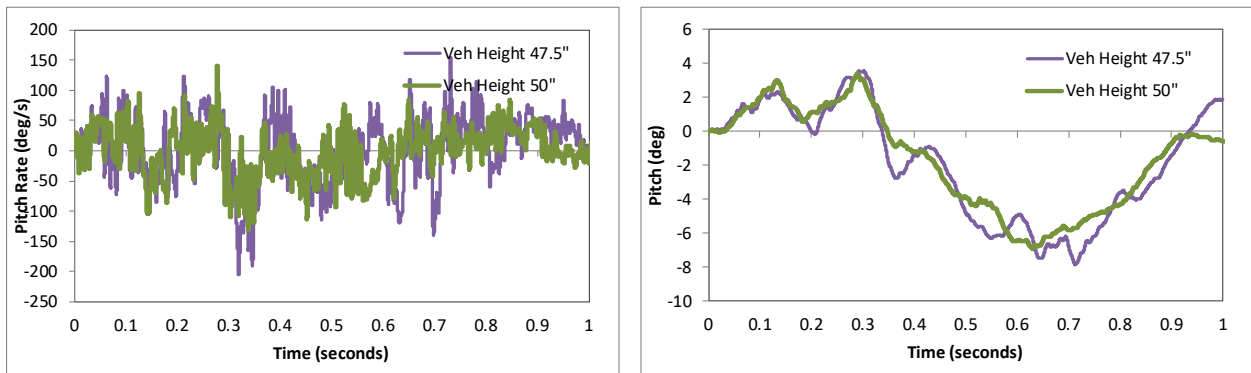


Figure 155. Pitch rate and pitch angle time-history from FEA of Test 4-12 on the NETC 3-bar bridge rail (cabin accelerometer).

9.3.3 Occupant Risk Measures

The acceleration-time histories and angular rate-time histories collected from inside the truck cabin were used to evaluate occupant risk metrics according to the procedures outlined in *MASH*. Table 74 shows the results for the occupant risk calculations. The results indicate that the occupant risk factors met safety criteria specified in *MASH*.

9.3.3.1 Case 1

The occupant impact velocities in the longitudinal and transverse directions for Case 1 were 2 ft/s and 14.8 ft/s, respectively. The highest 0.010-second occupant ridedown acceleration in the longitudinal and transverse directions were 7 g and 5.3 g, respectively. The maximum 50-ms moving average acceleration values in the longitudinal and transverse directions were 2.8 g and 6.4 g, respectively. The maximum roll and pitch angles of the vehicle were 20.8 degrees and 7.8 degrees, respectively. All metrics were within recommended limits specified in *MASH*.

9.3.3.2 Case 2

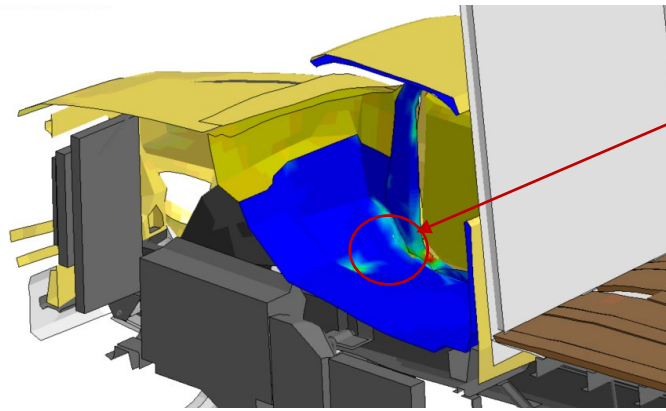
The occupant impact velocities in the longitudinal and transverse directions for Case 2 were 3 ft/s and 14.1 ft/s, respectively. The highest 0.010-second occupant ridedown acceleration in the longitudinal and transverse directions were 5.7 g and 5.9 g, respectively. The maximum 50-ms moving average acceleration values in the longitudinal and transverse directions were 2.3 g and 5.7 g, respectively. The maximum roll and pitch angles of the vehicle were 70.8 degrees and 6.9 degrees, respectively. The analysis was terminated at 1.5 seconds; the roll angle was still increasing, indicating the vehicle would roll onto its side. All metrics were within recommended limits specified in *MASH* except for the roll angle of Case 2.

Table 74. Summary of occupant risk metrics for Test 4-12 on the NETC 3-bar Bridge Rail.

Occupant Risk Factors		MASH T4-12		
		Case 1 (47.5")	Case 2 (50")	
Occupant Impact Velocity (ft/s)	x-direction	2.0	3.0	} < 30 ft/s (preferred) ✓ < 40 ft/s (limit)
	y-direction	-14.8	-14.1	
	at time	at 0.1407 seconds on left side of interior	at 0.1464 seconds on left side of interior	
THIV (ft/s)		15.4	14.4	}
		at 0.1407 seconds on left side of interior	at 0.1464 seconds on left side of interior	
Ridedown Acceleration (g's)	x-direction	(0.2038 - 0.2138 seconds)	(0.1784 - 0.1884 seconds)	} < 15 G (preferred) ✓ < 20.49 G (limit)
	y-direction	(0.1491 - 0.1591 seconds)	(0.1559 - 0.1659 seconds)	
PHD (g's)		7	7.4	}
		(0.2038 - 0.2138 seconds)	(0.1571 - 0.1671 seconds)	
ASI		0.76	0.66	}
		(0.0532 - 0.1032 seconds)	(0.0557 - 0.1057 seconds)	
Max 50-ms moving avg. acc. (g's)	x-direction	-2.8	-2.3	}
	y-direction	6.4	5.7	
	z-direction	3.5	2.4	
Maximum Angular Disp. (deg)	Roll	-20.8	-70.8	} < 75 deg ✓
		(0.9596 seconds)	(1.4987 seconds)	
	Pitch	-7.8	-6.9	
		(0.7127 seconds)	(0.6292 seconds)	
	Yaw	20.7	38	
		(1.0333 seconds)	(1.4969 seconds)	

9.3.4 Occupant Compartment Intrusion

The maximum deformation of the occupant compartment for impact on the NETC 3-bar bridge rail was approximately 1 inch for Case 1 and 3.3 inches for Case 2. The maximum deformation occurred at the lower right-front corner of the toe-pan and the wheel well in both cases. Figure 156 shows a view of the vehicle interior after the impact, with several components removed to facilitate viewing. The maximum deformation was less than the critical limit of 9 inches specified in *MASH* for this area of the occupant compartment.



Case 1 (47.5"):

Maximum OCI was ≈ 1 inch (27 mm) and occurred at the lower right-front corner of the top-pan at the wheel well.

Case 2 (50"):

Maximum OCI was 3.27" (83 mm) and occurred at the floor pan near the lower-front edge of the door.

Figure 156. Occupant compartment deformation resulting from Test 4-12 on the NETC 3-bar bridge rail system.

9.3.5 Damages to the Barrier System

Figure 157 shows images of the barrier at the time of maximum deflection with a contour plot of lateral displacement on the rail elements. The maximum dynamic deflections were 7.64 inches and 8.1 inches for Case 1 and Case 2, respectively, and occurred on the top rail at mid-span between Posts 7 and 8 when the rear of the cargo-box impacted the railing. Figure 158 shows contour plots of the maximum permanent deflection for the two cases. The maximum permanent deflections were 5.7 inches and 6.6 inches for Cases 1 and 2, respectively. The cargo bed contacted the side of the top rail in both cases. The deformation was slightly higher for Case 2 (e.g., higher center of gravity vehicle).

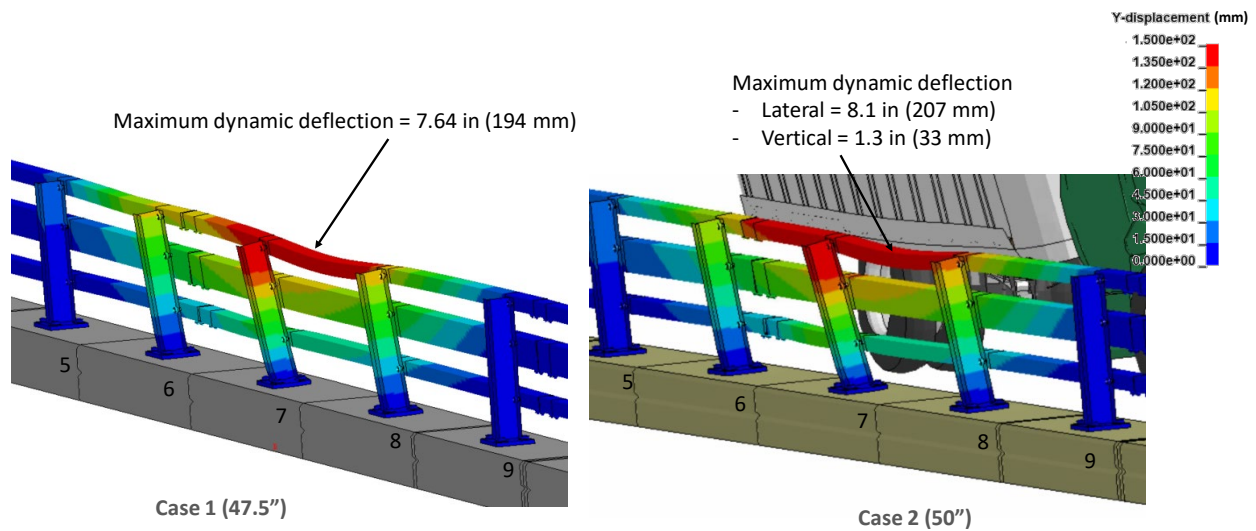


Figure 157. Contour plot of lateral displacement for the bridge rail from Test 4-12 at the time of maximum dynamic deflection for the NETC 3-bar bridge rail.

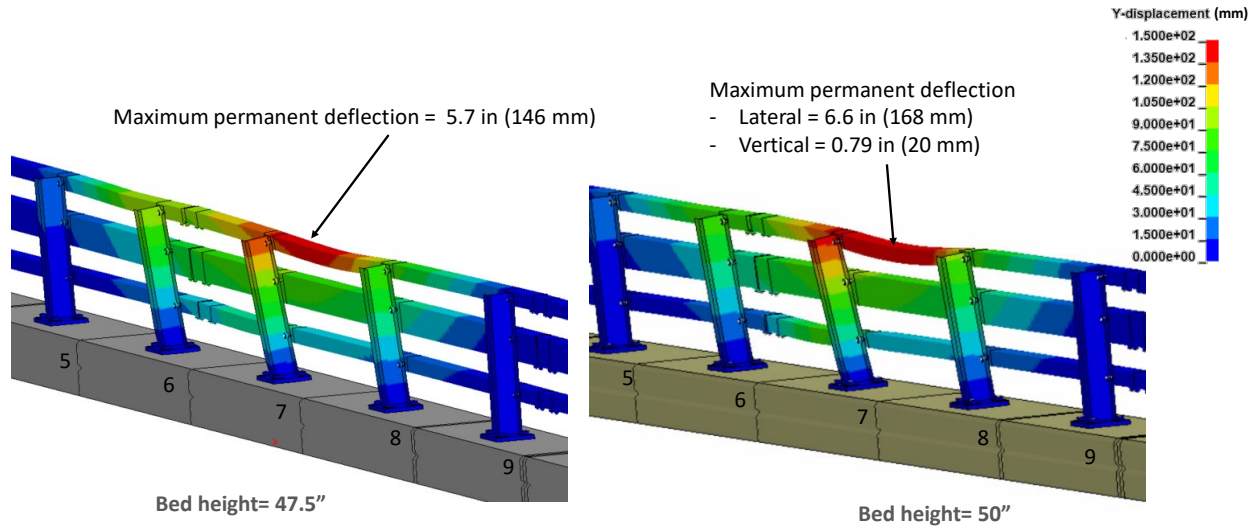


Figure 158. Contour plot of permanent deflection for the bridge rail from Test 4-12 for the NETC 3-bar bridge rail.

Figure 159 shows contours of true effective plastic strains on the bridge rail post and baseplate for the two analysis cases, which resulted in significant damage to post and baseplate at Posts 6 and 7. The post flanges buckled near the welded connection to the baseplate, and the front-center edge of the baseplate was deflected upward. The maximum vertical deflection of the baseplates was 1.28 inches for Case 1 and 1.24 inches for Case 2; the maximum permanent deflection of the baseplates was 0.9 inches for both cases. The vertical deflection at this location on the baseplate causes a stress concentration at the outer edges of the front flange of the post at the weld location. The maximum effective true plastic strain value was 0.32 at these points which corresponds to a nominal strain value that well exceeds the necking point for the material, as indicated on the nominal stress-strain curve for the material in Figure 160. The forces on the welds were not collected during the analysis, but they may be of concern for these analysis cases given that the welds on the front flange are in tension.

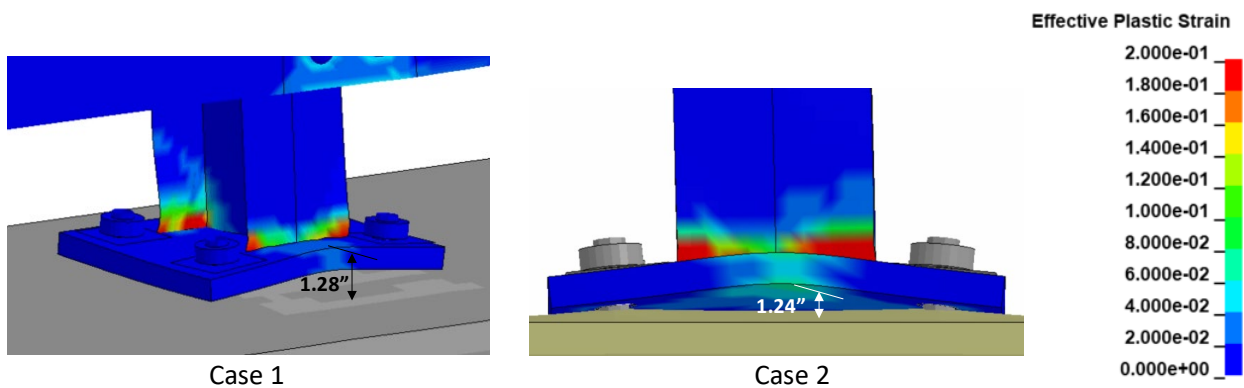


Figure 159. Contours of effective plastic strains on the critical post for Test 4-12 on the NETC 3-bar bridge rail.

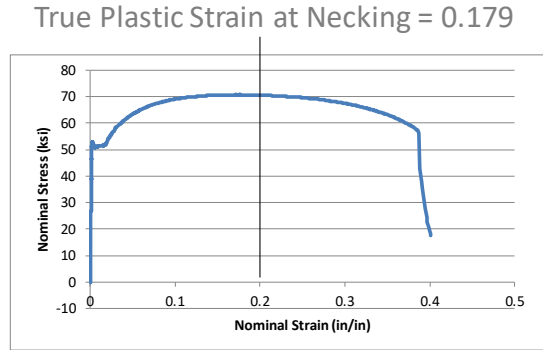


Figure 160. Plot of material stress-strain curve for Post with necking strain identified.

Figure 161 shows contours of 1st principal strain with contours cut off at strains of 0.1. The analysis resulted in notable concrete damage at two posts. These damages correspond to potential cracks around the front anchor bolts and/or anchor pullout.

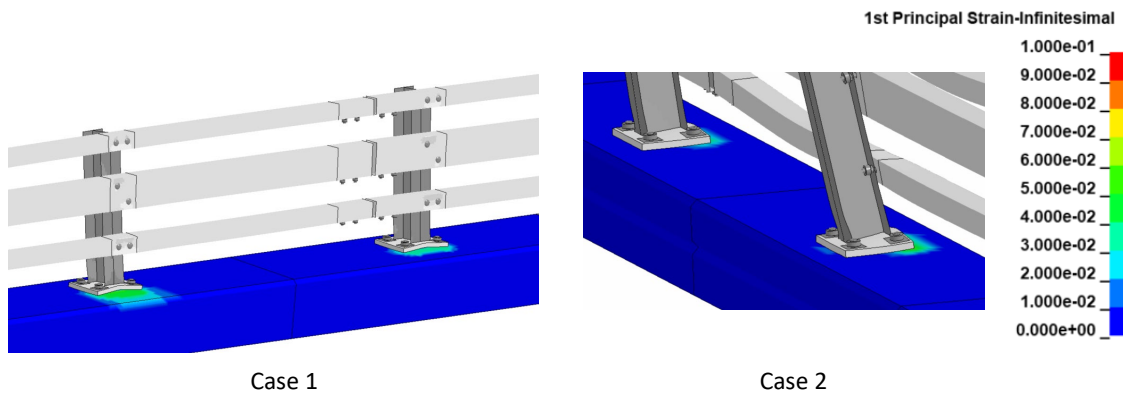


Figure 161. Contours of 1st principal strains for concrete at the critical post for Test 4-12 on the NETC 3-bar bridge rail.

9.3.6 Peak Forces on Barrier

The impact force between the vehicle and the barrier was computed to determine the peak loading on the barrier which could then be compared to the design strength of the bridge rail. The lateral force-time history results are shown in Figure 162 including the force data filtered with cutoff frequency of 60 Hz, the 25-millisecond moving average force and the 50-millisecond moving average force. The maximum impact force occurred when the rear tandem wheel set impacted against the bridge rail. The maximum 25-ms moving average force was 109 kips; the maximum 50-ms moving average force was 100 kips, which are both greater than the calculated strength of the barrier in Section 3.4.2.

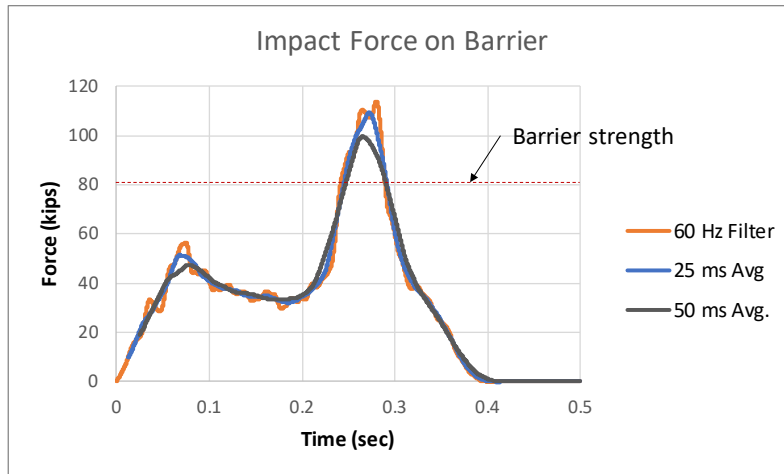


Figure 162. Lateral force-time history between vehicle and barrier for Test 4-12 on NETC 3-bar bridge rail.

9.3.7 Damages to Vehicle

Figure 163 shows contour plots of effective plastic strain for the vehicle, which were used to identify areas of the vehicle that suffered damage during the simulated impact event. The most severe damages were to the front bumper, the front fender, the front impact-side suspension, the front axle, the front impact-side corner of the cargo box, the cargo-box floor beams, and the cargo box main rail. These are typical damages for Test 4-12 on post-and-beam bridge rails. Note that the damages for Case 2 would also include further damage due to the vehicle rolling onto its side; the analysis was terminated prior to reaching final roll position.

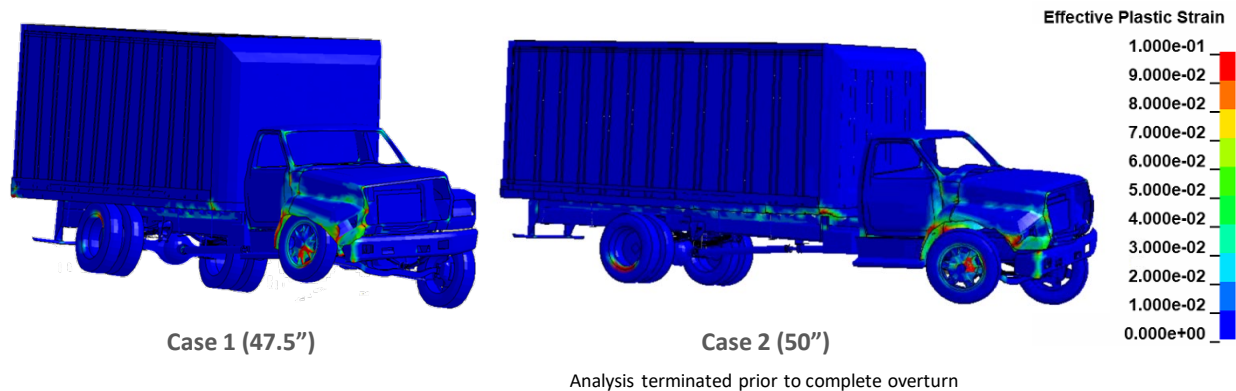


Figure 163. Damages to vehicle in Test 4-12 analysis of NETC 3-bar bridge rail for Cases 1 and 2.

9.3.8 Exit Box

Figures 164 and 165 show the exit box for Test 4-12 on the NETC 3-bar bridge rail system for Cases 1 and 2, respectively. Although the exit box analysis is not required in *MASH*, it was included here for completeness. The vehicle was smoothly redirected for Case 1 and, in both cases, the vehicle path was well within the exit box criteria of *MASH*.

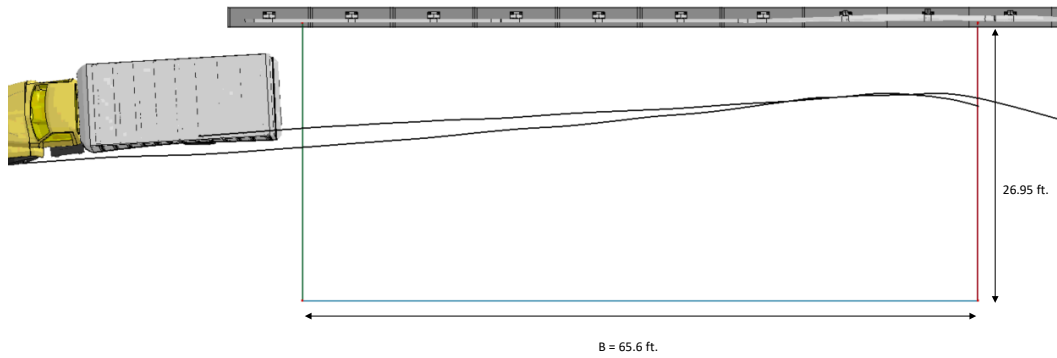


Figure 164. Exit box for Test 4-12 for Case 1 on the NETC 3-bar bridge rail.

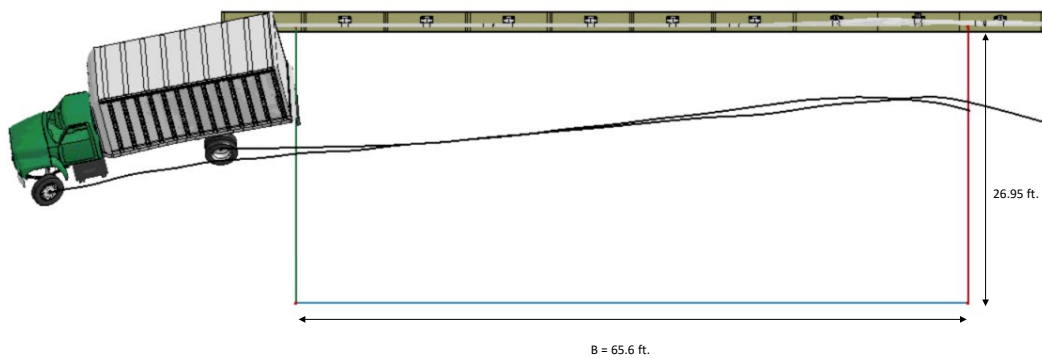


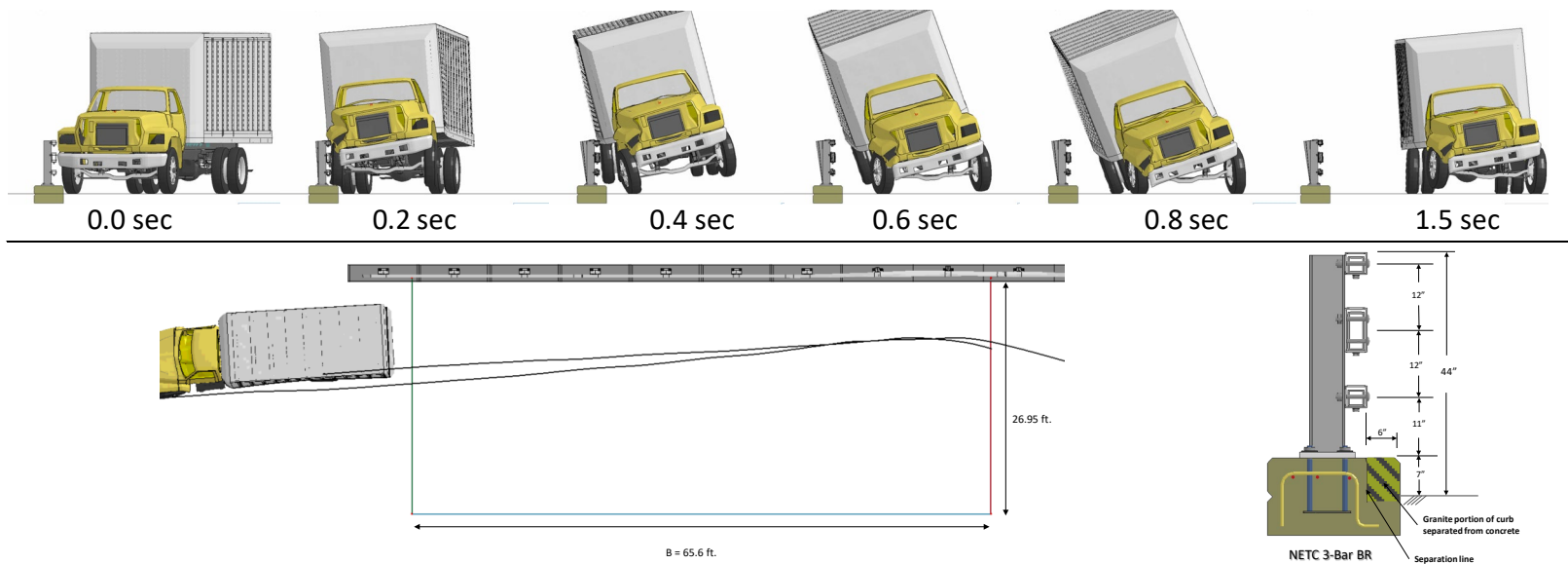
Figure 165. Exit box for Test 4-12 for Case 2 on the NETC 3-bar bridge rail.

9.3.9 Test 4-12 Results Summary

A summary of the *MASH* Test 4-12 results on the NETC 3-bar bridge rail is shown in Table 75 and Figures 166 and 167. The barrier adequately contained and redirected the 10000S vehicle (single unit truck) with moderate to extensive damage to the bridge rail. The damage included plastic deformation of posts and baseplates with high stress concentrations for the welds at the outside edges of the front flange. The analysis indicated only slight potential for concrete damage around the front anchor bolts. The maximum dynamic and permanent deflections of the railing were 8.1 inches and 6.6 inches, respectively. There were no detached elements from the barrier that showed potential for penetrating the occupant compartment or presenting undue hazard to other traffic. The vehicle remained upright and stable for Case 1 but rolled over onto its side for Case 2. It is preferred that the vehicle remain upright, but not required. Based on the results of this analysis, the barrier meets all structural and occupant risk criteria in *MASH* for Test 4-12 impact conditions. Additional discussion on crash performance compared to a similar system is provided in the Section 9.4 below.

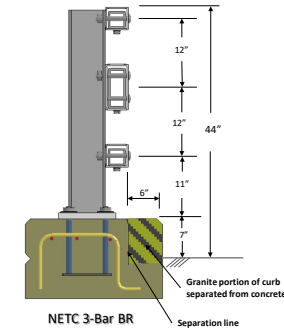
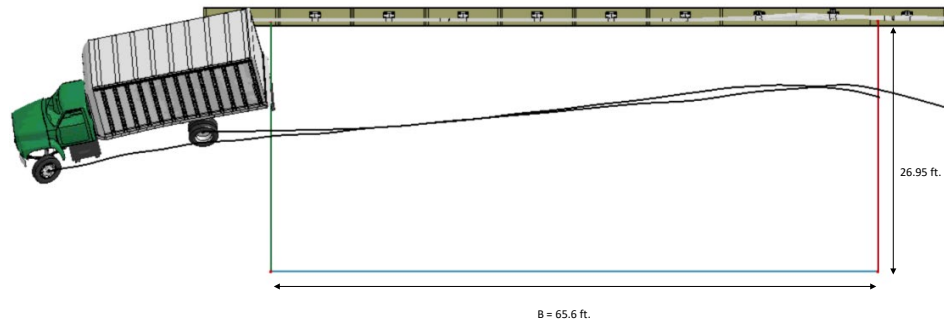
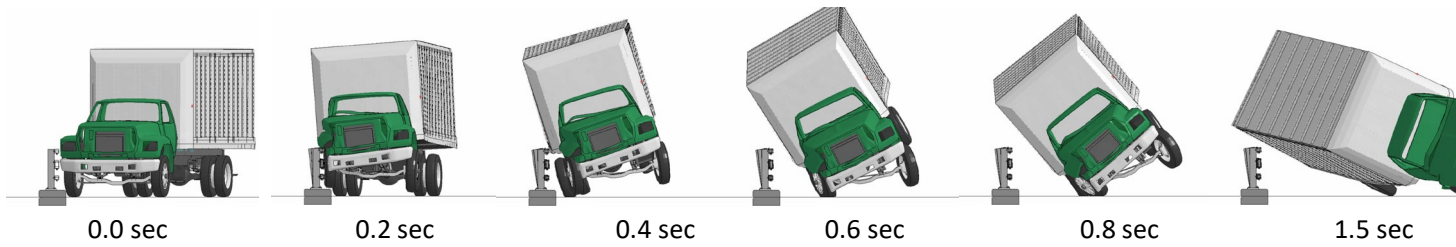
Table 75. Summary of MASH Test 4-12 results on the curb-mounted bridge rail.

Evaluation Factors	Evaluation Criteria	Results	
		Case 1	Case 2
Structural Adequacy	A Test article should contain and redirect the vehicle or bring the vehicle to a controlled stop; the vehicle should not penetrate, underride, or override the installation although controlled lateral deflection of the test article is acceptable.	Pass	Pass
Occupant Risk	D Detached elements, fragments, or other debris from the test article should not penetrate or show potential for penetrating the occupant compartment, or present undue hazard to other traffic, pedestrians, or personnel in a work zone. Deformations of, or intrusions into, to occupant compartment should not exceed limits set forth in Section 5.2.2 and Appendix E.	Pass	Pass
	G It is <u>preferable, although not essential</u> , that the vehicle remain upright during and after collision.	Pass	Fail



General Information		Impact Conditions		Max50-millisecond Avg. (G)	
Analysis Agency	Roadsafe LLC	Speed	56 mph	Longitudinal	2.8 g
Test Standard Test No.	MASH Test 4-12	Angle	15 degrees	Lateral	6.4 g
Analysis No.	NETC18_3BarBR_T412_Case1	Location	5.0 feet upstream of Post 7	Vertical	3.5 g
Analysis Date	2/5/2019				
Test Article		Impact Severity		Test Article Deflections (in)	
Type	Bridge Rail		155.6 kip-ft	Dynamic	7.6 inches
Name	NETC 3-Bar	Exit Conditions		Permanent	5.7 inch
Installation Length	120 feet	Speed	50.5 mph	Working Width	23.3 inches
Material or Key Elements		Angle	2.3 degrees		
		Time	0.47 seconds	Max. OCI	
				≈1 inch	
Soil Type and Condition		Occupant Risk Values		Vehicle Stability	
N.A.		Longitudinal OIV	2.0 ft/s	Roll	20.8 degees
Analysis Vehicle		Lateral OIV	14.8 ft/s	Pitch	7.8 degrees
Type / Designation	10000S	Longitudinal ORA	7.0 g	Yaw	20.7 degrees
FEA Model name	F800_No-Box_181114_UboltF0p17	Lateral ORA	5.3 g		
	502_TruckBox_181114	THIV	15.4 ft/s		
Mass	22,198 lb	PHD	7.0 g		
		ASI	0.76		

Figure 166. Summary results for MASH Test 4-12 on the NETC 3-bar bridge rail (Case 1).



General Information		Impact Conditions		Max50-millisecond Avg. (G)	
Analysis Agency	Roadsafe LLC	Speed	56 mph	Longitudinal	2.3 g
Test Standard Test No.	MASH Test 4-12	Angle	15 degrees	Lateral	5.7 g
Analysis No.	NETC18_3BarBR_T412_Case2	Location	5.0 feet upstream of Post 7	Vertical	2.4 g
Analysis Date	3/11/2019				
Test Article		Impact Severity		Test Article Deflections (in)	
Type	Bridge Rail	155.6 kip-ft		Dynamic	8.1 inches
Name	NETC 3-Bar	Exit Conditions		Permanent	6.6 inch
Installation Length	120 feet	Speed	49.4 mph	Working Width	23.3 inches
Material or Key Elements		Angle	parallel	Max. OCI	≈3.3 inch
Soil Type and Condition	N.A.	Time	0.41 seconds	Vehicle Stability	
Analysis Vehicle		Occupant Risk Values		Roll	*90 degrees
Type / Designation	10000S	Longitudinal OIV	3.0 ft/s	Pitch	6.9 degrees
FEA Model name	F800_No-Box_181114_UboltF0p17	Lateral OIV	14.1 ft/s	Yaw	38 degrees
	502_TruckBox_181114	Longitudinal ORA	5.7 g		
	Nodes3.k (50" cargo-bed height)	Lateral ORA	5.9 g		
Mass	22,198 lb	THIV	14.4 ft/s		
		PHD	7.4 g		
		ASI	0.66		

* The roll angle was 70.8 deg at 1.5 sec when the analysis was terminated, but 90 degree roll was expected.

Figure 167. Summary results for MASH Test 4-12 on the NETC 3-bar bridge rail (Case 2).

9.4 Conclusion for TL4 Evaluation of NETC 3-Bar Bridge Rail

Based on the results of this analysis, the NETC 3-bar bridge rail meets *MASH* TL4 criteria; however, relatively high barrier damages are likely under these conditions. The barrier system meets *MASH* TL3 criteria with only moderate barrier damages.

9.4.1 Structural Adequacy: (PASS)

- The barrier successfully contained and redirected the vehicle in all test cases, with controlled lateral deflections for the pickup and SUT tests.
- The barrier experienced relatively high plastic deformations of the posts, rails and baseplates for the Pickup and SUT vehicle test.
- Lateral deflections were relatively high for the SUT case (e.g., 8.1 inches).
- Concrete curb damage at two post locations was considered likely for the SUT test case (based on the 1st principle strain values in the concrete).
- The damages corresponded to potential cracks around the front anchor bolts and/or anchor pullout.

9.4.2 Occupant Risk (PASS)

- Occupant compartment intrusion was well below allowable limits.
- OIV and ORA
 - Small Car: OIV (within critical limits); ORA (within preferred limits). Values highly dependent on time of occupant impact.
 - Pickup: OIV (within preferred limits); ORA (within critical)

9.4.3 Vehicle Trajectory (PASS)

- Small car: Vehicle remained upright and stable through impact and redirection, with relatively low angular displacements.
- Pickup: Vehicle remained upright and stable through impact and redirection, with relatively low angular displacements.
- SUT: Vehicle remained upright and relatively stable for Case 1 (47.5" bed height) but rolled onto its side for Case 2 (50" bed height). *MASH* prefers that the vehicle remain upright, but this criterion is not required.

9.4.4 Full-Scale Test Results of Similar Bridge Rail Design

In the Summer of 2016, researchers at the Texas Transportation Institute conducted full-scale testing of the TxDOT C2P bridge rail, shown in Figure 168, which successfully met *MASH* TL4 performance criteria.[*Williams 17b*] Although there are several aspects of this design that are different from the NETC design, there are also many similarities such as, a 42-inch tall, 3-bar bridge rail mounted on top of a 9-inch curb with 8-ft post spacing. Some of the critical aspects of the C2P rail geometrics are inferior to that of the NETC design based on AASHTO LRFD Bridge Design Specifications Section A13. For example, the *vertical clear opening* for the C2P is 9-3/8 inches compared to 9 inches for the NETC design; the *post setback distance* is 3.5 inches for the C2P (i.e., for the two lower rails) compared to 4 inches for the NETC design; *ratio of*

contact width to height for the C2P is 0.38 compared to 0.52 for the NETC design. The C2P also uses smaller anchor rods (e.g., 3/4" dia. vs. 1" dia.) and a smaller base plate (e.g., 3/4" thick vs. 1" thick) compared to the NETC system. The LRFD strength calculations were not documented in the test report, but it is expected that the lateral strength of the C2P is similar to, or less than, that of the NETC 3-bar design. These comparisons, as well as other crash performance metrics, are shown in Table 76.



Figure 168. Photo and cross-section drawing of the MASH TL4 TxDOT C2P bridge rail.

Table 76. Comparison of NETC 3-bar design to TxDOT C2P.

		C2P	NETC	
	Dimensions	Rail height (in)	42	42
		Number of long. Bars	3	3
		Post spacing (ft)	8	8
		Curb height (in)	9	7-9
		Anchor rod dia (in)	0.75	1
		Base plate thickness (in)	0.75	1
LRFD Rail	Geometric Criteria	Vertical clear opening (in)	9-3/8	9
		Post setback distance (in)	3.5	4
		Contact width (in)	16.25	23
		Contact width/height	0.38	0.52
MASH CRITERIA	Test 4-10	OIV-x (ft/s)	26.2	25.6
		OIV-y (ft/s)	33.1	32.5
		ORA-x (G)	2.8	6.7
		ORA-y (G)	8.2	6
		Lateral Deflection (in)	0.8	3.35
	Test 4-11	OIV-x (ft/s)	18.4	22
		OIV-y (ft/s)	29.5	26.6
		ORA-x (G)	9.9	4.7
		ORA-y (G)	15.3	15.4
	Test 4-12	Lateral Deflection (in)	2.5	4.2
		Exit speed (mph)	54.1	50.5 (Case 1) 49.4 (Case 2)
		Exit angle (deg)	0	2.4 (Case 1) 0 (Case 2)
	Lateral Deflection (in)	11.4	8.1	

* Approximated from sequential views of Test 490026-4-3

The results of Test 4-12 on the C2P system were similar to that of the NETC 3-bar system, in that both systems sustained significant damage when the rear of the SUT vehicle impacted against the rail. The maximum dynamic deflection of the C2P was 11.4 inches, compared to 8.1 inches for the NETC system. Both systems also resulted in the vehicle exiting approximately parallel with the barrier and subsequently rolling onto its side during post trajectory.

10 EVALUATION OF THE NETC 3-BAR TRANSITION FOR *MASH TL4*

The FEA model of the NETC 3-bar transition was developed based on the baseline validated NETC 2-bar transition model (refer to Section 7). The modifications to the baseline transition model were primarily related to including the third rail and to matching the current design being installed (refer to Appendix B), which included:

- Replacing the 6"x8" wood posts with steel W6x9 posts made from AASHTO M183 steel (ASTM A36); the material characterization was based on stress-strain curves from tensile tests [*Wright97*] with yield strength = 45.7 ksi (true stress).
- Increasing w-beam rail height from 27 inches to 31 inches.
- Increasing the thrie-beam height from 32 inches to 34 inches.
- Adding the 3rd rail element and repositioning mounting holes for post attachments.
- Removing the deflector plate.
- Extending the continuum soil model to include all posts in the thrie-beam region.
- Replacing the NETC 2-bar bridge rail model with the NETC 3-bar bridge rail model developed in Section 9.
- Updating the splice connection to include bushing-spacers for the cap screws on both sides of the splice.

The model included 42 feet of w-beam guardrail and transition elements; and included 23.8 feet of the NETC 3-bar bridge rail, as illustrated in Figure 169. The geometric details of the system model were consistent with the drawings of Appendix B. Refer to Section 7 for additional details regarding model development and methodology.

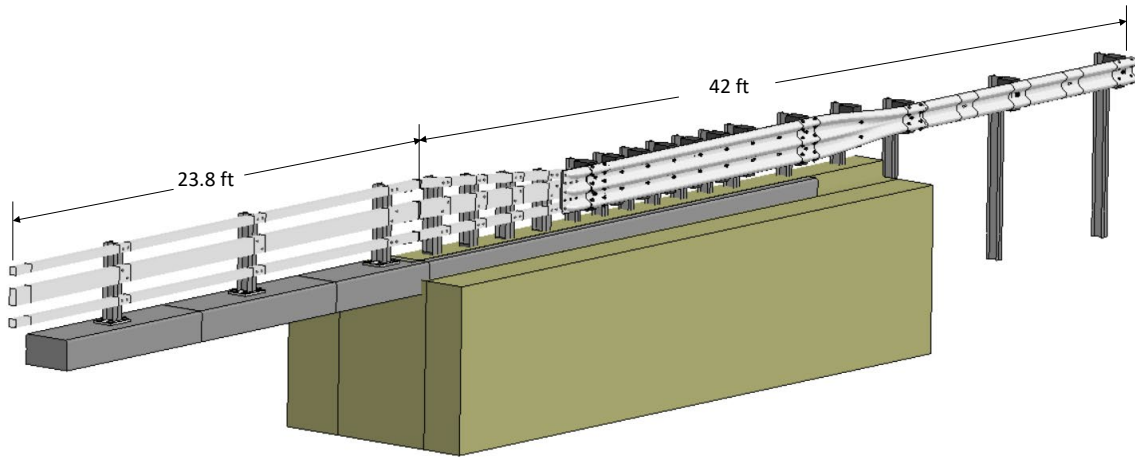


Figure 169. FEA model of the 3-bar transition (oblique viewpoint).

10.1 Determining Critical Impact Point

According to *MASH* the critical impact point for passenger vehicles must be planned to examine the potential for wheel snagging and pocking as well as structural failure of barrier elements. Wheel snagging and pocking are generally the most critical and the most sensitive to impact point. When the impact is too close to a potential snag point, the vehicle may not penetrate deep enough into the barrier prior to reaching the snag point. When the impact point is too far away from the potential snag point, the vehicle may begin to redirect and exit the barrier prior to reaching the snag point.

Two critical snag points were identified for the transition regarding impact with passenger vehicle: 1) the upstream end of the tube rails and 2) the first post of the tube-rail section of the transition, as illustrated in Figure 170. For the single unit truck the critical snag point was determined to be at the splice connection between the transition and the bridge rail, as illustrated in Figure 171.

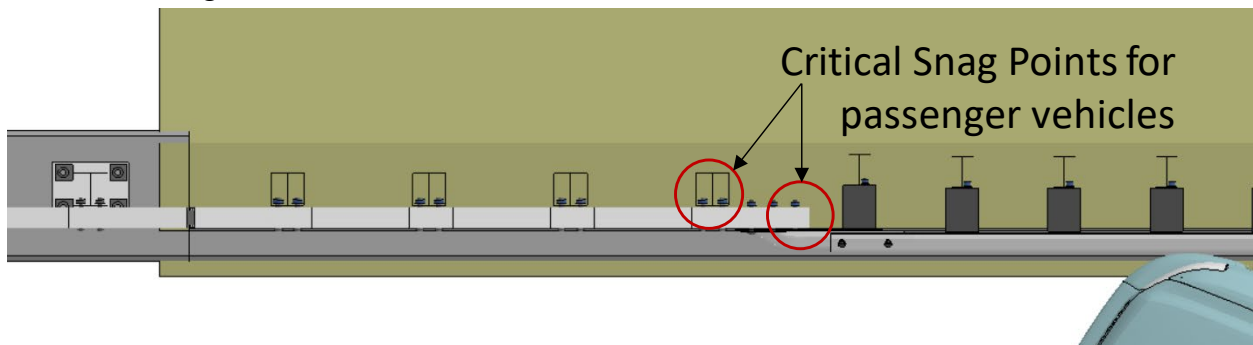


Figure 170. Illustration of potential snag points on the 3-bar transition for passenger vehicles.

Critical Snag Point for SUT

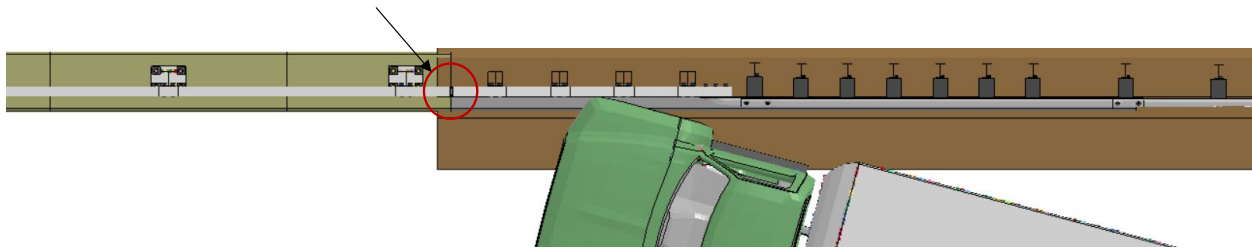


Figure 171. Illustration of potential snag point on the 3-bar transition for the single unit truck.

10.2 Test 4-20

10.2.1 CIP for Test 4-20

The critical impact point for Test 4-20 was determined using FEA with respect to maximum potential for wheel snag on the first post of the tube-rail section of the transition. Finite element analysis was used to simulate *MASH* Test 4-20 at impact points 3.6 ft, 4.0 ft, 4.5 ft, 5.0 ft, 5.5 ft and 6.0 ft from the centerline of the post. These analysis cases were conducted for 0.15 seconds of impact for the purpose of determining the critical impact point for maximizing the potential for wheel snag on the first post of the tubular-rail section of the transition. The results of the six analysis cases are shown in Figure 172. None of the analysis cases resulted in significant wheel contact with the post; however, impact at 5.5 feet upstream of the critical post resulted in the greatest chance for wheel contact with the post and was therefore selected as the CIP for the final evaluation to maximize potential for wheel snag.

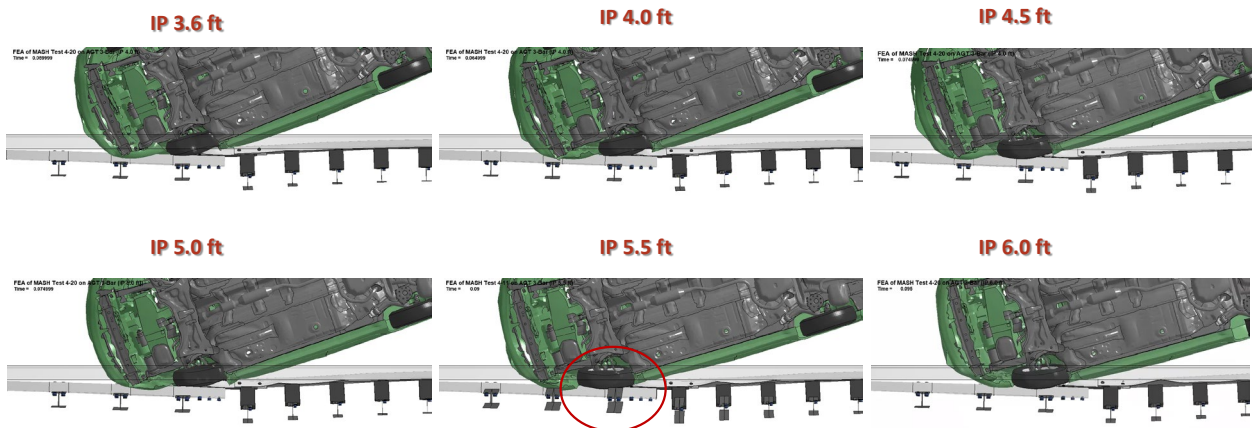


Figure 172. Results of Test 4-20 CIP evaluations for the 3-bar Transition.

The final analysis was performed for 0.6 seconds of the impact event. The following sections provide a summary of the results and include a commentary describing the timing and occurrence of various events during the simulated impact, time-history data evaluation, occupant risk assessments, and damages sustained by both the barrier and vehicle.

10.2.2 Summary of Key Phenomenological Events

The sequential views of the impact event are shown in Appendix N in Figures N-1 through N-3 from an overhead viewpoint, downstream and upstream viewpoint, and oblique viewpoint, respectively. At time equal zero seconds the front bumper of the car contacted the lower two corrugations of the nested thrie-beam rail at 5.5 feet upstream of Post 4, as illustrated in Figure 173. Before 0.005 seconds, the front-right tire struck the curb. At 0.01 seconds the front-right fender contacted the top corrugation of the thrie-beam, the front-right tire contacted the lower corrugation, and the barrier began to deflect. At 0.025 seconds the front-right tire was steered parallel to the barrier, and the front bumper of the vehicle was aligned with Post 5. At 0.035 seconds the lower edge of the front-right A-pillar deformed and cracked the lower edge of the windshield. At 0.05 seconds the front bumper was aligned with Post 4. At 0.06 seconds the front-right tire was fully mounted onto the curb. At 0.075 seconds the barrier reached maximum dynamic deflection of 5.8 inches at the lower corrugation of the thrie-beam at the point where the nested thrie-beam connects to the thrie-beam end shoe; Post 5 deflected 4.69 inches. At 0.076 seconds the occupant struck the right side of the interior at 24.3 ft/s in the longitudinal direction and 25.9 ft/s in the lateral direction. At 0.085 seconds the front-right tire was aligned with Post 4 (critical snag point) but did not contact the post. At 0.103 seconds the maximum longitudinal ORA occurred with magnitude 4.2 G. At 0.155 seconds the rear-right tire contacted the curb. At 0.195 seconds the rear-right tire was fully mounted onto the curb. At 0.21 seconds the rear-right tire contacted the lower tube railing near Post 4. At 0.227 seconds maximum lateral ORA occurred with magnitude 7.4 G. At 0.26 seconds the vehicle reached a maximum roll angle of 6.2 degrees (away from barrier). At 0.295 seconds the vehicle separated from the barrier at an exit speed and angle of 43.5 mph and 4 degrees. At 0.48 seconds the vehicle reached a maximum pitch of 3.9 degrees (rear pitching upward). The vehicle remained stable throughout post-impact trajectory. The analysis ended at 0.6 seconds, at which time:

- The roll, pitch, and yaw of the vehicle were, respectively, 1.8 degrees (toward barrier), 2.9 degrees (rear pitching up), and 19.29 degrees (5.71 degrees relative to and toward barrier).
- The forward velocity of the vehicle was 43 mph (69.1 km/h).

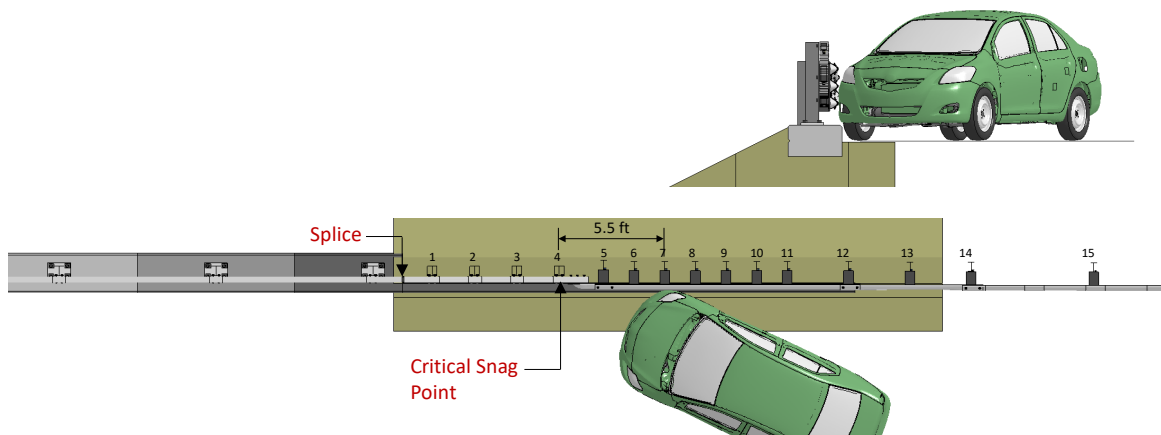


Figure 173. Impact point for Test 4-20 on the 3-bar transition.

10.2.3 Time History Data Evaluation

Figures 174 through 176 show the longitudinal, transverse, and vertical acceleration-time histories, respectively, computed from the center of gravity of the vehicle; Figures 177 through 179 show the comparison of the angular rates and angular displacements (i.e., yaw, roll and pitch) at the center of gravity of the vehicle.

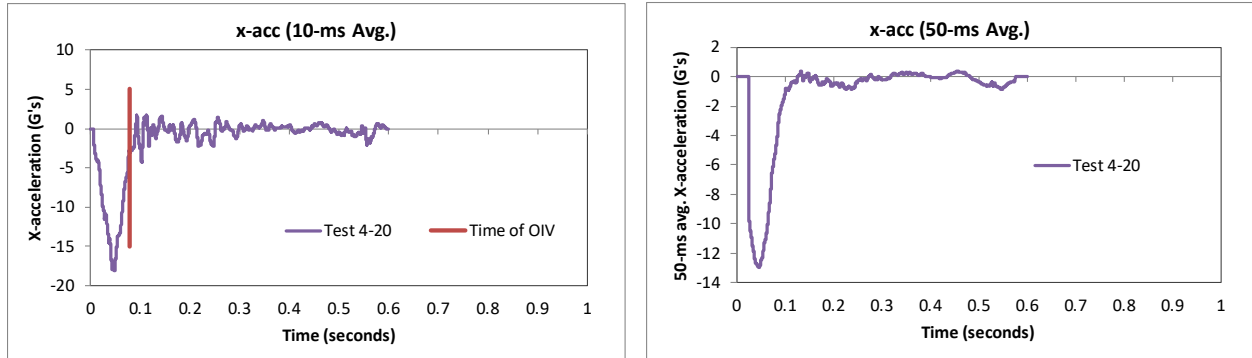


Figure 174. 10- and 50-millisecond average X-acceleration from FEA of Test 4-20 on the 3-bar transition.

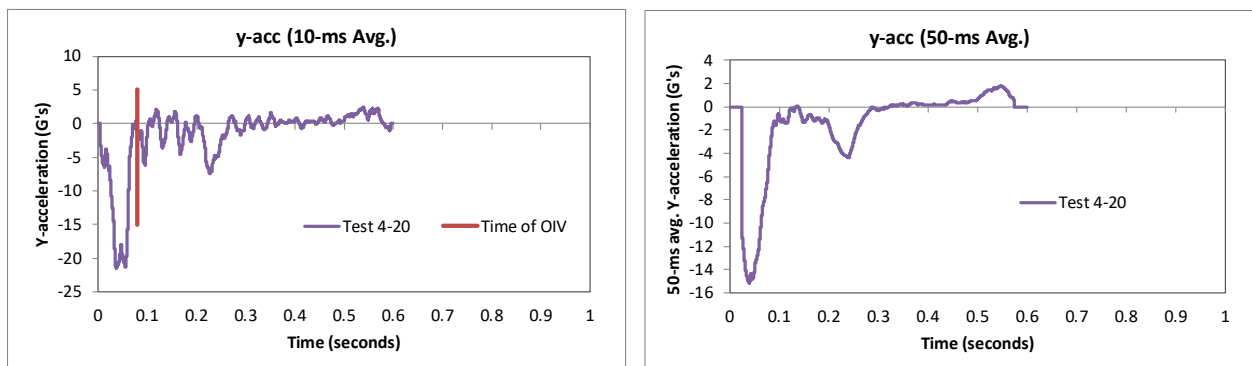


Figure 175. 10- and 50-millisecond average Y-acceleration from FEA of Test 4-20 on the 3-bar transition.

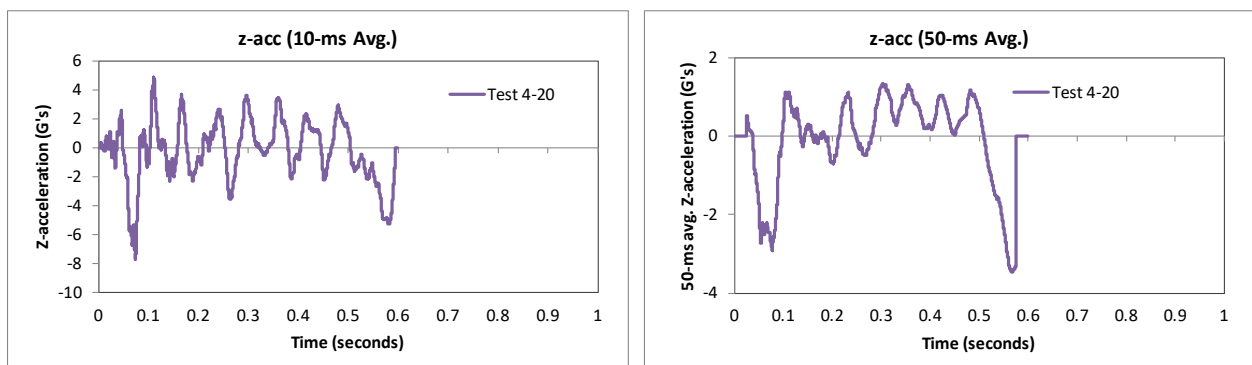


Figure 176. 10- and 50-millisecond average Z-acceleration from FEA of Test 4-20 on the 3-bar transition.

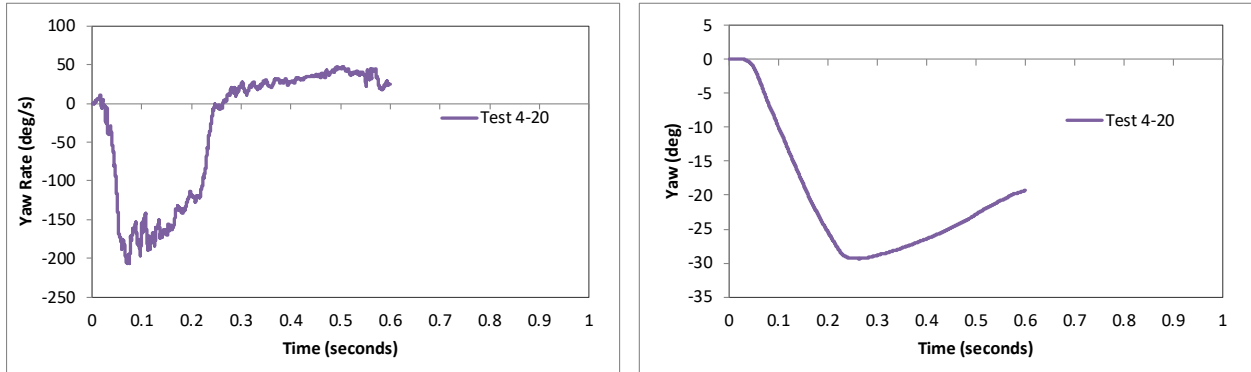


Figure 177. Yaw rate and yaw angle time-history from FEA of Test 4-20 on the 3-bar transition.

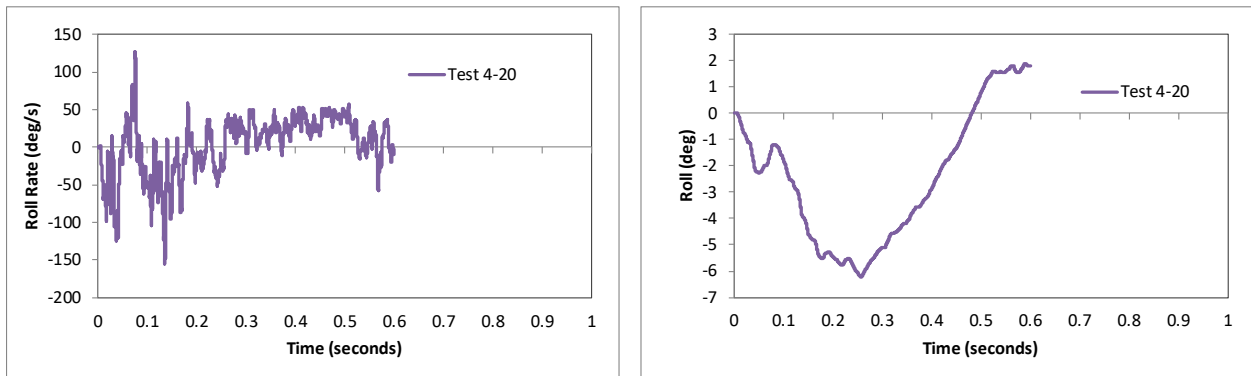


Figure 178. Roll rate and roll angle time-history from FEA of Test 4-20 on the 3-bar transition.

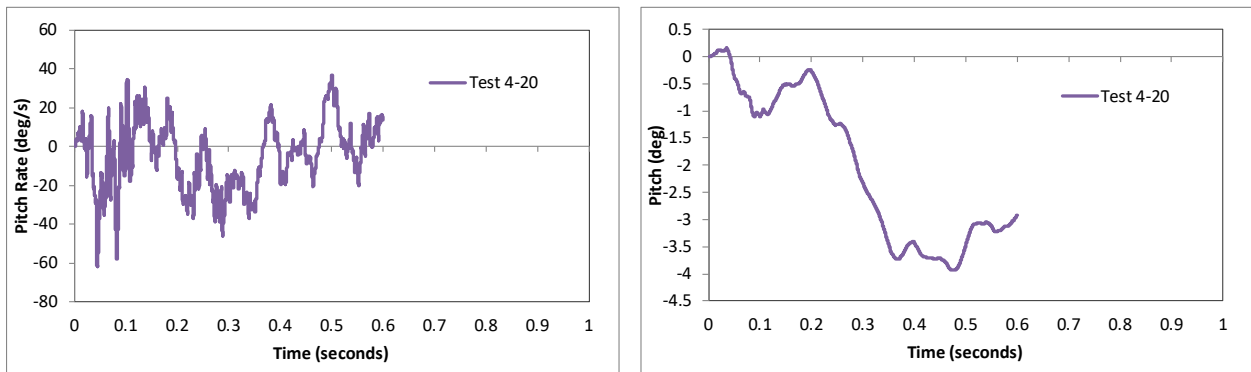


Figure 179. Pitch rate and pitch angle time-history from FEA of Test 4-20 on the 3-bar transition.

10.2.4 Occupant Risk Measures

The acceleration-time histories and angular rate-time histories collected at the center of gravity of the vehicle were used to evaluate occupant risk metrics according to the procedures outlined in *MASH*. Table 77 shows the results for the occupant risk calculations. The results indicate that the occupant risk factors meet safety criteria specified in *MASH*.

The occupant impact velocities in the longitudinal and transverse directions for the transition were 24.3 ft/s and 25.9 ft/s, respectively, which were within the recommended limits specified in *MASH*. The highest 0.010-second occupant ridedown acceleration in the longitudinal and transverse directions were 4.2 g and 7.4 g, respectively, which were well within preferred limits specified in *MASH*. The maximum 50-ms moving average acceleration values in the longitudinal and transverse directions were 13.0g and 15.1 g, respectively. The maximum roll and pitch angles of the vehicle were 6.2 degrees and 3.9 degrees, respectively, which were well below critical limits in *MASH*.

Table 77. Summary of *MASH* occupant risk metrics for Test 4-20 on the 3-bar transition.

Occupant Risk Factors		MASH T4-10	MASH Criteria
		Test 4-20	
Occupant Impact Velocity (ft/s)	x-direction	24.3	} < 30 ft/s (preferred) ✓ < 40 ft/s (limit)
	y-direction	25.9	
	at time	at 0.0761 seconds on right side of interior	
THIV (ft/s)		35.1	}
		at 0.0761 seconds on right side of interior	
Ridedown Acceleration (g's)	x-direction	-4.2 (0.0976 - 0.1076 seconds)	} < 15 G (preferred) ✓ < 20.49 G (limit)
	y-direction	-7.4 (0.2218 - 0.2318 seconds)	
PHD (g's)		7.5 (0.2218 - 0.2318 seconds)	
ASI		1.99 (0.0151 - 0.0651 seconds)	
Max 50-ms moving avg. acc. (g's)	x-direction	-13 (0.0219 - 0.0719 seconds)	}
	y-direction	-15.1 (0.0148 - 0.0648 seconds)	
	z-direction	-3.5 (0.5417 - 0.5917 seconds)	
Maximum Angular Disp. (deg)	Roll	-6.2 (0.2565 seconds)	} < 75 deg ✓
	Pitch	-3.9 (0.4753 seconds)	
	Yaw	-29.4 (0.2632 seconds)	

10.2.5 Occupant Compartment Intrusion

The maximum deformation of the occupant compartment was less than 1 inch at the lower right-front corner of the toe-pan at the wheel well. Figure 180 shows a view of the vehicle interior after the impact, with several components removed to facilitate viewing. The deformation was less than the critical limit of 9 inches specified in *MASH* for this area of the occupant compartment.

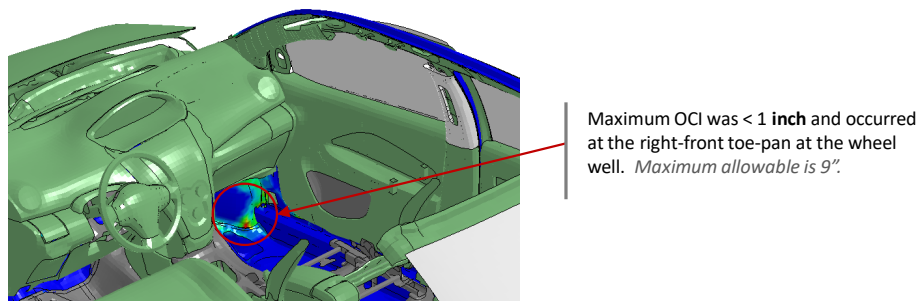


Figure 180. Occupant compartment deformation resulting from Test 4-20 on the 3-bar transition.

10.2.6 Damages to the Barrier System

The damages to the barrier were minimal. Figure 181 shows an overhead view of the post impact deformation of the transition indicating the extent of damage. The barrier was deformed over 16.7 ft of the system with deformation extending from the rail splice at the bridge rail to Post 11 of the transition. Figure 182 and Figure 183 show images of the maximum dynamic deflection and permanent deflection of the barrier, respectively, with a contour plot of lateral displacement on the rail elements. The maximum dynamic and permanent deflections were 5.8 inches and 4.65 inches, respectively, and occurred at the lower corrugation of the thrie-beam at the point where the nested thrie-beam connects to the thrie-beam end shoe, as illustrated in Figures 182 - 184.

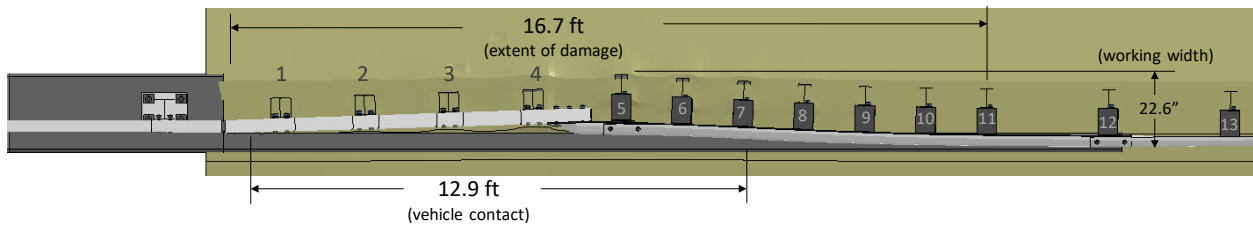


Figure 181. Overhead view of 3-bar transition after Test 4-20 showing extent of damage.

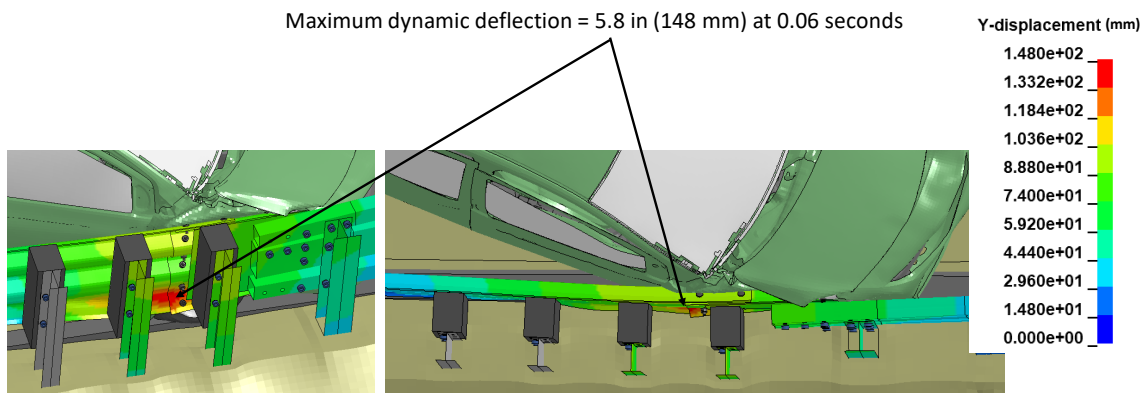


Figure 182. Contour plot of lateral displacement for the transition at the time of maximum dynamic deflection.

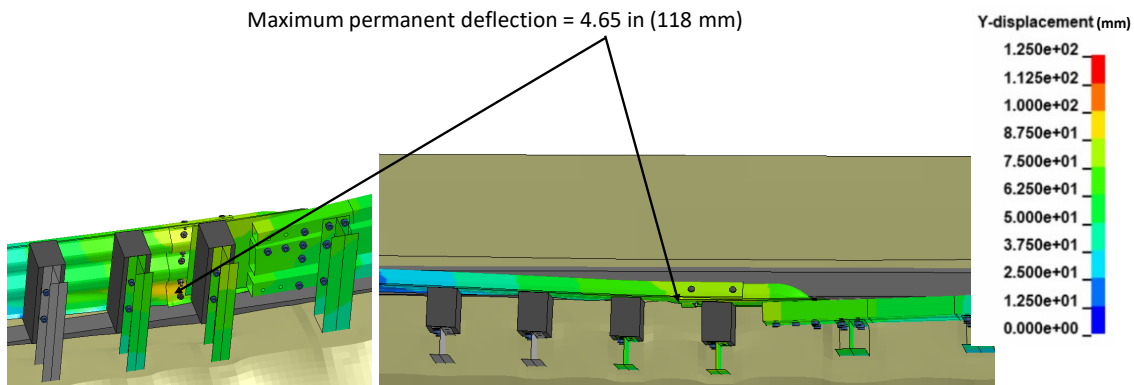


Figure 183. Contour plot of maximum permanent deflection for the transition.

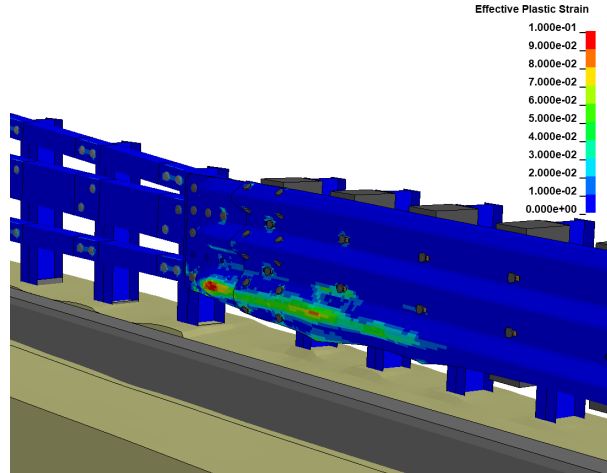


Figure 184. Contours of effective plastic strains on the steel rails and posts for 3-bar transition.

10.2.7 Damages to Vehicle

Figure 185 show contour plots of effective plastic strain for the vehicle, which were used to identify areas of the vehicle that suffered damage during the simulated impact event. The most severe damages were to the front fender, the upper and lower control arm of front suspension, front wheel, lower- impact edge of windshield (cracking), with light damage to the rear quarter panel of the vehicle.

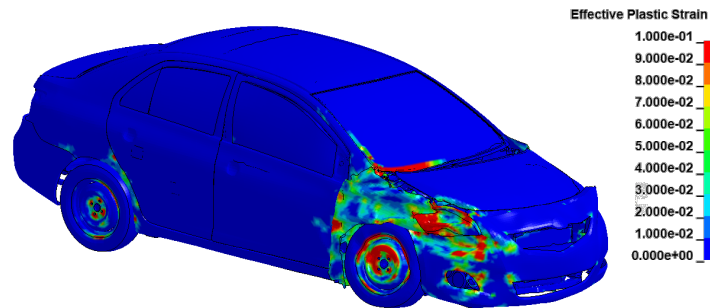


Figure 185. Damages to vehicle in Test 4-20 analysis of the 3-bar transition.

10.2.8 Exit Box

Figure 186 shows the exit box for Test 4-20 on the transition, where the vehicle was smoothly redirected and its path was well within the exit box criteria of *MASH*.

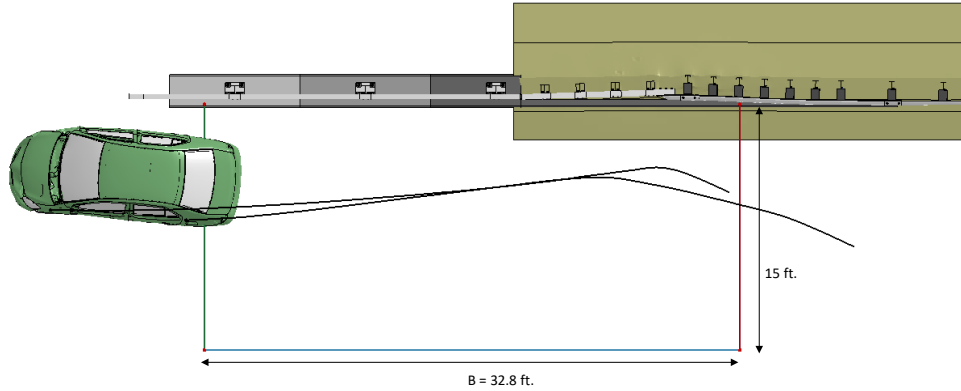


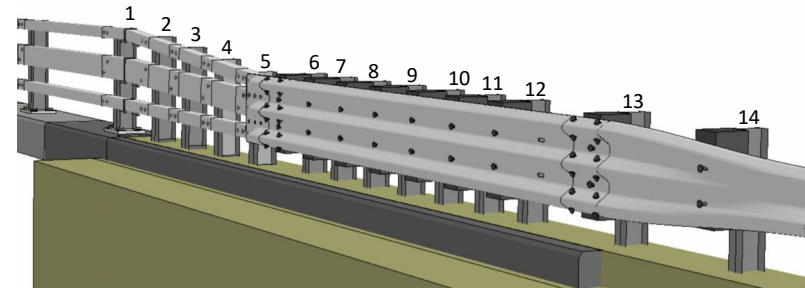
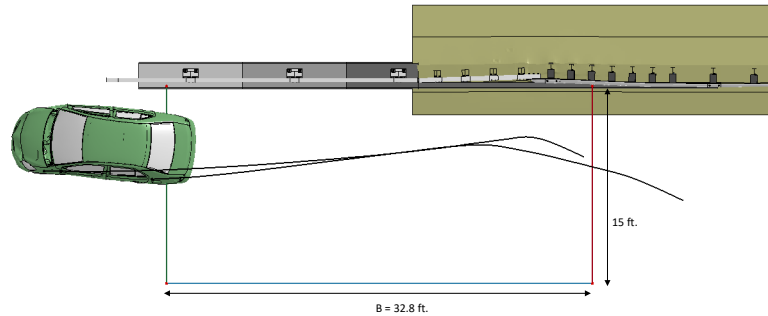
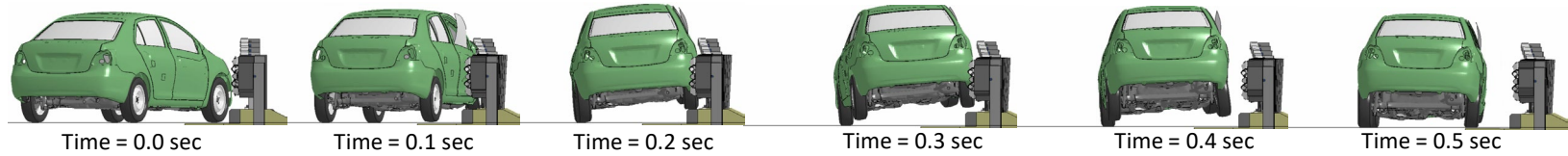
Figure 186. Exit box for Test 4-20 analysis of the 3-bar transition.

10.2.9 Results Summary

A summary of the *MASH* Test 4-20 results on the 3-bar transition is shown in Table 78 and Figures 187. The barrier successfully contained and redirected the small car with minimal damage to the system. There were no detached elements from the barrier that showed potential for penetrating the occupant compartment or presenting undue hazard to other traffic. The vehicle remained upright and very stable throughout impact and redirection. The OIV and maximum ORA values were within recommended limits specified in *MASH*. Based on the results of this analysis, the barrier meets all structural and occupant risk criteria in *MASH* for Test 4-20 impact conditions.

Table 78. Summary of *MASH* Test 4-20 results on the 3-bar transition.

Evaluation Factors	Evaluation Criteria	Results
Structural Adequacy	A Test article should contain and redirect the vehicle or bring the vehicle to a controlled stop; the vehicle should not penetrate, underride, or override the installation although controlled lateral deflection of the test article is acceptable.	Pass
Occupant Risk	D Detached elements, fragments, or other debris from the test article should not penetrate or show potential for penetrating the occupant compartment, or present undue hazard to other traffic, pedestrians, or personnel in a work zone. Deformations of, or intrusions into, to occupant compartment should not exceed limits set forth in Section 5.2.2 and Appendix E.	Pass
	F The vehicle should remain upright during and after collision. The maximum roll and pitch angles are not to exceed 75 degrees.	Pass
	H The longitudinal and lateral occupant impact velocity (OIV) shall not exceed 40 ft/s (12.2 m/s), with a preferred limit of 30 ft/s (9.1 m/s)	Pass
	I The longitudinal and lateral occupant ridedown acceleration (ORA) shall not exceed 20.49 G, with a preferred limit of 15.0 G	Pass



General Information

Analysis Agency Roadsafe LLC
 Test Standard Test No. MASH Test 4-20
 Analysis No. NETC18_3BarTrans_T420
 Analysis Date 4/2/2019

Test Article

Type Bridge Rail Transition
 Name NETC 3-Bar Transition
 Installation Length 65.8 feet
 Material or Key Elements

Soil Type and Condition MASH Strong Soil

Analysis Vehicle

Type / Designation 1100C
 FEA Model name 510_YarisC_V1I_R180228
 Mass 2,595 lb

Impact Conditions

Speed 62 mph
 Angle 25 degrees
 Location 5.5 ft upstream of Post 5

Impact Severity 59.5 kip-ft

Exit Conditions

Speed 43.5 mph
 Angle 4 degrees
 Time 0.295 seconds

Occupant Risk Values

Longitudinal OIV 24.3 ft/s
 Lateral OIV 25.9 ft/s
 Longitudinal ORA 4.2 g
 Lateral ORA 7.4 g
 THIV 35.1 ft/s
 PHD 7.5 g
 ASI 1.99

Max50-millisecond Avg. (G)

Longitudinal 13 g
 Lateral 15.1 g
 Vertical 3.5 g

Test Article Deflections (in)

Dynamic 5.8 inches
 Permanent 4.7 inches
 Working Width 1.9 ft

Max. OCI < 1 inch

Vehicle Stability

Roll 6.2 degrees
 Pitch 3.9 degrees
 Yaw 29.4 degrees

Figure 187. Summary results for MASH Test 4-20 on the 3-bar transition.

10.3 Test 4-21

10.3.1 CIP for Test 4-21

Finite element analysis was used to simulate *MASH* Test 4-21 at impact points 5.7 ft, 6.2 ft, 7.2 ft, 8.2 ft, 8.7 ft, 9.2 ft, 9.7 ft, 10.2 ft, 10.7 ft and 11.7 from the end of the tube rail. These analysis cases were conducted for 0.15 seconds of impact for the purpose of determining the critical impact point for maximizing vehicle accelerations and maximizing forces on the barrier at the junction point of the thrie-beam and the tubular rail section. The 0.15 seconds was sufficient time for the vehicle to reach peak lateral acceleration and almost fully redirect (e.g., the yaw angle ranged from 18-20 degrees). The assessment was based on three key factors; 1) pocketing, 2) peak accelerations, and 3) impact severity at the time when the vehicle approached the connection point. Vehicle stability was not assessed in these analyses due to the short time duration of the impact (i.e., 0.15 seconds); however, the roll and pitch angles were relatively low for all cases.

The potential for pocketing was evaluated by measuring the lateral displacement at six points on the thrie-beam near the connection point and comparing to the lateral deflection of the rail at the connection point, as illustrated in Figure 188. The results of the evaluations are shown in Figures 189 and 190. Based on these results, impact at 9.2 feet upstream of the tubular rails resulted in the highest relative deflections at Nodes 1 - 4; and was therefore considered the highest potential for snagging on the ends of the tubular rails related to pocketing.

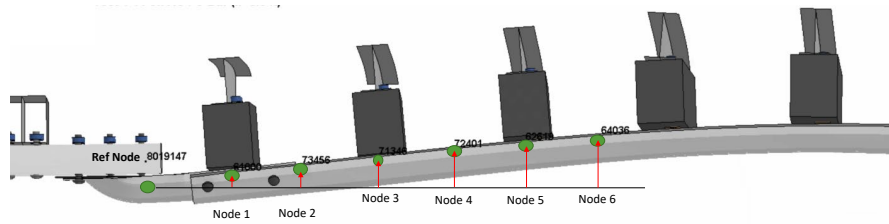


Figure 188. Measurement points for determining CIP for pocketing for Test 4-21.

IP (ft)	Max Pocket					
	Δ Node 1 (in)	Δ Node 2 (in)	Δ Node 3 (in)	Δ Node 4 (in)	Δ Node 5 (in)	Δ Node 6 (in)
5.7 ft	0.92	1.33	1.73	1.89	1.76	1.67
6.2 ft	1.02	2.13	2.54	2.74	2.68	2.49
7.2 ft	1.23	2.04	2.79	3.13	3.16	3.07
8.2 ft	1.47	2.47	3.44	4.16	4.49	4.51
8.7 ft	1.59	2.62	3.72	4.61	5.27	5.40
9.2 ft	1.71	2.86	4.09	5.12	5.80	6.26
9.7 ft	1.53	2.58	3.72	4.72	5.42	5.94
10.2 ft	1.60	2.74	4.04	5.16	6.05	6.49
10.7 ft	1.51	2.60	3.84	4.93	5.83	6.54
11.7 ft	1.36	2.38	3.65	4.78	5.78	6.75

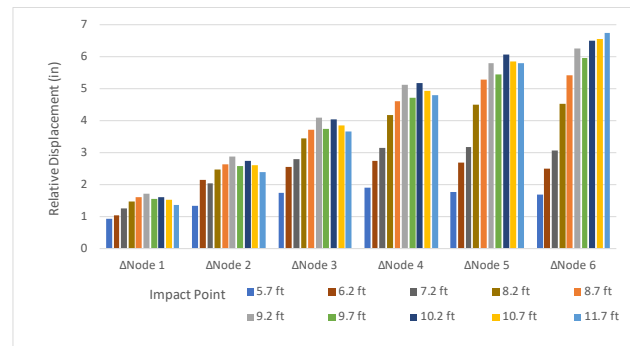


Figure 189. Relative displacements of rail for Test 4-21 simulations in CIP evaluations.

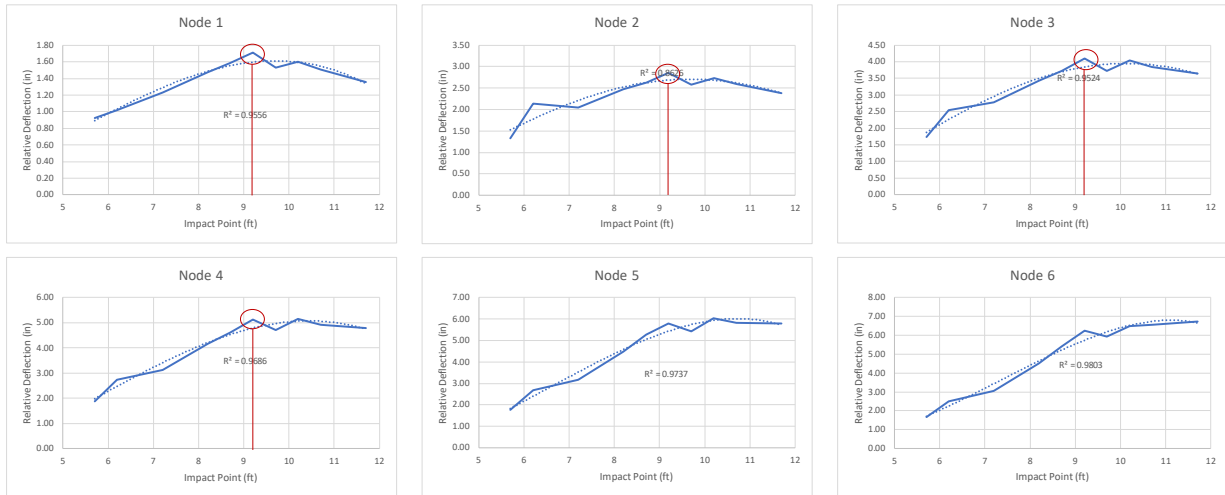


Figure 190. Plots of relative displacements for Test 4-21 simulations in CIP evaluations.

Figure 191 shows a plot of the total deflection of the transition at the critical snag point for each of the analysis cases, which indicates that impact at 7.2 feet resulted in the highest loading on the rail at the critical snag point, with impact at 6.2 feet resulting in the second highest loading. Figure 192 shows plots of vehicle resultant accelerations and impact severity at the time when the vehicle bumper is at the critical snag point. The initial peak accelerations are of similar magnitude and occur at approximately the same time for all cases; the results are also consistent with typical Test 3-11 or 3-21 results on rigid barriers. The highest resultant acceleration occurred for impact at 6.2 feet; however, the peak acceleration for that case occurred at 0.01 seconds before the bumper of the vehicle reached the critical snag point. The second highest acceleration peak was for the 5.7-ft case and occurred just before the bumper reached the critical snag point. Although impact at 9.2 feet resulted in the greatest potential for pocketing, the vehicle accelerations and the impact severity on the barrier was significantly reduced at the time when the vehicle reached the critical snag point.

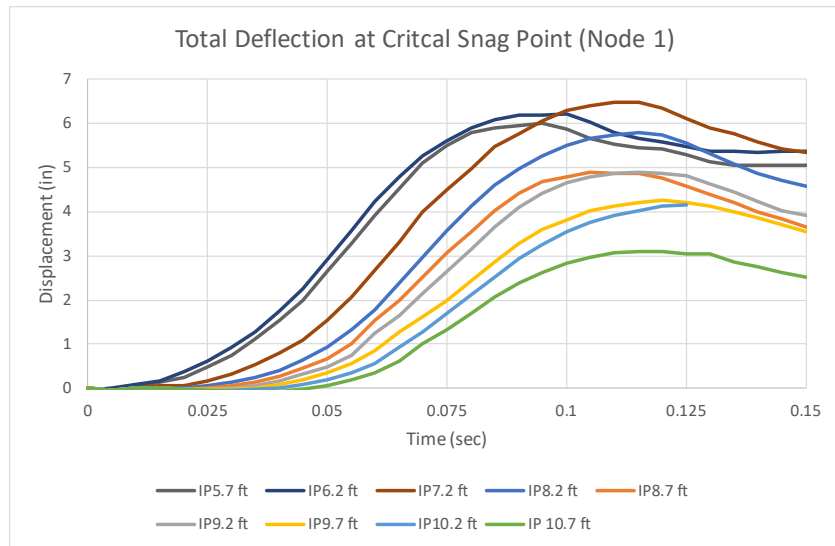


Figure 191. Total deflection of the rail at the critical snag point on the transition for Test 4-21.

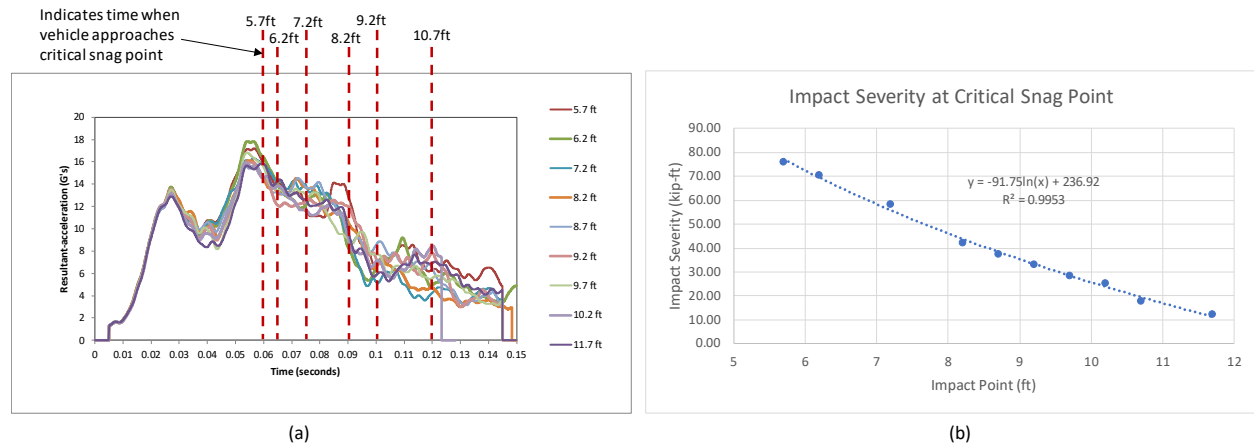


Figure 192. Plots of (a) vehicle accelerations and (b) impact severity at time when vehicle is positioned at critical snag point.

Based on the analysis results it was determined that there was very low potential for snags on the end of the transition tube rails, and that the curb sufficiently shields the posts from contact/snag with vehicle tires. In general, the results showed that:

- Impact at 7.2 ft resulted in largest displacement of rail (at Node 1) approaching end of transition tube rails
- Impact at 6.2 ft resulted in the highest accelerations and 2nd largest displacement of rail approaching end of rail tube
- Impact at 5.7 ft resulted in the highest accelerations occurring at time of potential snag on end of transition rails.
- Impact at 9.2 feet resulted in the greatest relative deflection at the snag point.

The CIP used for NCHRP Report 350 Test 3-21 (i.e., Test 401181-1) on the NETC 2-bar transition was 5.1 feet.[*Alberson06*]. The critical impact points used in recent *MASH* evaluations of bridge rail transitions included 6.7 feet for Test AGTB-1 [*Rosenbaugh18*] and 5.5 feet for simulation of MassDOT AGT [*Plaxico18*]; both cases involved a nested three-beam transition section connected to a rigid concrete buttress.

For the current study, two critical impact points were determined. The primary CIP was 6.2 feet upstream of the critical snag point at the end of the tubular rails and was based on overall results considering equal weight for pocketing and impact severity at time of vehicle approach to potential snag point. The secondary CIP was determined to be 9.2 feet upstream of the critical snag point which resulted in the greatest potential for pocketing. Only the primary CIP, however, was selected for further evaluation.

The final analysis was performed for 0.85 seconds of the impact event. The following sections provide a summary of the results and include a commentary describing the timing and occurrence of various events during the simulated impact, time-history data evaluation, occupant risk assessments, and damages sustained by both the barrier and vehicle.

10.3.2 Summary of Key Phenomenological Events

The 5,001-lb pickup struck the barrier at 6.2 feet upstream of the critical snag point at the end of the tubular rails at a speed of 62 mph and at an angle of 25 degrees, as illustrated in Figure

193. The sequential views of the impact event are shown in Appendix O in Figures O-1 through O-3 from an overhead viewpoint, downstream and upstream viewpoint, and isometric viewpoint, respectively.

At time equal zero seconds the front bumper of the pickup contacted the lower and middle corrugation of the thrie-beam, while the front-right fender contacted the upper corrugation. At 0.01 seconds the front-right tire contacted the curb and the barrier started to deflect. At 0.02 seconds the front-right tire was compressed to the rim at two points and would likely have deflated; however, tire deflation was not included in the model. At 0.04 seconds the front-right tire was fully mounted onto the curb and was steered parallel to the barrier. At 0.055 seconds the front bumper was aligned with Post 5. At 0.06 seconds the front-left tire lifted off the ground as the vehicle started to roll toward the barrier. At 0.065 seconds the front bumper was aligned with the end of the transition tube rails, and the front fender slightly snagged on the top of the blockout of Post 5. This resulted in a peak 10-millisecond average acceleration of 11.8 G in the longitudinal direction. At 0.08 seconds the front bumper was aligned with Post 4. At 0.0925 seconds the occupant struck the right side of the interior at 17.7 ft/s in the forward direction and 24.6 ft/s in the lateral direction. At 0.095 seconds the rear-left tire lifted off the ground as the vehicle continued to roll toward the barrier. The roll angle of the pickup at this time was 4.4 degrees. At 0.11 seconds the front-right tire was aligned with Post 4, but the tire did not contact the post. At 0.113 seconds the peak occupant ridedown acceleration in the longitudinal direction occurred with magnitude 5.2 G. At 0.12 seconds the vehicle reached peak roll angle of 5.8 degrees toward the barrier. At 0.17 seconds the rear-right tire contacted the curb and the pickup bed contacted the middle and lower corrugations of the thrie-beam. At 0.18 seconds the rear bumper contacted the middle corrugation of the thrie-beam at approximately 8.1 feet upstream from the end of the transition tube rails. At 0.185 seconds the vehicle was parallel to the barrier. At 0.19 seconds the rear-left tire was compressed laterally to the point the tire debanding would be likely. Also, at this time the front bumper of the vehicle was aligned with the splice connection at the bridge rail, and the front of the vehicle began to exit the system. At 0.202 the maximum occupant ridedown acceleration in the lateral direction occurred with magnitude 15.1 G. At 0.21 seconds the rear-left tire was fully mounted onto the curb. At 0.31 seconds the vehicle separated from the barrier traveling at 47.5 mph at an exit angle of 3 degrees. At 0.5 seconds the vehicle reached maximum roll angle of 8.1 degrees away from the barrier. At 0.56 seconds the vehicle reached maximum pitch angle of -3.7 degrees rear pitching up). The vehicle remained stable throughout post-impact trajectory. The analysis ended at 0.85 seconds, at which time:

- The roll, pitch, and yaw of the vehicle were, respectively, 0.8 degrees (toward barrier), 1.1 degrees (rear pitching up), and 26.9 degrees (1.9 degrees relative to and away from the barrier).
- The forward velocity of the vehicle was 45.6 mph (73.3 km/h).

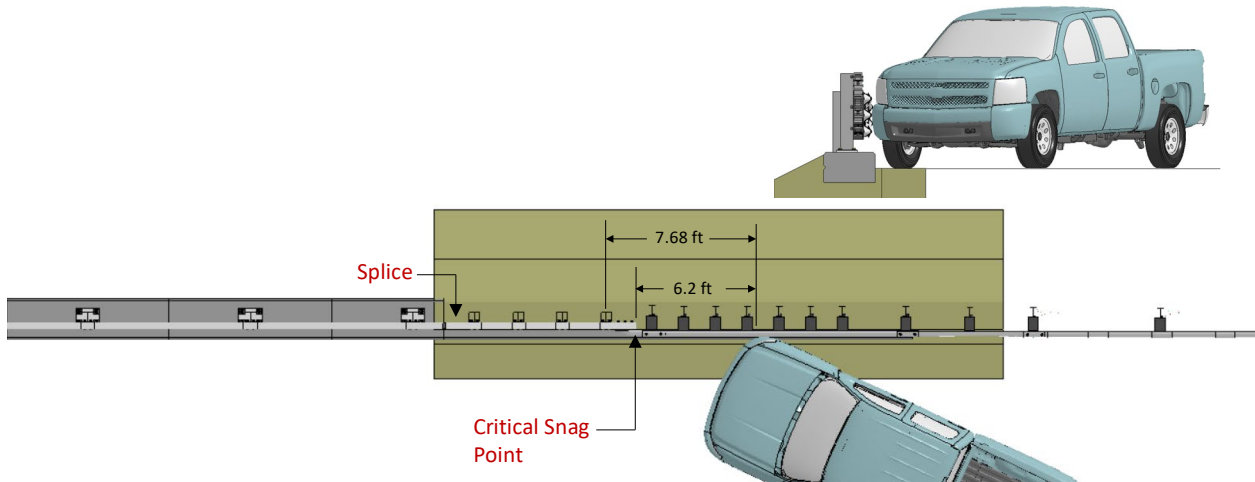


Figure 193. Impact point for Test 4-21 on the 3-bar transition.

10.3.3 Time History Data Evaluation

Figures 194 through 196 show the longitudinal, transverse, and vertical acceleration-time histories, respectively, computed from the center of gravity of the vehicle; Figures 197 through 199 show the angular rates and angular displacement about the x-, y-, and z-axis at the center of gravity of the vehicle.

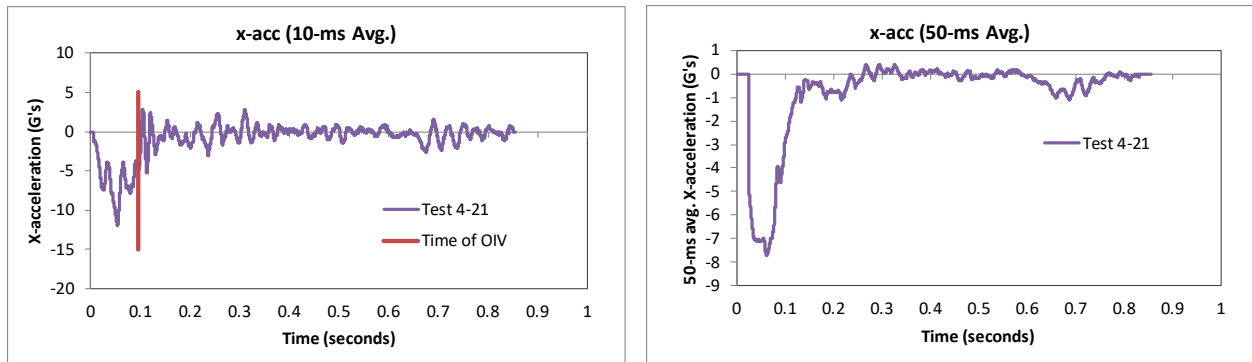


Figure 194. 10- and 50-millisecond average X-acceleration from FEA of Test 4-21 on the 3-bar transition.

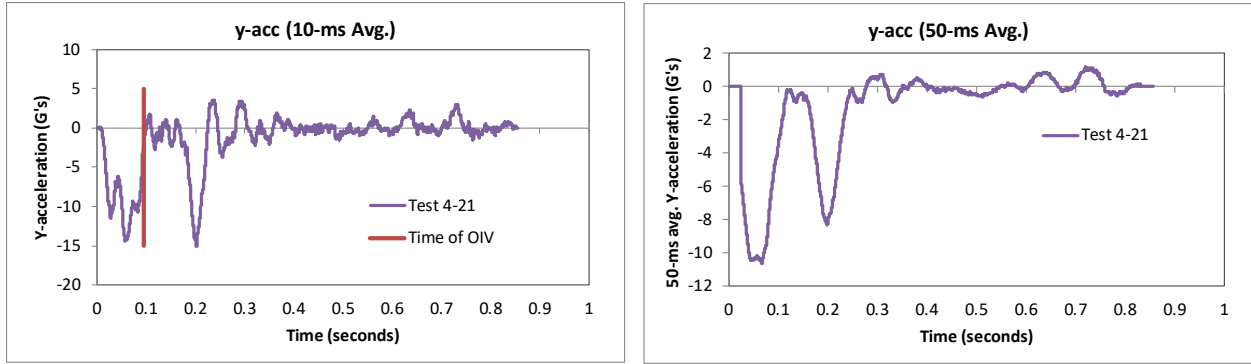


Figure 195. 10- and 50-millisecond average Y-acceleration from FEA of Test 4-21 on the 3-bar transition.

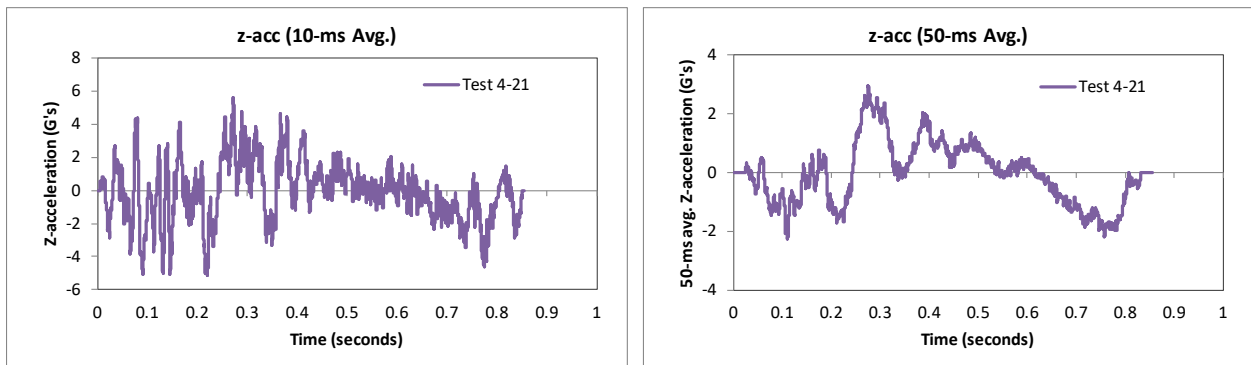


Figure 196. 10- and 50-millisecond average Z-acceleration from FEA of Test 4-21 on the 3-bar transition.

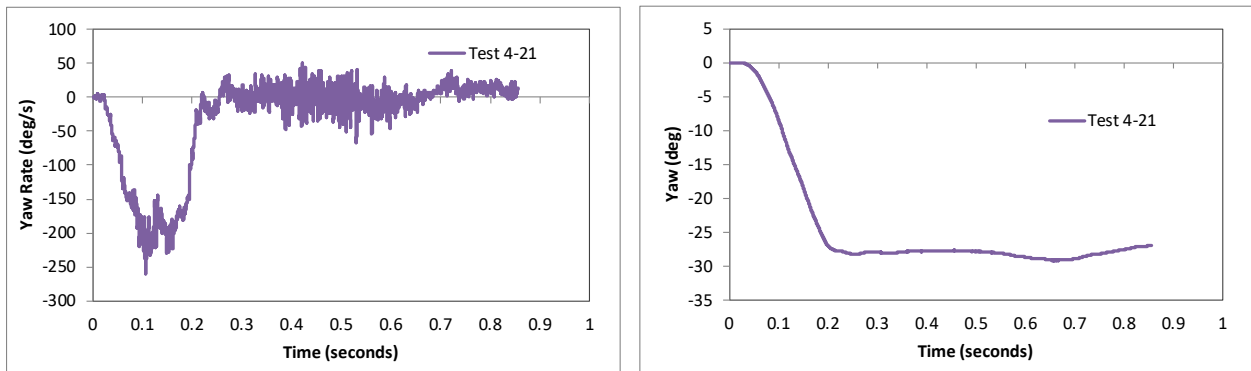


Figure 197. Yaw rate and yaw angle time-history from FEA of Test 4-21 on the 3-bar transition.

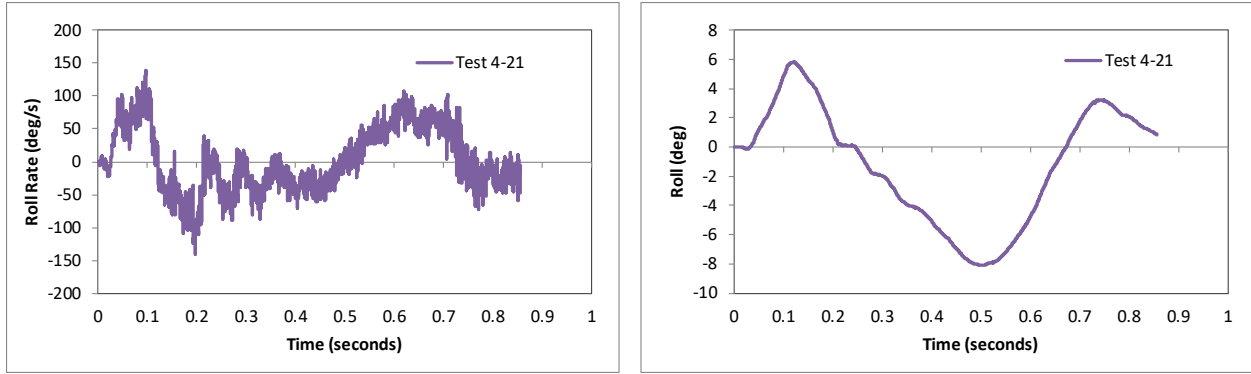


Figure 198. Roll rate and pitch angle time-history from FEA of Test 4-21 on the 3-bar transition.

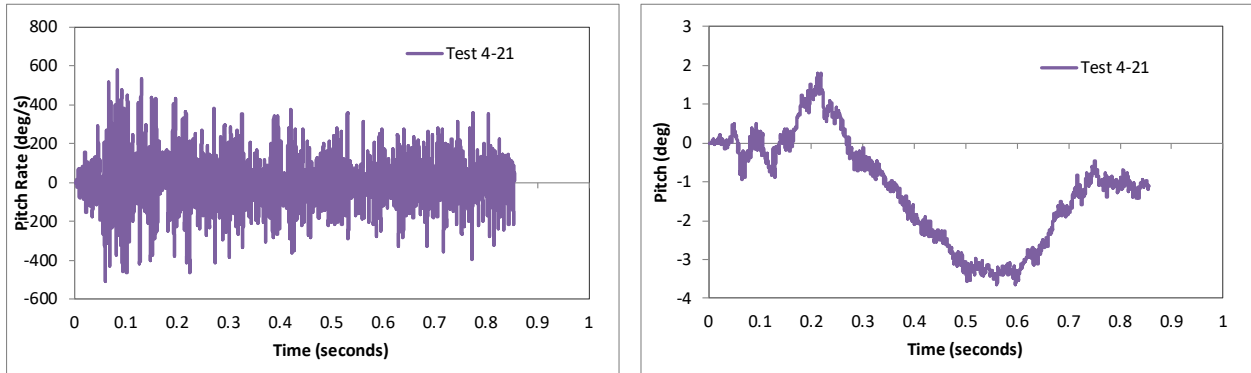


Figure 199. Pitch rate and pitch angle time-history from FEA of Test 4-21 on the 3-bar transition.

10.3.4 Occupant Risk Measures

The acceleration-time histories and angular rate-time histories collected at the center of gravity of the vehicle were used to evaluate occupant risk metrics according to the procedures outlined in *MASH*. Table 79 shows the results for the occupant risk calculations. The results indicate that the occupant risk factors met safety criteria specified in *MASH*.

The occupant impact velocities in the longitudinal and transverse directions for the curb-mounted system were 17.7 ft/s and 24.6 ft/s, respectively, which were within the recommended limits specified in *MASH*. The highest 0.010-second occupant ridedown acceleration in the longitudinal and transverse directions were 5.2 g and 15.1 g, respectively, which were just over the recommended limit within but with critical limits specified in *MASH*. The maximum 50-ms moving average acceleration values in the longitudinal and transverse directions were 7.7 g and 10.6 g, respectively. The maximum roll and pitch angles of the vehicle were 8.1 degrees and 3.7 degrees, respectively, which were well below critical limits in *MASH*. As mentioned previously in Section 5, the 2270P vehicle model often over-estimates the lateral ridedown acceleration [see Appendix E].

Table 79. Summary of occupant risk metrics for Test 4-11 on the 3-bar transition.

Occupant Risk Factors		MASH T4-11
		Test 4-21
Occupant Impact Velocity (ft/s)	x-direction	17.7
	y-direction	24.6
	at time	at 0.0925 seconds on right side of interior
THIV (ft/s)		30.5 at 0.0925 seconds on right side of interior
Ridedown Acceleration (g's)	x-direction	-5.2 (0.1082 - 0.1182 seconds)
	y-direction	-15.1 (0.1973 - 0.2073 seconds)
PHD (g's)		15.2 (0.1973 - 0.2073 seconds)
ASI		1.33 (0.0417 - 0.0917 seconds)
Max 50-ms moving avg. acc. (g's)	x-direction	-7.7 (0.0367 - 0.0867 seconds)
	y-direction	-10.6 (0.0419 - 0.0919 seconds)
	z-direction	2.9 (0.2506 - 0.3006 seconds)
Maximum Angular Disp. (deg)	Roll	-8.1 (0.4977 seconds)
	Pitch	-3.7 (0.5602 seconds)
	Yaw	-29.1 (0.6542 seconds)

MASH Criteria

- < 30 ft/s (preferred) ✓
- < 40 ft/s (limit)
- > 15 G (preferred)
- < 20.49 G (limit) ✓
- < 75 deg ✓

10.3.5 Occupant Compartment Intrusion

The maximum deformation of the occupant compartment was negligible for this analysis case. Figure 200 shows a view of the vehicle interior after the impact, with several components removed to facilitate viewing.

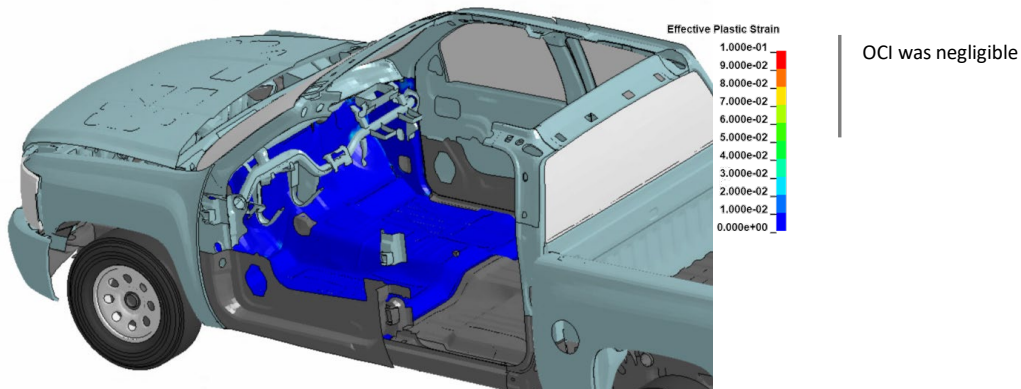


Figure 200. Occupant compartment deformation resulting from Test 4-21 on the 3-bar transition.

10.3.6 Damages to the Barrier System

The damages to the barrier were moderate. Figure 201 show an overhead view of the post impact deformation of the transition indicating the extent of damage. The barrier was deformed over 22.9 ft of the system with deformation extending from the rail splice at the bridge rail to Post 12 of the transition. The vehicle was in contact with the barrier for approximately 15.6 ft.

Figure 202 and Figure 203 show images of the maximum dynamic deflection and permanent deflection of the barrier, respectively, with a contour plot of lateral displacement on the rail elements. The maximum dynamic and permanent deflections were 7.95 inches and 6.8 inches, respectively, and occurred at the lower corrugation of the thrie-beam at the point where the nested thrie-beam connects to the thrie-beam end shoe, as illustrated in Figures 201 - 204.

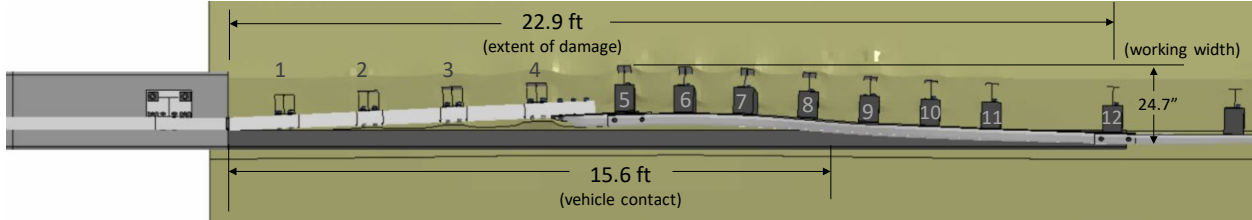


Figure 201. Overhead view of 3-bar transition after Test 4-21 showing extent of damage.

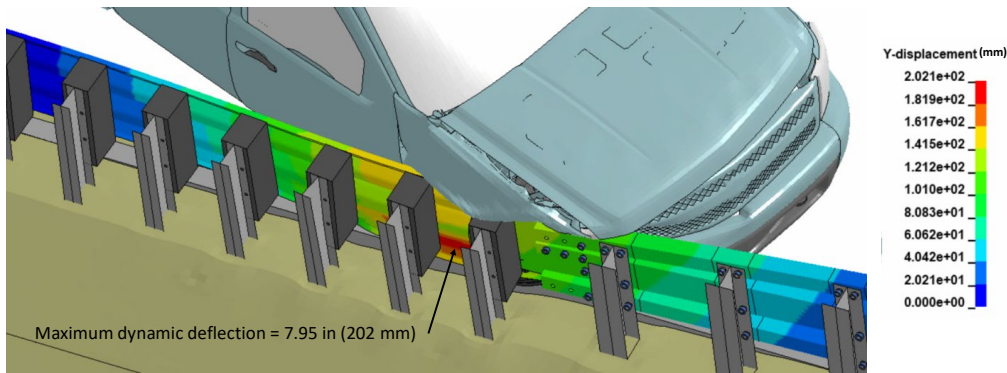


Figure 202. Contour plot of lateral displacement for Test 4-21 on the 3-bar transition at the time of maximum dynamic deflection.

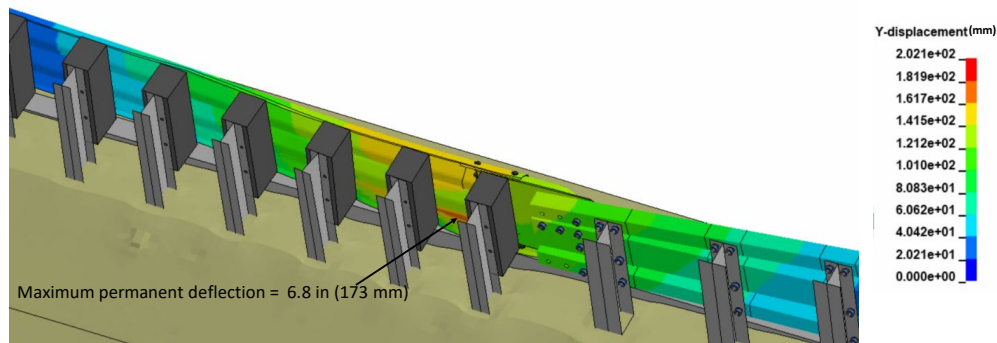


Figure 203. Contour plot of maximum permanent deflection for Test 4-21 on the 3-bar transition.

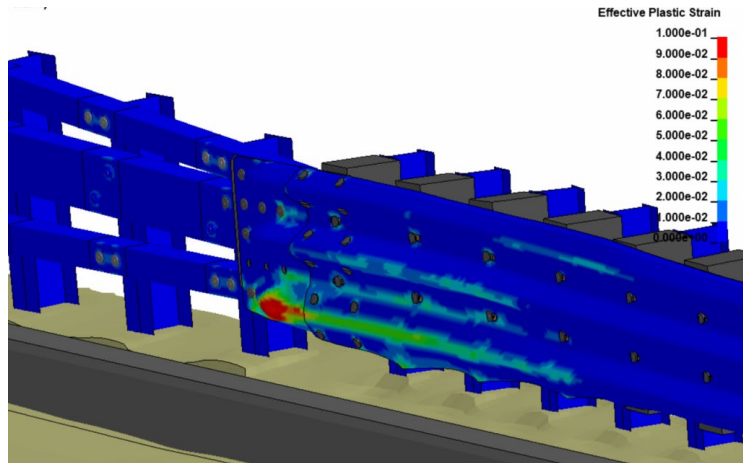


Figure 204. Contours of effective plastic strains on the steel rails and posts for Test 4-21 on 3-bar transition.

10.3.7 Damages to Vehicle

Figure 205 show contour plots of effective plastic strain for the vehicle, which were used to identify areas of the vehicle that suffered damage during the simulated impact event. The most severe damages were to the front bumper, the front fender, the upper control arm of front suspension, front and rear wheels, rear edge of rear door, front edge of truck bed, rear quarter panel of truck bed and rear bumper.

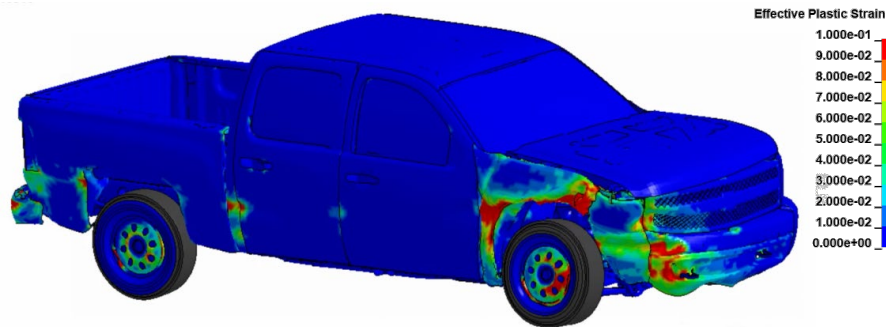


Figure 205. Damages to vehicle in Test 4-21 analysis of the 3-bar transition.

10.3.8 Exit Box

Figure 206 shows the exit box for Test 4-21 on the 3-bar transition system. The vehicle was smoothly redirected and its path was well within the exit box criteria of *MASH*.

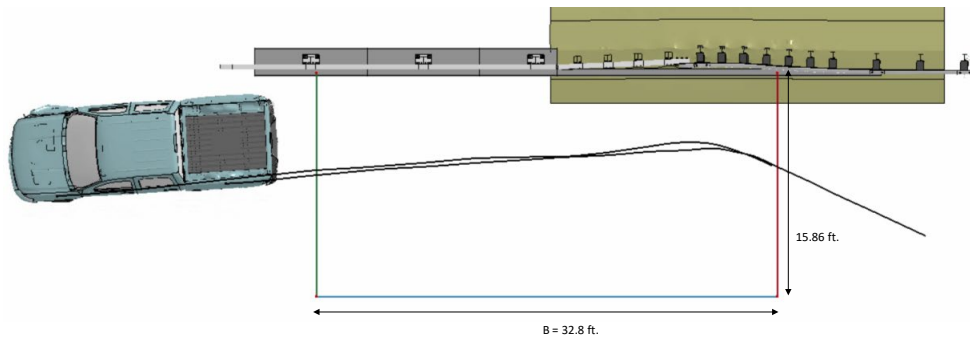


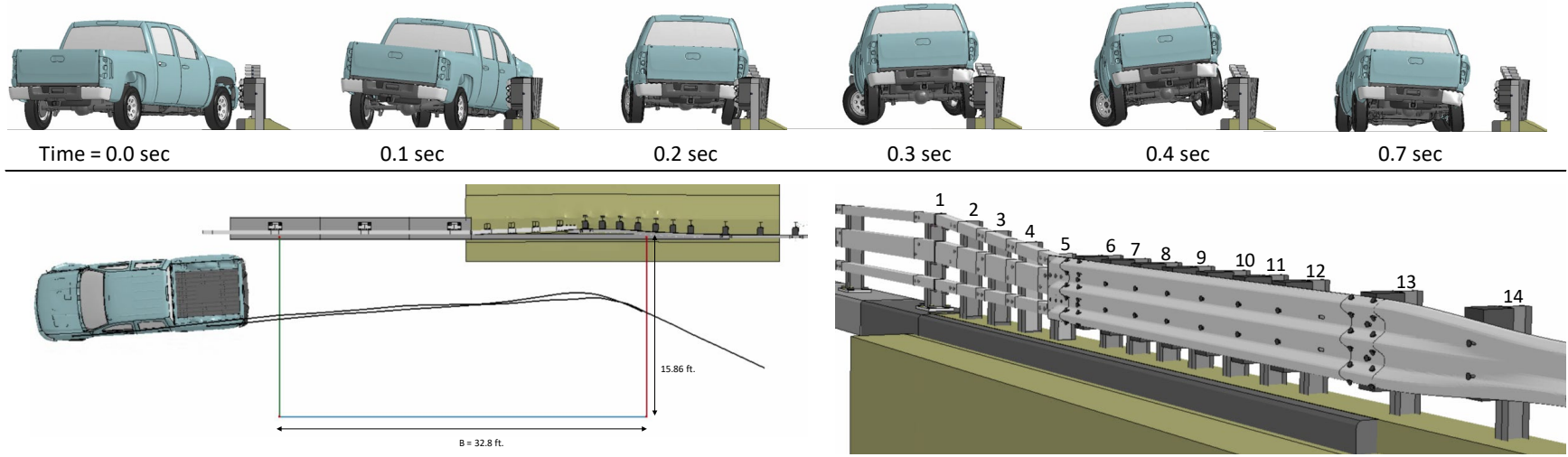
Figure 206. Exit box for Test 4-21 analysis of the 3-bar transition.

10.3.9 Results Summary

A summary of the *MASH* Test 4-21 results on the NETC 3-bar transition is shown in Table 80 and Figure 207. The barrier successfully contained and redirected the 2270P vehicle (pickup) with moderate damage to the transition. There were no detached elements from the barrier that showed potential for penetrating the occupant compartment or presenting undue hazard to other traffic. The vehicle remained upright and did not experience excessive roll or pitch angle displacements. The OIV and maximum ORA values were within critical limits specified in *MASH*. Based on the results of this analysis, the barrier meets all structural and occupant risk criteria in *MASH* for Test 4-21 impact conditions.

Table 80. Summary of *MASH* Test 4-21 results on the NETC 3-bar transition.

Evaluation Factors	Evaluation Criteria	Results
Structural Adequacy	A Test article should contain and redirect the vehicle or bring the vehicle to a controlled stop; the vehicle should not penetrate, underride, or override the installation although controlled lateral deflection of the test article is acceptable.	Pass
	D Detached elements, fragments, or other debris from the test article should not penetrate or show potential for penetrating the occupant compartment, or present undue hazard to other traffic, pedestrians, or personnel in a work zone. Deformations of, or intrusions into, to occupant compartment should not exceed limits set forth in Section 5.2.2 and Appendix E.	Pass
Occupant Risk	F The vehicle should remain upright during and after collision. The maximum roll and pitch angles are not to exceed 75 degrees.	Pass
	H The longitudinal and lateral occupant impact velocity (OIV) shall not exceed 40 ft/s (12.2 m/s), with a preferred limit of 30 ft/s (9.1 m/s)	Pass
	I The longitudinal and lateral occupant ridedown acceleration (ORA) shall not exceed 20.49 G, with a preferred limit of 15.0 G	Pass



General Information

Analysis Agency Roadsafe LLC
 Test Standard Test No. MASH Test 4-21
 Analysis No. NETC18_3BarTrans_T421
 Analysis Date 3/28/2019

Test Article

Type Bridge Rail Transition
 Name NETC 3-Bar Transition
 Installation Length 65.8 feet
 Material or Key Elements

Soil Type and Condition MASH Strong Soil

Analysis Vehicle

Type / Designation 2270P
 FEA Model name SilveradoC_V3a_V180201_TireRS_35psi
 Mass 5,001 lb

Impact Conditions

Speed 62 mph
 Angle 25 degrees
 Location 5.5 ft upstream of Post 5

Impact Severity 114.7 kip-ft

Exit Conditions

Speed 47.5 mph
 Angle 3 degrees
 Time 0.31 seconds

Occupant Risk Values

Longitudinal OIV 17.7 ft/s
 Lateral OIV 24.6 ft/s
 Longitudinal ORA 5.2 g
 Lateral ORA 15.1 g
 THIV 30.5 ft/s
 PHD 15.2 g
 ASI 1.33

Max50-millisecond Avg. (G)

Longitudinal 7.7 g
 Lateral 10.6 g
 Vertical 2.9 g

Test Article Deflections (in)

Dynamic 7.95 inches
 Permanent 6.8 inches
 Working Width 2.06 ft

Max. OCI < 1 inch

Vehicle Stability

Roll 8.1 degrees
 Pitch 3.7 degrees
 Yaw 29.1 degrees

Figure 207. Summary results for MASH Test 4-21 on the 3-bar transition system

10.4 Test 4-22

10.4.1 CIP for Test 4-22

The critical impact point for Test 4-22 was determined using FEA with respect to maximum potential for vehicle snag on the end of the bridge rail at the splice connection between transition rails and bridge rail, as illustrated in Figure 208. Finite element analysis was used to simulate *MASH* Test 4-22 at impact points 5 ft, 6 ft, 7 ft, 8 ft and 9 ft from the mid-point of the splice connection. These analysis cases were conducted for 0.4 seconds of impact which was sufficient to evaluate potential snags regarding both the front and rear of the vehicle.

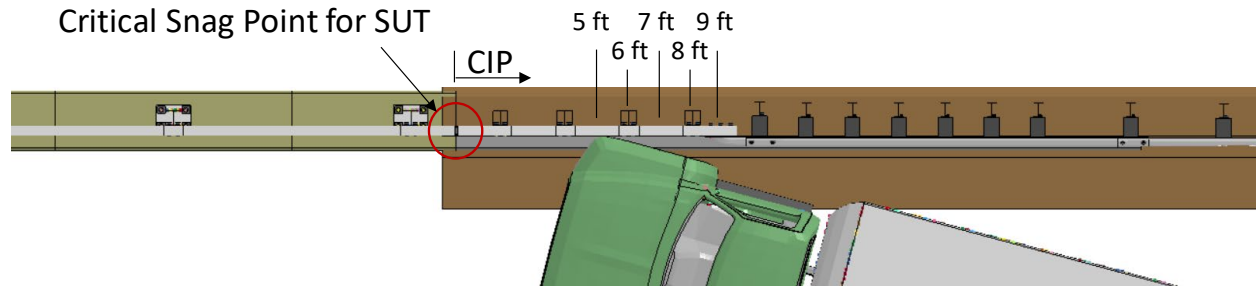


Figure 208. Illustration of potential snag point for Test 4-22 on the 3-bar transition and impact points evaluated.

The longitudinal, lateral and resultant forces on the barrier for each case is shown in Figure 209, and an overlay of all cases is shown in Figure 210. The force magnitudes were very similar for all cases. The impact at 9 feet upstream of the splice, however, resulted in the greatest potential for the cargo-box of the truck to extend over the top of the rail and snag on the tops of the bridge rail posts as the truck rolled toward and over the bridge rail, as illustrated in Figure 211. It was assumed that the potential for the vehicle bed extending over the rail and the potential for the vehicle rolling over the barrier would further increase as the impact point moved farther upstream onto the lower height section of the transition (e.g., thrie-beam section is 34 inches tall). However, at some point, the transition itself moves from a TL4 design to a TL3 design where it would not be expected or required to meet TL4. Therefore, the evaluations only considered impacts on the downstream section of the transition leading up to the TL4 bridge rail (i.e., the tubular transition section).

Based on these results, impact at 9 feet upstream of the bridge rail splice was selected as the critical impact point to maximize potential for vehicle snag on the end of the bridge rail and to also maximize potential for vehicle roll angle and contact between cargo-box and bridge rail posts. The analysis was performed for 1.5 seconds of the impact event. The following sections provide a summary of the results and include a commentary describing the timing and occurrence of various events during the simulated impact, time-history data evaluation, occupant risk assessments, and damages sustained by both the barrier and vehicle.



Figure 209. Longitudinal, lateral and resultant forces on barrier for each analysis case.

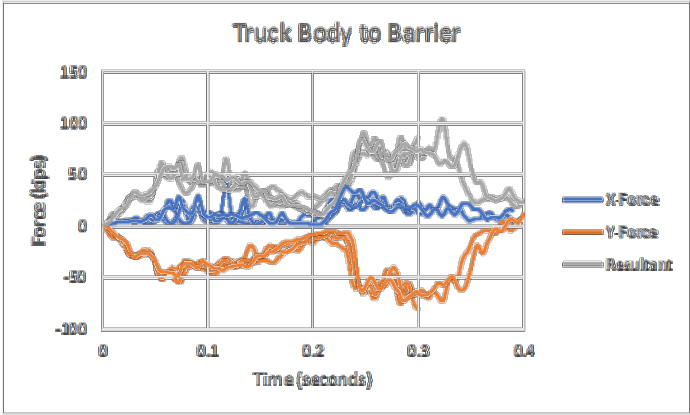


Figure 210. Overlay of force-time history for all cases.

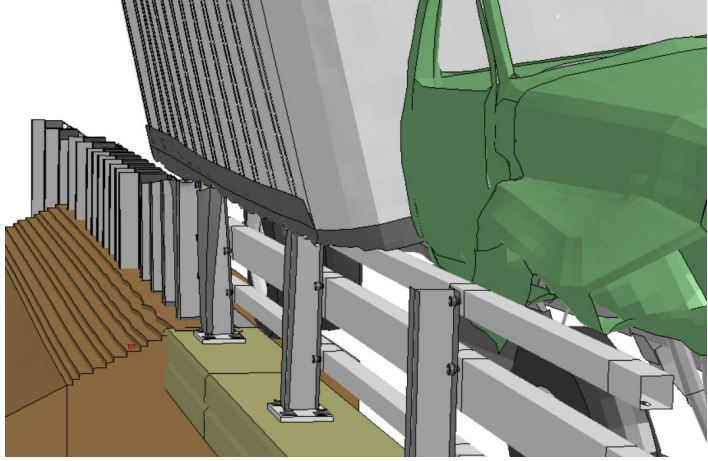


Figure 211. Cargo-box bed rails snag on top of bridge rail posts.

10.4.2 Summary of Key Phenomenological Events

The 22,198-lb single unit truck struck the barrier at 9.0 feet upstream of the bridge rail splice at a speed of 56 mph and at an angle of 15 degrees, as illustrated in Figure 208. The sequential views of the event are shown in Appendix P in Figures P-1 through P-3 from an overhead viewpoint, downstream and upstream viewpoint, and an oblique viewpoint, respectively.

At time equal zero seconds the front bumper of the vehicle made slight contact with the top and middle corrugations of the thrie-beam end shoe, and then immediately lost contact as the vehicle moved forward toward the tubular rail section of the transition. At 0.01 seconds the front-right tire made slight contact with the lower and middle corrugations of the thrie-beam end shoe, and the front bumper contacted the tubular section of the transition at Post 4. Also, at this time, the tire contacted the curb. At 0.015 seconds the front bumper contacted the upper and middle tube rails of the transition, and at 0.02 seconds the front fender contacted the upper rail tube. At 0.025 seconds the system started to deflect. At 0.035 seconds the front-right tire started to steer away from the barrier, and the front bumper was aligned with Post 3 of the transition. At 0.055 seconds the front-right tire was fully mounted onto the curb, and the front bumper was aligned with Post 2 of the transition. At 0.065 seconds the tire had steered parallel to the barrier. At 0.08 seconds the front bumper was aligned with Post 1 of the transition. At 0.105 seconds the front bumper moved across the splice connection of the middle rail tube to the bridge rail. At 0.12 seconds the front fender moved across the splice connection of the top tube rail. At 0.125 seconds the front-right wheel began to move across the splice connection of the lower tube rail. At 0.145 seconds the front-lower edge of the cargo-box passed over the top of the top rail just upstream of Post 3 of the transition. At 0.215 seconds the lower-leading edge of the cargo-box contacted the top of the tube rails at the splice connection. At 0.22 seconds the rear-right wheel contacted the curb. At 0.23 seconds the lower-leading edge of the cargo-box contacted the first post of the bridge rail and began to deform. At 0.24 seconds the rear-right wheel simultaneously contacted the thrie-beam end shoe and all three tube rails of the transition. Also, at this time, the lower edge of the cargo-box contacted the top of Post 1 of the transition. At 0.245 seconds the lower-edge of the cargo-box snagged on Post 1 of the bridge rail, and the post began to twist and deflect longitudinally. The under-side of the cargo-box then remained in contact with the top of the bridge rail and continued to snag on the tops of the bridge rail posts until the truck exited the end of the bridge rail. At 0.265 seconds the rear-right tire was fully mounted onto the curb. At 0.304 seconds the vehicle was parallel to the barrier. At 0.335 seconds the rear-right tire began to pass the splice connection with no snag with the splice. At 0.365 seconds the lower-side of the cargo-box contacted and snagged the top of Post 2 of the bridge rail. At 0.455 seconds the lower-side of the cargo-box contacted and snagged the top of Post 3 of the bridge rail. At 0.6 seconds the vehicle exited the rail as the cargo-box slide off the end of the bridge rail a 44.4 mph with yaw angle of 5.5 degrees toward the barrier. At 0.76 seconds the truck cabin reached maximum roll angle of 26.3 degrees. At 0.81 seconds the cargo box reached peak pitch angle of 11.8 degrees with rear pitching upward. At 0.82 seconds the cargo-box reached peak roll angle of 34 degrees toward the barrier. At 0.873 seconds the truck cabin reached maximum pitch angle of 11.9 degrees with rear pitching upward. The vehicle remained upright and relatively stable throughout impact, although post trajectory indicated that the vehicle would likely roll onto its side. The analysis ended at 1.5 seconds, at which time:

- The roll, pitch, and yaw of the truck cabin were, respectively, 16.7 degrees (toward barrier), 0.82 degrees (rear pitching up), and 35.2 degrees (20.2 degrees relative to and toward barrier).
- The roll, pitch, and yaw of the cargo-box were, respectively, 14.2 degrees (toward barrier), 1.94 degrees (rear pitching up), and 33.6 degrees (18.6 degrees relative to and toward barrier).
- The forward velocity of the vehicle was 48.6 mph (78.1 km/h).

10.4.3 Time History Data Evaluation

Acceleration-time histories and angular rate-time histories were collected at two locations on the vehicle: (1) on the cargo box at the center of gravity of the vehicle, and (2) a point inside the cabin of the truck, as shown in Figure 111. The acceleration and angular rate data used for the occupant risk measures came from the cabin location. Figures 212 through 214 show the longitudinal, transverse, and vertical acceleration-time histories, respectively, computed from near the center of gravity of the vehicle which falls inside the cargo-box near the front of the ballast.

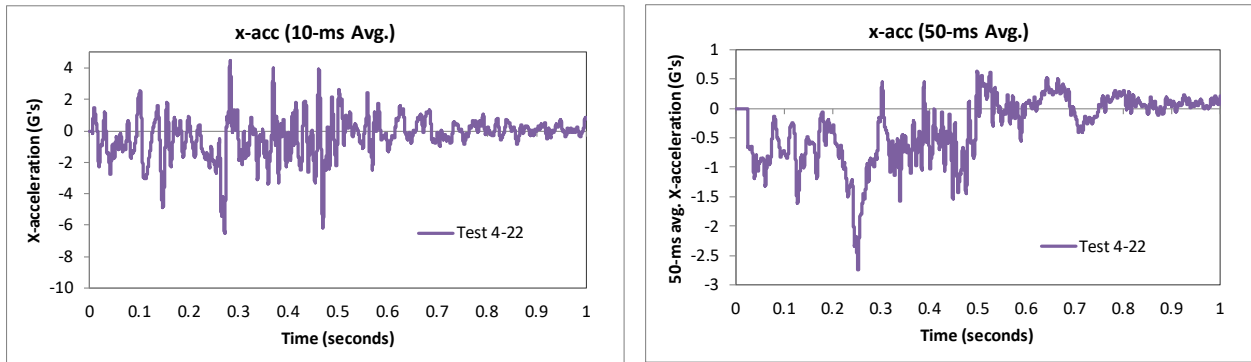


Figure 212. 10- and 50-millisecond average X-acceleration from FEA of Test 4-22 on the 3-bar transition (c.g. accelerometer).

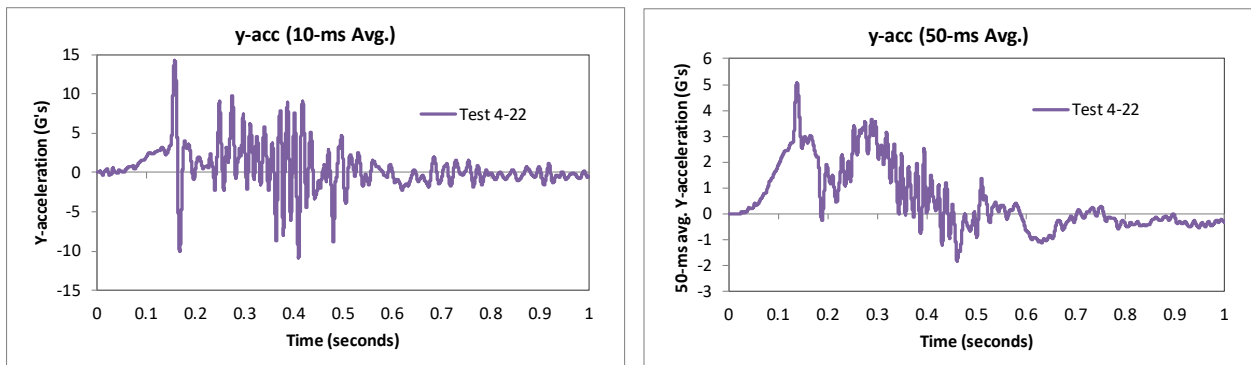


Figure 213. 10- and 50-millisecond average Y-acceleration from FEA of Test 4-22 on the 3-bar transition (c.g. accelerometer).

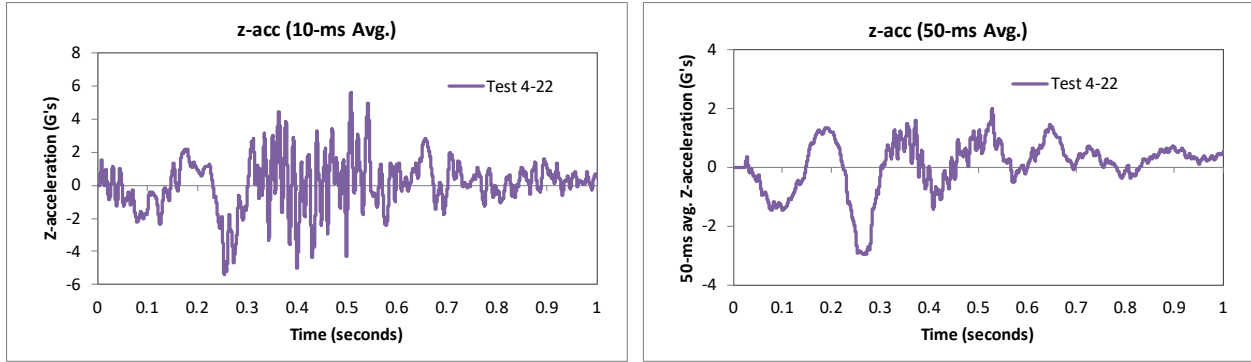


Figure 214. 10- and 50-millisecond average Z-acceleration from FEA of Test 4-22 on the 3-bar transition (c.g. accelerometer).

Figures 215 through 217 show the longitudinal, transverse, and vertical acceleration-time histories, respectively, computed from the inside the cabin of the vehicle; Figures 218 through 220 show the comparison of the angular rates and angular displacements about the x-, y-, and z-axis from the cabin location. These data are used for calculating the occupant risk metrics. *MASH* does not require that occupant risk be evaluated; however, they are reported herein for completeness (see following section).

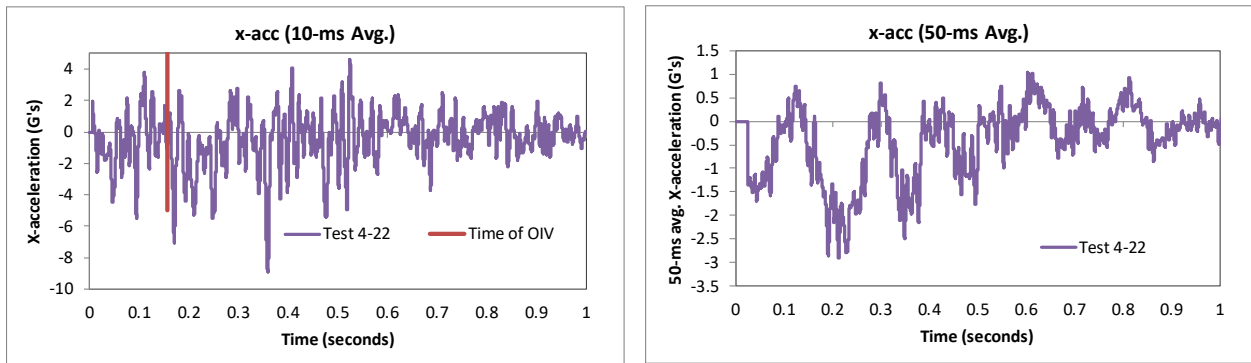


Figure 215. 10- and 50-millisecond average X-acceleration from FEA of Test 4-22 on the 3-bar transition (cabin accelerometer).

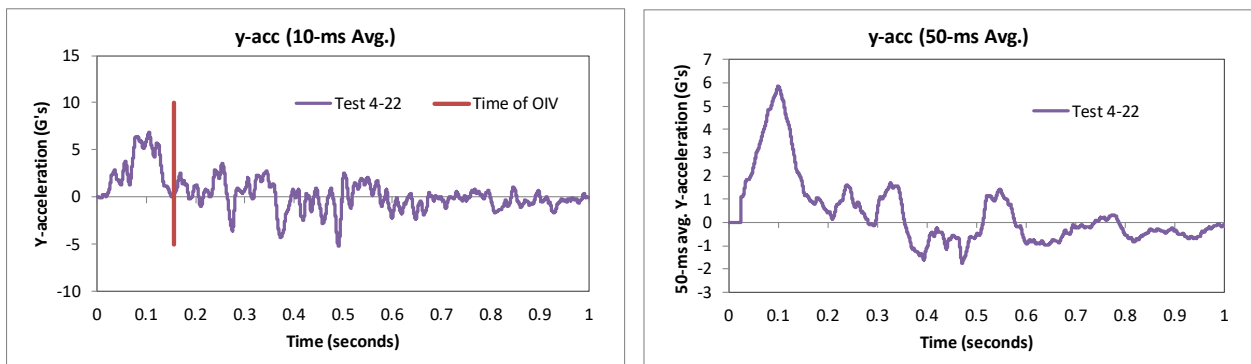


Figure 216. 10- and 50-millisecond average Y-acceleration from FEA of Test 4-22 on the 3-bar transition (cabin accelerometer).

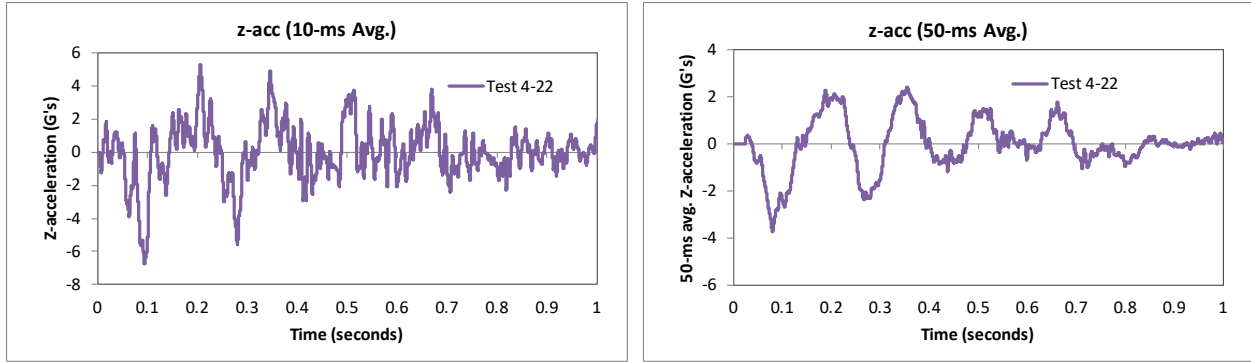


Figure 217. 10- and 50-millisecond average Z-acceleration from FEA of Test 4-22 on the 3-bar transition (cabin accelerometer).

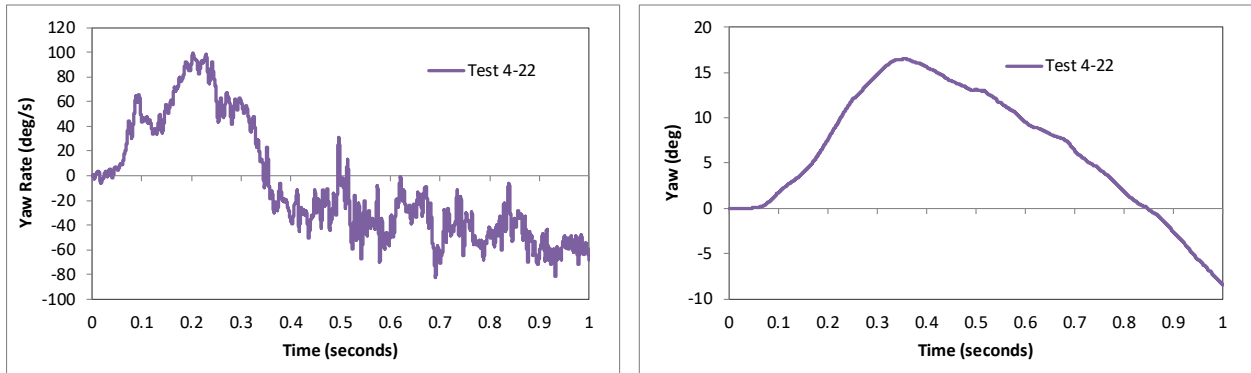


Figure 218. Yaw rate and yaw angle time-history from FEA of Test 4-22 on the 3-bar transition (cabin accelerometer).

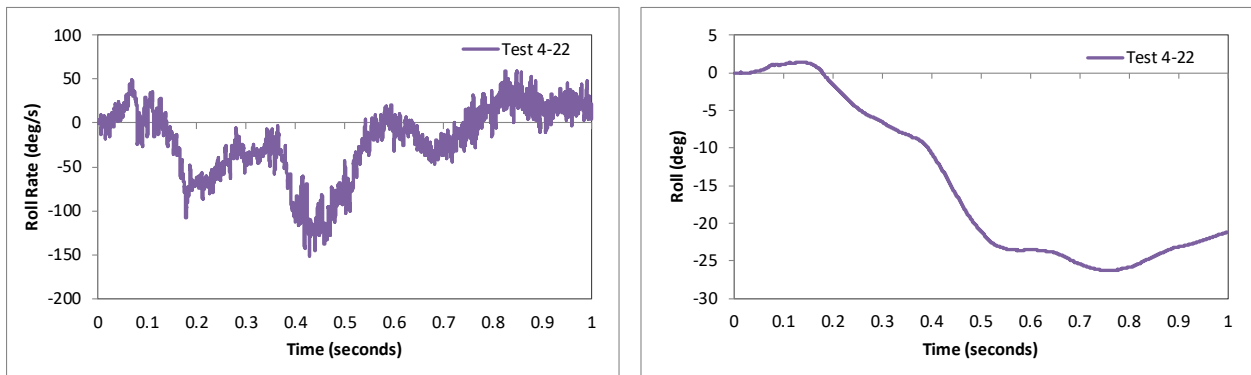


Figure 219. Roll rate and roll angle time-history from FEA of Test 4-22 on the 3-bar transition (cabin accelerometer).

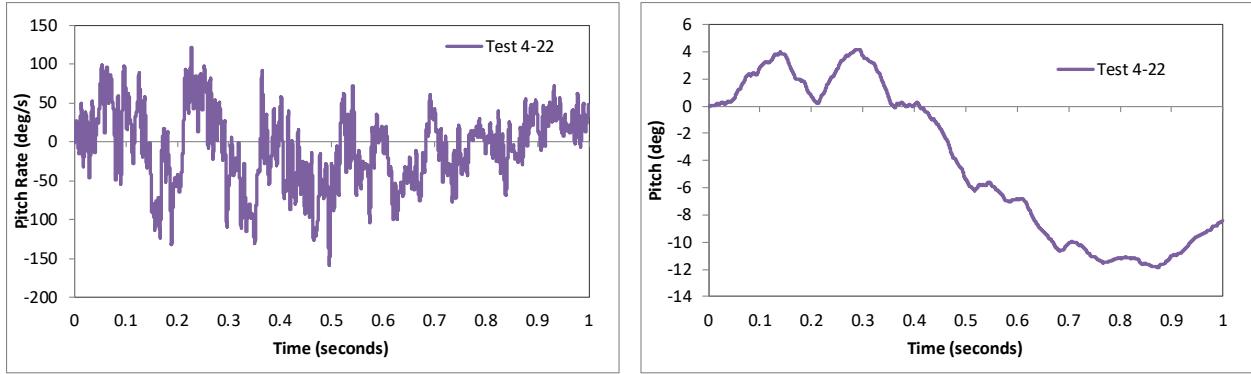


Figure 220. Pitch rate and pitch angle time-history from FEA of Test 4-22 on the 3-bar transition (cabin accelerometer).

10.4.4 Occupant Risk Measures

The acceleration-time histories and angular rate-time histories collected from inside the truck cabin were used to evaluate occupant risk metrics according to the procedures outlined in *MASH*. Table 81 shows the results for the occupant risk calculations. The results indicate that the occupant risk factors met safety criteria specified in *MASH*.

The occupant impact velocities in the longitudinal and transverse directions were 2.3 ft/s and 14.8 ft/s, respectively. The highest 0.010-second occupant ridedown acceleration in the longitudinal and transverse directions were 8.9 g and 5.5 g, respectively. The maximum 50-ms moving average acceleration values in the longitudinal and transverse directions were 2.9 g and 5.9 g, respectively. The maximum roll and pitch angles of the vehicle were 26.3 degrees and 11.9 degrees, respectively. All metrics were within recommended limits specified in *MASH*.

Table 81. Summary of occupant risk metrics for Test 4-22 on the 3-bar transition.

Occupant Risk Factors		MASH	
		Test 4-22	
Occupant Impact Velocity (ft/s)	x-direction	2.3	} < 30 ft/s (preferred) ✓ < 40 ft/s (limit)
	y-direction	-14.8	
	at time	at 0.1553 seconds on left side of interior	
THIV (ft/s)		15.1	
		at 0.1553 seconds on left side of interior	
Ridedown Acceleration (g's)	x-direction	-8.9	} < 15 G (preferred) ✓ < 20.49 G (limit)
	y-direction	-5.5	
		(0.3536 - 0.3636 seconds)	
		(1.4779 - 1.4879 seconds)	
PHD (g's)		9	
		(0.3536 - 0.3636 seconds)	
ASI		0.69	
		(0.0757 - 0.1257 seconds)	
Max 50-ms moving avg. acc. (g's)	x-direction	-2.9	
	y-direction	5.9	
	z-direction	-3.7	
		(0.1877 - 0.2377 seconds)	
		(0.0750 - 0.1250 seconds)	
		(0.0552 - 0.1052 seconds)	
Maximum Angular Disp. (deg)	Roll	-26.3	} < 75 deg ✓
	Pitch	-11.9	
	Yaw	-35.3	
		(0.7569 seconds)	
		(0.8730 seconds)	
		(1.4987 seconds)	

10.4.5 Occupant Compartment Intrusion

The maximum deformation of the occupant compartment for impact on the 3-bar transition was approximately 2.6 inches. The maximum deformation occurred at the lower right-front corner of the toe-pan and the wheel well. Figure 221 shows a view of the vehicle interior

after the impact, with several components removed to facilitate viewing. The maximum deformation was less than the critical limit of 9 inches specified in *MASH* for this area of the occupant compartment.

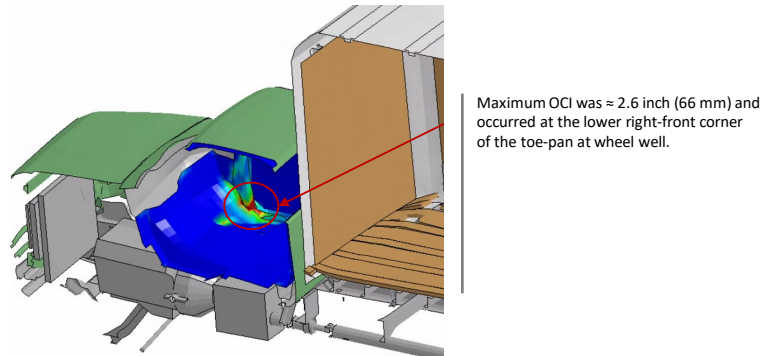


Figure 221. Occupant compartment deformation resulting from Test 4-12 on the NETC 3-bar bridge rail system.

10.4.6 Damages to the Barrier System

Figure 222 shows images of the barrier at the time of maximum deflection with a contour plot of lateral displacement on the rail elements. The maximum dynamic deflection was 4.29 inches and occurred on the top rail at the critical splice connection. Figure 223 shows contour plots of the maximum permanent deflection. The maximum permanent deflection was 2.8 inches.

Maximum dynamic deflection = 4.29 in (109 mm)

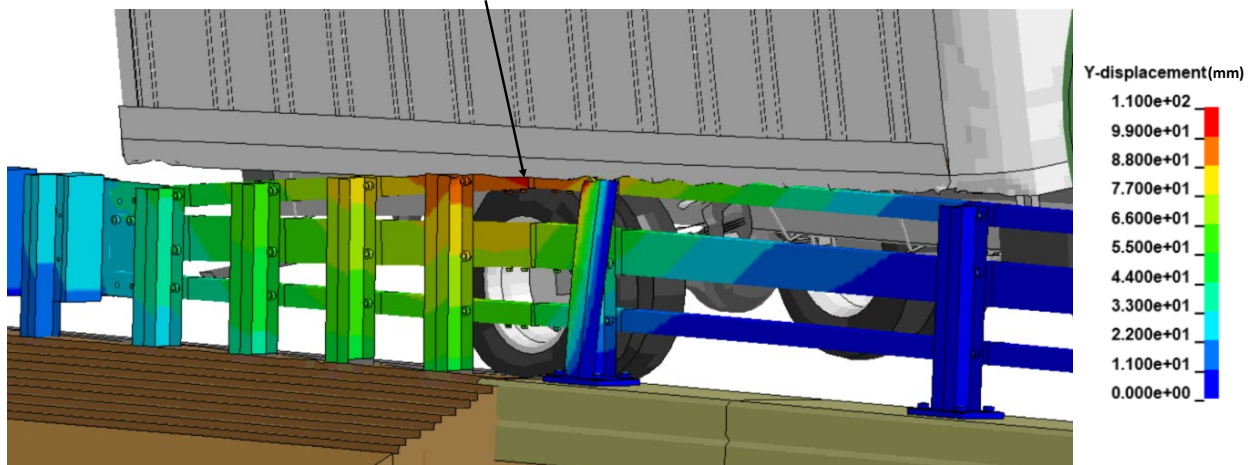


Figure 222. Contour plot of lateral displacement for the 3-bar transition for Test 4-22 at the time of maximum dynamic deflection.

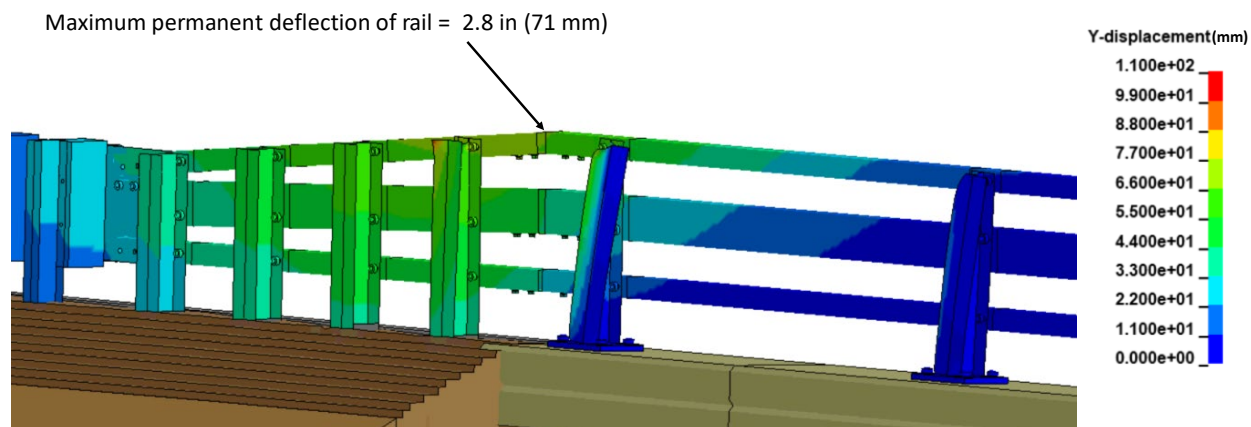


Figure 223. Contour plot of permanent deflection for the 3-bar transition for Test 4-22.

Figure 224 shows contours of true effective plastic strains on the steel components of the transition and bridge rail. The plastic deformations were primarily limited to the top of Post 1 of the transition and to the three bridge rail posts. The plastic deformations of the transition rail elements were minimal. The damage to the posts were due to the bottom of the cargo-box snagging on the top of the posts. This caused torque rotation and lateral deformation of the posts. There was also soil displacement at transition Posts 1 through 6.

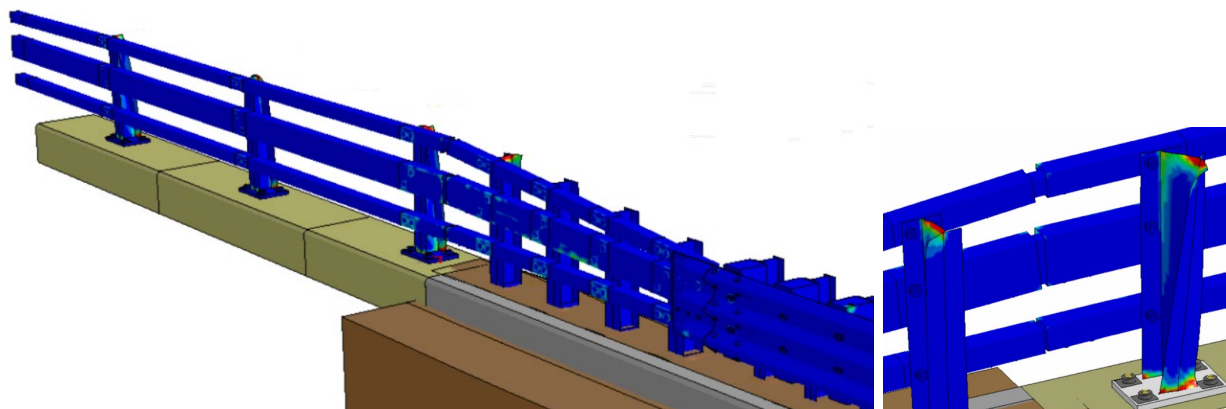


Figure 224. Contours of effective plastic strains on the transition and bridge rail for Test 4-22 on the 3-bar transition.

The vehicle was in contact with the barrier from the point of contact until the truck box slid off the end of the bridge rail at 0.55 seconds. The maximum working width prior to exiting the barrier was 3.9 ft resulting from the top of the cargo box extending over the bridge rail, as illustrated in Figure 225.

10.4.7 Peak Forces on Barrier

The longitudinal, lateral and resultant force-time history results are shown in Figure 226 including the force data filtered with cutoff frequency of 60 Hz. The maximum impact forces occurred when the rear tandem wheel set impacted against the transition, with approximate magnitudes of 38 kips, 75 kips, and 80 kips for the longitudinal, lateral and resultant components, respectively.

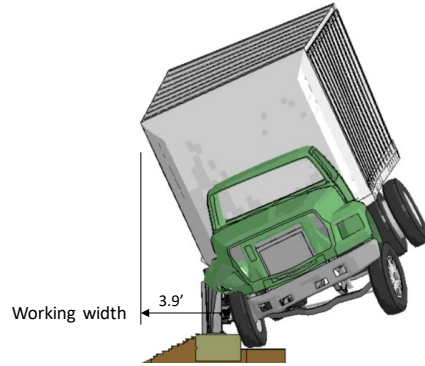


Figure 225. Working width for Test 4-22 on 3-bar transition.

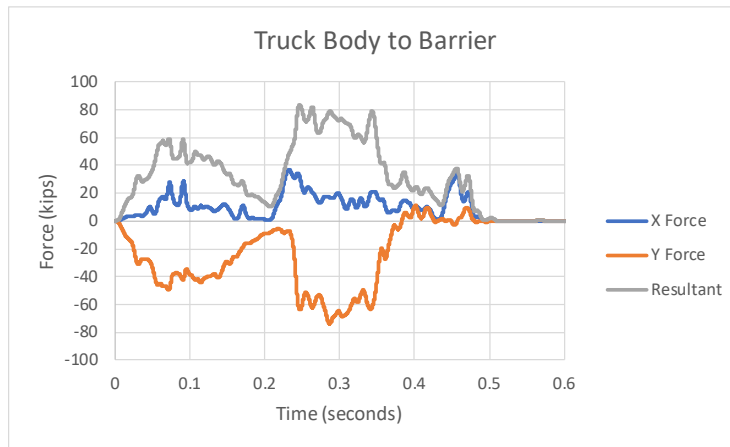


Figure 226. Longitudinal, lateral and resultant force-time history between vehicle and barrier for Test 4-22 on the 3-bar transition.

10.4.8 Damages to Vehicle

Figure 227 shows contour plots of effective plastic strain for the vehicle, which were used to identify areas of the vehicle that suffered damage during the simulated impact event. The damages to the truck included the front bumper, the front fender, the front impact-side suspension, the front axle and wheel, and rear wheel. The damages to the cargo-box included lower-front corner of the box, the lateral floor beams, main bed rail, wood flooring, and the exterior lower side-rail of the box.

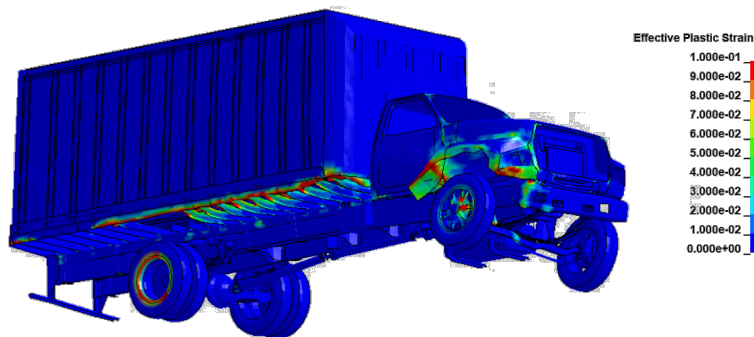


Figure 227. Damages to vehicle in Test 4-22 analysis of the 3-bar transition.

10.4.9 Exit Box

Figure 228 shows the exit box for Test 4-22 on the 3-bar transition. Although the exit box analysis is not required in *MASH*, it was included here for completeness. The vehicle was smoothly redirected, and the vehicle path was well within the exit box criteria of *MASH*. The vehicle remained upright during the 1.5 seconds of the impact evaluated; however, the roll rate at the termination of the analysis indicated that it was probable that the vehicle would roll onto its side.

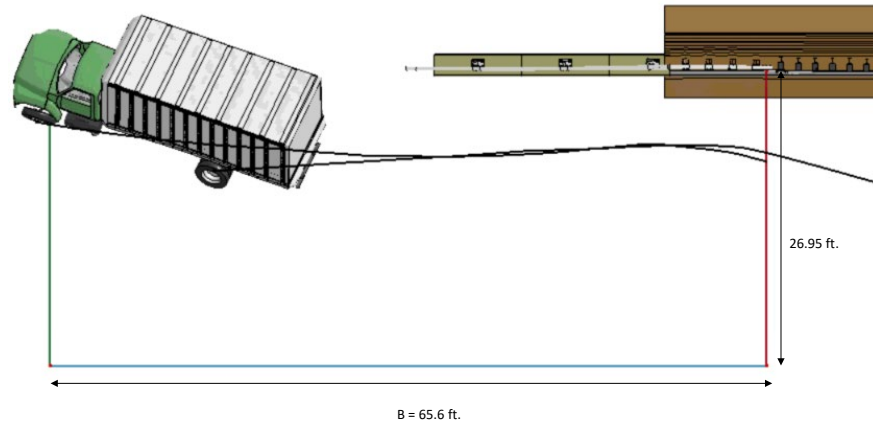


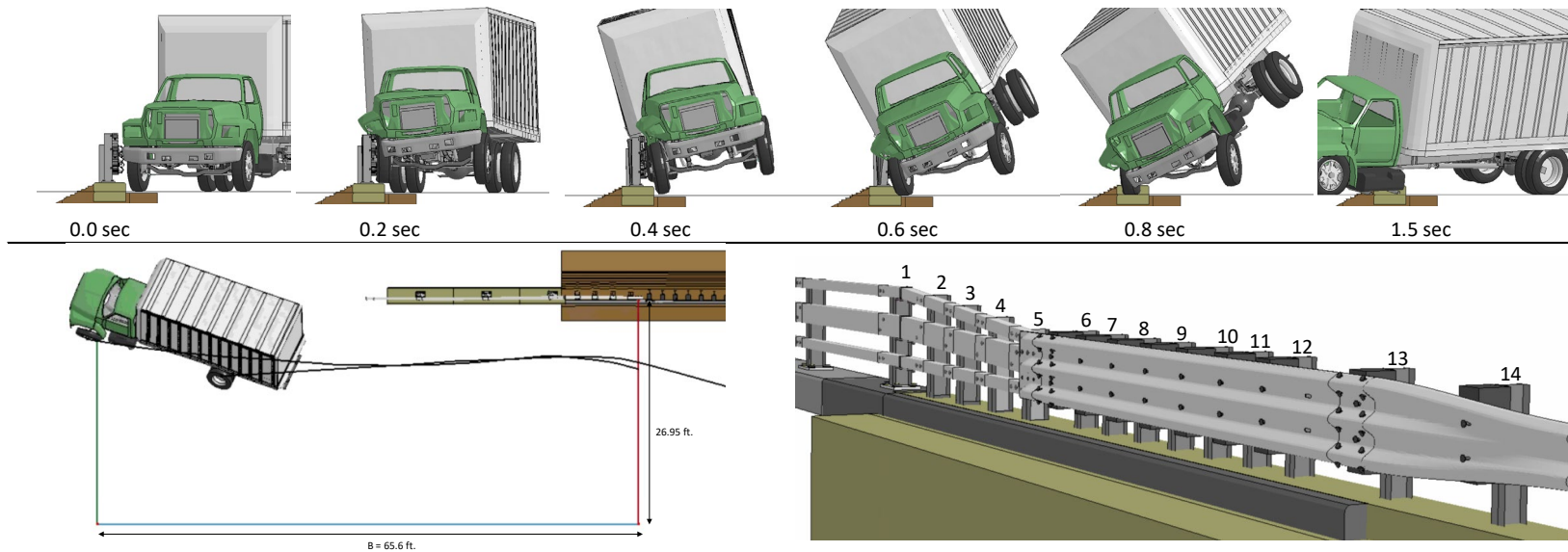
Figure 228. Exit box for Test 4-22 for the 3-bar transition.

10.4.10 Test 4-22 Results Summary

A summary of the *MASH* Test 4-22 results on the 3-bar transition is shown in Table 82 and Figure 229. The barrier adequately contained and redirected the 10000S vehicle (single unit truck) with low to moderate damage to the transition. The damages to the bridge rail posts were significant due to the bottom of the cargo-box leaning over the rail and snagging on the tops of the posts. The maximum dynamic and permanent deflections of the railing were 4.3 inches and 2.8 inches, respectively. There were no detached elements from the barrier that showed potential for penetrating the occupant compartment or presenting undue hazard to other traffic. The vehicle remained upright during the 1.5 seconds of the impact evaluated; however, the roll rate at the termination of the analysis indicated that it was probable that the vehicle would roll onto its side. It is preferred that the vehicle remain upright, but not required. Based on the results of this analysis, the barrier meets all structural and occupant risk criteria in *MASH* for Test 4-22 impact conditions.

Table 82. Summary of *MASH* Test 4-12 results on the curb-mounted bridge rail.

Evaluation Factors	Evaluation Criteria	Results
Structural Adequacy	A Test article should contain and redirect the vehicle or bring the vehicle to a controlled stop; the vehicle should not penetrate, underride, or override the installation although controlled lateral deflection of the test article is acceptable.	Pass
Occupant Risk	D Detached elements, fragments, or other debris from the test article should not penetrate or show potential for penetrating the occupant compartment, or present undue hazard to other traffic, pedestrians, or personnel in a work zone. Deformations of, or intrusions into, to occupant compartment should not exceed limits set forth in Section 5.2.2 and Appendix E.	Pass
	G It is <u>preferable, although not essential</u> , that the vehicle remain upright during and after collision.	Probable Fail



General Information		Impact Conditions		Max50-millisecond Avg. (G)	
Analysis Agency	Roadsafe LLC	Speed	56 mph	Longitudinal	2.9 g
Test Standard Test No.	MASH Test 4-22	Angle	15 degrees	Lateral	5.9 g
Analysis No.	NETC18_3BarTrans_T422	Location	9.0 feet upstream of bridge rail	Vertical	3.7 g
Analysis Date	4/20/2019	Impact Severity	155.6 kip-ft	Test Article Deflections (in)	
Test Article		Exit Conditions		Dynamic	7.6 inches
Type	Bridge Rail Transition	Speed	44.4 mph	Permanent	5.7 inch
Name	NETC 3-Bar Transition	Angle	5.5 degrees toward barrier	Working Width	23.3 inches
Installation Length	65.8 feet	Time	0.6 seconds	Max. OCI	≈1 inch
Material or Key Elements		Occupant Risk Values		Vehicle Stability	
Soil Type and Condition	MASH Strong Soil	Longitudinal OIV	2.3 ft/s	Roll	*26.3 degrees
Analysis Vehicle		Lateral OIV	14.8 ft/s	Pitch	11.9 degrees
Type / Designation	10000S	Longitudinal ORA	8.9 g	Yaw	-35.3 degrees
FEA Model name	F800_No-Box_181114_UboltF0p17	Lateral ORA	5.5 g	<i>* Value corresponds to peak roll angle during interaction with barrier. At termination of analysis, the vehicle was rolling the opposite direction and 90 degree roll was considered probable.</i>	
	502_TruckBox_181114	THIV	15.1 ft/s		
Mass	22,198 lb	PHD	9.0 g		
		ASI	0.69		

Figure 229. Summary results for MASH Test 4-22 on the 3-bar transition.

10.5 Conclusions for *MASH* TL4 Evaluation of the 3-Bar Transition

Based on the results of this analysis, the 3-bar transition is expected to meet all structural and occupant risk criteria in *MASH* Test Level 4.

10.5.1 *Structural Adequacy: (PASS)*

- The barrier successfully contained and redirected the vehicle in all test cases.
- There was low-to-moderate damage to the transition in all cases.
- Test 4-22 resulted in the bottom of the cargo-bed contacting and snagging on the tops of the bridge rail posts and deforming those posts.

10.5.2 *Occupant Risk (PASS)*

- Occupant compartment intrusion was well below allowable limits for all cases
- OIV and ORA
 - Test 4-20 (small car): OIV and ORA were within preferred limits (values highly dependent on time of occupant impact); however, peak accelerations were below critical limits throughout the acceleration-time history.
 - Test 4-21 (pickup): OIV was within preferred limits; ORA was within critical limits

10.5.3 *Vehicle Trajectory (PASS)*

- Vehicle remained upright through impact and redirection.
- Roll and Pitch for Tests 4-20 (small car) and 4-21 (pickup) were relatively low.
- Roll and pitch for Test 4-22 (SUT) were relatively high. Final vehicle stability was undetermined at 1.5 seconds; however, *MASH* states that it is preferred that the vehicle remain upright, but it is not required.

11 EVALUATION OF THE NETC 4-BAR BRIDGE RAIL FOR *MASH* TL4

The FEA model of the sidewalk-mounted NETC 4-bar bridge rail was developed and validated in Section 6. The model was updated with modifications described in Section 9, including:

- Updated splice model (refer to Figure 54),
- Moved rail splice to opposite side of post to permit CIP for splice from primary direction impact, and
- Revised anchor plate model.

The FEA model for the NETC 4-bar bridge rail is shown in Figure 230. The dimensions of the sidewalk and reinforcing were modeled based on the NHDOT design (refer to Appendix B), as illustrated in Figures 56 and 57. To maximize the potential for snags on the tube-rail splice, reverse-direction impact cases were simulated by moving the splice to the opposite side of the post, as described in Section 9.

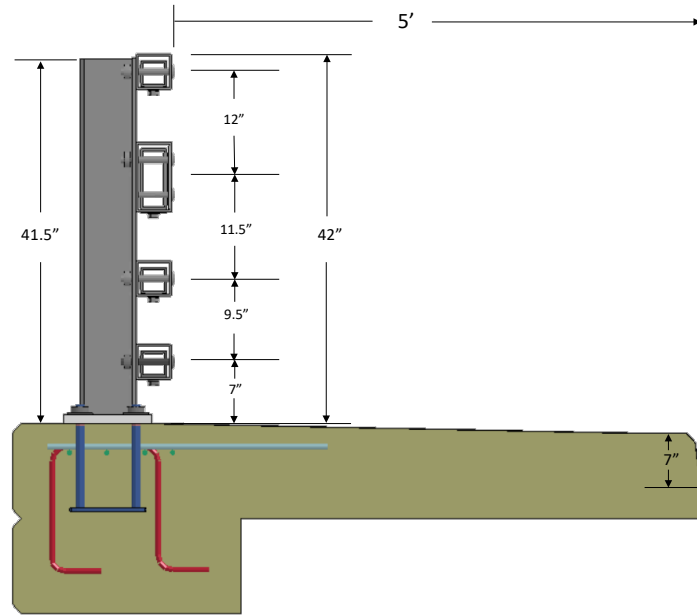


Figure 230. FEA model of sidewalk-mounted NETC 4-Bar bridge rail.

FEA was used to evaluate the crash performance of the NETC 4-bar bridge rail based on structural adequacy, vehicle stability during and after redirection, and occupant risk factors using criteria specified in *MASH* for Test Level 4. Three impact cases were evaluated:

- Simulation of Test 4-10 included the 1100C Yaris model ballasted to 2,595 lb (1177 kg) impacting the barrier at 62.2 mph and 25 degrees. The critical impact point was selected as 3.6 feet (1.1 m) upstream of a bridge rail post.
- Simulation of Test 4-11 included the 2270P Chevrolet Silverado model ballasted to 5,001lb (2,269 kg) impacting the railing at 62.2 mph and 25 degrees. The critical impact point was selected as 4.3 feet (1.3 m) upstream of a bridge rail post.
- Simulation of Test 4-12 included the 10000S model ballasted to 22,198 lb (10,068 kg) impacting at 56 mph and 15 degrees. Cargo-bed height = 47.5 inches. The impact point was set to 5.0 feet (1.52 m) upstream of a bridge rail post.

The analysis in all cases was performed using LS-DYNA version mpp_s_R8.0.0 revision number 95309. The analysis was conducted with a time-step of 1.0 microsecond for a time period of 0.8 seconds for Test 4-10, 1.0 seconds for Test 4-11, and 1.5 seconds for Test 4-12.

11.1 Test 4-10

The critical impact condition for Test 4-10 was selected based the *MASH* recommended CIP for rigid barrier tests with a target impact point of 3.6 feet upstream of Post 7 to maximize potential for snagging at the post, while also providing adequate opportunity for snag at the splice connection the tubular rails.[*AASHTO16*] The splice is located 1.5 feet upstream of the post. The vehicle was backed up to the face of the sidewalk curb, as shown in Figure 231, for the initial start point of the impact event. After crossing the curb, the vehicle struck the bridge at 3.8 feet upstream of Post 7, as shown in Figure 232. The following sections provide a summary of the results and include a commentary describing the timing and occurrence of various events

during the simulated impact, time-history data evaluation, occupant risk assessments, and damages sustained by both the barrier and vehicle.

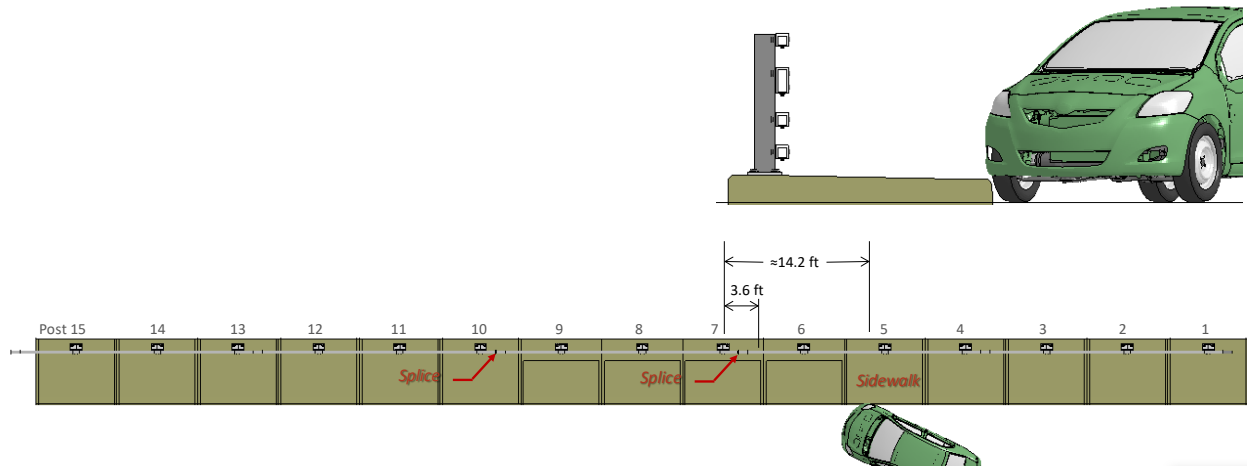


Figure 231. Initial starting point and target impact point for Test 4-10 on the NETC 4-bar bridge rail.

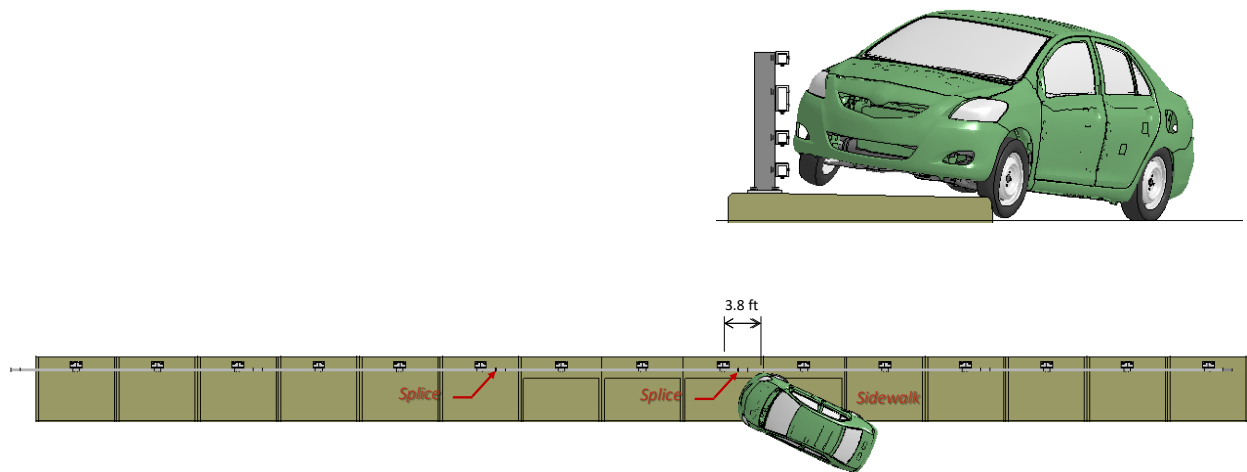


Figure 232. Actual impact point on barrier for test 4-10 on the NETC 4-bar bridge rail.

11.1.1 Summary of Key Phenomenological Events

The sequential views of the impact event are shown in Appendix Q in Figures Q-1 through Q-3 from an overhead viewpoint, downstream and upstream viewpoint, and oblique viewpoint, respectively.

The front impact side tire of the vehicle model struck the sidewalk curb within a few milliseconds of the start of the analysis at a speed and angle of 62.1 mph and 25 degrees, respectively. At 0.005 seconds, the front-right tire compressed at the point of contact with the curb, and at 0.01 seconds the wheel rim was noticeably deformed from the impact. At 0.03 seconds the tire had fully mounted the sidewalk and the vehicle began to roll away from the barrier. The tire was, at this time, compressed fully flat. The ability of the tire to deflate was not incorporated into the model; therefore, the tire immediately began to rebound from the top of the sidewalk and lift the front of the vehicle. The rear-right tire began to lift off the ground at 0.06 seconds. At 0.065 seconds the front-right tire rebounded off the sidewalk. At 0.095 seconds, the

rear-right tire contacted the curb and was fully mounted onto the sidewalk at 0.115 seconds. Also, at this time, the front-left tire impacted against the curb face of the sidewalk. At 0.125, the front-left rim was significantly deformed at the point of contact with the curb; also, at this time, the rear-right tire rebounded off the sidewalk. At 0.13 seconds the lower edge of the front bumper contacted the lower-middle railing of the barrier 3.8 ft upstream of Post 7 traveling at 60.3 mph and 24.9 degrees. Immediately afterward, the front fender contacted the upper-middle railing and the front-right tire contacted the lower railing. At 0.145 seconds the front-right tire was fully mounted on the sidewalk. Also, at this time, Post 7 began to deflect back. At 0.155 seconds the vehicle's right fender was fully engaged with the top railing and the front-right tire was steered parallel to the barrier. At 0.17 seconds the front-left tire rim snagged on the rail tube at the splice connection resulting in maximum vehicle accelerations peaks of 21.6 G and 25.8 G in the longitudinal and lateral directions, respectively. At 0.19 seconds Post 7 reached maximum dynamic deflection of 2.57 inches, and the vehicle reached peak roll angle of 10.8 degrees away from the barrier. At 0.1971 seconds the vehicle occupant contacted the right side of the interior with OIV's in the longitudinal and lateral directions of 24.0 ft/s and of 31.5 ft/s, respectively. At 0.2 seconds the vehicle reached a peak pitch angle of 4.3 degrees (front pitching upward). At 0.206 seconds the maximum ORA in the longitudinal direction occurred with magnitude 7.1 G. At 0.25 seconds the front of the car lost contact with the barrier as the rear of the vehicle continued to yaw toward the barrier. At 0.294 seconds the vehicle was parallel to the barrier. At 0.32 seconds the rear fender of the car contacted the upper-middle rail just downstream of Post 7. At 0.325 seconds the rear-right tire contacted the lower and lower-middle railings. At 0.352 seconds the maximum ORA in the lateral direction occurred with magnitude 10.3 G. At 0.4 seconds the vehicle lost contact with the barrier traveling at 43.4 mph with an exit angle of 13.3 degrees (53 percent of the impact angle). At 0.603 seconds the vehicle reached maximum pitch angle of 6.5 degrees (rear pitching up). At 0.7 seconds the vehicle reached maximum roll angle of 10.9 degrees (rolling away from the barrier). The vehicle remained stable throughout post-impact trajectory. The analysis ended at 0.8 seconds, at which time:

- The roll, pitch, and yaw of the vehicle were, respectively, 7.1 degrees (toward barrier), 2.6 degrees (rear pitching up), and 51.8 degrees (26.8 degrees relative to and away from barrier).
- The forward velocity of the vehicle was 43.2 mph (69.5 km/h).

11.1.2 Time History Data Evaluation

Figures 233 through 235 show the longitudinal, transverse, and vertical acceleration-time histories, respectively, computed from the center of gravity of the vehicle; Figures 236 through 99 show the comparison of the angular rates and angular displacements (i.e., yaw, roll and pitch) at the center of gravity of the vehicle.

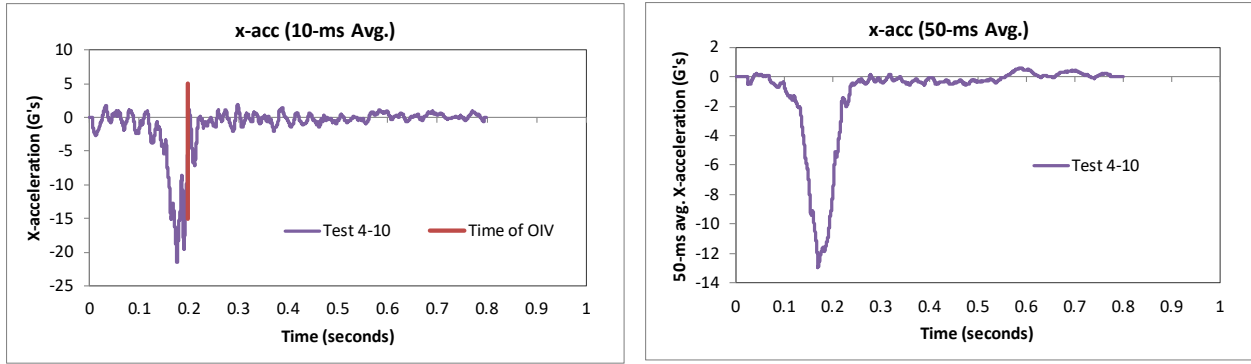


Figure 233. 10- and 50-millisecond average X-acceleration from FEA of Test 4-10 on the NETC 4-bar bridge rail.

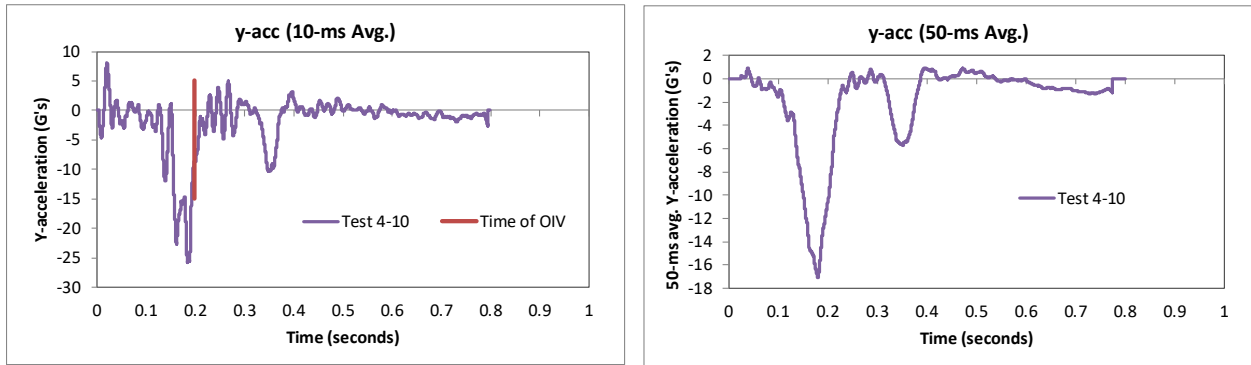


Figure 234. 10- and 50-millisecond average Y-acceleration from FEA of Test 4-10 on the NETC 4-bar bridge rail.

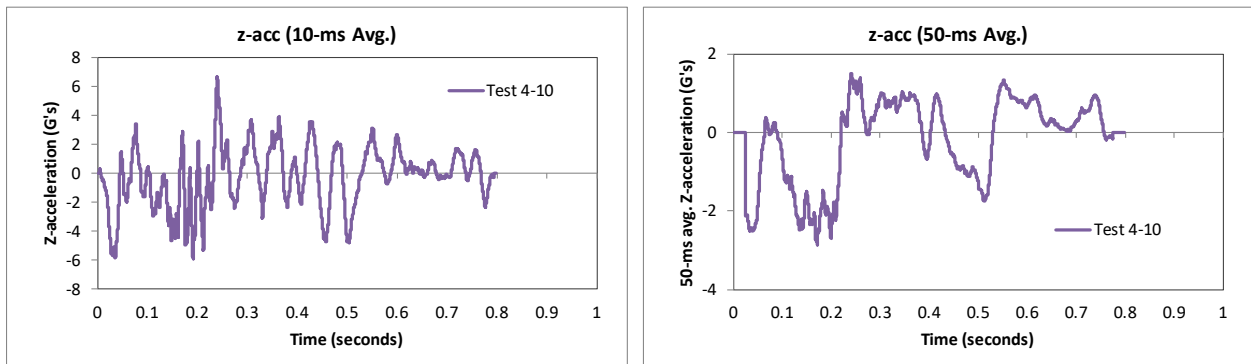


Figure 235. 10- and 50-millisecond average Z-acceleration from FEA of Test 4-10 on the NETC 4-bar bridge rail.

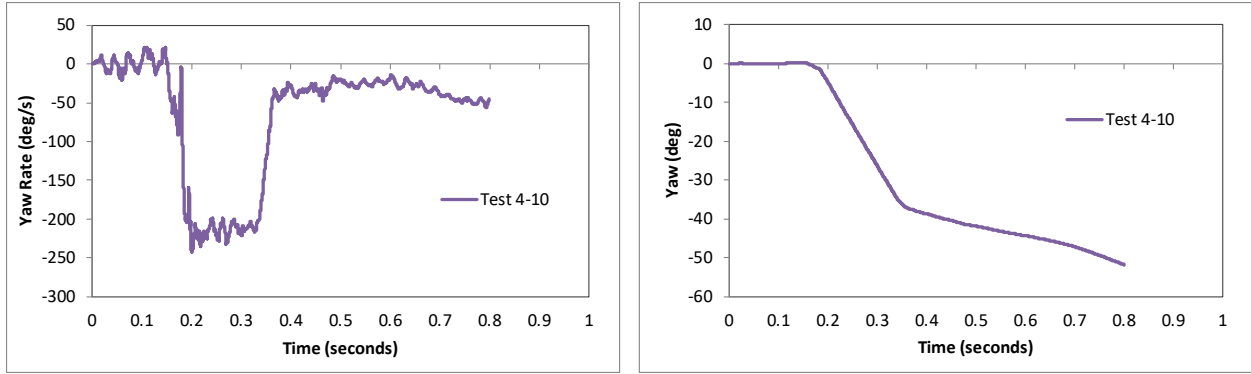


Figure 236. Yaw rate and yaw angle time-history from FEA of Test 4-10 on the NETC 4-bar bridge rail.

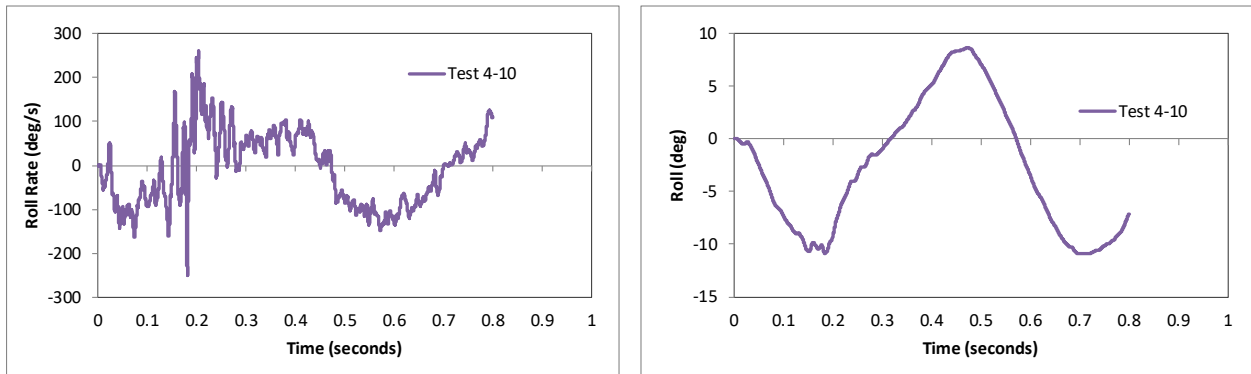


Figure 237. Roll rate and roll angle time-history from FEA of Test 4-10 on the NETC 4-bar bridge rail.

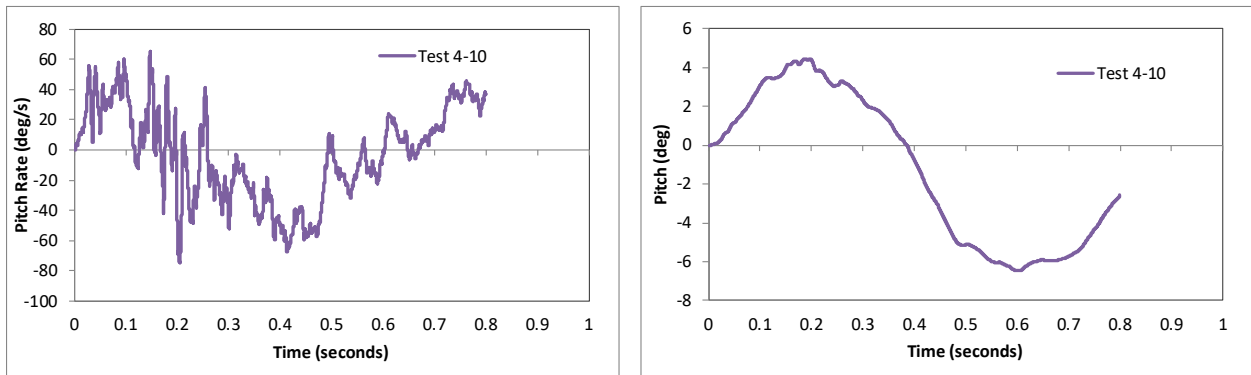


Figure 238. Pitch rate and pitch angle time-history from FEA of Test 4-10 on the NETC 4-bar bridge rail.

11.1.3 Occupant Risk Measures

The acceleration-time histories and angular rate-time histories collected at the center of gravity of the vehicle were used to evaluate occupant risk metrics according to the procedures outlined in *MASH*. Table 83 shows the results for the occupant risk calculations. The results indicate that the occupant risk factors meet safety criteria specified in *MASH*.

The occupant impact velocities in the longitudinal and transverse directions were 24.0 ft/s and 31.5 ft/s, respectively, which were within critical limits specified in *MASH*. The highest

0.010-second occupant ridedown acceleration in the longitudinal and transverse directions were 7.1 g and 10.3 g, respectively, which were within preferred limits specified in *MASH*. However, as in previous test 4-10 cases, these values are highly dependent on time of occupant impact with the interior, as shown in Figures 233 and 234. The maximum 50-ms moving average acceleration values in the longitudinal and transverse directions were 12.9 g and 17.1 g, respectively. The maximum roll and pitch angles of the vehicle were 10.9 degrees and 6.5 degrees, respectively, which were well below critical limits in *MASH*.

Table 83. Summary of *MASH* occupant risk metrics for Test 4-10 on the NETC 4-bar bridge rail.

Occupant Risk Factors		MASH T4-10	
		NETC 3-Bar	
Occupant Impact Velocity (ft/s)	x-direction	24.0	} > 30 ft/s (preferred) < 40 ft/s (limit) ✓
	y-direction	31.5	
	at time	at 0.1971 seconds on right side of interior	
THIV (ft/s)		39.4	
		at 0.1971 seconds on right side of interior	
Ridedown Acceleration (g's)	x-direction	-7.1	} < 15 G (preferred) ✓ < 20.49 G (limit)
	y-direction	-10.3	
		(0.2064 - 0.2164 seconds)	
		(0.3473 - 0.3573 seconds)	
PHD (g's)		10.3	
		(0.3473 - 0.3573 seconds)	
ASI		2.14	
		(0.1550 - 0.2050 seconds)	
Max 50-ms moving avg. acc. (g's)	x-direction	-12.9	} < 75 deg ✓
	y-direction	-17.1	
	z-direction	-2.9	
		(0.1453 - 0.1953 seconds)	
		(0.1550 - 0.2050 seconds)	
		(0.1463 - 0.1963 seconds)	
Maximum Angular Disp. (deg)	Roll	-10.9	} < 75 deg ✓
	Pitch	-6.5	
	Yaw	-51.8	
		(0.6998 seconds)	
		(0.6029 seconds)	
		(0.7996 seconds)	

11.1.4 Occupant Compartment Intrusion

The maximum deformation of the occupant compartment was approximately 3.4 inches at the lower right-front corner of the toe-pan at the wheel well. Figure 239 shows a view of the vehicle interior after the impact, with several components removed to facilitate viewing. The deformation was less than the critical limit of 9 inches specified in *MASH* for this area of the occupant compartment.

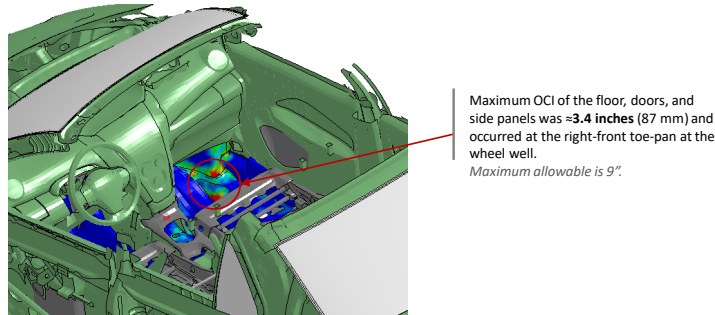


Figure 239. Occupant compartment deformation resulting from Test 4-10 on the NETC 4-bar bridge rail.

11.1.5 Damages to the Barrier System

The damages to the barrier were low with the highest deflection occurring on the top railing at the splice connection upstream of the Post 7. Figure 240 and Figure 241 show images of the maximum dynamic deflection and permanent deflection of the barrier, respectively, with a contour plot of lateral displacement on the rail elements. The maximum dynamic and permanent deflections were 2.8 inches and 1.25 inches, respectively, and occurred at the top tube rail at the splice.

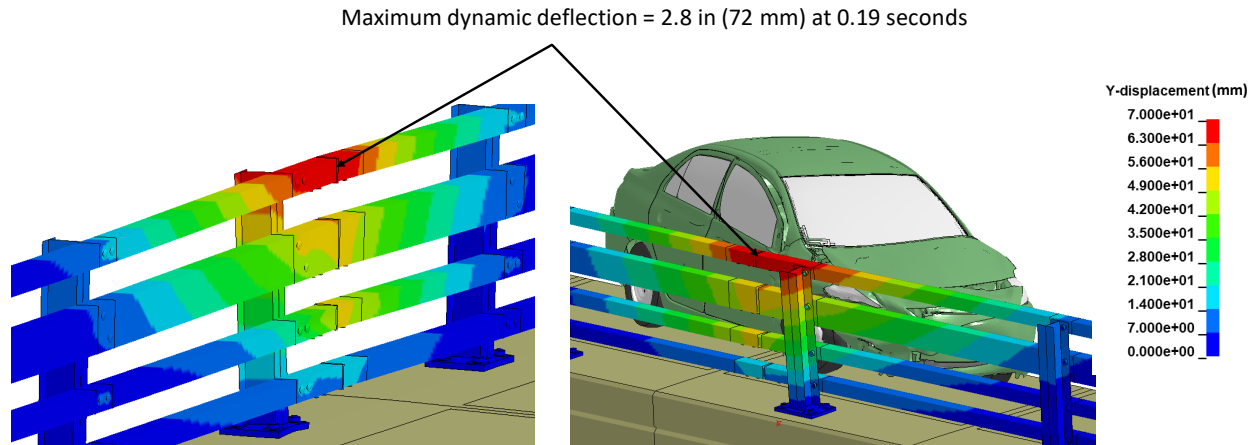


Figure 240. Contour plot of lateral displacement for the bridge rail for Test 4-10 at the time of maximum dynamic deflection.

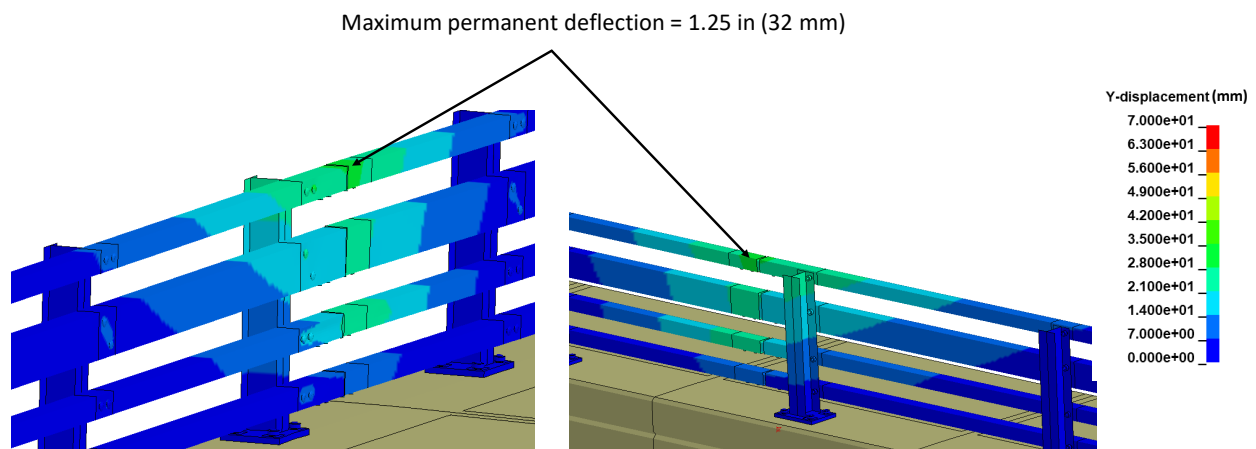


Figure 241. Contour plot of maximum permanent deflection of the bridge rail for Test 4-10.

Figure 242 shows contours of true effective plastic strains on the bridge rail. There was low to moderate damage to the post, and baseplate and rails. The damage was primarily limited to plastic deformations of the lower-middle rail at the splice connection, as well as, the post and the baseplate at Post 7. The maximum vertical dynamic deflection of the baseplate was 0.41 inches (10.5 mm) and the maximum permanent deflection of the baseplate was 0.18 inches (4.5 mm).

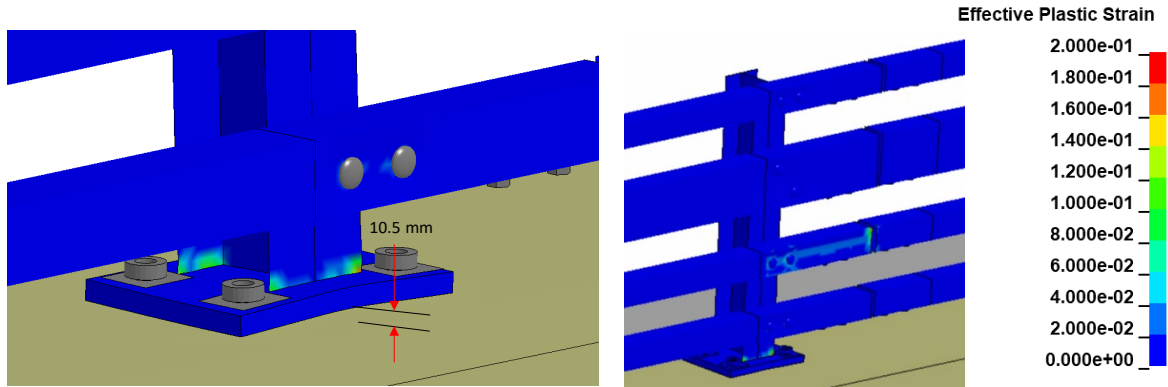


Figure 242. Contours of effective plastic strains for Test 4-10 on the NETC 4-bar bridge rail.

Figure 243 shows contours of 1st principal strain with contours cut off at strains of 0.1. The 1st Principal strain values for the concrete in these cases was 0.046 dynamic strain and was 0.0 permanent, which indicates a relatively low probability for concrete failure.

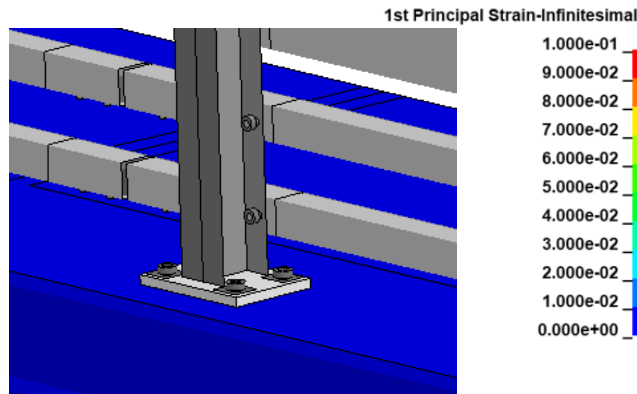


Figure 243. Contours of 1st principal strains for concrete at the critical post for Test 4-10 on the NETC 4-bar bridge rail.

11.1.6 Damages to Vehicle

Figure 244 shows contour plots of effective plastic strain for the vehicle, which were used to identify areas of the vehicle that suffered damage during the simulated impact event. The most severe damages were to the front fender, the upper and lower control arm of front suspension, front wheel, and the leading edge of the front door on the impact side.

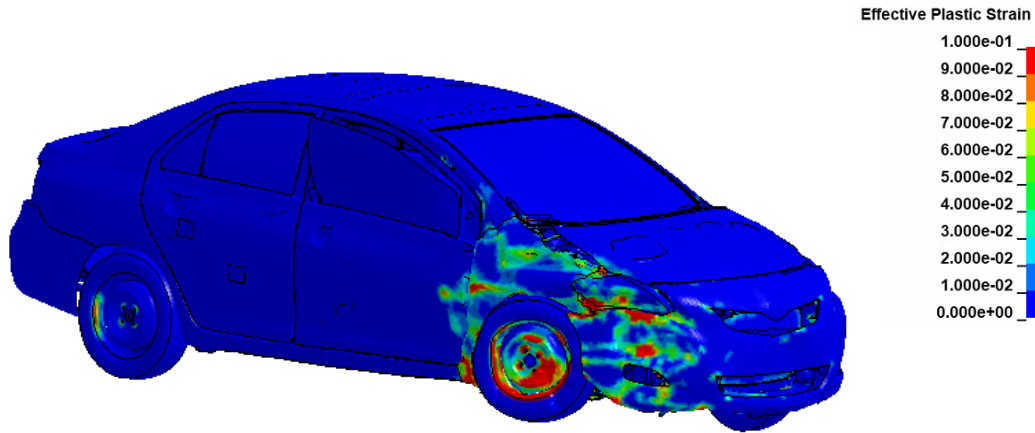


Figure 244. Damages to vehicle in Test 4-10 analysis of the NETC 4-bar bridge rail.

11.1.7 Exit Box

Figure 245 shows the exit box for Test 4-10 on the bridge rail, where the vehicle was smoothly redirected, and its path was well within the exit box criteria of *MASH*.

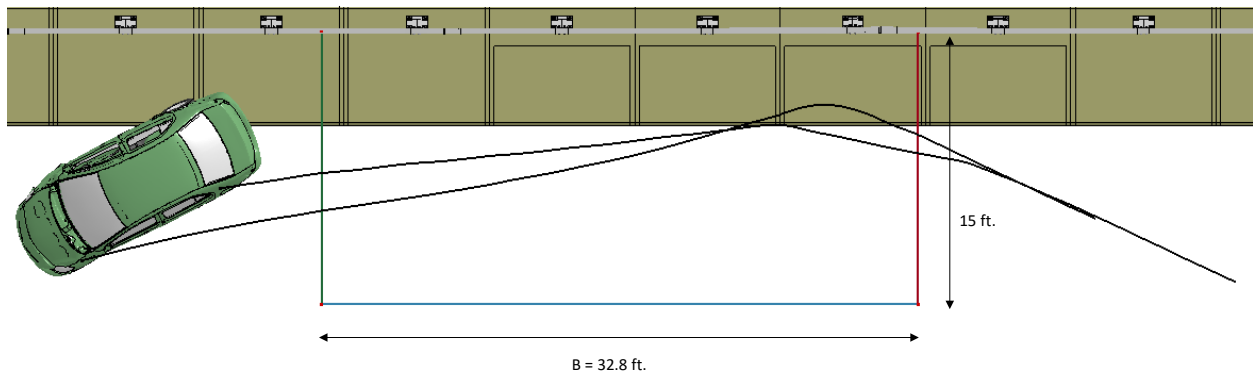


Figure 245. Exit box for Test 4-10 analysis of the NETC 4-bar bridge rail.

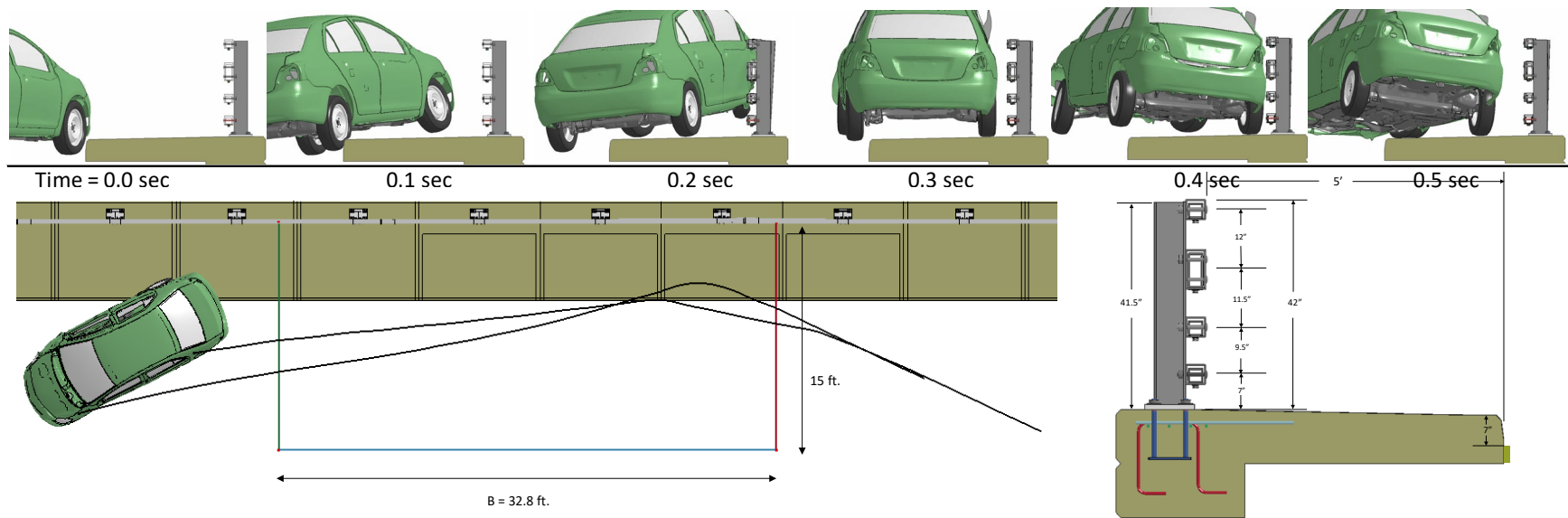
11.1.8 Results Summary

A summary of the *MASH* Test 4-10 results on the NETC 4-bar bridge rail is shown in Table 84 and Figure 246. The barrier successfully contained and redirected the small car with minimal damage to the system. There were no detached elements from the barrier that showed potential for penetrating the occupant compartment or presenting undue hazard to other traffic. The vehicle remained upright and very stable throughout impact and redirection. The OIV was within critical limits and the maximum ORA values were within recommended limits specified in *MASH*. Based on the results of this analysis, the barrier meets all structural and occupant risk criteria in *MASH* for Test 4-10 impact conditions.

As discussed in Section 11.1.1, the trajectory of the vehicle was affected by the tire rebound after it impacted and traversed the sidewalk. The tire model for this vehicle is very simplistic and does not have enough detail to accurately simulate tire compression, debanding and/or deflation. It is expected that the vehicle would likely impact much lower on the bridge rail in a full-scale test, in which the barrier damage and vehicle response would be similar to that reported for the NETC 3-bar bridge rail in Section 9.1.

Table 84. Summary of *MASH* Test 4-10 results on the NETC 4-bar bridge rail.

Evaluation Factors	Evaluation Criteria	Results
Structural Adequacy	A Test article should contain and redirect the vehicle or bring the vehicle to a controlled stop; the vehicle should not penetrate, underide, or override the installation although controlled lateral deflection of the test article is acceptable.	Pass
Occupant Risk	D Detached elements, fragments, or other debris from the test article should not penetrate or show potential for penetrating the occupant compartment, or present undue hazard to other traffic, pedestrians, or personnel in a work zone. Deformations of, or intrusions into, to occupant compartment should not exceed limits set forth in Section 5.2.2 and Appendix E.	Pass
	F The vehicle should remain upright during and after collision. The maximum roll and pitch angles are not to exceed 75 degrees.	Pass
	H The longitudinal and lateral occupant impact velocity (OIV) shall not exceed 40 ft/s (12.2 m/s), with a preferred limit of 30 ft/s (9.1 m/s)	Pass
	I The longitudinal and lateral occupant ridedown acceleration (ORA) shall not exceed 20.49 G, with a preferred limit of 15.0 G	Pass



General Information		Impact Conditions		Max50-millisecond Avg. (G)	
Analysis Agency	Roadsafe LLC	Speed	62 mph	Longitudinal	12.9 g
Test Standard Test No.	MASH Test 4-10	Angle	25 degrees	Lateral	17.1 g
Analysis No.	NETC18_4BarBR_T410	Location	3.6 ft upstream of Post 7	Vertical	2.9 g
Analysis Date	4/10/2019				
Test Article		Impact Severity		Test Article Deflections (in)	
Type	Bridge Rail	59.5 kip-ft		Dynamic	2.8 inches
Name	NETC 4-Bar	Exit Conditions		Permanent	1.25 inches
Installation Length	120 feet	Speed	43.4 mph	Working Width	
Material or Key Elements		Angle	13.3 degrees		
		Time	0.4 seconds		
Soil Type and Condition		N.A.		Max. OCI	
				3.4 inch	
Analysis Vehicle		Occupant Risk Values		Vehicle Stability	
Type / Designation	1100C	Longitudinal OIV	24.0 ft/s	Roll	10.9 degrees
FEA Model name	510_YarisC_V1I_R180228	Lateral OIV	31.5 ft/s	Pitch	6.5 degrees
Mass	2,595 lb	Longitudinal ORA	7.1 g	Yaw	51.8 degrees
		Lateral ORA	10.3 g		
		THIV	39.4 ft/s		
		PHD	10.3 g		
		ASI	2.14		

Figure 246. Summary results for MASH Test 4-10 on the NETC 4-bar bridge rail.

11.2 Test 4-11

The critical impact condition for *MASH* Test 4-11 was selected based the *MASH* recommended CIP for rigid barrier tests. The target impact point was 4.3 feet upstream of Post 7, as shown in Figure 130, and was selected to maximize potential for snagging at the post, while also providing adequate opportunity for snag at the splice connection of the tubular rails. [AASHTO16] The vehicle was backed up to the face of the sidewalk curb, as shown in Figure 247, as the initial start point of the impact event. After crossing the curb, the vehicle struck the bridge at 4.23 feet upstream of Post 7, as shown in Figure 248. The following sections provide a summary of the results and include a commentary describing the timing and occurrence of various events during the simulated impact, time-history data evaluation, occupant risk assessments, and damages sustained by both the barrier and vehicle.

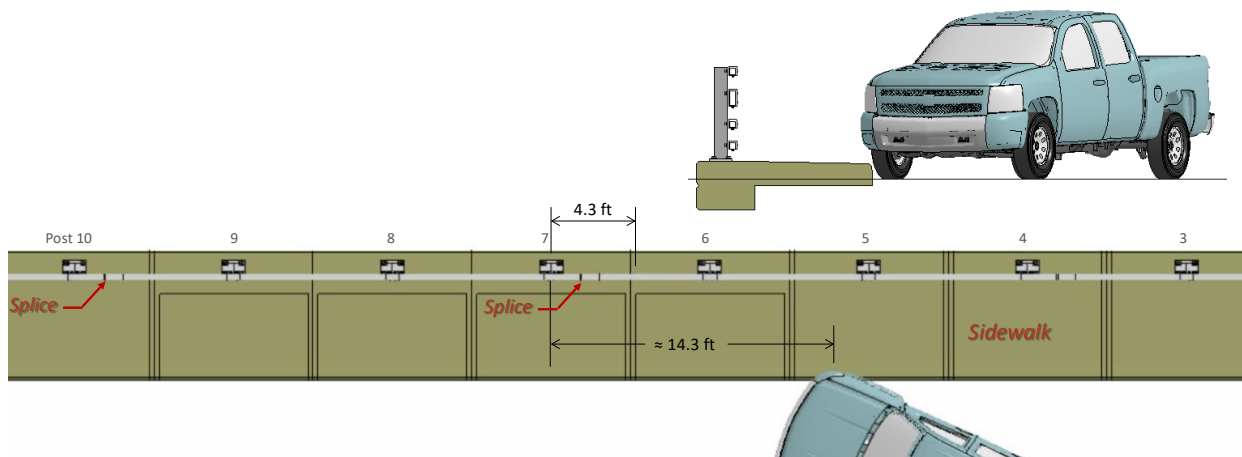


Figure 247. Initial starting point and target impact point for Test 4-11 on the NETC 4-bar bridge rail.

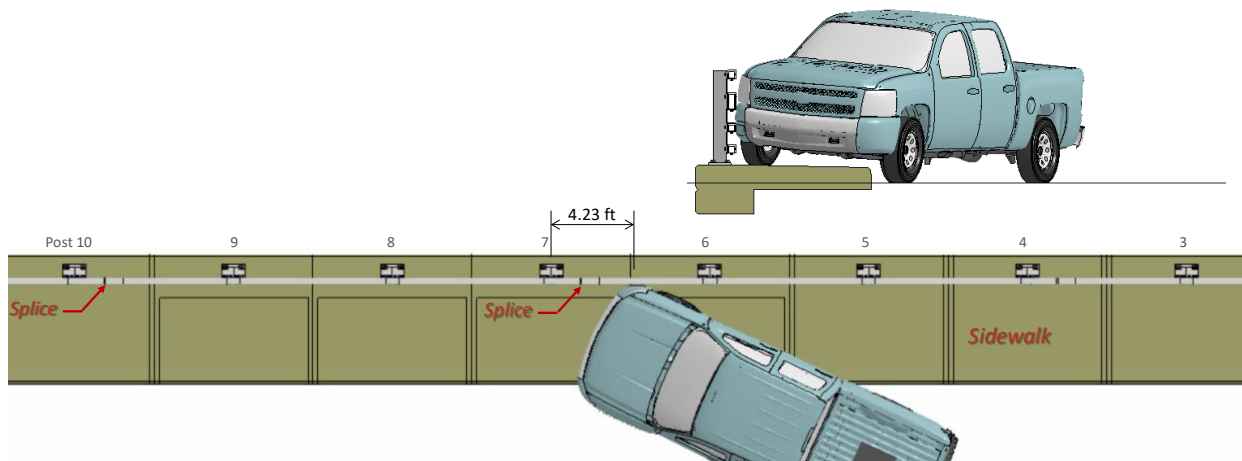


Figure 248. Actual impact point on barrier for test 4-11 on the NETC 4-bar bridge rail.

11.2.1 Summary of Key Phenomenological Events

The sequential views of the impact event are shown in Appendix R in Figures R-1 through R-3 from an overhead viewpoint, downstream and upstream viewpoint, and oblique viewpoint, respectively.

The 5,001-lb pickup struck the curb-face of the sidewalk at a speed of 62 mph and at an angle of 25 degrees per *MASH* Test 4-11 specifications. The impact point of the front-right tire with the curb was approximately 15.1 feet upstream of Post 7, the front bumper was 14.3 feet upstream of Post 7 at this time. At 0.005 seconds, the front-right tire compressed at the point of contact with the curb. At 0.015 seconds the deformation of the tire indicated that deflation was likely; however, tire deflation was not included in the model. At 0.03 seconds the tire had fully mounted the sidewalk, and the vehicle began to roll away from the barrier. The tire rebounded slightly from the sidewalk at 0.040 seconds but then recontacted the sidewalk at 0.060 seconds and remained in contact until impact with the barrier. At 0.125 seconds the front bumper impacted against the two middle rails at 4.3 feet upstream of Post 7. The speed and angle of the vehicle at the time of impact was 61.9 mph and 24.8 degrees, as illustrated in Figure 248. At 0.13 seconds the front-right corner of the vehicle impacted the upper-middle rail, and the front-right tire impacted the two lower rails, and the bridge rail began to deflect. At 0.135 seconds the front fender contacted the upper rail. At 0.14 seconds the front-left tire and the rear-right tire contacted the sidewalk curb simultaneously. At 0.155 seconds the front-right tire was parallel to the barrier. The rear-right tire was fully mounted onto the sidewalk at 0.165 seconds. At 0.15 seconds the lower wheel joint on the front-right tire failed. At 0.175 seconds, the rear-right tire lifted off the sidewalk. Also, at 0.175 seconds, the front-left tire partially mounted onto the sidewalk. At 0.185 seconds Post 7 reached an initial peak lateral deflection of 3.43 inches. At 0.2039 seconds the vehicle occupant contacted the right side of the vehicle interior, with a maximum longitudinal and lateral OIV of 17.7 ft/s and 26.6 ft/s, respectively. At 0.291 seconds the vehicle was parallel to the barrier traveling at 49.3 mph. At 0.295 seconds the rear quarter panel of the pickup contacted the two upper rails (i.e., Rails 3 and 4), and the rear-right tire contacted the three lower rails (i.e., Rails 1, 2 and 3). At 0.32 seconds the barrier reached maximum dynamic deflection of 5.4 inches at the splice connection between Post 6 and 7. At 0.321 seconds the maximum longitudinal acceleration occurred with magnitude 13.8 g. At 0.325 seconds Post 7 reached a second peak dynamic deflection of 4.1 inches, and Post 6 reached a peak dynamic deflection of 2 inches. The peak dynamic deflection of Post 8 downstream of the impact was 1.18 inches; while the deflection of Post 5 upstream of the impact was negligible. At 0.331 seconds the maximum lateral acceleration occurred with magnitude 18 g. At 0.395 seconds the vehicle separated from barrier at 47.2 mph and 5.9 degrees. At 0.465 seconds the lower control arm of the vehicle contacted the top of the sidewalk. At 0.595 seconds the front-left tire recontacted the roadway. At 0.75 seconds the rear-right tire recontacted the top of the sidewalk and the rear left tire recontacted the roadway. At 0.83 seconds the front right tire dropped off the sidewalk. At 0.91 seconds the rear right tire dropped off the sidewalk. The analysis ended at 1.0 seconds, at which time:

- The roll, pitch, and yaw of the vehicle were 2.63 degrees (toward the barrier), 3.75 degrees (rear pitching up), and 30.4 degrees (5.4 degrees relative to and away from the barrier), respectively.
- The forward velocity of the vehicle was 41.3 mph (66.6 km/h).

11.2.2 Time History Data Evaluation

Figures 249 through 251 show the longitudinal, transverse, and vertical acceleration-time histories, respectively, computed from the center of gravity of the vehicle; Figures 252 through 254 show the comparison of the angular rates and angular displacements (i.e., yaw, roll and pitch) at the center of gravity of the vehicle.

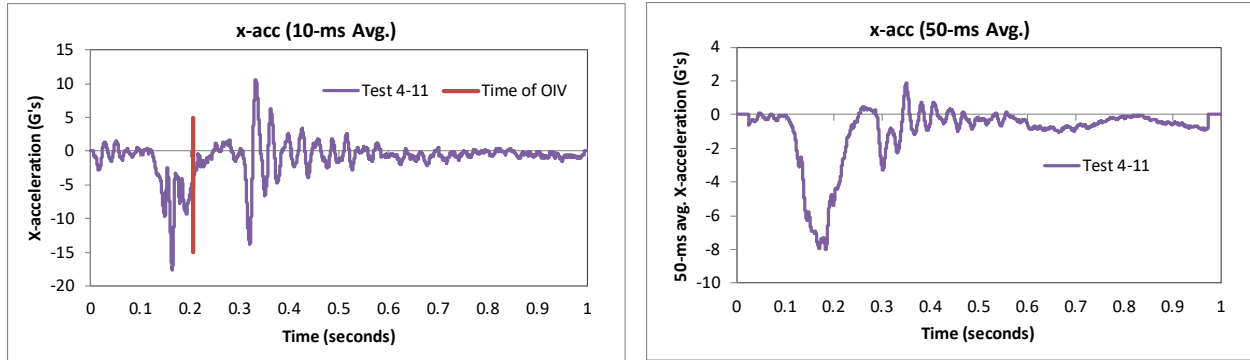


Figure 249. 10- and 50-millisecond average X-acceleration from FEA of Test 4-11 on the NETC 4-bar bridge rail.

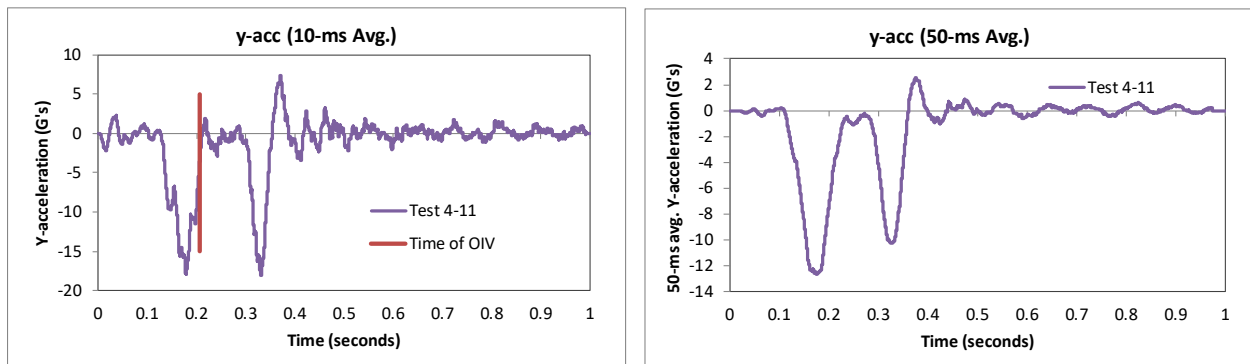


Figure 250. 10- and 50-millisecond average Y-acceleration from FEA of Test 4-11 on the NETC 4-bar bridge rail.

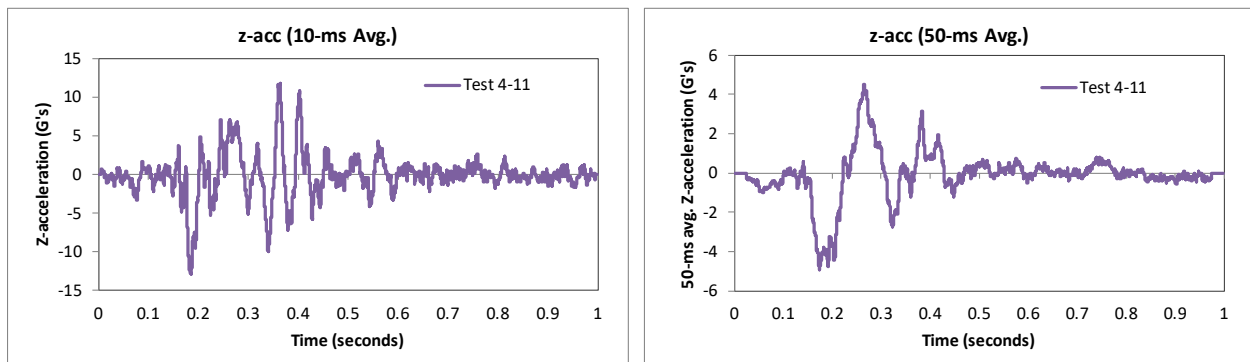


Figure 251. 10- and 50-millisecond average Z-acceleration from FEA of Test 4-11 on the NETC 4-bar bridge rail.

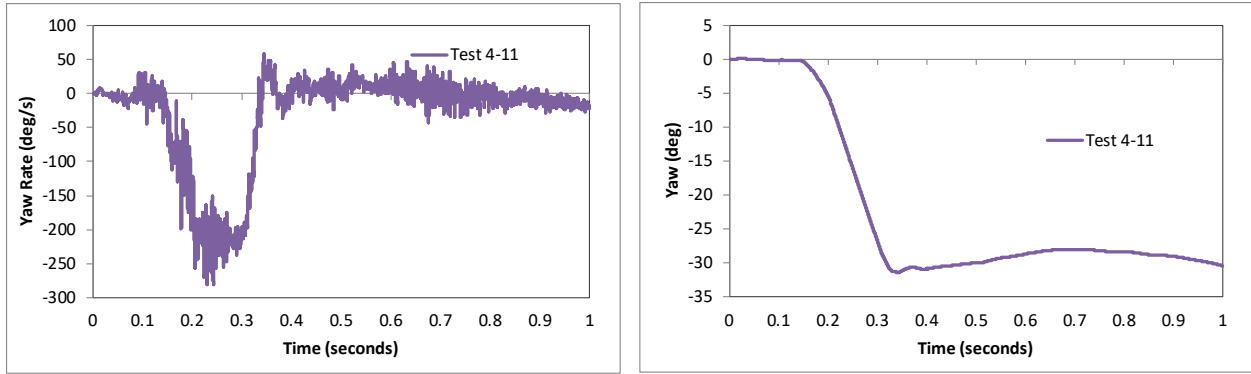


Figure 252. Yaw rate and yaw angle time-history from FEA of Test 4-11 on the NETC 4-bar bridge rail.

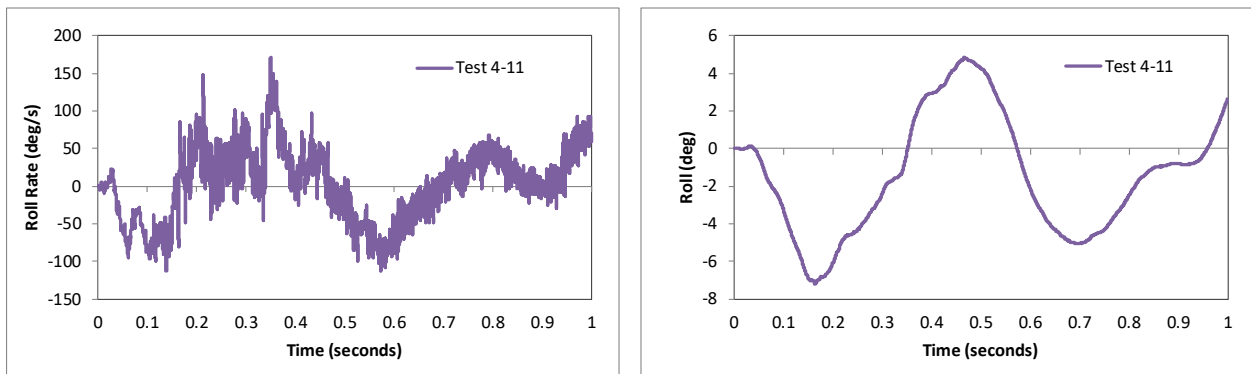


Figure 253. Roll rate and roll angle time-history from FEA of Test 4-11 on the NETC 4-bar bridge rail.

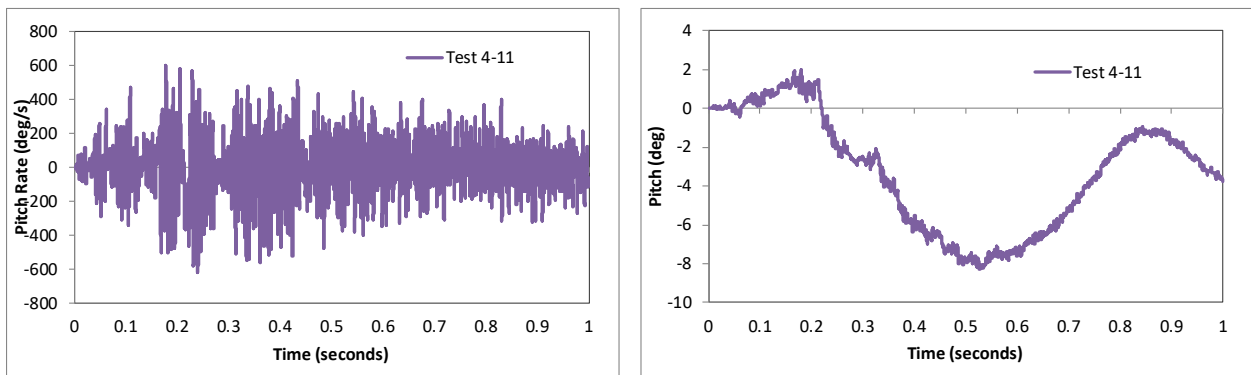


Figure 254. Pitch rate and pitch angle time-history from FEA of Test 4-11 on the NETC 4-bar bridge rail.

11.2.3 Occupant Risk Measures

The acceleration-time histories and angular rate-time histories collected at the center of gravity of the vehicle were used to evaluate occupant risk metrics according to the procedures outlined in *MASH*. Table 85 shows the results for the occupant risk calculations. The results indicate that the occupant risk factors meet safety criteria specified in *MASH*.

The occupant impact velocities in the longitudinal and transverse directions were 17.7 ft/s and 26.6 ft/s, respectively, which were within recommended limits specified in *MASH*. The

highest 0.010-second occupant ridedown acceleration in the longitudinal and transverse directions were 13.8 g and 18 g, respectively, which were within critical limits specified in *MASH*. The maximum ORA occurred when the rear tire rim snagged on the splice connection upstream of Post 7. The maximum 50-ms moving average acceleration values in the longitudinal and transverse directions were 8 g and 18 g, respectively. The maximum roll and pitch angles of the vehicle were 7.2 degrees and 8.3 degrees, respectively, which were well below critical limits in *MASH*.

Table 85. Summary of *MASH* occupant risk metrics for Test 4-11 on the NETC 4-bar bridge rail.

Occupant Risk Factors		MASH T4-11	MASH Criteria
		Test 4-11	
Occupant Impact Velocity (ft/s)	x-direction	17.7	} < 30 ft/s (preferred) ✓ < 40 ft/s (limit)
	y-direction	26.6	
	at time	at 0.2039 seconds on right side of interior	
THIV (ft/s)		32.2 at 0.2039 seconds on right side of interior	
Ridedown Acceleration (g's)	x-direction	-13.8 (0.3157 - 0.3257 seconds)	} > 15 G (preferred) < 20.49 G (limit) ✓
	y-direction	-18 (0.3264 - 0.3364 seconds)	
PHD (g's)		20.8 (0.3268 - 0.3368 seconds)	
ASI		1.61 (0.1482 - 0.1982 seconds)	
Max 50-ms moving avg. acc. (g's)	x-direction	-8 (0.1589 - 0.2089 seconds)	}
	y-direction	-12.7 (0.1512 - 0.2012 seconds)	
	z-direction	-4.9 (0.1487 - 0.1987 seconds)	
Maximum Angular Disp. (deg)	Roll	-7.2 (0.1642 seconds)	} < 75 deg ✓
	Pitch	-8.3 (0.5264 seconds)	
	Yaw	-31.4 (0.3422 seconds)	

11.2.4 Occupant Compartment Intrusion

The maximum deformation of the occupant compartment was approximately 2.2 inches at the right-front toe pan at the wheel well. Figure 255 shows a view of the vehicle interior after the impact, with several components removed to facilitate viewing. The deformation was less than the critical limit of 9 inches specified in *MASH* for this area of the occupant compartment.

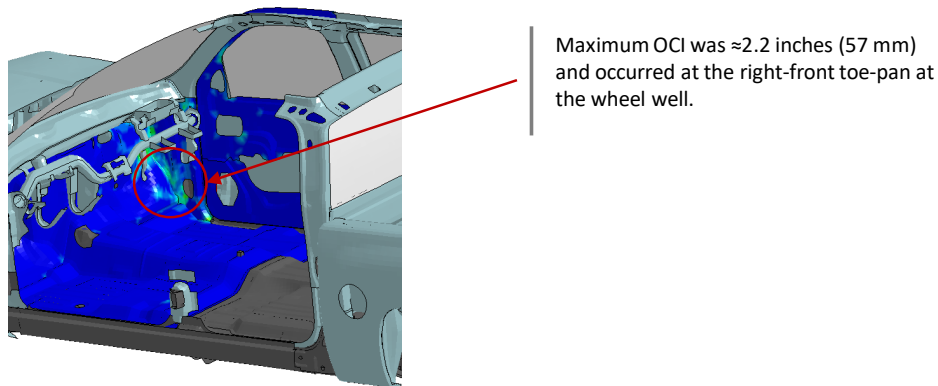


Figure 255. Occupant compartment deformation resulting from Test 4-11 on the NETC 4-bar bridge rail.

11.2.5 Damages to the Barrier System

The damages to the barrier were moderate. Figure 256 and Figure 257 show images of the maximum dynamic deflection and permanent deflection of the barrier, respectively, with a contour plot of lateral displacement on the rail elements. The maximum dynamic and permanent deflections were 5.4 inches and 2.4 inches, respectively, and occurred at the top rail tube at the splice.

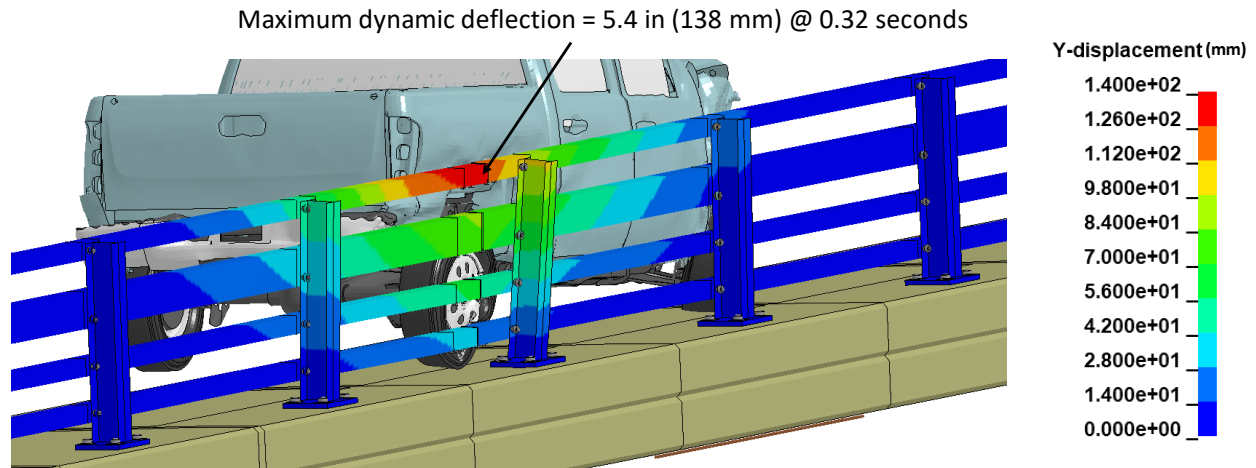


Figure 256. Contour plot of lateral displacement for the bridge rail for Test 4-11 at the time of maximum dynamic deflection.

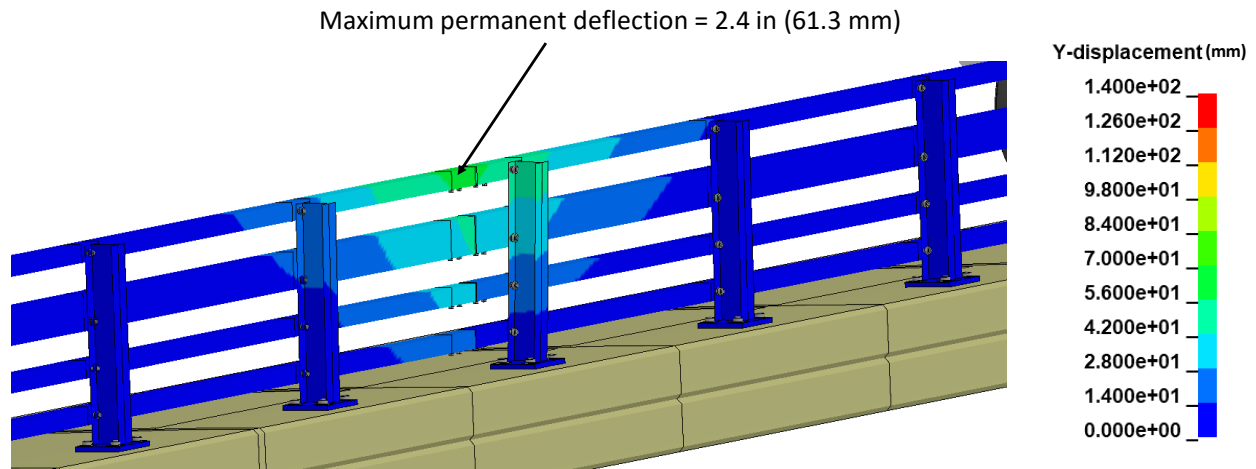


Figure 257. Contour plot of maximum permanent deflection of the bridge rail for test 4-11.

Figure 258 shows contours of true effective plastic strains on the bridge rail. There was moderate damage to the rail tubes between Post 6 and 7, with additional damage at the end of the lower-middle and lower rails at the splice. There was moderate damage to Post 6 and 7 and their baseplates. The true plastic strain at the outer edge of post flange at the weld of Post 7 was 0.34, which indicates possible material failure at those points (refer to Figure 257). The vertical deflection of baseplate at Post 6 was 0.29 inches (7.5 mm) dynamic deflection and 0.13 inches (3.4 mm) final permanent deflection. The vertical deflection of baseplate at Post 7 was 0.6 inches (15 mm) dynamic deflection and 0.31 (8 mm) final permanent deflection.

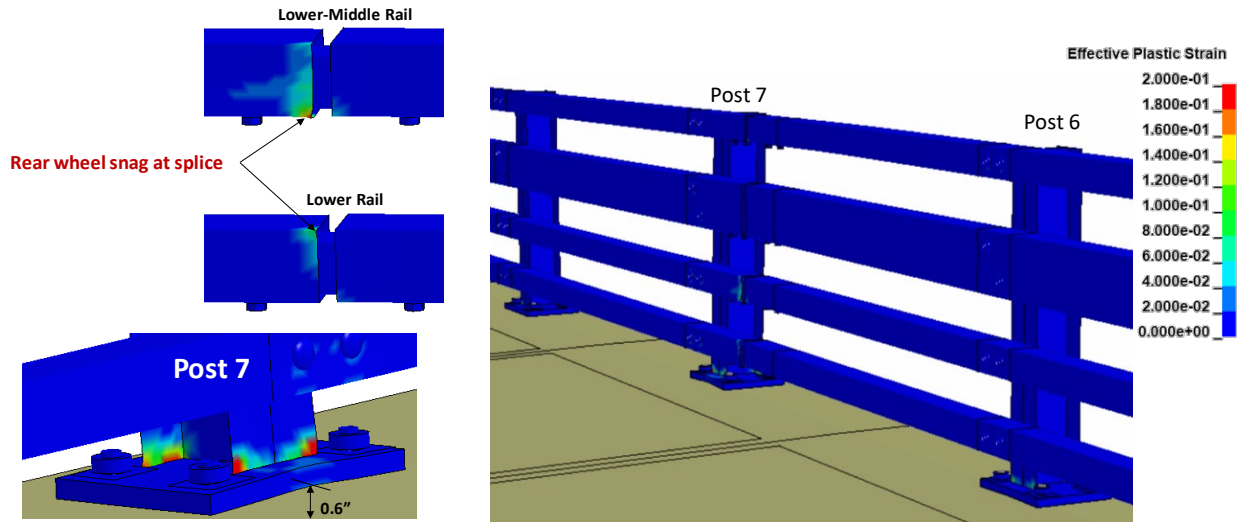


Figure 258. Contours of effective plastic strains for Test 4-11 on the NETC 4-bar bridge rail.

Figure 259 shows contours of 1st principal strain with contours cut off at strains of 0.1. The 1st Principal strain values for the concrete in these cases was 0.048 dynamic strain with final permanent strain of 0.024, which indicated no damage to the concrete sidewalk/deck.

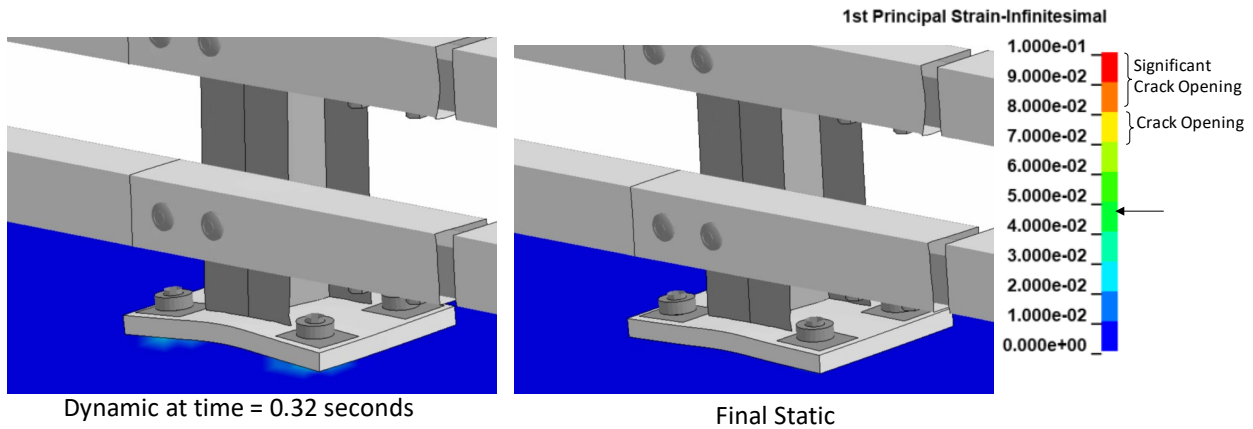


Figure 259. Contours of 1st principal strains for concrete at the critical post for Test 4-11 on the NETC 4-bar bridge rail.

11.2.6 Damages to Vehicle

Figure 260 shows contour plots of effective plastic strain for the vehicle, which were used to identify areas of the vehicle that suffered damage during the simulated impact event. The most severe damages were to the front bumper, front fender, lower edge of the passenger front door, the upper and lower control arm of front suspension, front wheel, rear wheel, rear edge of truck cabin, rear fender, rear quarter panel and rear bumper on the impact side.

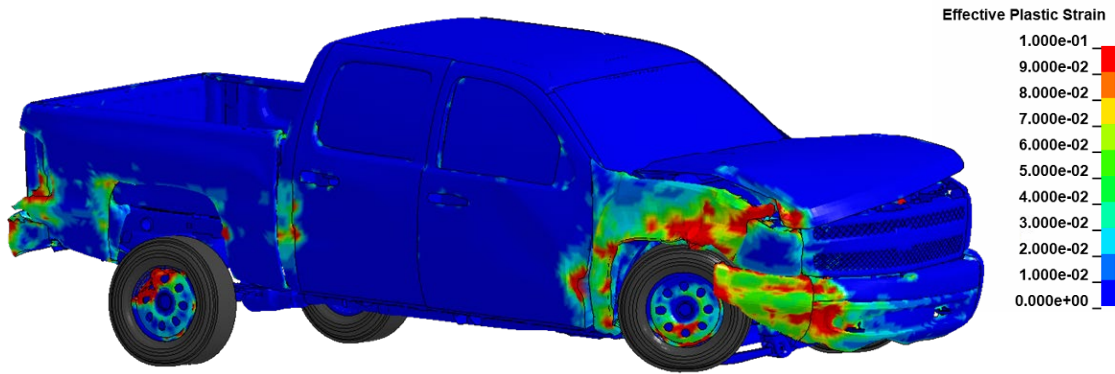


Figure 260. Damages to vehicle in Test 4-11 analysis of the NETC 4-bar bridge rail.

11.2.7 Exit Box

Figure 144 shows the exit box for Test 4-11 on the bridge rail, where the vehicle was smoothly redirected, and its path was well within the exit box criteria of *MASH*.

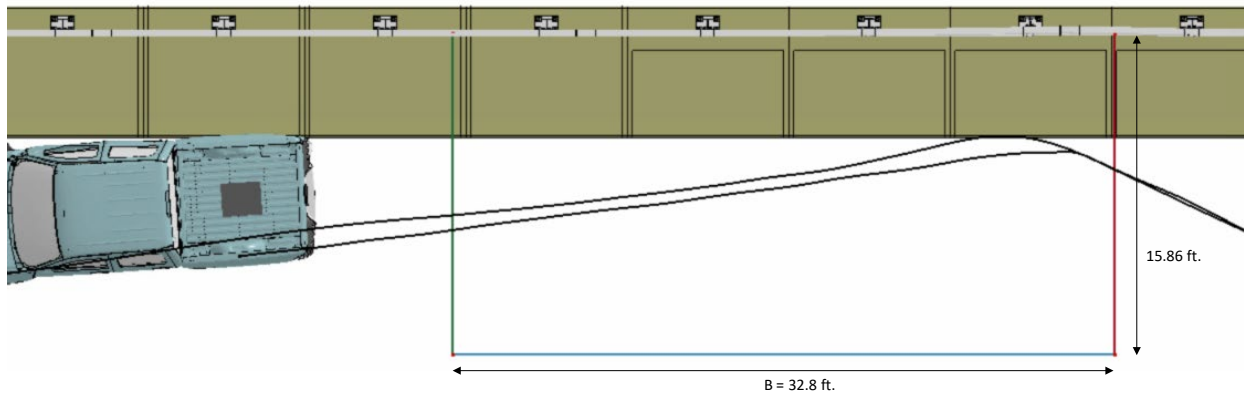


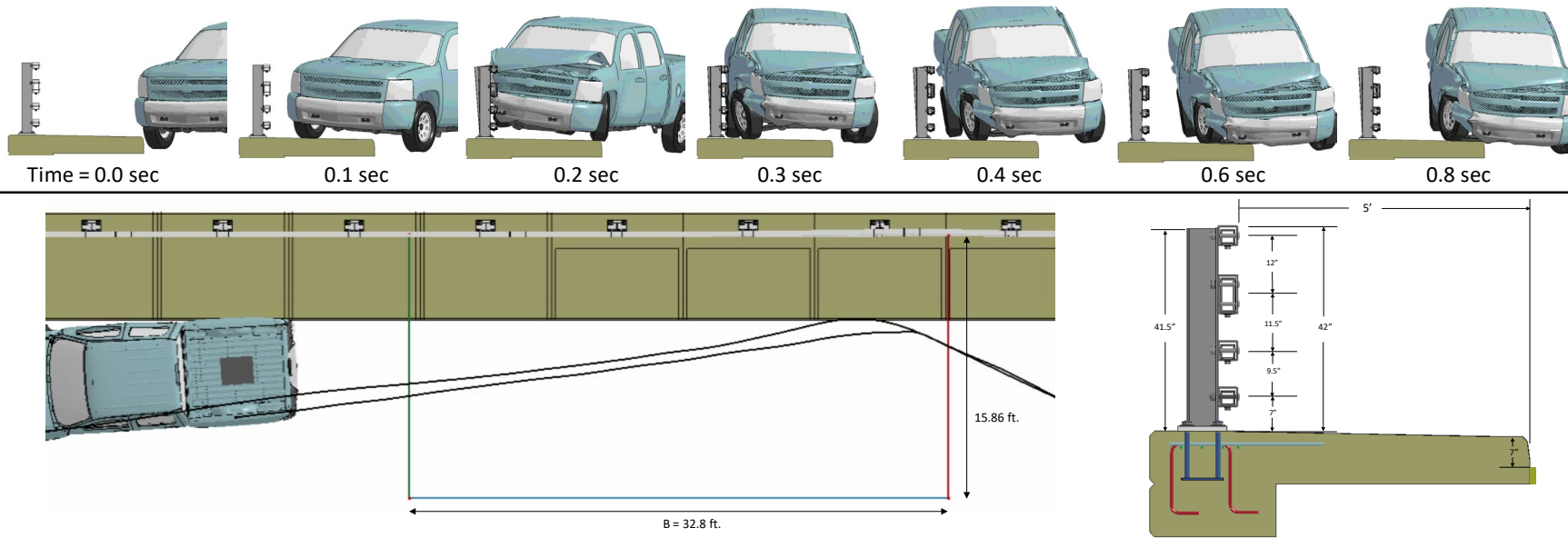
Figure 261. Exit box for Test 4-11 analysis of the NETC 4-bar bridge rail.

11.2.8 Results Summary

A summary of the *MASH* Test 4-11 results on the NETC 4-bar bridge rail is shown in Table 86 and Figure 262. The barrier successfully contained and redirected the pickup with moderate damage to the system. There were no detached elements from the barrier that showed potential for penetrating the occupant compartment or presenting undue hazard to other traffic. The vehicle remained upright and very stable throughout impact and redirection. The OIV was within preferred limits and the ORA was within critical limits as specified in *MASH*. Based on the results of this analysis, the barrier meets all structural and occupant risk criteria in *MASH* for Test 4-11 impact conditions.

Table 86. Summary of *MASH* Test 4-11 results on the NETC 4-bar bridge rail.

Evaluation Factors	Evaluation Criteria	Results
Structural Adequacy	A Test article should contain and redirect the vehicle or bring the vehicle to a controlled stop; the vehicle should not penetrate, underride, or override the installation although controlled lateral deflection of the test article is acceptable.	Pass
Occupant Risk	D Detached elements, fragments, or other debris from the test article should not penetrate or show potential for penetrating the occupant compartment, or present undue hazard to other traffic, pedestrians, or personnel in a work zone. Deformations of, or intrusions into, to occupant compartment should not exceed limits set forth in Section 5.2.2 and Appendix E.	Pass
	F The vehicle should remain upright during and after collision. The maximum roll and pitch angles are not to exceed 75 degrees.	Pass
	H The longitudinal and lateral occupant impact velocity (OIV) shall not exceed 40 ft/s (12.2 m/s), with a preferred limit of 30 ft/s (9.1 m/s)	Pass
	I The longitudinal and lateral occupant ridedown acceleration (ORA) shall not exceed 20.49 G, with a preferred limit of 15.0 G	Pass



General Information		Impact Conditions		Max50-millisecond Avg. (G)	
Analysis Agency	Roadsafe LLC	Speed	62 mph	Longitudinal	8.0 g
Test Standard Test No.	MASH Test 4-11	Angle	25 degrees	Lateral	12.7 g
Analysis No.	NETC18_4BarBR_T411	Location	4.23 ft upstream of Post 7	Vertical	4.9 g
Analysis Date	4/8/2019				
Test Article		Impact Severity		Test Article Deflections (in)	
Type	Bridge Rail		114.7 kip-ft	Dynamic	5.4 inches
Name	NETC 4-Bar	Exit Conditions		Permanent	2.4 inches
Installation Length	120 feet	Speed	47.5 mph	Working Width	1.16 feet
Material or Key Elements		Angle	5.88 degrees		
		Time	0.4 seconds	Max. OCI	
				2.2 inch	
Soil Type and Condition				Vehicle Stability	
N.A.		Longitudinal OIV	17.7 ft/s	Roll	7.2 degrees
Analysis Vehicle		Lateral OIV	26.6 ft/s	Pitch	8.3 degrees
Type / Designation	2270P	Longitudinal ORA	13.8 g	Yaw	31.4 degrees
FEA Model name	SilveradoC_V3a_V180201_TireRS_35psi	Lateral ORA	18.0 g		
Mass	5,001 lb	THIV	32.2 ft/s		
		PHD	20.8 g		
		ASI	1.61		

Figure 262. Summary results for MASH Test 4-11 on the NETC 4-bar bridge rail.

11.3 Test 4-12

The critical impact condition for *MASH* Test 4-12 was selected based the *MASH* recommended CIP for rigid barrier tests. The target impact point was 5.0 feet upstream of Post 7, as shown in Figure 263 and was selected to maximize loading on the post.[*AASHTO16*] The vehicle was backed up to the face of the sidewalk curb, as shown in Figure 263(a), as the initial start point of the impact event. After crossing the curb, the vehicle struck the bridge at 4.4 feet upstream of Post 7, as shown in Figure 263(b).

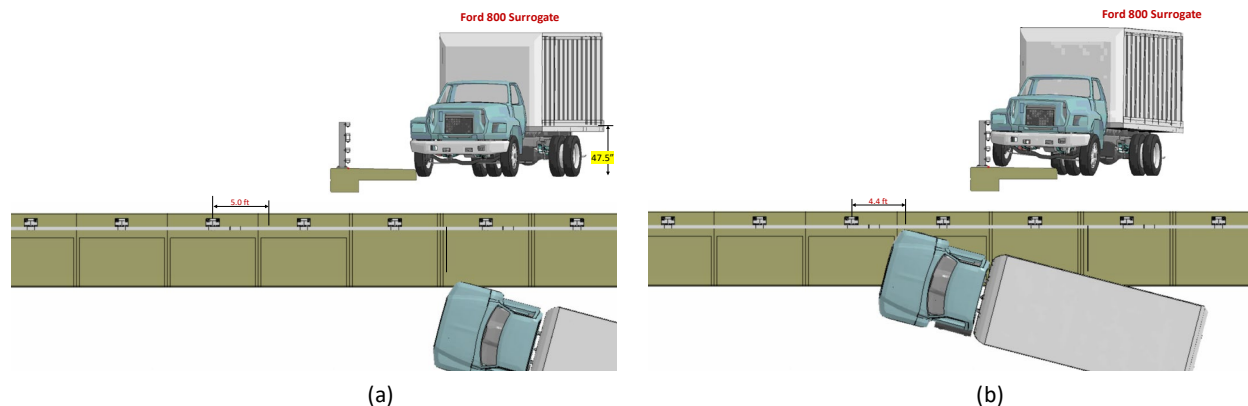


Figure 263. (a) Target and (b) actual impact point for Test 4-12 on the NETC 4-bar bridge rail.

The analysis of NETC 3-bar bridge (see Section 9) included single unit truck vehicles with two different cargo-bed heights. The results of that analysis indicated that the loading on the barrier was similar for both cases; therefore, only one analysis case was performed for the NETC 4-bar bridge rail. The cargo-bed height for the FEA model was 47.5 inches measured from the ground to the top of the cargo-bed floor, consistent with the Ford 800 which was the basis for the model. The following sections provide a summary of the results and include a commentary describing the timing and occurrence of various events during the simulated impact, time-history data evaluation, occupant risk assessments, and damages sustained by both the barrier and vehicle.

11.3.1 Summary of Key Phenomenological Events

The sequential views of the Case 1 impact event are shown in Appendix S in Figures S-1 through S-3 from an overhead viewpoint, downstream and upstream viewpoint, and an oblique viewpoint, respectively.

At 0.005 seconds, the front-right tire compressed at the point of contact with the sidewalk curb, and at 0.04 seconds the tire had fully mounted the sidewalk and the vehicle began to roll away from the barrier. The tire model for the SUT is relatively stiff and immediately rebounded of the surface of the sidewalk. At 0.08 seconds the front-right tire recontacted the sidewalk as the vehicle was yawing slightly counter-clockwise away from the barrier. At 0.205 seconds the rear-right tire contacted the curb face of the sidewalk. At 0.22 seconds the front bumper impacted against the upper-middle railing and the front fender impacted against the upper railing of the bridge rail at 4.4 feet upstream of Post 7, as illustrated in Figure 263, at a speed of 55.3 mph and impact angle of 14.1 degrees. At 0.225 seconds the barrier began to deflect. At 0.245

seconds the rear-right tire was fully mounted onto the sidewalk. At 0.265 seconds the front-right tire was parallel to the bridge rail. At 0.3 seconds the front-right tire was centered with Post 7 and the vehicle started to roll toward the barrier. Also, at this time, one of the u-bolts connecting the front axle to the front-right suspension failed and the wheel began to push back in the rear of the wheel well. At 0.345 seconds the lower, front corner of the cargo-box impacted the top rail. This event corresponded to the maximum lateral acceleration of at the c.g. of the vehicle (e.g., located inside the cargo-box) with magnitudes of 15 G and 5.8 G for the 10-ms running average and 50-ms running average, respectively. At 0.352 seconds the theoretical occupant struck the right side of the interior at a longitudinal and lateral velocity of 3.9 ft/s and 16.7 ft/s, respectively. At 0.355 seconds the front-left tire and the rear-left tires lifted off the roadway as the vehicle continued to roll toward the barrier. At 0.378 seconds the maximum longitudinal ORA of 4.3 g occurred, and at 0.384 seconds the maximum lateral ORA of 6.7 g occurred, both measured from inside the truck cabin. At 0.46 seconds the rear-right tandem wheel set impacted against the barrier at 35 inches upstream of Post 7. At 0.475 seconds the rear lower edge of the cargo-box impacted against the top rail of the barrier. At 0.5 inches Post 5 reached a peak lateral deflection of 1.5 inches. At 0.504 seconds the truck was parallel to the barrier traveling at 50.6 mph. At 0.505 seconds Post 6 reached a peak lateral deflection of 5.7 inches. At 0.51 seconds a maximum dynamic deflection of 8.15 inches occurred at the splice connection on the top rail. At 0.515 seconds Post 7 reached a peak lateral deflection of 7.6 inches. At 0.56 seconds Posts 8 and 9 reached peak lateral deflections of 5.7 inches and 1.52 inches, respectively. The vehicle separated from the barrier at 0.71 seconds but continued to roll toward the barrier. At 0.72 seconds the cargo-box reached a maximum pitch angle of 3.5 degrees; and at 0.81 seconds the cabin reached a maximum pitch angle of 5.6 degrees (rear pitching up). At 0.82 seconds the cargo-box reached a maximum roll angle of 21.3 degrees; and at 0.91 seconds the cabin reached a maximum roll angle of 18.8 degrees toward the barrier. This resulted in the top of the cargo box extending 29 inches behind the face of the bridge rail. At 0.935 seconds the front-right tire dropped off the sidewalk curb; at 0.97 seconds the tire recontacted the roadway. At 1.07 seconds the front-left tire recontacted the roadway. At 1.29 seconds the rear-left tire recontacted the roadway. The analysis was terminated at 1.5 seconds, at which time:

- The roll, pitch, and yaw angles for the truck cabin were 3.9 degrees (toward barrier and stable), 0.31 degrees (front pitching upward and stable), and 39.7 degrees (24.7 degrees relative to and away from barrier), respectively.
- The roll, pitch, and yaw angles for the cargo box were 5.6 degrees (toward barrier and stable), 1.5 degrees (front pitching upward and stable), and 40.8 degrees (25.8 degrees relative to and away from barrier), respectively.
- The forward velocity was 50.9 mph (81.9 km/hr).

11.3.2 Time History Data Evaluation

Acceleration-time histories and angular rate-time histories were collected at two locations on the vehicle: (1) on the cargo box at the center of gravity of the vehicle, and (2) a point inside the cabin of the truck, as shown in Figure 111. The acceleration and angular rate data used for the occupant risk measures came from the cabin location. Figures 264 through 266 show the longitudinal, transverse, and vertical acceleration-time histories, respectively, computed from near the center of gravity of the vehicle which falls inside the cargo-box near the front of the ballast.

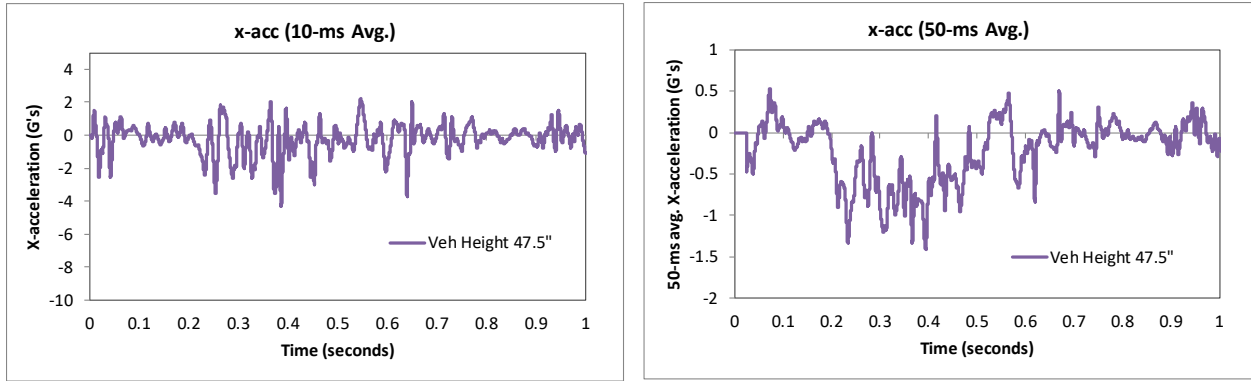


Figure 264. 10- and 50-millisecond average X-acceleration from FEA of Test 4-12 on the NETC 4-bar bridge rail (c.g. accelerometer).

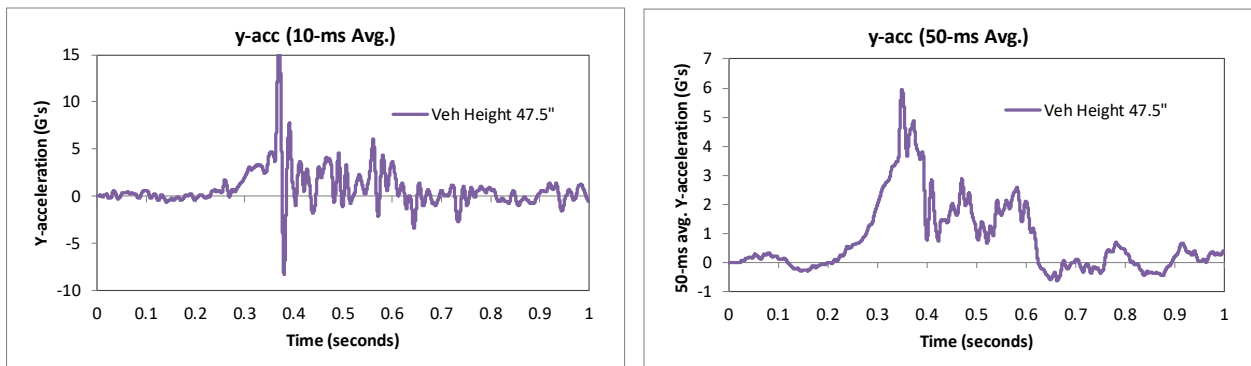


Figure 265. 10- and 50-millisecond average Y-acceleration from FEA of Test 4-12 on the NETC 4-bar bridge rail (c.g. accelerometer).

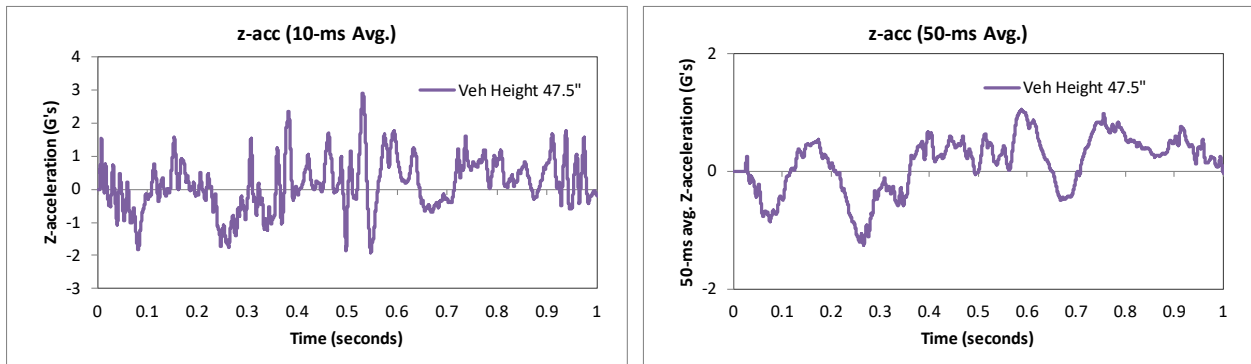


Figure 266. 10- and 50-millisecond average Z-acceleration from FEA of Test 4-12 on the NETC 4-bar bridge rail (c.g. accelerometer).

Figures 267 through 269 show the longitudinal, transverse, and vertical acceleration-time histories, respectively, computed from the inside the cabin of the vehicle; Figures 270 and 272 show the comparison of the angular rates and angular displacements about the x-, y-, and z-axis from the cabin location. These data are used for calculating the occupant risk metrics. *MASH* does not require that occupant risk be evaluated; however, they are reported herein for completeness (see following section).

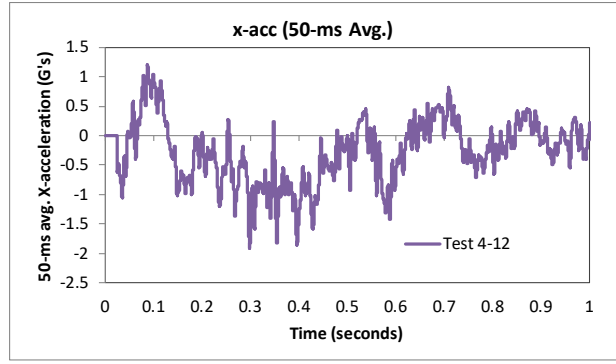
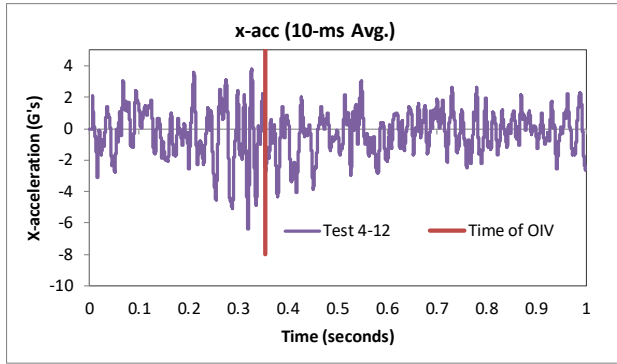


Figure 267. 10- and 50-millisecond average X-acceleration from FEA of Test 4-12 on the NETC 4-bar bridge rail (cabin accelerometer).

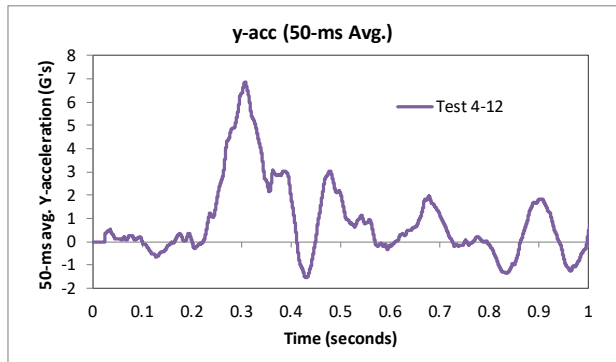
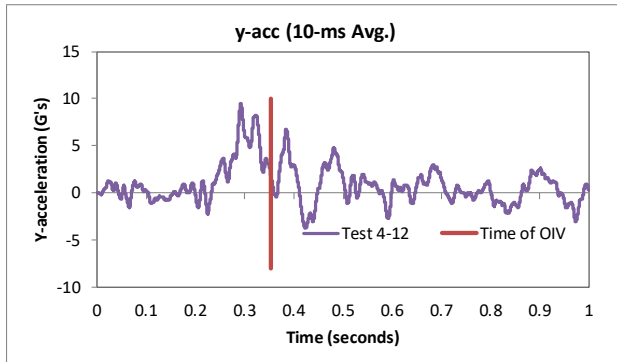


Figure 268. 10- and 50-millisecond average Y-acceleration from FEA of Test 4-12 on the NETC 4-bar bridge rail (cabin accelerometer).

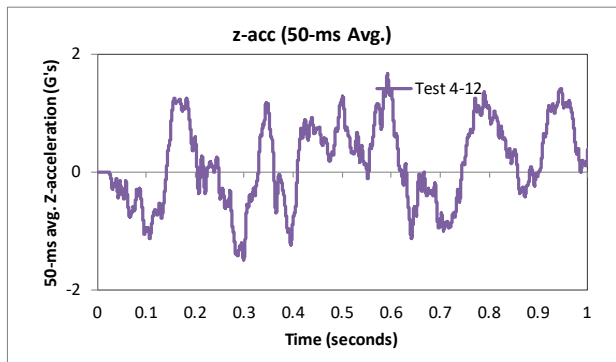
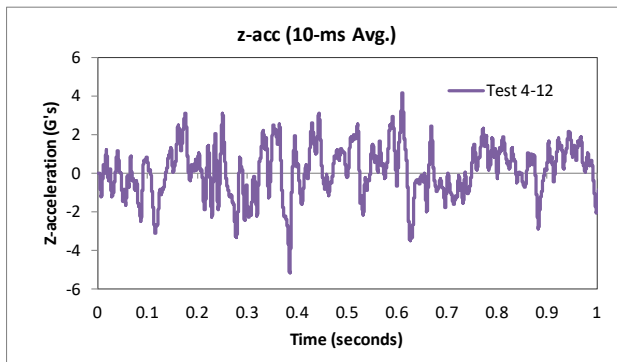


Figure 269. 10- and 50-millisecond average Z-acceleration from FEA of Test 4-12 on the NETC 4-bar bridge rail (cabin accelerometer).

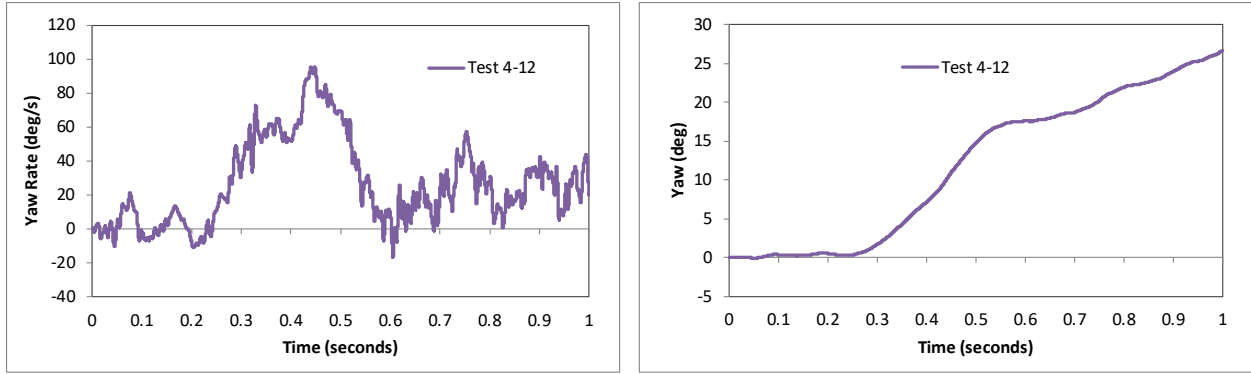


Figure 270. Yaw rate and yaw angle time-history from FEA of Test 4-12 on the NETC 4-bar bridge rail (cabin accelerometer).

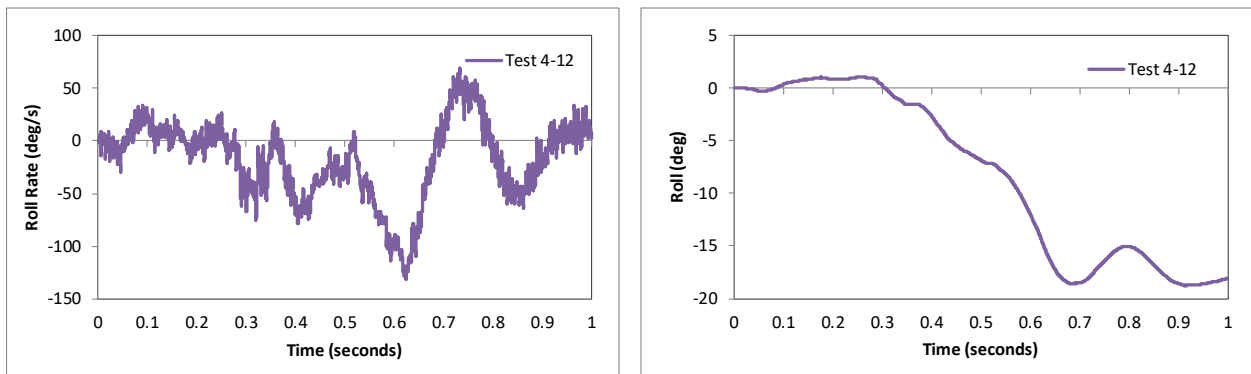


Figure 271. Roll rate and roll angle time-history from FEA of Test 4-12 on the NETC 4-bar bridge rail (cabin accelerometer).

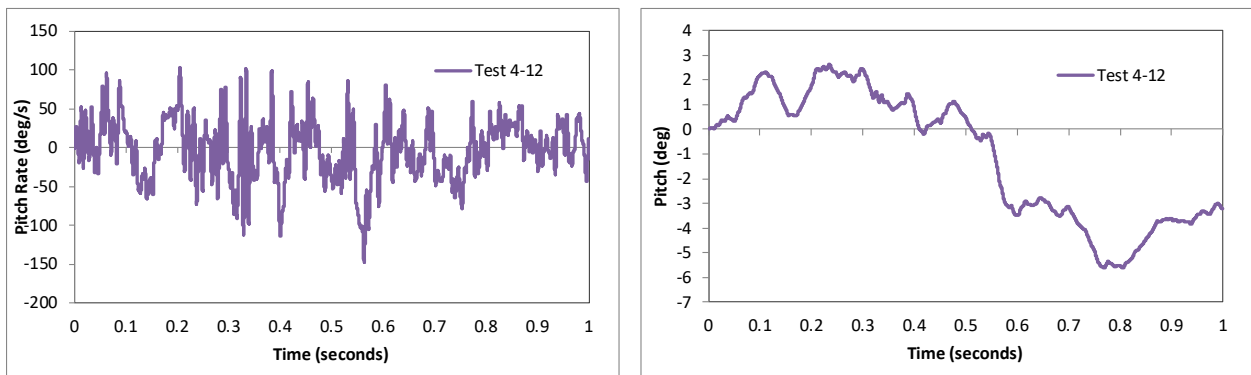


Figure 272. Pitch rate and pitch angle time-history from FEA of Test 4-12 on the NETC 4-bar bridge rail (cabin accelerometer).

11.3.3 Occupant Risk Measures

The acceleration-time histories and angular rate-time histories collected from inside the truck cabin were used to evaluate occupant risk metrics according to the procedures outlined in *MASH*. Table 87 shows the results for the occupant risk calculations. The results indicate that the occupant risk factors met safety criteria specified in *MASH*.

The occupant impact velocities in the longitudinal and transverse directions were 3.9 ft/s and 16.7 ft/s, respectively. The highest 0.010-second occupant ridedown acceleration in the

longitudinal and transverse directions were 4.3 g and 6.7 g, respectively. The maximum 50-ms moving average acceleration values in the longitudinal and transverse directions were 1.9 g and 6.9 g, respectively. The maximum roll and pitch angles of the vehicle were 18.8 degrees and 5.6 degrees, respectively. All metrics were within recommended limits specified in *MASH*.

Table 87. Summary of occupant risk metrics for Test 4-12 on the NETC 4-bar Bridge Rail.

Occupant Risk Factors		MASH T4-12	MASH Criteria
		Test 4-12	
Occupant Impact Velocity (ft/s)	x-direction	3.9	} < 30 ft/s (preferred) ✓ < 40 ft/s (limit)
	y-direction	-16.7	
	at time	at 0.3519 seconds on left side of interior	
THIV (ft/s)		17.4	
		at 0.3519 seconds on left side of interior	
Ridedown Acceleration (g's)	x-direction	-4.3 (0.3734 - 0.3834 seconds)	} < 15 G (preferred) ✓ < 20.49 G (limit)
	y-direction	6.7 (0.3793 - 0.3893 seconds)	
PHD (g's)		6.7 (0.3791 - 0.3891 seconds)	
ASI		0.77 (0.2828 - 0.3328 seconds)	
Max 50-ms moving avg. acc. (g's)	x-direction	-1.9 (0.2735 - 0.3235 seconds)	
	y-direction	6.9 (0.2823 - 0.3323 seconds)	
	z-direction	1.7 (0.5674 - 0.6174 seconds)	
Maximum Angular Disp. (deg)	Roll	-18.8 (0.9140 seconds)	} < 75 deg ✓
	Pitch	-5.6 (0.8050 seconds)	
	Yaw	39.7 (1.4987 seconds)	

11.3.4 Occupant Compartment Intrusion

The maximum deformation of the occupant compartment for impact on the NETC 4-bar bridge rail was approximately 1 inch and occurred at the lower right-front corner of the toe-pan and the wheel well. Figure 273 shows a view of the vehicle interior after the impact, with several components removed to facilitate viewing. The maximum deformation was less than the critical limit of 9 inches specified in *MASH* for this area of the occupant compartment.

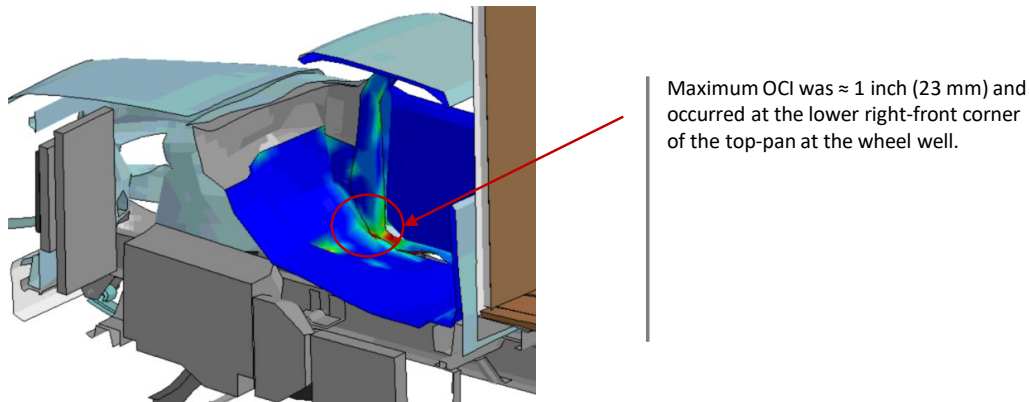


Figure 273. Occupant compartment deformation resulting from Test 4-12 on the NETC 4-bar bridge rail system.

11.3.5 Damages to the Barrier System

The extent damage was 48 feet starting at approximately 2.8 feet upstream of Post 5, as shown in Figure 274. There was moderate damage to the rail tubes between Post 5 and 9. The vehicle was in contact with the barrier for 53.25' starting at the point of impact and extending to Post 13. Figure 275 shows images of the barrier at the time of maximum deflection with a contour plot of lateral displacement on the rail elements. The maximum dynamic deflection was 8.15 inches and occurred on the top rail at the splice connection upstream of Post 7 when the rear of the cargo-box impacted the railing. Figure 276 shows a contour plot of maximum permanent deflection which was 5.8 inches.

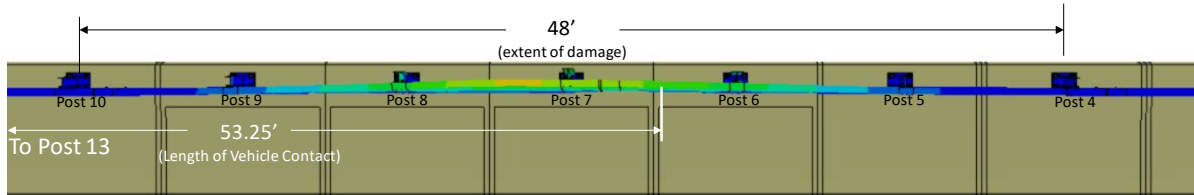


Figure 274. Extent of damage to the bridge rail for Test 4-12 on the NETC 4-bar bridge rail system.

Maximum dynamic deflection = 8.15 in (207 mm) @ 0.32 seconds

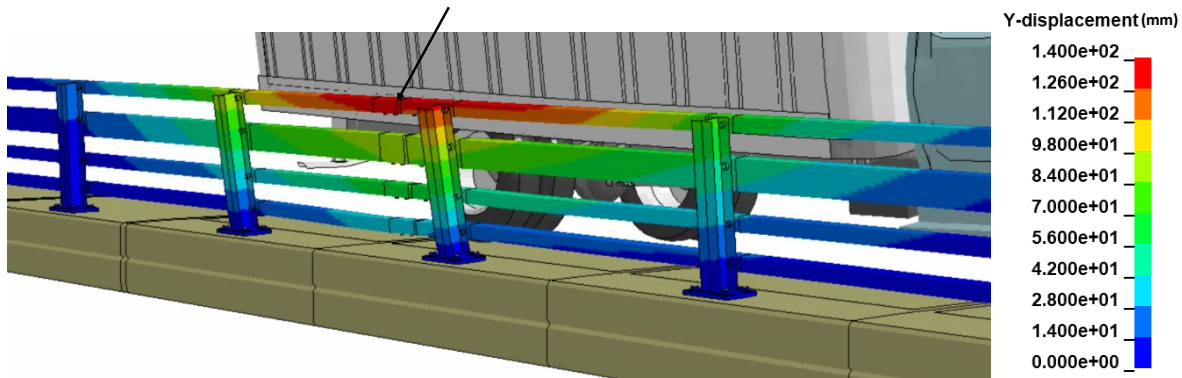


Figure 275. Contour plot of lateral displacement for the bridge rail from Test 4-12 at the time of maximum dynamic deflection for the NETC 4-bar bridge rail.

Maximum permanent deflection = 5.8 in (147 mm)

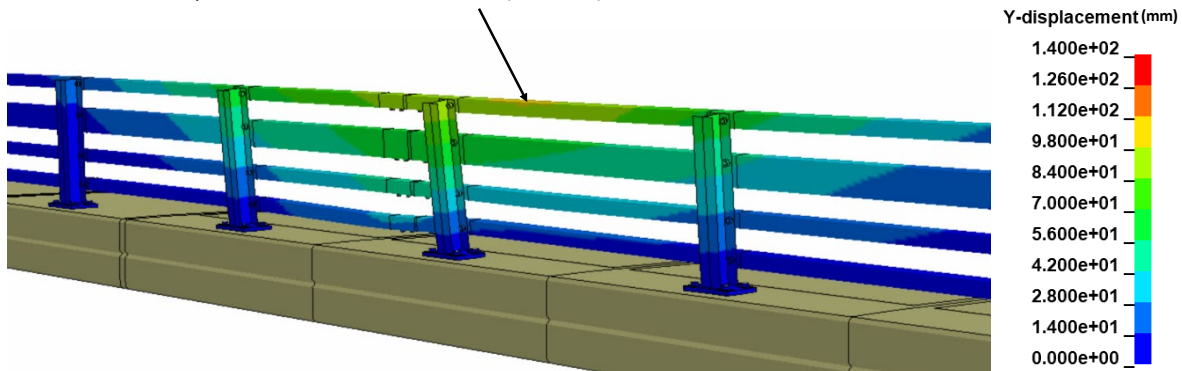


Figure 276. Contour plot of permanent deflection for the bridge rail from Test 4-12 for the NETC 4-bar bridge rail.

Figure 277 shows contours of true effective plastic strains on the bridge rail post and baseplate for the two analysis cases, which resulted in significant damage to post and baseplate at Posts 6 - 8. The post flanges buckled near the welded connection to the baseplate, and the front-center edge of the baseplate was deflected upward. The maximum vertical dynamic deflections of the baseplates were 0.82 inches, 1.11 inches and 0.78 inches, for Posts 6-8 respectively. The maximum permanent deflections of the baseplates were 0.53 inches, 0.82 inches and 0.52 inches, respectively. The vertical deflection of the baseplate caused a stress concentration at the outer edges of the front flange of the post at the weld location. The maximum effective true plastic strain values were 0.29, 0.33 and 0.28 for Posts 6 – 8, respectively, which correspond to nominal strain values that exceeds the necking point for the material, as indicated on the nominal stress-strain curve for the material in Figure 160. The forces on the welds were not collected during the analysis, but they may be of concern for these analysis cases given that the welds on the front flange are in tension.

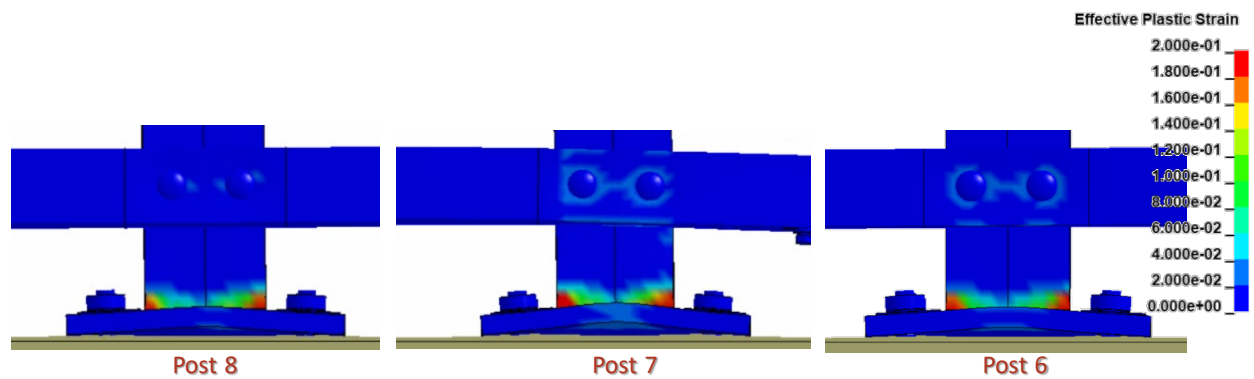


Figure 277. Contours of effective plastic strains on the critical post for Test 4-12 on the NETC 4-bar bridge rail.

Figure 278 shows contours of 1st principal strain with contours cut off at strains of 0.1. The 1st Principal strain value for the concrete was 0.079 at the front anchor bolt locations at Post 7, which indicates probable crack opening in the concrete at those locations.

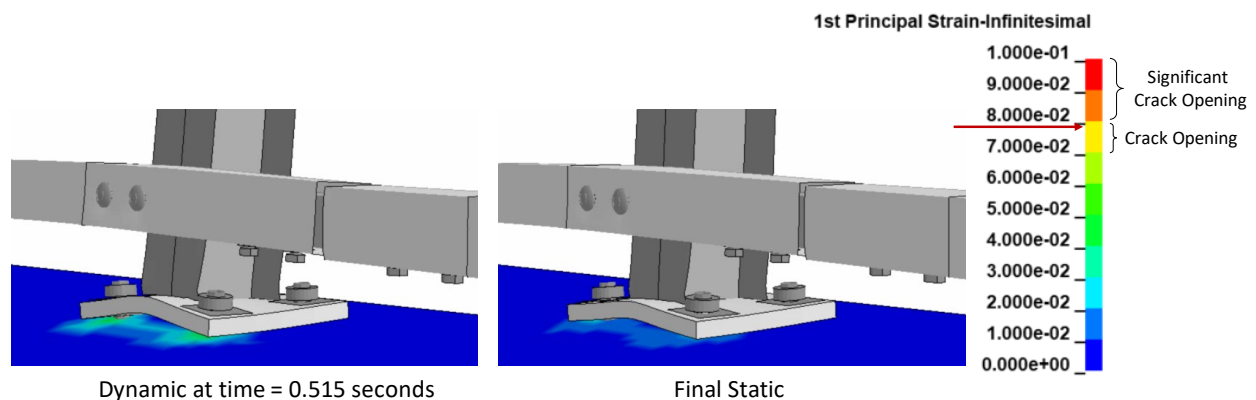


Figure 278. Contours of 1st principal strains for concrete at the critical post for Test 4-12 on the NETC 4-bar bridge rail.

11.3.6 Peak Forces on Barrier

The impact force between the vehicle and the barrier was computed to determine the peak loading on the barrier which could then be compared to the design strength of the bridge rail. The longitudinal and lateral force-time history results are shown in Figure 279 including the force data filtered with cutoff frequency of 60 Hz, the 25-millisecond moving average force and the 50-millisecond moving average force. The maximum lateral impact force occurred when the rear tandem wheel set impacted against the bridge rail. The maximum 25-ms moving average force was 110 kips; the maximum 50-ms moving average force was 97 kips, which are both greater than the calculated strength of the barrier in Section 3.4.2.3 (see Table 13). Since the peak lateral forces result from the “backslap” rather than the front of the vehicle, then the vehicle would already be passing (or passed) the damaged section as the failure was occurring, thus containment was successful.

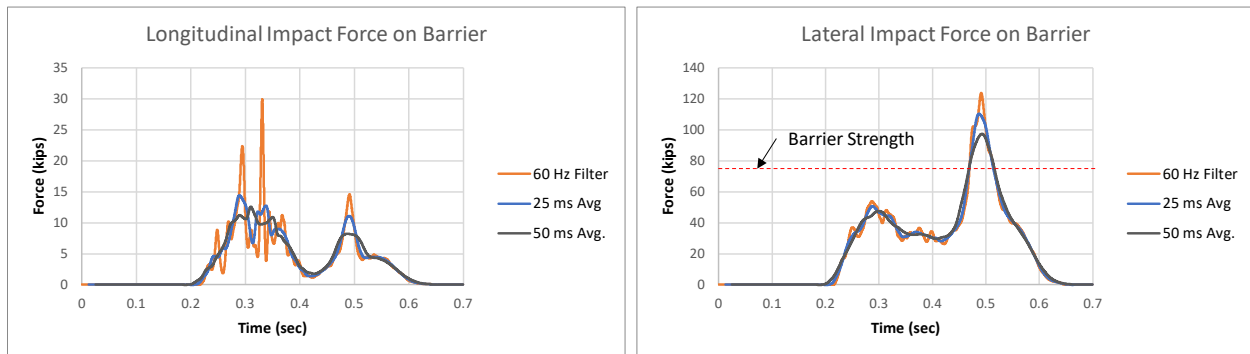


Figure 279. Longitudinal and lateral force-time history between vehicle and barrier for Test 4-12 on NETC 4-bar bridge rail.

11.3.7 Damages to Vehicle

Figure 280 shows contour plots of effective plastic strain for the vehicle, which were used to identify areas of the vehicle that suffered damage during the simulated impact event. The most severe damages were to the front bumper, the front fender, the front impact-side suspension, the front axle, the longitudinal rail at the lower edge of the cargo box, and the rear wheel. These are typical damages for Test 4-12 on post-and-beam bridge rails.



Figure 280. Damages to vehicle in Test 4-12 analysis of NETC 4-bar bridge rail.

11.3.8 Exit Box

Figure 281 show the exit box for Test 4-12 on the NETC 4-bar bridge rail system. Although the exit box analysis is not required in *MASH*, it was included here for completeness. The vehicle was smoothly redirected and the vehicle path was well within the exit box criteria of *MASH*.

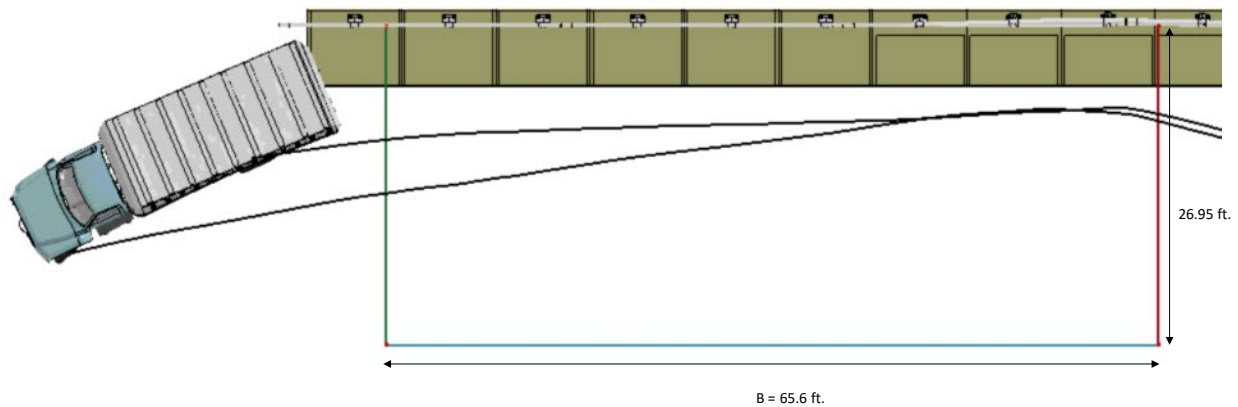


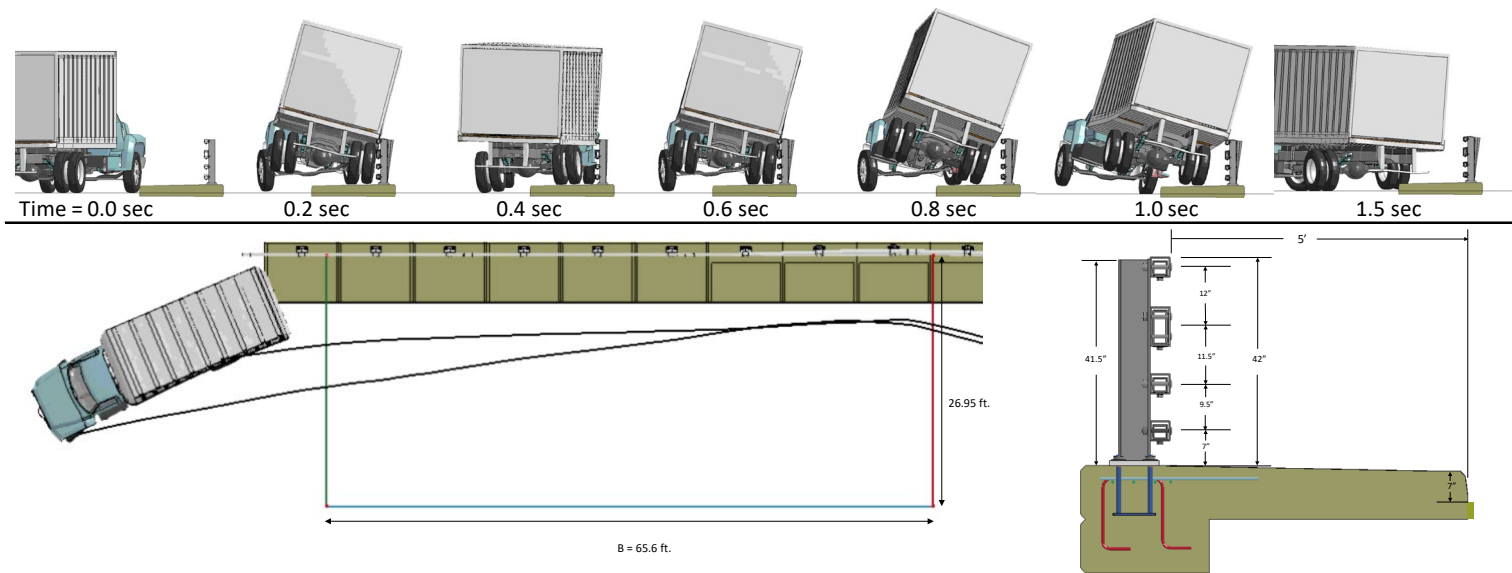
Figure 281. Exit box for Test 4-12 for Case 1 on the NETC 4-bar bridge rail.

11.3.9 Test 4-12 Results Summary

A summary of the *MASH* Test 4-12 results on the NETC 4-bar bridge rail is shown in Table 88 and Figure 282. The barrier adequately contained and redirected the 10000S vehicle (single unit truck) with moderate to extensive damage to the bridge rail. The damage included plastic deformation of posts and baseplates with high stress concentrations for the welds at the outside edges of the front flange at three post locations. The analysis also indicated probable concrete damage around the front anchor bolts. The maximum dynamic and permanent deflections of the railing were 8.2 inches and 5.8 inches, respectively. There were no detached elements from the barrier that showed potential for penetrating the occupant compartment or presenting undue hazard to other traffic. The vehicle remained upright and stable throughout impact and post trajectory. Based on the results of this analysis, the barrier meets all structural and occupant risk criteria in *MASH* for Test 4-12 impact conditions.

Table 88. Summary of *MASH* Test 4-12 results on the sidewalk-mounted NETC 4-bar bridge rail.

Evaluation Factors	Evaluation Criteria	Results
Structural Adequacy	A Test article should contain and redirect the vehicle or bring the vehicle to a controlled stop; the vehicle should not penetrate, underide, or override the installation although controlled lateral deflection of the test article is acceptable.	Pass
Occupant Risk	D Detached elements, fragments, or other debris from the test article should not penetrate or show potential for penetrating the occupant compartment, or present undue hazard to other traffic, pedestrians, or personnel in a work zone. Deformations of, or intrusions into, to occupant compartment should not exceed limits set forth in Section 5.2.2 and Appendix E.	Pass
	G It is <u>preferable, although not essential</u> , that the vehicle remain upright during and after collision.	Fail



General Information		Impact Conditions		Max50-millisecond Avg. (G)	
Analysis Agency	Roadsafe LLC	Speed	56 mph	Longitudinal	1.9 g
Test Standard Test No.	MASH Test 4-12	Angle	15 degrees	Lateral	6.9 g
Analysis No.	NETC18_4BarBR_T411	Location	Target: 5 feet upstream of Post 7	Vertical	1.7 g
Analysis Date	4/16/2019	Actual: 4.4 ft			
Test Article		Impact Severity		Test Article Deflections (in)	
Type	Bridge Rail	155.6 kip-ft		Dynamic	8.15 inches
Name	NETC 4-Bar	Exit Conditions		Permanent	5.8 inch
Installation Length	120 feet	Speed	49.8 mph	Working Width	2.4 feet
Material or Key Elements		Angle	4.3 degrees		
Soil Type and Condition		Time	0.725 seconds	Max. OCI	
N.A.		Occupant Risk Values		≈1 inch	
Analysis Vehicle		Longitudinal OIV	3.9 ft/s	Vehicle Stability	
Type / Designation	10000S	Lateral OIV	16.7 ft/s	Roll	18.8 degees
FEA Model name	F800_No-Box_181114_UboltF0p17	Longitudinal ORA	4.3 g	Pitch	5.6 degrees
	502_TruckBox_181114	Lateral ORA	6.7 g	Yaw	39.7 degrees
Mass	22,198 lb	THIV	17.4 ft/s		
		PHD	6.7 g		
		ASI	0.77		

Figure 282. Summary results for MASH Test 4-12 on the NETC 4-bar bridge rail.

11.4 Conclusion for TL4 Evaluation of NETC 4-Bar Bridge Rail

Based on the results of this analysis, the NETC 4-bar bridge rail meets all structural and occupant risk criteria in *MASH* Test Level 4; however, relatively high barrier damages are likely under these conditions. The barrier system meets *MASH* TL3 criteria with only moderate barrier damages.

11.4.1 Structural Adequacy: (PASS)

- The barrier successfully contained and redirected the vehicle in all test cases, but with significant barrier deflections for Test 4-12.
- The barrier experienced moderate plastic deformations of the posts, rails and baseplates for Test 4-11 (Pickup), but more significant damage for Test 4-12 (SUT).
- Lateral deflections were relatively high for 4-12 (e.g., 8.2”)
- Concrete curb damage at Post 7 was likely for Test 4-12. The damages corresponded to potential cracks around the front anchor bolts and/or pryout damage.

11.4.2 Occupant Risk (PASS)

- Occupant compartment intrusion was well below allowable limits for all cases
- OIV and ORA
 - Small Car: OIV (within critical limits); ORA (within preferred limits) (values highly dependent on time of occupant impact)
 - Pickup: OIV (within preferred limits); ORA (within critical)

11.4.3 Vehicle Trajectory (PASS)

- Vehicle remained upright and stable through impact and redirection, with relatively low angular displacements for all cases.

12 EVALUATION OF THE CONCRETE TRANSITION TO THRIE-BEAM FOR 4-BAR BRIDGE RAILS

12.1 Model Development

The FEA model of the MaineDOT Concrete Transition Barrier and the Bridge Transition Type 1 was developed based on the MaineDOT standard drawings (see Appendix A). Elevation views of the transition system are shown in Figures 283 and 284. This system is used in Maine for all the NETC steel post-and-beam bridge rail designs and is installed with either a 9-inch tall curb or with a 5-ft wide sidewalk with 9-inch curb face. Only the sidewalk case was evaluated here since it provided the greatest opportunity for snags on the concrete buttress. The 9-inch curb face for these designs begins at the end of the concrete transition nose and tapers to the height of the approach curb over a 7-ft distance. The height of the approach curb varies depending on site details. For these evaluations, the approach curb was modeled as 7 inches. The analyses presented herein only involve evaluations of the crashworthiness of the transition from the thrie beam section to the buttress. The evaluations for the transition from the w-beam to the thrie beam section have been presented elsewhere. [FHWA12]

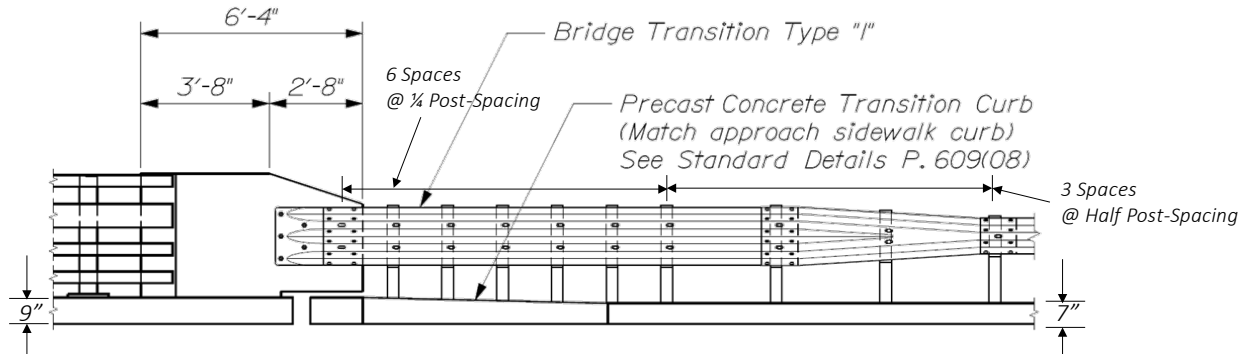


Figure 283. Elevation view of the concrete transition barrier for the NETC 4-bar bridge rail.

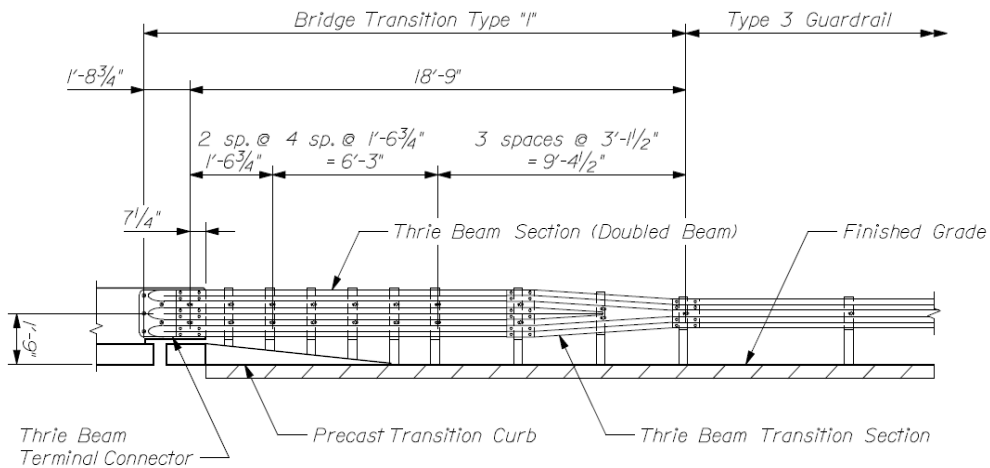


Figure 284. MaineDOT Bridge Transition Type 1.

The transition design includes four primary elements: (1) 10-gauge w-beam to thrie-beam transition with “half post-spacing”, (2) a two-layer, 12-gauge thrie-beam section with further decreased post spacing, (3) a 10-gauge thrie-beam terminal connector, and (4) a shaped concrete buttress, as illustrated in Figure 285. The concrete strength for the buttress and bridge deck was modeled with an unconfined compressive strength of 5000 psi. The transition posts are all W6x9 and 7 feet long with post spacing as shown in Figure 286. The material for the posts conformed to AASHTO M183. This part of the transition is identical to that of the 3-bar transition evaluated in Section 10.

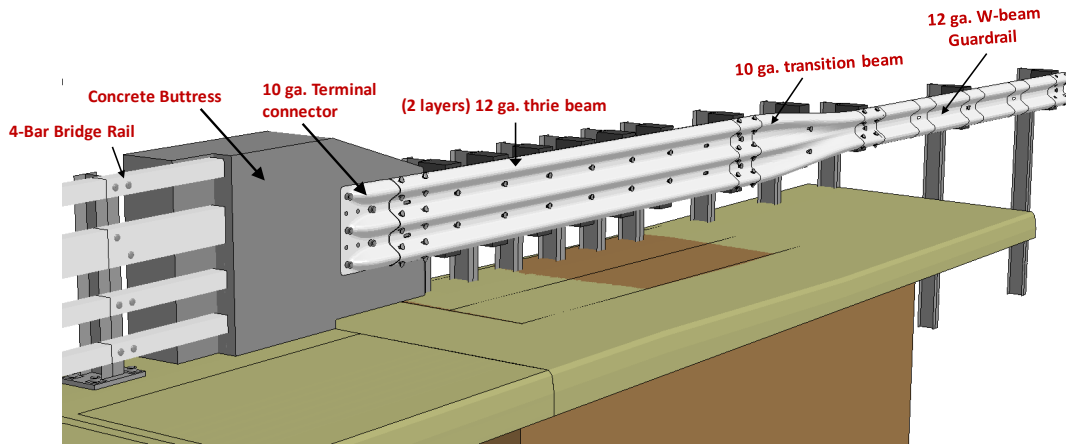


Figure 285. FEA model illustrating the various components of the system.

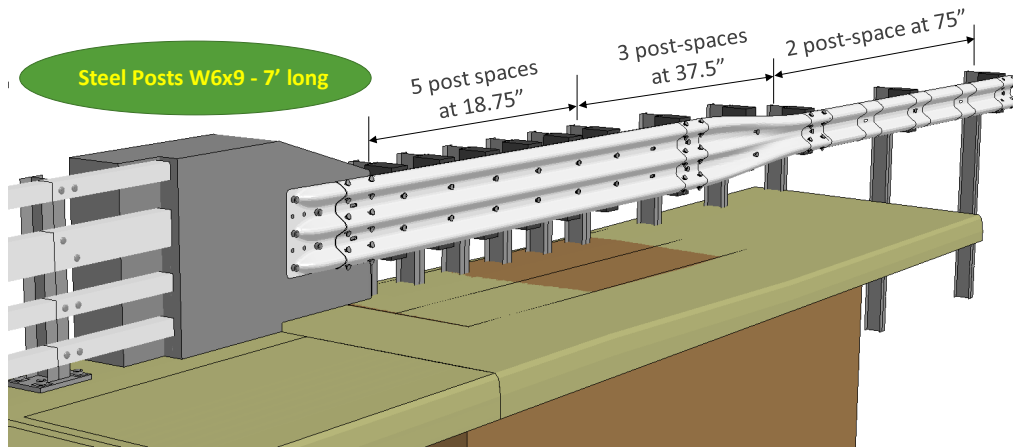


Figure 286. FEA model illustrating the post types and post spacing.

The model included 37.5 feet of w-beam guardrail and transition elements; and included 22.9 feet of the NETC 4-bar bridge rail, as illustrated in Figure 287. The bridge rail overlaps the buttress 12 inches at the recessed section of the buttress.

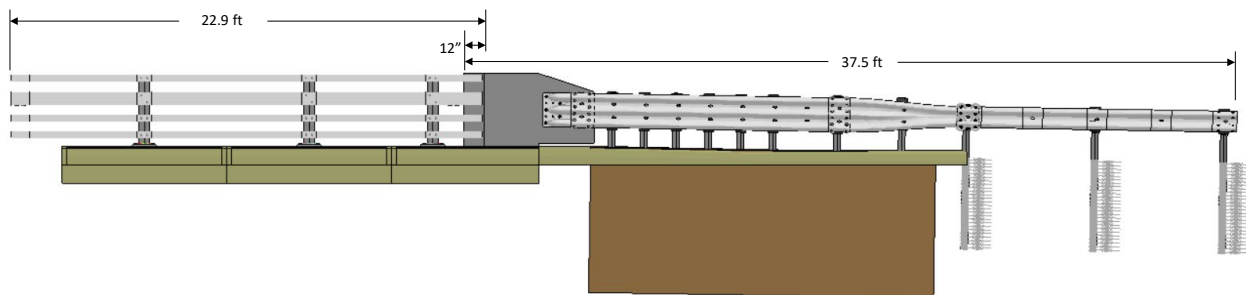


Figure 287. Complete FEA model of the MaineDOT transition and bridge rail.

The soil was modeled using two different methods depending on post location. Discrete elements (i.e., springs and dampers) were used to model the soil in the w-beam section for computational efficiency. Solid elements were used in the impact region on the transition where the posts were closely spaced (i.e., thrie-beam sections). The continuum soil model was 16.7 feet long, 8.34 feet wide and 7 feet deep and included a 2:1 slope starting just behind the thrie-

beam posts. A section view of the soil model is shown in Figure 288. Both models were calibrated to the MGSATB test series performed by MwRSF (refer to Task 2b for details).

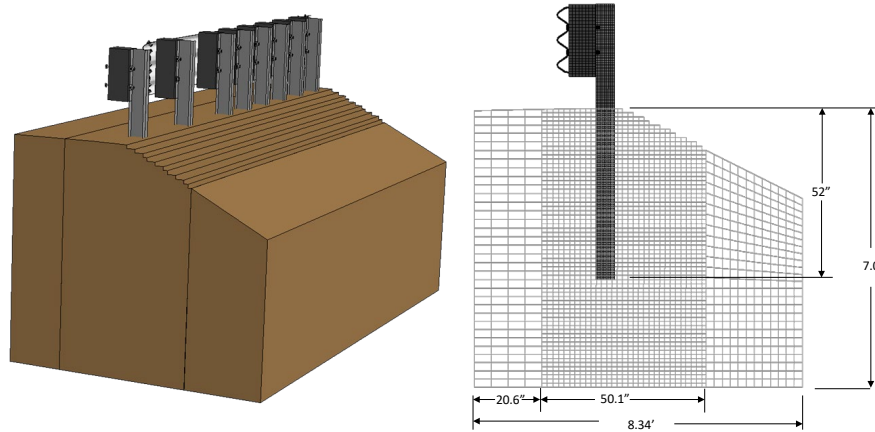


Figure 288. Soil continuum model from an oblique and section view.

The model for the shaped concrete buttress section was developed based on the drawing details in the MaineDOT standard drawings (see Appendix A). Figures 289 and 290 show the FEA model of the buttress, illustrating the overall dimensions, steel reinforcement details and anchorage details. The concrete was modeled using Mat_RHT in LS-DYNA with properties consistent with 5000-psi concrete. The material properties for the reinforcing steel conformed to ASTM A615 Grade 60 steel with properties measured at Turner Fairbanks Highway Research Center.[*TFHRC15*] The stress-strain characterization is shown in Figure 58. The buttress includes two bar sizes. The “dark shaded” bars in Figure 289 are #6 bars, and the lighter shaded bars are #5 bars.

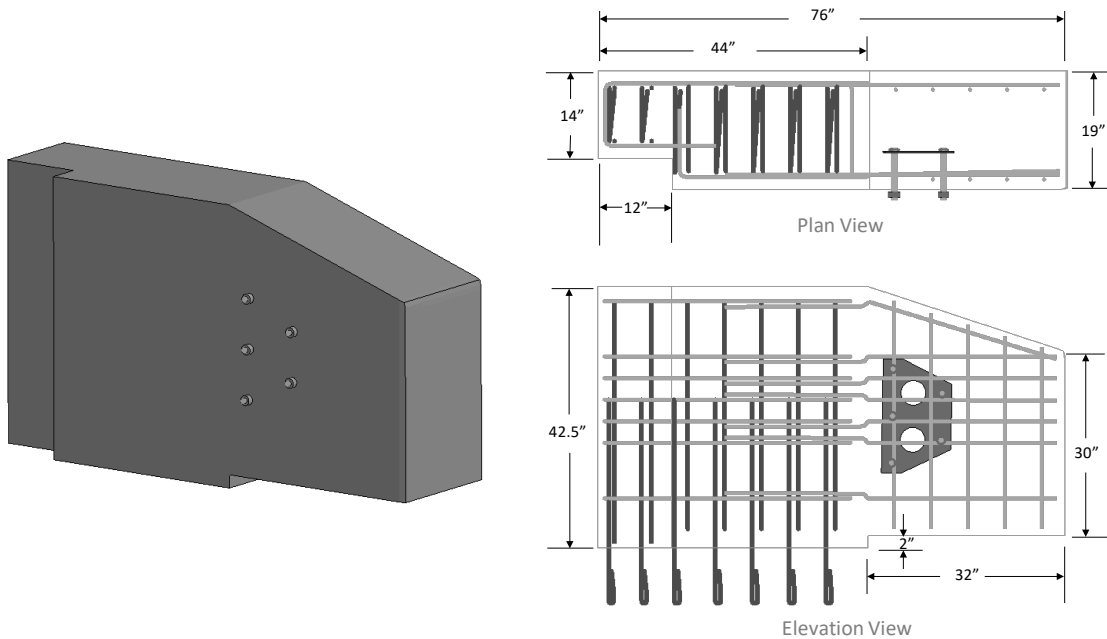


Figure 289. FEA model of transition buttress with dimensions and steel reinforcement details.

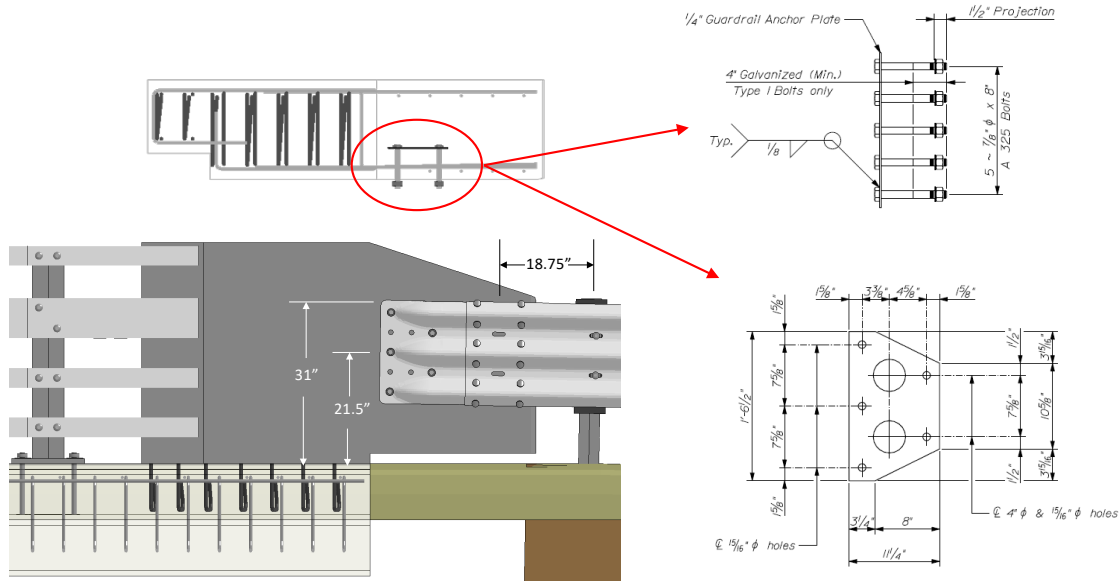


Figure 290. FEA model of buttress illustrating attachment details to three-beam and bridge deck.

The end of the w-beam in the model was not constrained for simulations of Test 4-20 (small car test) and Test 4-21 (pickup test). The lateral deflection of the rail in those cases was small enough to not warrant an end treatment on the rail. In a field installation, however, the rail would either continue on upstream or be terminated with a guardrail anchor system. For simulation of Test 4-22, the upstream end of the unanchored w-beam experienced relatively large longitudinal deflection. It was therefore necessary to include an end-treatment model for the rail for evaluation of Test 4-22 that accurately simulates the force-deflection response of a generic end-terminal with anchor cable and groundline strut.

The anchor was modeled as a nonlinear spring attached to the end of the w-beam rail with a force-deflection response developed and calibrated based on full-scale low-speed tests on a generic anchor system shown in Figure 291, which was performed at the Federal Outdoor Impact Laboratory (FOIL) test facility at the Federal Highway Administration’s Turner Fairbank Highway Research Center (TFHRC) in McLean, Virginia, as part of NCHRP Project 22-28. [Plaxico15] Chapter 9, as well as Chapter 13, of that report discusses the testing and characterization for the anchor model.



Figure 291. Test set-up for measuring force-deflection response of a standard two-post guardrail end-terminal anchor.

The force-deflection response of the anchor test is shown in Figure 292. The effect of loading rate on the anchor response was accounted for in the finite element model using a dynamic magnification factor of 1.5 to scale the quasi-static force-deflection curve.

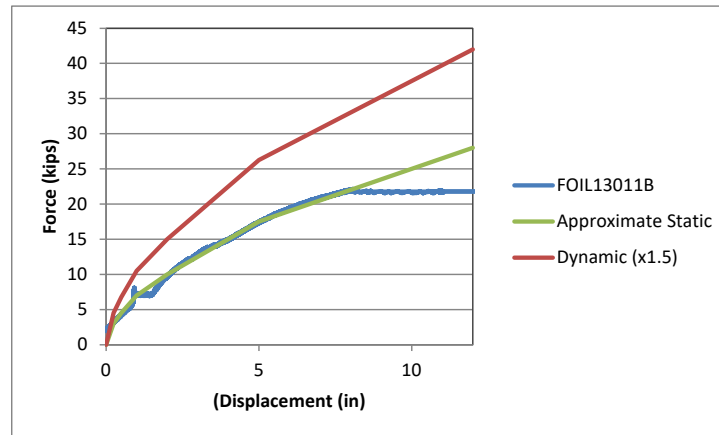


Figure 292. Measured and approximated force-deflection response for the end-anchor.

12.2 Test 4-20

12.2.1 CIP for Test 4-20

The critical impact point for all cases were designed to maximize potential for snag on the end of the concrete buttress. FEA was used to simulate impact of the 1100C vehicle into the transition system under *MASH* Test 4-20 conditions. Five analysis cases were performed which included impact at 4.0 ft, 4.5 ft, 5.0 ft, 5.5 ft, and 6.0 ft from the end of the concrete buttress. These analysis cases were conducted for 0.15 seconds of impact for the purpose of determining the critical impact point for maximizing vehicle accelerations and maximizing forces on the barrier at the junction point of the thrie-beam and the concrete buttress.

Figure 293 shows the results of the Test 4-20 simulations showing the deformation and position of the vehicle just before the tire impacted against the buttress in each case. Figure 294 shows the longitudinal and lateral 10-ms running average acceleration-time history data collected at the center of gravity of the vehicle in each case. Figure 295 shows plots of the OIV and maximum ORA values for each case.

From visual inspection of the analysis videos, the greatest potential for the wheel of the vehicle to snag on the abutment was at IP 5.5 ft, which corresponded to the greatest penetration of the wheel underneath the thrie-beam rail at the time of impact with the buttress. In all cases the OIVs were at or just above recommended limits. The longitudinal ORA was relatively high for impact points between 5 – 6 feet upstream of the buttress; however, impact at 5.5 feet resulted in ORA of 26 G (thus failing *MASH* criteria), and impact at 6.0 feet resulted in longitudinal ORA near critical limits.

Based on the results of these analyses the CIP for Test 4-20 was selected as 5.5 ft upstream of the buttress, which corresponds to the greatest potential for pocketing and highest ORA. This CIP is consistent with that determined for a similar system tested by MwRSF, which involved a shaped concrete transition to thrie-beam.[*Rosenbaugh19*]



Figure 293. Results of the Test 4-20 simulations showing the deformation and position of the vehicle just before the tire impacted against the buttruss for each case.

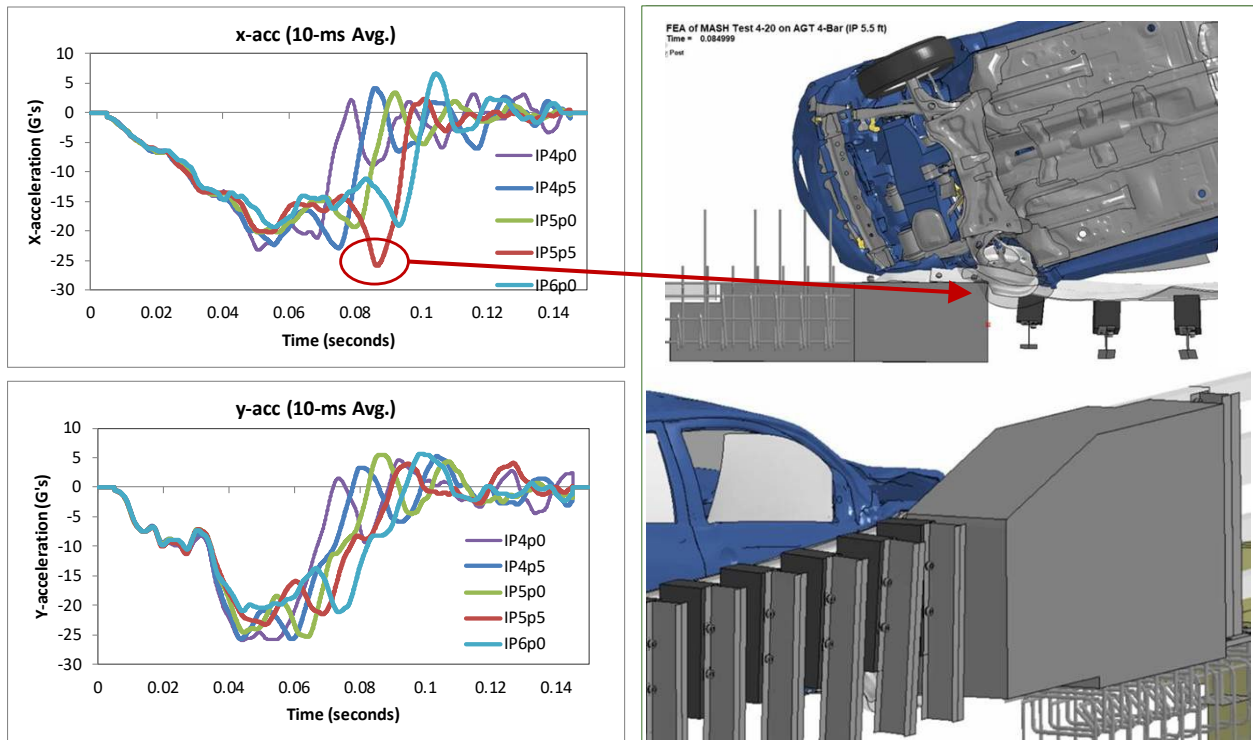


Figure 294. Acceleration data collected at the c.g. of the vehicle for each case.

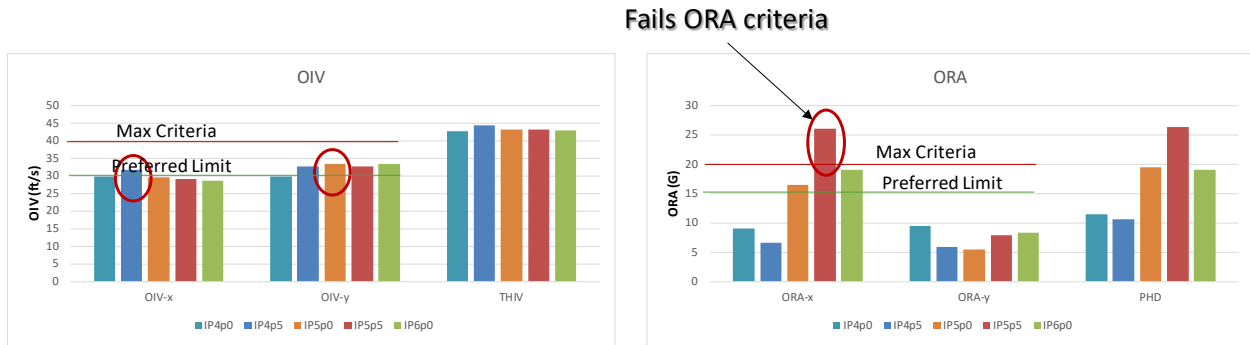


Figure 295. Plots of OIV and maximum ORA for each case.

12.2.2 Summary of Key Phenomenological Events

The sequential views of the impact event are shown in Appendix T in Figures T-1 through T-3 from an overhead viewpoint, downstream and upstream viewpoint, and isometric viewpoint, respectively. For this analysis case, the vehicle was not repositioned to the edge of the sidewalk, based on previous analysis results with this vehicle model that suggested that the tire interaction with the curb likely over-exaggerated the vertical trajectory of the vehicle (see Section 11.1.8).

At time equal zero seconds the vehicle struck the rail at 62.1 mph and 25 degrees. The front bumper of the car contacted the lower two corrugations of the nested thrie-beam rail at 5.5 feet upstream of the concrete buttress, as illustrated in Figure 296. At 0.005 seconds, the front-right tire contacted the lower corrugation of the thrie-beam, and the front-right fender contacted the top corrugation of the thrie-beam. At 0.01 seconds the barrier began to deflect. At 0.015 seconds the front-right tire began to steer away from the barrier, and at 0.02 seconds the tire was parallel to the barrier. At 0.04 seconds the top-back edge of the front fender kinked and cracked the lower edge of the windshield. At 0.05 seconds the front bumper of the vehicle was at the edge of the buttress, and the front-right tire was pushed underneath the rail between Posts 2 and 3. At 0.55 seconds the passenger side window failed, but the failure was not due to direct contact with the barrier. At 0.07 seconds the right-front tire was pushed underneath the thrie-beam rail approximately 12 inches, which was the maximum lateral position of the tire. Also, at this time, the rail reached maximum lateral deflection of 6.93 inches at the lower corrugation of the thrie-beam at the upstream edge of Post 2. At 0.0767 seconds the occupant struck the right side of the interior at 29.2 ft/s in the longitudinal direction and 32.8 ft/s in the lateral direction. At 0.08 seconds the wheel rim of the vehicle contacted and snagged the leading edge of the buttress. At 0.0837 seconds the maximum lateral ORA occurred with magnitude 7.9 G. At 0.087 seconds the maximum longitudinal ORA occurred with magnitude 26 G, which exceeded the maximum allowable limit of 20.49 G in *MASH*. At 0.085 seconds a substantial portion of the windshield had cracked due to the deformations of the fender and lower portion of the A-pillar. At 0.135 seconds the front of the vehicle separated from the barrier (the front-right tire was at the end of the thrie-beam terminal connector). At 0.25 seconds the vehicle reached maximum pitch angle of 6.8 degrees (rear of vehicle pitching upward). At 0.345 seconds the rear bumper of the vehicle contacted the bridge rail just upstream of Post 1 of the bridge rail on the two upper rails. The rear bumper remained in contact with the bridge rail until 0.47 seconds, at which time the vehicle exited the system at 36.3 mph and 35 degrees. At 0.63 seconds the vehicle reached a

maximum roll angle of 5.4 degrees (toward barrier). The vehicle remained stable throughout post-impact trajectory. The analysis ended at 0.63 seconds, at which time:

- The roll, pitch, and yaw of the vehicle were, respectively, 5.4 degrees (toward barrier), 4.1 degrees (rear pitching up), and 73.7 degrees (48.7 degrees relative to and away from barrier).
- The roll and pitch rate were stable at termination; however, the yaw rate was relatively high at 73.2 deg/s.
- The forward velocity of the vehicle was 34.7 mph (55.9 km/h).

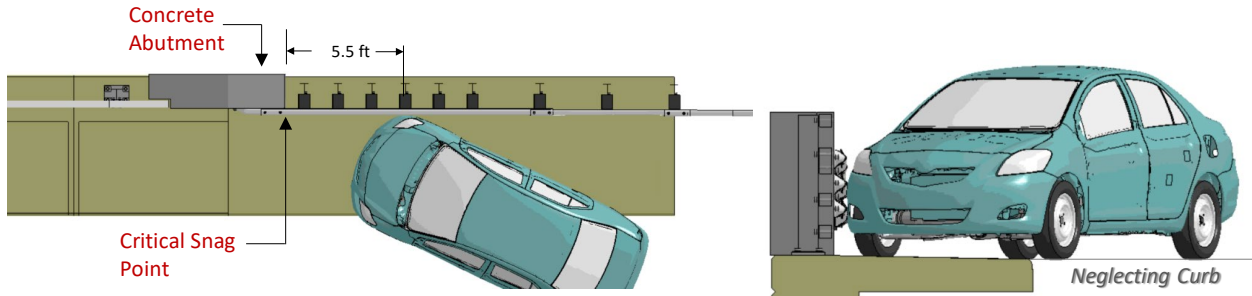


Figure 296. Impact point for Test 4-20 on the MaineDOT transition for 4-bar bridge rail.

12.2.3 Time History Data Evaluation

Figures 297 through 299 show the longitudinal, transverse, and vertical acceleration-time histories, respectively, computed from the center of gravity of the vehicle; Figures 300 through 302 show the comparison of the angular rates and angular displacements (i.e., yaw, roll and pitch) at the center of gravity of the vehicle.

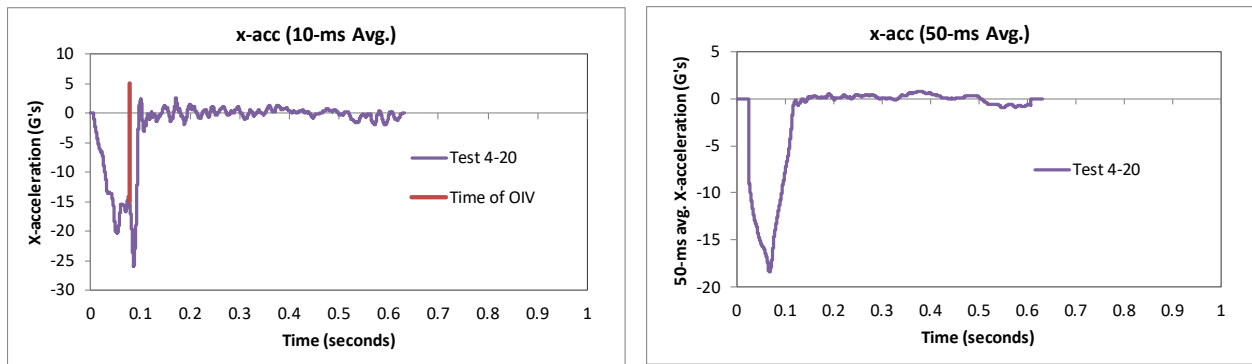


Figure 297. 10- and 50-millisecond average X-acceleration from FEA of Test 4-20 on the MaineDOT transition.

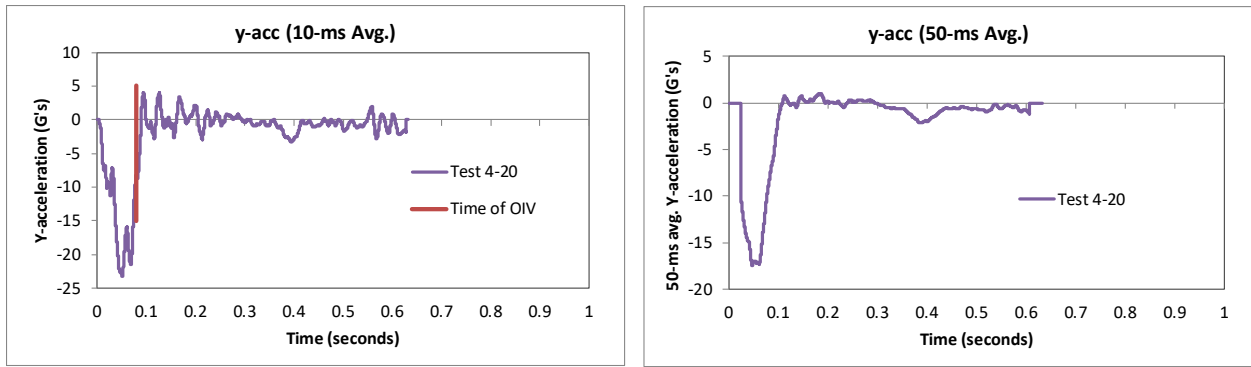


Figure 298. 10- and 50-millisecond average Y-acceleration from FEA of Test 4-20 on the MaineDOT transition.

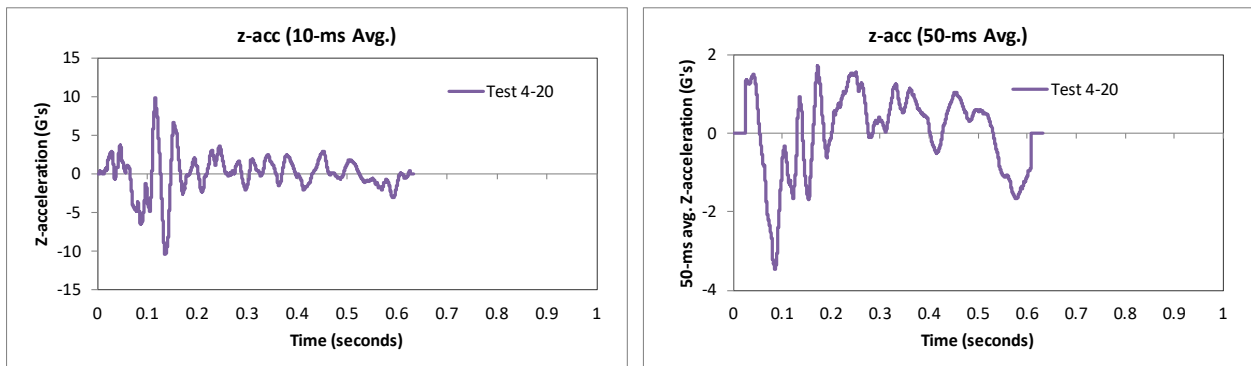


Figure 299. 10- and 50-millisecond average Z-acceleration from FEA of Test 4-20 on the MaineDOT transition.

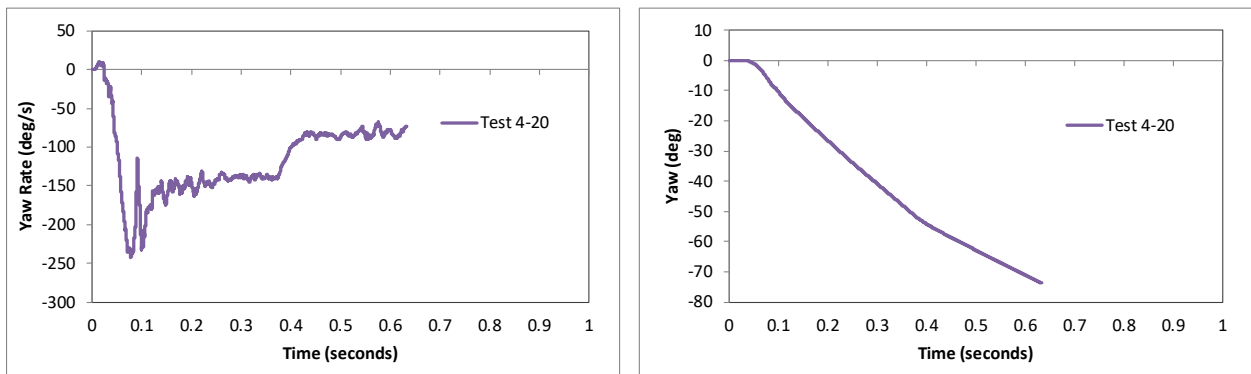


Figure 300. Yaw rate and yaw angle time-history from FEA of Test 4-20 on the MaineDOT transition.

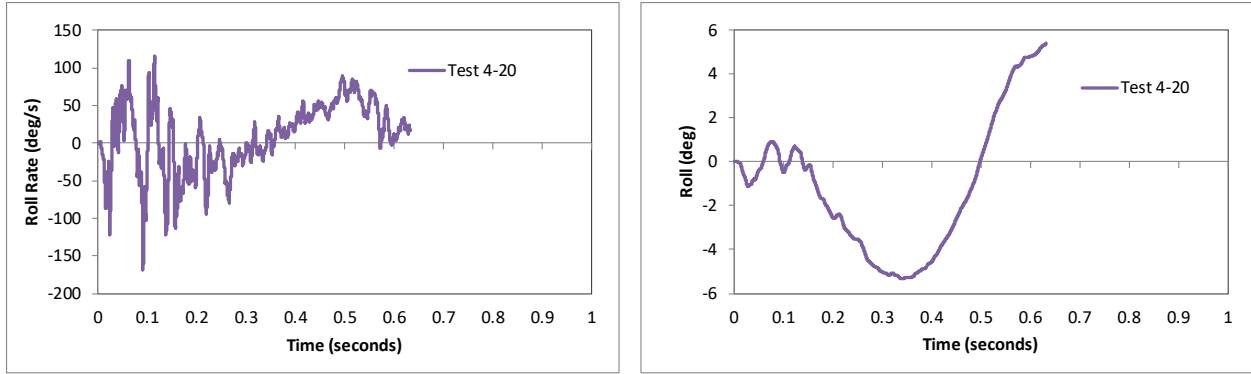


Figure 301. Roll rate and roll angle time-history from FEA of Test 4-20 on the MaineDOT transition.

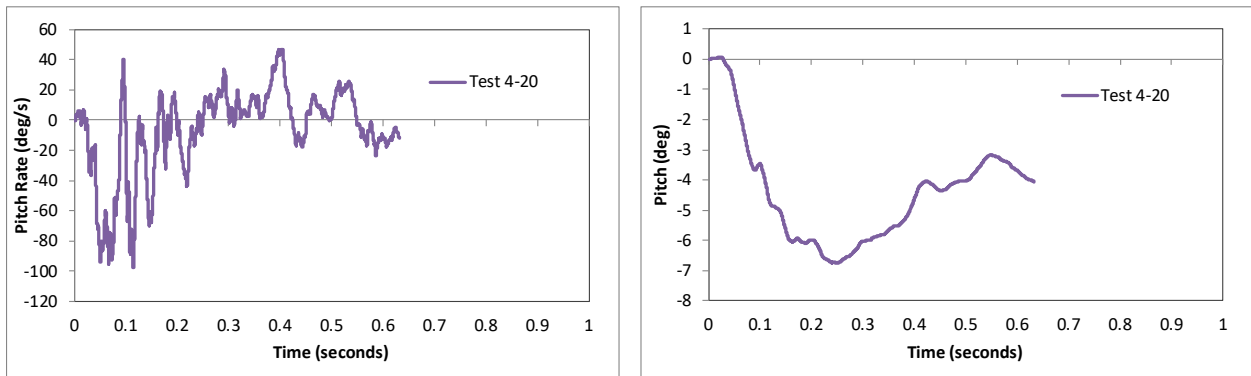


Figure 302. Pitch rate and pitch angle time-history from FEA of Test 4-20 on the MaineDOT transition.

12.2.4 Occupant Risk Measures

The acceleration-time histories and angular rate-time histories collected at the center of gravity of the vehicle were used to evaluate occupant risk metrics according to the procedures outlined in *MASH*. Table 89 shows the results for the occupant risk calculations. The results indicate that the longitudinal ORA does not meet safety criteria specified in *MASH*.

The occupant impact velocities in the longitudinal and transverse directions for the transition were 29.2 ft/s and 32.8 ft/s, respectively, which were within the critical limits specified in *MASH*. The highest 0.010-second occupant ridedown acceleration in the longitudinal and transverse directions were 26 g and 7.9 g, respectively, which exceeded the maximum critical limit of 20.49 g specified in *MASH*. The maximum 50-ms moving average acceleration values in the longitudinal and transverse directions were 18.4 g and 17.4 g, respectively. The maximum roll and pitch angles of the vehicle were 5.4 degrees and 6.8 degrees, respectively, which were well below critical limits in *MASH*.

Table 89. Summary of *MASH* occupant risk metrics for Test 4-20 on the MaineDOT transition.

Occupant Risk Factors		MASH	MASH Criteria
		Test 4-20	
Occupant Impact Velocity (ft/s)	x-direction	29.2	} > 30 ft/s (preferred) < 40 ft/s (limit) ✓
	y-direction	32.8	
	at time	at 0.0767 seconds on right side of interior	
THIV (ft/s)		43.3	}
		at 0.0767 seconds on right side of interior	
Ridedown Acceleration (g's)	x-direction	-26 (0.0816 - 0.0916 seconds)	} > 15 G (preferred) > 20.49 G (limit) ✗
	y-direction	-7.9 (0.0787 - 0.0887 seconds)	
PHD (g's)		26.4 (0.0814 - 0.0914 seconds)	
ASI		2.37 (0.0371 - 0.0871 seconds)	
Max 50-ms moving avg. acc. (g's)	x-direction	-18.4 (0.0427 - 0.0927 seconds)	}
	y-direction	-17.4 (0.0225 - 0.0725 seconds)	
	z-direction	-3.5 (0.0605 - 0.1105 seconds)	
Maximum Angular Disp. (deg)		5.4	} < 75 deg ✓
	Roll	(0.6324 seconds)	
	Pitch	(0.2502 seconds)	
	Yaw	(0.6324 seconds)	

12.2.5 Occupant Compartment Intrusion

The maximum deformation of the occupant compartment was approximately 3.4 inches at the lower right-front corner of the toe-pan at the wheel well. The deformation was less than the critical limit of 9 inches specified in *MASH* for this area of the occupant compartment. The lateral deformation of the A-pillar was 2 inches, which was less than the critical limit of 3 inches for this area of the vehicle. Figure 180 shows a view of the vehicle interior after the impact, with several components removed to facilitate viewing.

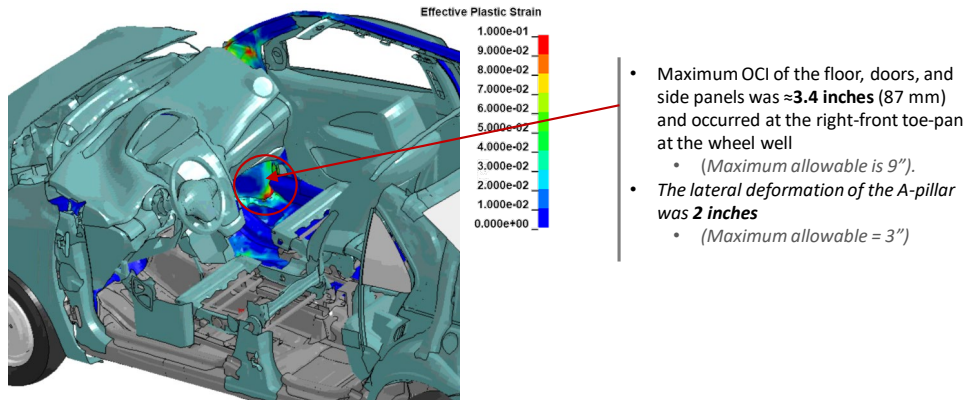


Figure 303. Occupant compartment deformation resulting from Test 4-20 on the MaineDOT transition.

12.2.6 Damages to the Barrier System

The damages to the transition were moderate to significant, but within expectations, and included kinking of the thrie-beam, lateral deflection of several posts and corresponding soil displacement at those posts. Figure 304 shows an overhead view of the post impact deformation of the transition indicating the length of vehicle contact. The vehicle was in contact with the

barrier system for 19.9 feet, although much of the contact on the bridge rail section was from light contact with the rear of the vehicle. Primary plastic deformations of the steel components of the transition were limited to the thrie-beam and thrie-beam terminal connector, with a sharp kink in the rail at the edge of the buttress, as shown in Figure 305. There was also soil displacement at Posts 1 – 6 approaching the buttress. Figure 306 and Figure 307 show contour plots of the maximum dynamic and permanent lateral deflection of the barrier, respectively, which occurred at the lower corrugation of the thrie-beam at the upstream edge of the blockout at Post 2. The maximum dynamic deflection was 6.73 inches, and the maximum permanent deflection was 5.7 inches. Figure 308 shows a contour plot of 1st principle strain on the concrete buttress. The damage to the concrete was negligible with strains limited to the joint connection between the buttress and bridge deck. The maximum dynamic strain was 0.054 at the vertical rebar joint on the upstream end of the buttress on the traffic side.

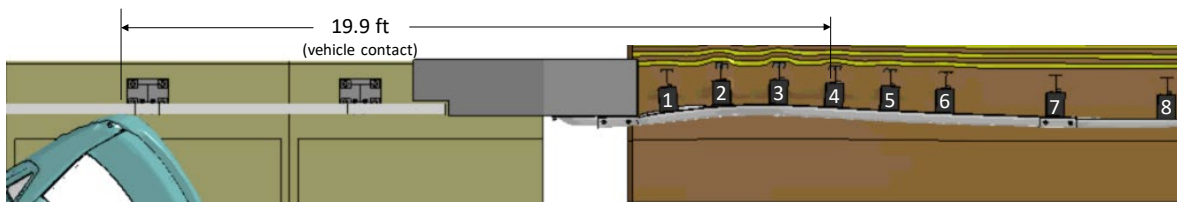


Figure 304. Overhead view of MaineDOT transition after Test 4-20 showing extent of damage.

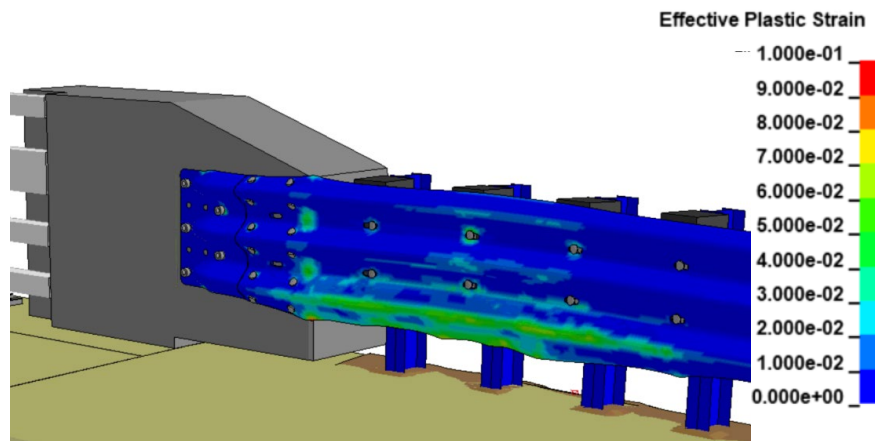


Figure 305. Contours of effective plastic strains on the steel rails and posts for Test 4-20 on the MaineDOT transition.

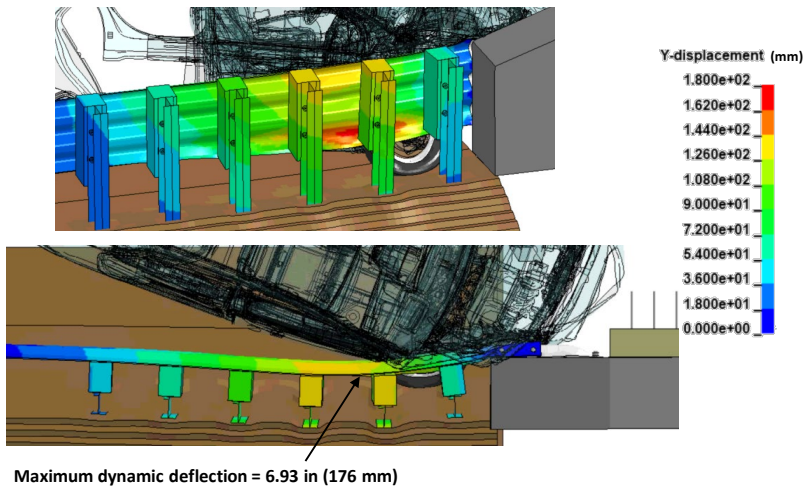


Figure 306. Contour plot of lateral displacement for the MaineDOT transition at the time of maximum dynamic deflection.

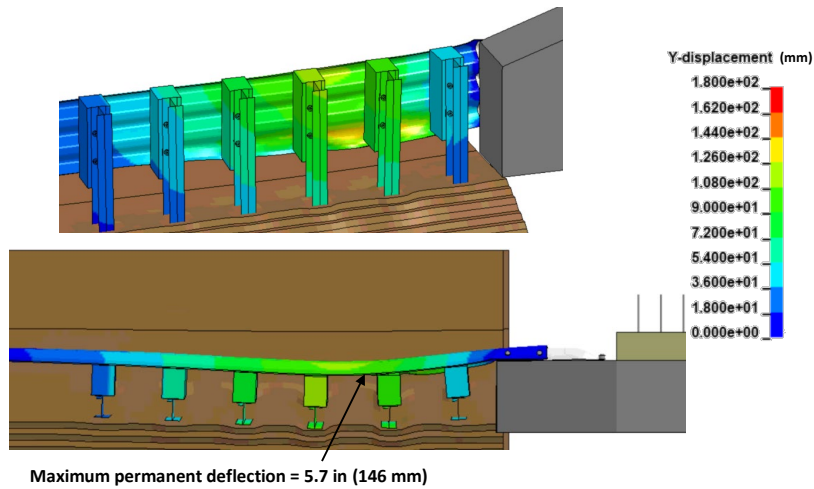


Figure 307. Contour plot of maximum permanent deflection for the MaineDOT transition.

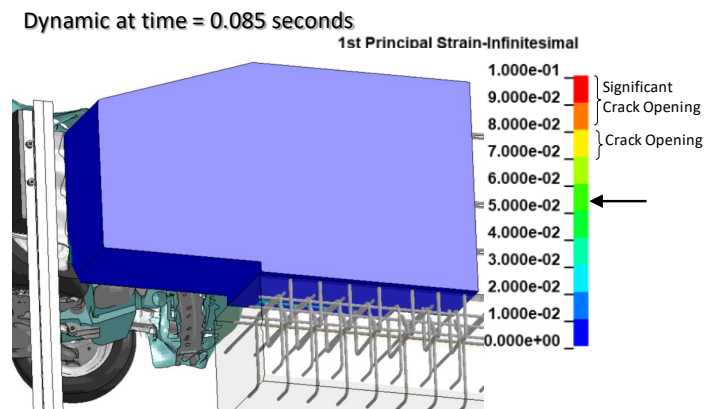


Figure 308. Contour plot of 1st principle strain on concrete buttress.

12.2.7 Damages to Vehicle

Figure 309 shows contour plots of effective plastic strain for the vehicle, which were used to identify areas of the vehicle that suffered damage during the simulated impact event. There was significant damages to the front-right corner of the vehicle, including the front fender, the front suspension, front wheel, and the leading edge of the front door on the impact side, the A-pillar, both passenger windows, and the right edge of the windshield at the A-pillar on the impact side.

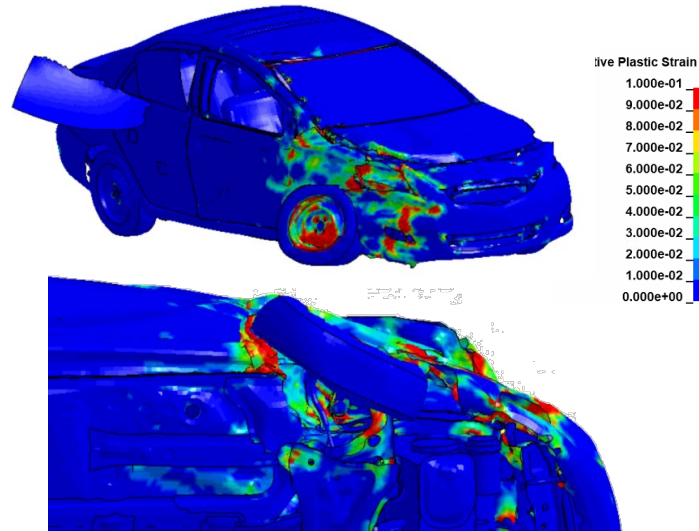


Figure 309. Damages to vehicle in Test 4-20 analysis of the MaineDOT transition.

12.2.8 Exit Box

Figure 310 shows the exit box for Test 4-20 on the MaineDOT transition, where the vehicle was redirected with its path within the exit box criteria of *MASH*; however, the yaw angle (i.e., 48.7 degrees relative to the barrier) and the yaw rate (i.e., 75 deg/s) were somewhat aggressive during post trajectory as the vehicle was redirected toward traffic lanes.

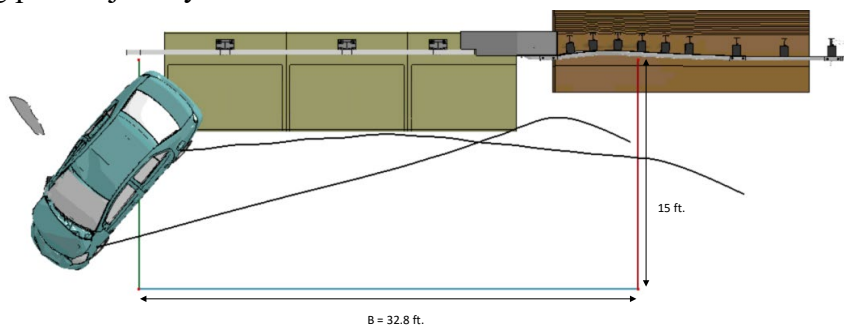


Figure 310. Exit box for Test 4-20 analysis of the 3-bar transition.

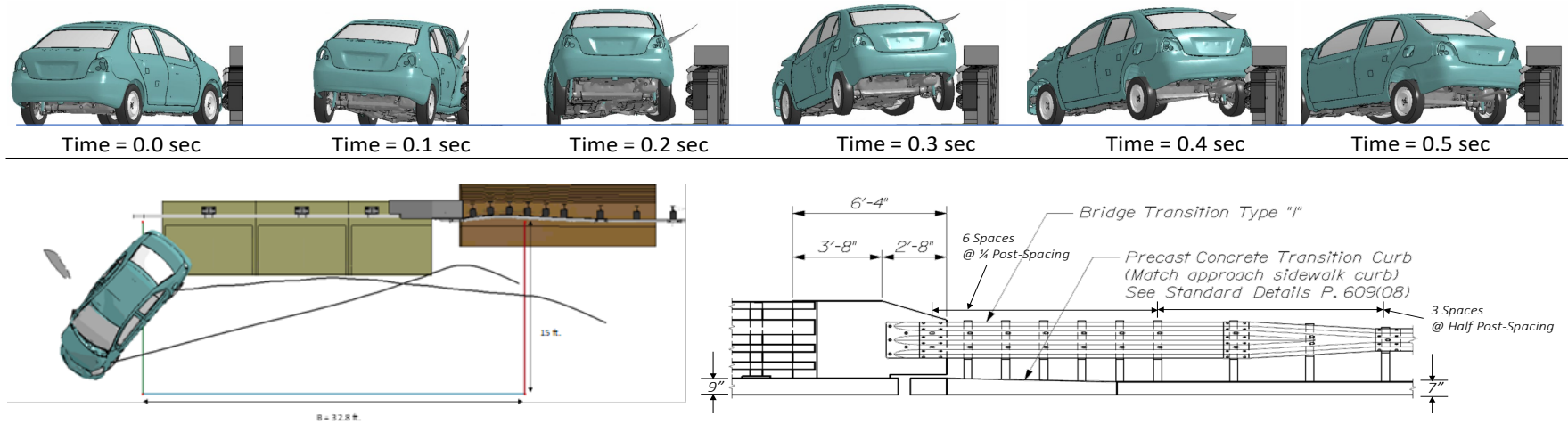
12.2.9 Results Summary

A summary of the *MASH* Test 4-20 results on the MaineDOT transition is shown in Table 90 and Figure 311. The barrier contained and redirected the small car with significant deformations to the thrie-beam section of the transition. There were no detached elements from the barrier that showed potential for penetrating the occupant compartment or presenting undue

hazard to other traffic. The vehicle remained upright and stable throughout impact and redirection. The OIV metrics were within critical limits; but the longitudinal ORA value of 26 G exceeded the maximum limit of 20.49 G. Based on the results of this analysis, the barrier does not meet the occupant risk criteria in *MASH* for Test 4-20 impact conditions.

Table 90. Summary of *MASH* Test 4-20 results on the MaineDOT transition for 4-bar bridge rail.

Evaluation Factors	Evaluation Criteria	Results
Structural Adequacy	A Test article should contain and redirect the vehicle or bring the vehicle to a controlled stop; the vehicle should not penetrate, underide, or override the installation although controlled lateral deflection of the test article is acceptable.	Pass
Occupant Risk	D Detached elements, fragments, or other debris from the test article should not penetrate or show potential for penetrating the occupant compartment, or present undue hazard to other traffic, pedestrians, or personnel in a work zone. Deformations of, or intrusions into, to occupant compartment should not exceed limits set forth in Section 5.2.2 and Appendix E.	Pass
	F The vehicle should remain upright during and after collision. The maximum roll and pitch angles are not to exceed 75 degrees.	Pass
	H The longitudinal and lateral occupant impact velocity (OIV) shall not exceed 40 ft/s (12.2 m/s), with a preferred limit of 30 ft/s (9.1 m/s)	Pass
	I The longitudinal and lateral occupant ridedown acceleration (ORA) shall not exceed 20.49 G, with a preferred limit of 15.0 G	Fail



General Information		Impact Conditions		Max50-millisecond Avg. (G)	
Analysis Agency	Roadsafe LLC	Speed	62 mph	Longitudinal	18.4 g
Test Standard Test No.	MASH Test 4-20	Angle	25 degrees	Lateral	17.4 g
Analysis No.	NETC18_MEDOT-Trans_T420	Location	5.5 ft upstream of buttress	Vertical	3.5 g
Analysis Date	4/16/2019				
Test Article		Impact Severity		Test Article Deflections (in)	
Type	Bridge Rail Transition	59.5 kip-ft		Dynamic	6.93 inches
Name	MEDOT Transition for 4-Bar BR	Exit Conditions		Permanent	5.7 inches
Installation Length	59.4 feet	Speed	36.3 mph	Working Width	
Material or Key Elements		Angle	35 degrees		
Soil Type and Condition		Time	0.47 seconds	Max. OCI	
MASH Strong Soil		Occupant Risk Values		3.4 inches	
Analysis Vehicle		Longitudinal OIV	29.2 ft/s	Vehicle Stability	
Type / Designation	1100C	Lateral OIV	32.8 ft/s	Roll	5.4 degrees
FEA Model name	510_YarisC_V11_R180228	Longitudinal ORA	26 g	Pitch	6.8 degrees
Mass	2,595 lb	Lateral ORA	7.9 g	Yaw	73.7 degrees
		THIV	43.3 ft/s		
		PHD	26.4 g		
		ASI	2.37		

Figure 311. Summary results for MASH Test 4-20 on the 3-bar transition.

12.2.10 Comparison to MASH Test 4-20 on Similar AGT System

Since the results of the analysis indicated poor performance for the concrete transition, it is meaningful to compare the results of the analysis to those of a full-scale test on a similar concrete AGT system. On May 9, 2017 the MwRSF conducted a *MASH* Test 4-20 on a 34-inch tall concrete AGT, which is shown in Figure 312. This design incorporates a taper at the nose of the concrete transition buttress to help mitigate wheel snag and uses W6x15 posts spaced at 3'-1.5" on center at the approach to the buttress. Additional details of the MwRSF AGT can be found in Rosenbaugh et.al. [Rosenbaugh18; Rosenbaugh19] The designs are not the same for these two systems; however, they are similar in that they both entail a relatively stiff, nested thrie-beam section connected to a rigid concrete buttress, and they both resulted in the tire of the vehicle pushing underneath the thrie-beam and snagging on the end of the concrete buttress. The resulting vehicle accelerations were also similar in both cases, as shown in Figure 315.

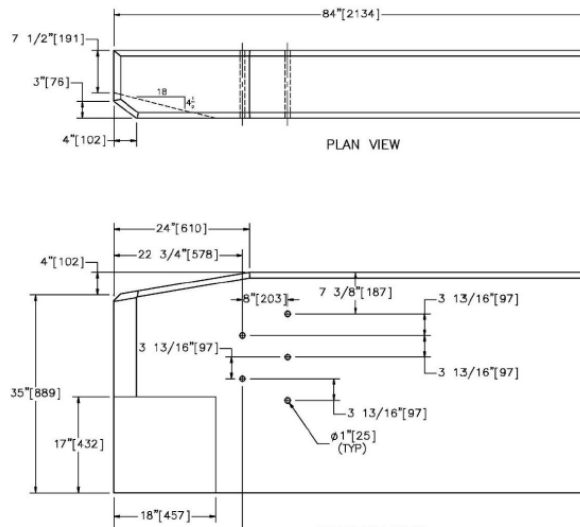


Figure 312. Concrete AGT tested by MwRSF (Test 34AGT-2). [Rosenbaugh19]

The full-scale test involved a 2,420-lb small car impacting at 62.1 mph and 25.5 degrees at 5.41-ft upstream from the nose of the MwRSF buttress; whereas, the FEA involved a 2,595-lb small car impacting at 62.1 mph and 25 degrees at 5.5 ft upstream from the nose of the MaineDOT buttress. For the full-scale test the acceleration-time histories of the vehicle were collected from two accelerometer blocks. One of the blocks was located at the vehicle c.g. (i.e., Slice-2), and the other was located near the c.g. (Slice-1). The longitudinal and lateral acceleration-time histories from these two blocks are overlaid with each other in Figure 315, and the occupant risk metrics from each data set is shown in Table 91.

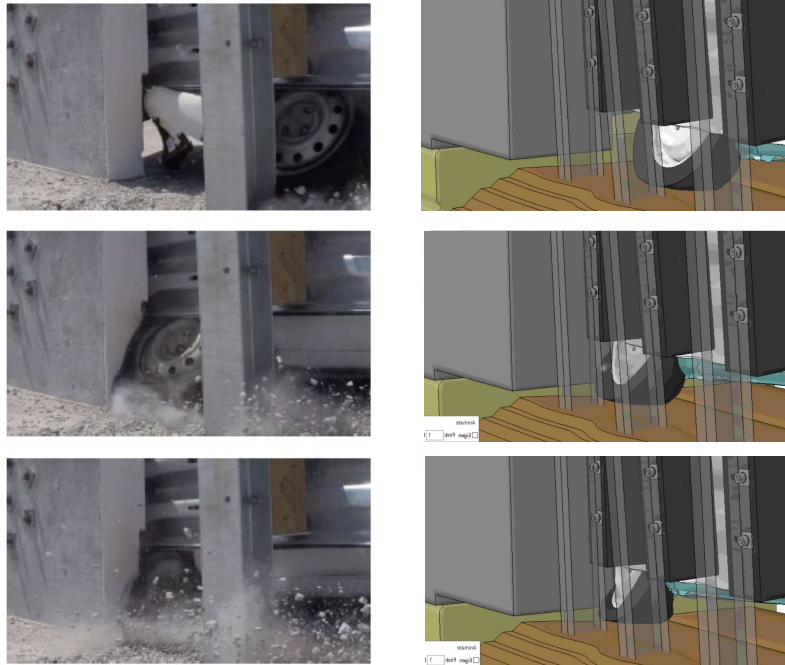


Figure 313. Tire snag on the buttress for Test 34AGT-2 and the FEA analysis.

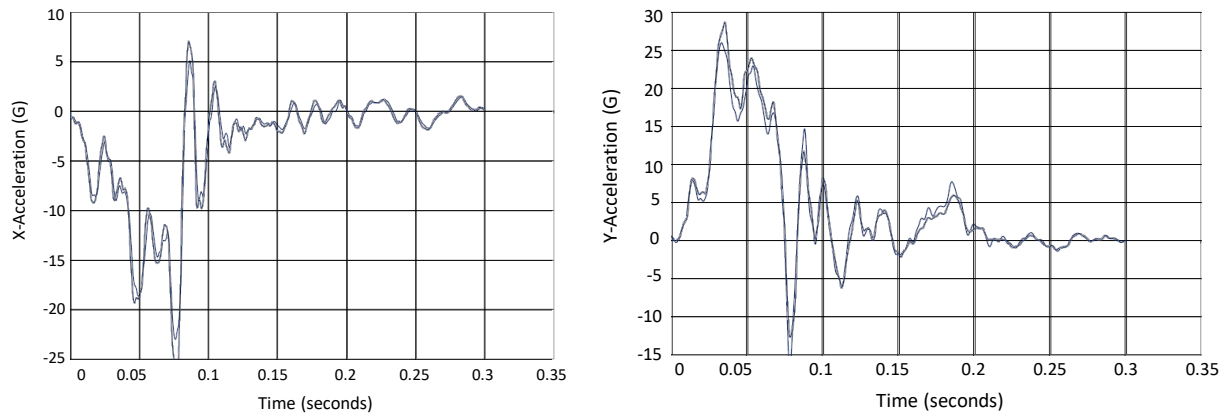


Figure 314. Overlay of the accelerations from Slice 1 and Slice 2 from full-scale test 34AGT-2. [Rosenbaugh19]

Table 91. Occupant risk metrics from Test 34AGT-2 and the FEA analysis.

Evaluation Criteria		Test 34AGT-2		MEDOT	MASH 2016 Limit
		Slice -1	Slice -2 (Primary)	FEA	
OIV ft/s	Longitudinal	20.5	22.7	29.5	±40
	Lateral	35.3	32.7	32.8	
ORA g's	Longitudinal	-25.6	-10.84	-26.0	±20.49
	lateral	-12.7	+14.7	7.9	

Although the acceleration-time histories are very similar for the two acceleration blocks, the resulting ORA values are very different for Slice-1 and Slice-2. It is assumed, based on the plot overlays, that the likely cause for these differences is that the theoretical occupant would have contacted the interior slightly sooner for Slice-1 than Slice-2, since the acceleration peaks were higher magnitude for Slice-1.

Figure 315 shows an overlay of the FEA results with each of the test accelerometers. The vertical line in each of the plots in Figure 315 represents the time of occupant impact with the interior as determined from the FEA analysis. The acceleration trace for the FEA is similar to the test in each case, with the exception that the peak acceleration occurs approximately 0.01 seconds sooner in the test because the impact point in the test was nearer to the buttress (e.g., 5.41 ft vs. 5.5 ft). The time of occupant impact was not reported for the full-scale test; however, based on the FEA results the time of occupant impact occurs at approximately the same time of the peak acceleration in the test. So, a very slight delay in the time of occupant impact could result in a significant reduction in ORA for the test, which appears to be the case based on the time of ORA for the two acceleration blocks in the test, as indicated in Figure 315. For the longitudinal ORA it was a difference of -25.6 G vs. -10.8 G; and for the lateral ORA it was a difference of -12.7 G vs. +14.7 G. The longitudinal ORA for the FEA was essentially the same as Slice-1 in the test (i.e., 26 G vs. 25.6 G).

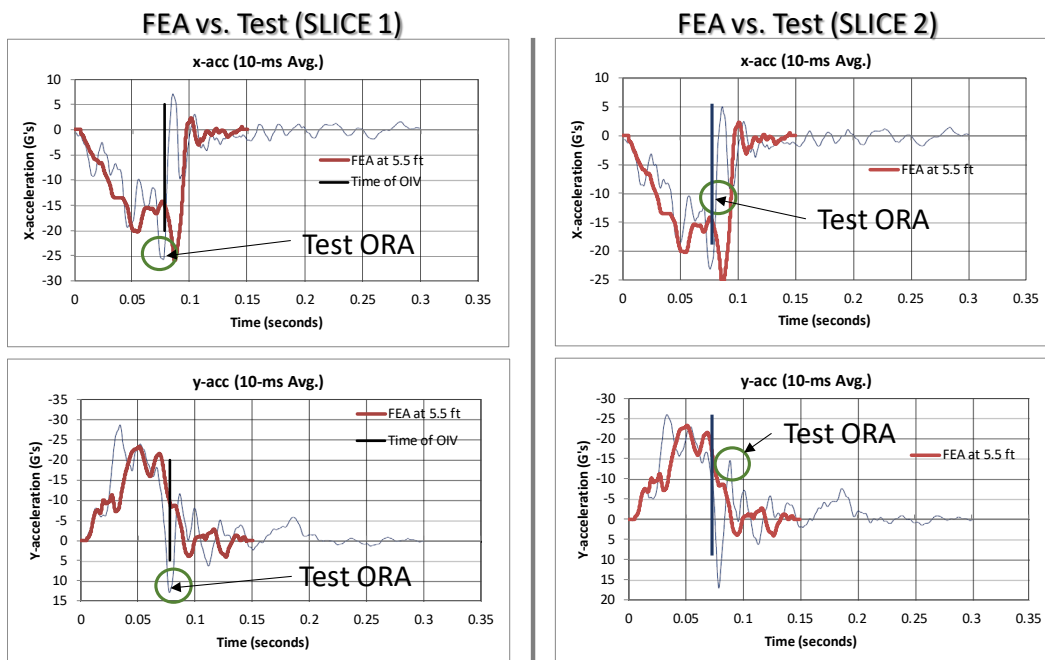


Figure 315. Overlay of acceleration-time histories for FEA and tests.

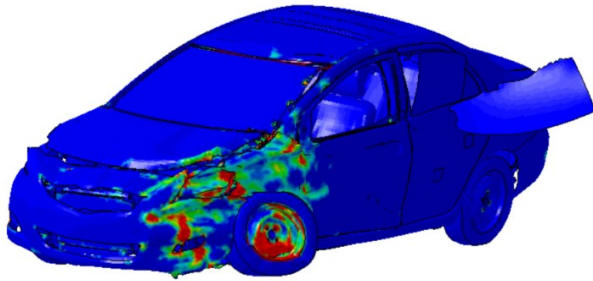


Figure 316. Comparison of vehicle damage for FEA (MaineDOT transition) and full-scale test (MwRSF transition).

12.3 Test 4-21

12.3.1 CIP for Test 4-21

Finite element analysis was used to simulate *MASH* Test 4-21 at impact points 5.5 ft, 6.0 ft, 6.5 ft, 7.0 ft and 7.5 ft from the end of the nose of the buttress. These analysis cases were conducted for 0.15 seconds of impact for the purpose of determining the critical impact point for maximizing the potential for snagging on the upstream end of the buttress. For computational efficiency the dynamic effects of the vehicle crossing the sidewalk were neglected, and the vehicle was positioned on top of the sidewalk with the bumper a few millimeters away from the barrier at the target impact point. The assessment was based on five key factors:

1. Pocketing – Maximum relative deflection between thrie-beam and buttress
2. Peak accelerations relative to critical snag point – Peak longitudinal acceleration (e.g., generally identifies snag), and peak lateral acceleration (e.g., point of highest lateral force)
3. OIV and ORA – These metrics are used directly in crashworthy assessments in *MASH*
4. Impact severity and kinetic energy at time of impact with critical snag point
5. Maximize potential for component failure – maximizing forces on the barrier at the junction point of the thrie-beam and the concrete buttress. Also, the strains in concrete were evaluated to determine potential for cracking and spalling.

The potential for pocketing was evaluated by measuring the lateral displacement of the thrie-beam at 12 inches upstream of the nose of the buttress, as illustrated in 271Figure 188. The results of the evaluations are shown in Figure 318, which also includes plots of impact severity and kinetic energy of the vehicle at the time of impact with the buttress. Based on these results, impact at 7.0 feet upstream of the buttress resulted in the highest relative deflections and was therefore considered the highest potential for snagging on the ends of the buttress.

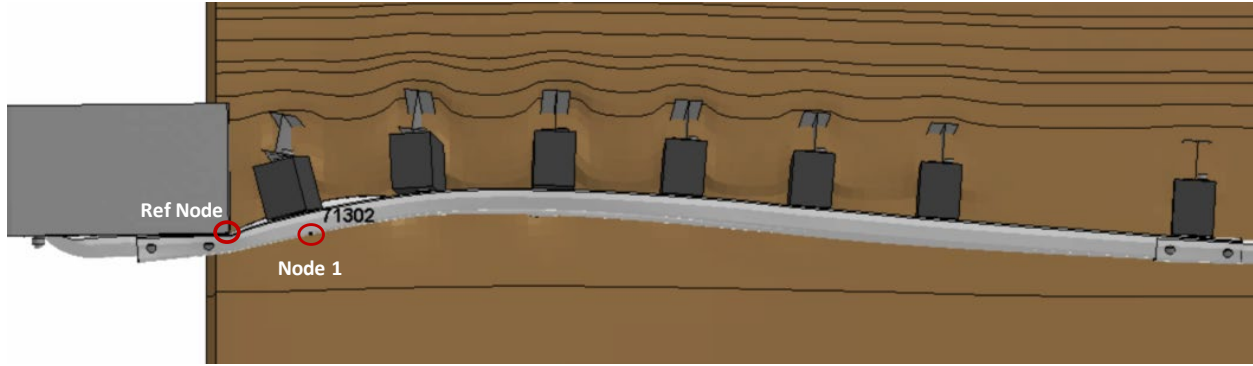


Figure 317. Measurement points for determining CIP for pocketing for Test 4-21.

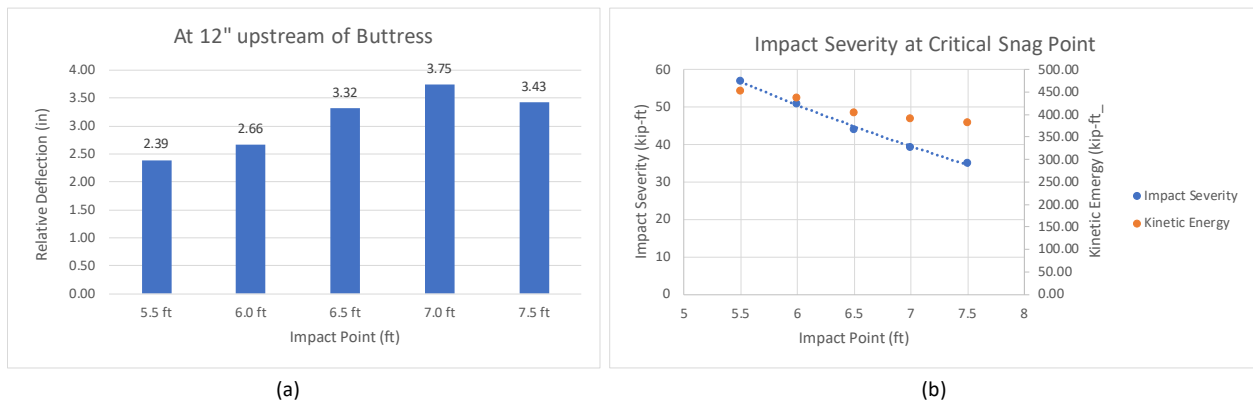


Figure 318. (a) Relative displacements of rail and (b) impact severity and kinetic energy at time of impact with buttress for Test 4-21 CIP evaluations.

Figure 319 shows plots of the 10-millisecond running average accelerations and the 50-millisecond running average accelerations measured at the center of gravity of the vehicle for the longitudinal and lateral directions for each of the analysis cases. The highest longitudinal acceleration occurring at the time when the vehicle impacts the buttress occurred for impact case 6.5 feet. The highest lateral accelerations at the time of impact with the buttress were highest for impact cases 5.5 – 6.5 feet, each with similar magnitudes.

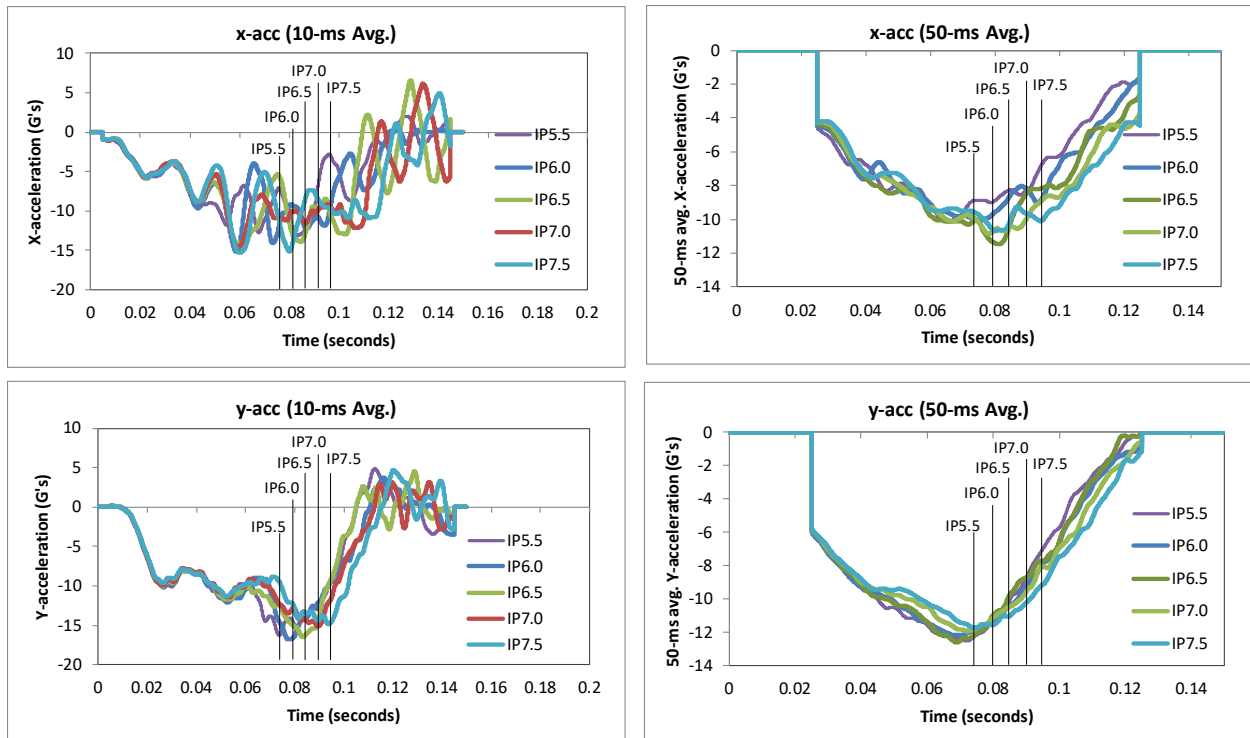


Figure 319. Plots of longitudinal and lateral accelerations indicating the time of vehicle contact with the buttress.

Figure 320 shows a comparison of the occupant risk metrics computed using the TRAP software, including the OIV, ORA, THIV, PHD, ASI, and 50-millisecond average accelerations. The highest values for some of the key metrics are circled on the plots. Note that the rear of the vehicle had not impacted the rail at the time of analysis termination, so maximum ORA in the lateral direction was not yet determined. The impact case at 6.5 feet resulted in the highest values for each of the key metrics, although the OIV, THIV and ASI were very similar for all cases.

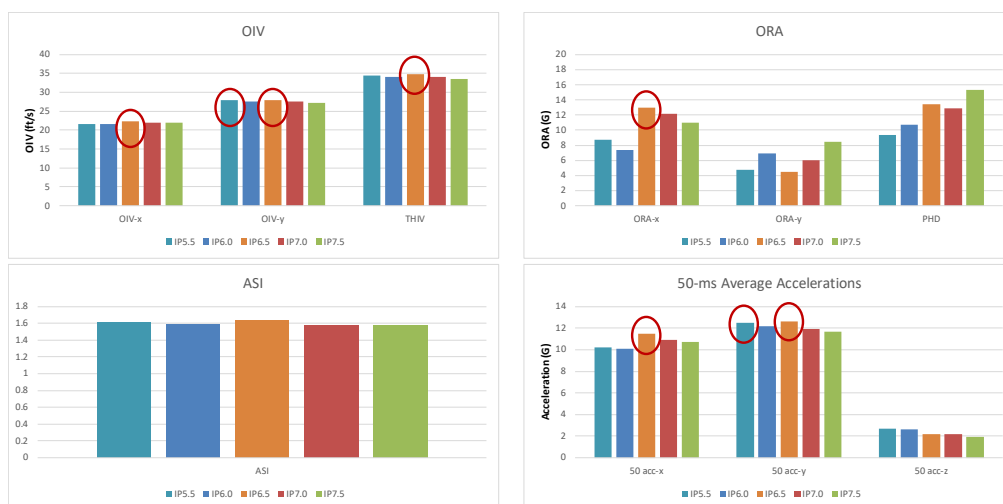


Figure 320. Comparison of occupant risk metrics computed in TRAP for Test 4-21.

Figure 321 and Figure 322 show contour plots of 1st principle strain for the buttress and the bridge deck, respectively, with the maximum values identified for each case. The damage to the buttress was limited to the rebar-joint between the buttress and the curb at two stirrup locations on the upstream end of the buttress on the traffic side. The magnitude of the strains on the buttress for impact cases 5.5 – 7.0 feet indicated that concrete failure around the first two or three stirrups on the traffic side was likely, with the highest strains occurring for the impact case at 6.5 feet. Similarly, the damage to the concrete deck was limited to the rebar-joint at three stirrup locations at the upstream end of the buttress on the field side. The magnitude of the strains for impact cases at 5.5 feet and 6.5 feet indicated that significant cracks were likely for the concrete deck at the upstream stirrups on the field side.

Based on the analysis results it was determined that the impact case at 7.0 ft upstream of the buttress provided the greatest potential for pocketing, and the impact case at 6.5 ft provided the highest occupant risk (e.g., ORA). Thus, the CIP was selected as the midpoint between those two cases at 6.75 ft upstream of the buttress. The local damages to the concrete buttress and sidewalk did not significantly influence the crashworthiness of the system.

The final analysis was performed with the pickup moved back to the curb-face of the sidewalk with a target impact point on the transition at 6.75 feet upstream of the buttress. The analysis was performed for 0.9 seconds of the impact event. The following sections provide a summary of the results and include a commentary describing the timing and occurrence of various events during the simulated impact, time-history data evaluation, occupant risk assessments, and damages sustained by both the barrier and vehicle.

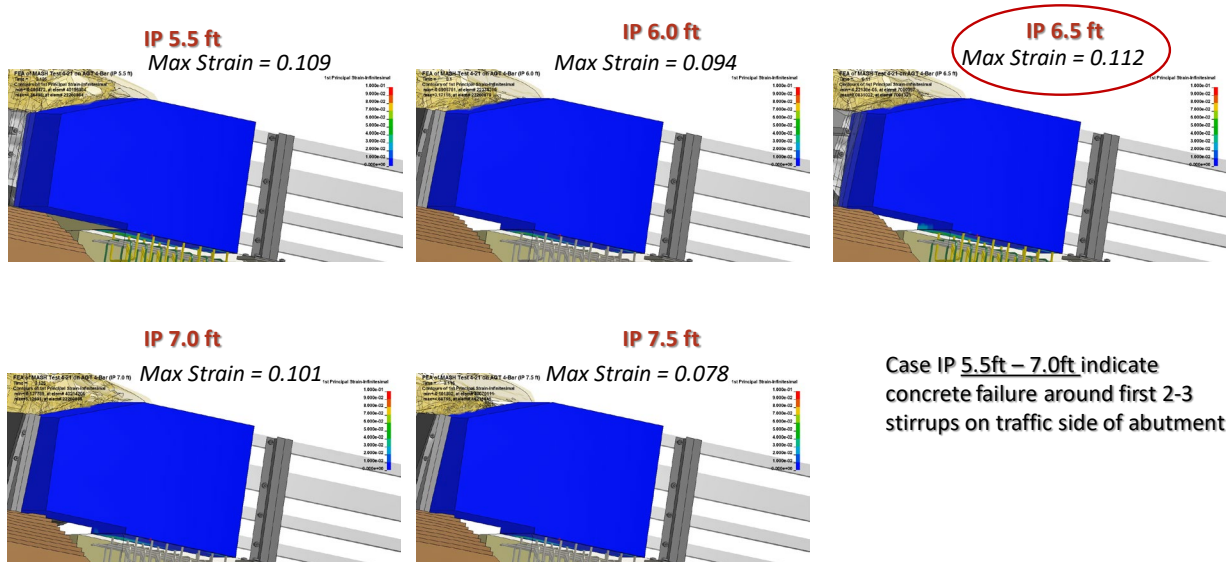


Figure 321. Contour plots of 1st principle strain for the buttress.

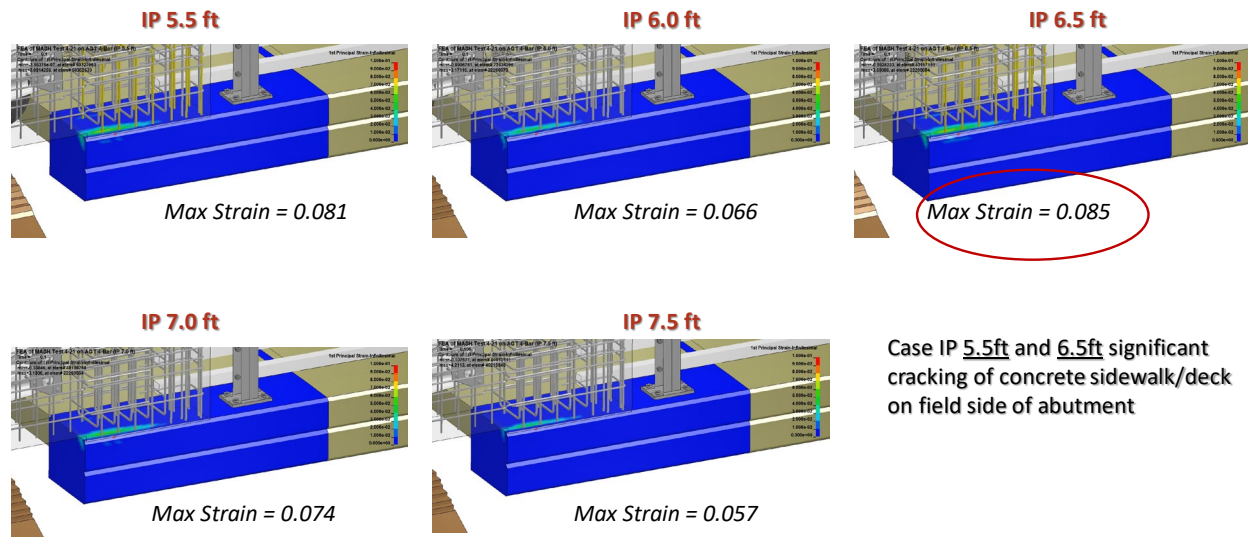


Figure 322. Contour plots of 1st principle strain for the deck.

12.3.2 Summary of Key Phenomenological Events

The sequential views of the impact event are shown in Appendix U in Figures U-1 through U-3 from an overhead viewpoint, downstream and upstream viewpoint, and isometric viewpoint, respectively. For this analysis case, the vehicle was repositioned to the edge of the sidewalk with a target impact point of 6.75 feet upstream of the nose of the concrete buttress, as illustrated in Figure 323.

The 5,001-lb pickup struck the curb-face of the sidewalk at a speed of 62 mph and at an angle of 25 degrees per *MASH* Test 4-21 specifications. The impact point of the front-right tire with the curb was approximately 16.5 feet upstream of the concrete buttress, the front bumper was 15.2 feet upstream of the buttress at this time. At 0.005 seconds, the front-right tire compressed at the point of contact with the curb. At 0.015 seconds the deformation of the tire indicated that deflation was likely; however, tire deflation was not included in the model. At 0.03 seconds the tire had fully mounted the sidewalk, and the vehicle began to roll away from the barrier. The tire rebounded slightly from the sidewalk at 0.040 seconds but then recontacted the sidewalk at 0.060 seconds and remained in contact until impact with the barrier. At 0.11 seconds the front bumper impacted against the two lower corrugations of the nested thrie-beam rails at 6.5 feet upstream of the buttress. The speed and angle of the vehicle at the time of impact was 61.4 mph and 24.8 degrees, as illustrated in Figure 324. The roll and pitch angle of the vehicle was 4.25 deg (rolling away from the barrier) and 0.86 degrees (front pitching up), respectively. At 0.115 seconds the front-right fender contacted the top corrugation of the thrie-beam. At 0.12 seconds the barrier began to deflect. At 0.13 seconds the front-right tire began to steer away from the barrier, and at 0.14 seconds the tire was parallel to the barrier. At 0.135 seconds the rear-right tire contacted the curb-face of the sidewalk and began to mount the curb. At 0.145 seconds the front-left tire contacted the curb-face of the sidewalk and began to steer away (the tire did not mount the curb). At 0.165 seconds the front fender extended over the top of the thrie beam and impacted against the blockout at Post 2. Also, at this time, the rear-right tire was fully mounted onto the sidewalk, and the front-left tire was steered parallel to the sidewalk. At 0.17 seconds the front bumper of the pickup contacted the leading edge of the buttress. At 0.175 seconds the barrier experienced a maximum dynamic deflection of 8.11 inches at the lower

corrugation of the thrie-beam at 35.2 inches upstream of the buttress. At 0.19 seconds the ball-joint of the lower control arm on the front-left wheel failed. At 0.1943 seconds the occupant struck the right side of the interior at 21.0 ft/s in the longitudinal direction and 28.2 ft/s in the lateral direction. At 0.195 seconds the front fender extended over the top of the thrie beam and impacted against the blockout at Post 1 and the top edge of the buttress. At 0.2 seconds the front-left tire was pressed slightly underneath the thrie-beam and contacted the lower edge of the buttress. The maximum longitudinal ORA of 9.4 G also occurred at this time. At 0.305 seconds the rear-right tire contacted the two lower corrugations of the thrie-beam and the bumper contacted the top corrugation. The barrier again began to deflect. At 0.335 seconds Posts 1 and 2 reached a maximum lateral deflection of 6.9 inches, resulting in a barrier working width of 24.2 inches. At 0.345 seconds the rear-right tire contacted the buttress, and at 0.36 seconds the vehicle reached a peak lateral acceleration of 17.3 G due to impact with the buttress, resulting in the maximum ORA. At 0.42 seconds the vehicle separated from the barrier at a speed and angle of 42.6 mph and 8.9 degrees as the rear bumper was passing the thrie-beam terminal connector on the buttress. At 0.69 seconds the vehicle reached a maximum roll angle of 15.4 degrees (toward barrier). At 0.74 seconds the vehicle reached maximum pitch angle of 9.6 degrees (rear of vehicle pitching upward). The vehicle remained stable throughout post-impact trajectory. The analysis ended at 0.9 seconds, at which time:

- The roll, pitch, and yaw of the vehicle were, respectively, 0.9 degrees (toward barrier), 3.5 degrees (rear pitching up), and 8.84 degrees (16.16 degrees relative to and toward barrier).
- The roll and pitch rate were stable at termination.
- The forward velocity of the vehicle was 37.5 mph (60.4 km/h).

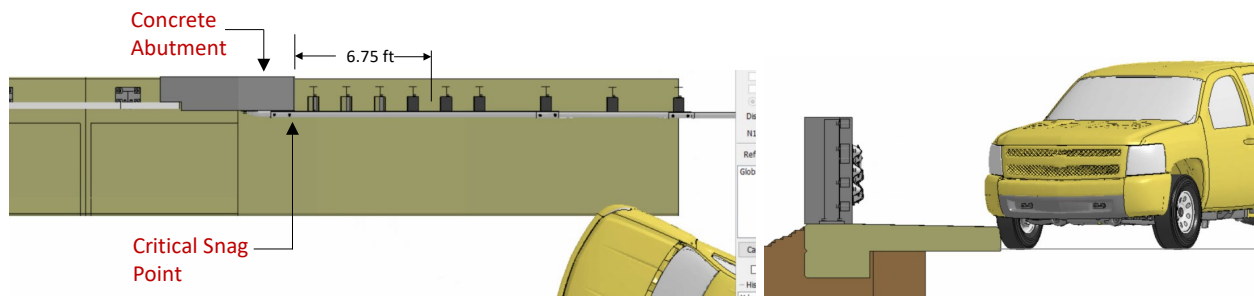


Figure 323. Starting point and target impact point for Test 4-21 on the MaineDOT transition for 4-bar bridge rail.

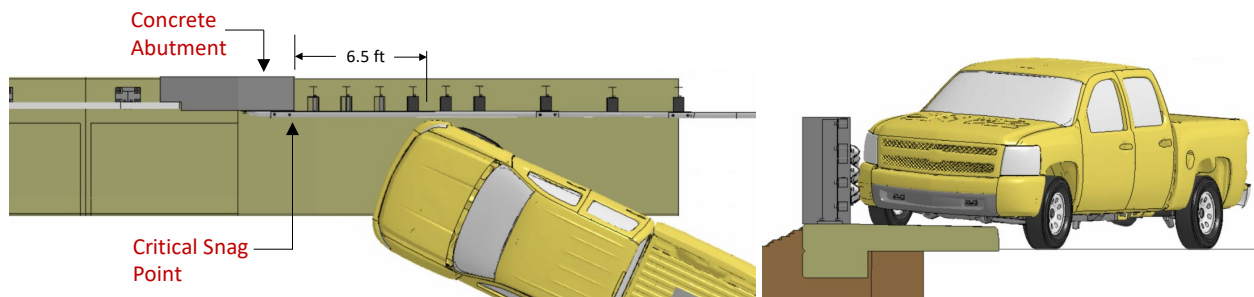


Figure 324. Actual impact point for Test 4-21 on the MaineDOT transition for 4-bar bridge rail.

12.3.3 Time History Data Evaluation

Figures 325 through 327 show the longitudinal, transverse, and vertical acceleration-time histories, respectively, computed from the center of gravity of the vehicle; Figures 328 through 330 show the angular rates and angular displacement about the x-, y-, and z-axis at the center of gravity of the vehicle.

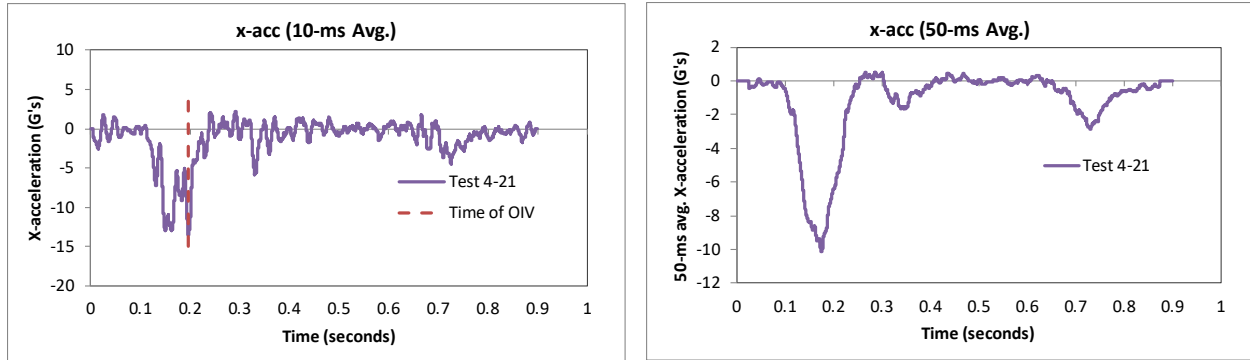


Figure 325. 10- and 50-millisecond average X-acceleration from FEA of Test 4-21 on the MaineDOT transition.

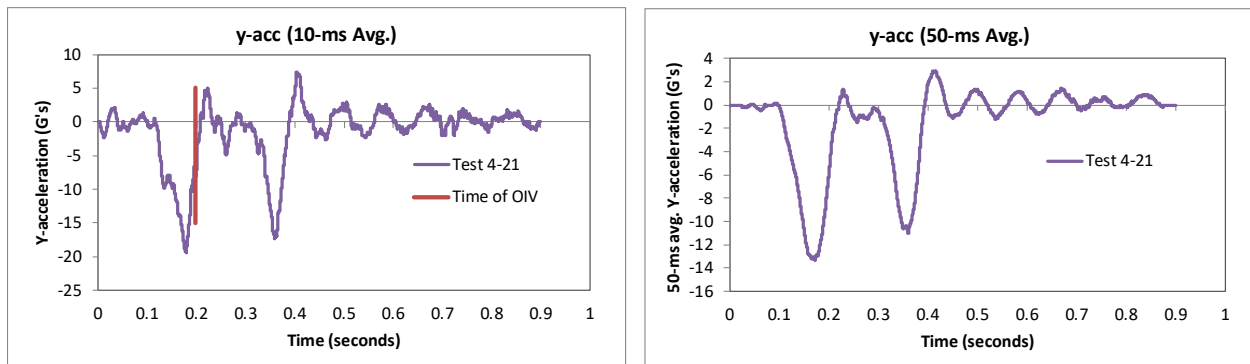


Figure 326. 10- and 50-millisecond average Y-acceleration from FEA of Test 4-21 on the MaineDOT transition.

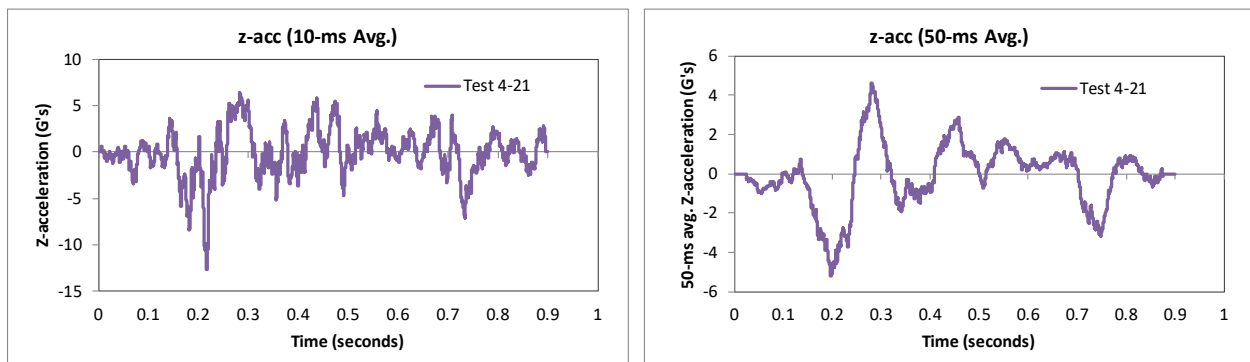


Figure 327. 10- and 50-millisecond average Z-acceleration from FEA of Test 4-21 on the MainedOT transition.

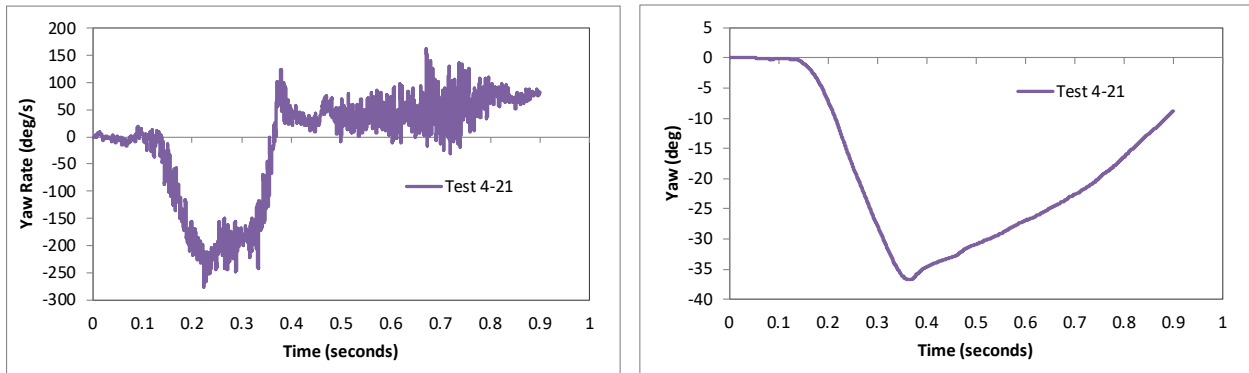


Figure 328. Yaw rate and roll angle time-history from FEA of Test 4-21 on the MainedOT transition.

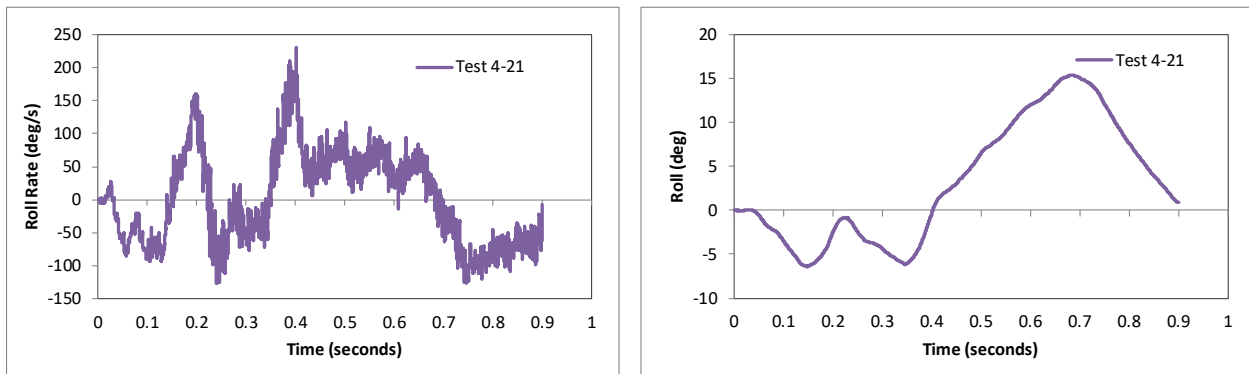
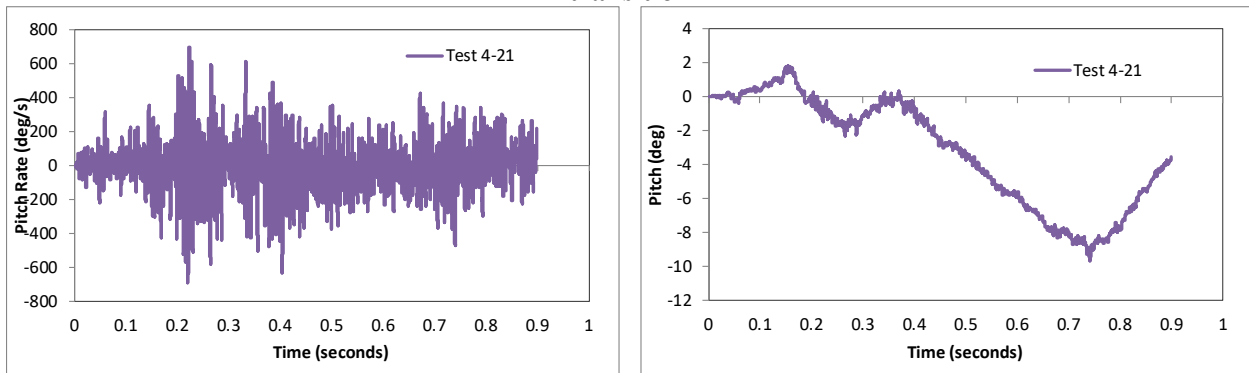


Figure 329. Roll rate and pitch angle time-history from FEA of Test 4-21 on the MainedOT transition



n.

Figure 330. Pitch rate and yaw angle time-history from FEA of Test 4-21 on the MainedOT transition.

12.3.4 Occupant Risk Measures

The acceleration-time histories and angular rate-time histories collected at the center of gravity of the vehicle were used to evaluate occupant risk metrics according to the procedures outlined in *MASH*. Table 92 shows the results for the occupant risk calculations. The results indicate that the occupant risk factors met safety criteria specified in *MASH*.

The occupant impact velocities in the longitudinal and transverse directions were 21.0 ft/s and 28.2 ft/s, respectively, which were within the recommended limits specified in *MASH*. The highest 0.010-second occupant ridedown acceleration in the longitudinal and transverse directions were 9.4 g and 17.3 g, respectively, which were over the recommended limit within but with critical limits specified in *MASH*. The maximum 50-ms moving average acceleration values in the longitudinal and transverse directions were 10.2 g and 13.3 g, respectively. The maximum roll and pitch angles of the vehicle were 15.4 degrees and 9.6 degrees, respectively, which were well below critical limits in *MASH*. As mentioned previously in Section 5, the 2270P vehicle model often over-estimates the lateral ridedown acceleration [see Appendix E].

Table 92. Summary of occupant risk metrics for Test 4-21 on the MaineDOT transition.

Occupant Risk Factors		MASH	MASH Criteria
		Test 4-21	
Occupant Impact Velocity (ft/s)	x-direction	21.0	} < 30 ft/s (preferred) ✓ < 40 ft/s (limit)
	y-direction	28.2	
	at time	at 0.1943 seconds on right side of interior	
THIV (ft/s)		34.1 at 0.1943 seconds on right side of interior	
Ridedown Acceleration (g's)	x-direction	-9.4 (0.1970 - 0.2070 seconds)	} > 15 G (preferred) < 20.49 G (limit) ✓
	y-direction	-17.3 (0.3543 - 0.3643 seconds)	
PHD (g's)		17.6 (0.3543 - 0.3643 seconds)	
ASI		1.72 (0.1474 - 0.1974 seconds)	
Max 50-ms moving avg. acc. (g's)	x-direction	-10.2 (0.1496 - 0.1996 seconds)	
	y-direction	-13.3 (0.1470 - 0.1970 seconds)	
	z-direction	-5.2 (0.1721 - 0.2221 seconds)	
Maximum Angular Disp. (deg)		15.4	} < 75 deg ✓
	Roll	(0.6858 seconds)	
	Pitch	-9.6 (0.7410 seconds)	
	Yaw	-36.8 (0.3638 seconds)	

12.3.5 Occupant Compartment Intrusion

The maximum deformation of the occupant compartment was approximately 1 inch. Figure 331 shows a view of the vehicle interior after the impact, with several components removed to facilitate viewing.

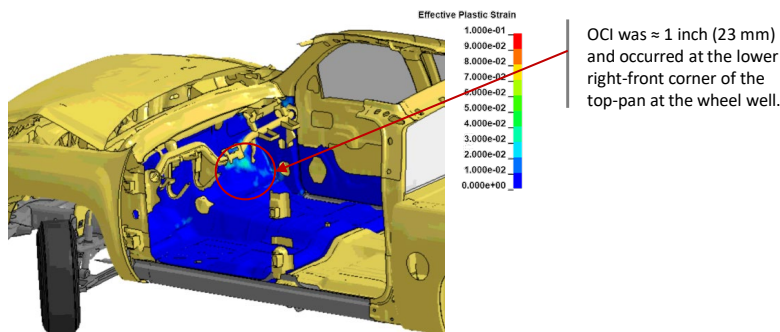


Figure 331. Occupant compartment deformation resulting from Test 4-21 on the MaineDOT transition.

12.3.6 Damages to the Barrier System

The damages to the barrier were moderate to significant but considered typical for this type of system. Figure 332 shows an overhead view of the post impact deformation of the transition indicating the extent of damage. The barrier was deformed over 14.2 feet of the system with deformation extending from Post 7 to the end of the thrie-beam terminal connector. The vehicle was in contact with the barrier for approximately 10.2 feet. The maximum working width for the system was 24.2 inches, measured as the maximum dynamic lateral position of Post 3 (top-back of post) relative to the initial face of the thrie-beam. The maximum deflection of the system occurred on the lower corrugation of the thrie-beam at the upstream end of the blackout at Post 2. Figure 333 and Figure 334 show contour plot images of the 1st peak dynamic deflection and maximum dynamic deflection, respectively. The first peak deflection was 8.11 inches resulting from the front of vehicle impacting the system, and the maximum dynamic deflection was 8.34 inches resulting from the rear of the vehicle impacting the system. Figure 335 shows a contour plot of final permanent lateral displacement of the system, which was 7.17 inches. Figure 336 shows a contour plot of effective plastic strain on the steel components of the transition. The plastic deformations were limited to the thrie-beam and thrie-beam terminal connector. There was also soil displacement at 7 posts approaching the concrete buttress.

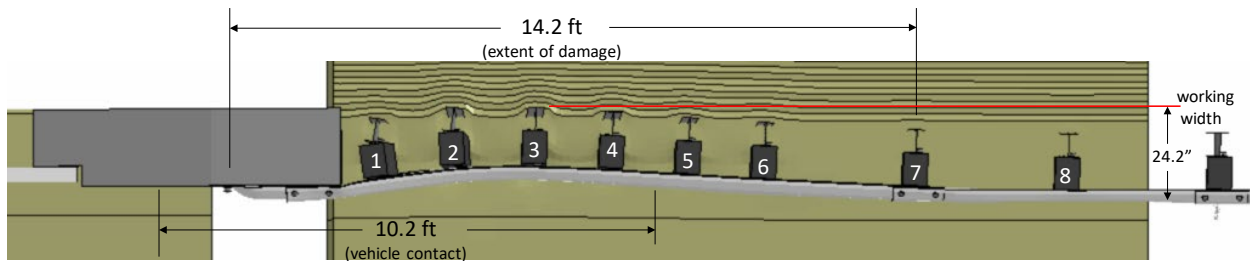


Figure 332. Overhead view of MaineDOT transition after Test 4-21 showing extent of damage.

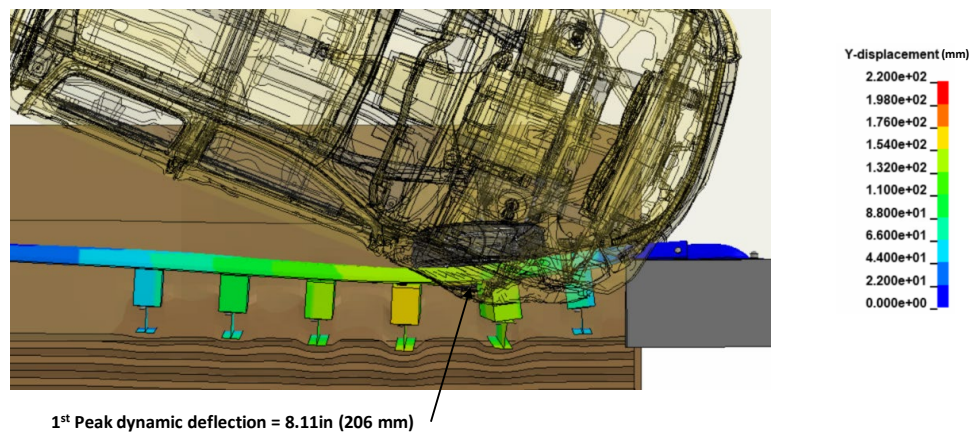


Figure 333. Contour plot of lateral displacement for Test 4-21 on the MaineDOT transition at the 1st peak deflection.

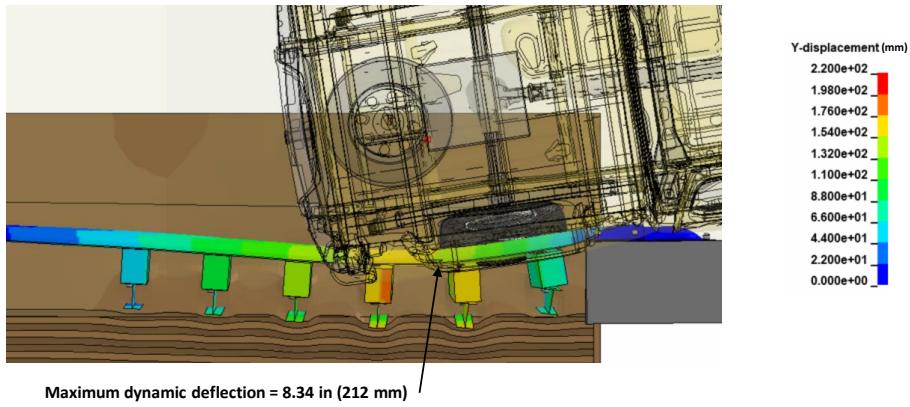


Figure 334. Contour plot of lateral displacement for Test 4-21 on the MaineDOT transition at maximum dynamic deflection.

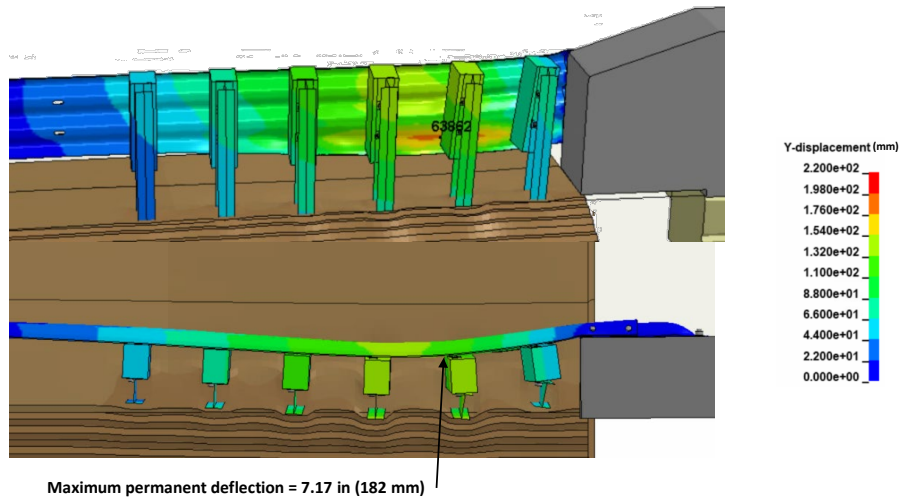


Figure 335. Contour plot of maximum permanent deflection for Test 4-21 on the MaineDOT transition.

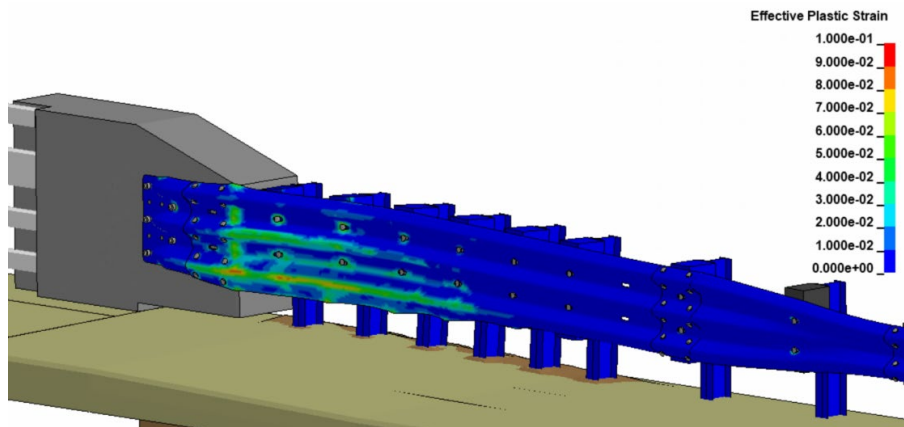


Figure 336. Contours of effective plastic strains on the steel rails and posts for Test 4-21 on MaineDOT transition.

12.3.7 Damages to Vehicle

Figure 337 shows contour plots of effective plastic strain for the vehicle, which were used to identify areas of the vehicle that suffered damage during the simulated impact event. The most severe damages were to the front bumper, the front fender, the upper control arm of front suspension, fail ball joint on lower control arm, front and rear wheels, rear edge of rear door, front edge of truck bed, rear quarter panel of truck bed and rear bumper.

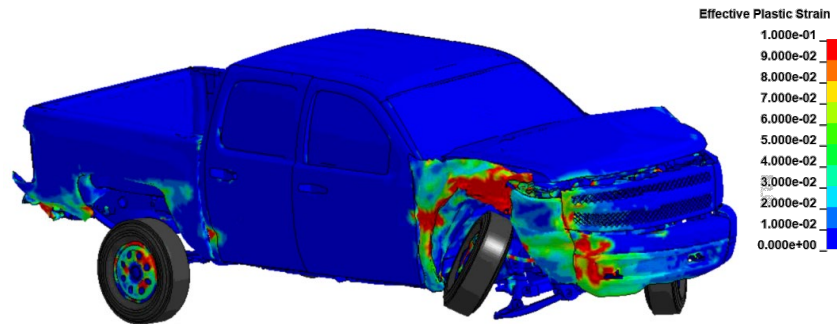


Figure 337. Damages to vehicle in Test 4-21 analysis of the MaineDOT transition.

12.3.8 Exit Box

Figure 338 shows the exit box for Test 4-21 on the MaineDOT transition system. The vehicle was redirected within the exit box criteria of *MASH* and the vehicle did not show signs of re-entering traffic lanes at aggressive angle.

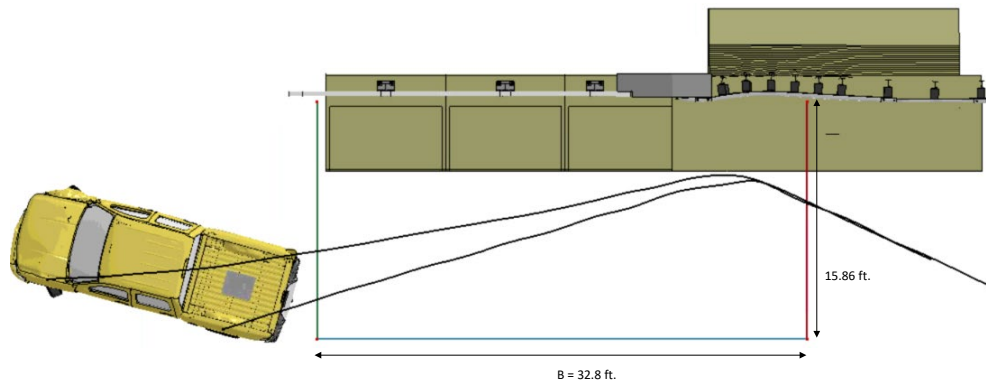


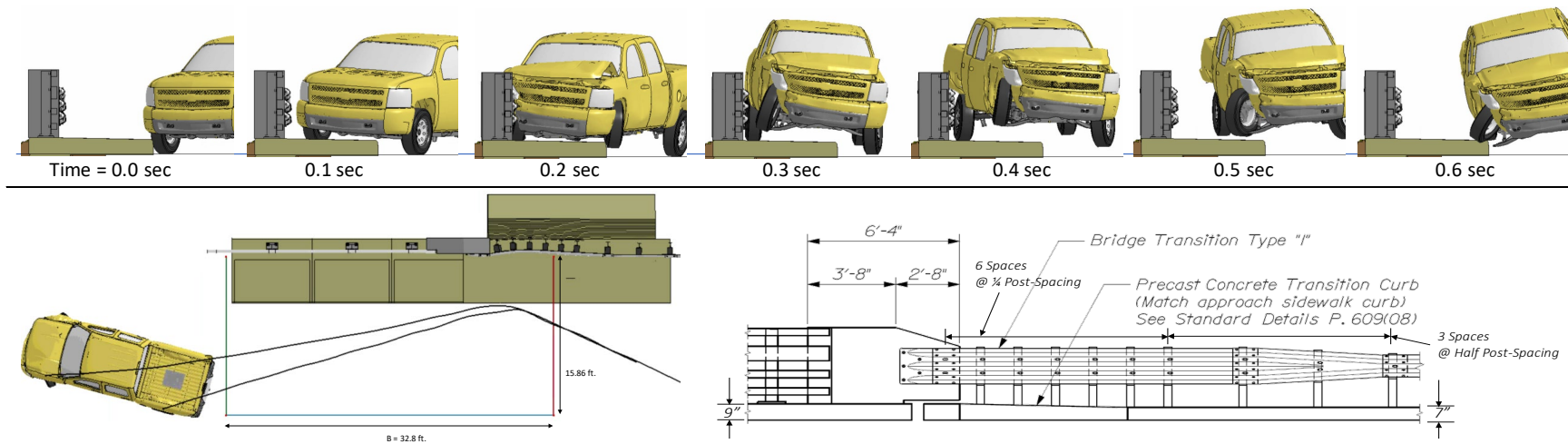
Figure 338. Exit box for Test 4-21 analysis of the MaineDOT transition.

12.3.9 Results Summary

A summary of the *MASH* Test 4-21 results on the MaineDOT transition is shown in Table 93 and Figure 339. The barrier successfully contained and redirected the 2270P vehicle (pickup) with significant damage to the transition. There were no detached elements from the barrier that showed potential for penetrating the occupant compartment or presenting undue hazard to other traffic. The vehicle remained upright and did not experience excessive roll or pitch angle displacements. The OIV and maximum ORA values were within critical limits specified in *MASH*. Based on the results of this analysis, the barrier meets all structural and occupant risk criteria in *MASH* for Test 4-21 impact conditions.

Table 93. Summary of MASH Test 4-11 results on the MaineDOT transition.

Evaluation Factors	Evaluation Criteria	Results
Structural Adequacy	A Test article should contain and redirect the vehicle or bring the vehicle to a controlled stop; the vehicle should not penetrate, underride, or override the installation although controlled lateral deflection of the test article is acceptable.	Pass
Occupant Risk	D Detached elements, fragments, or other debris from the test article should not penetrate or show potential for penetrating the occupant compartment, or present undue hazard to other traffic, pedestrians, or personnel in a work zone. Deformations of, or intrusions into, to occupant compartment should not exceed limits set forth in Section 5.2.2 and Appendix E.	Pass
	F The vehicle should remain upright during and after collision. The maximum roll and pitch angles are not to exceed 75 degrees.	Pass
	H The longitudinal and lateral occupant impact velocity (OIV) shall not exceed 40 ft/s (12.2 m/s), with a preferred limit of 30 ft/s (9.1 m/s)	Pass
	I The longitudinal and lateral occupant ridedown acceleration (ORA) shall not exceed 20.49 G, with a preferred limit of 15.0 G	Pass



General Information		Impact Conditions		Max50-millisecond Avg. (G)	
Analysis Agency	Roadsafe LLC	Speed	62 mph	Longitudinal	10.2 g
Test Standard Test No.	MASH Test 4-21	Angle	25 degrees	Lateral	13.3 g
Analysis No.	NETC18_MEDOT-Trans_T421	Location	6.5 ft upstream of buttress	Vertical	5.2 g
Analysis Date	5/12/2019				
Test Article		Impact Severity		Test Article Deflections (in)	
Type	Bridge Rail Transition	114.7 kip-ft	Dynamic	8.34 inches
Name	MEDOT Transition for 4-Bar BR	Exit Conditions		Permanent	7.17 inches
Installation Length	59.4 feet	Speed	42.6 mph	Working Width	24.2 inches
Material or Key Elements		Angle	8.9 degrees		
		Time	0.42 seconds		
Soil Type and Condition		Occupant Risk Values		Max. OCI	
MASH Strong Soil		Longitudinal OIV	21 ft/s	1 inch	
Analysis Vehicle		Lateral OIV	28.2 ft/s	Vehicle Stability	
Type / Designation	2270P	Longitudinal ORA	9.4 g	Roll	15.4 degees
FEA Model name	SilveradoC_V3a_V180201_TireRS_35psi	Lateral ORA	17.3 g	Pitch	9.6 degrees
Mass	5,001 lb	THIV	34.1 ft/s	Yaw	36.8 degrees
		PHD	17.5 g		
		ASI	1.72		

Figure 339. Summary results for MASH Test 4-21 on the MaineDOT transition system

12.4 Test 4-22

12.4.1 CIP for Test 4-22

The critical impact point for Test 4-22 was determined using FEA with respect to maximum potential for vehicle snag on the end of the transition buttress, as illustrated in Figure 340. Finite element analysis was used to simulate *MASH* Test 4-22 at impact points 9 ft, 10 ft, 11 ft and 12 ft from the end of the buttress nose. The effects of the sidewalk on vehicle dynamics prior to impact were ignored for the CIP determination. These analysis cases were conducted for 0.4 seconds of impact which was sufficient to evaluate potential snags regarding both the front and rear of the vehicle.

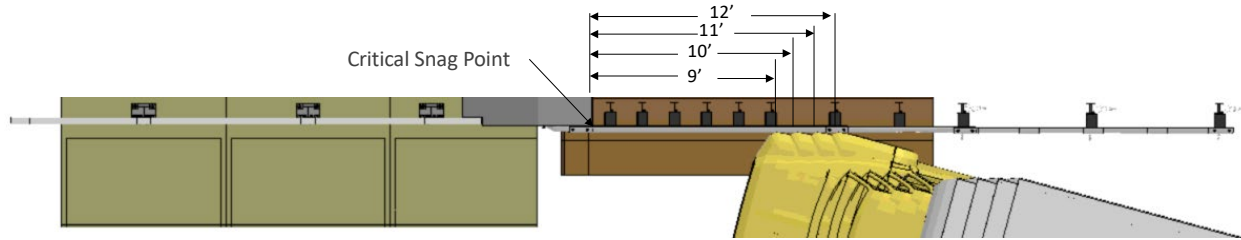


Figure 340. Illustration of potential snag point for Test 4-22 on the MaineDOT transition and impact points evaluated.

The longitudinal, lateral and resultant forces on the barrier for each case is shown in Figure 341. The impact force from the rear tandem wheel set was essentially equal for all cases except for impact at 11 feet. In all cases, the rear suspension failed when the right tire of the tandem wheel set impacted the end of the buttress; however, for impact at 11 feet the suspension failed during impact against the blockout on Post 1 of the transition, which resulted in lower forces when the tire subsequently contacted the buttress. Figure 342 shows an overhead image for each impact case with the cargo-box components shown as transparent to facilitate viewing the interaction between the rear wheel set and the end of the concrete buttress.

The impact at 12 feet upstream of the splice resulted in the highest force resulting from the front of the cargo box impacting against the top surface of the concrete buttress, and the greatest potential for the cargo-box of the truck to extend over the top of the rail and snag on the tops of the bridge rail posts as the truck rolled toward and over the bridge rail, as illustrated in Figure 343.

Based on these results, impact at 12 feet upstream of the buttress was selected as the critical impact point to maximize potential for vehicle snag on the end of the buttress and to also maximize potential for vehicle roll angle and contact between cargo-box and bridge rail posts. The analysis was performed for 1.5 seconds of the impact event. The following sections provide a summary of the results and include a commentary describing the timing and occurrence of various events during the simulated impact, time-history data evaluation, occupant risk assessments, and damages sustained by both the barrier and vehicle.

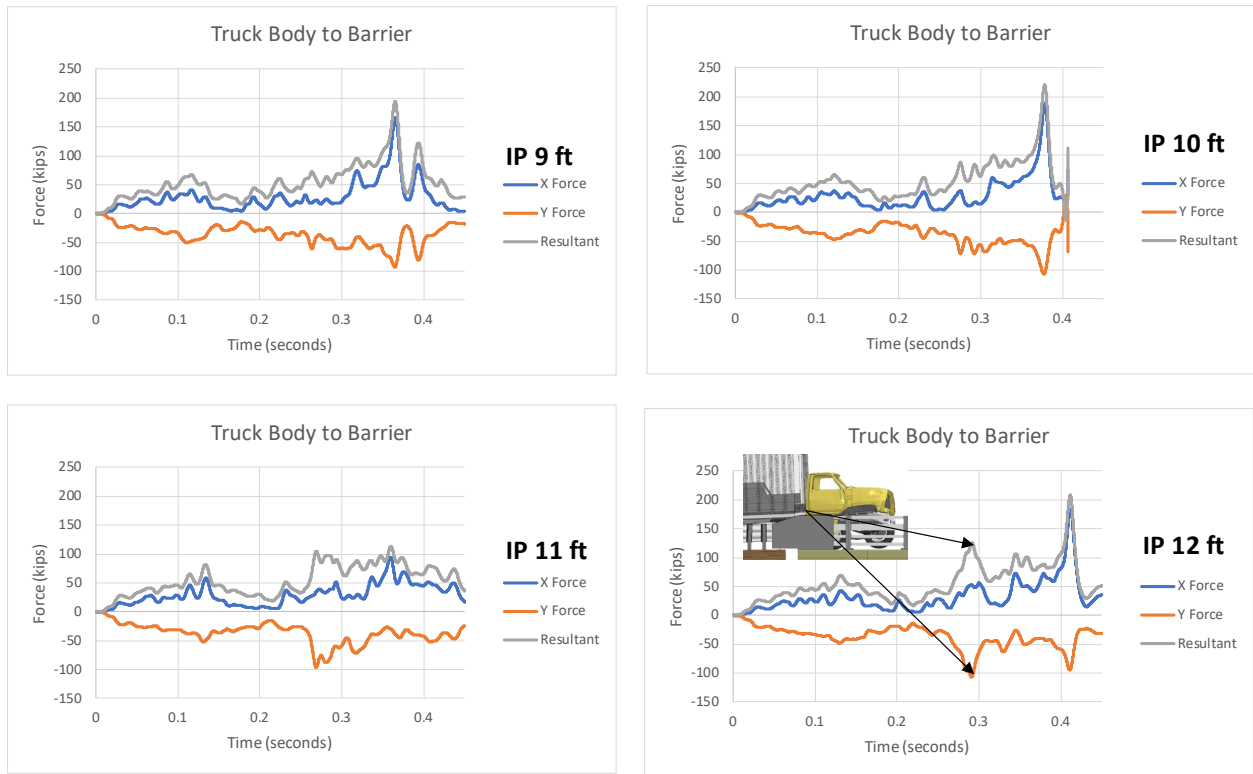


Figure 341. Longitudinal, lateral and resultant forces on barrier for each analysis case.



Figure 342. Overhead images with transparent cargo-box showing the interaction of the rear wheel set and the concrete buttress.

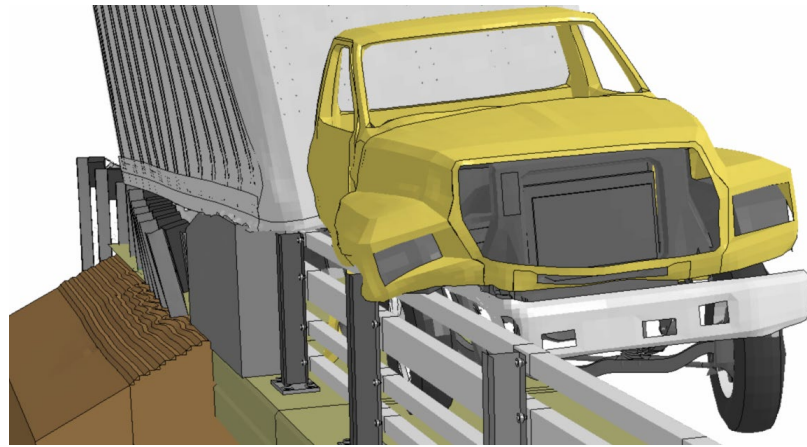


Figure 343. Cargo-box bed rails snag on top of bridge rail posts.

12.4.2 Summary of Key Phenomenological Events

The 22,198-lb single unit truck struck the curb-face of the sidewalk at 28.5 feet upstream of the end of the concrete buttress at a speed of 56 mph and at an angle of 15 degrees, as illustrated in Figure 344, with a target impact point on the barrier of 12 feet upstream of the end of the buttress. The sequential views of the impact event are shown in Appendix V in Figures V-22 through V-24 from an overhead viewpoint, downstream and upstream viewpoint, and isometric viewpoint, respectively.

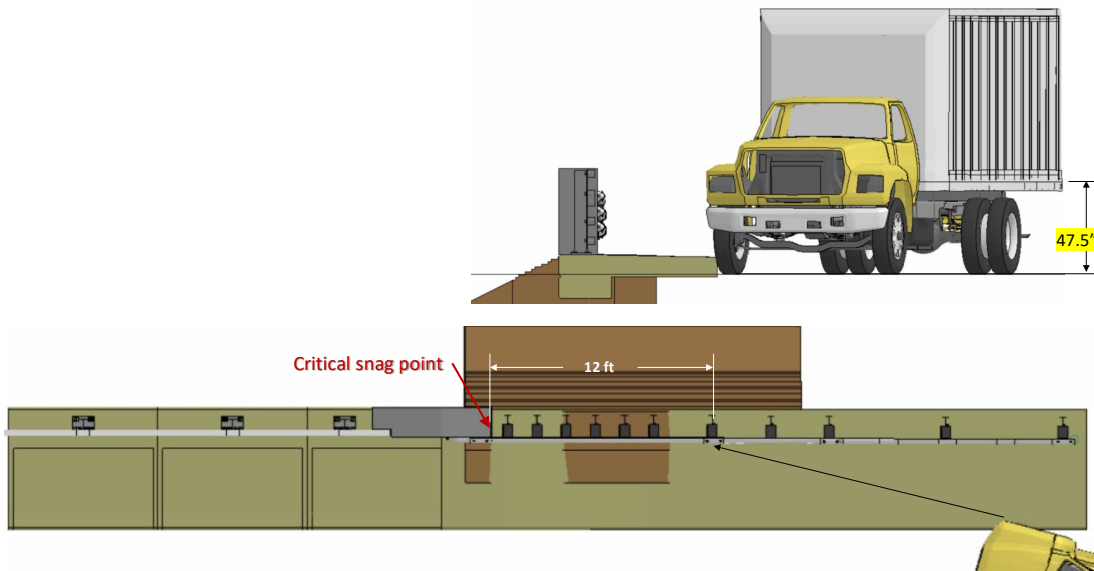


Figure 344. Initial impact point on the curb-face for Test 4-22 on the sidewalk-mounted MaineDOT transition.

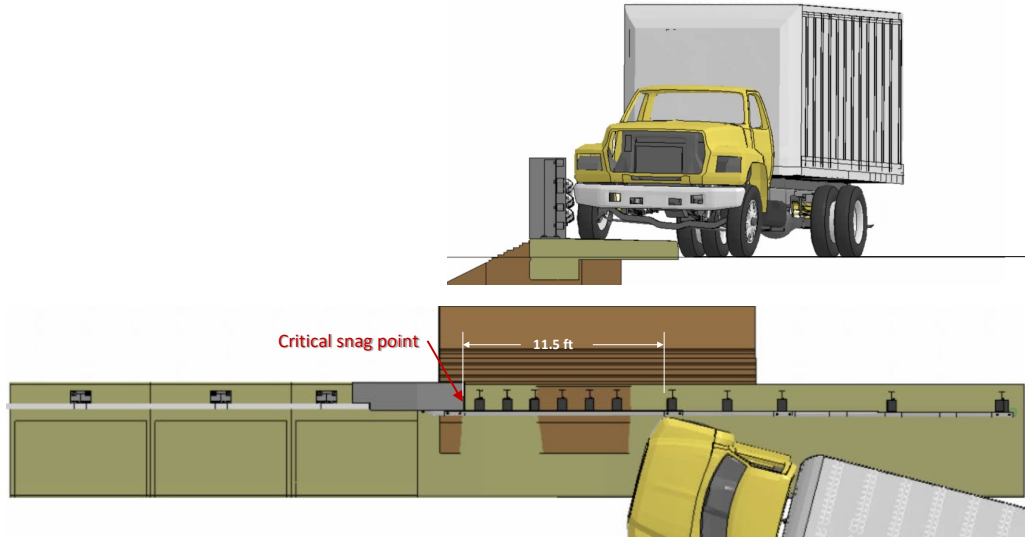


Figure 345. Impact point on the barrier for Test 4-22 on the sidewalk-mounted MaineDOT transition.

At 0.005 seconds, the front-right tire compressed at the point of contact with the sidewalk curb, and at 0.04 seconds the tire had fully mounted the sidewalk and the vehicle began to roll away from the barrier. The tire model for the SUT is relatively stiff and immediately rebounded off the surface of the sidewalk. At 0.09 seconds the front-right tire recontacted the sidewalk as the vehicle was yawing slightly counter-clockwise away from the barrier. At 0.205 seconds the rear-right tire contacted the curb face of the sidewalk; also, at this time, the front bumper of the truck impacted the top and middle corrugations of the thrie-beam at 11.5 feet upstream of the end of the buttress, traveling at 55.1 mph and 14.5 degrees, as shown in Figure 345. At 0.21 seconds the front-right tire impacted the lower two corrugations of the thrie-beam, and at 0.215 seconds the tire began to steer counter-clockwise (away from the barrier). At 0.25 seconds the rear-right tandem wheel was fully mounted onto the sidewalk. At 0.28 seconds one of the u-bolts connecting the front axle to the right suspension failed. At 0.335 seconds the second u-bolt failed connecting the front axle to the right suspension. At 0.37 seconds the front-left tire contacted the curb face of the sidewalk and began to slowly climb the curb. At 0.43 seconds the rear-left tandem wheel set lifted off the ground, and the front-left wheel began to push away from the curb face. At 0.42 seconds the front bumper of the truck began to pass the downstream end of the buttress. At 0.46 seconds the front-right tire began to pass the downstream end of the buttress and continued in contact with the barrier onto the bridge rail. At 0.47 seconds the rear-right wheel set impacted the thrie-beam at approximately 8.85 feet upstream of the buttress, and the posts began to deflect back at this section of the barrier. Also, at this time, the front-lower edge of the cargo box struck the top surface of the buttress at 20 inches from the end of the buttress nose. The lower edge of the cargo box deformed as it rode up the sloped surface of the buttress. At 0.51 seconds the longitudinal deflection of the transition rail began to increase significantly due to pocketing of the thrie-beam as the rear tandem wheel set approached the end of the buttress. At 0.55 seconds, Post 4 reached peak dynamic lateral deflection of 12.28 inches, and the truck cabin experienced maximum lateral acceleration of 7.9 g. At 0.565 seconds the wheel rim on the rear-right wheel deformed during interaction with the post blockout at Post 2, and the truck experienced maximum lateral acceleration of 10.8 g at the center of gravity of the vehicle. At 0.57 seconds the rear-right tandem wheel set began to climb the thrie-beam rail as

the tires approached closer to the buttress, resulting in significant damage to the truck suspension and causing increased pitch of the rear of the truck bed. At 0.58 seconds, Post 3 reached peak dynamic lateral deflection of 14.17 inches. At 0.59 seconds, the maximum lateral deflection of the barrier was 17 inches and occurred at the front-top corner of the blockout at Post 2. Also, at this time, Post 2 reached peak dynamic lateral deflection of 15.83 inches. At 0.595 seconds the rear tandem wheel set contacted and snagged on the end of the buttress, causing failure of the leaf spring at the forward connection bracket. At 0.6 seconds the maximum longitudinal deflection of the terminal-end of the transition occurred with magnitude 6.2 inches. At 0.605 seconds, Post 1 reached peak dynamic lateral deflection of 10.79 inches. At 0.614 seconds the truck experienced maximum longitudinal acceleration of 16.8 g at the center of gravity of the vehicle. At 0.62 seconds the lower edge of the cargo box contacted the top of the bridge rail near the first post in the bridge rail section. The lower edge of the cargo box was extended over the top of the rail approximately 19 inches, and the cargo box snagged slightly on Post 1. At 0.637 seconds the truck cabin experienced maximum longitudinal acceleration of 13.9 g. At 0.67 seconds the bottom of the cargo box snagged slightly on the top of Post 2 of the bridge rail and continued to these snags until 0.755 seconds. At 0.745 seconds the front of the truck was passing the downstream end of the bridge rail. The yaw angle of the vehicle resulted in the vehicle moving toward the field-side as it progressed forward. At 0.79 seconds the front-lower edge of the cargo box impacted against the 3rd post of the bridge rail, resulting in a significant snag with the post. The snag resulted in shearing post-bolts and significantly deforming the Post 3, but also bending Posts 1 and 2 of the bridge rail. At 0.842 seconds the vehicle reached maximum roll angle of 17.8 degrees (toward barrier). At 1.01 seconds the vehicle exited the barrier at 35.8 mph and 8.49 degrees toward the barrier as the lower edge of the truck box slid off the end of the railing. At 1.081 seconds the vehicle reached maximum pitch angle of -13.4 degrees (rear pitching up). The analysis was terminated at 1.35 seconds, at which time:

- The roll, pitch, and yaw angles for the truck cabin were -8.7 degrees and increasing, -2.25 degrees (rear pitching upward) and stable, and 30.4 degrees (toward field-side) and increasing, respectively.
- The roll, pitch, and yaw angles for the cargo box were 3.81 degrees (toward the field-side) and decreasing, -4.4 degrees (rear pitching upward) and stable, and 25.9 degrees (toward field-side) and increasing, respectively.
- It is possible that the vehicle would have rolled onto its side if the analysis had continued.
- The SUT was no longer in contact with the barrier as it reached the end of the bridge rail and was moving toward the field-side.
- The forward speed of the vehicle was 37.5 mph (60.42 km/hr)

12.4.3 Time History Data Evaluation

Acceleration-time histories and angular rate-time histories were collected at two locations on the vehicle: (1) on the cargo box at the center of gravity of the vehicle, and (2) a point inside the cabin of the truck, as shown in Figure 111. The acceleration and angular rate data used for the occupant risk measures came from the cabin location. Figures 346 through 348 show the longitudinal, transverse, and vertical acceleration-time histories, respectively, computed from near the center of gravity of the vehicle which falls inside the cargo-box near the front of the ballast.

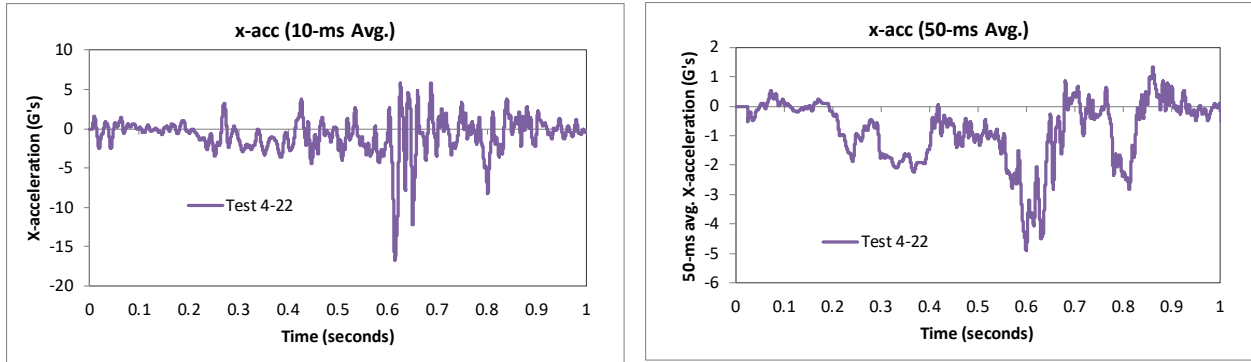


Figure 346. 10- and 50-millisecond average X-acceleration from FEA of Test 4-22 on the MaineDOT transition (c.g. accelerometer).

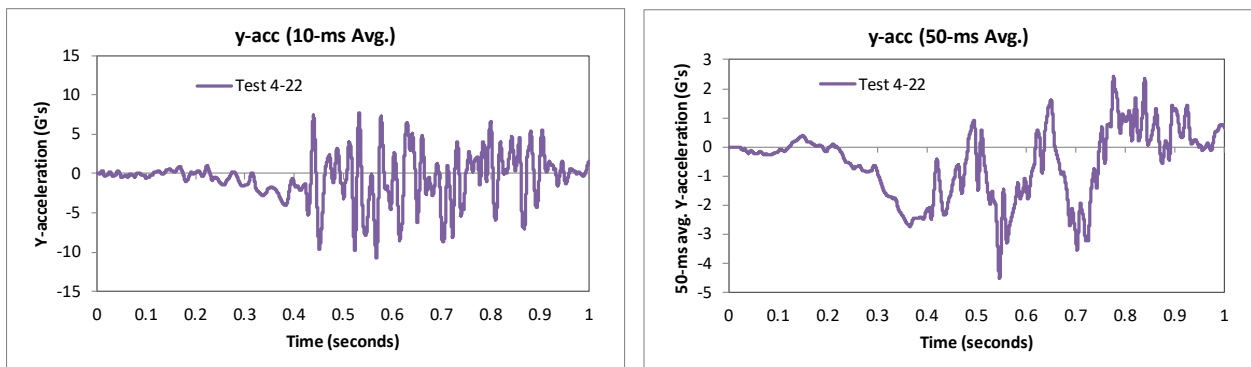


Figure 347. 10- and 50-millisecond average Y-acceleration from FEA of Test 4-22 on the MaineDOT transition (c.g. accelerometer).

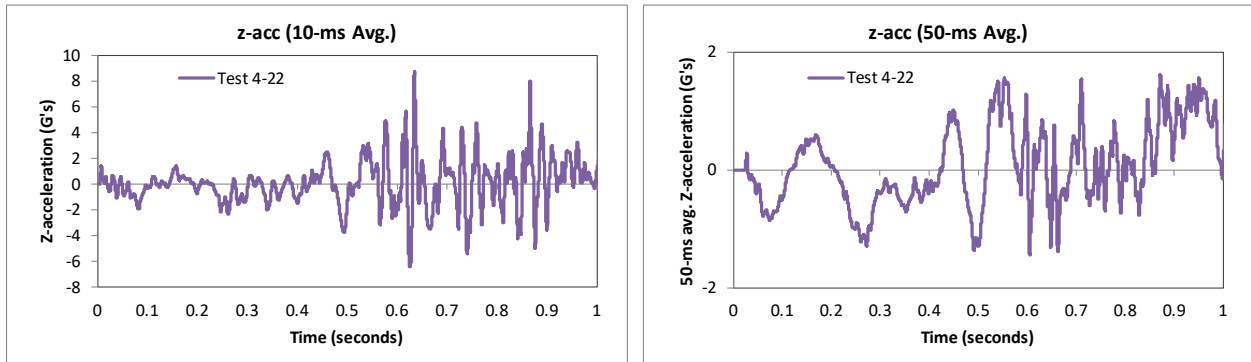


Figure 348. 10- and 50-millisecond average Z-acceleration from FEA of Test 4-22 on the MaineDOT transition (c.g. accelerometer).

Figures 349 through 351 show the longitudinal, transverse, and vertical acceleration-time histories, respectively, computed from the inside the cabin of the vehicle; Figures 352 through 354 show the comparison of the angular rates and angular displacements about the x-, y-, and z-axis from the cabin location. These data are used for calculating the occupant risk metrics. *MASH* does not require that occupant risk be evaluated; however, they are reported herein for completeness (see following section).

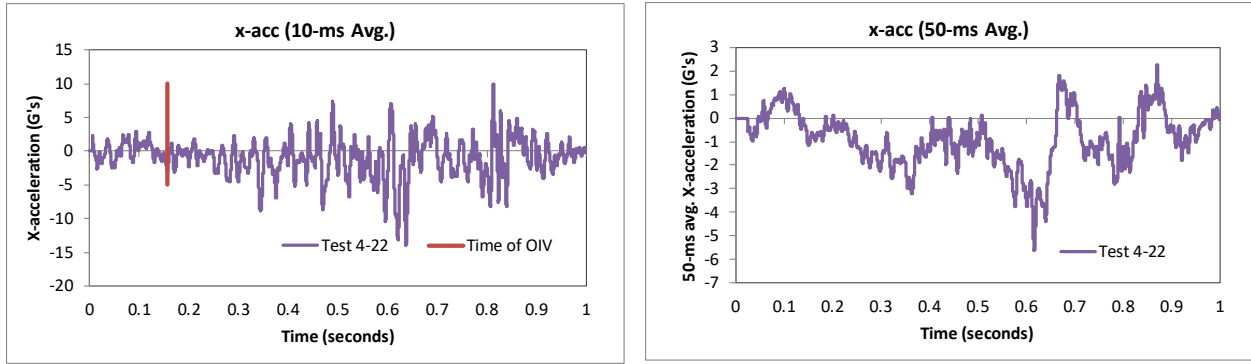


Figure 349. 10- and 50-millisecond average X-acceleration from FEA of Test 4-22 on the MaineDOT transition (cabin accelerometer).

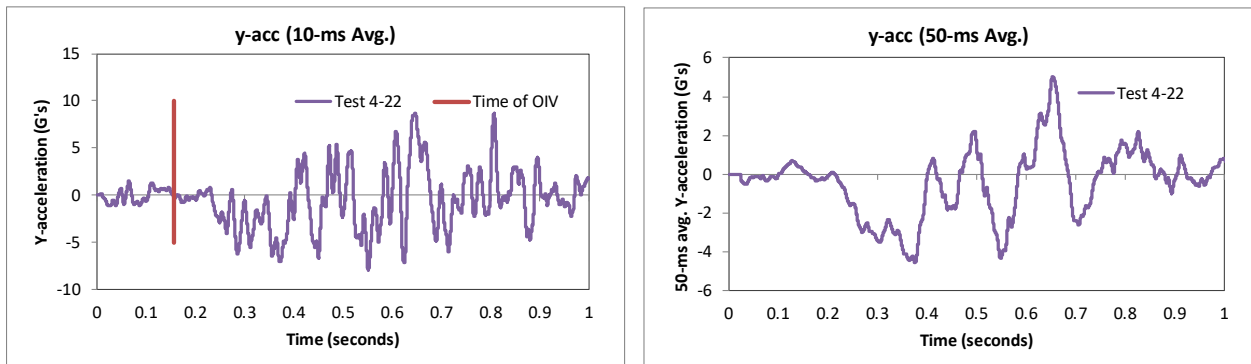


Figure 350. 10- and 50-millisecond average Y-acceleration from FEA of Test 4-22 on the MaineDOT transition (cabin accelerometer).

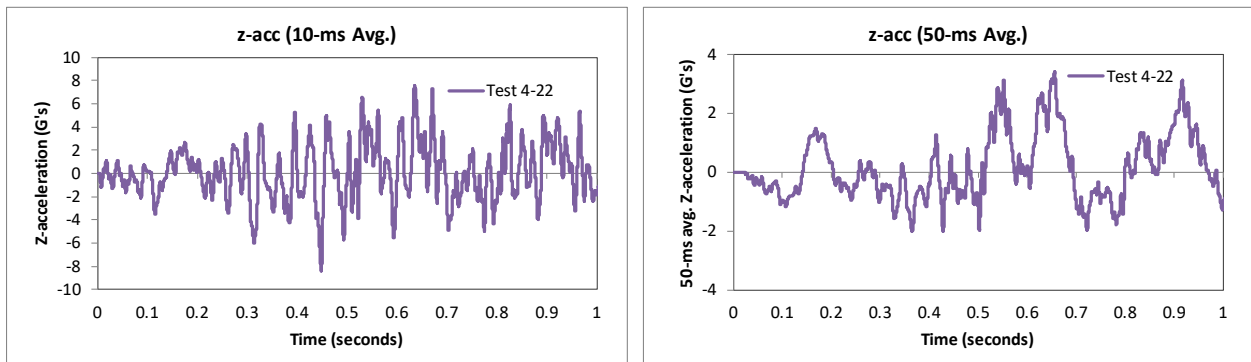


Figure 351. 10- and 50-millisecond average Z-acceleration from FEA of Test 4-22 on the MaineDOT transition (cabin accelerometer).

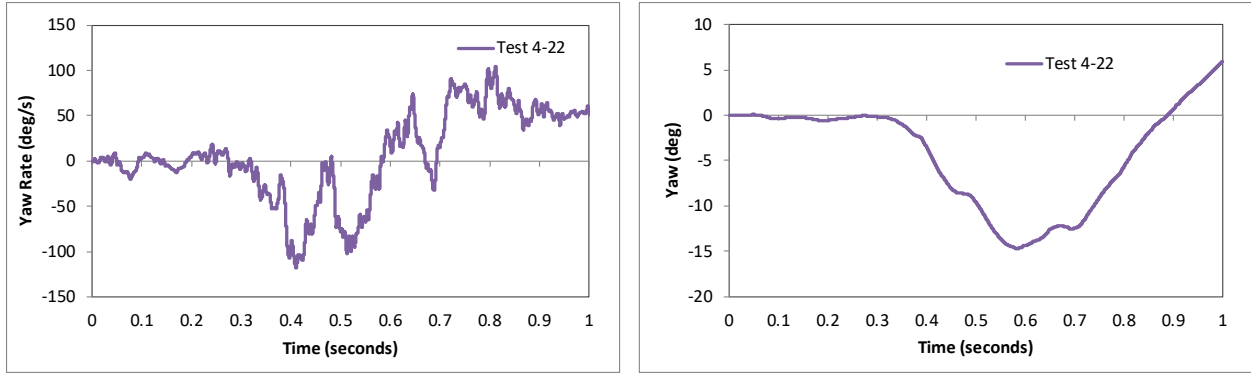


Figure 352. Yaw rate and yaw angle time-history from FEA of Test 4-22 on the MaineDOT transition (cabin accelerometer).

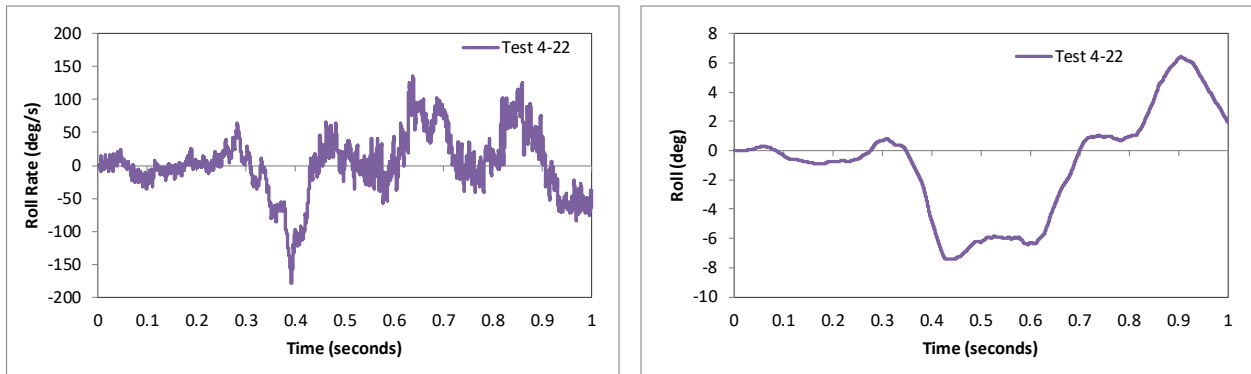


Figure 353. Roll rate and roll angle time-history from FEA of Test 4-22 on the MaineDOT transition (cabin accelerometer).

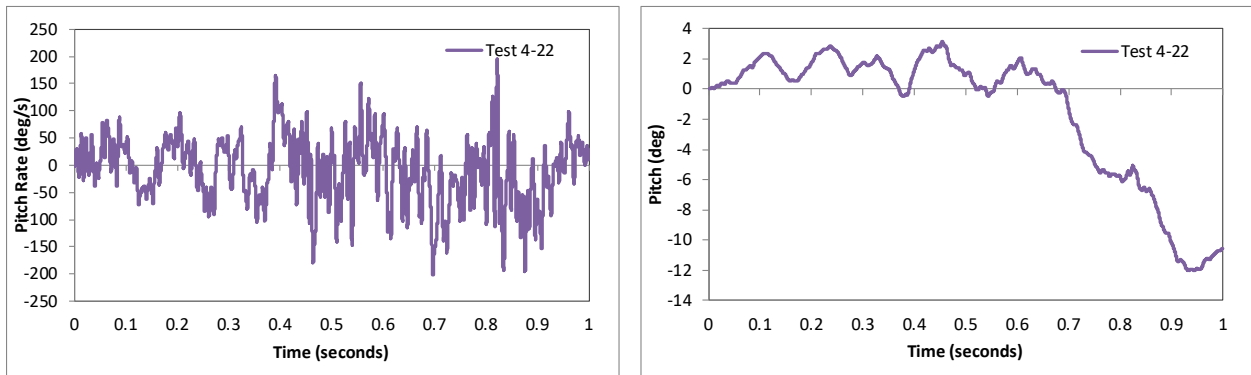


Figure 354. Pitch rate and pitch angle time-history from FEA of Test 4-22 on the MaineDOT transition (cabin accelerometer).

12.4.4 Occupant Risk Measures

The acceleration-time histories and angular rate-time histories collected from inside the truck cabin were used to evaluate occupant risk metrics according to the procedures outlined in *MASH*. Table 94 shows the results for the occupant risk calculations. The results indicate that the occupant risk factors met safety criteria specified in *MASH*.

The occupant impact velocities in the longitudinal and transverse directions were 8.9 ft/s and 14.4 ft/s, respectively. The highest 0.010-second occupant ridedown acceleration in the

longitudinal and transverse directions were 13.9 g and 8.7 g, respectively. The maximum 50-ms moving average acceleration values in the longitudinal and transverse directions were 5.6 g and 5 g, respectively. The maximum roll and pitch angles of the vehicle were 8.7 degrees and 12.0 degrees, respectively. All metrics were within recommended limits specified in *MASH*.

Table 94. Summary of occupant risk metrics for Test 4-22 on the MaineDOT transition.

Occupant Risk Factors		MASH	MASH Criteria
		Test 4-22	
Occupant Impact Velocity (ft/s)	x-direction	8.9	} < 30 ft/s (preferred) ✓ < 40 ft/s (limit)
	y-direction	14.4	
	at time	at 0.3726 seconds on right side of interior	
THIV (ft/s)		16.4	}
		at 0.3726 seconds on right side of interior	
Ridedown Acceleration (g's)	x-direction	-13.9 (0.6320 - 0.6420 seconds)	} < 15 G (preferred) ✓ < 20.49 G (limit)
	y-direction	8.7 (0.6419 - 0.6519 seconds)	
PHD (g's)		15 (0.6322 - 0.6422 seconds)	
ASI		0.66 (0.6306 - 0.6806 seconds)	
Max 50-ms moving avg. acc. (g's)	x-direction	-5.6 (0.5916 - 0.6416 seconds)	}
	y-direction	5 (0.6284 - 0.6784 seconds)	
	z-direction	3.4 (0.6310 - 0.6810 seconds)	
Maximum Angular Disp. (deg)	Roll	-8.7 (1.3455 seconds)	} < 75 deg ✓
	Pitch	-12 (0.9437 seconds)	
	Yaw	30.4 (1.3455 seconds)	

12.4.5 Occupant Compartment Intrusion

The maximum deformation of the occupant compartment for impact on the MaineDOT transition was approximately 5.5 inches. The maximum deformation occurred at the lower right-front corner of the toe-pan at the wheel well. Figure 355 shows a view of the vehicle interior after the impact, with several components removed to facilitate viewing. The maximum deformation was less than the critical limit of 9 inches specified in *MASH* for this area of the occupant compartment.

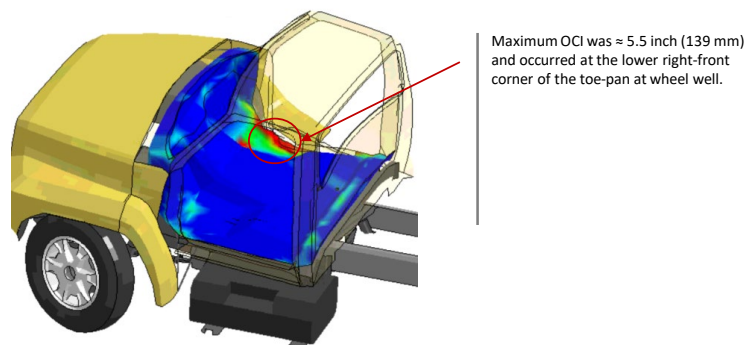


Figure 355. Occupant compartment deformation resulting from Test 4-22 on the MaineDOT transition.

12.4.6 Damages to the Barrier System

Figure 356 shows images of the barrier at maximum deflection and final displacement with a contour plot of lateral displacement on the rail elements. The maximum dynamic deflection was 17 inches and occurred at the top of Post 2 on the thrie-beam section of the transition. The maximum permanent deflection was 15.4 inches at the same location.

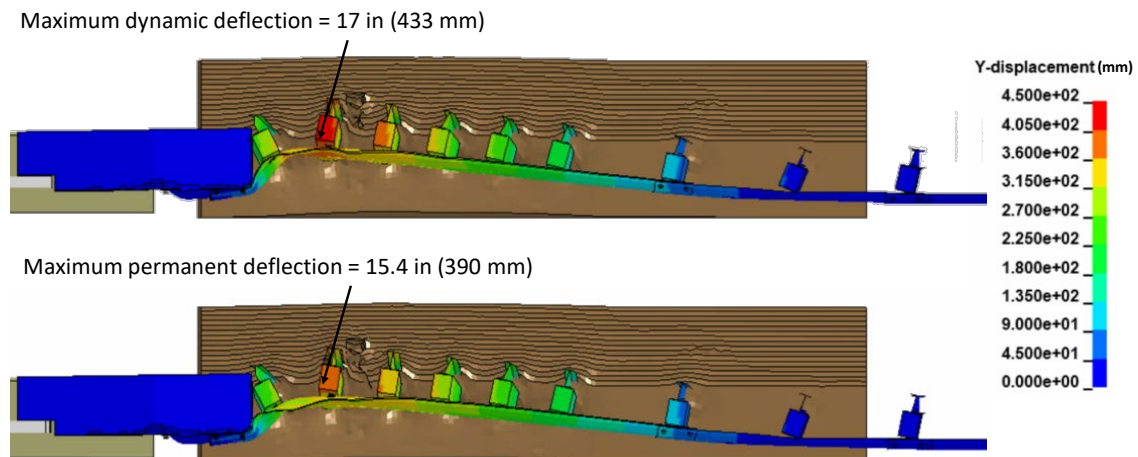


Figure 356. Contour plot of lateral displacement for the MaineDOT transition for Test 4-22 at the time of maximum dynamic deflection.

Figure 357 shows contours of true effective plastic strains on the steel components of the transition and bridge rail with contour range cut off at 0.2. Figure 358 shows a close-up view of the bridge rail end-post and the thrie-beam rail at the buttress. Plastic deformations of the thrie-beam rail were significant at, and near to, the end of the buttress. The maximum effective plastic strain was 0.5 at the top edge of the thrie-beam where the rail was pressed against the top corner of the buttress. Several of the transition posts near the buttress were deformed. The bridge rail was also damaged, due to the bottom of the cargo box snagging on the tops of the posts. The most significant damage to the bridge rail was to the downstream end post, in which the rail mounting bolts sheared off, and the post bent along the longitudinal direction of the rail.

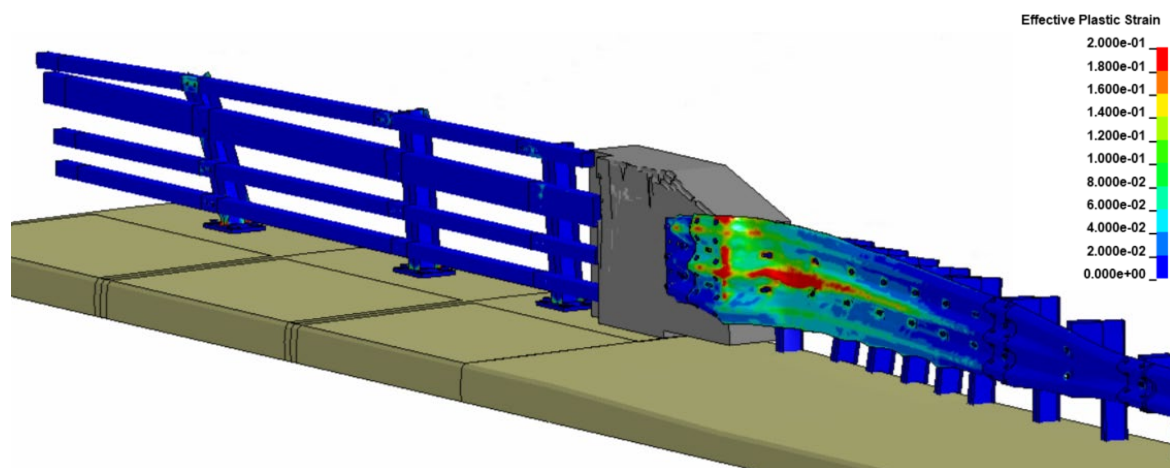


Figure 357. Contours of effective plastic strains on the transition and bridge rail for Test 4-22 on the MaineDOT transition.

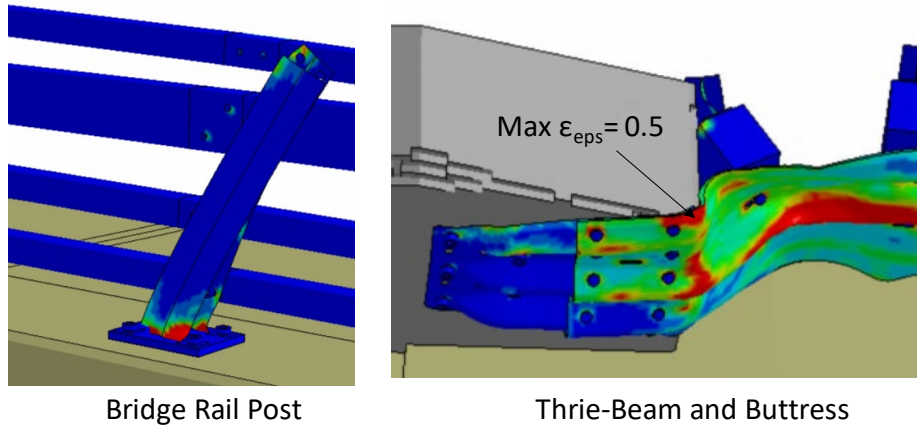


Figure 358. Close-up view of end-post on bridge rail and the high deformation area of the thrie-beam at the buttress.

The vehicle was in contact with the barrier from the point of contact until the truck box slid off the end of the bridge rail at 1.01 seconds. The maximum working width prior to exiting the barrier was 3.88 ft resulting from the top-front corner of the cargo box extending over the bridge rail, as illustrated in Figure 359.



Figure 359. Working width for Test 4-22 on MaineDOT transition.

12.4.7 Peak Forces on Barrier

The longitudinal, lateral and resultant force-time history results are shown in Figure 360 with data filtered with cutoff frequency of 60 Hz. The peak forces are annotated with images showing truck at time of peak force. The maximum impact force occurred when the rear tandem wheel set impacted against the transition, with approximate magnitudes of 100 kips, 85 kips, and 135 kips for the longitudinal, lateral and resultant components, respectively.

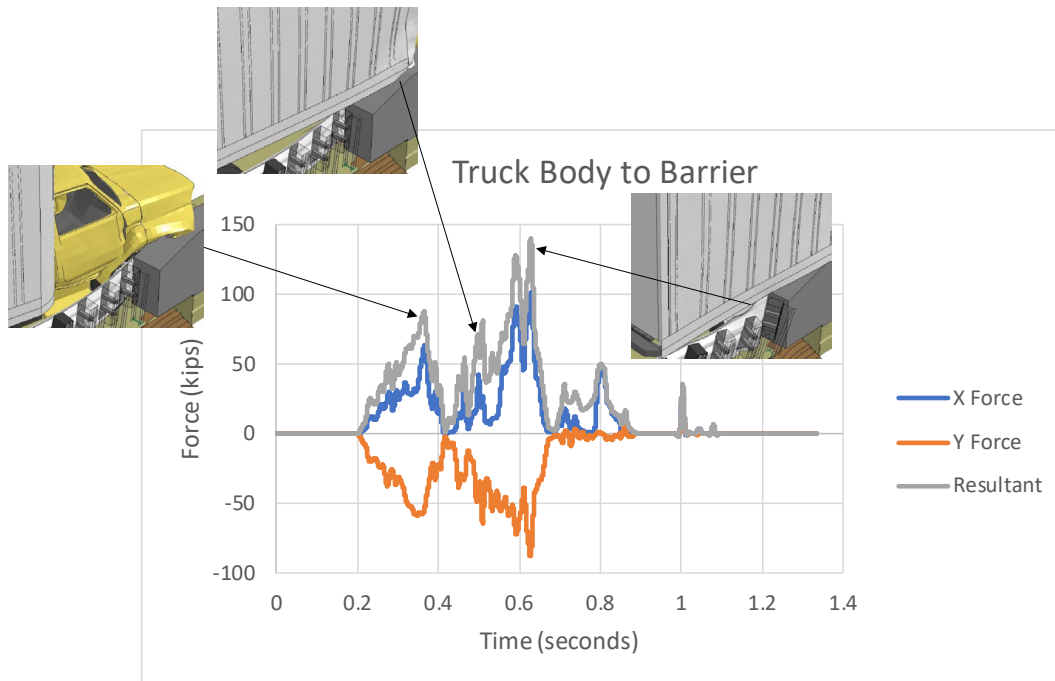


Figure 360. Longitudinal, lateral and resultant force-time history between vehicle and barrier for Test 4-22 on the MaineDOT transition.

12.4.8 Damages to Vehicle

Figure 361 shows contour plots of effective plastic strain for the vehicle, which were used to identify areas of the vehicle that suffered damage during the simulated impact event. The damages to the truck included the front bumper, front fender, front-right suspension failure, front axle and wheel, side step, lower edge of door and cabin, frame rails, rear suspension failure, and rear outside tandem wheel. The damages to the cargo-box included front-lower corner of box, lateral floor beams, main bed rail, wood flooring, and side rail.

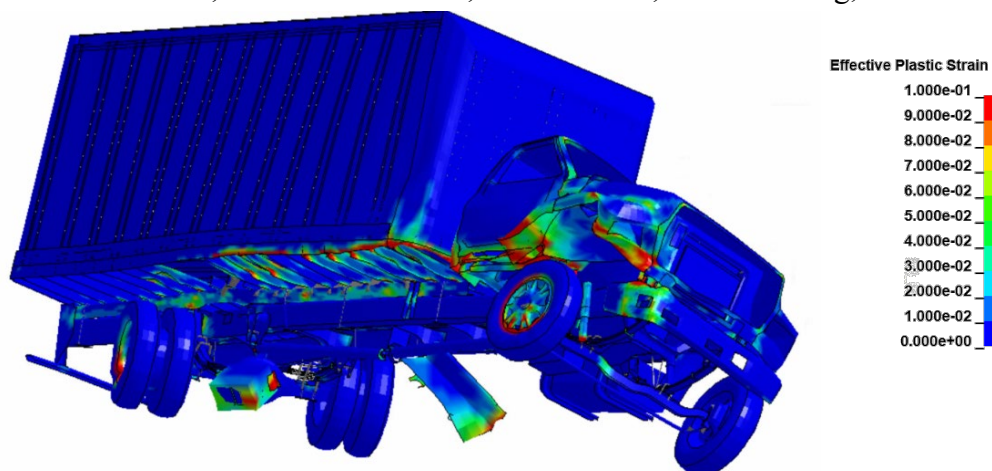


Figure 361. Damages to vehicle in Test 4-22 analysis of the MaineDOT transition.

12.4.9 Exit Box

Figure 362 shows the exit box for Test 4-22 on the MaineDOT transition. Although the exit box analysis is not required in *MASH*, it was included here for completeness. The vehicle was smoothly redirected, and the vehicle path was well within the exit box criteria of *MASH*. The vehicle remained upright during the 1.35 seconds of the impact evaluated; however, the roll rate and yaw angle at the termination of the analysis indicated that it was probable that the vehicle would roll onto its side. If a greater length of the bridge rail had been modeled, the contact between the truck and barrier would have reduce the yaw angle and improved the post trajectory of the vehicle.

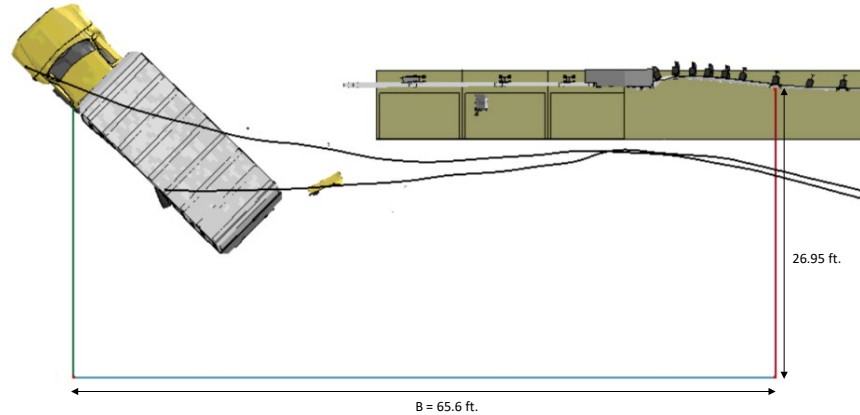


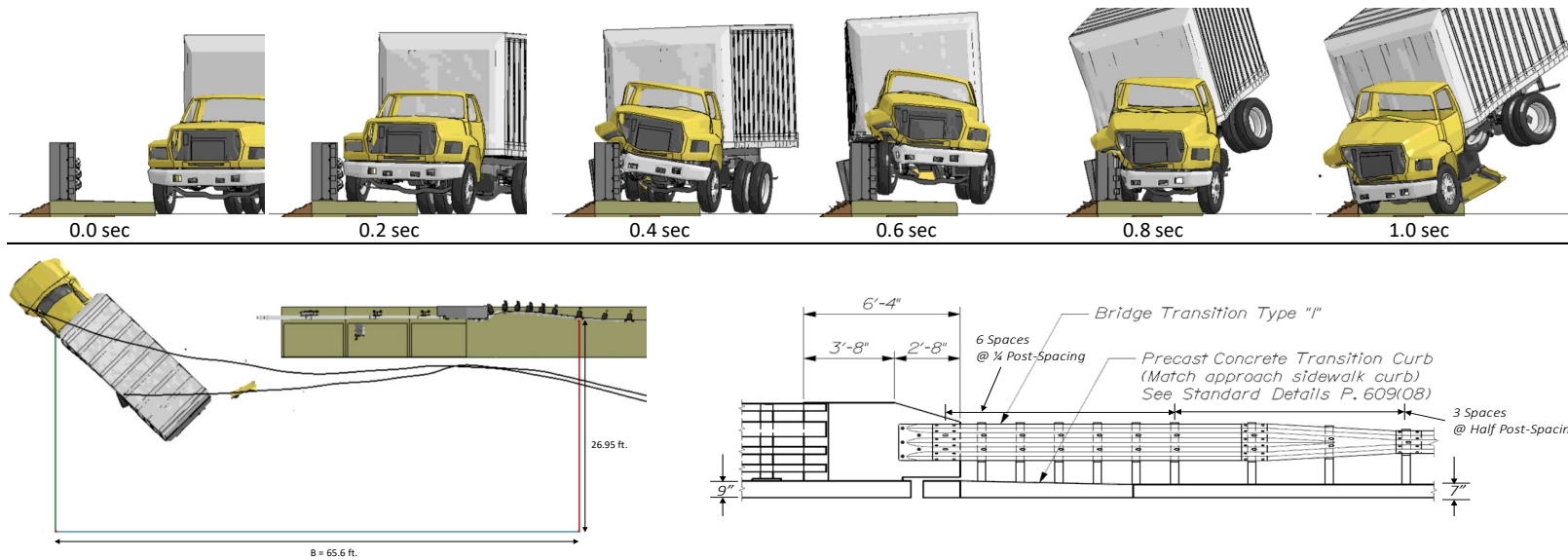
Figure 362. Exit box for Test 4-22 for the MaineDOT transition.

12.4.10 Test 4-22 Results Summary

A summary of the *MASH* Test 4-22 results on the MaineDOT transition is shown in Table 95 and Figure 363. The analysis showed that the barrier contained and redirected the 10,000S vehicle, but with significant damage to the transition and bridge rail elements. The damages to the transition included lateral soil displacement at 6 posts, significant plastic deformation of barrier three-beam components, with maximum dynamic deflection of 17 inches at Post 2 in transition. The maximum plastic strain on the three-beam was 0.5, which indicates possible rail rupture. The damages to the bridge rail posts were due to the bottom of the cargo-box leaning over the rail and snagging on the tops of the posts. There were no detached elements from the barrier that showed potential for penetrating the occupant compartment or presenting undue hazard to other traffic. The vehicle remained upright during the 1.5 seconds of the impact evaluated; however, the roll rate at the termination of the analysis indicated that it was probable that the vehicle would roll onto its side. It is preferred that the vehicle remain upright, but not required. Based on the results of this analysis, the barrier marginally meets all structural and occupant risk criteria in *MASH* for Test 4-22 impact conditions.

Table 95. Summary of MASH Test 4-12 results on the concrete transition to thrie-beam.

Evaluation Factors	Evaluation Criteria	Results
Structural Adequacy	A Test article should contain and redirect the vehicle or bring the vehicle to a controlled stop; the vehicle should not penetrate, underride, or override the installation although controlled lateral deflection of the test article is acceptable.	Marginal
Occupant Risk	D Detached elements, fragments, or other debris from the test article should not penetrate or show potential for penetrating the occupant compartment, or present undue hazard to other traffic, pedestrians, or personnel in a work zone. Deformations of, or intrusions into, to occupant compartment should not exceed limits set forth in Section 5.2.2 and Appendix E.	Pass
	G It is <u>preferable, although not essential</u> , that the vehicle remain upright during and after collision.	Probable Fail



General Information		Impact Conditions		Max50-millisecond Avg. (G)	
Analysis Agency	Roadsafe LLC	Speed	56 mph	Longitudinal	5.6 g
Test Standard Test No.	MASH Test 4-22	Angle	15 degrees	Lateral	5.0 g
Analysis No.	NETC18_MEDOT-Trans_T422	Location	12 feet upstream of bridge rail	Vertical	3.4 g
Analysis Date	6/21/2019				
Test Article		Impact Severity		Test Article Deflections (in)	
Type	Bridge Rail Transition		155.6 kip-ft	Dynamic	17 inches
Name	MEDOT Transition to 4-Bar BR	Exit Conditions		Permanent	15.4 inch
Installation Length	59.4 feet	Speed	35.9 mph	Working Width	3.9 ft
Material or Key Elements		Angle	8.5 degrees toward barrier		
		Time	1.01 seconds	Max. OCI	
				5.5 inch	
Soil Type and Condition		Occupant Risk Values		Vehicle Stability	
	MASH Strong Soil	Longitudinal OIV	8.9 ft/s	Roll	8.7 degees
Analysis Vehicle		Lateral OIV	14.4 ft/s	Pitch	12 degrees
Type / Designation	10000S	Longitudinal ORA	13.9 g	Yaw	30.4 degrees
FEA Model name	F800_No-Box_181114_UboltF0p17	Lateral ORA	8.7 g		
	502_TruckBox_181114	THIV	16.4 ft/s		
		PHD	15 g		
Mass	22,198 lb	ASI	0.66		

Figure 363. Summary results for MASH Test 4-22 on the MainedOT transition.

12.5 Conclusions for *MASH* TL4 Evaluation of the Concrete Transition to Thrie-Beam System

Based on the results of this analysis, the concrete transition to thrie-beam system is not expected to meet *MASH* safety criteria for Test Level 3 or 4.

12.5.1 *Structural Adequacy: (Marginal Pass)*

- The barrier contained and redirected the vehicle for Tests 4-20 and 4-21, but containment was marginal for Test 4-22.
- There was moderate to significant damage to the transition for Tests 4-20 and 4-21, but highly significant damage for Test 4-22.
- Test 4-22 also resulted in the bottom of the cargo-bed contacting and snagging on the tops of the bridge rail posts and deforming those posts.

12.5.2 *Occupant Risk (Fail)*

- Occupant compartment intrusion was below allowable limits for all cases
- OIV and ORA
 - Small Car : OIV was within critical limits, but ORA exceeded critical limits.
 - Pickup: OIV was within preferred limits; ORA was within critical limits

12.5.3 *Vehicle Trajectory (PASS)*

- Roll and Pitch for Tests 4-20 (small car) and 4-21 (pickup) were relatively low, and the vehicle remained upright through impact and redirection.
- Roll and pitch for Test 4-22 (SUT) were relatively low through 1.34 seconds of the impact event; however, given the final orientation, speed and roll rate of the vehicle, it is likely that the truck will roll over onto its side.

13 EVALUATION OF THE NETC 2-BAR BRIDGE RAIL FOR *MASH* TL3

The finite element model of the NETC 3-bar bridge rail was developed in Tasks 3. That model was used as a baseline for developing the NETC 2-bar bridge rail. In the 3-bar model, the deck and granite curb extension were modeled based on RIDOT design, as shown in Figure 113 (see Appendix D for drawings), in which adjacent surfaces between the granite curb and the concrete curb were not connected and the vertical leg of the hoop steel was positioned near to front anchor rods. Other states such as Vermont and New Hampshire use an integral concrete curb extension, as shown in Figure 364. Based on recommendations from the technical advisory committee for the project, the 2-bar bridge rail was modeled with the integral curb, as illustrated in Figure 364.

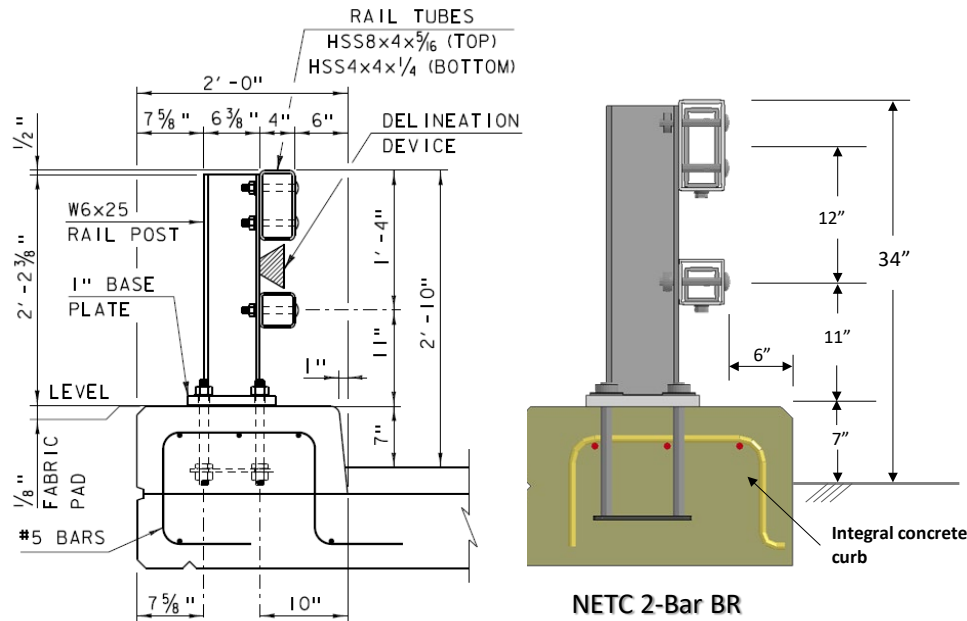


Figure 364. Section view drawing and the FEA model of the NETC 2-Bar bridge rail.

As with the 3-bar design, the splice for the tubular rails are placed on the downstream side of the posts to minimize potential for vehicles snagging at the joint in primary-direction impacts. The critical impact condition for the splice is therefore a reverse-direction impact where the vehicle impacts from the opposite direction. To simulate reverse-direction impact cases, the splice was moved to the opposite side of the post, consistent with the analysis of the 3-bar design.

FEA was used to evaluate the crash performance of the NETC 2-bar bridge rail based on structural adequacy, vehicle stability during and after redirection, and occupant risk factors using criteria specified in *MASH* for Test Level 3. Two impact cases were evaluated:

- Simulation of Test 3-10 included the 1100C Yaris model ballasted to 2,595 lb (1177 kg) impacting the barrier at 62.2 mph and 25 degrees. The critical impact point was selected as 3.6 feet (1.1 m) upstream of a bridge rail post.
- Simulation of Test 3-11 included the 2270P Chevrolet Silverado model ballasted to 5,001lb (2,269 kg) impacting the railing at 62.2 mph and 25 degrees. The critical impact point was selected as 4.3 feet (1.3 m) upstream of a bridge rail post.

The analysis in all cases was performed using LS-DYNA version mpp_s_R8.1.0 revision number 105896. The analysis was conducted with a time-step of 1.0 microsecond for a time period of 1.0 seconds for Test 3-10 and 0.9 seconds for Test 3-11.

13.1 Test 3-10

The critical impact condition for Test 3-10 was selected based the *MASH* recommended CIP for rigid barrier tests (see Table 2-7 of *MASH*). [AASHTO16] The target impact point was 3.6 feet upstream of Post 7 and was selected to maximize potential for snagging at the post, while also providing adequate opportunity for snag at the splice connection for the tubular rails. The splice is located 1.5 feet upstream of the post. The following sections provide a summary of

the results and include a commentary describing the timing and occurrence of various events during the simulated impact, time-history data evaluation, occupant risk assessments, and damages sustained by both the barrier and vehicle.

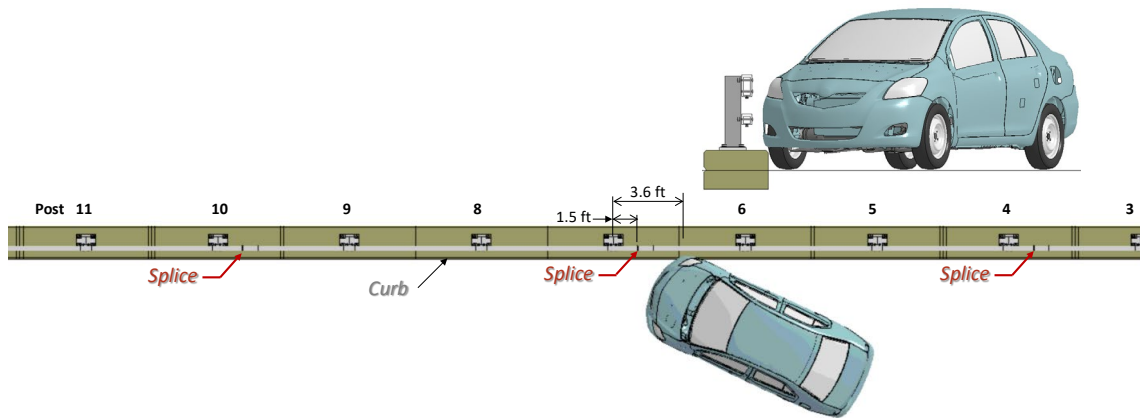


Figure 365. Impact point for Test 3-10 on the NETC 2-bar bridge rail.

13.1.1 Summary of Key Phenomenological Events

The sequential views of the impact event are shown in Appendix W in Figures W-1 through W-3 from an overhead viewpoint, downstream and upstream viewpoint, and oblique viewpoint, respectively. At time equal zero seconds the front-right tire contacted the curb, and 0.01 seconds the front bumper contacted the lower railing. At 0.015 seconds the front fender contacted the top railing. Also, at this time, the front-right tire was deformed enough to indicate debanding and deflation; however, that attribute was not included in the FEA model. At 0.02 seconds the middle and lower railings began to deflect. At 0.025 seconds the front bumper contacted the splice but did not snag; also, at this time, Post 7 began to deflect. At 0.035 seconds the front bumper was aligned with Post 7, and the front-right tire was fully mounted onto the curb. At 0.04 seconds the front bumper contacted Post 7 but did not snag on the post. At 0.045 seconds the front-right tire contacted and snagged the splice on the lower rail, which resulted in deforming the wheel, but vehicle deceleration was mostly unaffected. At 0.06 seconds the lower railing reached maximum dynamic deflection of 3.6 inches at the splice, and Post 7 reached maximum dynamic deflection of 1.75 inches. Also, at this time, the vehicle reached maximum longitudinal and lateral acceleration values of 26.2 G and 29.6 G, respectively. At 0.065 seconds the front-right tire contacted Post 7 but did not snag on the post. Also, at this time, the deformation at the lower edge of the A-Pillar caused the windshield to crack. At 0.0793 seconds the vehicle occupant contacted the right side of the interior at longitudinal velocity of 26.2 ft/s and lateral velocity of 33.1 ft/s. At 0.0862 seconds the maximum ORA in the longitudinal direction occurred with magnitude 5.5 G. At 0.13 seconds the front of the vehicle separated from the barrier. At 0.15 seconds the rear-right tire contacted the curb. At 0.165 seconds the rear-right tire rim began to bend. At 0.166 seconds the vehicle was parallel to the barrier. At 0.185 seconds the rear quarter panel and rear bumper contacted the upper and lower railings, respectively, at Post 7. Also, at this time the tire damage indicated that tire deflation was likely. At 0.2 seconds the rear-left tire lifted off the ground. At 0.205 seconds the rear-right tire was fully mounted onto the curb. At 0.222 seconds the maximum ORA in the lateral direction occurred with magnitude 6.4 G. At 0.28 seconds the vehicle separated from the barrier traveling at 42.1 mph with exit angle of 10.7 degrees (42.8 percent of impact angle). At 0.375 seconds the

vehicle reached a maximum pitch of 5.4 degrees (rear pitching upward). At 0.529 seconds the vehicle reached a maximum roll angle of 7.0 degrees (toward barrier). The vehicle remained stable throughout post-impact trajectory. The analysis ended at 1.0 seconds, at which time:

- The roll, pitch, and yaw of the vehicle were, respectively, 0.3 degrees (toward barrier), 1.3 degrees (rear pitching up), and 27.7 degrees (2.7 degrees relative to and away from barrier).
- The forward velocity of the vehicle was 39.5 mph (63.6 km/h).

13.1.2 Time History Data Evaluation

Figures 366 through 368 show the longitudinal, transverse, and vertical acceleration-time histories, respectively, computed from the center of gravity of the vehicle; Figures 369 through 371 show the comparison of the angular rates and angular displacements (i.e., yaw, roll and pitch) at the center of gravity of the vehicle.

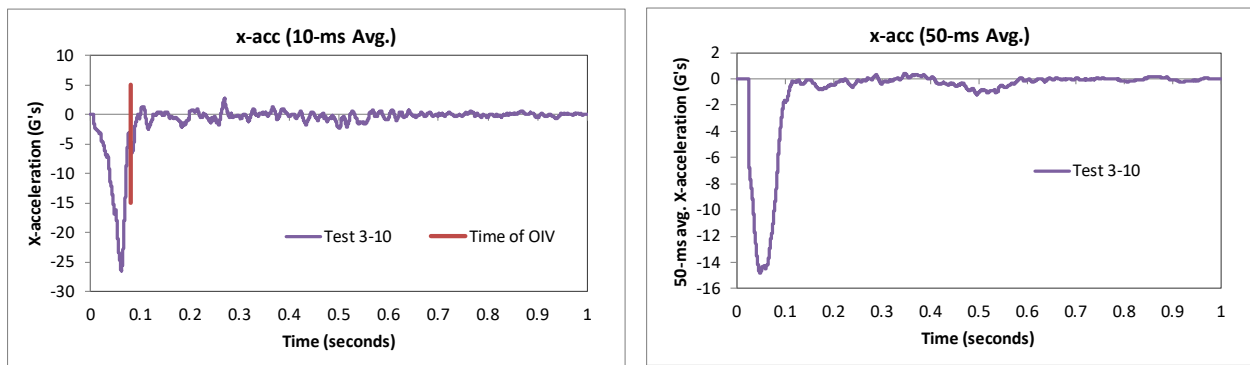


Figure 366. 10- and 50-millisecond average X-acceleration from FEA of Test 3-10 on the NETC 2-bar bridge rail.

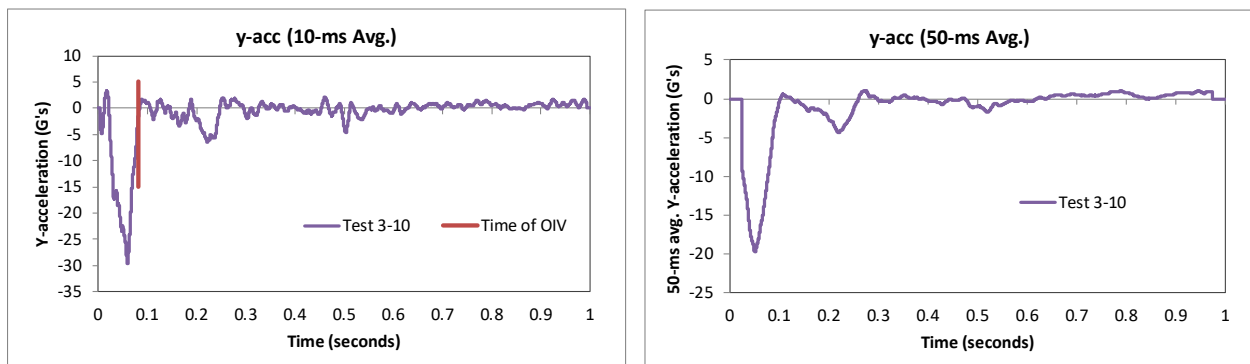


Figure 367. 10- and 50-millisecond average Y-acceleration from FEA of Test 3-10 on the NETC 2-bar bridge rail.

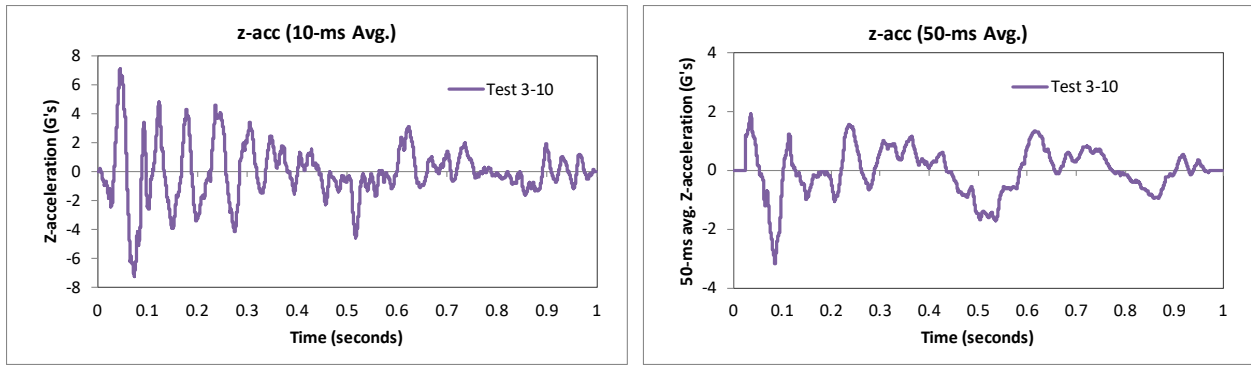


Figure 368. 10- and 50-millisecond average Z-acceleration from FEA of Test 3-10 on the NETC 2-bar bridge rail.

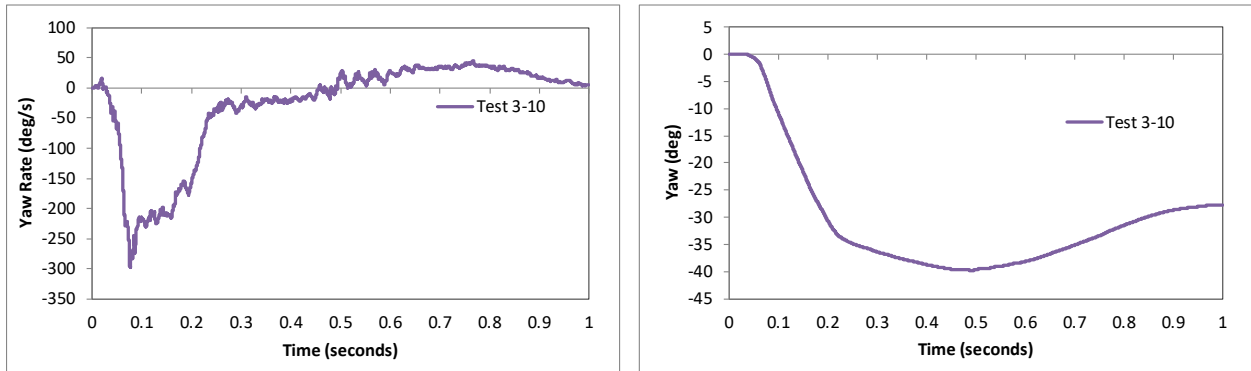


Figure 369. Yaw rate and yaw angle time-history from FEA of Test 3-10 on the NETC 2-bar bridge rail.

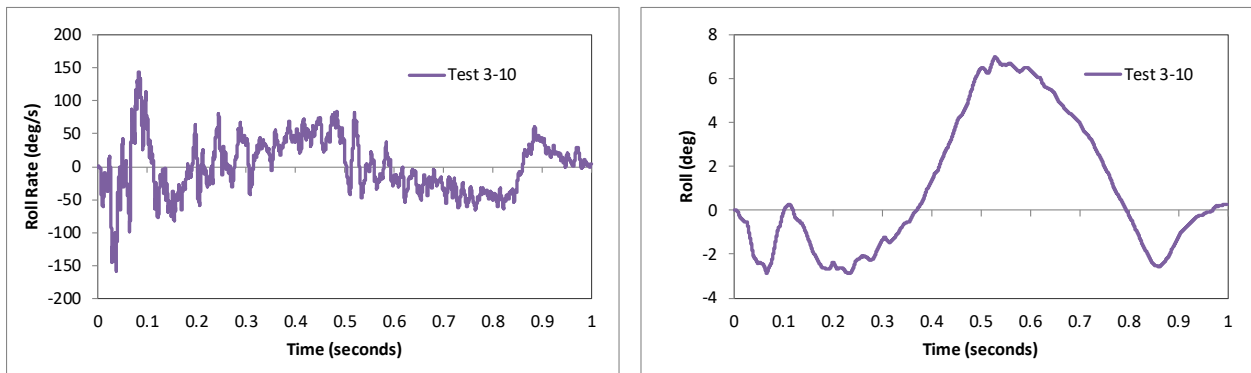


Figure 370. Roll rate and roll angle time-history from FEA of Test 3-10 on the NETC 2-bar bridge rail.

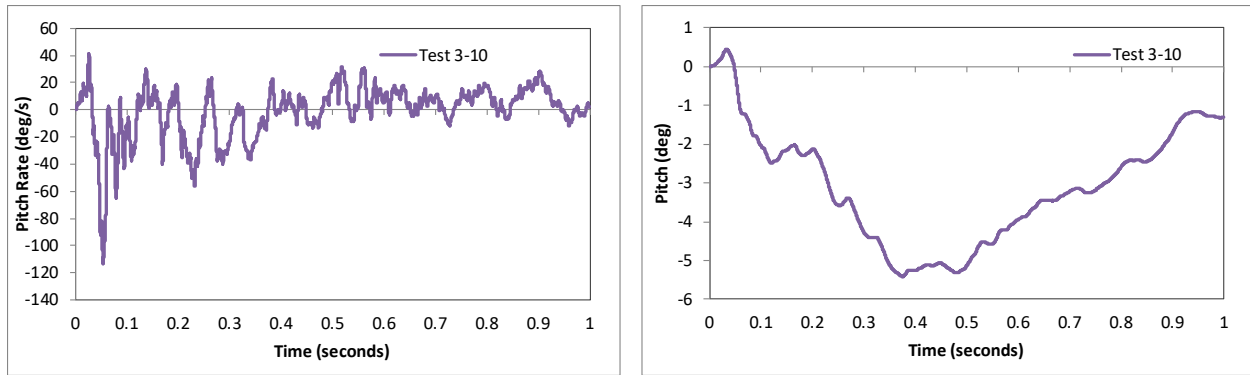


Figure 371. Pitch rate and pitch angle time-history from FEA of Test 3-10 on the NETC 2-bar bridge rail.

13.1.3 Occupant Risk Measures

The acceleration-time histories and angular rate-time histories collected at the center of gravity of the vehicle were used to evaluate occupant risk metrics according to the procedures outlined in *MASH*. Table 96 shows the results for the occupant risk calculations. The results indicate that the occupant risk factors meet safety criteria specified in *MASH*.

The occupant impact velocities in the longitudinal and transverse directions were 26.2 ft/s and 33.1 ft/s, respectively, which were within critical limits specified in *MASH*. The highest 0.010-second occupant ridedown acceleration in the longitudinal and transverse directions were 5.5 g and 6.4 g, respectively, which were well within preferred limits specified in *MASH*. However, these values are highly dependent on time of occupant impact with the interior, as shown in Figures 366 and 367. The maximum 50-ms moving average acceleration values in the longitudinal and transverse directions were 14.8 g and 19.8 g, respectively, which are considered relatively high. The maximum roll and pitch angles of the vehicle were 7.0 degrees and 5.4 degrees, respectively, which were well below critical limits in *MASH*.

Table 96. Summary of *MASH* occupant risk metrics for Test 3-10 on the NETC 2-bar bridge rail.

Occupant Risk Factors		MASH	MASH Criteria
		Test 3-10	
Occupant Impact Velocity (ft/s)	x-direction	26.2	} > 30 ft/s (preferred) < 40 ft/s (limit) ✓
	y-direction	33.1	
	at time	at 0.0793 seconds on right side of interior	
THIV (ft/s)		42.0 at 0.0793 seconds on right side of interior	
Ridedown Acceleration (g's)	x-direction	-5.5 (0.0812 - 0.0912 seconds)	} < 15 G (preferred) ✓ < 20.49 G (limit)
	y-direction	-6.4 (0.2169 - 0.2269 seconds)	
PHD (g's)		6.4 (0.2169 - 0.2269 seconds)	
ASI		2.51 (0.0257 - 0.0757 seconds)	
Max 50-ms moving avg. acc. (g's)	x-direction	-14.8 (0.0241 - 0.0741 seconds)	} < 75 deg ✓
	y-direction	-19.8 (0.0263 - 0.0763 seconds)	
	z-direction	-3.2 (0.0603 - 0.1103 seconds)	
Maximum Angular Disp. (deg)	Roll	7 (0.5291 seconds)	} < 75 deg ✓
	Pitch	-5.4 (0.3745 seconds)	
	Yaw	-39.8 (0.4896 seconds)	

13.1.4 Occupant Compartment Intrusion

The maximum deformation of the occupant compartment was approximately 3.3 inches at the lower right-front corner of the toe-pan at the wheel well. Figure 372 shows a view of the vehicle interior after the impact, with several components removed to facilitate viewing. The deformation was less than the critical limit of 9 inches specified in *MASH* for this area of the occupant compartment.

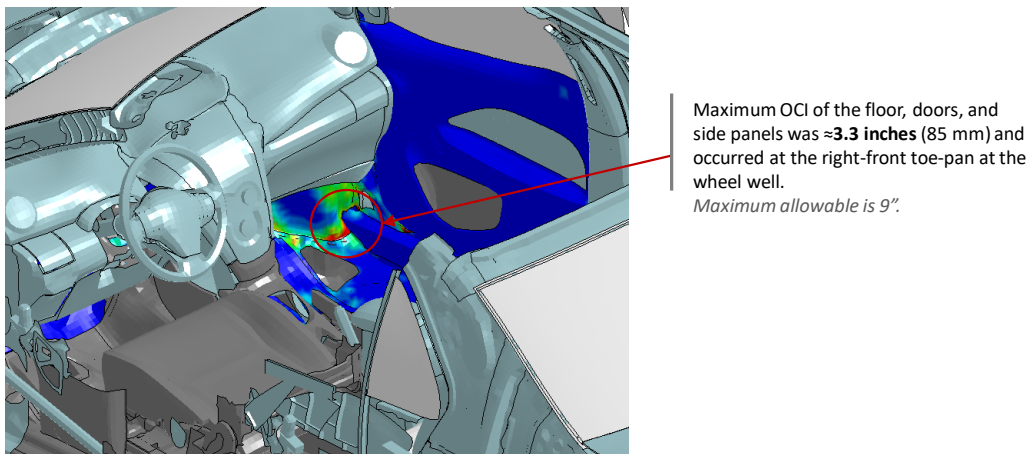


Figure 372. Occupant compartment deformation resulting from Test 3-10 on the NETC 2-bar bridge rail.

13.1.5 Damages to the Barrier System

The damages to the barrier were minimal. Figure 373 shows an overhead view of the post impact deformation of the bridge rail. The vehicle was in contact with the barrier for 11 feet, with damages limited to region between Posts 6 and 7. Figure 374 and Figure 375 show images of the maximum dynamic deflection and permanent deflection of the barrier, respectively, with a contour plot of lateral displacement on the rail elements. The maximum dynamic and permanent deflections were 3.6 inches and 2.03 inches, respectively, and occurred at the lower tube rail at the splice.

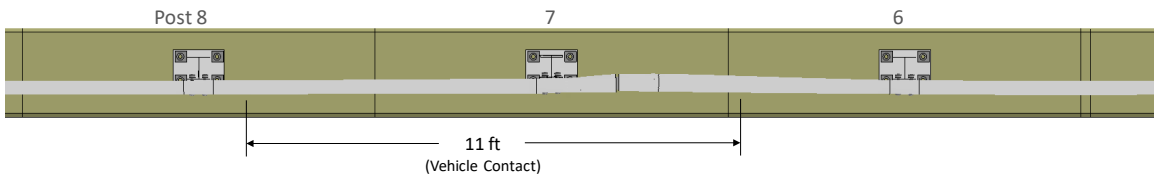


Figure 373. Overhead view of NETC 3-bar bridge rail after Test 3-10 showing extent of damage.

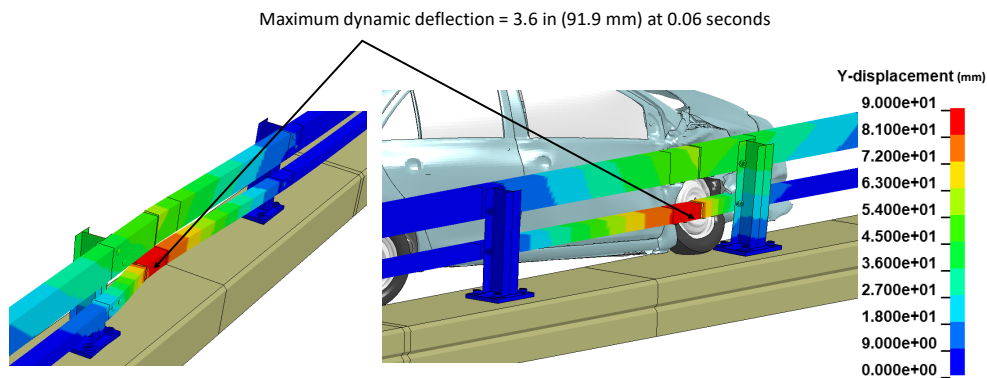


Figure 374. Contour plot of lateral displacement for the bridge rail for Test 3-10 at the time of maximum dynamic deflection.

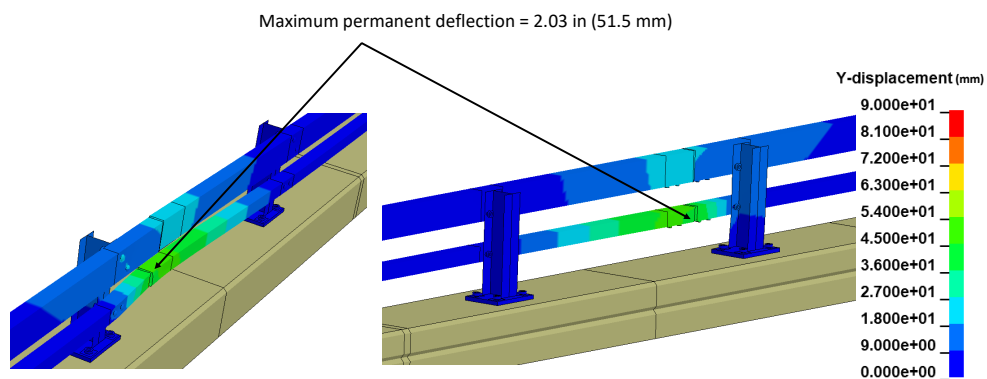


Figure 375. Contour plot of maximum permanent deflection of the NETC 2-bar bridge rail for test 3-10.

Figure 376 shows contours of true effective plastic strains on the bridge rail and of vertical displacement on the baseplate. The damage was limited to deformations of the lower rail at the splice connection, as well as, the post and the baseplate at the critical post location. The plastic strain values for those components were well below critical values. The maximum vertical dynamic deflection of the baseplate was 0.49 inches (12.4 mm), and the maximum permanent deflection of the baseplate was 0.16 inches (4.1 mm).

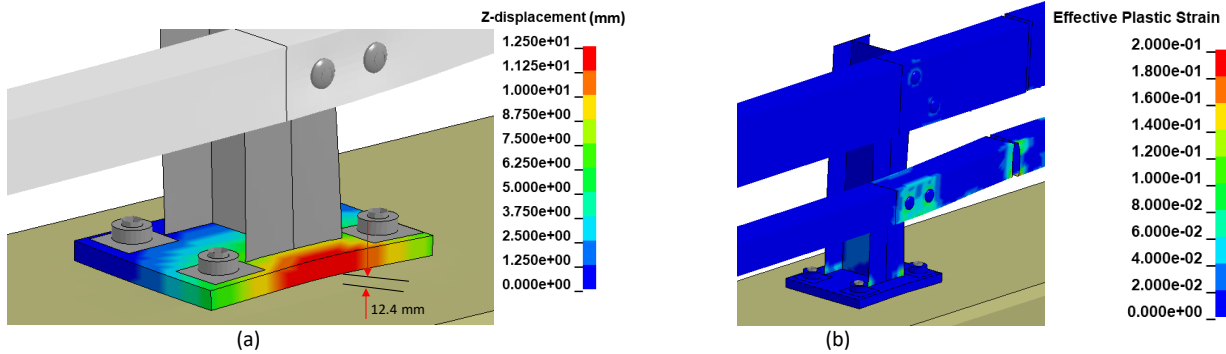


Figure 376. Contours of (a) vertical displacement on baseplate and (b) effective plastic strains on barrier for Test 3-10 on the NETC 2-bar bridge rail.

Figure 377 shows contours of 1st principal strain with contours cut off at strains of 0.1. The 1st Principal strain values for the concrete in these cases was 0.073 dynamic strain and was 0.02 permanent, which indicates a slight possibility for crack openings in the concrete curb near the front anchor rods.

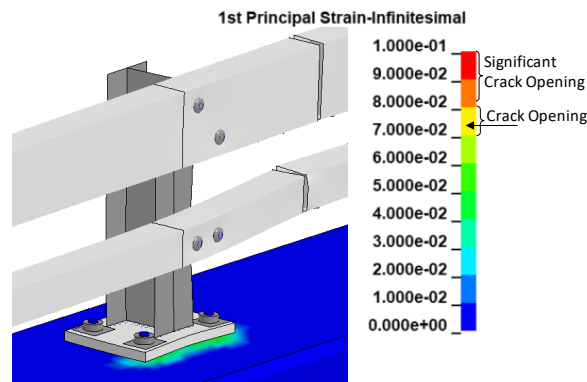


Figure 377. Contours of 1st principal strains for concrete at the critical post for Test 3-10 on the NETC 2-bar bridge rail.

13.1.6 Damages to Vehicle

Figure 378 shows contour plots of effective plastic strain for the vehicle, which were used to identify areas of the vehicle that suffered damage during the simulated impact event. The most severe damages were to the front fender, the upper and lower control arm of front suspension, front wheel, and the leading edge of the front door on the impact side. The impact-side windows were broken, and the windshield was fractured on the impact side caused from vehicle deformation. The rear-left wheel was also deformed resulting from impact with the curb.

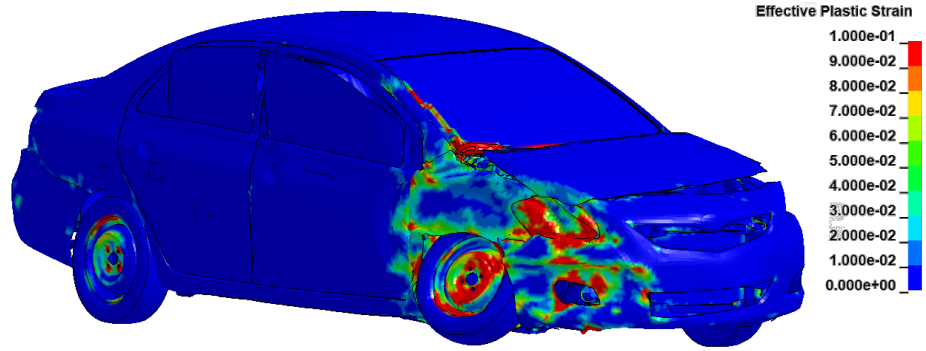


Figure 378. Damages to vehicle in Test 3-10 analysis of the NETC 2-bar bridge rail.

13.1.7 Exit Box

Figure 379 shows the exit box for Test 3-10 on the bridge rail, where the vehicle was smoothly redirected, and its path was well within the exit box criteria of *MASH*.

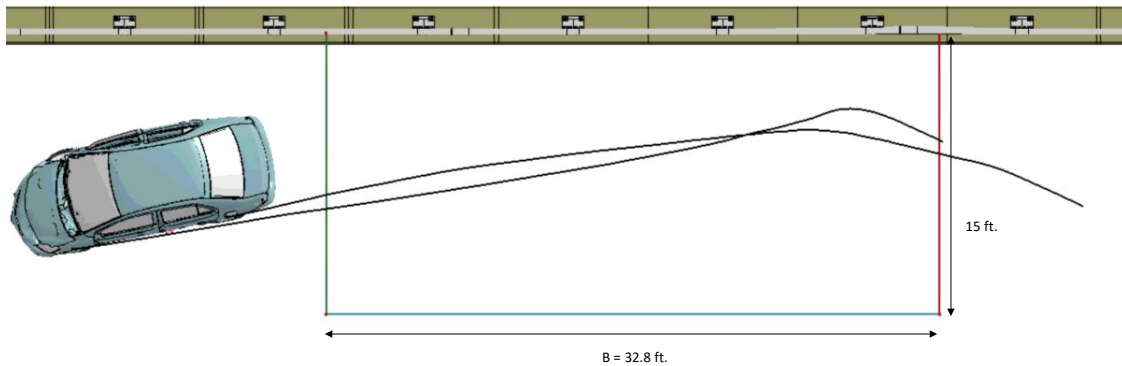


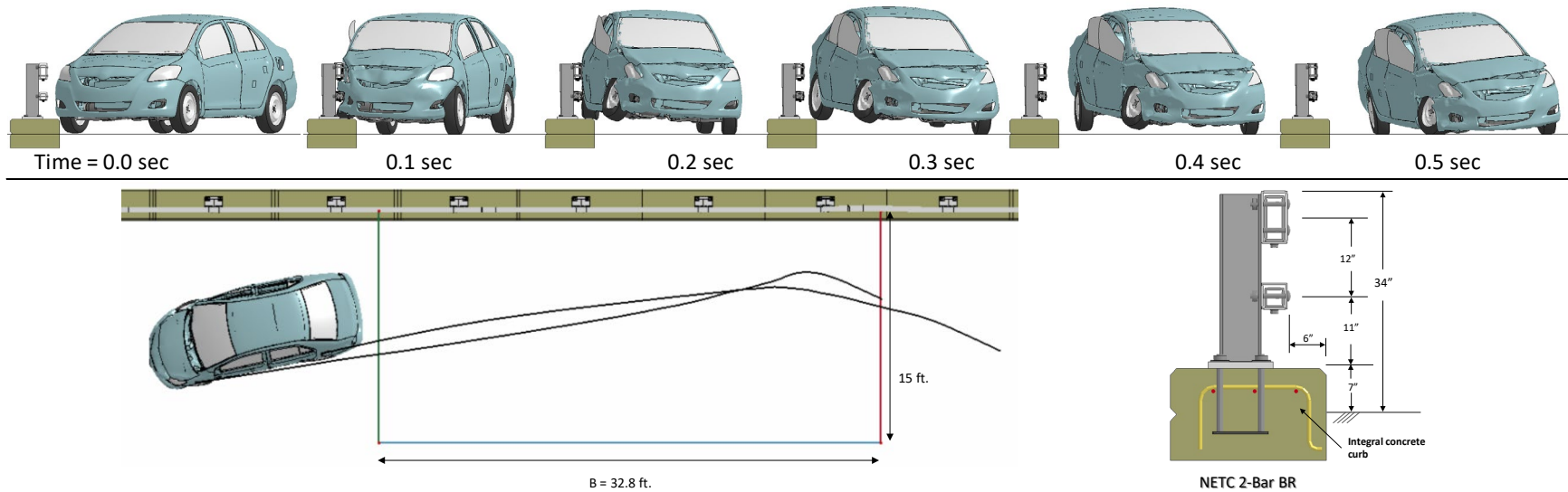
Figure 379. Exit box for Test 3-10 analysis of the NETC 2-bar bridge rail.

13.1.8 Results Summary

A summary of the *MASH* Test 3-10 results on the NETC 2-bar bridge rail is shown in Table 97 and Figure 380. The barrier successfully contained and redirected the small car with minimal damage to the system. There were no detached elements from the barrier that showed potential for penetrating the occupant compartment or presenting undue hazard to other traffic. The vehicle remained upright and very stable throughout impact and redirection. The OIV values were within critical limits, and the maximum ORA values were within recommended limits specified in *MASH*. Based on the results of this analysis, the barrier meets all structural and occupant risk criteria in *MASH* for Test 3-10 impact conditions.

Table 97. Summary of MASH Test 3-10 results on the NETC 2-bar bridge rail.

Evaluation Factors	Evaluation Criteria	Results
Structural Adequacy	A Test article should contain and redirect the vehicle or bring the vehicle to a controlled stop; the vehicle should not penetrate, underride, or override the installation although controlled lateral deflection of the test article is acceptable.	Pass
Occupant Risk	D Detached elements, fragments, or other debris from the test article should not penetrate or show potential for penetrating the occupant compartment, or present undue hazard to other traffic, pedestrians, or personnel in a work zone. Deformations of, or intrusions into, to occupant compartment should not exceed limits set forth in Section 5.2.2 and Appendix E.	Pass
	F The vehicle should remain upright during and after collision. The maximum roll and pitch angles are not to exceed 75 degrees.	Pass
	H The longitudinal and lateral occupant impact velocity (OIV) shall not exceed 40 ft/s (12.2 m/s), with a preferred limit of 30 ft/s (9.1 m/s)	Pass
	I The longitudinal and lateral occupant ridedown acceleration (ORA) shall not exceed 20.49 G, with a preferred limit of 15.0 G	Pass



General Information		Impact Conditions		Max50-millisecond Avg. (G)	
Analysis Agency	Roadsafe LLC	Speed	62 mph	Longitudinal	14.8 g
Test Standard Test No.	MASH Test 3-10	Angle	25 degrees	Lateral	19.8 g
Analysis No.	NETC18_2BarBR_T410	Location	3.6 ft upstream of Post 7	Vertical	3.2 g
Analysis Date	4/30/2019				
Test Article		Impact Severity		Test Article Deflections (in)	
Type	Bridge Rail	59.5 kip-ft		Dynamic	3.6 inches
Name	NETC 2-Bar	Exit Conditions		Permanent	2.03 inches
Installation Length	120 feet	Speed	42.1 mph	Working Width	
Material or Key Elements		Angle	10.7 degrees		
		Time	0.28 seconds	Max. OCI	
				3.3 inch	
Soil Type and Condition		Occupant Risk Values		Vehicle Stability	
N.A.		Longitudinal OIV	26.2 ft/s	Roll	7.0 degees
Analysis Vehicle		Lateral OIV	33.1 ft/s	Pitch	5.4 degrees
Type / Designation	1100C	Longitudinal ORA	5.5 g	Yaw	39.8 degrees
FEA Model name	510_YarisC_V1I_R180228	Lateral ORA	6.4 g		
Mass	2,595 lb	THIV	42.0 ft/s		
		PHD	6.4 g		
		ASI	2.51		

Figure 380. Summary results for MASH Test 3-10 on the NETC 2-bar bridge rail.

13.2 Test 3-11

The critical impact condition for *MASH* Test 3-11 was selected based the *MASH* recommended CIP for rigid barrier tests. The target impact point was 4.3 feet upstream of Post 7, as shown in Figure 381, and was selected to maximize potential for snagging at the post, while also providing adequate opportunity for snag at the splice connection of the tubular rails. [AASHTO16] The following sections provide a summary of the results and include a commentary describing the timing and occurrence of various events during the simulated impact, time-history data evaluation, occupant risk assessments, and damages sustained by both the barrier and vehicle.

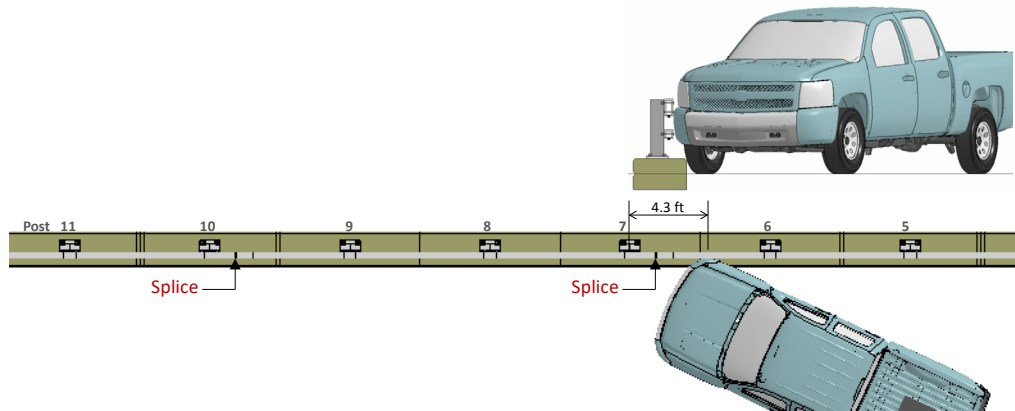


Figure 381. Impact point for Test 3-11 on the NETC 2-bar bridge rail.

13.2.1 Summary of Key Phenomenological Events

The sequential views of the impact event are shown in Appendix X in Figures X-1 through X-3 from an overhead viewpoint, downstream and upstream viewpoint, and oblique viewpoint, respectively. At time equal zero seconds the front-right tire contacted the curb, and the front bumper contacted the upper and lower railing. At 0.005 seconds the front fender contacted the top railing. At 0.01 seconds the front-right tire contacted the lower railing, and Post 7 began to deflect. At 0.015 seconds the tire front-right tire contacted the middle railing. Also, at this time, the tire was deformed enough to indicate debanding and deflation; however, that attribute was not included in the FEA model. At 0.03 seconds the front-right tire was fully mounted onto the curb. At 0.035 seconds the front-right tire was steered parallel to the barrier. At 0.04 seconds the front bumper was aligned with Post 7. At 0.05 seconds the rim of the front-right tire snagged on the end of the lower rail at the splice connection. Also, at this time, the lower control arm joint failed. At 0.065 seconds the rail reached an initial peak dynamic deflection of 2.7 inches at the splice connection on the top rail. At 0.07 seconds Post 7 reached a peak lateral deformation of 2.37 inches. At 0.08 seconds the front-right tire was aligned with Post 7 but did not contact the post. At 0.0919 seconds the vehicle occupant contacted the right side of the interior at longitudinal velocity of 20.7 ft/s and lateral velocity of 26.9 ft/s. At 0.105 seconds the ear-left tire lifted off the ground. At 0.13 seconds the front bumper was aligned with Post 8. At 0.17 seconds the rear-right tire contacted the curb. At 0.175 seconds the front-right tire was aligned with Post 8. At 0.18 seconds the rear quarter panel of the vehicle impacted the upper rail. At 0.181 the vehicle was parallel to the barrier traveling at 46 mph. At 0.185 seconds the rear bumper impacted against the middle rail. At 0.19 seconds the rear-right tire contacted

the upper rail. Also, at this time, the tire was deformed enough to indicate deflation (not included in model). At 0.196 seconds the maximum ORA in the lateral direction occurred with magnitude 15.4 G. At 0.2 seconds Post 6 reached peak dynamic deflection of 0.58 inch. At 0.205 seconds the rear-right tire contacted the lower rail. Also, at this time, Post 7 reached a second peak deflection of 2 inches. At 0.21 seconds the front of the vehicle separated from the barrier, and the rear-right tire was fully mounted onto the curb. At 0.228 seconds the maximum ORA in the longitudinal direction occurred with magnitude 4.6 G. At 0.25 seconds the rail reached a second peak dynamic deflection of 2.7 inches at the splice connection on the top rail. At 0.27 seconds the vehicle separated from the rail traveling at 45.6 mph and at an exit angle of 3.6 degrees. At 0.464 seconds the vehicle reached a maximum pitch angle of 10.1 degrees (rear pitching up), and at 0.786 seconds the vehicle reached maximum roll angle of 9.0 degrees (rolling toward barrier). The vehicle remained stable throughout post-impact trajectory. The analysis ended at 0.9 seconds, at which time:

- The roll, pitch, and yaw of the vehicle were, respectively, 4.2 degrees (toward barrier), 1.4 degrees (rear pitching up), and 18.2 degrees (6.78 degrees relative to and toward barrier).
- The forward velocity of the vehicle was 39.2 mph (63.1 km/h).

13.2.2 Time History Data Evaluation

Figures 382 through 384 show the longitudinal, transverse, and vertical acceleration-time histories, respectively, computed from the center of gravity of the vehicle; Figures 385 through 387 show the comparison of the angular rates and angular displacements (i.e., yaw, roll and pitch) at the center of gravity of the vehicle.

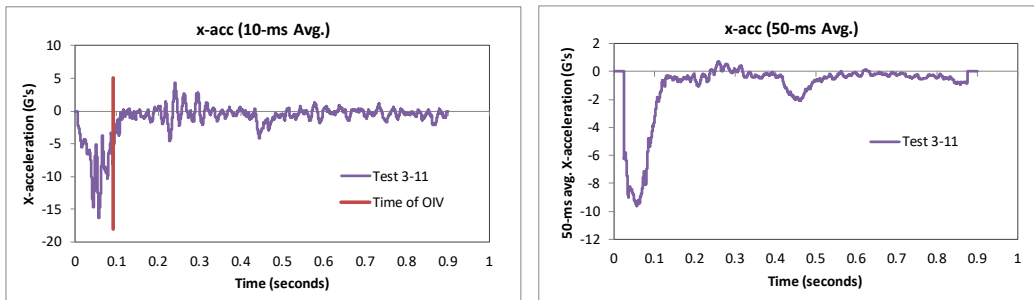


Figure 382. 10- and 50-millisecond average X-acceleration from FEA of Test 3-11 on the NETC 2-bar bridge rail.

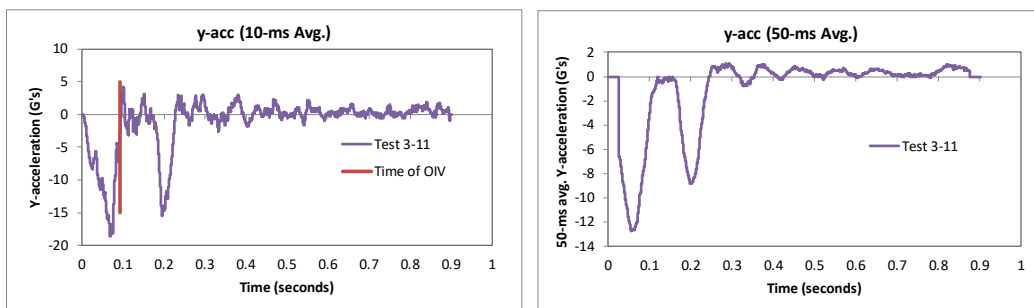


Figure 383. 10- and 50-millisecond average Y-acceleration from FEA of Test 3-11 on the NETC 2-bar bridge rail.

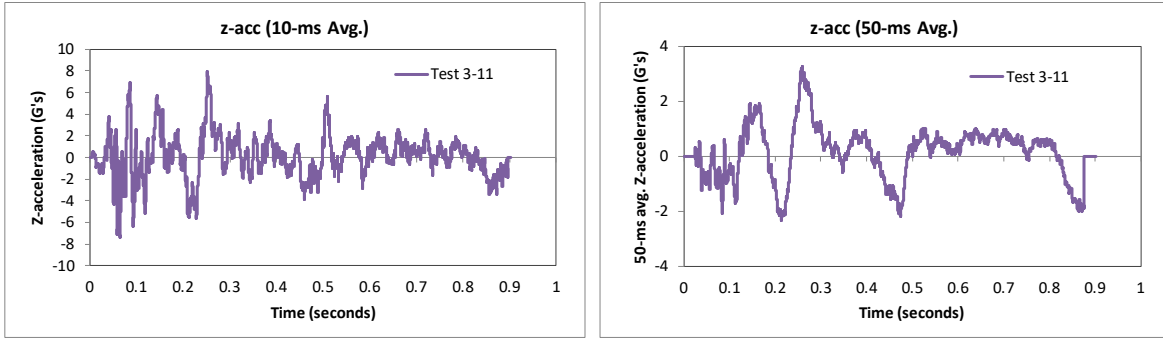


Figure 384. 10- and 50-millisecond average Z-acceleration from FEA of Test 3-11 on the NETC 2-bar bridge rail.

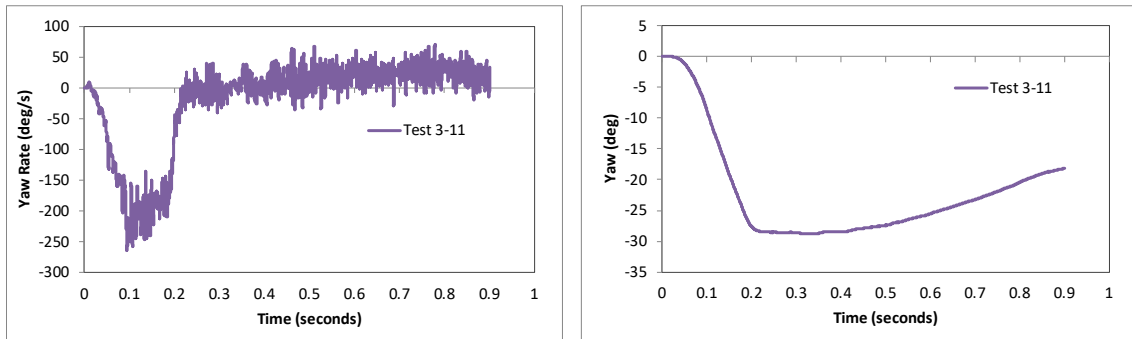


Figure 385. Yaw rate and yaw angle time-history from FEA of Test 3-11 on the NETC 2-bar bridge rail.

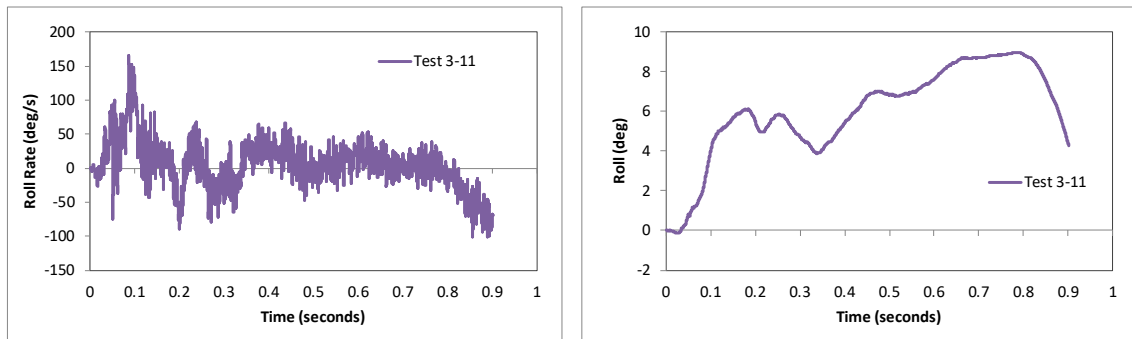


Figure 386. Roll rate and roll angle time-history from FEA of Test 3-11 on the NETC 2-bar bridge rail.

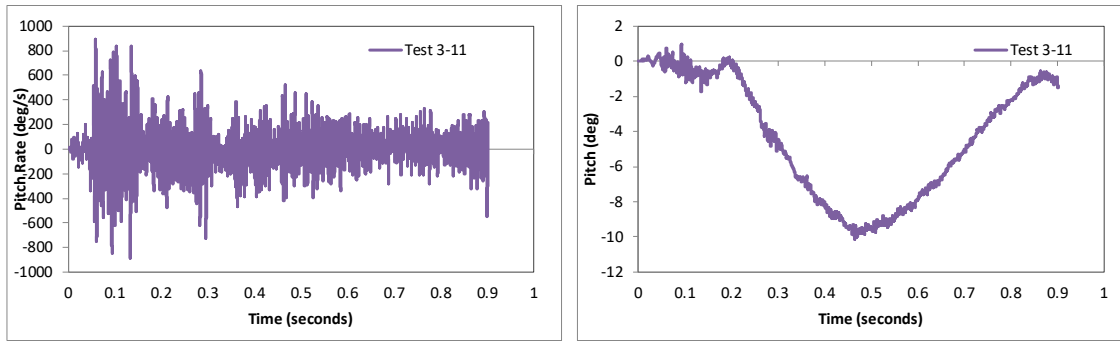


Figure 387. Pitch rate and pitch angle time-history from FEA of Test 3-11 on the NETC 2-bar bridge rail.

13.2.3 Occupant Risk Measures

The acceleration-time histories and angular rate-time histories collected at the center of gravity of the vehicle were used to evaluate occupant risk metrics according to the procedures outlined in *MASH*. Table 98 shows the results for the occupant risk calculations. The results indicate that the occupant risk factors meet safety criteria specified in *MASH*.

The occupant impact velocities in the longitudinal and transverse directions were 20.7 ft/s and 26.9 ft/s, respectively, which were within critical limits specified in *MASH*. The highest 0.010-second occupant ridedown acceleration in the longitudinal and transverse directions were 4.6 g and 15.4 g, respectively, which were within preferred limits specified in *MASH*. The maximum 50-ms moving average acceleration values in the longitudinal and transverse directions were 9.6 g and 12.7 g, respectively. The maximum roll and pitch angles of the vehicle were 9.0 degrees and 10.1 degrees, respectively, which were well below critical limits in *MASH*.

Table 98. Summary of *MASH* occupant risk metrics for Test 3-11 on the NETC 2-bar bridge rail.

Occupant Risk Factors		MASH	
		Test 3-11	
Occupant Impact Velocity (ft/s)	x-direction	20.7	} < 30 ft/s (preferred) ✓ < 40 ft/s (limit)
	y-direction	26.9	
	at time	at 0.0919 seconds on right side of interior	
THIV (ft/s)		33.5	
		at 0.0893 seconds on right side of interior	
Ridedown Acceleration (g's)	x-direction	-4.6	} > 15 G (preferred) < 20.49 G (limit) ✓
	y-direction	-15.4	
		(0.2233 - 0.2333 seconds)	
		(0.1905 - 0.2005 seconds)	
PHD (g's)		15.4	
		(0.1905 - 0.2005 seconds)	
ASI		1.63	
		(0.0308 - 0.0808 seconds)	
Max 50-ms moving avg. acc. (g's)	x-direction	-9.6	} < 75 deg ✓
	y-direction	-12.7	
	z-direction	3.3	
		(0.0320 - 0.0820 seconds)	
		(0.0303 - 0.0803 seconds)	
		(0.2342 - 0.2842 seconds)	
Maximum Angular Disp. (deg)	Roll	9	
	Pitch	-10.1	
	Yaw	-28.8	
		(0.7864 seconds)	
		(0.4644 seconds)	
		(0.3265 seconds)	

13.2.4 Occupant Compartment Intrusion

The maximum deformation of the occupant compartment was approximately 5.4 inches at the right-front corner of the toe-pan at the wheel well. Figure 388 shows a view of the vehicle interior after the impact, with several components removed to facilitate viewing. The deformation was less than the critical limit of 9 inches specified in *MASH* for this area of the occupant compartment.

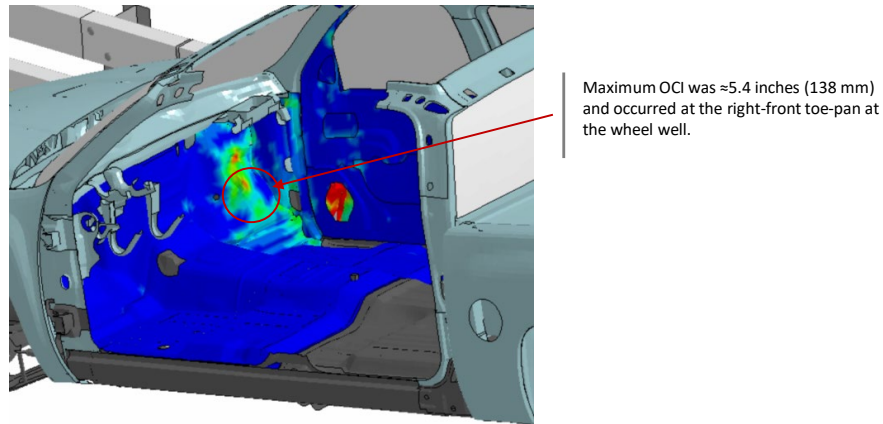


Figure 388. Occupant compartment deformation resulting from Test 3-11 on the NETC 2-bar bridge rail.

13.2.5 Damages to the Barrier System

The damages to the barrier were minimal to moderate. Figure 389 shows an overhead view of the post impact deformation of the bridge rail. The vehicle was in contact with the barrier for 16.3 feet. The barrier was deformed between Posts 6 and 9. Figure 390 and Figure 391 show images of the maximum dynamic deflection and permanent deflection of the barrier, respectively, with a contour plot of lateral displacement on the rail elements. The maximum dynamic and permanent deflections were 2.7 inches and 1.27 inches, respectively, and occurred at the top rail tube at the splice. The maximum working width of the barrier was 1.03 feet based on maximum dynamic lateral extent of the barrier during impact; and was 1.17 feet based on the maximum lateral extent of the front fender of the vehicle over the top of the rail during impact.

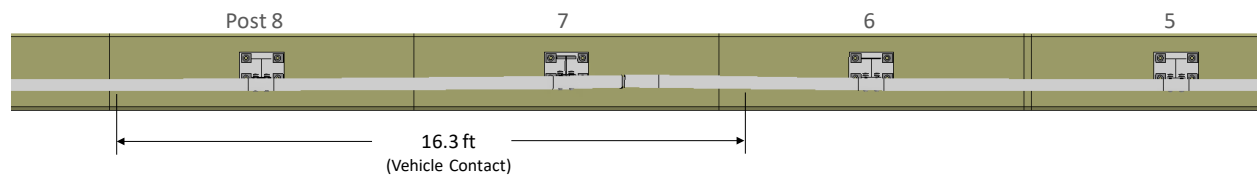


Figure 389. Overhead view of NETC 3-bar bridge rail after Test 3-11.

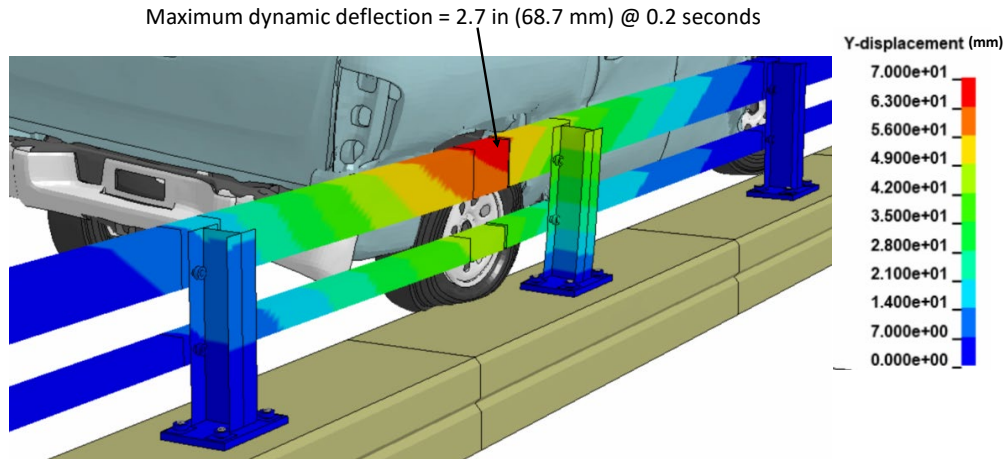


Figure 390. Contour plot of lateral displacement for the bridge rail for Test 3-11 on NETC 2-bar bridge rail at the time of maximum dynamic deflection.

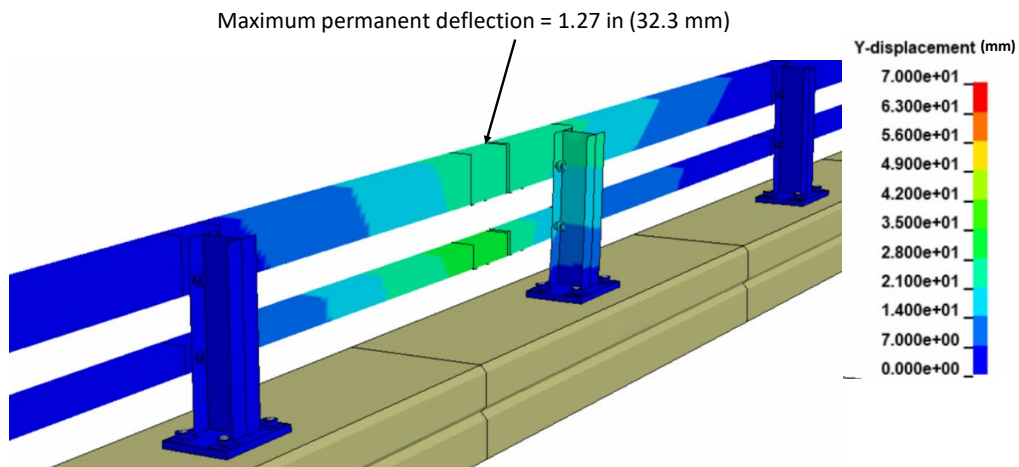


Figure 391. Contour plot of maximum permanent deflection of the NETC 2-bar bridge rail for test 3-11.

Figure 392 shows contours of true effective plastic strains on the bridge rail. The damage was primarily focused at Post 7 and included plastic deformation of the post, baseplate and both rails. The plastic deformation at the ends of the rail tubes at the splice connection was a result of a snag with the front impact-side wheel and the leading edge of the passenger door. The maximum vertical dynamic deflection of the baseplate at Post 7 was 0.62 inches (15.7 mm) and the maximum permanent deflection was 0.24 inches (6.2 mm). There was also slight vertical deformation of the baseplate at Post 6 of 0.14 inch (3.5 mm) maximum dynamic and 0.04 inch (1 mm) permanent.

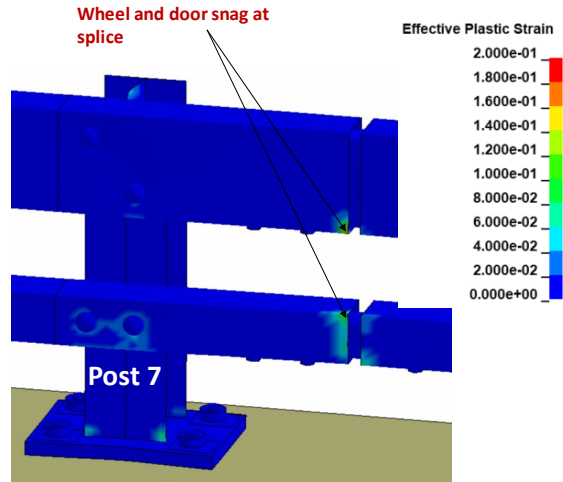


Figure 392. Contours of effective plastic strains for Test 3-11 on the NETC 2-bar bridge rail.

Figure 393 shows contours of 1st principal strain with contours cut off at strains of 0.1. The 1st Principal strain values for the concrete in these cases was 0.092 dynamic strain and was 0.076 permanent, which indicated a relatively high probability for damage to the concrete curb, although complete failure is not predicted.

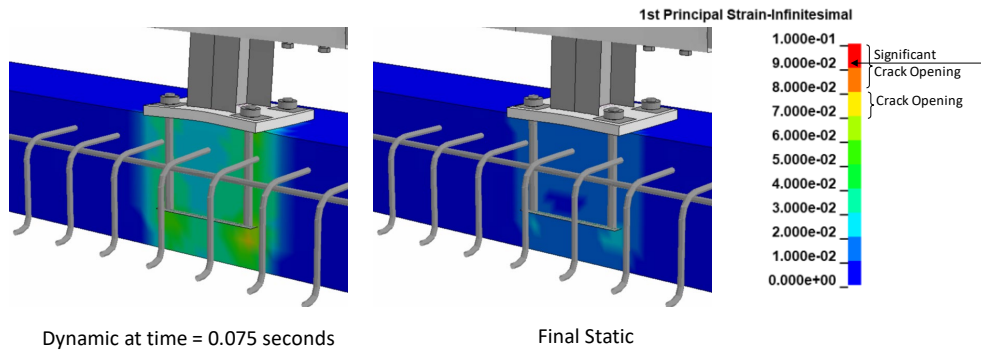


Figure 393. Contours of 1st principal strains for concrete at the critical post for Test 3-11 on the NETC 2-bar bridge rail.

13.2.6 Damages to Vehicle

Figure 394 shows contour plots of effective plastic strain for the vehicle, which were used to identify areas of the vehicle that suffered damage during the simulated impact event. The most severe damages were to the front bumper, front fender, passenger front door, the upper and lower control arm of front suspension, front wheel, rear wheel, and the rear quarter panel of the vehicle on the impact side.

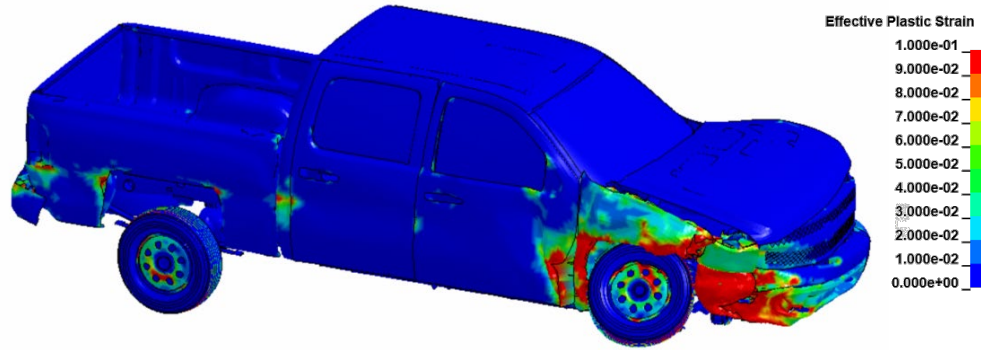


Figure 394. Damages to vehicle in Test 3-11 analysis of the NETC 2-bar bridge rail.

13.2.7 Exit Box

Figure 395 shows the exit box for Test 3-11 on the bridge rail, where the vehicle was smoothly redirected and its path was well within the exit box criteria of *MASH*.

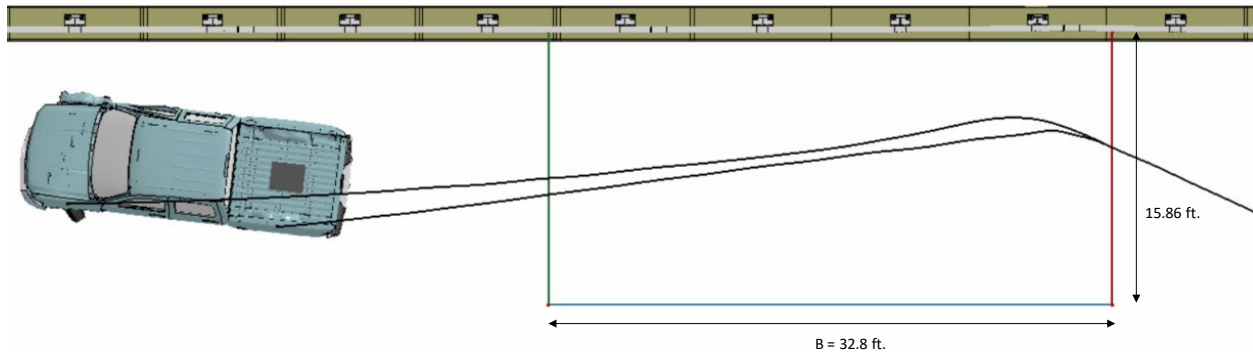


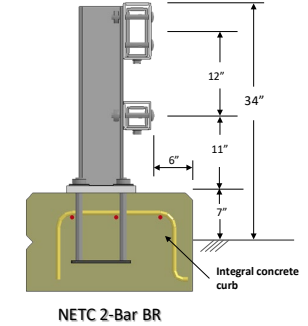
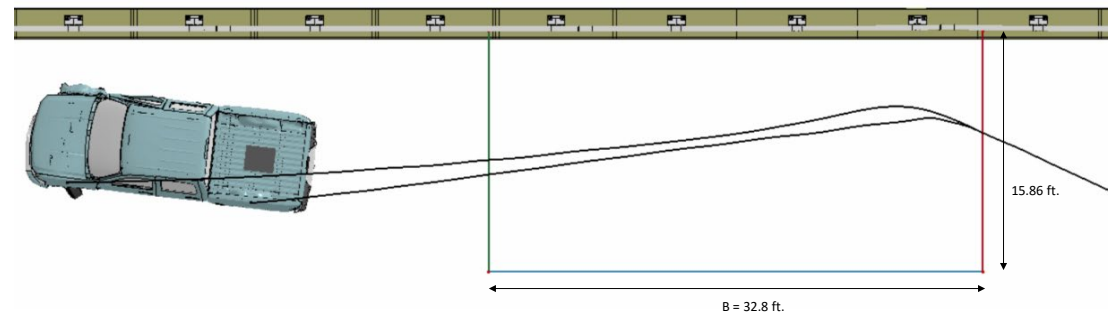
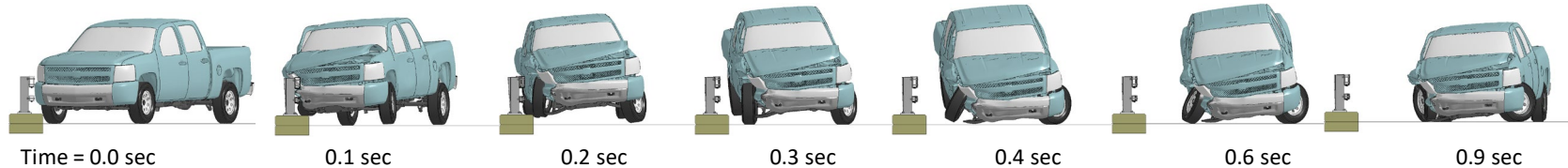
Figure 395. Exit box for Test 3-11 analysis of the NETC 2-bar bridge rail.

13.2.8 Results Summary

A summary of the *MASH* Test 3-11 results on the NETC 2-bar bridge rail is shown in Table 99 and Figure 396. The barrier successfully contained and redirected the pickup with minimal to moderate damage of the system. There were no detached elements from the barrier that showed potential for penetrating the occupant compartment or presenting undue hazard to other traffic. The vehicle remained upright and very stable throughout impact and redirection. The OIV values were with recommended limits, and the ORA values were within critical limits as specified in *MASH*. Based on the results of this analysis, the barrier meets all structural and occupant risk criteria in *MASH* for Test 3-11 impact conditions.

Table 99. Summary of MASH Test 3-11 results on the NETC 2-bar bridge rail.

Evaluation Factors	Evaluation Criteria	Results
Structural Adequacy	A Test article should contain and redirect the vehicle or bring the vehicle to a controlled stop; the vehicle should not penetrate, underride, or override the installation although controlled lateral deflection of the test article is acceptable.	Pass
Occupant Risk	D Detached elements, fragments, or other debris from the test article should not penetrate or show potential for penetrating the occupant compartment, or present undue hazard to other traffic, pedestrians, or personnel in a work zone. Deformations of, or intrusions into, to occupant compartment should not exceed limits set forth in Section 5.2.2 and Appendix E.	Pass
	F The vehicle should remain upright during and after collision. The maximum roll and pitch angles are not to exceed 75 degrees.	Pass
	H The longitudinal and lateral occupant impact velocity (OIV) shall not exceed 40 ft/s (12.2 m/s), with a preferred limit of 30 ft/s (9.1 m/s)	Pass
	I The longitudinal and lateral occupant ridedown acceleration (ORA) shall not exceed 20.49 G, with a preferred limit of 15.0 G	Pass



General Information		Impact Conditions		Max50-millisecond Avg. (G)	
Analysis Agency	Roadsafe LLC	Speed	62 mph	Longitudinal	9.6 g
Test Standard Test No.	MASH Test 3-11	Angle	25 degrees	Lateral	12.7 g
Analysis No.	NETC18_2BarBR_T311	Location	4.3 ft upstream of Post 7	Vertical	3.3 g
Analysis Date	5/1/2019				
Test Article		Impact Severity		Test Article Deflections (in)	
Type	Bridge Rail	114.7 kip-ft		Dynamic	2.7 inches
Name	NETC 2-Bar	Exit Conditions		Permanent	1.3 inches
Installation Length	120 feet	Speed	45.6 mph	Working Width (barrier deflection)	1.03 feet
Material or Key Elements		Angle	3.6 degrees	Working Width (vehicle penetration)	1.17 feet
Soil Type and Condition	N.A.	Time	0.295 seconds	Max. OCI	2.76 inch
Analysis Vehicle		Occupant Risk Values		Vehicle Stability	
Type / Designation	2270P	Longitudinal OIV	20.7 ft/s	Roll	9.0 degees
FEA Model name	SilveradoC_V3a_V180201_TireRS_35psi	Lateral OIV	26.9 ft/s	Pitch	10.1 degrees
Mass	5,001 lb	Longitudinal ORA	4.6 g	Yaw	28.8 degrees
		Lateral ORA	15.4 g		
		THIV	33.5 ft/s		
		PHD	15.4 g		
		ASI	1.63		

Figure 396. Summary results for MASH Test 3-11 on the NETC 2-bar bridge rail.

13.3 Conclusion for TL3 Evaluation of NETC 2-Bar Bridge Rail

Based on the results of this analysis, the NETC 2-bar bridge rail meets all structural and occupant risk criteria in *MASH* for Test Level 3; however, relatively high barrier damages are likely under these conditions. The barrier system meets *MASH* TL3 criteria with only moderate barrier damages.

13.3.1 Structural Adequacy: (PASS)

- The barrier successfully contained and redirected the vehicle in all test cases.

13.3.2 Occupant Risk (PASS)

- Occupant compartment intrusion was below allowable limits for all cases
- OIV and ORA:
 - Small Car : OIV (within critical limits); ORA (within preferred limits) (values highly dependent on time of occupant impact)
 - Pickup: OIV (within preferred limits); ORA (within critical)

13.3.3 Vehicle Trajectory (PASS)

- Vehicle remained upright and stable through impact and redirection, with relatively low angular displacements for all cases.

13.3.4 Barrier Damages

- The barrier experienced moderate plastic deformations of the posts, rails and baseplates for Test 3-11 (Pickup).
- Concrete curb damage at Post 7 was likely for Test 3-11. The damages corresponded to potential cracks around the front anchor bolts and/or pryout damage.

14 EVALUATION OF THE NETC 2-BAR TRANSITION FOR *MASH* TL3

The baseline finite element model of the NETC 2-bar transition system was developed in Task 2b (refer to Section 7). For the *MASH* evaluation of the 2-bar transition, the baseline model was updated to reflect the current design standard for the 2-bar system (per NHDOT design) and to include the general model improvements presented in Task 4 for the NETC 3-bar transition. The detail drawings for this system is provided in Appendix B. The primary modifications to the baseline transition model were primarily related to matching the current design standards, which included:

- Replacing the 6"x8" wood posts with steel W6x9 posts made from AASHTO M183 steel (ASTM A36); the material characterization was based on stress-strain curves from tensile tests [*Wright97*] with yield strength = 45.7 ksi (true stress).
- Increasing w-beam rail height from 27 inches to 31 inches.
- Increasing the thrie-beam height from 32 inches to 34 inches.

- Adding the 3rd rail element and repositioning mounting holes for post attachments.
- Extending the continuum soil model to include all posts in the thrie-beam region.
- Updating the splice connection to include bushing-spacers for the cap screws on both sides of the splice.

The model included 42 feet of w-beam guardrail and transition elements; and included 23.8 feet of the NETC 2-bar bridge rail, as illustrated in Figure 397. The geometric details of the system model were consistent with the drawings of Appendix B. Refer to Section 7 for additional details regarding model development and methodology.

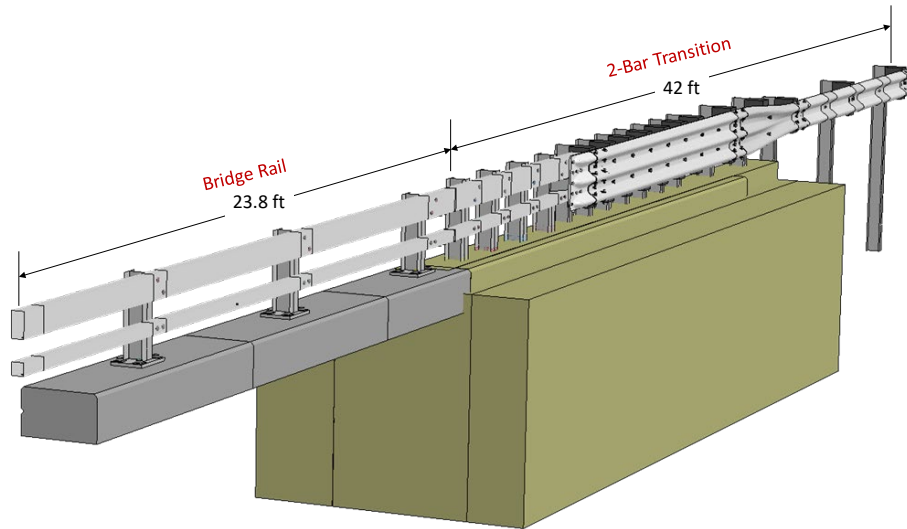


Figure 397. FEA model of the 2-bar transition (oblique viewpoint).

14.1 Determining Critical Impact Point

MASH guidance on selecting critical impact points was provided in Section 10.1 and deals primarily with identifying critical snagging hazards and structural failure of barrier elements. The determination of critical impact point for the current case also included maximizing occupant risk metrics, which are used directly in crashworthy evaluations in *MASH*.

For the 2-bar transition, two critical snag points were identified for the system regarding impact with passenger vehicle: 1) the upstream end of the tube rails and 2) the first post of the tube-rail section of the transition, as illustrated in Figure 398.

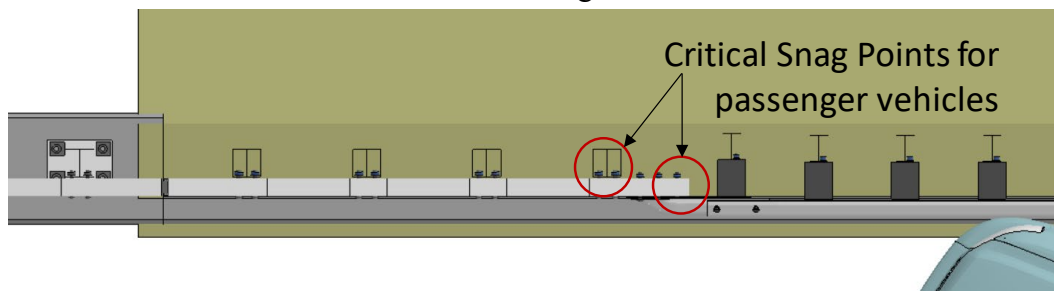


Figure 398. Illustration of potential snag points on the 2-bar transition for passenger vehicles.

14.2 Test 3-20

14.2.1 CIP for Test 3-20

The critical impact point for Test 3-20 was determined using FEA with respect to maximum potential for wheel snag on the first post of the tube-rail section of the transition and on maximizing OIV and ORA metrics. Finite element analysis was used to simulate *MASH* Test 3-20 at impact points 5.0 ft, 5.5 ft, 6.0 ft, 6.5 ft and 7.0 ft from the centerline of the post. These analysis cases were conducted for 0.15 seconds of impact, which was sufficient for capturing the full impact and initial redirection of the vehicle. The results of analysis cases for impact point of 5.0 ft to 6.5 ft are shown in Figure 399. The image for the analysis case with impact at 7.0 ft upstream of the critical snag point is not shown but was very similar to the impact case at 6.5 ft. None of the analysis cases resulted in significant wheel contact with the post.

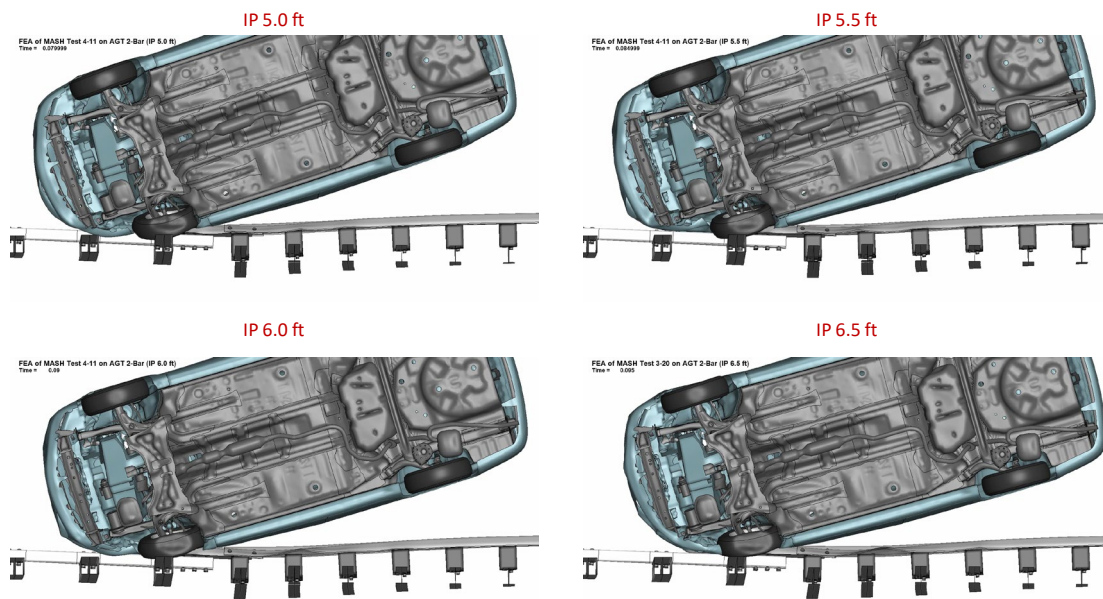


Figure 399. Results of Test 3-20 CIP evaluations for the 2-bar Transition.

An overlay of the acceleration-time histories for the five analysis cases is shown in Figure 400, and plots of OIV and ORA values are shown in Figure 401. The peak acceleration and the shape of the acceleration pulse was very similar for all cases, with slightly higher impulse for Cases IP6.5 and IP7.0 (e.g., similar peak but wider pulse). The OIV and ORA metrics were below recommended limits for all cases. The OIV values in the x-direction were the same for Cases IP5.5 – IP7.0, with IP5.0 being slightly lower. The OIV-y was highest for Cases IP6.5 and IP7.0. The ORA-x was highest for Case IP6.5, and the ORA-y was highest for Case IP5.0, although all cases were well below recommended limits.

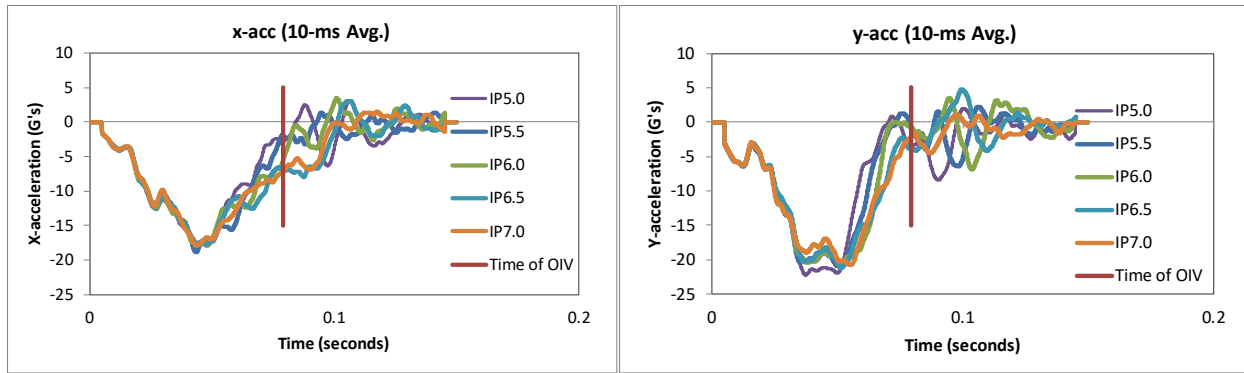


Figure 400. Plots of x-acceleration and y-acceleration measured at the c.g. of the vehicle.

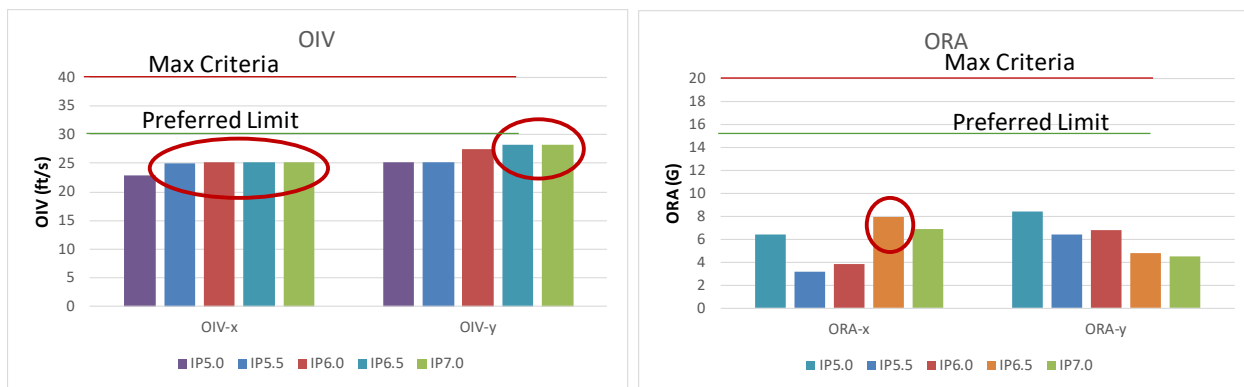


Figure 401. OIV and ORA metrics calculated for the five Test 3-20 analysis cases on the 2-bar transition.

Based on these data, the critical impact point was selected as 6.5 feet upstream of the critical post to maximize OIV (which was close to preferred limits). The final analysis was performed for 0.8 seconds of the impact event. The following sections provide a summary of the results and include a commentary describing the timing and occurrence of various events during the simulated impact, time-history data evaluation, occupant risk assessments, and damages sustained by both the barrier and vehicle.

14.2.2 Summary of Key Phenomenological Events

The sequential views of the impact event are shown in Appendix Y in Figures Y-1 through Y-3 from an overhead viewpoint, downstream and upstream viewpoint, and oblique viewpoint, respectively. At time equal zero seconds the front bumper of the car contacted the lower two corrugations of the nested thrie-beam rail at 6.5 feet upstream of Post 4, as illustrated in Figure 402.

Before 0.005 seconds, the front-right tire struck the curb, the front-right fender contacted the top corrugation of the thrie-beam and the front-right tire contacted the lower corrugation. At 0.01 seconds the barrier began to deflect. At 0.025 seconds the front-right tire was steered parallel to the barrier, and the right corner of the front bumper was aligned with Post 6. At 0.035 seconds the lower edge of the front-right A-pillar deformed and cracked the lower edge of the windshield. At 0.04 seconds the front bumper was aligned with Post 5. At 0.055 seconds the front-right tire was fully mounted onto the curb. At 0.07 seconds the barrier reached maximum

dynamic deflection of 6.3 inches at the lower corrugation of the thrie-beam at the point where the nested thrie-beam connects to the thrie-beam end shoe; Post 5 deflected 4.8 inches. At 0.0725 seconds the hub of the front-right tire was aligned with Post 5. At 0.0789 seconds the occupant contacted the right side of the interior at 25.26 ft/s in the forward direction and 28.21 ft/s in the lateral direction. At 0.0874 seconds the maximum longitudinal ORA occurred with magnitude 7.9 G. At 0.0996 seconds the maximum lateral ORA occurred with magnitude 4.8 G. At 0.1 seconds the hub of the front-right tire was aligned with Post 4 (critical snag point) but was at least 2 inches away from contact with the post. Also, at this time, the rear-right tire began to lift off the roadway as the vehicle rolled away from the barrier. At 0.165 seconds the rear-right tire contacted the curb. At 0.18 seconds the rear-right tire contacted the lower and middle corrugations of the nested thrie-beam and terminal connector near Post 5. At 0.2 seconds the vehicle was parallel to the barrier traveling at 42.2 mph. At 0.21 seconds the rear-right tire was fully mounted onto the curb. At 0.235 seconds the rear-quarter panel of the vehicle contacted the lower and top tube railings of the transition near Post 3. At 0.27 seconds the vehicle reached a maximum roll angle of -6.7 degrees (away from barrier). At 0.28 seconds the vehicle separated from the barrier at an exit speed and angle of 41.3 mph and 7.3 degrees. At 0.49 seconds the vehicle reached a maximum pitch of -3.6 degrees (rear pitching upward). The vehicle remained stable throughout post-impact trajectory. The analysis ended at 0.8 seconds, at which time:

- The roll, pitch, and yaw of the vehicle were, respectively, -2.6 degrees (away from barrier), 0.08 degrees (front pitching up), and -24.9 degrees (0.1 degrees relative to and toward barrier).
- The forward velocity of the vehicle was 38.7 mph (62.4 km/h).

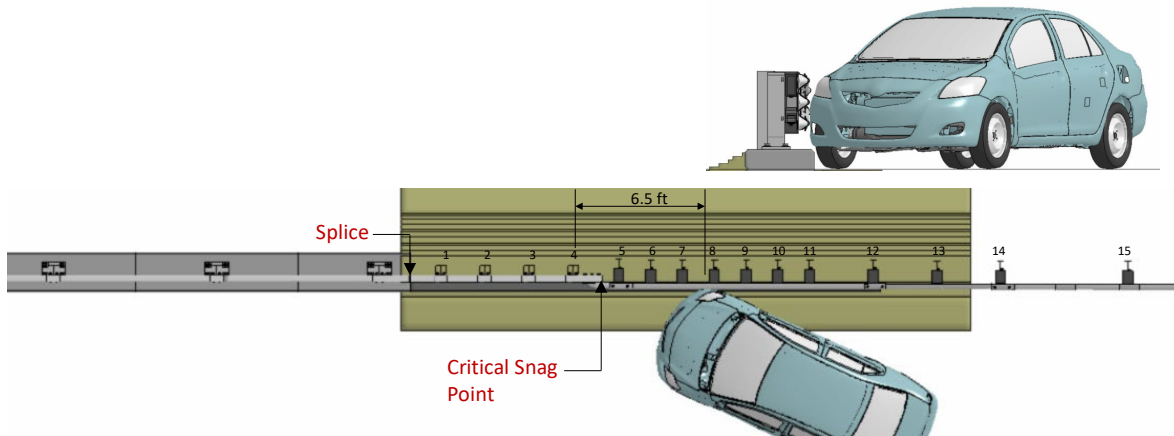


Figure 402. Impact point for Test 3-20 on the 2-bar transition.

14.2.3 Time History Data Evaluation

Figures 403 through 405 show the longitudinal, transverse, and vertical acceleration-time histories, respectively, computed from the center of gravity of the vehicle; Figures 406 through 408 show the comparison of the angular rates and angular displacements (i.e., yaw, roll and pitch) at the center of gravity of the vehicle.

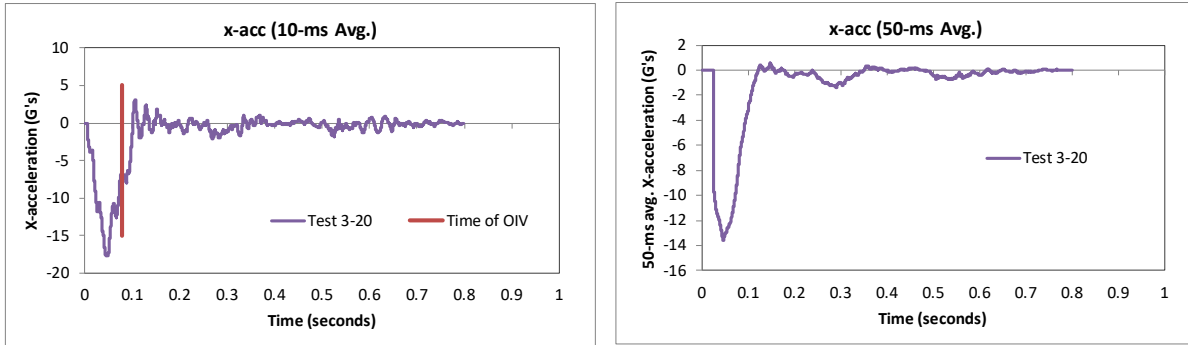


Figure 403. 10- and 50-millisecond average X-acceleration from FEA of Test 3-20 on the 2-bar transition.

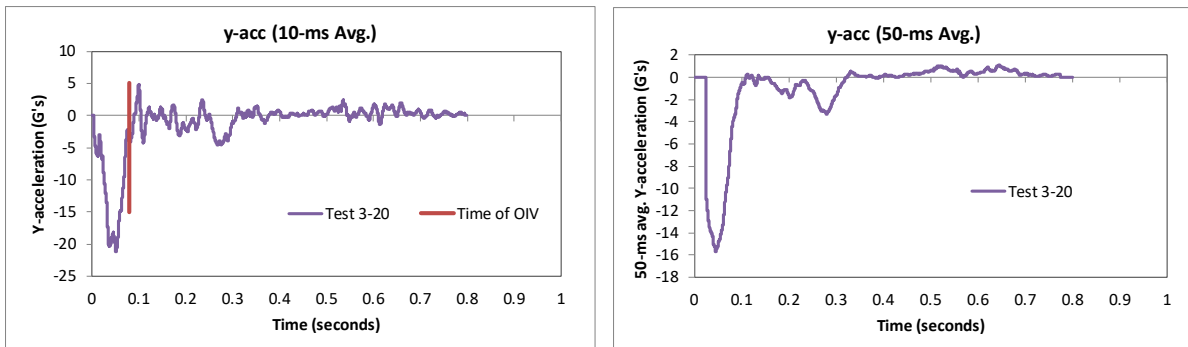


Figure 404. 10- and 50-millisecond average Y-acceleration from FEA of Test 3-20 on the 2-bar transition.

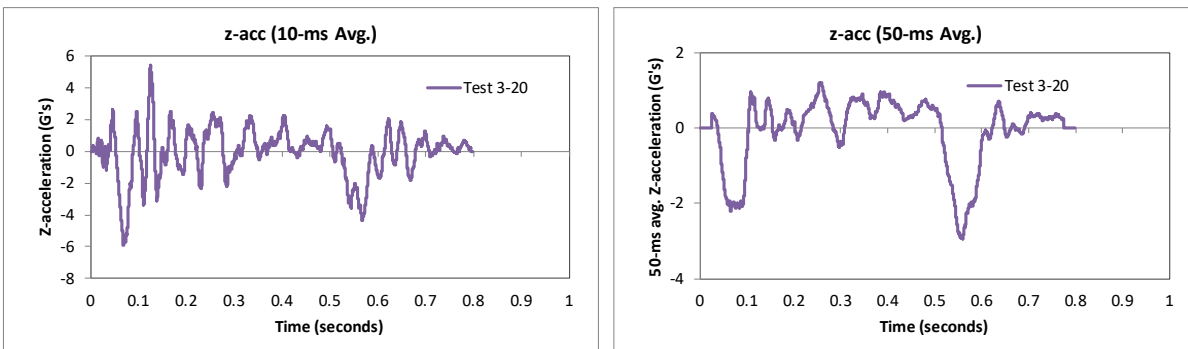


Figure 405. 10- and 50-millisecond average Z-acceleration from FEA of Test 3-20 on the 2-bar transition.

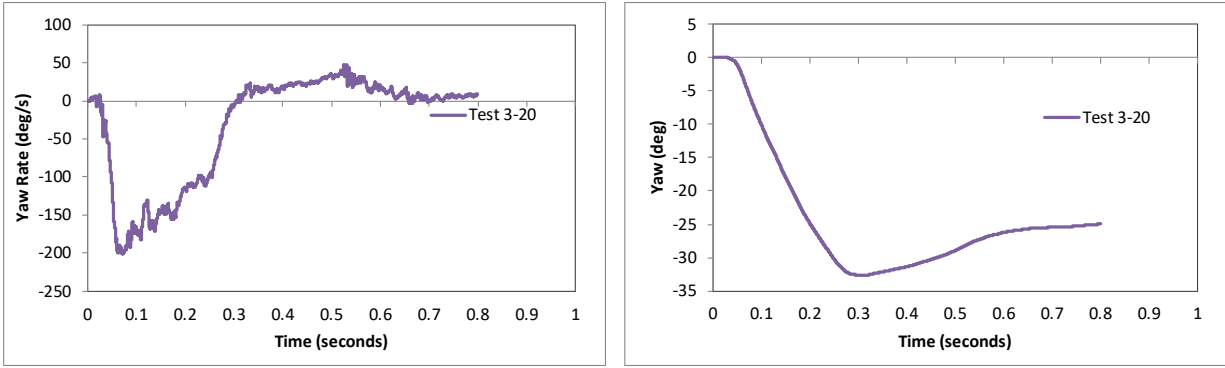


Figure 406. Yaw rate and yaw angle time-history from FEA of Test 3-20 on the 2-bar transition.

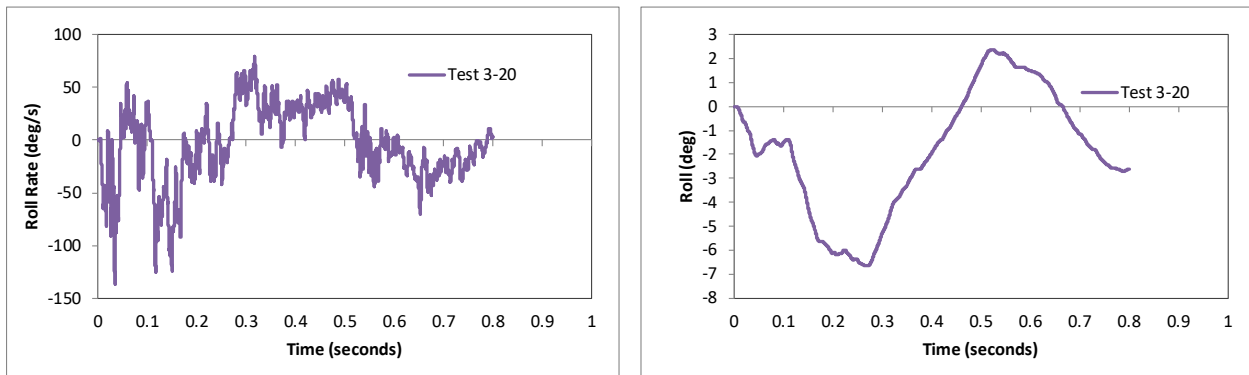


Figure 407. Roll rate and roll angle time-history from FEA of Test 3-20 on the 2-bar transition.

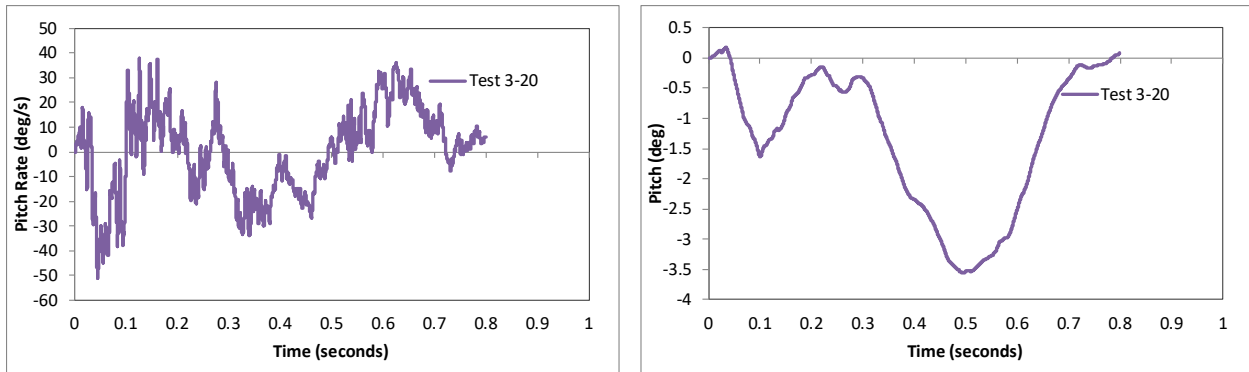


Figure 408. Pitch rate and pitch angle time-history from FEA of Test 3-20 on the 2-bar transition.

14.2.4 Occupant Risk Measures

The acceleration-time histories and angular rate-time histories collected at the center of gravity of the vehicle were used to evaluate occupant risk metrics according to the procedures outlined in *MASH*. Table 100 shows the results for the occupant risk calculations. The results indicate that the occupant risk factors meet safety criteria specified in *MASH*.

The occupant impact velocities in the longitudinal and transverse directions for the transition were 25.3 ft/s and 28.2 ft/s, respectively, which were within the recommended limits

specified in *MASH*. The highest 0.010-second occupant ridedown acceleration in the longitudinal and transverse directions were 7.9 g and 4.8 g, respectively, which were well within preferred limits specified in *MASH*. The maximum 50-ms moving average acceleration values in the longitudinal and transverse directions were 13.6 g and 15.7 g, respectively. The maximum roll and pitch angles of the vehicle were 6.7 degrees and 3.6 degrees, respectively, which were well below critical limits in *MASH*.

Table 100. Summary of *MASH* occupant risk metrics for Test 3-20 on the 2-bar transition.

Occupant Risk Factors		MASH	
		Test 4-20	
Occupant Impact Velocity (ft/s)	x-direction	25.3	
	y-direction	28.2	
	at time	at 0.0765 seconds on right side of interior	
THIV (ft/s)		37.7	
		at 0.0765 seconds on right side of interior	
Ridedown Acceleration (g's)	x-direction	-7.9 (0.0824 - 0.0924 seconds)	
	y-direction	4.8 (0.0946 - 0.1046 seconds)	
PHD (g's)		8.2 (0.0822 - 0.0922 seconds)	
ASI		2.08 (0.0211 - 0.0711 seconds)	
Max 50-ms moving avg. acc. (g's)	x-direction	-13.6 (0.0216 - 0.0716 seconds)	
	y-direction	-15.7 (0.0209 - 0.0709 seconds)	
	z-direction	-2.9 (0.5346 - 0.5846 seconds)	
Maximum Angular Disp. (deg)	Roll	-6.7 (0.2664 seconds)	
	Pitch	-3.6 (0.4934 seconds)	
	Yaw	-32.6 (0.3077 seconds)	

MASH Criteria

< 30 ft/s (preferred) ✓
< 40 ft/s (limit)

< 15 G (preferred) ✓
< 20.49 G (limit)

< 75 deg ✓

14.2.5 Occupant Compartment Intrusion

The maximum deformation of the occupant compartment was approximately 1.4 inches at the lower right-front corner of the toe-pan at the wheel well. Figure 409 shows a view of the vehicle interior after the impact, with several components removed to facilitate viewing. The deformation was less than the critical limit of 9 inches specified in *MASH* for this area of the occupant compartment.

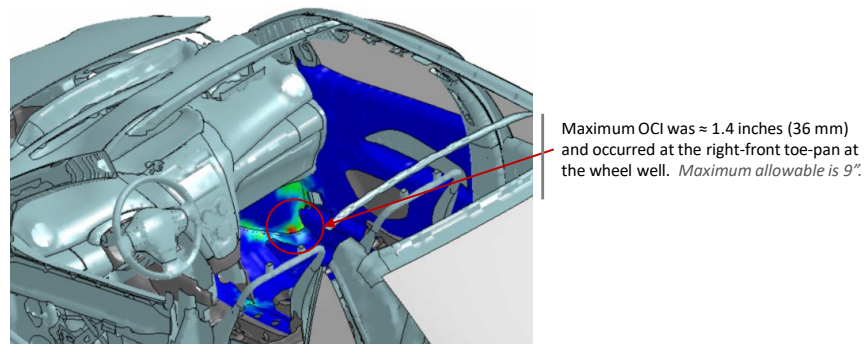


Figure 409. Occupant compartment deformation resulting from Test 3-20 on the 2-bar transition.

Damages to the Barrier System

The damages to the barrier were minimal. Figure 410 shows an overhead view of the post impact deformation of the transition indicating the extent of damage. The barrier was deformed over 20.6 ft of the system with deformation extending from the rail splice at the bridge rail to approximately the midpoint between Post 11 and 12 of the transition. Figure 411 and Figure 412 show images of the maximum dynamic deflection and permanent deflection of the barrier, respectively, with a contour plot of lateral displacement on the rail elements. The maximum dynamic and permanent deflections were 6.3 inches and 5.2 inches, respectively, and occurred at the lower corrugation of the thrie-beam at the point where the nested thrie-beam connects to the thrie-beam end shoe, as illustrated in Figures 411 - 413.

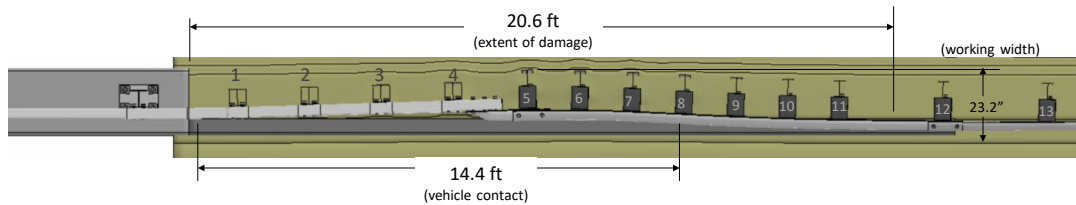


Figure 410. Overhead view of 2-bar transition after Test 3-20 showing extent of damage.

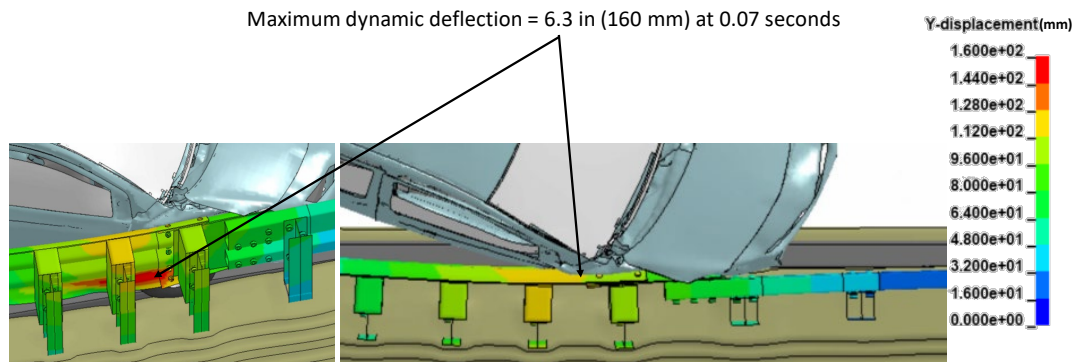


Figure 411. Contour plot of lateral displacement for the transition at the time of maximum dynamic deflection.

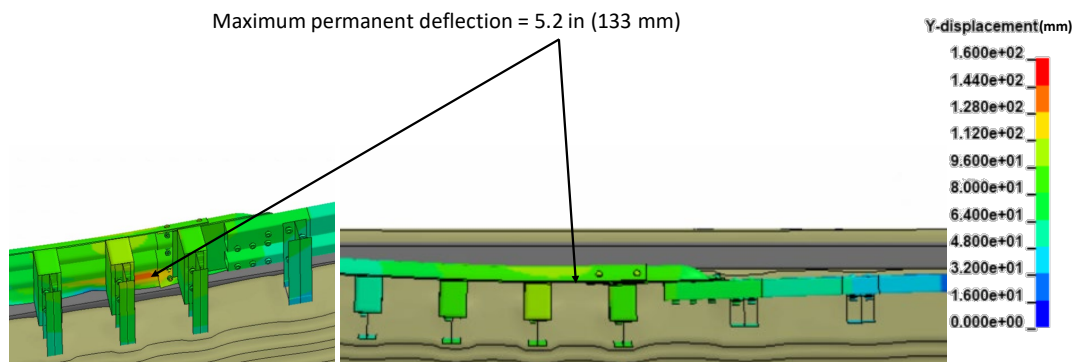


Figure 412. Contour plot of maximum permanent deflection for the transition.

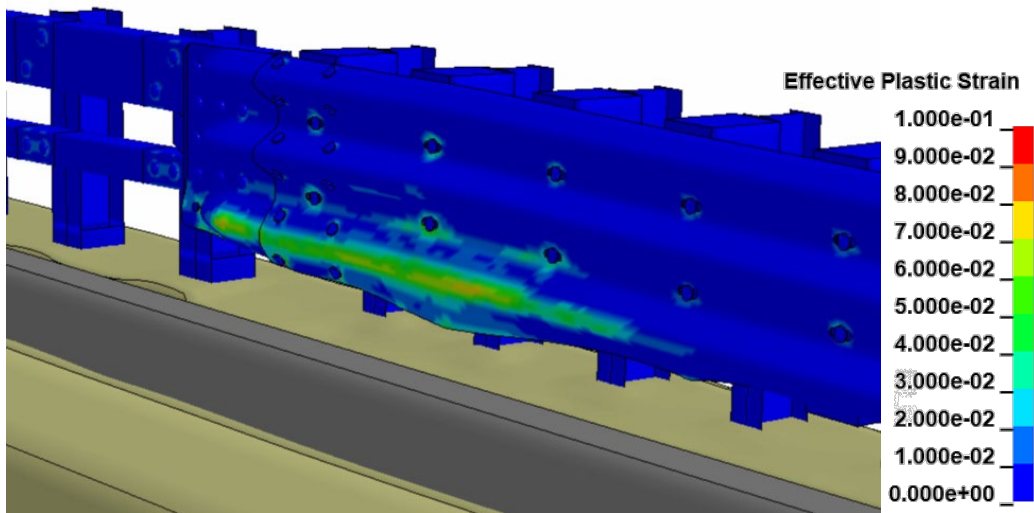


Figure 413. Contours of effective plastic strains on the steel rails and posts for 2-bar transition.

14.2.6 Damages to Vehicle

Figure 414 shows contour plots of effective plastic strain for the vehicle, which were used to identify areas of the vehicle that suffered damage during the simulated impact event. The most severe damages were to the front fender, the upper and lower control arm of front suspension, front wheel, lower- impact-side edge of windshield (cracking), with light damage to the rear wheel of the vehicle.

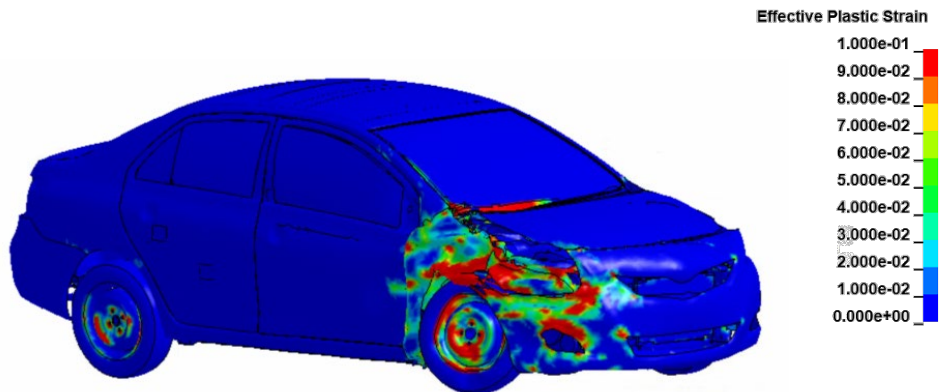


Figure 414. Damages to vehicle in Test 3-20 analysis of the 2-bar transition.

14.2.7 Exit Box

Figure 415 shows the exit box for Test 3-20 on the transition, where the vehicle was smoothly redirected, and its path was well within the exit box criteria of *MASH*.

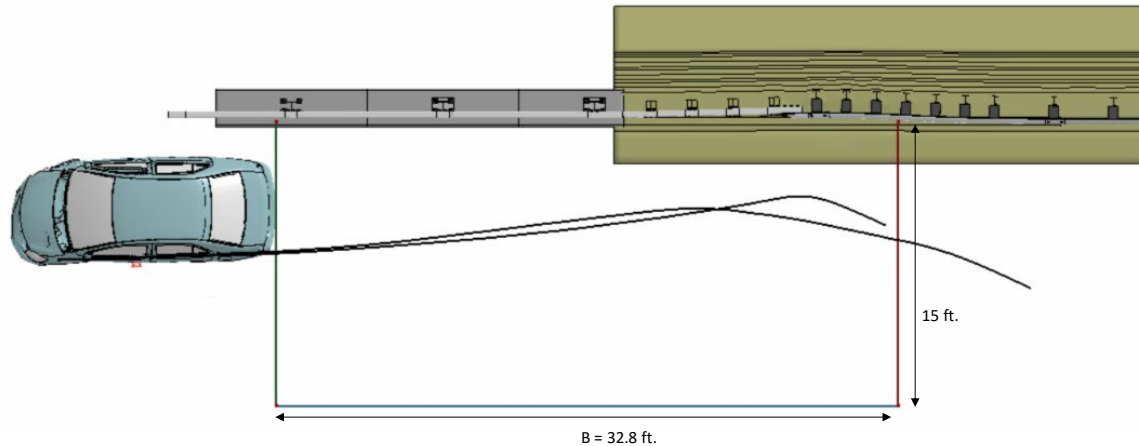


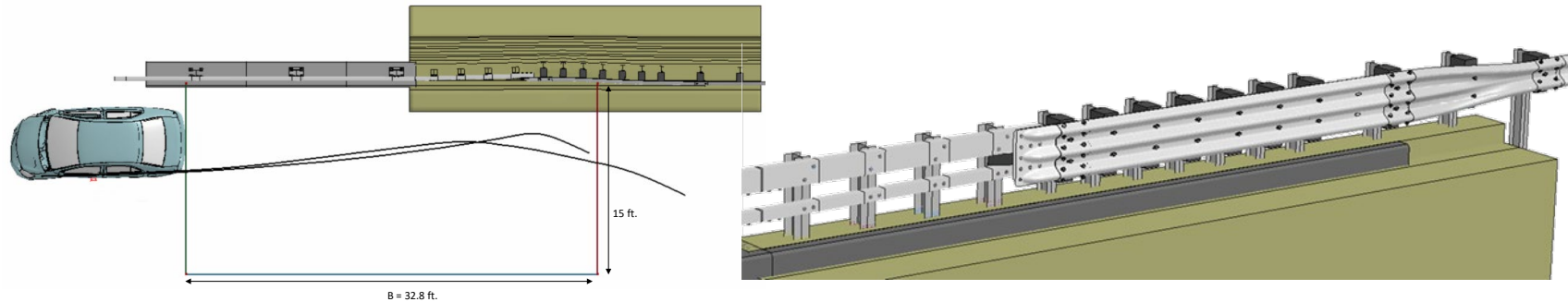
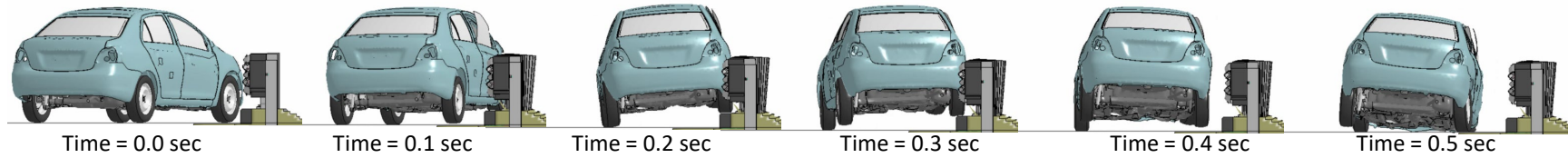
Figure 415. Exit box for Test 3-20 analysis of the 2-bar transition.

14.2.8 Results Summary

A summary of the *MASH* Test 3-20 results on the 2-bar transition is shown in Table 101 and Figure 416. The barrier successfully contained and redirected the small car with minimal damage to the system. There were no detached elements from the barrier that showed potential for penetrating the occupant compartment or presenting undue hazard to other traffic. The vehicle remained upright and very stable throughout impact and redirection. The OIV and maximum ORA values were within recommended limits specified in *MASH*. Based on the results of this analysis, the barrier meets all structural and occupant risk criteria in *MASH* for Test 3-20 impact conditions.

Table 101. Summary of *MASH* Test 3-20 results on the 2-bar transition.

Evaluation Factors	Evaluation Criteria	Results
Structural Adequacy	A Test article should contain and redirect the vehicle or bring the vehicle to a controlled stop; the vehicle should not penetrate, underride, or override the installation although controlled lateral deflection of the test article is acceptable.	Pass
Occupant Risk	D Detached elements, fragments, or other debris from the test article should not penetrate or show potential for penetrating the occupant compartment, or present undue hazard to other traffic, pedestrians, or personnel in a work zone. Deformations of, or intrusions into, to occupant compartment should not exceed limits set forth in Section 5.2.2 and Appendix E.	Pass
	F The vehicle should remain upright during and after collision. The maximum roll and pitch angles are not to exceed 75 degrees.	Pass
	H The longitudinal and lateral occupant impact velocity (OIV) shall not exceed 40 ft/s (12.2 m/s), with a preferred limit of 30 ft/s (9.1 m/s)	Pass
	I The longitudinal and lateral occupant ridedown acceleration (ORA) shall not exceed 20.49 G, with a preferred limit of 15.0 G	Pass



General Information

Analysis Agency Roadsafe LLC
 Test Standard Test No. MASH Test 3-20
 Analysis No. NETC18_2BarTrans_T320
 Analysis Date 7/15/2019

Test Article

Type Bridge Rail Transition
 Name NETC 2-Bar Transition
 Installation Length 65.8 feet
 Material or Key Elements

Soil Type and Condition MASH Strong Soil

Analysis Vehicle

Type / Designation 1100C
 FEA Model name 510_YarisC_V1I_R180228
 Mass 2,595 lb

Impact Conditions

Speed 62 mph
 Angle 25 degrees
 Location 6.5 ft upstream of Post 4

Impact Severity 59.5 kip-ft

Exit Conditions

Speed 41.3 mph
 Angle 7.3 degrees
 Time 0.28 seconds

Occupant Risk Values

Longitudinal OIV 25.3 ft/s
 Lateral OIV 28.2 ft/s
 Longitudinal ORA 7.9 g
 Lateral ORA 4.8 g
 THIV 25.7 ft/s
 PHD 8.2 g
 ASI 2.08

Max50-millisecond Avg. (G)

Longitudinal 13.6 g
 Lateral 15.7 g
 Vertical 2.9 g

Test Article Deflections (in)

Dynamic 6.3 inches
 Permanent 5.2 inches
 Working Width 1.9 ft

Max. OCI ≈ 1.4 inch

Vehicle Stability

Roll -6.7 degrees
 Pitch -3.6 degrees
 Yaw -32.6 degrees

Figure 416. Summary results for MASH Test 3-20 on the 2-bar transition.

14.3 Test 3-21

14.3.1 CIP for Test 3-21

The critical impact point for Test 3-21 was determined using FEA with respect to maximizing the potential for wheel snag on the end of the tube rail section of the transition. Finite element analysis was used to simulate *MASH* Test 3-21 at impact points 6.0 ft, 6.5 ft, 7.0 ft, 7.5 ft, 8.0 ft, 8.5 ft, 9.0 ft and 9.5 ft from the end of the tube rail. These analysis cases were conducted for 0.25 seconds of impact for the purpose of determining the critical impact point for maximizing vehicle accelerations and maximizing forces on the barrier at the junction point of the thrie-beam and the tubular rail section. The 0.25 seconds was sufficient time for determining both maximum OIV and ORA for the impact event. The assessment was based on four key factors; 1) pocketing, 2) peak accelerations relative to critical snag point, 3) OIV and ORA values and 4) impact severity and kinetic energy at the time when the vehicle approached the connection point. Vehicle stability was not assessed in these analyses due to the short time duration of the impact (i.e., 0.25 seconds); however, the roll and pitch angles were relatively low for all cases.

The potential for pocketing was evaluated by measuring the lateral displacement at four points on the thrie-beam near the connection point and comparing to the lateral deflection of the rail at the connection point, as illustrated in Figure 417. The results of the evaluations are shown in Figures 418 and 419. Based on these results, impact at 9.0 ft and 9.5 ft upstream of the critical snag point were the same and resulted in the highest relative deflection at Points 1 and 2 on the thrie-beam (i.e., pocketing nearest to the snag point), while the relative deflection at 9.5 ft was slightly higher at Points 3 and 4 and was therefore considered the highest potential for snagging on the ends of the tubular rails related to pocketing. Figure 418 shows a plot of the total deflection of the transition at the critical snag point for each of the analysis cases. The maximum deflection was similar for impacts at 6.0 ft – 8.0 ft; while deflection values began to decrease as the impact point moved farther away from the critical snag point.

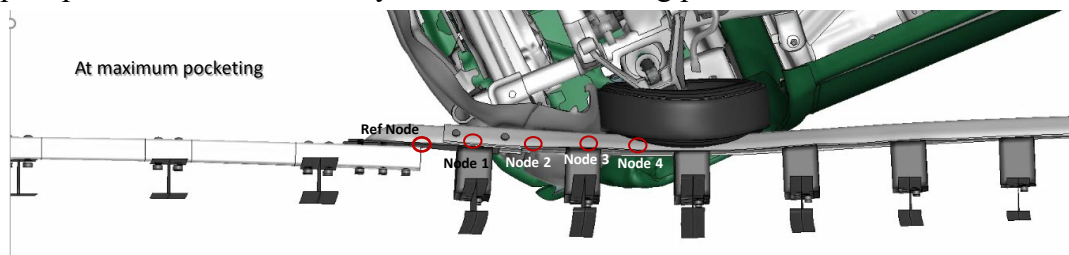


Figure 417. Measurement points for determining CIP for pocketing for Test 3-21.

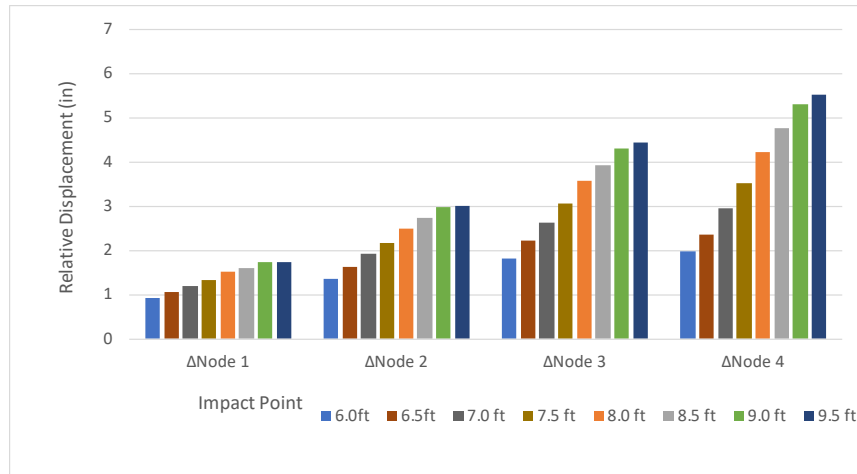


Figure 418. Relative displacements of rail for Test 3-21 simulations in CIP evaluations.

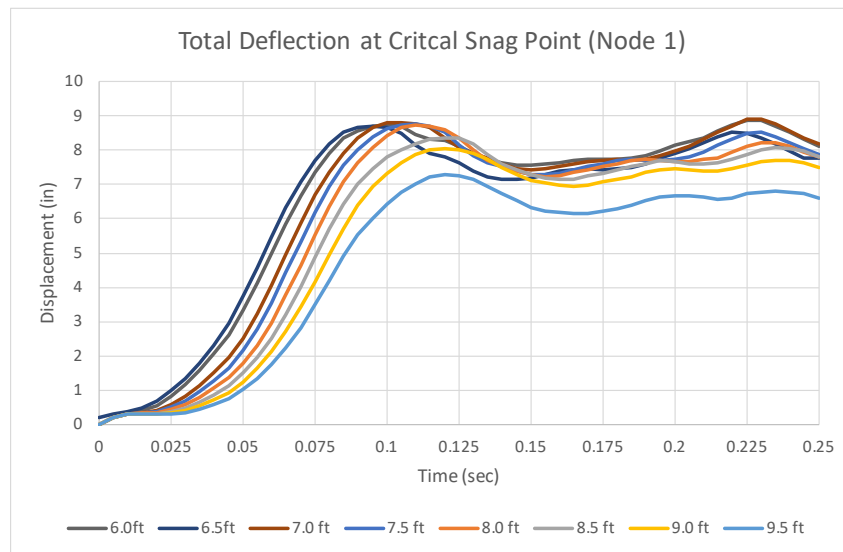


Figure 419. Total deflection of the rail at the critical snag point on the transition for Test 3-21.

Figure 420 shows plots of vehicle longitudinal and lateral accelerations, and Figure 421 shows a plot of impact severity and kinetic energy of the vehicle at the time when the vehicle bumper is at the critical snag point. The peak accelerations are of similar magnitude and occur at approximately the same time for all cases; the results are also consistent with typical Test 3-11 or 3-21 results on rigid barriers. Figure 422 shows the maximum OIV and ORA for each of the analysis cases.

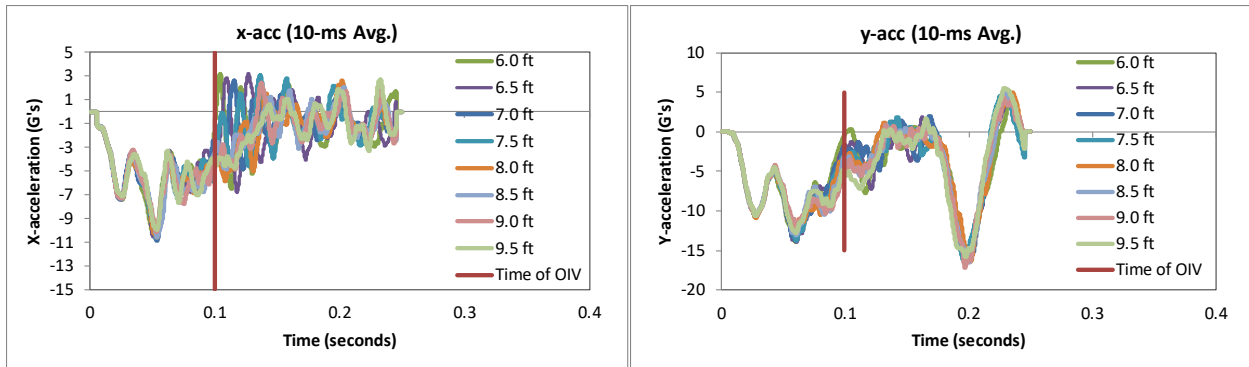


Figure 420. Plots of vehicle longitudinal and lateral accelerations measured at the c.g. of the vehicle.

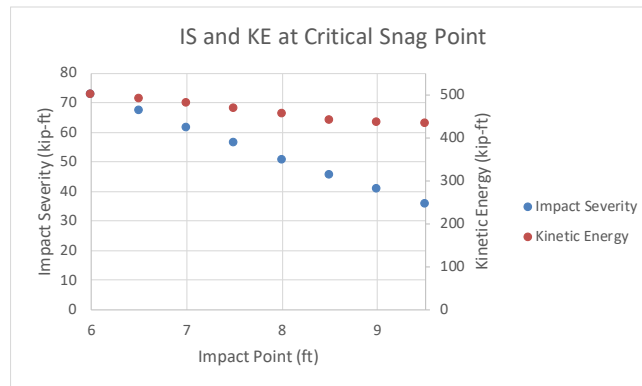


Figure 421. Impact severity and kinetic energy of the vehicle at the time when the vehicle is positioned at the critical snag point.

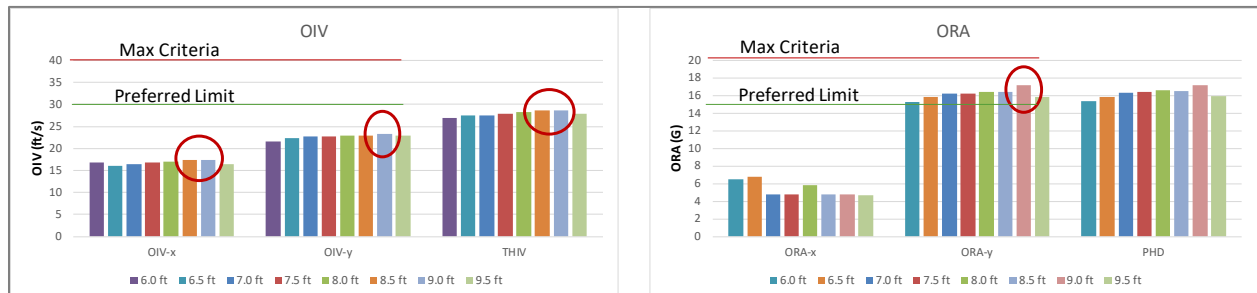


Figure 422. maximum OIV and ORA values for the Test 4-21 cases.

Based on the analysis results it was determined that there was very low potential for snags on the end of the transition tube rails, and that the curb sufficiently shields the posts from contact/snag with vehicle tires. In general, the results showed that:

- Considering pocketing, Impact at 9.0 ft and 9.5 ft resulted in the greatest relative deflection of the rail at the snag point.
- Considering OIV, all cases were essentially the same; however, the highest lateral acceleration occurred at impact cases 8.5 ft and 9 ft.
- Considering ORA, the highest longitudinal ORA occurred for impact at 6.5 ft and the highest lateral ORA occurred for impact at 9.0 ft.

- Additional comparisons were made for the 3-bar transition case (see Section 10.3.1), which are not repeated here but are considered relevant to the 2-bar system.

Given that this system is very similar to the 3-bar transition evaluated in Task 4, the results are essentially identical to that system. Any differences correspond to the fact that the CIP for the 3-bar was based on results up to 0.15 seconds of the impact; whereas, for the 2-bar system the analysis was extended to 0.25 seconds to include the backslap of the pickup into the barrier.

Based on these data, the critical impact point was selected as 9.0 ft upstream of the end of the tube rails in the transition section. This was also considered as a secondary CIP for the 3-bar system, but that analysis case was not performed for the full impact event (e.g., 1.0 second). It is further assumed that the results for the 2-bar at impact point 9.0 ft would also pertain to the 3-bar system. The final analysis was performed for 1.0 seconds of the impact event. The following sections provide a summary of the results and include a commentary describing the timing and occurrence of various events during the simulated impact, time-history data evaluation, occupant risk assessments, and damages sustained by both the barrier and vehicle.

14.3.2 Summary of Key Phenomenological Events

The 5,001-lb pickup struck the barrier at 9.0 feet upstream of the critical snag point at the end of the tubular rails at a speed of 62 mph and at an angle of 25 degrees, as illustrated in Figure 423. The sequential views of the impact event are shown in Appendix Z in Figures Z-1 through Z-3 from an overhead viewpoint, downstream and upstream viewpoint, and isometric viewpoint, respectively.

At time equal zero seconds the front bumper of the pickup contacted the lower and middle corrugation of the thrie-beam, while the front-right fender contacted the upper corrugation. At 0.01 seconds the front-right tire contacted the curb and the barrier started to deflect. At 0.02 seconds the front-right tire was compressed to the rim at two points and would likely have deflated; however, tire deflation was not included in the model. At 0.04 seconds the front-right tire was fully mounted onto the curb and was steered parallel to the barrier. At 0.065 seconds the front-left tire lifted off the ground as the vehicle started to roll toward the barrier. At 0.085 seconds the front bumper was aligned with Post 5. At 0.95 seconds the front bumper was aligned with the end of the transition tube rails. At 0.105 seconds the front-right fender slightly snagged on the top of the blockout at Post 5. At 0.11 seconds the front bumper was aligned with Post 4. At 0.1 seconds the rear-left tire lifted off the ground as the vehicle continued to roll toward the barrier. The roll angle of the pickup at this time was 4.0 degrees. At 0.0973 seconds the occupant struck the right side of the interior at 17.4 ft/s in the forward direction and 23.3 ft/s in the lateral direction. At 0.116 seconds the peak occupant ridedown acceleration in the longitudinal direction occurred with magnitude 4.8 G. At 0.145 seconds the hub of the front-right tire was aligned with Post 4, but the tire did not contact the post. At 0.165 seconds the rear-right tire contacted the curb and the pickup bed contacted the middle and lower corrugations of the thrie-beam. At 0.175 seconds the rear bumper contacted the middle corrugation of the thrie-beam at approximately 11.1 feet upstream from the end of the transition tube rails. At 0.176 seconds the vehicle was parallel to the barrier. At 0.185 seconds the rear-left tire was compressed laterally to the point the tire debanding would be likely. At 0.197 the maximum occupant ridedown acceleration in the lateral direction occurred with magnitude 17.2 G. At

0.205 seconds the rear-left tire was fully mounted onto the curb. At 0.21 seconds the front bumper was aligned with the splice connection at the bridge rail, and the front of the vehicle began to exit the system. At 0.31 seconds the vehicle separated from the barrier traveling at 46.9 mph at an exit angle of 7.45 degrees. At 0.41 seconds the vehicle reached peak roll angle of 9.3 degrees toward the barrier. At 0.5 seconds the vehicle reached maximum pitch angle of -5.5 degrees rear pitching up). The vehicle remained stable throughout post-impact trajectory. The analysis ended at 1.0 seconds, at which time:

- The roll, pitch, and yaw of the vehicle were, respectively, 1.28 degrees (toward barrier), -1.4 degrees (rear pitching up), and -31.3 degrees (6.3 degrees relative to and away from the barrier).
- The forward velocity of the vehicle was 45.4 mph (73 km/h).

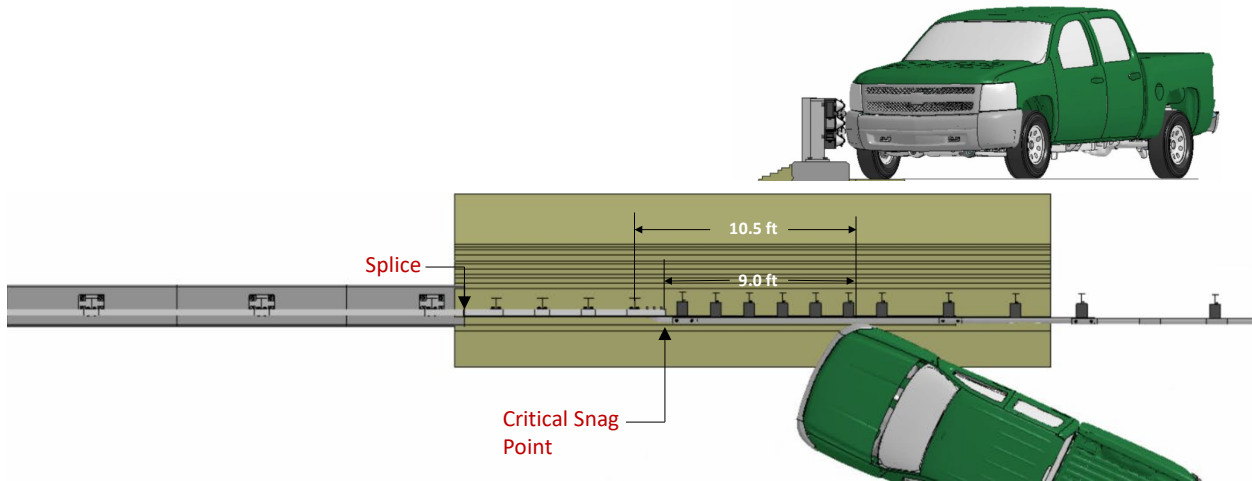


Figure 423. Impact point for Test 3-21 on the 2-bar transition.

14.3.3 Time History Data Evaluation

Figures 424 through 426 show the longitudinal, transverse, and vertical acceleration-time histories, respectively, computed from the center of gravity of the vehicle; Figures 427 through 429 show the angular rates and angular displacement about the x-, y-, and z-axis at the center of gravity of the vehicle.

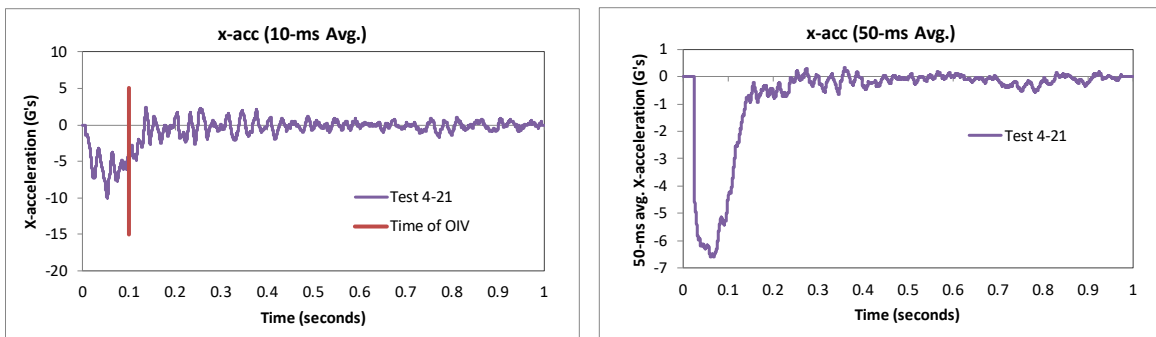


Figure 424. 10- and 50-millisecond average X-acceleration from FEA of Test 3-21 on the 3-bar transition.

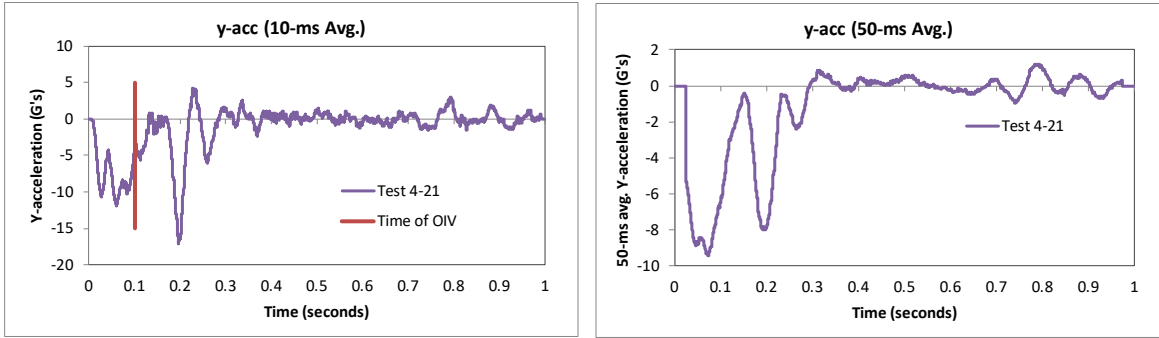


Figure 425. 10- and 50-millisecond average Y-acceleration from FEA of Test 3-21 on the 2-bar transition.

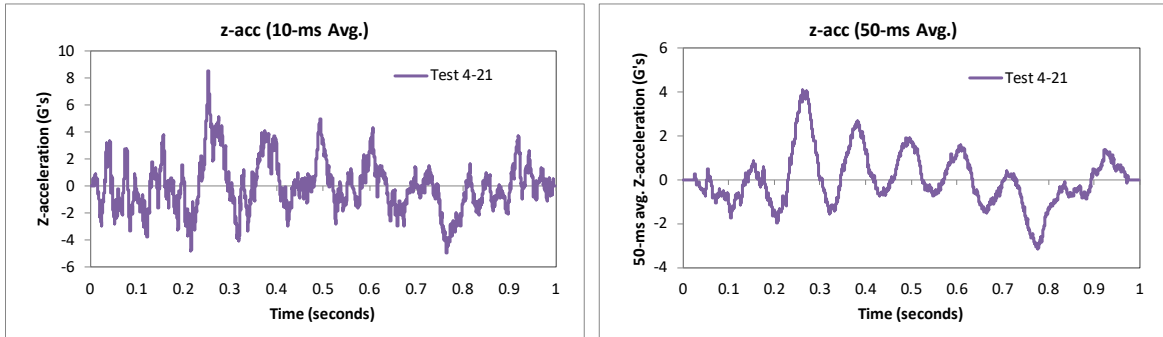


Figure 426. 10- and 50-millisecond average Z-acceleration from FEA of Test 3-21 on the 2-bar transition.

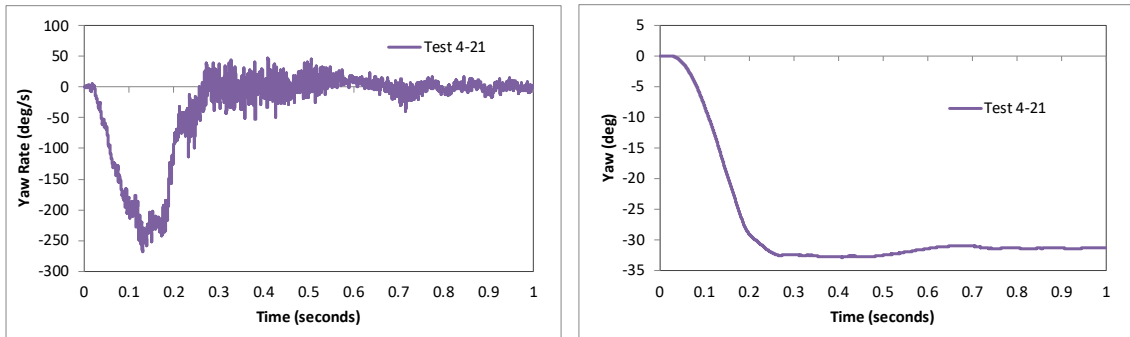


Figure 427. Yaw rate and yaw angle time-history from FEA of Test 3-21 on the 2-bar transition.

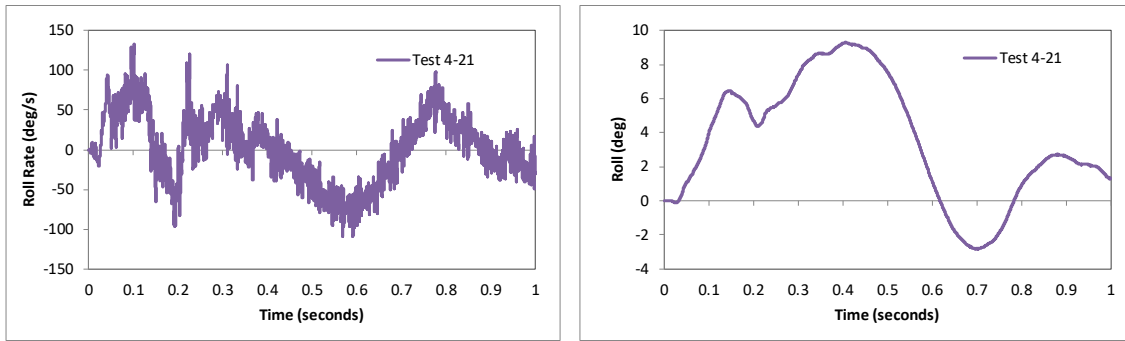


Figure 428. Roll rate and pitch angle time-history from FEA of Test 3-21 on the 2-bar transition.

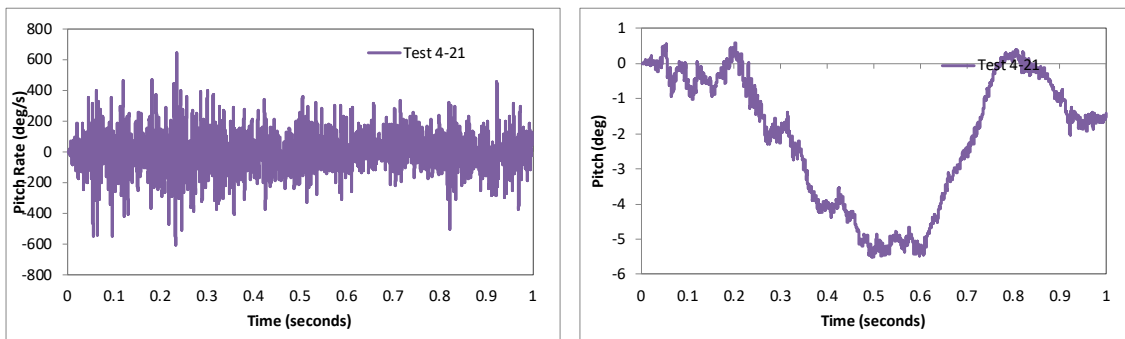


Figure 429. Pitch rate and pitch angle time-history from FEA of Test 3-21 on the 2-bar transition.

14.3.4 Occupant Risk Measures

The acceleration-time histories and angular rate-time histories collected at the center of gravity of the vehicle were used to evaluate occupant risk metrics according to the procedures outlined in *MASH*. Table 102 shows the results for the occupant risk calculations. The results indicate that the occupant risk factors met safety criteria specified in *MASH*.

The occupant impact velocities in the longitudinal and transverse directions for the curb-mounted system were 17.4 ft/s and 23.3 ft/s, respectively, which were within the recommended limits specified in *MASH*. The highest 0.010-second occupant ridedown acceleration in the longitudinal and transverse directions were 4.8 g and 17.2 g, respectively, which were just over the recommended limit within but with critical limits specified in *MASH*. The maximum 50-ms moving average acceleration values in the longitudinal and transverse directions were 6.6 g and 9.4 g, respectively. The maximum roll and pitch angles of the vehicle were 9.3 degrees and 5.5 degrees, respectively, which were well below critical limits in *MASH*. As mentioned previously in Section 5, the 2270P vehicle model often over-estimates the lateral ridedown acceleration for rigid barrier impacts [see Appendix E].

Table 102. Summary of occupant risk metrics for Test 3-21 on the 2-bar transition.

Occupant Risk Factors		MASH	
		Test 4-21	
Occupant Impact Velocity (ft/s)	x-direction	17.4	
	y-direction	23.3	
	at time	at 0.0973 seconds on right side of interior	
THIV (ft/s)		28.5 at 0.0973 seconds on right side of interior	
Ridedown Acceleration (g's)	x-direction	-4.8 (0.1112 - 0.1212 seconds)	
	y-direction	-17.2 (0.1919 - 0.2019 seconds)	
PHD (g's)		17.2 (0.1919 - 0.2019 seconds)	
ASI		1.18 (0.0484 - 0.0984 seconds)	
Max 50-ms moving avg. acc. (g's)	x-direction	-6.6 (0.0377 - 0.0877 seconds)	
	y-direction	-9.4 (0.0485 - 0.0985 seconds)	
	z-direction	4.1 (0.2373 - 0.2873 seconds)	
Maximum Angular Disp. (deg)	Roll	9.3 (0.4070 seconds)	
	Pitch	-5.5 (0.4992 seconds)	
	Yaw	-32.8 (0.4083 seconds)	

MASH Criteria

- < 30 ft/s (preferred) ✓
- < 40 ft/s (limit)
- > 15 G (preferred)
- < 20.49 G (limit) ✓
- < 75 deg ✓

14.3.5 Occupant Compartment Intrusion

The maximum deformation of the occupant compartment was negligible for this analysis case. Figure 430 shows a view of the vehicle interior after the impact, with several components removed to facilitate viewing.

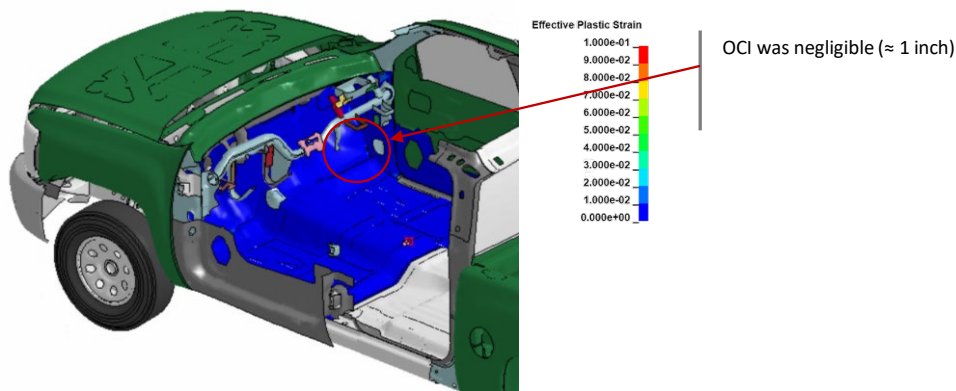


Figure 430. Occupant compartment deformation resulting from Test 3-21 on the 2-bar transition.

14.3.6 Damages to the Barrier System

The damages to the barrier were moderate. Figure 431 shows an overhead view of the post impact deformation of the transition indicating the extent of damage. The barrier was deformed over 25.6 feet of the system with deformation extending from the rail splice at the bridge rail to Post 13 of the transition. The vehicle was in contact with the barrier for approximately 15.9 ft. Figure 432 shows images of the maximum dynamic deflection and

permanent deflection of the barrier with a contour plot of lateral displacement on the rail elements. The maximum dynamic and permanent deflections were 11.8 inches and 10.4 inches, respectively, and occurred at the lower corrugation of the thrie-beam at the point where the nested thrie-beam connects to the thrie-beam end shoe, as illustrated in Figure 433.

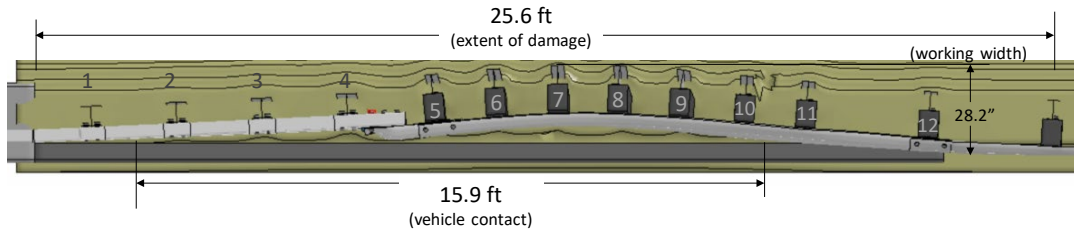


Figure 431. Overhead view of 2-bar transition after Test 3-21 showing extent of damage.

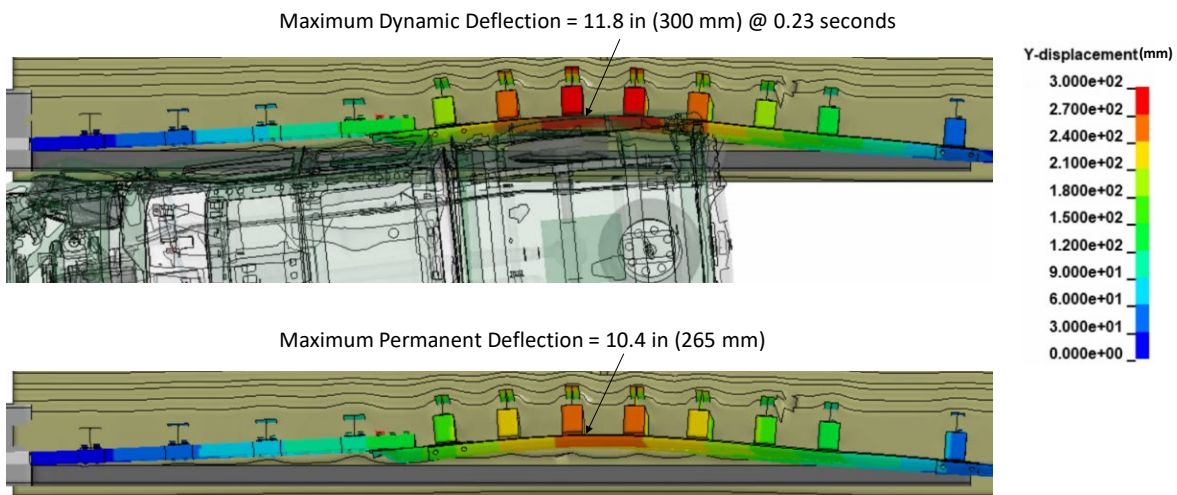


Figure 432. Contour plot of lateral displacement for Test 3-21 on the 3-bar transition at the time of maximum dynamic deflection and maximum permanent deflection.

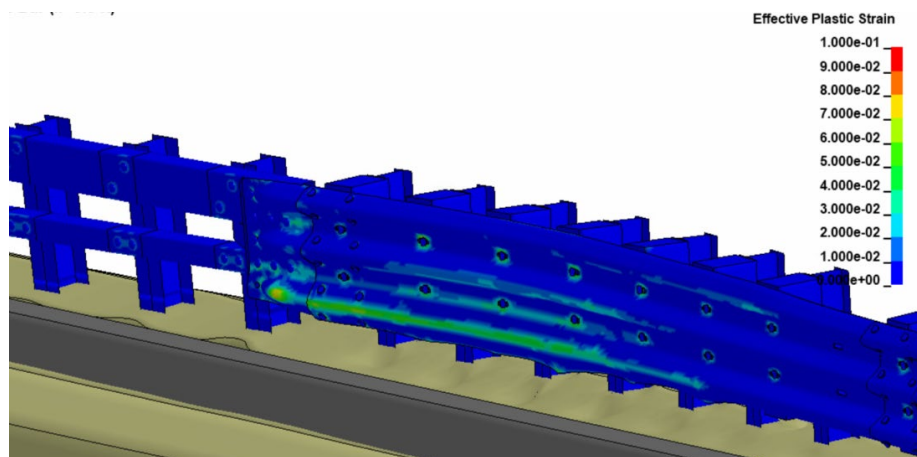


Figure 433. Contours of effective plastic strains on the steel rails and posts for Test 3-21 on 2-bar transition.

14.3.7 Damages to Vehicle

Figure 434 shows contour plots of effective plastic strain for the vehicle, which were used to identify areas of the vehicle that suffered damage during the simulated impact event. The most severe damages were to the front bumper, the front fender, the upper control arm of front suspension, front and rear wheels, rear edge of rear door, front edge of truck bed, rear quarter panel of truck bed and rear bumper.

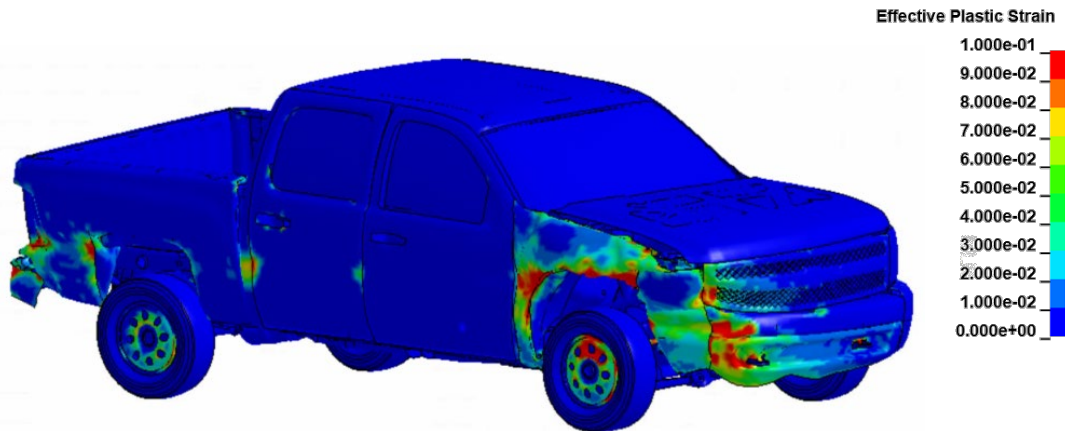


Figure 434. Damages to vehicle in Test 3-21 analysis of the 2-bar transition.

14.3.8 Exit Box

Figure 435 shows the exit box for Test 3-21 on the 2-bar transition system. The vehicle was smoothly redirected, and its path was well within the exit box criteria of *MASH*.

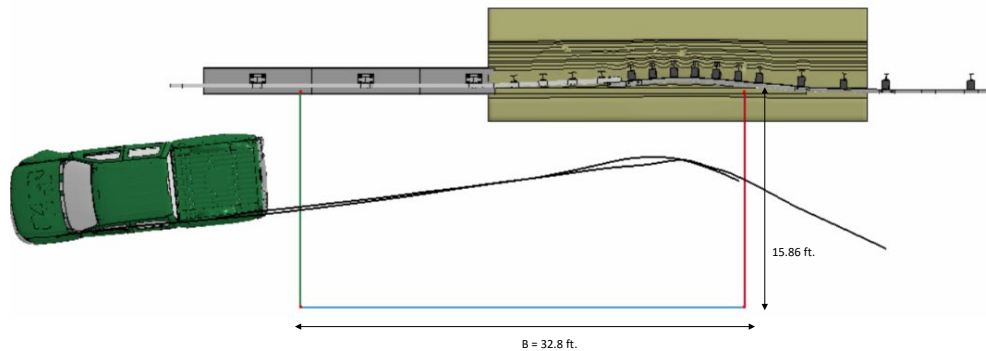


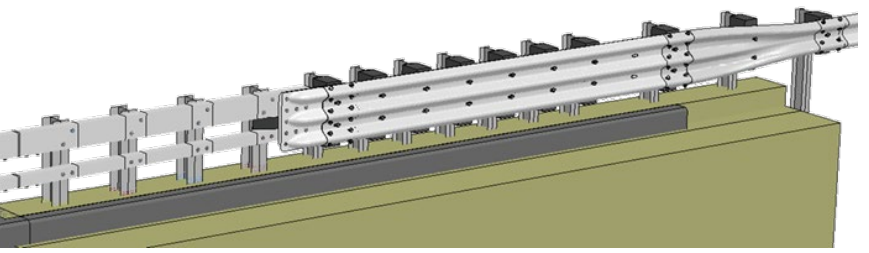
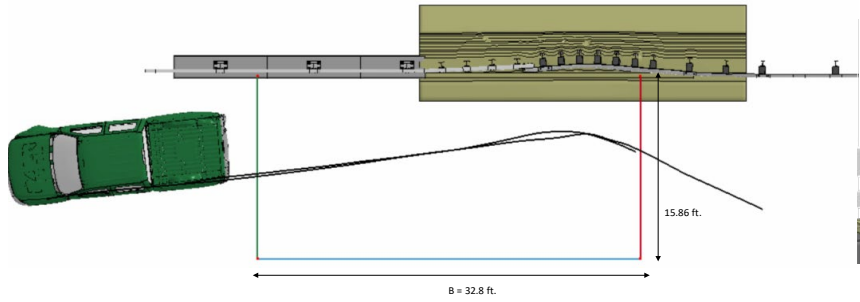
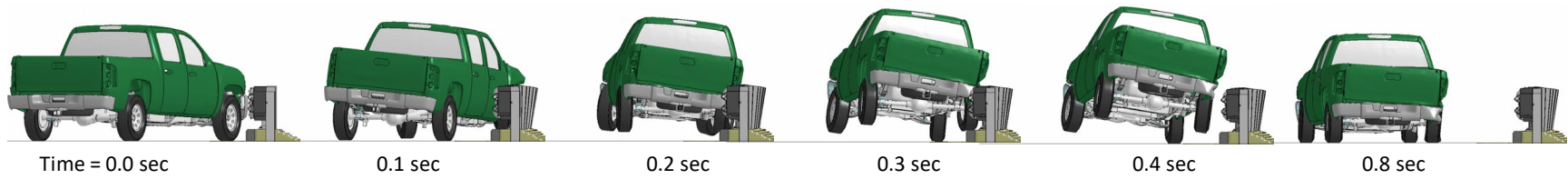
Figure 435. Exit box for Test 3-21 analysis of the 2-bar transition.

14.3.9 Results Summary

A summary of the *MASH* Test 3-21 results on the NETC 2-bar transition is shown in Table 103 and Figure 436. The barrier successfully contained and redirected the 2270P vehicle (pickup) with moderate damage to the transition. There were no detached elements from the barrier that showed potential for penetrating the occupant compartment or presenting undue hazard to other traffic. The vehicle remained upright and did not experience excessive roll or pitch angle displacements. The maximum OIV values were within recommended limits and the maximum ORA values were within critical limits specified in *MASH*. Based on the results of this analysis, the barrier meets all structural and occupant risk criteria in *MASH* for Test 3-21 impact conditions.

Table 103. Summary of MASH Test 3-21 results on the NETC 2-bar transition.

Evaluation Factors	Evaluation Criteria	Results
Structural Adequacy	A Test article should contain and redirect the vehicle or bring the vehicle to a controlled stop; the vehicle should not penetrate, underride, or override the installation although controlled lateral deflection of the test article is acceptable.	Pass
Occupant Risk	D Detached elements, fragments, or other debris from the test article should not penetrate or show potential for penetrating the occupant compartment, or present undue hazard to other traffic, pedestrians, or personnel in a work zone. Deformations of, or intrusions into, to occupant compartment should not exceed limits set forth in Section 5.2.2 and Appendix E.	Pass
	F The vehicle should remain upright during and after collision. The maximum roll and pitch angles are not to exceed 75 degrees.	Pass
	H The longitudinal and lateral occupant impact velocity (OIV) shall not exceed 40 ft/s (12.2 m/s), with a preferred limit of 30 ft/s (9.1 m/s)	Pass
	I The longitudinal and lateral occupant ridedown acceleration (ORA) shall not exceed 20.49 G, with a preferred limit of 15.0 G	Pass



General Information		Impact Conditions		Max50-millisecond Avg. (G)	
Analysis Agency	Roadsafe LLC	Speed	62 mph	Longitudinal	6.6 g
Test Standard Test No.	MASH Test 3-21	Angle	25 degrees	Lateral	9.4 g
Analysis No.	NETC18_2BarTrans_T321	Location	9.0 ft upstream of end of transition tube rail	Vertical	4.1 g
Analysis Date	7/4/2019				
Test Article		Impact Severity		Test Article Deflections (in)	
Type	Bridge Rail Transition		114.7 kip-ft	Dynamic	11.8 inches
Name	NETC 2-Bar Transition	Exit Conditions		Permanent	10.4 inches
Installation Length	65.8 feet	Speed	46.9 mph	Working Width	2.35 ft
Material or Key Elements		Angle	7.45 degrees		
		Time	0.31 seconds		
Soil Type and Condition		Occupant Risk Values		Max. OCI	
	MASH Strong Soil			< 1 inch	
Analysis Vehicle		Longitudinal OIV	17.4 ft/s	Vehicle Stability	
Type / Designation	2270P	Lateral OIV	23.3 ft/s	Roll	9.3 degees
FEA Model name	SilveradoC_V3a_V180201_TireRS_35psi	Longitudinal ORA	4.8 g	Pitch	5.5 degrees
Mass	5,001 lb	Lateral ORA	17.2 g	Yaw	32.8 degrees
		THIV	28.5 ft/s		
		PHD	17.2 g		
		ASI	1.18		

Figure 436. Summary results for MASH Test 3-21 on the 2-bar transition system

14.4 Conclusions for *MASH* TL3 Evaluation of the 2-Bar Transition

Based on the results of this analysis, the 2-bar transition is expected to meet all structural and occupant risk criteria for *MASH* Test Level 3.

14.4.1 Structural Adequacy: (*PASS*)

- The barrier successfully contained and redirected the vehicle in all test cases.
- There was low-to-moderate damage to the transition in all cases.

14.4.2 Occupant Risk (*PASS*)

- Occupant compartment intrusion was well below allowable limits for all cases
- OIV and ORA
 - Small Car: OIV and ORA were within preferred limits
 - Pickup: OIV was within preferred limits; ORA was within critical limits

14.4.3 Vehicle Trajectory (*PASS*)

- Vehicle remained upright through impact and redirection.
- Roll and Pitch for Tests 3-20 (small car) and 3-21 (pickup) were relatively low.

15 MODIFIED DESIGNS AND EVALUATIONS

Based on the results of this study, the project panel and the NETC advisory board identified three additional issues to be resolved, which included:

- 1) Would increasing the strength of the lower railing mitigate pocketing for the small car test and thereby reduce longitudinal OIV and ORA values?
- 2) What are the implications of exceeding the specified maximum allowable post spacing of 3-feet between the last bridge rail post and the first transition post for the 3-bar system?
- 3) Would increasing strength of the bridge rail posts improve crash performance for the 4-bar bridge rail?

15.1 Modified NETC 3-Bar Bridge Rail with Stiffer Lower Rail

The evaluation of the 3-bar bridge rail was presented in Section 9. FEA simulations showed that the mid-span deflections for the rails for the 2-bar and 3-bar systems lead to pocketing, particularly for Test 4-10 in which the forces from the small car were largely concentrated on the lower HSS 4 x 4 x ¼" rail. The maximum dynamic deflection of the lower rail for that case was 3.35 inches, as shown in Figure 123, and resulted in peak longitudinal and lateral accelerations of 26 G and 30 G, respectively. The NETC 3-bar bridge rail model was modified to include a larger HSS section for the lower rail to: (1) increase stiffness and lower deflection and (2) increase rail dimension in vertical direction to provide additional contact width at the lower portion of the bridge railing to reduce potential for wheel-sag on the posts.

The bar size options that were considered for the lower rail are shown in Table 104. For the modified design, the standoff distance between the post and rail face was to remain at 4 inches so that the face of the barrier remains flush. Three vertical height dimensions were considered for the low rail, including 5, 6, and 7 inches, as well as two thickness options of 1/4-inch and 5/16-inch.

Table 104. Bar size options for the lower rail of the Modified NETC 3-bar bridge rail.

	Bar Size	Area		Z _y		Ratio
		(in ²)	ΔA	(in ³)	ΔZ _y	ΔA/ ΔZ _y
Original	HSS 4 x 4 x 1/4	3.59	-	4.97	-	-
	HSS 5 x 4 x 1/4	4.09	14%	5.9	19%	1.36
*	HSS 5 x 4 x 5/16	4.98	39%	7.05	42%	1.08
	HSS 6 x 4 x 1/4	4.59	28%	6.84	38%	1.36
*	HSS 6 x 4 x 5/16	5.61	56%	8.21	65%	1.16
*	HSS 7 x 4 x 1/4	5.09	42%	7.78	57%	1.36
	HSS 7 x 4 x 5/16	3.23	74%	9.36	88%	1.19

* Selected for evaluation



15.1.1 Analysis Cases

Of the potential options listed in Table 104, three were selected for further evaluation using FEA, including:

- Case 1: HSS 5 x 4 x 5/16
- Case 2: HSS 6 x 4 x 5/16
- Case 3: HSS 7 x 4 x 1/4 (all units are inches).

Figure 437 shows a cross-section view of these three design options compared with the baseline design. The splice design was fundamentally unchanged for these analysis cases. The splice consisted of a 20-inch long HSS splice bar which was inserted into the ends of the two connecting rails and fastened with four 5/8-inch diameter A307 cap screws and washers (refer to Figures 53 and 54 and Appendix B). The splice tubes for the lower rail were 5/16 inches thick in all cases and included HSS 4 x 3 x 5/16, HSS 5 x 3 x 5/16 and HSS 6 x 3 x 5/16 for Cases 1, 2, and 3, respectively. Figure 438 shows a cross-section view of the splice connection for each case and identifies tube sizes and internal gap size for the splice.

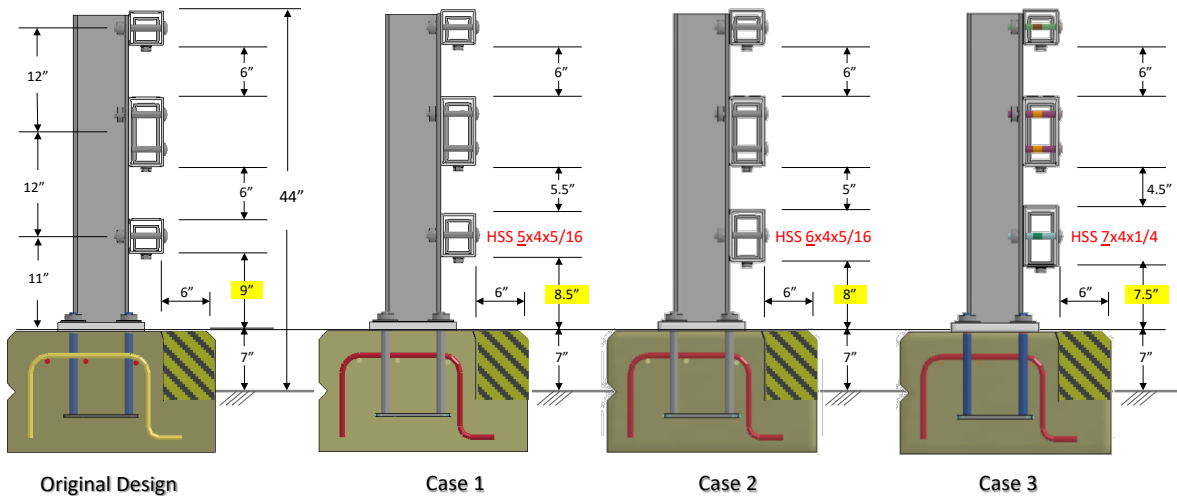


Figure 437. Analysis cases evaluated for the Modified NETC 3-bar with stiffer lower rail.

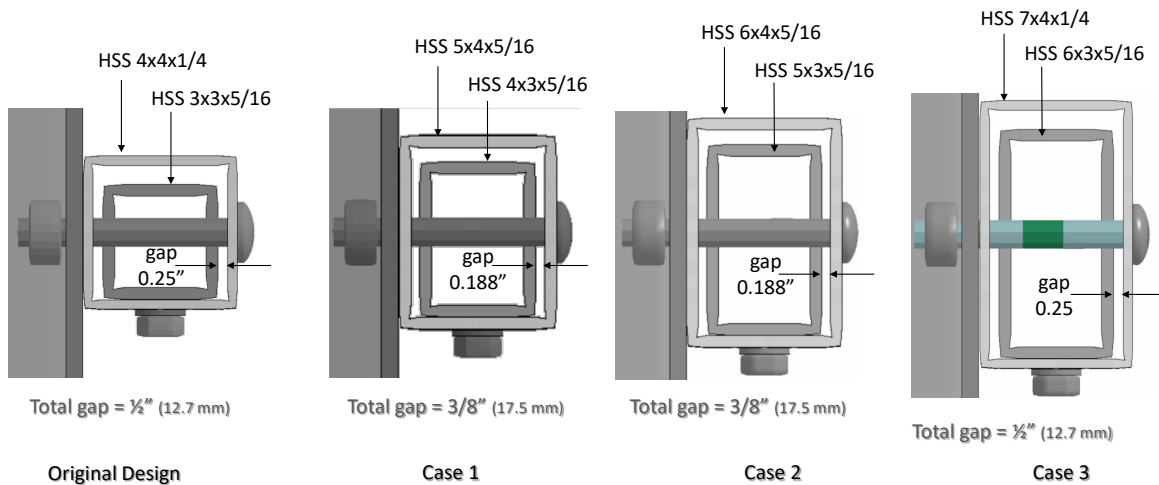


Figure 438. Cross-section view of splice for each case identifying tube size and internal gap size.

The HSS 5 x 4 x 5/16 bar provided the overall lowest cost solution and was assumed adequate to reduce pocketing; however, it also resulted in the lowest stiffness per added cost (i.e., 39/42). Both the HSS 5 x 4 x 5/16 and the HSS 6 x 4 x 5/16 reduced the internal gap between the splice bar and the main railing from 1/2 inch to 3/8 inch (neglecting galvanizing). The HSS 6 x 4 x 5/16 was also the highest cost option among the three selected but provided good stiffness-to-cost ratio. The HSS 7 x 4 x 1/4 bar provided the highest increase in stiffness per added cost (i.e., 57/42) and the largest contact area; but, the internal gap between the splice tube and rail remained at 1/2 inch.

15.1.2 Test 4-10

FEA was used to evaluate the crash performance of the Modified NETC 3-bar bridge rail using criteria specified in *MASH* for Test 4-10. The impact conditions included the 1100C Yaris model ballasted to 2,595 lb (1177 kg) impacting the barrier at 62.2 mph and 25 degrees, as illustrated in Figure 439. The critical impact point was selected as 3.6 feet (1.1 m) upstream of a bridge rail post and 2.1 feet (0.64 m) upstream of the splice. These impact conditions were

consistent with the those used in the baseline evaluation of the NETC 3-bar bridge rail in Section 9.

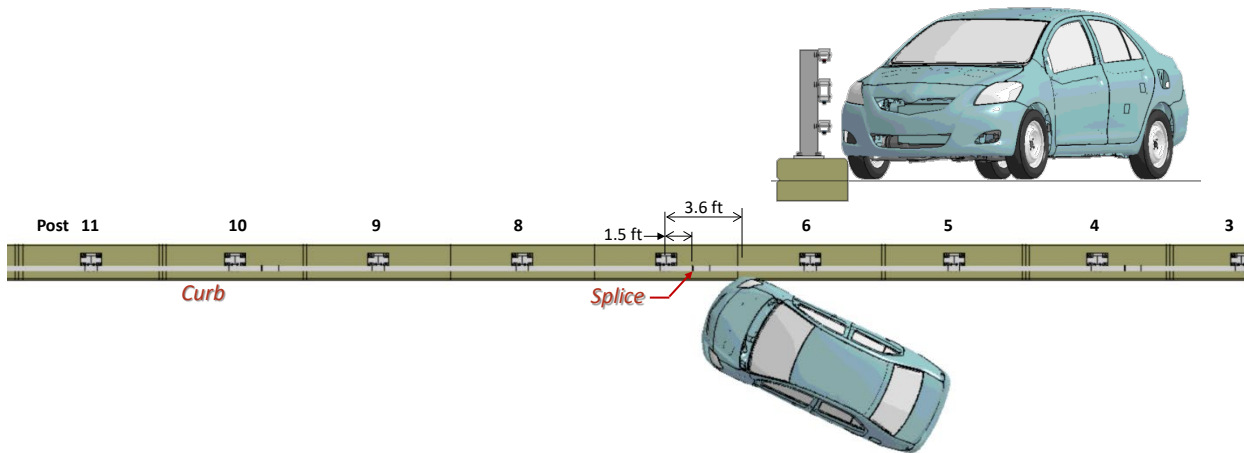


Figure 439. Impact point for Test 4-10 on the Modified NETC 3-bar bridge rail.

15.1.2.1 Damages to the Barrier System Compared

Figures 440 and 441 show maximum deflections for each case compared to the baseline from overhead and oblique view points, respectively. Each of the modified designs resulted in reduced deflection of the lower rail as well as reduced potential for vehicle contact with the post. The maximum dynamic deflections for Case 1, 2, and 3 were 2.3 inches (58 mm), 2.1 inches (52 mm) and 2.8 inches (63 mm), respectively. It was anticipated that Case 3 (i.e., stiffest rail option) would result in lower deflections than the other cases; however, the larger internal gap in the splice for Case 3 increased the relative lateral deflection between the rail tubes, as can be seen in Figure 440.

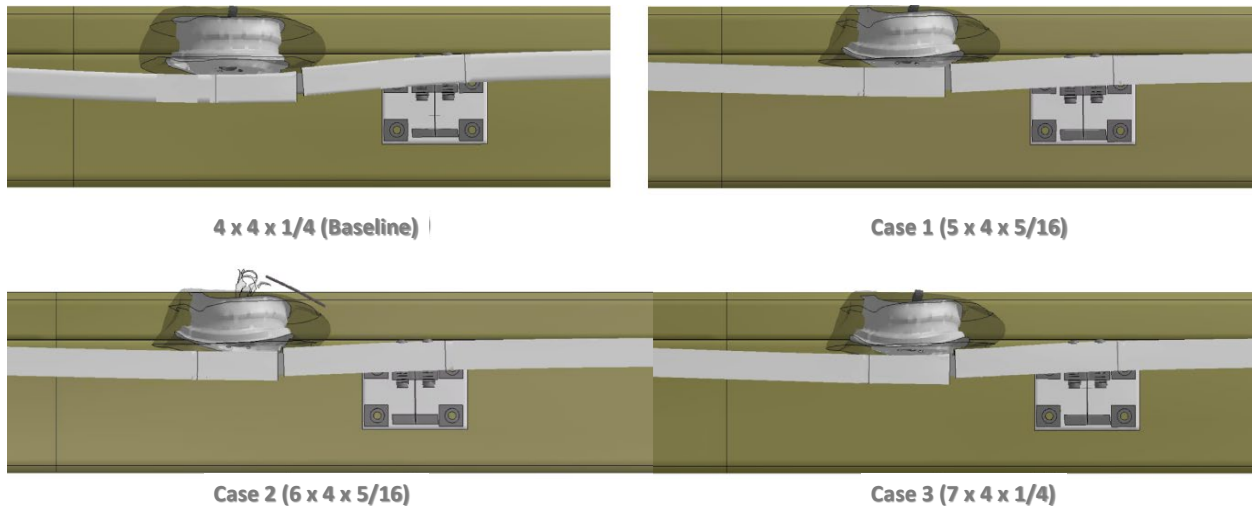


Figure 440. Overhead transparent view showing maximum deflections of the lower rail for each analysis case compared to baseline.

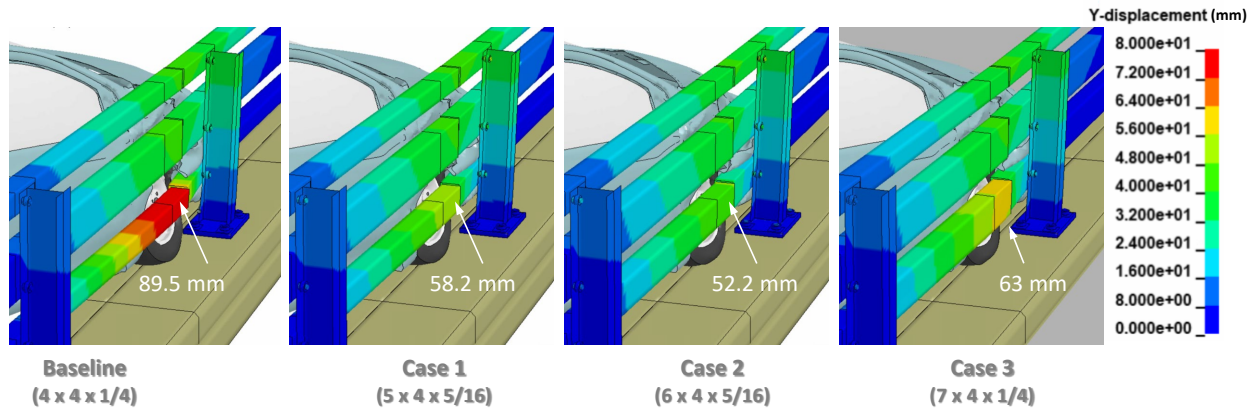


Figure 441. Oblique view showing maximum dynamic deflections of the barrier for each analysis case compared to baseline.

15.1.2.2 Time History Data Compared

Figures 442 through 444 show the longitudinal, transverse, and vertical acceleration-time histories, respectively, computed from the center of gravity of the vehicle; Figures 445 through 447 show the comparison of the angular rates and angular displacements (i.e., yaw, roll and pitch) at the center of gravity of the vehicle. The peak 10-ms moving average longitudinal acceleration was reduced for all modified design cases compared to the baseline (i.e., from 26 G to ≈ 23 G), as shown in Table 105; while the peak accelerations for the y- and z-directions were essentially unchanged. The yaw, roll and pitch attitudes of the vehicle were also similar for all cases; although roll and pitch angular displacements were slightly reduced 2 or 3 degrees for the modified cases.

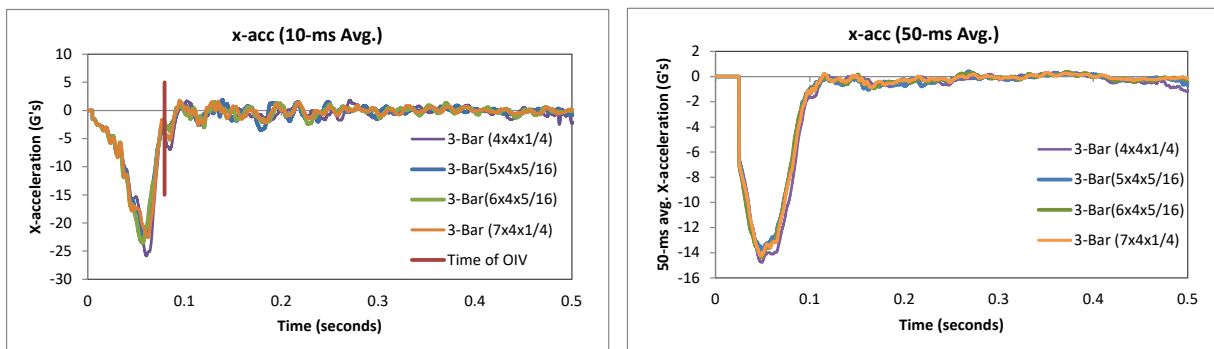


Figure 442. 10- and 50-millisecond average x-acceleration from FEA of Test 4-10 on the Modified NETC 3-bar bridge rail.

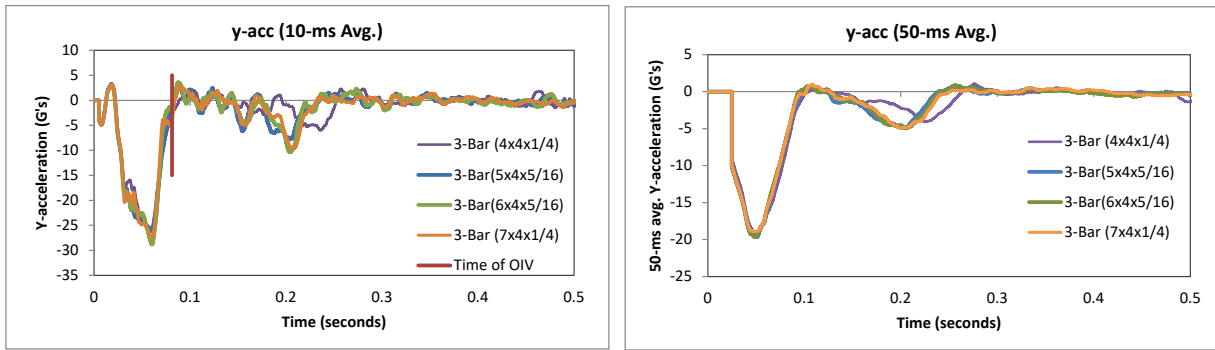


Figure 443. 10- and 50-millisecond average y-acceleration from FEA of Test 4-10 on the Modified NETC 3-bar bridge rail design cases.

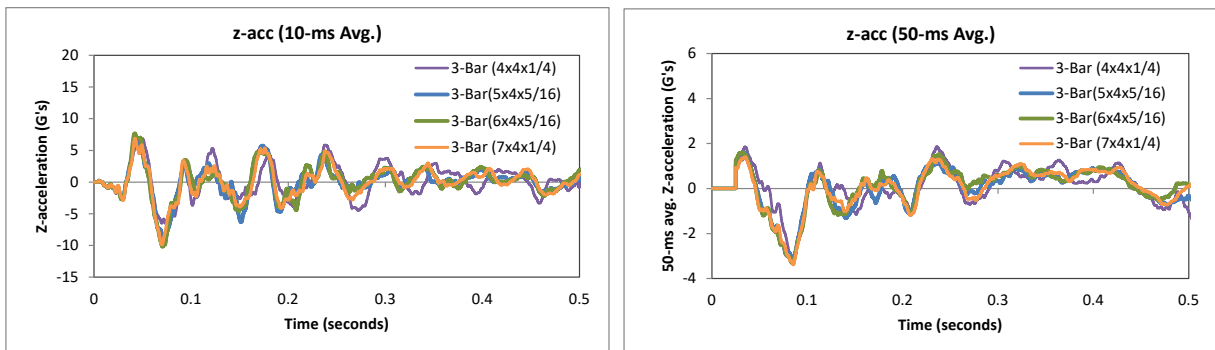


Figure 444. 10- and 50-millisecond average z-acceleration from FEA of Test 4-10 on the Modified NETC 3-bar bridge rail design cases.

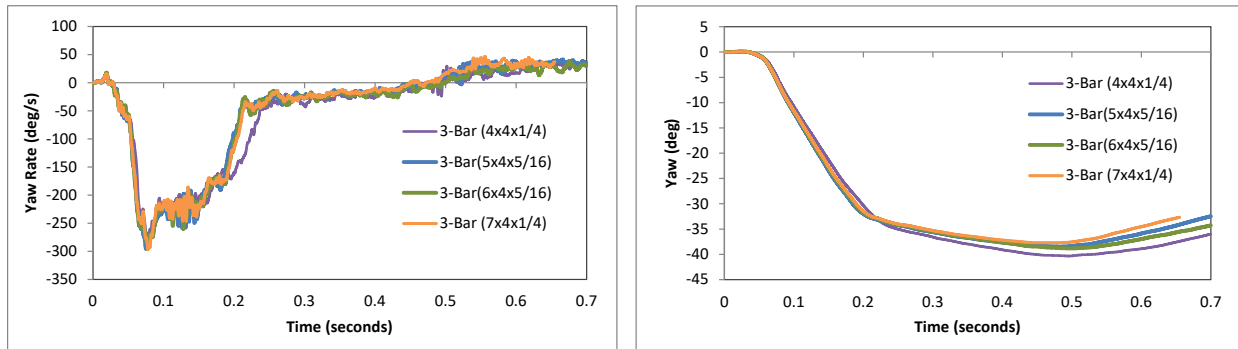


Figure 445. Yaw rate and yaw angle time-history from FEA of Test 4-10 on the Modified NETC 3-bar bridge rail design cases.

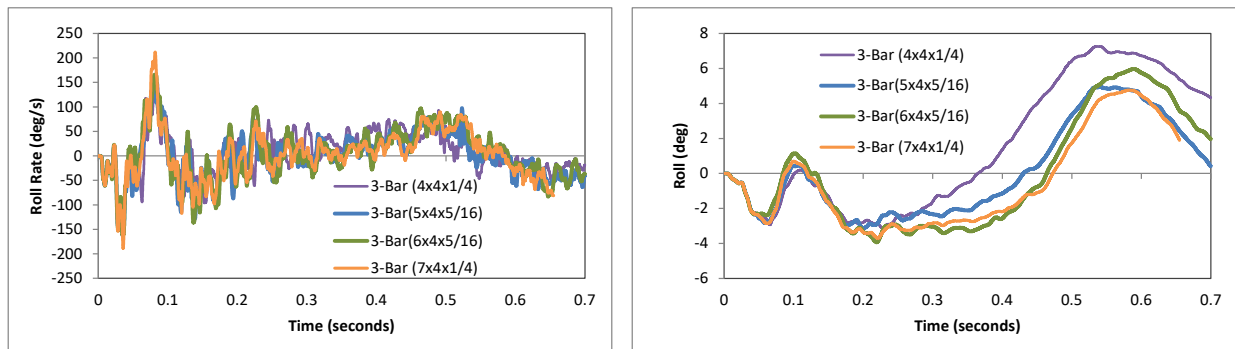


Figure 446. Roll rate and roll angle time-history from FEA of Test 4-10 on the Modified NETC 3-bar bridge rail design cases.

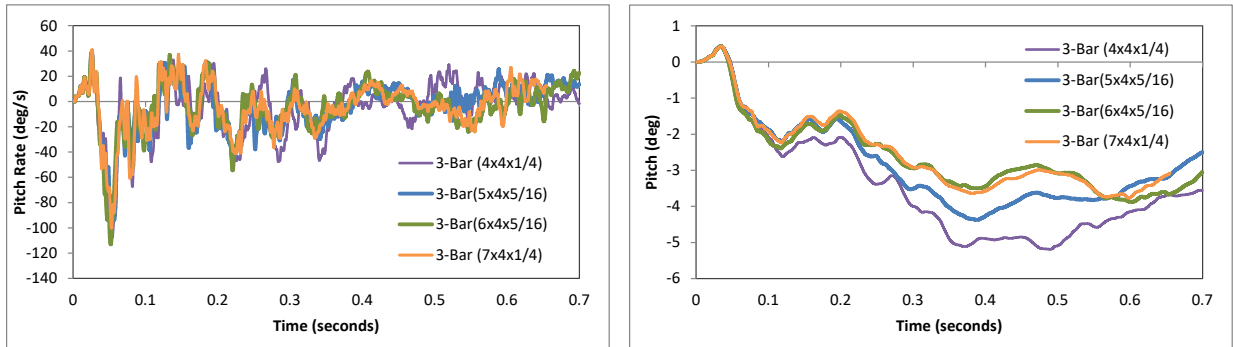


Figure 447. Pitch rate and pitch angle time-history from FEA of Test 4-10 on the Modified NETC 3-bar bridge rail design cases.

Table 105. Peak accelerations for Test 4-10 on the Modified NETC 3-bar bridge rail design cases.

Design	Peak Accelerations	
	X-acc (G)	Y-acc (G)
3-Bar (4x4x1/4)	25.87	28.86
3-Bar(5x4x5/16)	22.42	26.18
3-Bar(6x4x5/16)	23.51	28.83
3-Bar (7x4x1/4)	22.62	27.46

15.1.2.3 Occupant Risk Metrics Compared

The acceleration-time histories and angular rate-time histories collected at the center of gravity of the vehicle were used to evaluate occupant risk metrics according to the procedures outlined in *MASH*. Figure 448 shows the results for the occupant risk calculations compared with the baseline. The OIV values were essentially unchanged. The ORA-x was slightly reduced, and the ORA-y was slightly increased for the modified design cases; however, all cases were well below the failure threshold of 20.45 G specified in *MASH*.

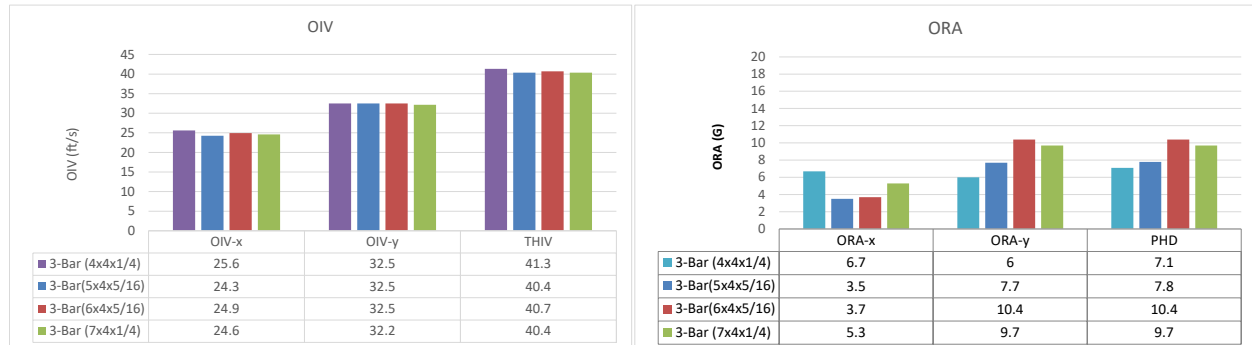


Figure 448. OI32.5V and ORA values for Test 4-10 on the Modified NETC 3-bar design case.

15.1.2.4 Results Summary and Recommendations

The modified NETC 3-bar system with larger lower rail showed slightly improved performance for all cases evaluated. The deflection of the lower rail was reduced 30% - 42%.

The peak longitudinal acceleration was reduced 9.3% - 13.5%. A wheel-slag still occurred at the splice connection for all cases, which likely affected peak acceleration magnitudes. Much of the deflection could be mitigated by minimizing the internal gap-space in the splice (recall that tested design only had 1/8" total gap-space). It is anticipated that the rail deflection and the potential for wheel snag would be reduced considerably if the internal gap-space in the splice were eliminated. Although not detailed in this report, the ORA-x was found to be the least sensitive to time-of-occupant-impact for Case 1, HSS 5x4x5/16, which was also the least costly revision.

Table 106 provides an overall summary of the modified lower rail design options and the analysis results. The barrier successfully contained and redirected the small car with minimal damage to the system. There were no detached elements from the barrier that showed potential for penetrating the occupant compartment or presenting undue hazard to other traffic. The vehicle remained upright and very stable throughout impact and redirection. The OIV and maximum ORA values were within recommended limits specified in *MASH*. Based on the results of this analysis, the barrier with each of the modified lower rail alternatives is expected to meet all structural and occupant risk criteria in *MASH* for Test 4-10 impact conditions.

It is recommended that the HSS 5x4x5/16 be used for the lower rail; however, the overall improvement may not be significant enough to warrant changing the design. It is further recommended that the splice design be revised to minimize the amount of internal gap-space between the splice tube and the main rails, since the lateral movement within the splice appears to be a key factor in causing the excessive deflection of the rail as well as wheel snag at the splice.

Table 106. Summary of results for Test 4-10 on the Modified NETC 3-bar bridge rail with larger lower rail.

Bar Size	Physical Properties					Results					
	Area		Zy		Splice Gap	Deflect	Peak Acc _x	OIV _x	OIV _y	ORA _x	ORA _y
	(in ²)	% Change	(in ³)	% Change	(in)	(in)	(G)	(ft/s)	(ft/s)	(G)	(G)
HSS 4 x 4 x ¼	3.59	-	4.97	-	3/4	3.5	25.9	25.6	32.5	6.7	6
HSS 5 x 4 x 5/16	4.98	39%	7.05	42%	11/16	2.3	22.4	24.3	32.5	3.5	7.7
HSS 6 x 4 x 5/16	5.61	56%	8.21	65%	11/16	2.1	23.5	24.9	32.5	3.7	10.4
HSS 7 x 4 x ¼	5.09	42%	7.78	57%	3/4	2.5	22.6	24.6	32.2	5.3	9.7

15.2 3-Bar Transition with Increased Post Spacing at First Bridge Rail Post

The maximum spacing between the first post of the bridge rail and the last post of the transition is currently specified as 3 feet; however, when spanning certain types of expansion joints, such as strip joints, compression seals, finger joints and modular joints, it is not always possible to meet this condition. One such example is shown in Figure 449, which involves the railing spanning a skew joint. A common practice for dealing with these situations is to use greater post spacing. Typical post spacing used by NHDOT include:

- 4'-9" spacing for strips or compression seals, 45-deg skew
- 5'-6" spacing for finger joints, 43-deg skew
- 7'-0" spacing for modular joints, 0-deg skew



Figure 449. Skew Joint

In Section 10, the original NETC 3-bar transition design was shown to meet *MASH* TL4 performance criteria (based on the FEA crash simulations). The only recommended design change was to taper the tops of the transition posts and bridge rail posts down and toward the field side to avoid contact with the front-lower edge and bottom of the cargo-box during impacts with single unit trucks.

It was of concern that the increased post spacing between the last post of the bridge rail and the first post of the transition would reduce the strength of the railing and have the greatest effect on performance in Tests 4-22 (i.e., SUT vehicle) and 4-20 (i.e., small car) impact cases. For example, Test 4-22 would subject the barrier to the greatest loading conditions overall, while Test 4-20 would tend to impart a concentrated load onto the lower railing, which could result in excessive pocketing at the approach to the first bridge rail post. Therefore, extending the post spacing between the transition and bridge rail may lead to greater potential for mid-span rail deflections and pocketing as described in the previous section. The consensus of the project technical committee was to evaluate a post spacing of 5'-6" for the 3-bar transition-to-bridge rail for *MASH* TL4 impact conditions. This post spacing should account for most of the non-conforming field installation cases.

15.2.1 Design Cases Evaluated

The finite element analysis model from Section 10 was modified for use in this evaluation by (1) extending the bridge rail tubes and deck to attain desired post spacing of 5.5-ft between first post of bridge rail and last post of the transition, (2) tapering the tops of the W6x25 posts, and (3) widening the expansion splice gap opening from 0.75 inches to 2 inches. An elevation view of the original and modified models is shown in Figure 450. Two different expansion splice options were included in the evaluation, as illustrated in Figure 451. Expansion splice Model01 included a nominal 3/4-inch opening at the splice, and expansion splice Model02 included a nominal 2-inch opening at the splice. Due to the angle of the transition rails, the maximum longitudinal gap opening in the splice joint was 1.4 inches and 2.4 inches for Model01 and Model02, respectively, at the top rail element.

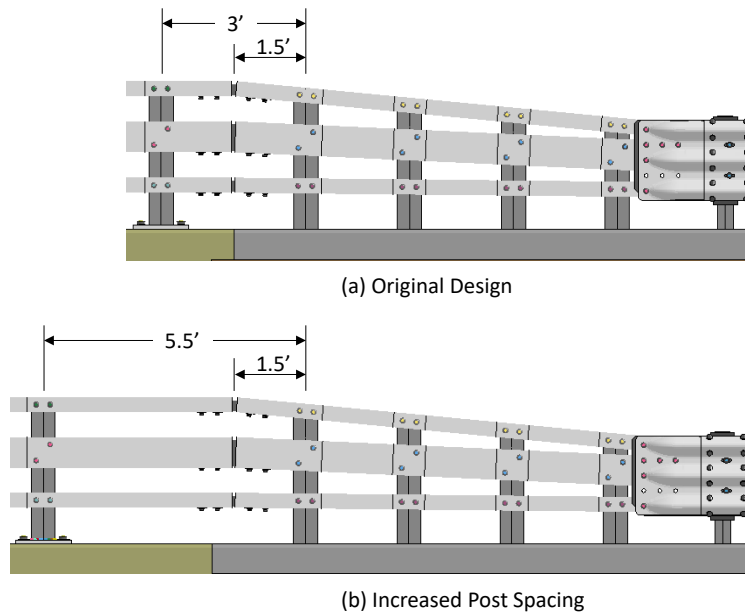


Figure 450. Post and splice spacing for (a) original and (b) modified designs.

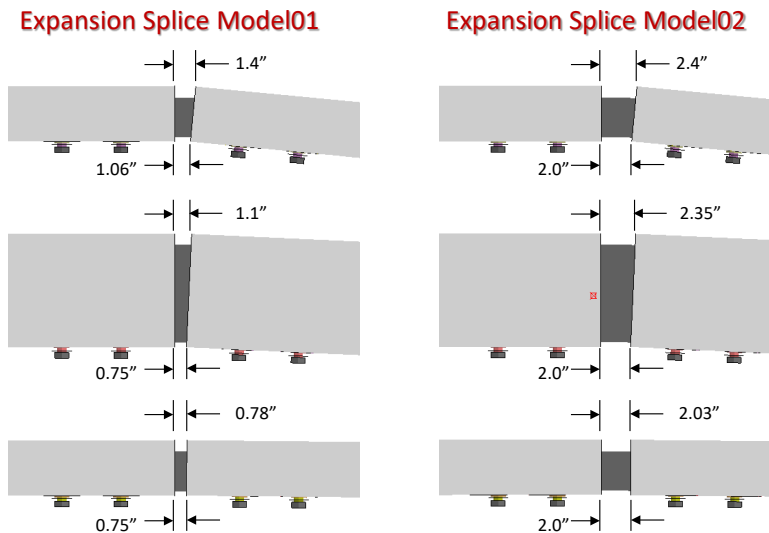


Figure 451. Expansion splice cases evaluated.

Expansion splice Model01 was used in the previous analysis of the 3-bar transition in Section 10. Recall, however, that only Test 4-22 (single-unit truck test) was evaluated at the expansion splice connection to the bridge rail. The critical snag point for passenger vehicles in those evaluations was determined to be at the connection point of the thrie-beam to the tube rail, which is located farther upstream on the transition (see Figure 170). In those evaluations, passenger vehicles did not contact the expansion splice during the impact event. For the current analysis case, with the increased span between the transition and bridge rail posts, the expansion splice may be more critical for the passenger vehicle tests.

Two different post designs were also evaluated: one did not include a taper on the post (e.g., original design), while the second included a 51-degree taper starting at 2 inches behind the face of the post, which was adopted from an existing MassDOT design, as illustrated in Figure 452. The taper is important for avoiding contact with the single-unit truck during impact, but it will not likely affect the passenger vehicle tests, since those vehicles do not contact the tops of the posts.

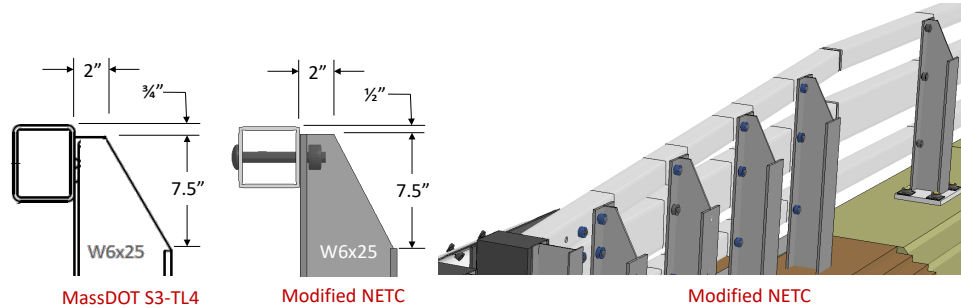


Figure 452. Tapered post based on MassDOT S3-TL4 bridge rail design.

Two potential critical snag points were identified for the passenger vehicle tests: 1) at the expansion splice joint and 2) at the first post of the bridge rail, as annotated on Figure 453. Only one critical snag point was identified for the single-unit truck which was also at the expansion splice. FEA was then used to evaluate the crash performance of the modified system for *MASH* TL4.

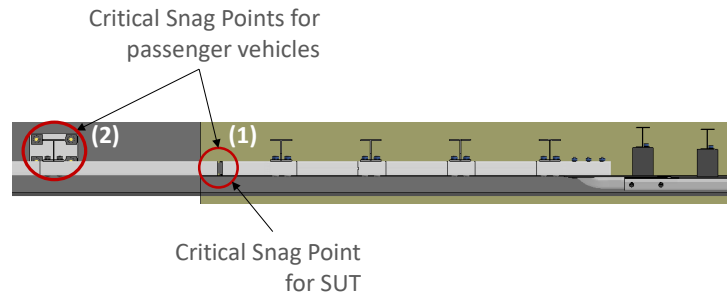


Figure 453. Critical impact point locations.

15.2.2 Test 4-20

For Test 4-20, two barrier designs were evaluated:

- 1) Design 1 – Original barrier components (e.g., same rails, posts and hardware) including:
 - 5.5' post spacing for first bridge rail post
 - Expansion Splice Model02 (Gap = 2 inches)
- 2) Design 2 – Modified Design including:
 - 5.5' post spacing for first bridge rail post
 - Expansion Splice Model02 (Gap = 2 inches)
 - Larger HSS 5x4x5/16 for lower rail as determined in previous section
 - Tapered posts

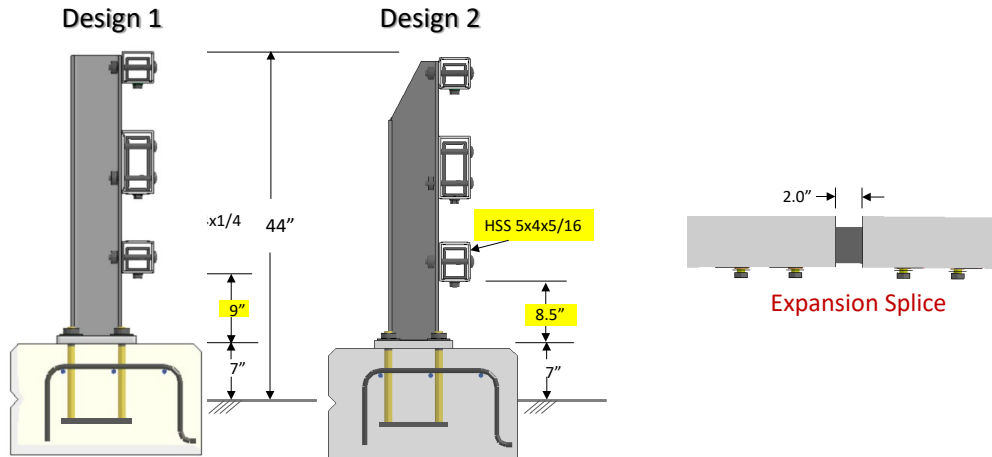


Figure 454. Bridge rail and splice designs used for the Test 4-20 evaluations.

15.2.2.1 Design Case 1 (Original System Components)

The critical impact point for Test 4-20 was determined using FEA with respect to maximizing the potential for wheel snag on the first post of the bridge rail and on the splice connection. Finite element analysis was used to simulate *MASH* Test 4-20 at ten (10) impact locations ranging from 3.6 feet to 8 feet upstream from the first post on the bridge rail, as shown in Figure 455. The third column in the table in Figure 455 provides the distance from the impact point in each case to the center of the expansion splice. These analyses were conducted for 0.15 seconds of impact, and the results of the ten impact cases are shown in the following sections.

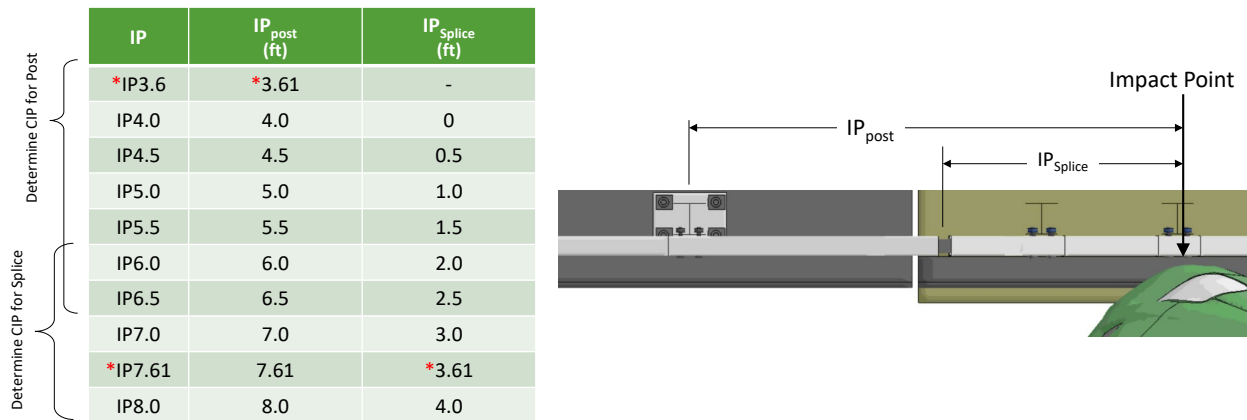


Figure 455. Impact point locations for Test 4-20 on the 3-bar transition with increased post spacing.

None of the impact points resulted in significant wheel contact with the post; however, impact at 4.0 feet upstream of the critical post resulted in the greatest chance for contacting the post, as illustrated in Figure 456. The analysis case with impact point at 8 feet upstream from the post (i.e., 4 ft upstream of expansion splice) was the critical impact point for snag on the splice, but the analysis results indicated a low potential for wheel snag due to the splice being located on the downstream side of the post, as shown in Figure 457. A reverse direction impact may be more critical for assessing snag on the splice.

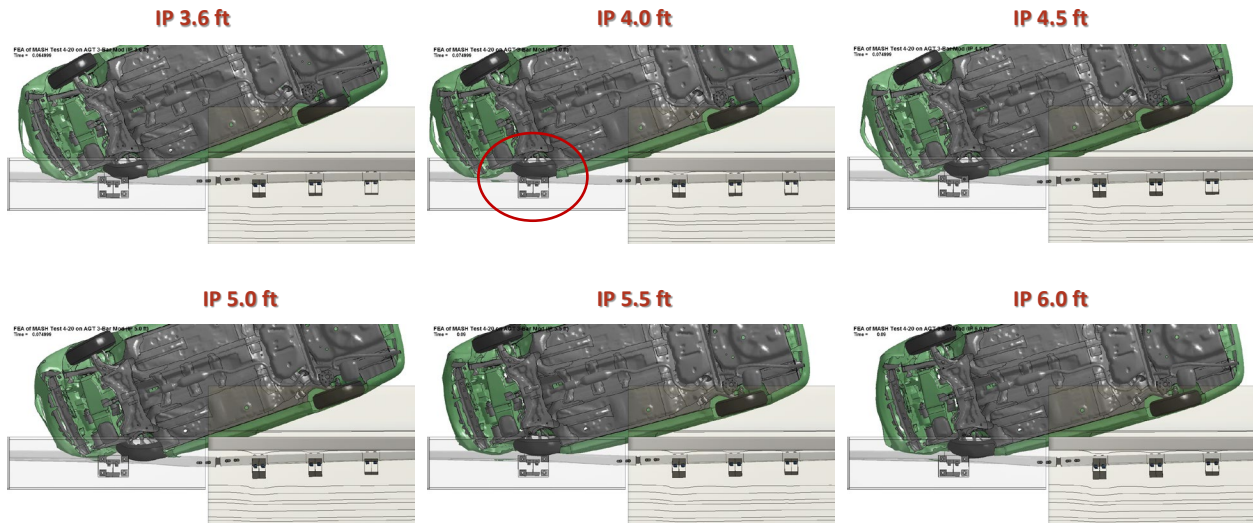


Figure 456. Test 4-20 results at time of potential impact with critical post.

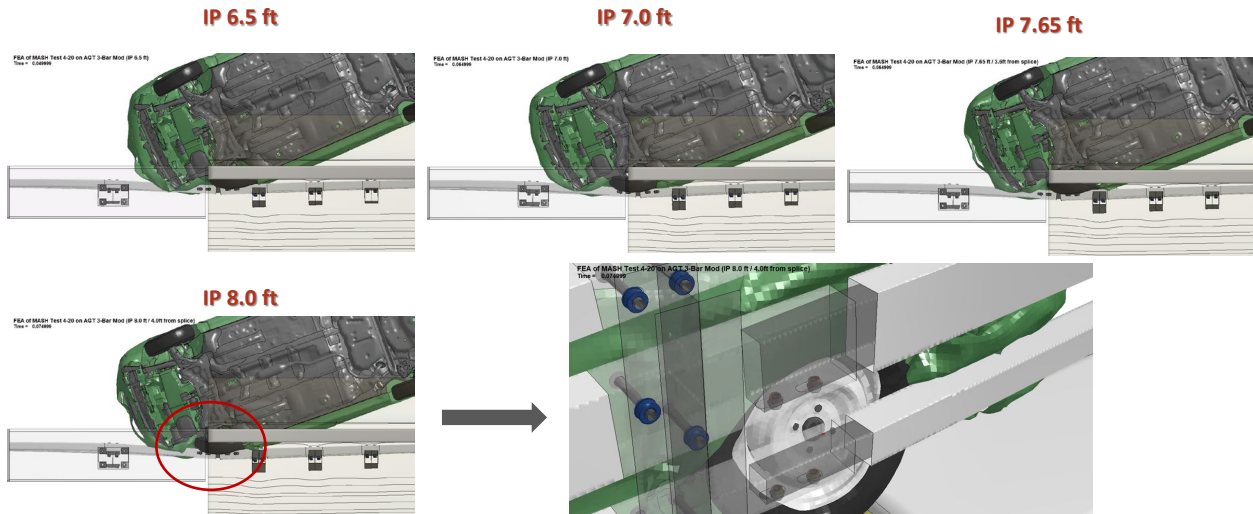


Figure 457. Test 4-20 results at time of potential snag on critical splice.

Peak accelerations

The acceleration-time histories collected at the center of gravity of the vehicle were used to assess peak acceleration values for the ten impact cases. As denoted in Figure 455, impact cases IP3.6 to IP6.5 were designed for assessing critical snag on the bridge rail posts. For those cases, IP4.0 was determined as the most critical for snag on the post. This impact case also corresponded to the highest peak longitudinal acceleration (x-direction), the 2nd highest lateral acceleration and the highest resultant acceleration, as shown in Figure 458. Impact cases IP6.0 to IP8.0 were designed for assessing critical snag on the expansion splice, in which IP8.0 was determined as the critical impact point for that case. However, as shown previously in Figure 457 and confirmed here in Figure 458, snagging on the splice does not appear to be an issue for primary impact direction for Test 4-20.

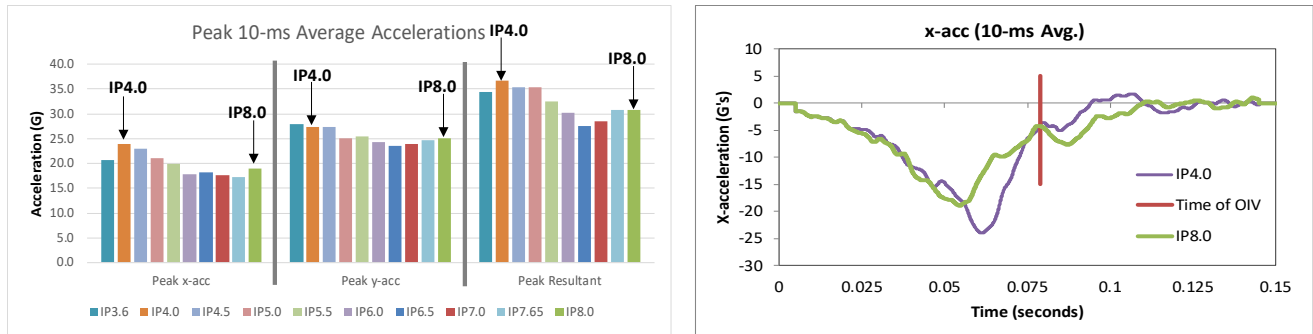


Figure 458. Peak 10-ms moving average acceleration data for Test 4-20 impact cases.

Occupant Risk Metrics

The acceleration-time histories and angular rate-time histories collected at the center of gravity of the vehicle were used to evaluate occupant risk metrics according to the procedures outlined in *MASH*. Table 107 shows the results for the occupant risk calculations, and Figure 459 shows a graphical representation of the peak OIV and ORA results. In all cases the OIV-x values were within preferred limits; while the OIV-y values exceeded preferred limits but were within critical limits. The ORA values were well within preferred limits for both the x- and y-directions. The highest OIV values occurred for IP 5.0, which were 26.2 ft/s and 35.1 ft/s in x-direction and y-direction, respectively. The highest ORA values occurred for IP7.6, which were 7.4 G and 7.9 G for x- and y-directions, respectively. The second highest ORA values occurred for IP8.0, which were 7.4 G and 6.2 G for x- and y-directions, respectively. It should be noted that the analyses were not conducted for a long enough period of time for the rear of the vehicle to impact against the barrier, which is usually the event that results in the highest lateral ORA for Test 4-20. However, based on previous full-scale test results on similar systems and the previous results in this study presented in Section 10.2.4, the peak lateral ORA was expected to be well below preferred limits for all cases evaluated here.

15.2.2.2 Design Case 2 – Modified Design with HSS 5 x 4 x 5/16 Lower Rail and Tapered Post

The FEA model developed in Section 15.2.2.1 (i.e., Design 1) was modified for the current analysis case (i.e., Design 2), as illustrated in Figure 454. The modifications included an HSS 5 x 4 x 5/16 lower rail for the NETC 3-bar bridge rail, and a taper on the W6x25 posts as recommended in Section 10. Based on the results of Design Case 1, the critical impact point for this case was selected as 4 feet upstream of the first bridge rail post, as shown in Figure 460, to maximum potential for wheel snag on the first post of the bridge rail and to maximize peak accelerations of the vehicle during impact. The impact conditions were consistent with *MASH* Test 4-20 and included the 2,595-lb Yaris model impacting the rail at 62.1 mph and 25 degrees. The analysis was performed for 0.5 seconds of the impact event, and all results presented in the following sections include comparison to Design Case 1.

Table 107. Occupant risk metrics for Test 4-20 impact cases on the 3-bar transition with increased post spacing.

Occupant Risk Factors		MASH Test 4-20									
		IP3.6	IP4.0	IP4.5	IP5.0	IP5.5	IP6.0	IP6.5	IP7.0	IP7.65	IP8.0
Occupant Impact Velocity (ft/s)	x-direction	24.0	25.3	25.6	26.2	24.9	24.9	23.9	N.A.	21.65328	22.63752
	y-direction	33.1	33.1	35.1	35.1	35.4	35.1	33.5	N.A.	31.1676	30.83952
	at time	at 0.0775 seconds on right side of interior	at 0.0788 seconds on right side of interior	at 0.0789 seconds on right side of interior	at 0.0794 seconds on right side of interior	at 0.0795 seconds on right side of interior	at 0.0804 seconds on right side of interior	at 0.0805 seconds on right side of interior	0	at 0.0810 seconds on right side of interior	at 0.0813 seconds on right side of interior
THIV (ft/s)	40.7 at 0.0775 seconds on right side of interior	41.7 at 0.0788 seconds on right side of interior	43.6 at 0.0789 seconds on right side of interior	43.3 at 0.0794 seconds on right side of interior	43.0 at 0.0795 seconds on right side of interior	42.3 at 0.0804 seconds on right side of interior	40.7 at 0.0805 seconds on right side of interior	0.0 0	37.07304 at 0.0810 seconds on right side of interior	37.7292 at 0.0813 seconds on right side of interior	
Ridedown Acceleration (g's)	x-direction	-3.3 (0.0794 - 0.0894 seconds)	-4.9 (0.0806 - 0.0906 seconds)	-3.5 (0.0813 - 0.0913 seconds)	-4.6 (0.0812 - 0.0912 seconds)	-6.7 (0.0813 - 0.0913 seconds)	-6.6 (0.0822 - 0.0922 seconds)	-7.5 (0.0825 - 0.0925 seconds)	ant does not impact vehi 0	-7.4 (0.0830 - 0.0930 seconds)	-7.4 (0.0834 - 0.0934 seconds)
	y-direction	4.1 (0.0846 - 0.0946 seconds)	2.9 (0.0901 - 0.1001 seconds)	3.6 (0.0950 - 0.1050 seconds)	-2.7 (0.1104 - 0.1204 seconds)	-2.8 (0.1081 - 0.1181 seconds)	-3.3 (0.1169 - 0.1269 seconds)	-5.1 (0.0825 - 0.0925 seconds)	ant does not impact vehi 0	-7.9 (0.0851 - 0.0951 seconds)	-6.2 (0.0834 - 0.0934 seconds)
PHD (g's)		4.2 (0.0846 - 0.0946 seconds)	5.3 (0.0798 - 0.0898 seconds)	4 (0.0789 - 0.0889 seconds)	6.3 (0.0794 - 0.0894 seconds)	8.8 (0.0795 - 0.0895 seconds)	9.8 (0.0803 - 0.0903 seconds)	11.1 (0.0805 - 0.0905 seconds)	ant does not impact vehi 0	12.4 (0.0809 - 0.0909 seconds)	10.8 (0.0812 - 0.0912 seconds)
ASI		2.49 (0.0253 - 0.0753 seconds)	2.53 (0.0251 - 0.0751 seconds)	2.58 (0.0265 - 0.0765 seconds)	2.51 (0.0274 - 0.0774 seconds)	2.47 (0.0266 - 0.0766 seconds)	2.41 (0.0337 - 0.0837 seconds)	2.28 (0.0338 - 0.0838 seconds)	2.07 (0.0231 - 0.0731 seconds)	2.07 (0.0263 - 0.0763 seconds)	2.06 (0.0304 - 0.0804 seconds)
Max 50-ms moving avg. acc.	x-direction	-13.4 (0.0242 - 0.0742 seconds)	-14 (0.0247 - 0.0747 seconds)	-14 (0.0298 - 0.0798 seconds)	-14.6 (0.0352 - 0.0852 seconds)	-13.4 (0.0314 - 0.0814 seconds)	-13.3 (0.0318 - 0.0818 seconds)	-12.9 (0.0377 - 0.0877 seconds)	-11.5 (0.0221 - 0.0721 seconds)	-11.2 (0.0241 - 0.0741 seconds)	-12.1 (0.0239 - 0.0739 seconds)
	y-direction	-20.1 (0.0267 - 0.0767 seconds)	-20.2 (0.0252 - 0.0752 seconds)	-20.7 (0.0266 - 0.0766 seconds)	-20 (0.0271 - 0.0771 seconds)	-19.9 (0.0265 - 0.0765 seconds)	-19.3 (0.0339 - 0.0839 seconds)	-18.2 (0.0266 - 0.0766 seconds)	-16.5 (0.0221 - 0.0721 seconds)	-16.7 (0.0332 - 0.0832 seconds)	-16.3 (0.0335 - 0.0835 seconds)
	z-direction	-2.9 (0.0610 - 0.1110 seconds)	-3.1 (0.0621 - 0.1121 seconds)	-2.8 (0.0608 - 0.1108 seconds)	-2.5 (0.0604 - 0.1104 seconds)	-2.3 (0.0598 - 0.1098 seconds)	-2.3 (0.0573 - 0.1073 seconds)	-2.5 (0.0539 - 0.1039 seconds)	-0.8 (0.0213 - 0.0713 seconds)	-3.1 (0.0554 - 0.1054 seconds)	-2.9 (0.0555 - 0.1055 seconds)
	Resultant	25.6	25.6	25.9	25.9	24.4	24.1	22.8	21.6	22.1	22.1
	Peak 10 ms Avg. Accelerations	x-direction	-20.7	-24.0	-22.9	-21.1	-20.0	-17.9	-18.3	-17.6	-17.3
	y-direction	-27.9	-27.3	-27.4	-25.1	-25.5	-24.4	-23.5	-23.9	-24.8	-25.0
	Resultant	34.5	36.6	35.3	35.3	32.5	30.2	27.5	28.5	30.8	30.8

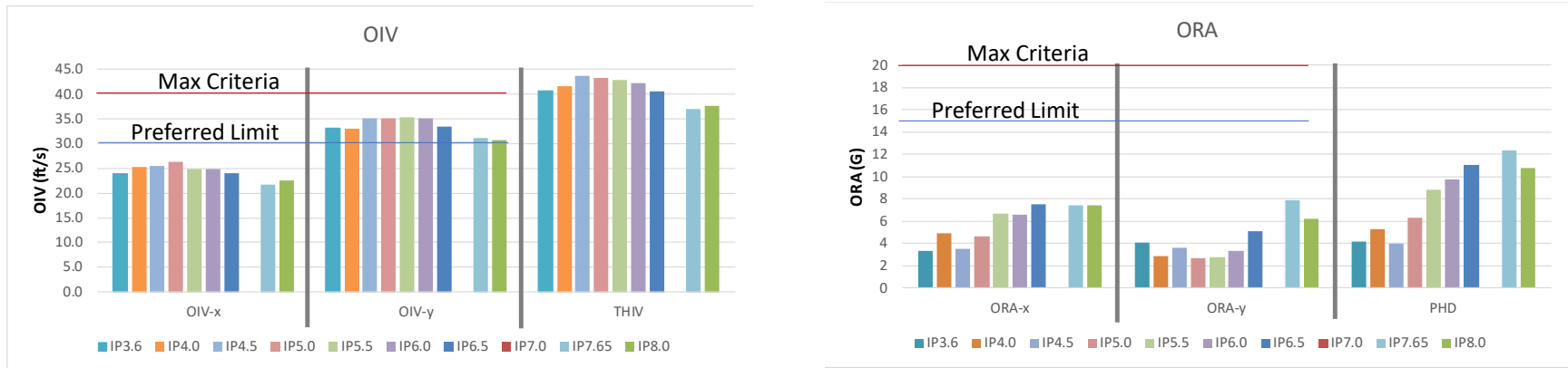


Figure 459. Graphical representation of OIV, THIV, ORA and PHD metrics for Test 4-20.

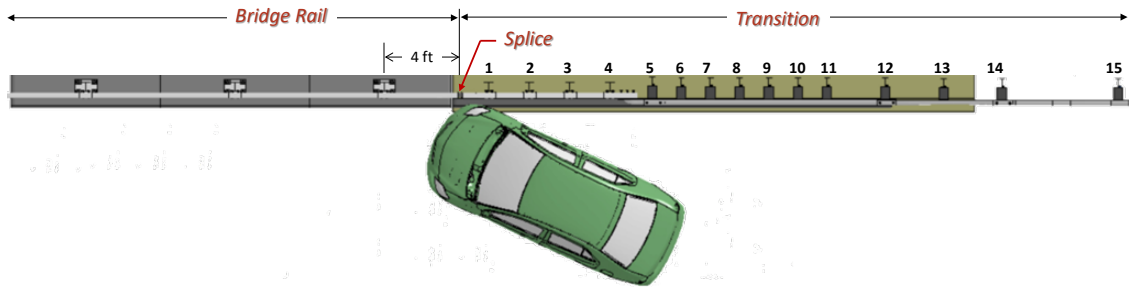


Figure 460. Impact point for Test 4-20 on Design Case 2.

Time History Evaluation

Figures 461 through 463 show the longitudinal, transverse, and vertical acceleration-time histories, respectively, computed from the center of gravity of the vehicle; Figures 464 through 466 show the comparison of the angular rates and angular displacements (i.e., yaw, roll and pitch) at the center of gravity of the vehicle. The accelerations and angular displacements were essentially the same for both Design Cases 1 and 2, except that peak longitudinal acceleration was 19.7 G for Design Case 2, which was approximately 20% less than Design Case 1.

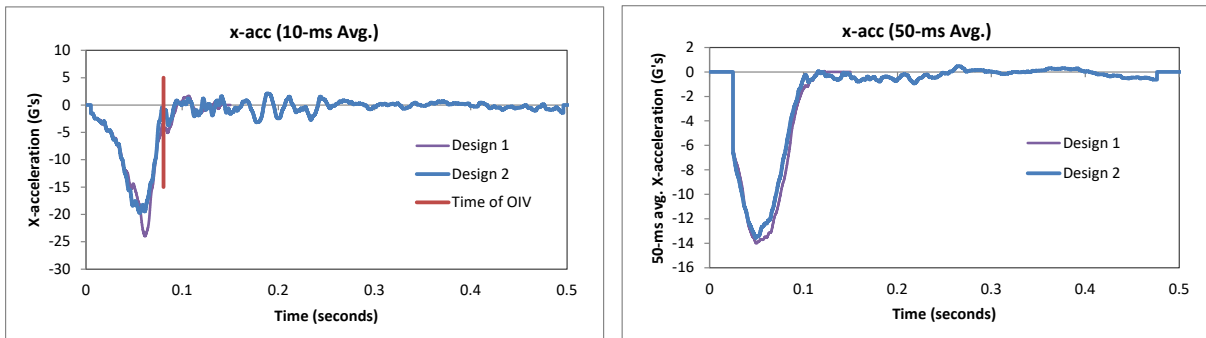


Figure 461. 10- and 50-millisecond average X-acceleration from FEA of Test 4-20 on the 3-bar transition with 5.5-ft post spacing.

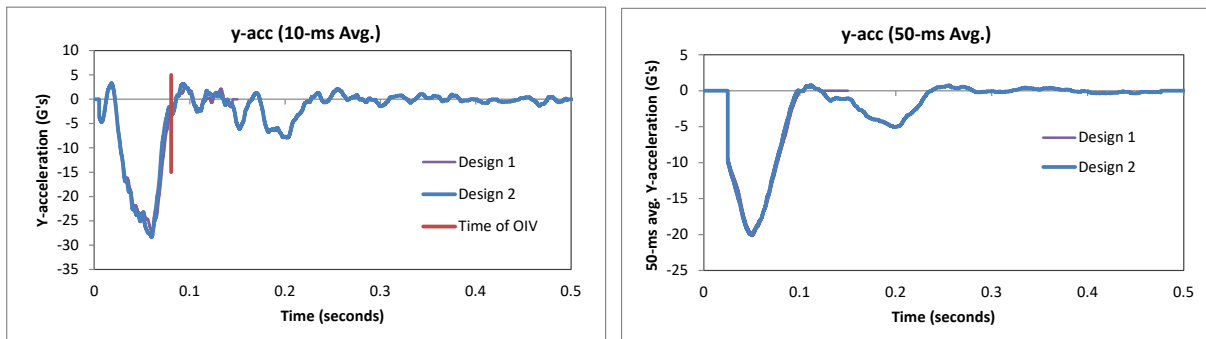


Figure 462. 10- and 50-millisecond average Y-acceleration from FEA of Test 4-20 on the 3-bar transition with 5.5-ft post spacing.

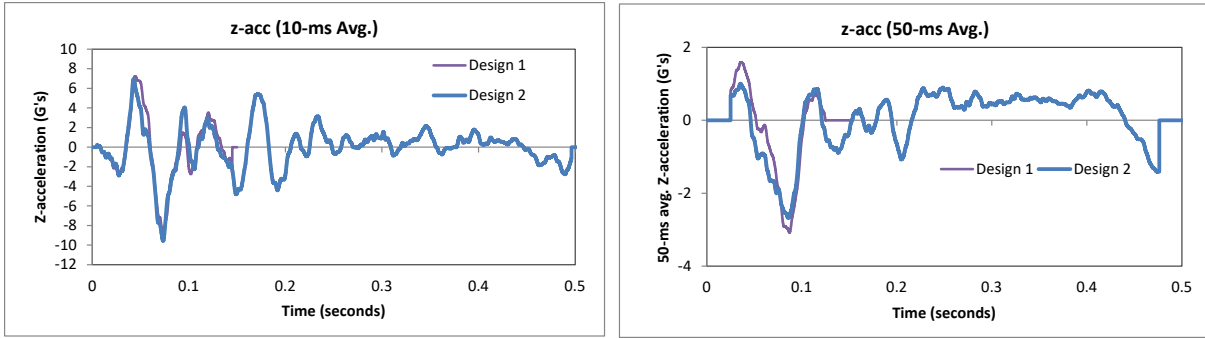


Figure 463. 10- and 50-millisecond average Z-acceleration from FEA of Test 4-20 on the 3-bar transition with 5.5-ft post spacing.

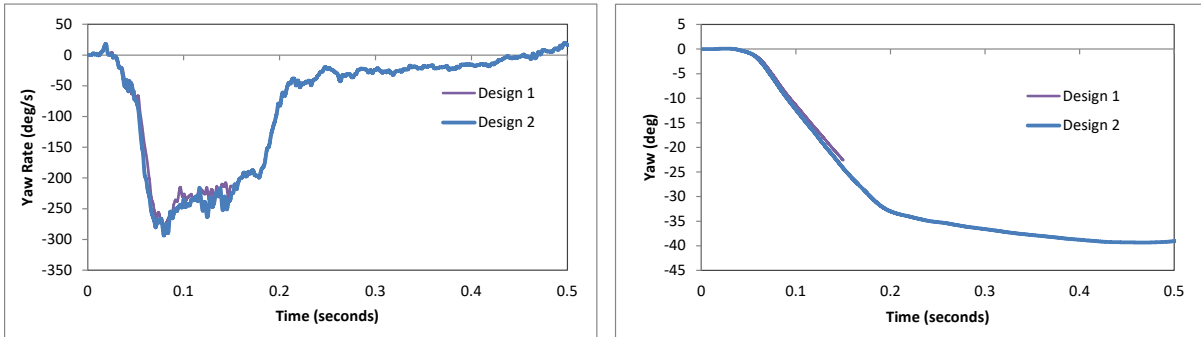


Figure 464. Yaw rate and yaw angle time-history from FEA of Test 4-20 on the 3-bar transition with 5.5-ft post spacing.

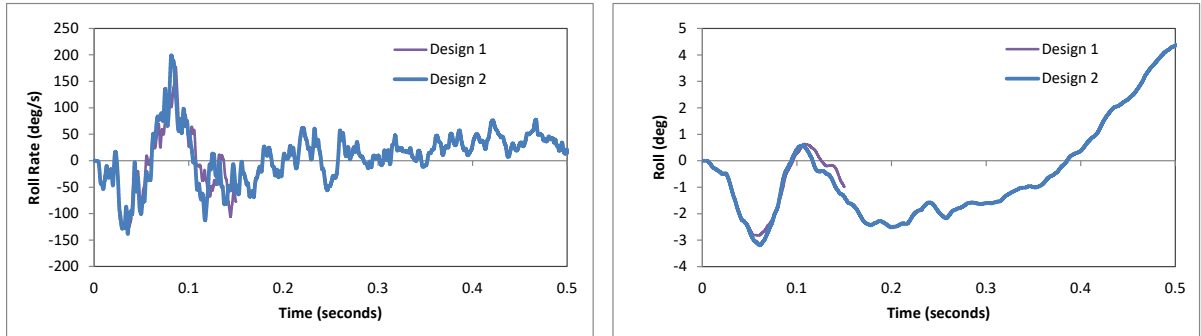


Figure 465. Roll rate and roll angle time-history from FEA of Test 4-20 on the 3-bar transition with 5.5-ft post spacing.

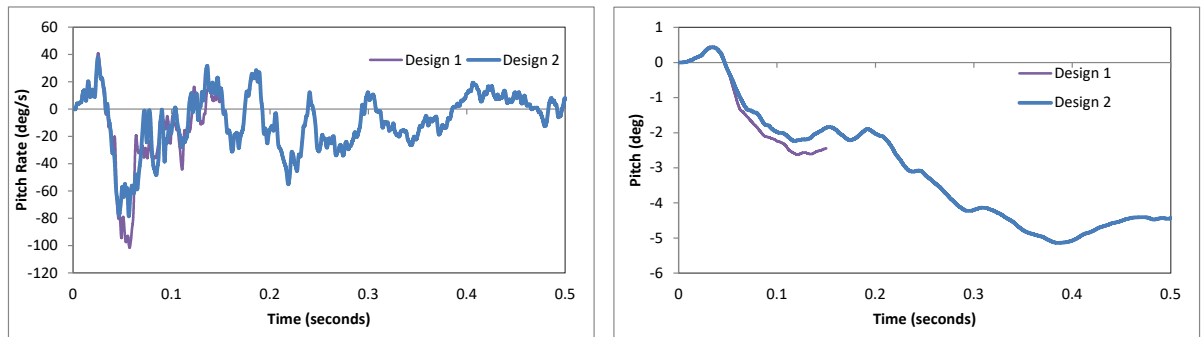


Figure 466. Pitch rate and pitch angle time-history from FEA of Test 4-20 on the 3-bar transition with 5.5-ft post spacing.

Occupant Risk Measures

The acceleration-time histories and angular rate-time histories collected at the center of gravity of the vehicle were used to evaluate occupant risk metrics according to the procedures outlined in *MASH*. Table 108 shows the results for the occupant risk calculations. The results indicate that the occupant risk factors meet safety criteria specified in *MASH*.

The occupant impact velocities in the longitudinal and transverse directions for the transition were 23.6 ft/s and 32.8 ft/s, respectively, which were within the recommended limits specified in *MASH* and slightly less than those same metrics for Design Case 1. The highest 0.010-second occupant ridedown acceleration in the longitudinal and transverse directions were 3.7 g and 7.9 g, respectively, which were well within preferred limits specified in *MASH*. The ORA-x value was slightly reduced compared to Design Case 1. The ORA-y values could not be compared since Design Case 1 was terminated prior to achieving peak values. The maximum 50-ms moving average acceleration values in the longitudinal and transverse directions were 1.5 g and 20 g, respectively. These values were also slightly lower than those for Design Case 1. The maximum roll and pitch angles of the vehicle were 4.4 degrees and 5.1 degrees, respectively, which were well below critical limits in *MASH*.

Table 108. Summary of *MASH* occupant risk metrics for Test 4-20 on the 3-bar transition with 5.5-ft post spacing.

Occupant Risk Factors		MASH	
		Design 1	Design 2
Occupant Impact Velocity (ft/s)	x-direction	25.3	23.6
	y-direction	33.1	32.8
	at time	at 0.0788 seconds on right side of interior	at 0.0776 seconds on right side of interior
THIV (ft/s)		41.7	40.7
		at 0.0788 seconds on right side of interior	at 0.0776 seconds on right side of interior
Ridedown Acceleration (g's)	x-direction	-4.9 (0.0806 - 0.0906 seconds)	-3.7 (0.0804 - 0.0904 seconds)
	y-direction	N/A	-7.9 (0.1972 - 0.2072 seconds)
PHD (g's)		N/A	8.2 (0.1966 - 0.2066 seconds)
ASI		2.53 (0.0251 - 0.0751 seconds)	2.49 (0.0241 - 0.0741 seconds)
Max 50-ms moving avg. acc. (g's)	x-direction	-14 (0.0247 - 0.0747 seconds)	-13.5 (0.0242 - 0.0742 seconds)
	y-direction	-20.2 (0.0252 - 0.0752 seconds)	-20 (0.0241 - 0.0741 seconds)
	z-direction	-3.1 (0.0621 - 0.1121 seconds)	-2.7 (0.0607 - 0.1107 seconds)
Maximum Angular Disp. (deg)	Roll	N/A	4.4 (0.5013 seconds)
	Pitch	N/A	-5.1 (0.3851 seconds)
	Yaw	N/A	-39.4 (0.4683 seconds)

MASH Criteria

< 30 ft/s (preferred) ✓
< 40 ft/s (limit)

< 15 G (preferred) ✓
< 20.49 G (limit)

< 75 deg ✓

N/A – Not applicable since the analysis was terminated prior to achieving peak values.

Damages to the Barrier System

Figure 467 shows images of the maximum dynamic deflection of the barrier and maximum dynamic deflection of the lower rail from an overhead and oblique view with a contour plot of lateral displacement on the rail elements. The maximum dynamic and permanent deflections were 2.65 inches and 1.36 inches, respectively, and occurred at the top railing at the expansion splice. For Design Case 1, the maximum dynamic and permanent deflections occurred on the lower rail at the expansion splice with values of 3.25 inches and 1.52 inches, respectively. For Design Case 2 with the larger HSS 5 x 4 x 5/16 lower rail, the dynamic and permanent deflections of the lower rail reduced to 2.44 inches and 1 inch, respectively. The

lower deflections and the larger contact area of the HSS 5 x 4 x 4/16 rail also resulted in a lower potential for the tire to contact the bridge rail post, as shown in Figure 468.

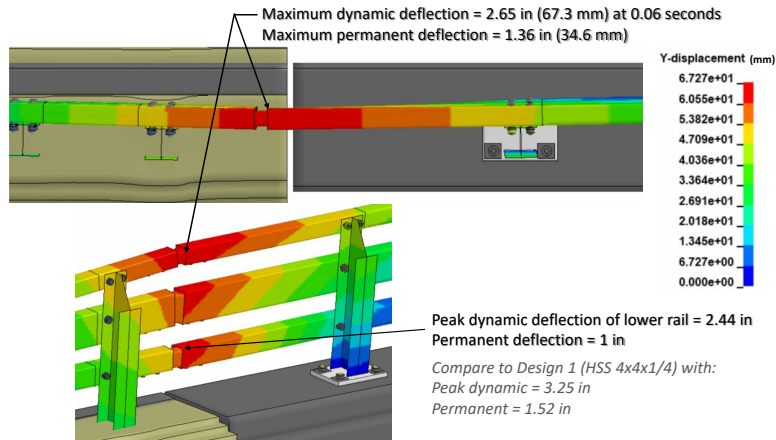


Figure 467. Contour plot of lateral displacement for the system at the time of maximum dynamic deflection.

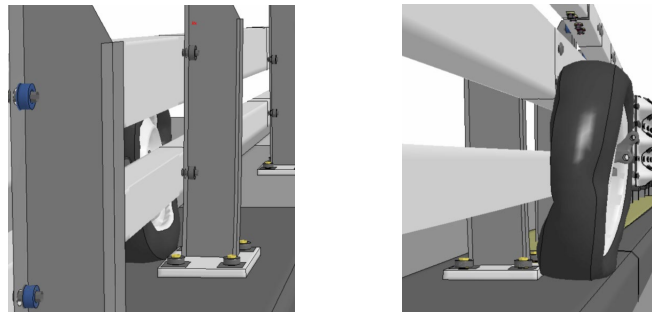


Figure 468. Test 4-20 results at time of potential impact with critical post.

Damages to Vehicle

Figure 469 show contour plots of effective plastic strain for the vehicle, which were used to identify areas of the vehicle that suffered damage during the simulated impact event. The damages to the vehicle were very similar to those for Test 4-10 on the NETC 3-bar bridge rail in Section 9.1.6. The most severe damages were to the front fender, the upper and lower control arm of front suspension, front wheel, lower edge of windshield, and light damage to the rear quarter panel of the vehicle.

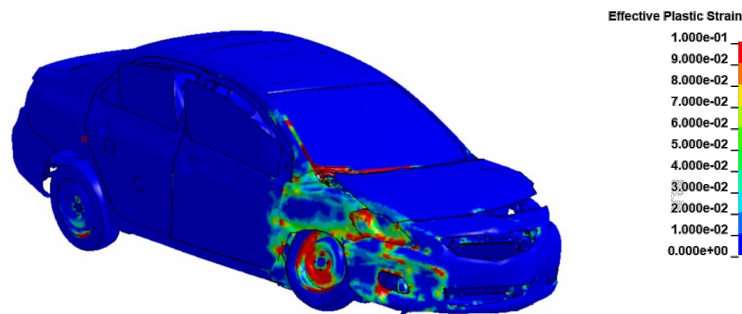


Figure 469. Damages to vehicle in Test 4-20 analysis of the 3-bar transition.

Exit Box

Figure 470 shows the exit box during the Test 4-20 analysis for Design Case 2 on the 3-bar transition with 5.5-ft post spacing. The vehicle was smoothly redirected, and its path was well within the exit box criteria of *MASH*.

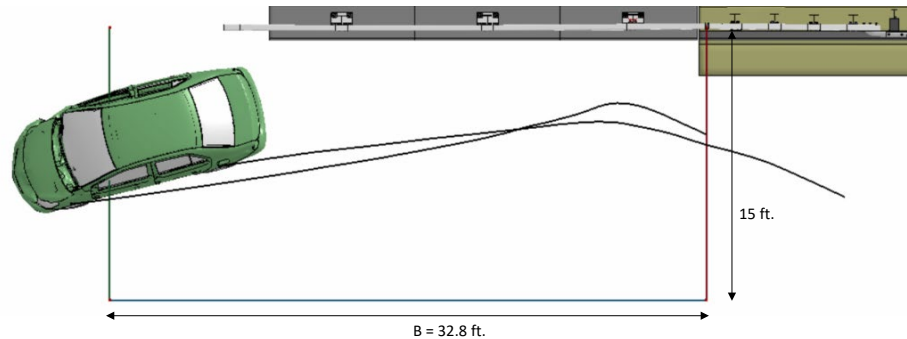


Figure 470. Exit box for Test 4-20 analysis of the 3-bar transition.

15.2.2.3 Results Summary for Test 4-20

The FEA results for *MASH* Test 4-20 on the 3-bar transition with 5.5-ft post spacing at the first bridge rail post indicated that the system would meet all structural adequacy, occupant safety and vehicle stability criteria according to *MASH* for both Design Case 1 and Design Case 2. The barrier successfully contained and redirected the small car with minimal damage to the system. There were no detached elements from the barrier that showed potential for penetrating the occupant compartment or presenting undue hazard to other traffic. The vehicle remained upright and very stable throughout impact and redirection. The OIV and maximum ORA values were within critical limits specified in *MASH*. Both design cases were shown to meet *MASH* safety criteria; however, Design Case 2 with the HSS 5 x 4 x 5/16 lower rail resulted in improved performance compared to Design Case 1 with the HSS 4 x 4 x 5/16 lower rail.

15.2.3 Test 4-21

For Test 4-21, only Design Case 1 was evaluated, which included the original system components with an expansion splice gap of 2 inches (nominal). This case represents current field installations and is also considered to be a less conservative analysis case compared to Design Case 2 (e.g., with larger lower rail). Therefore, if this system meets *MASH* crash performance criteria, then the improved design for Design Case 2 would be considered *MASH* compliant as well.

Finite element analysis was used to simulate *MASH* Test 4-21 at five (5) impact locations ranging from 5 feet to 9 feet upstream from the first post on the bridge rail in 1-foot increments, as shown in Figure 471. The third column in the table in Figure 471 provides the distance from the impact point in each case to the center of the expansion splice. These analyses were conducted for 0.25 seconds of impact and were sufficient for determining all occupant risk metrics in *MASH*.

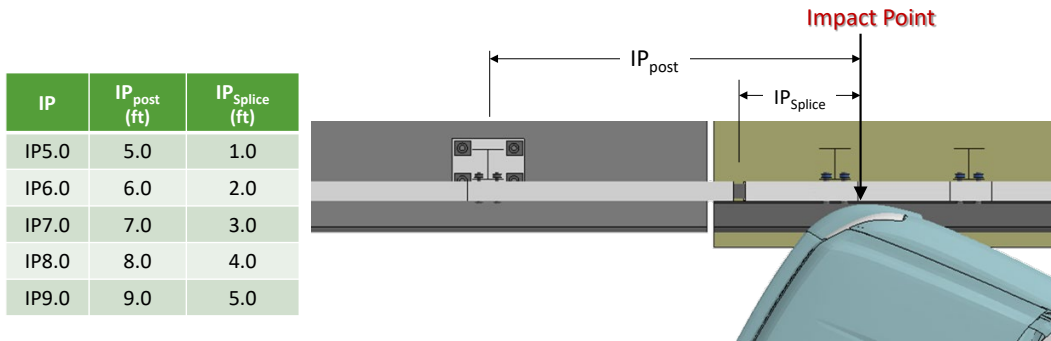


Figure 471. Impact point locations for Test 4-21 on the 3-bar transition with increased post spacing.

None of the impact points resulted in significant potential for wheel contact with the post; however, impact at 6.0 feet upstream of the critical post (i.e., 2-ft upstream of expansion splice) resulted in the highest potential for snag on the expansion splice. Images from analysis cases IP 6.0 ft – IP 9.0 ft at the time of tire contact with the expansion splice are shown in Figures 472 – 474 from an oblique viewpoint, underneath viewpoint, and tire-only view point, respectively.

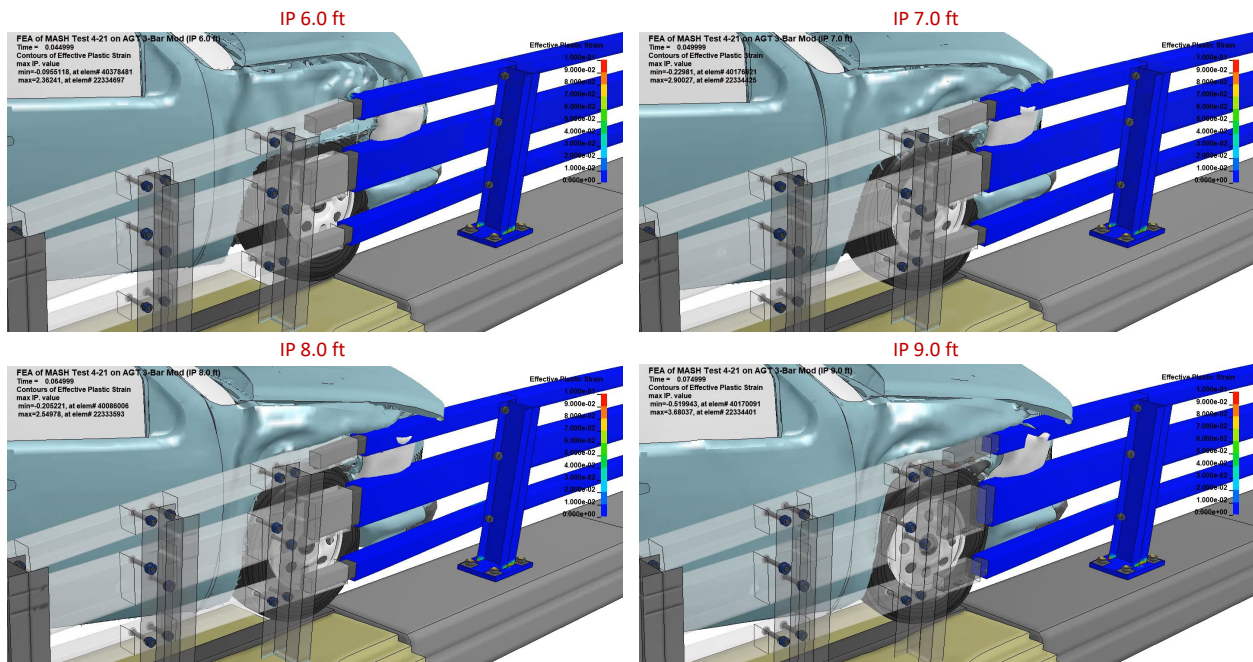


Figure 472. Test 4-21 results at time of impact with expansion splice (oblique view).

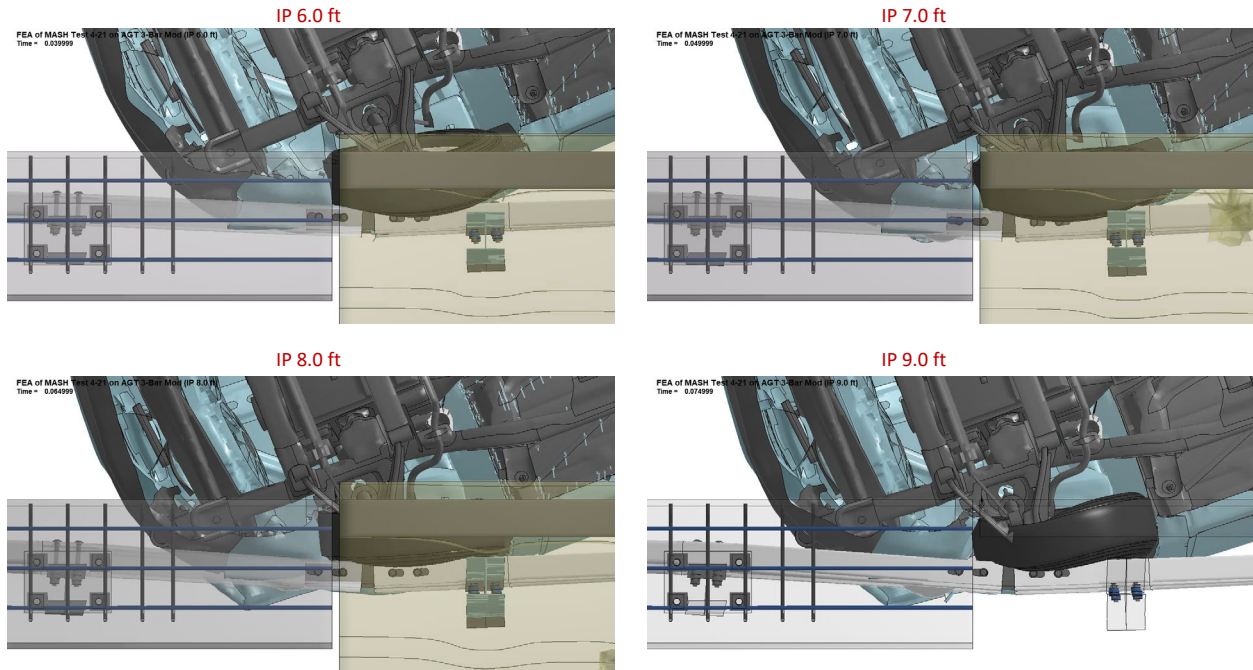


Figure 473. Test 4-21 results at time of impact with expansion splice (underneath view).

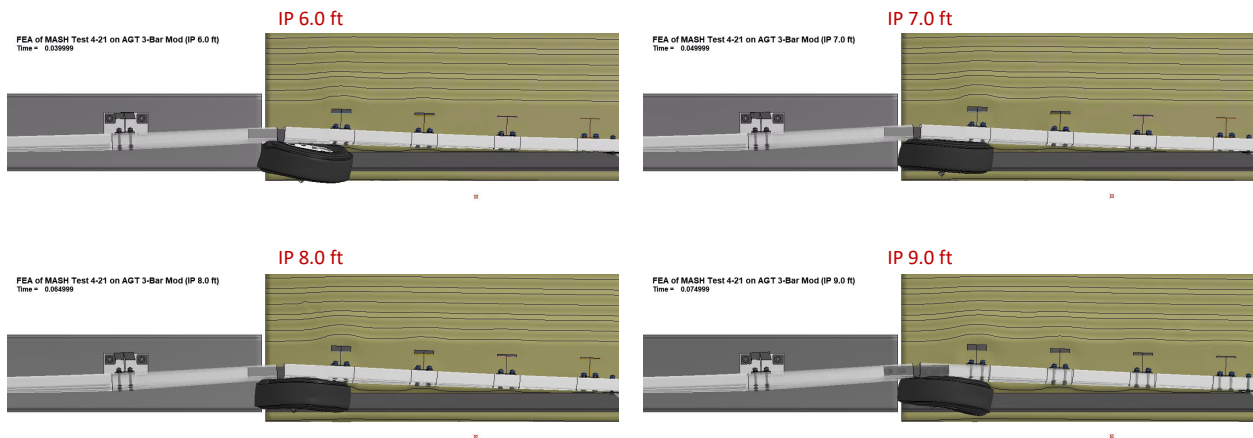


Figure 474. Test 4-21 results at time of impact with expansion splice (tire-only view).

Case IP6.0 appeared to be the critical impact point for the splice for Test 4-21. As shown in Figure 475, the fender snagged on the splice at the top rail. Although the snag did result in severely damaging the fender, it did not greatly affect vehicle accelerations. Neither the wheel rims nor the leading edge of the door (which would have been a more severe snag) showed propensity for snag in any of the cases. Cases IP 7.0 ft and IP 8.0 ft showed higher potential for snag at the leading edge of the door on the splice; however, no snags occurred in those analysis cases, likely due to the splice location on the downstream side of the post. As with the small car test, a reverse impact case may be more critical for assessing snag on the splice.

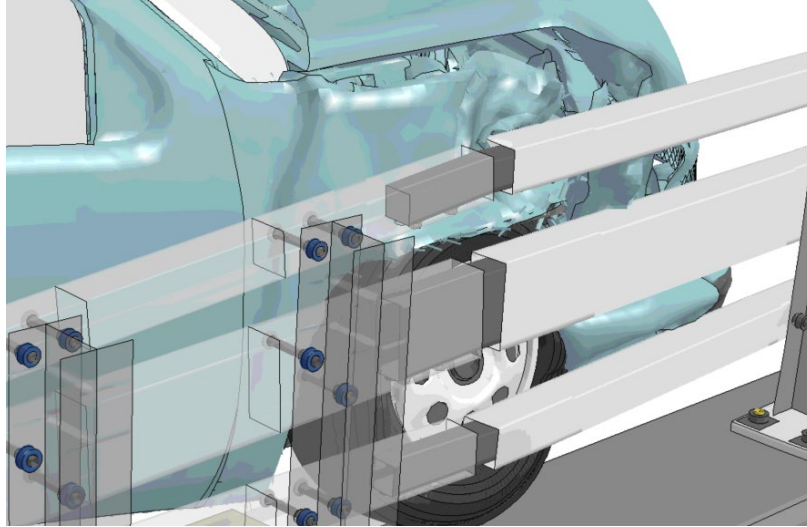


Figure 475. Closeup view of splice for Test 4-21 impact case IP 6.0 ft.

15.2.3.1 Peak accelerations

The acceleration-time histories collected at the center of gravity of the vehicle were used to assess peak acceleration values for the five impact cases. IP 6.0 ft was determined as the most critical for snag on both the post and the expansion splice. This impact case also corresponded to the highest peak longitudinal acceleration (x-direction), the 2nd highest lateral acceleration, and the highest resultant acceleration, as shown in Figure 476; it was also the only case to result in the fender snagging on the splice. The snag on the fender caused the higher x-acceleration peak for this case; however, the model did not allow for metal tearing of the fender which may have over-predicted the snag force since the material could not fail. Impact case IP 5.0 ft yielded the highest peak lateral acceleration.

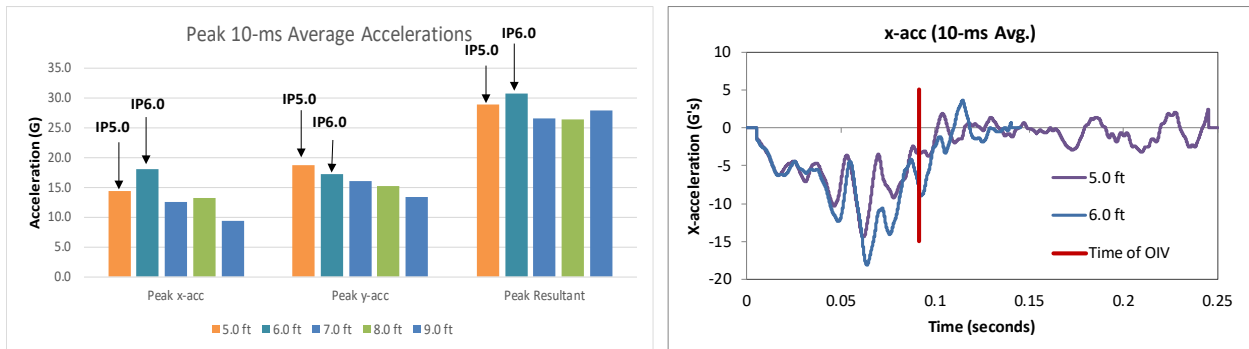


Figure 476. Peak 10-ms moving average acceleration data for Test 4-21 impact cases.

15.2.3.2 Occupant Risk Metrics

The acceleration-time histories and angular rate-time histories collected at the center of gravity of the vehicle were used to evaluate occupant risk metrics according to the procedures outlined in *MASH*. Table 109 shows the results for the occupant risk calculations, and Figure 477 shows a graphical representation of the peak OIV and ORA results. In all cases the OIV values were within preferred limits. The peak ORA values were well within preferred limits for the ORA in the x-direction, while the peak ORA values in the y-direction exceeded preferred limits but were within critical limits. The highest OIV in the x-direction was 22.6 mph for case

IP 6.0 ft. The highest OIV in the y-direction occurred for all cases from IP 5.0 ft to 8.0 ft with values ranging from 27.9 mph to 28.5 mph. The highest ORA in the x-direction was 6.0 G and occurred for cases IP 6.0 ft and 9.0 ft. Analysis case IP 6.0 ft terminated prematurely before peak ORA in y-direction occurred; however, the ORA-y was expected to be similar to the values for IP 5.0 ft and 7.0 ft. Also, recall that the Silverado model tends to over-predict the lateral acceleration for the “backslap” of the vehicle impacting rigid barriers (see Section 5).

Table 109. Occupant risk metrics for Test 4-21 impact cases on the 3-bar transition with increased post spacing.

Occupant Risk Factors		MASH Test 4-20				
		5.0 ft	6.0 ft	7.0 ft	8.0 ft	9.0 ft
Occupant Impact Velocity (ft/s)	x-direction	18.0	22.6	18.4	18.4	16.7
	y-direction	28.5	27.9	27.9	28.2	25.3
	at time	at 0.0878 seconds on right side of interior	at 0.0888 seconds on right side of interior	at 0.0898 seconds on right side of interior	at 0.0894 seconds on right side of interior	at 0.0904 seconds on right side of interior
THIV (ft/s)		33.8 at 0.0878 seconds on right side of interior	35.4 at 0.0888 seconds on right side of interior	33.1 at 0.0898 seconds on right side of interior	32.8 at 0.0894 seconds on right side of interior	29.5 at 0.0904 seconds on right side of interior
Ridedown Acceleration (g's)	x-direction	-3.8 (0.0914 - 0.1014 seconds)	-5.8 (0.0913 - 0.1013 seconds)	-5.6 (0.0923 - 0.1023 seconds)	-4.4 (0.2318 - 0.2418 seconds)	-6 (0.2075 - 0.2175 seconds)
	y-direction	-18.1 (0.1846 - 0.1946 seconds)	N.A.	-19.1 (0.1853 - 0.1953 seconds)	-17.9 (0.1858 - 0.1958 seconds)	-18.7 (0.1823 - 0.1923 seconds)
PHD (g's)		18.1 (0.1846 - 0.1946 seconds)	10 (0.0888 - 0.0988 seconds)	19.2 (0.1852 - 0.1952 seconds)	18.1 (0.1855 - 0.1955 seconds)	18.9 (0.1822 - 0.1922 seconds)
ASI		1.68 (0.0390 - 0.0890 seconds)	1.73 (0.0360 - 0.0860 seconds)	1.59 (0.0388 - 0.0888 seconds)	1.57 (0.0442 - 0.0942 seconds)	1.33 (0.0398 - 0.0898 seconds)
Max 50-ms moving avg. acc.	x-direction	-8 (0.0391 - 0.0891 seconds)	-10.7 (0.0334 - 0.0834 seconds)	-8.2 (0.0378 - 0.0878 seconds)	-7.8 (0.0361 - 0.0861 seconds)	-6.6 (0.0519 - 0.1019 seconds)
	y-direction	-13.9 (0.0354 - 0.0854 seconds)	-13.5 (0.0363 - 0.0863 seconds)	-13 (0.0390 - 0.0890 seconds)	-12.8 (0.0439 - 0.0939 seconds)	-10.8 (0.0391 - 0.0891 seconds)
	z-direction	-2.5 (0.1886 - 0.2386 seconds)	-2.4 (0.0654 - 0.1154 seconds)	-3.3 (0.1813 - 0.2313 seconds)	-2.5 (0.0502 - 0.1002 seconds)	-3 (0.1653 - 0.2153 seconds)
	Resultant	20.6	21.3	20.5	20.4	19.4
Peak 10 ms Avg. Accelerations	x-direction	-14.4	-18.1	-12.6	-13.3	-9.4
	y-direction	-18.7	-17.2	-16.0	-15.2	-13.5
	Resultant	28.9	30.8	26.7	26.4	27.9

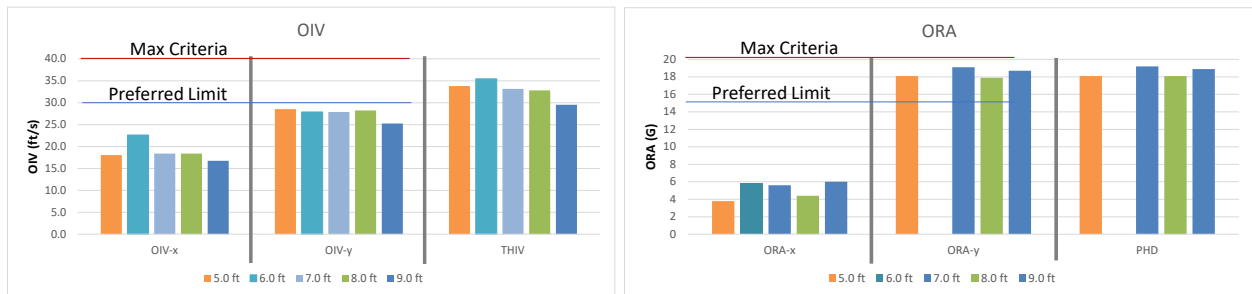


Figure 477. Graphical representation of OIV, THIV, ORA and PHD metrics for Test 4-21.

15.2.3.3 Results Summary for Test 4-21

The FEA results for *MASH* Test 4-21 on the 3-bar transition with 5.5-ft post spacing at the first bridge rail post indicated that the system would meet all structural adequacy, occupant safety and vehicle stability criteria according to *MASH* for Design Case 1 (i.e., with original system components). The barrier successfully contained and redirected the pickup with moderate damage to the system. There were no detached elements from the barrier that showed potential for penetrating the occupant compartment or presenting undue hazard to other traffic.

The vehicle remained upright and very stable throughout impact and redirection. The OIV and maximum ORA values were within critical limits specified in *MASH*. Design Case 1 was shown to meet *MASH* safety criteria; however, Design Case 2 with the larger HSS 5 x 4 x 5/16 lower rail is expected to result in lower rail deflections and improved overall crash performance compared to Design Case 1.

15.2.4 Test 4-22

For Test 4-22, three analysis cases were evaluated which involved two expansion splice gaps (i.e., $\frac{3}{4}$ -inch and 2-inch) and two different post designs (i.e., original and tapered posts). Those design details were shown previously in Figures 451 and 452, respectively. The three analysis cases included:

- Case 1 – $\frac{3}{4}$ -inch splice gap and original post design (i.e., non-tapered posts)
- Case 2 – $\frac{3}{4}$ -inch splice gap and tapered post design
- Case 3 – 2-inch splice gap and tapered post design

The critical impact point for all cases was 9 feet upstream of the expansion splice, as illustrated in Figure 478, which was adopted from the previous analysis of the original design in Section 10.4.1. The 10000S vehicle model corresponded to the Ford 800 with cargo bed height of 47.5 inches and gross-static weight of 22,198 lbs. The analyses were conducted for 0.7 seconds of the impact event, which was sufficient for the vehicle to redirect and exit the downstream end of the bridge rail system.

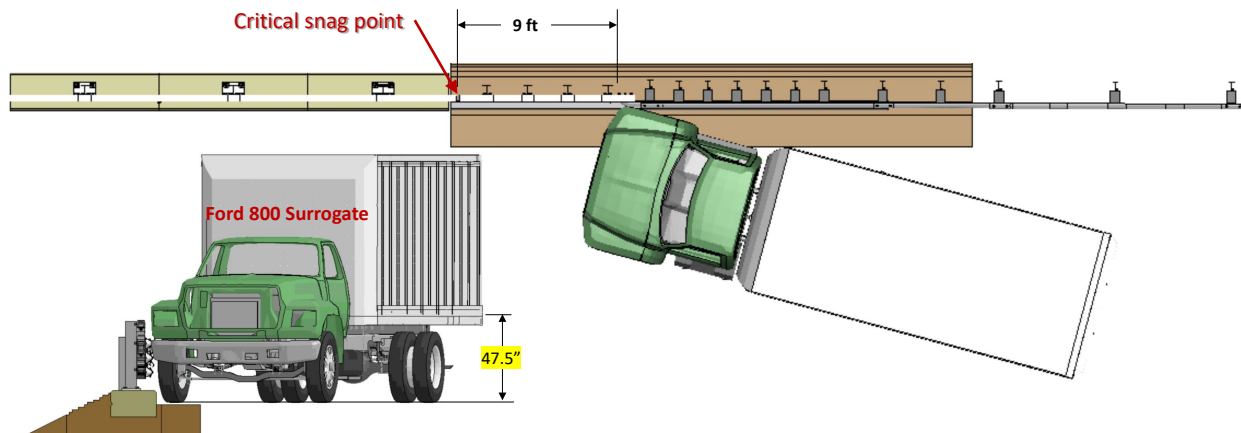


Figure 478. Critical impact point and 10000S vehicle selected for the Test 4-22 simulations.

15.2.4.1 Peak impact forces

In each case, the bottom of the cargo box snagged on the expansion splice but did not result in excessive forces or adverse performance of the system. As shown in Figure 479, the only significant snag was between the bottom of the cargo box and the top of the posts in Case 1, in which the tops of the posts were not tapered (i.e., original design). This result was very similar to that of the baseline case in Section 10.4. The bottom of the cargo box did not snag on the posts for Cases 2 and 3 in which the tops of the posts were tapered. The highest longitudinal and resultant impact forces occurred in Case 1 with magnitude of 44 kips, as shown in Figure 480. Cases 2 and 3 resulted in peak longitudinal forces of 34 and 39 kips, respectively. The lateral impact force for Cases 1-3 (i.e., 5-5-ft post spacing) were all very similar with magnitudes

ranging from 68-71 kips. The highest lateral impact force was 74 kips and occurred in the baseline case, which was expected since the closer post spacing results in a more rigid barrier.

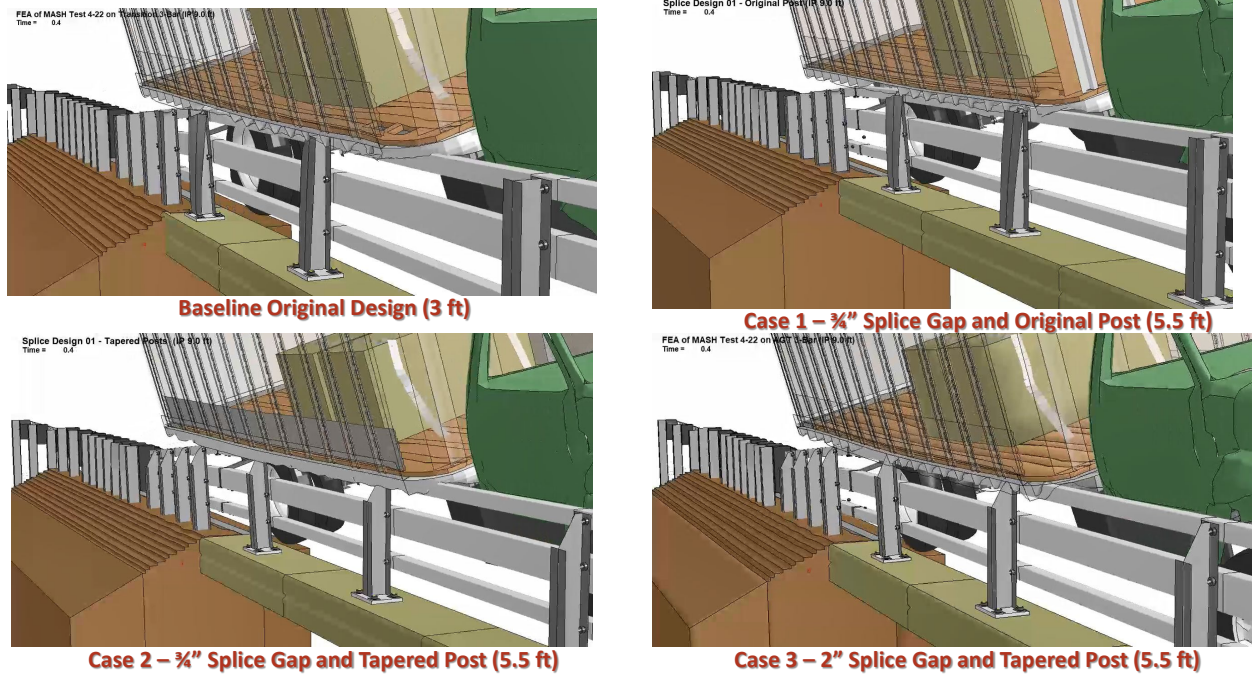


Figure 479. Images of the analysis results for Cases 1 – 3 compared to the baseline case at 0.4 seconds of the impact (cargo box transparent).

	Peak Forces (kips)		
	longitudinal	lateral	Resultant
Baseline Original	36.9	73.6	84
Case 1	43.8	68.1	96.2
Case 2	34.1	67.9	93.2
Case 3	38.6	71.3	90.7

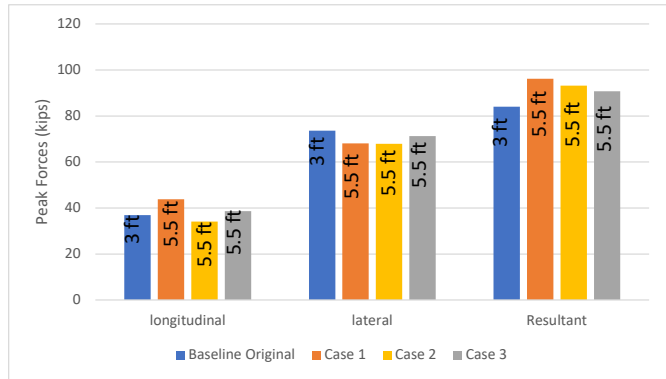


Figure 480. Peak impact forces on the barrier for Case 1 – 3 compared with baseline case.

15.2.4.2 Time History Data Evaluation

Acceleration-time histories and angular rate-time histories were collected at two locations on the vehicle: (1) inside the cargo box at the center of gravity of the vehicle, and (2) inside the cabin of the truck, as previously illustrated in Figure 111. Figures 481 through 483 show the longitudinal, transverse, and vertical acceleration-time histories, respectively, computed from near the center of gravity of the vehicle which falls inside the cargo-box near the front of the ballast.

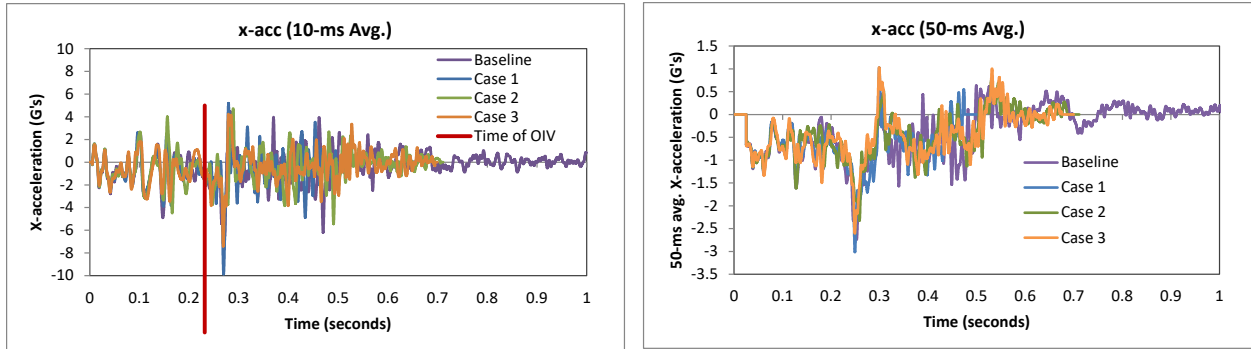


Figure 481. 10- and 50-millisecond average X-acceleration from FEA of Test 4-22 for Case 1-3 on the 3-bar transition with 5.5-ft post spacing compared with baseline (c.g. accelerometer).

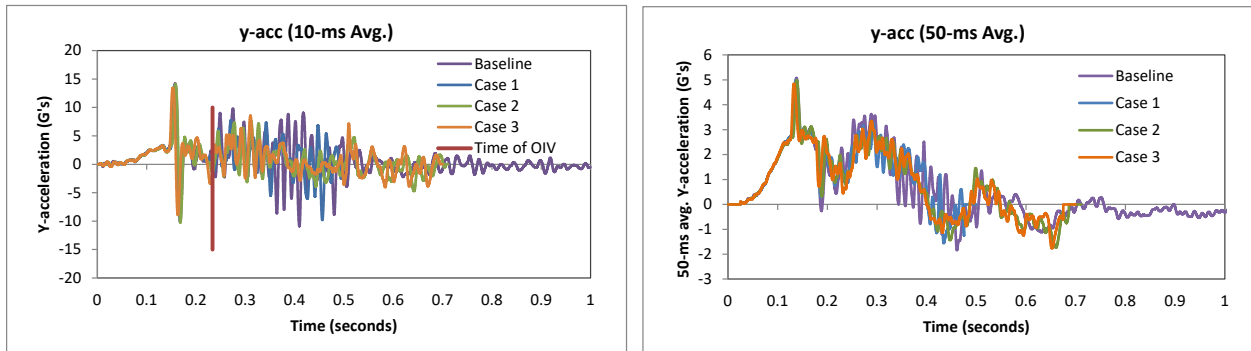


Figure 482. 10- and 50-millisecond average Y-acceleration from FEA of Test 4-22 for Case 1-3 on the 3-bar transition with 5.5-ft post spacing compared with baseline (c.g. accelerometer).

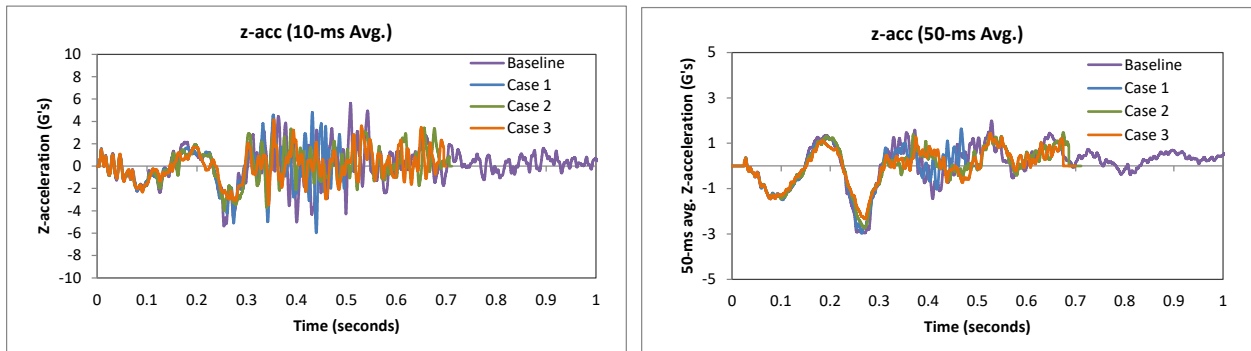


Figure 483. 10- and 50-millisecond average Z-acceleration from FEA of Test 4-22 for Case 1-3 on the 3-bar transition with 5.5-ft post spacing compared with baseline (c.g. accelerometer).

Figures 484 through 486 show the longitudinal, transverse, and vertical acceleration-time histories, respectively, computed from the inside the cabin of the vehicle; Figures 487 through 489 show the comparison of the angular rates and angular displacements about the x-, y-, and z-axis from the c.g. location. The comparison of the time-history data show that the increase in post span as well as the increase in splice gap do not adversely affect the overall accelerations of the vehicle during impact, i.e., the results were very similar for all analysis cases.

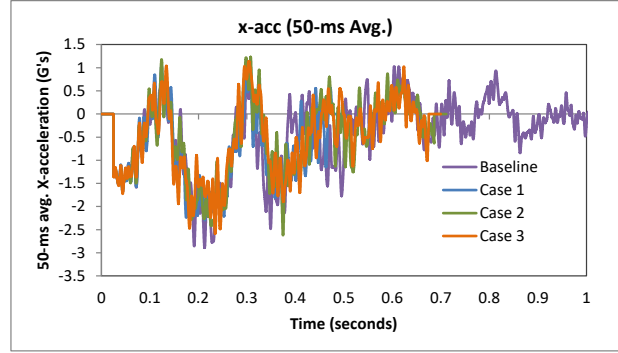
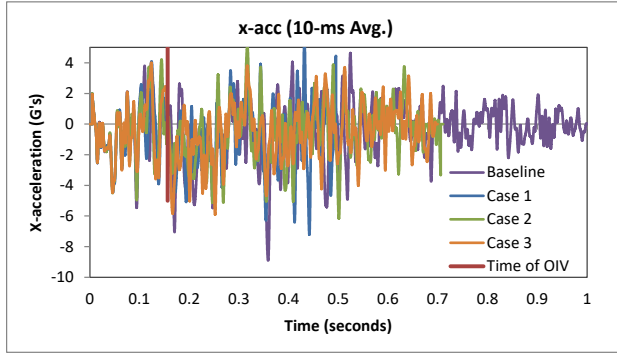


Figure 484. 10- and 50-millisecond average X-acceleration from FEA of Test 4-22 for Case 1-3 on the 3-bar transition with 5.5-ft post spacing compared with baseline (cabin accelerometer).

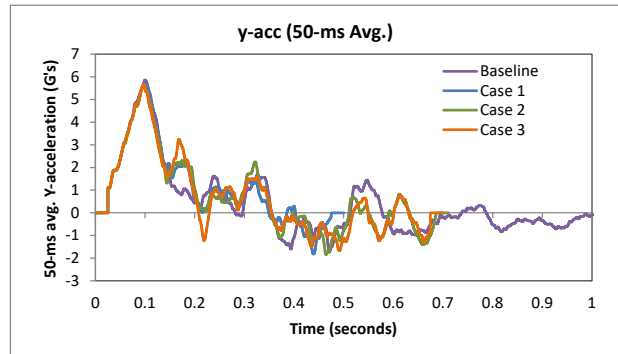
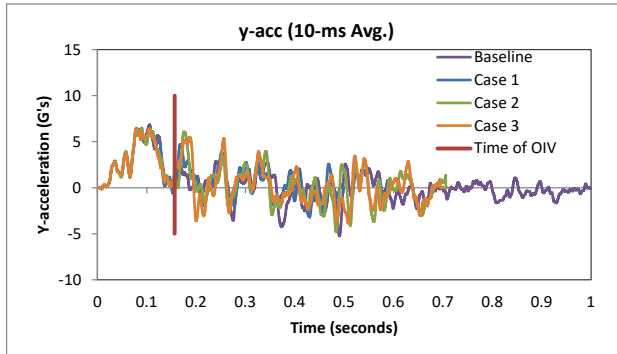


Figure 485. 10- and 50-millisecond average Y-acceleration from FEA of Test 4-22 for Case 1-3 on the 3-bar transition with 5.5-ft post spacing compared with baseline (cabin accelerometer).

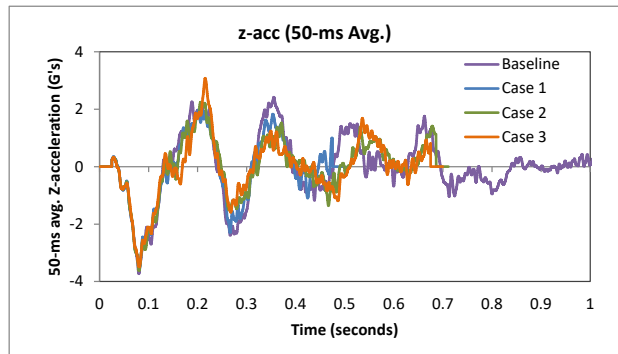
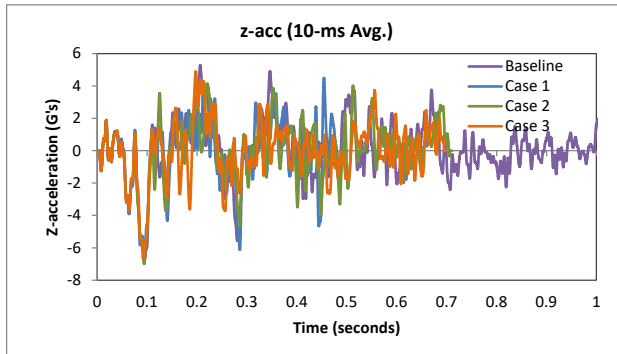


Figure 486. 10- and 50-millisecond average Z-acceleration from FEA of Test 4-22 for Case 1-3 on the 3-bar transition with 5.5-ft post spacing compared with baseline (cabin accelerometer).

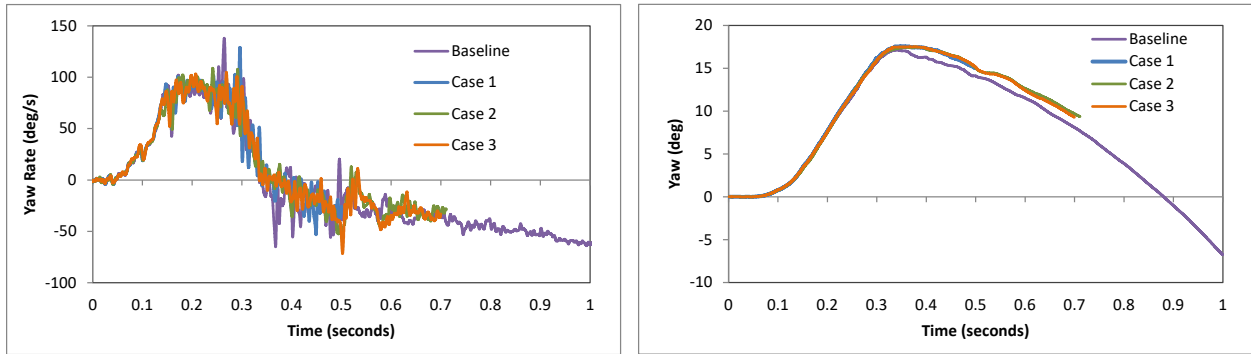


Figure 487. Yaw rate and yaw angle time-history from FEA of Test 4-22 for Case 1-3 on the 3-bar transition with 5.5-ft post spacing compared with baseline (c.g. accelerometer).

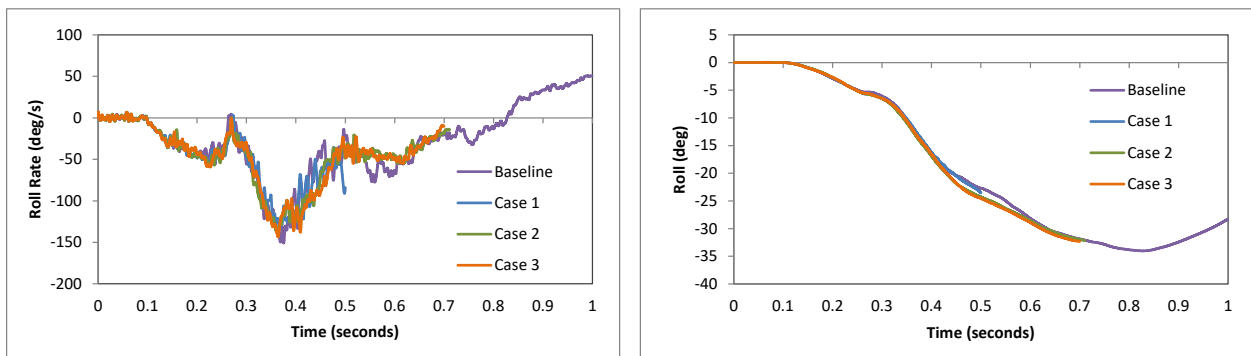


Figure 488. Roll rate and roll angle time-history from FEA of Test 4-22 for Case 1-3 on the 3-bar transition with 5.5-ft post spacing compared with baseline (c.g. accelerometer).

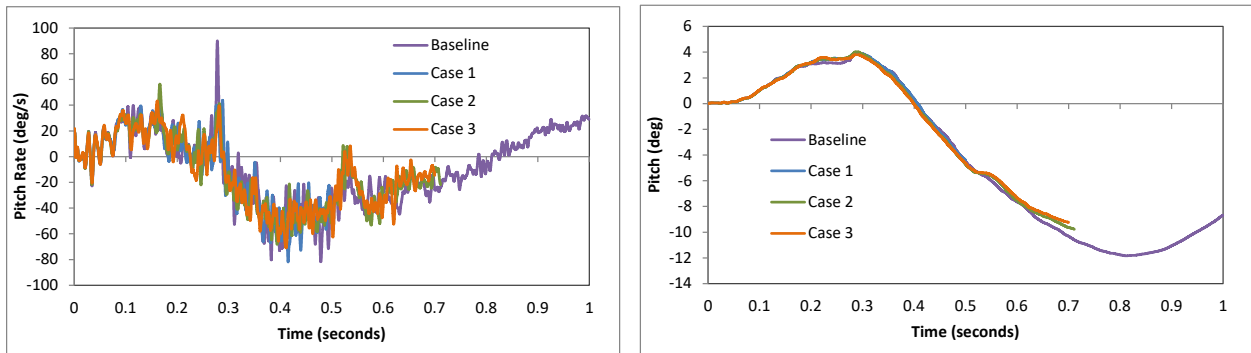


Figure 489. Pitch rate and pitch angle time-history from FEA of Test 4-22 for Case 1-3 on the 3-bar transition with 5.5-ft post spacing compared with baseline (c.g. accelerometer).

15.2.4.3 Damages to the Barrier

Figure 490 shows the deflection-time history of the rail at the expansion splice for Cases 1 through 3 compared with the baseline case, and Figure 491 shows peak dynamic and permanent lateral deflection values. The maximum dynamic deflection was 6 inches at the top rail expansion splice (i.e., 2nd peak) and occurred for Case 2 during the backslap of the rear tandem axel against the barrier. The maximum permanent deflection for that case was 4 inches at the same location. The maximum dynamic and permanent for the baseline case (i.e., post spacing 3 ft) was 4 inches and 2.8 inches, respectively.

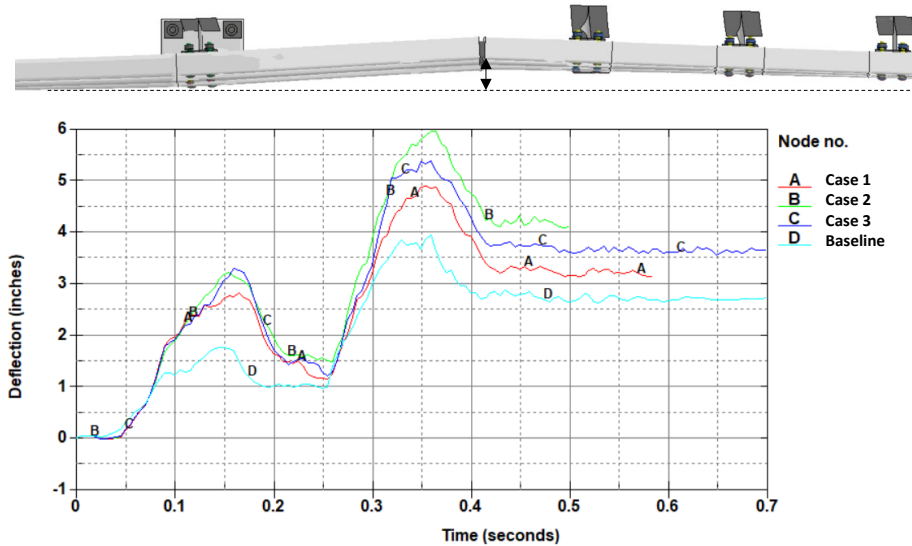


Figure 490. Deflection-time history at expansion splice for Cases 1-3 compared with baseline case.

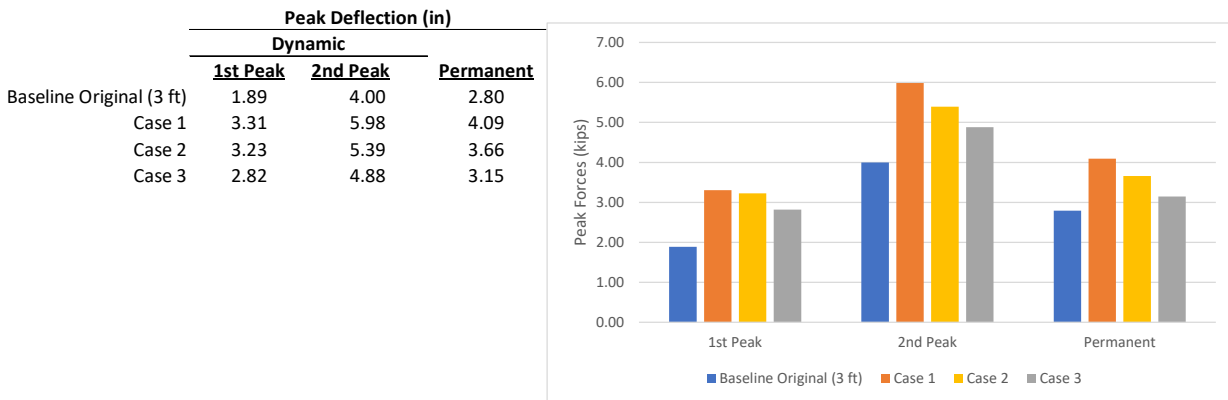


Figure 491. Peak lateral deflections of the barrier for Cases 1-3 compared with baseline case.

Figure 492 shows contours of true effective plastic strains on the steel components of the transition and bridge rail for each of the analysis cases. The damages to the baseline case and Case 1 were primarily limited to the top of Post 1 of the transition and to the three bridge rail posts. The damage to the posts were due to the bottom of the cargo-box snagging on the top of the posts. This caused torque rotation and lateral deformation of the posts. The damages to the posts were negligible for Case 2 and 3, which included the taper at the top of the post. A closeup view of the damages for the two different post designs is shown in Figure 493. The plastic

deformations of the transition rail elements were minimal for all cases. There was also soil displacement at transition Posts 1 through 6 for all cases.

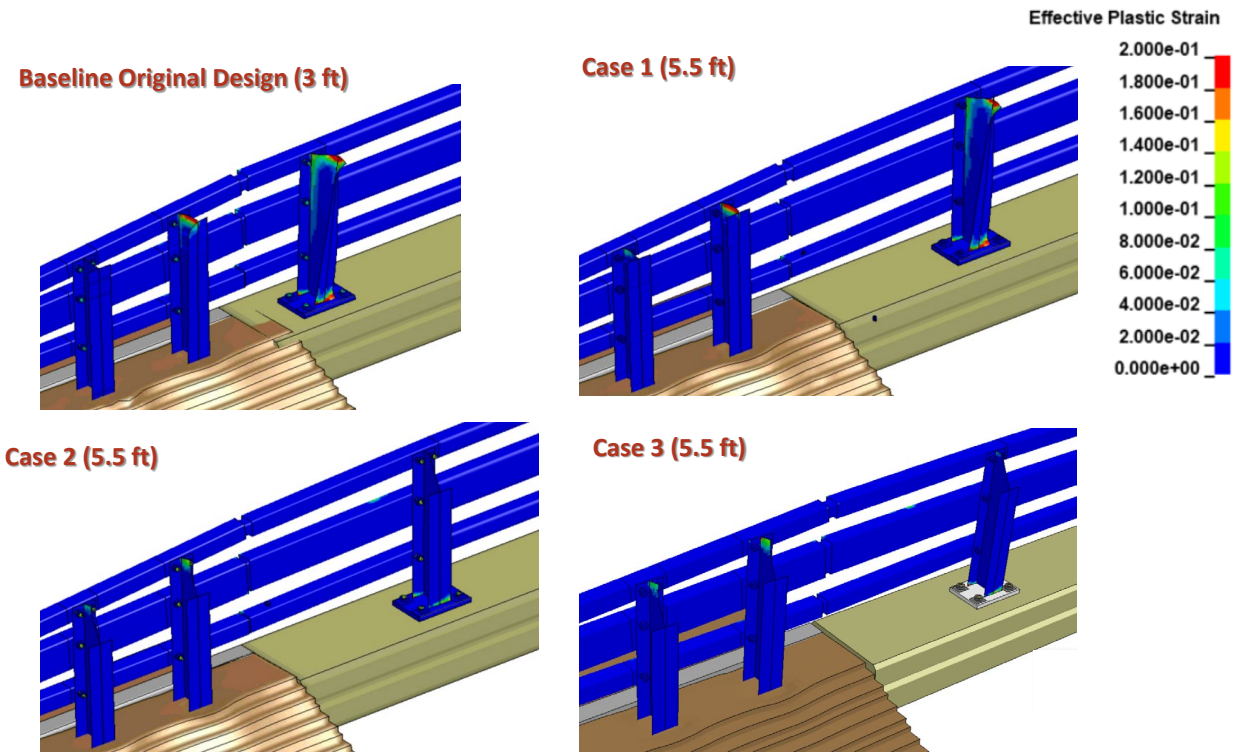


Figure 492. Contour plot of effective plastic strain for Cases 1-3 compared with baseline case.

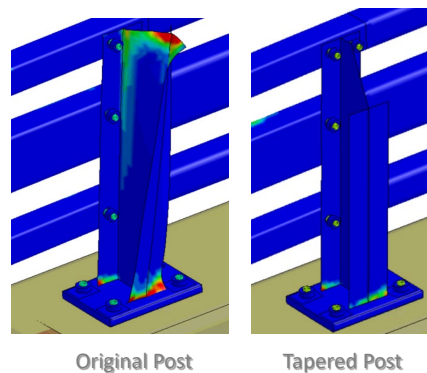


Figure 493. Typical damage to Post 1 of the bridge rail for original (non-tapered) and modified (tapered) post designs.

15.2.4.4 Results Summary for Test 4-22

The FEA results for *MASH* Test 4-22 on the 3-bar transition with 5.5-ft post spacing at the first bridge rail post indicated that the system would meet all structural adequacy, occupant safety and vehicle stability criteria according to *MASH* for all design cases evaluated. The barrier successfully contained and redirected the 10000S vehicle with moderate damage to the system. There were no detached elements from the barrier that showed potential for penetrating the occupant compartment or presenting undue hazard to other traffic. The analyses were

terminated before post-impact stability could be determined, but the vehicle attitude at termination (i.e., 0.7 seconds) was essentially the same for all cases, and it was determined in Section 10.4.9 that the baseline case would likely result in the vehicle rolling over onto its side. It is preferred that the vehicle remain upright, but not required in *MASH*.

It is noted that the wheels of the SUT model do not include protruding lug bolts (which are common on many SUT vehicles); therefore, snag from lug bolts was not evaluated. The longitudinal impact force on the barrier increased approximately 19% due to the increase in post spacing with the non-tapered posts (43.8 vs. 36.9 kips); but was slightly reduced for the tapered posts (34.1 vs. 36.9 kips). The lateral force was reduced with the increase in post spacing, while the resultant force was higher for the increased post spacing cases; the highest resultant force occurred for Case 1 with the non-tapered posts (96.2 vs. 84 kips).

The maximum lateral deflection occurred at the expansion splice in all cases. The lateral deflection was higher for 5.5-ft post spacing compared to the baseline with 3-ft post spacing (i.e., 6" vs. 4.3"). The highest deflection occurred for the 5.5-ft spacing case with non-tapered posts. The plastic deformations of the transition components were very similar to the baseline case which were low to moderate. The plastic deformations of the bridge rail for the non-tapered posts was significant due to the bottom of the cargo-box snagging on the tops of the posts, while the deformations for the tapered post cases were minimal.

15.2.5 Conclusions and Recommendations

The FEA simulations of the NETC 3-bar transition with an increased post spacing of 5.5 feet was shown to meet *MASH* TL4 performance criteria. The increased spacing generally resulted in increased rail deflections, increased longitudinal forces and accelerations and reduced lateral forces and accelerations. However, tapering the tops of the posts resulted in a notable reduction in magnitude for longitudinal forces during Test 4-22 (SUT test) by mitigating snag on the backs of the post.

The 2-inch wide expansion splice joint did not result in significant snag in the FEA, but the research team believes a potential exists – particularly for reverse-direction impact scenarios (not evaluated). Previous full-scale tests on a similar system with 3¾-inch splice gap resulted in significant snag for the pickup test. [Buth99b] It is therefore recommended that the splice designs be revised to minimize the amount of internal gap-space between the splice tube and the main rails.

It is also recommended that the lower rail for the bridge rail, and consequently the lower rail of the transition, be changed to the HSS 5x4x5/16. The larger rail resulted in a 25% decrease in rail deflection for the small car test compared to the baseline analysis with HSS4x4x1/4, and a 17.9% decrease in peak longitudinal acceleration.

15.3 Modified NETC 4-Bar Bridge Rail with W8x28 Posts

The objective of this part of the study was to use FEA to determine if increasing the size of the bridge rail post from W6x25 to W8x28 would improve crash performance for *MASH* Test 4-12. The evaluation of the baseline 4-bar bridge rail was performed in Section 11 where FEA simulations of Test 4-12 showed that the 4-bar bridge rail resulted in more severe damage to the post, base plate and curb than the 2-bar and 3-bar designs. The W8x28, which is a readily available shape, has a plastic modulus that is approximately 40% higher than the W6x25

resulting in greater static strength calculations (e.g., LRFD ch. 13). The lengths of the flange and web of the W8x28 are also longer than that of the current post design which will increase weld strength. Further, the larger post requires that the base plate be extended 2 inches which should reduce the tensile forces on the front anchor bolts but increase the chance of pushout shear failure of the concrete deck at the back of the post.

The finite element model of the NETC 4-bar bridge rail developed in Task 5 was updated for this analysis. The changes to the design are illustrated in Figure 494. The W6x25 posts were replaced with W8x28 posts, and the posts were tapered at the top. The 12"x10"x1" baseplate was replaced with a 14"x12.75"x1" baseplate for proper fitting of the larger post, and the anchor bolts were repositioned accordingly. For the analysis, the position of the front face of the barrier was not changed nor was the curb/deck size. Therefore, the resulting distance from the anchor bolts on the backside of the posts to the back edge of the deck was reduced from 7.625" to 6".

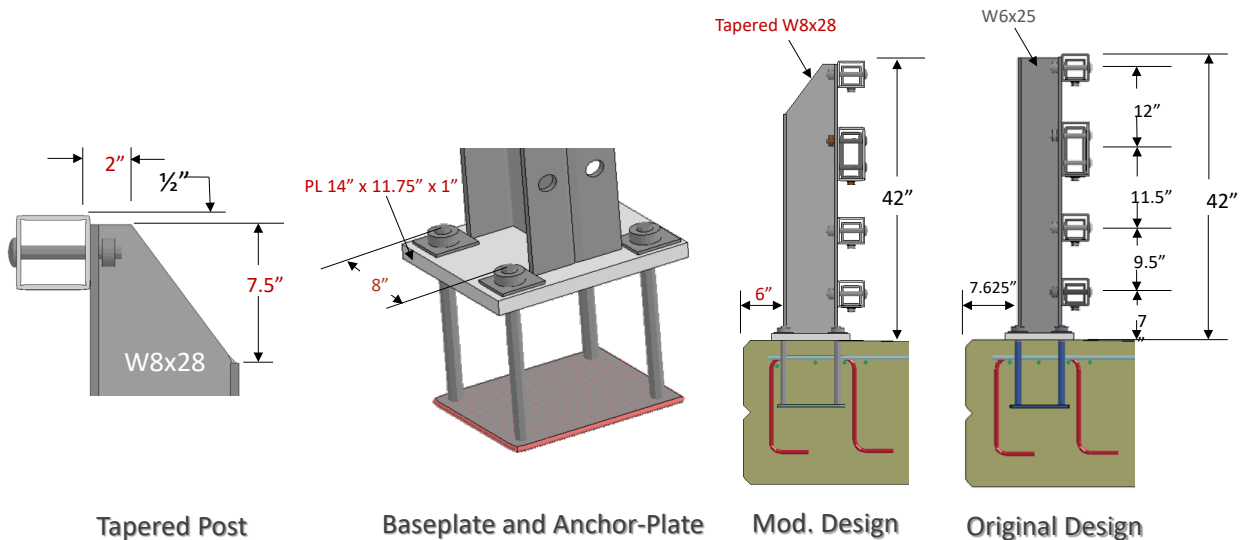


Figure 494. Design modifications for the 4-bar bridge rail.

15.3.1 Test 4-12

The 10000S vehicle model corresponded to the Ford 800 with cargo bed height of 47.5 inches and gross-static weight of 22,198 lbs. The critical impact condition for *MASH* Test 4-12 was selected based the *MASH* recommended CIP for rigid barrier tests. The target impact point was 5.0 feet upstream of Post 7, as shown in Figure 495 and was selected to maximize loading on the post.[*AASHTO16*] This impact condition was consistent with the analysis performed on the baseline design in Section 11.3. The vehicle was backed up to the face of the sidewalk curb, as shown in Figure 495(a), as the initial start point of the impact event. After crossing the curb, the vehicle struck the bridge at 4.4 feet upstream of Post 7, as shown in Figure 495(b). The analyses were conducted for 1.5 seconds of the impact event. The results from the analysis is presented below and is compared to the baseline analysis on the original design.

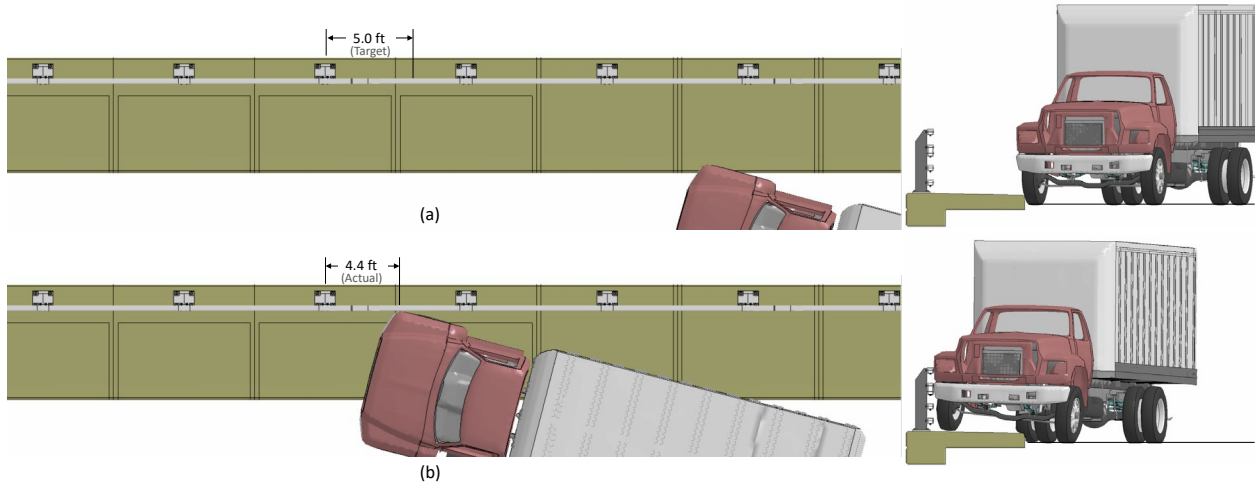


Figure 495. (a) Target and (b) actual impact point for Test 4-12 on the modified NETC 4-Bar bridge rail.

Sequential views from the FEA simulations of the baseline (original) and the modified designs are shown in Figure 496 from a downstream viewpoint. The overall attitude of the vehicle was very similar for the two cases through 0.7 seconds of the impact, while the modified design resulted in better vehicle stability during the latter stages of the post-impact trajectory.

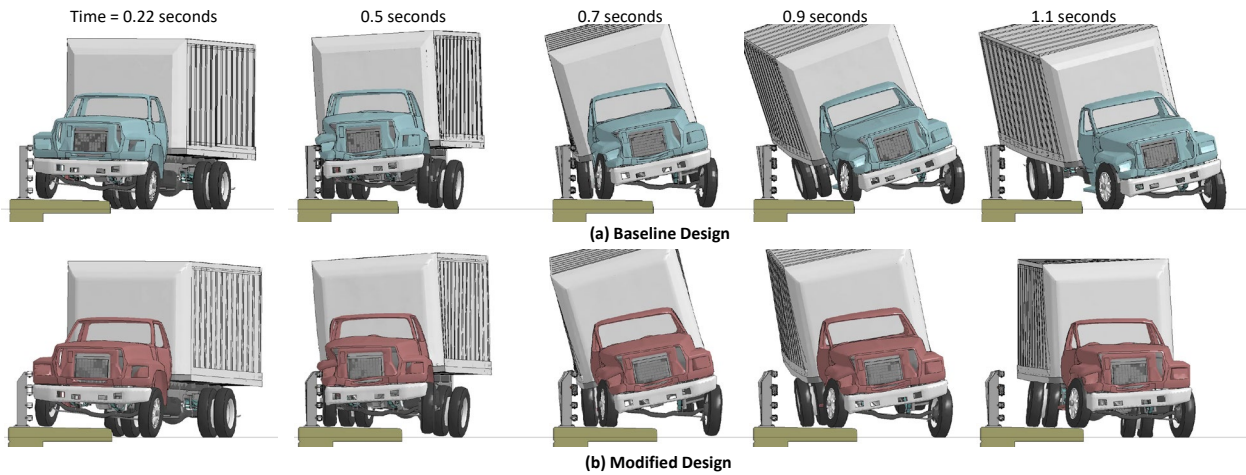


Figure 496. Sequential views for analyses of (a) baseline design and (b) modified design.

15.3.1.1 Time History Data Evaluation

Acceleration-time histories and angular rate-time histories were collected at two locations on the vehicle: (1) inside the cargo box at the center of gravity of the vehicle, and (2) inside the cabin of the truck, as shown previously in Figure 111. Figures 497 through 499 show the longitudinal, transverse, and vertical acceleration-time histories, respectively, computed from the cabin location for the baseline and modified design cases.

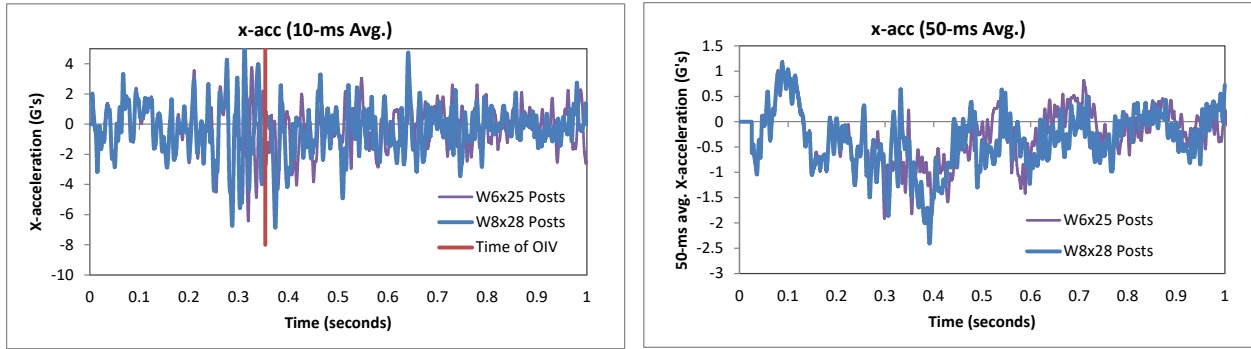


Figure 497. 10- and 50-millisecond average X-acceleration from FEA of Test 4-12 on the baseline and modified NETC 4-bar bridge rail (cabin accelerometer).

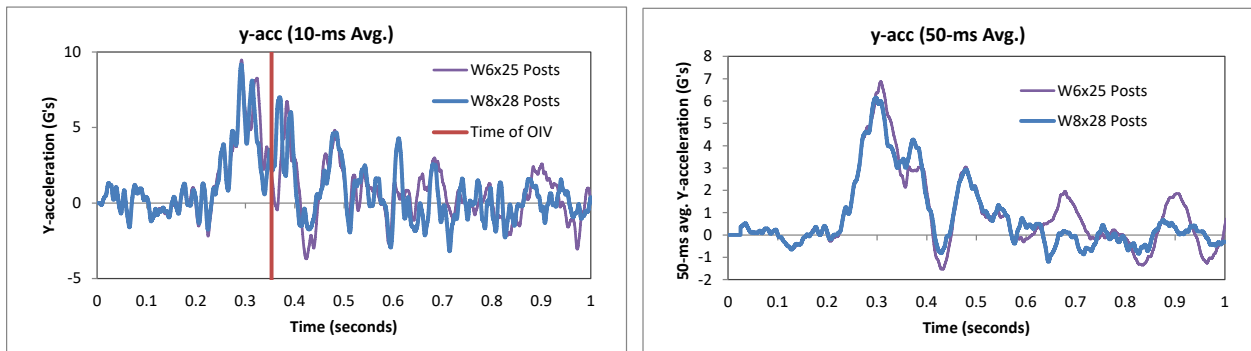


Figure 498. 10- and 50-millisecond average Y-acceleration from FEA of Test 4-12 on the baseline and modified NETC 4-bar bridge rail (cabin accelerometer).

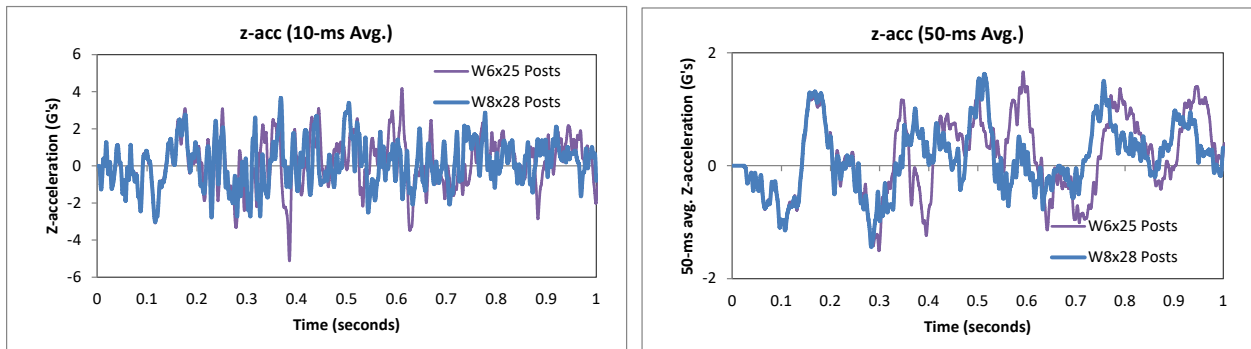


Figure 499. 10- and 50-millisecond average Z-acceleration from FEA of Test 4-12 on the baseline and modified NETC 4-bar bridge rail (cabin accelerometer).

Figures 500 through 502 show the longitudinal, transverse, and vertical acceleration-time histories, respectively, computed from near the center of gravity of the vehicle which falls inside the cargo-box near the front of the ballast; Figures 503 and 505 show the comparison of the angular rates and angular displacements about the x-, y-, and z-axis from the c.g. location. The comparison of the time-history data show that the larger W8x28 posts does not adversely affect the overall accelerations of the vehicle during impact; the results were very similar for all analysis cases. The modified design did, however, result in more stable yaw, pitch and roll behavior of the vehicle during impact and redirection.

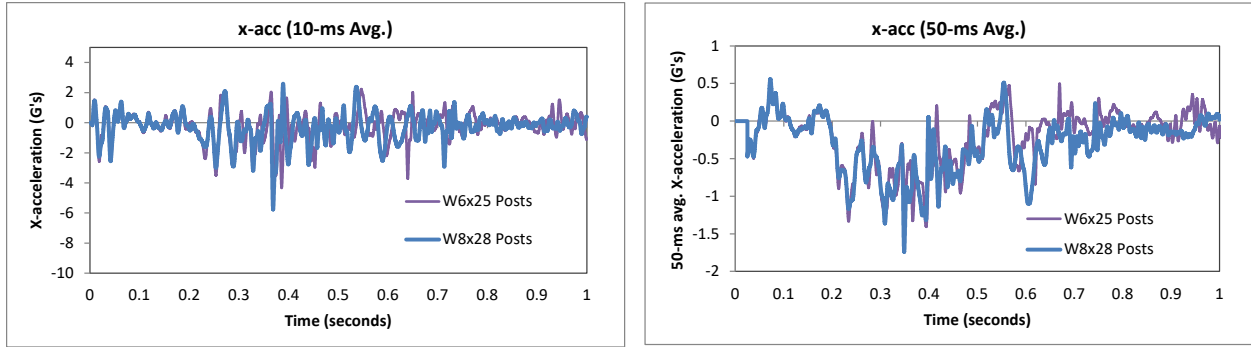


Figure 500. 10- and 50-millisecond average X-acceleration from FEA of Test 4-12 on the baseline and modified NETC 4-bar bridge rail (c.g. accelerometer).

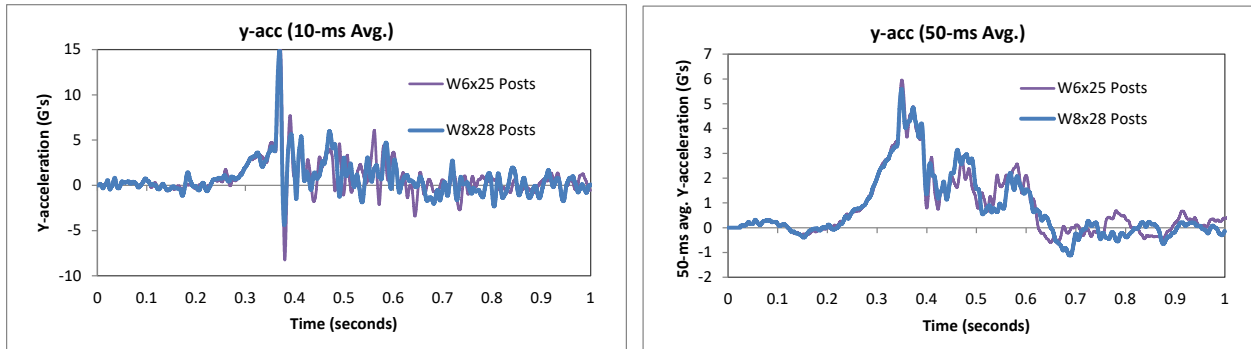


Figure 501. 10- and 50-millisecond average Y-acceleration from FEA of Test 4-12 on the baseline and modified NETC 4-bar bridge rail (c.g. accelerometer).

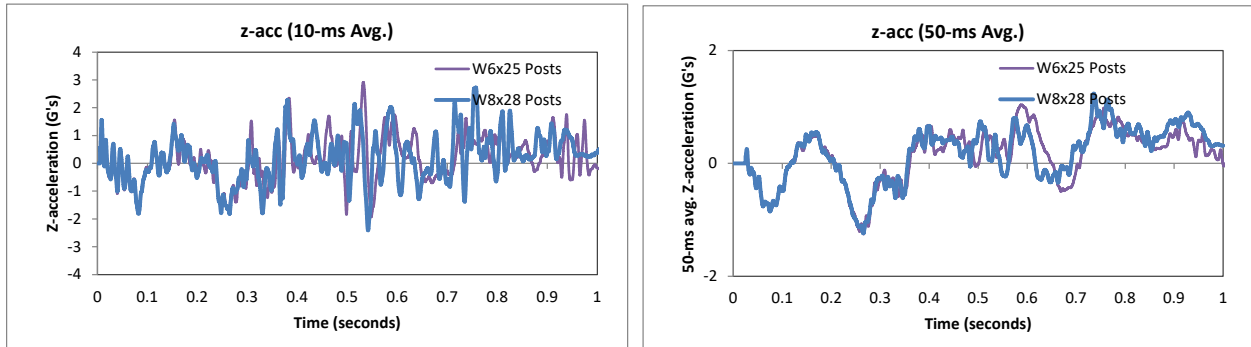


Figure 502. 10- and 50-millisecond average Z-acceleration from FEA of Test 4-12 on the baseline and modified NETC 4-bar bridge rail (c.g. accelerometer).

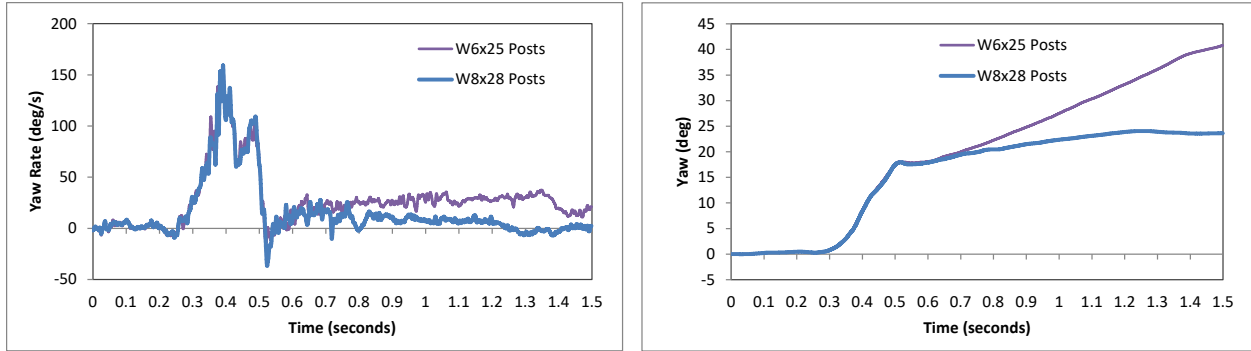


Figure 503. Yaw rate and yaw angle time-history from FEA of Test 4-12 on the baseline and modified NETC 4-bar bridge rail (c.g. accelerometer).

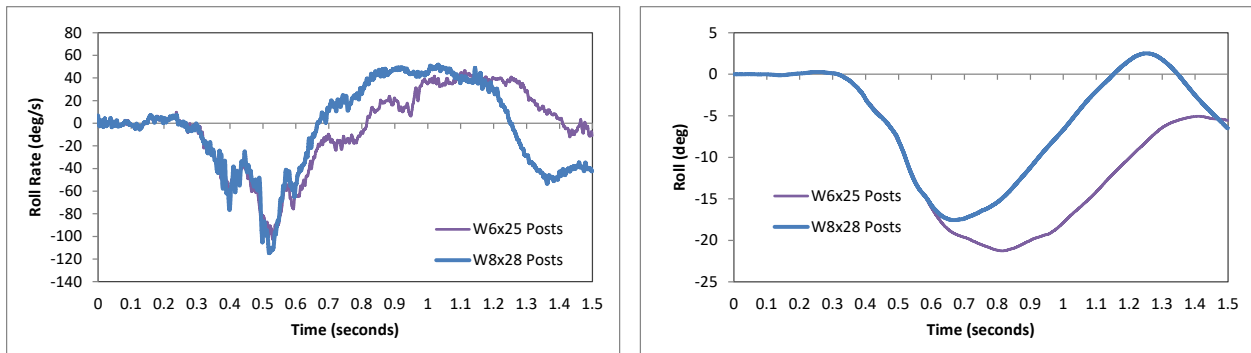


Figure 504. Roll rate and roll angle time-history from FEA of Test 4-12 on the baseline and modified NETC 4-bar bridge rail (c.g. accelerometer).

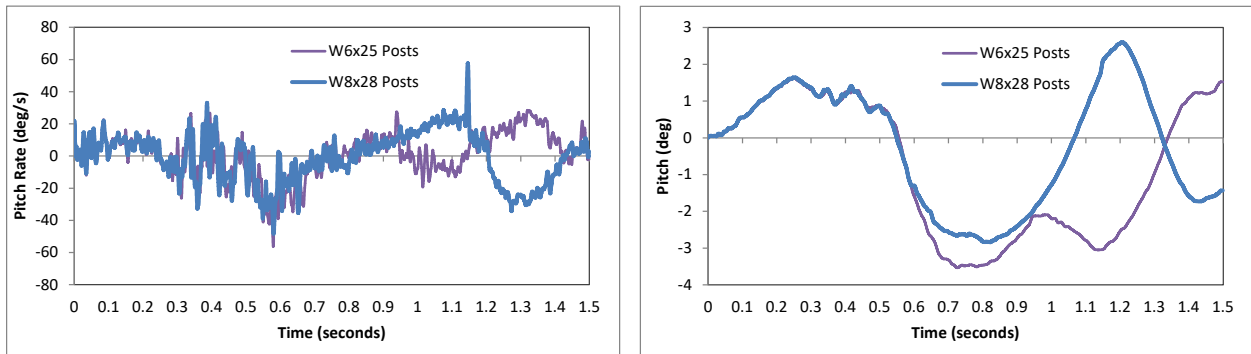


Figure 505. Pitch rate and pitch angle time-history from FEA of Test 4-12 on the baseline and modified NETC 4-bar bridge rail (c.g. accelerometer).

15.3.1.2 Peak impact forces

In both analysis cases, the cargo box did not pass over the top of the bridge rail. Consequently, the effect of post taper on the modified design could not be directly evaluated, since there was no potential for contact with the top of the posts. The impact forces on the barrier were only slightly higher for the modified design with stiffer W8x28 post. The highest 25-ms average longitudinal impact force was 14.4 and 17.6 kips for the baseline and modified designs, respectively. The increase in longitudinal force occurred at approximately 0.37 seconds and was due to the lower rail on the outside edge of the cargo-box snagging on top of the rail splice, as indicated in Figure 506(a). The highest 25-ms average impact force in the transverse

direction was 110.2 and 125.8 kips for the baseline and modified designs, respectively. The higher lateral force for the modified design is consistent with the increased stiffness of the W8x28 posts.

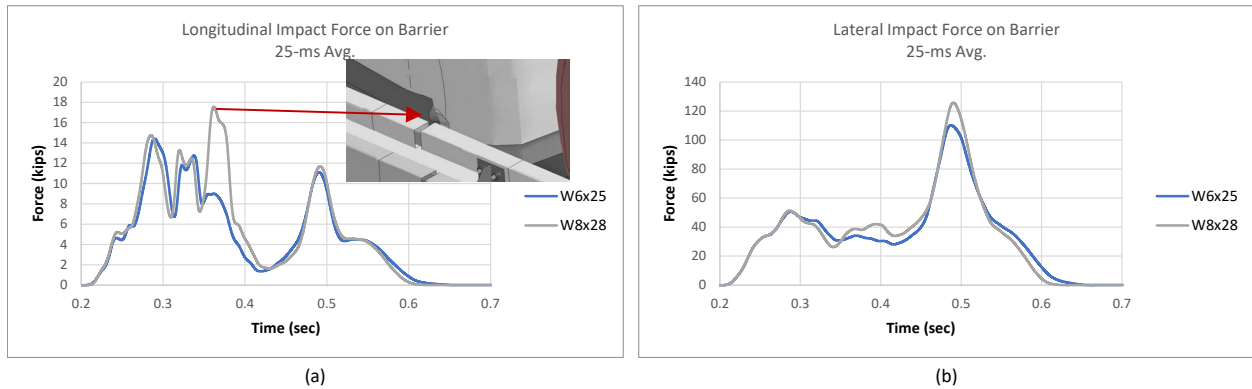


Figure 506. (a) longitudinal and (b) lateral impact force-time history for the baseline and modified design cases.

15.3.1.3 Damages to the Barrier

Figure 507 shows images of the barrier at the time of maximum deflection with a contour plot of lateral displacement on the rail elements. The maximum dynamic deflection was 6.5 inches for the modified design, compared to 8.15 inches for the original design, and occurred on the top rail at the splice connection upstream of Post 7 when the rear of the cargo-box impacted the railing. The maximum permanent deflection for the modified design was 3.7 inches, compared with 5.8 inches for the original design.

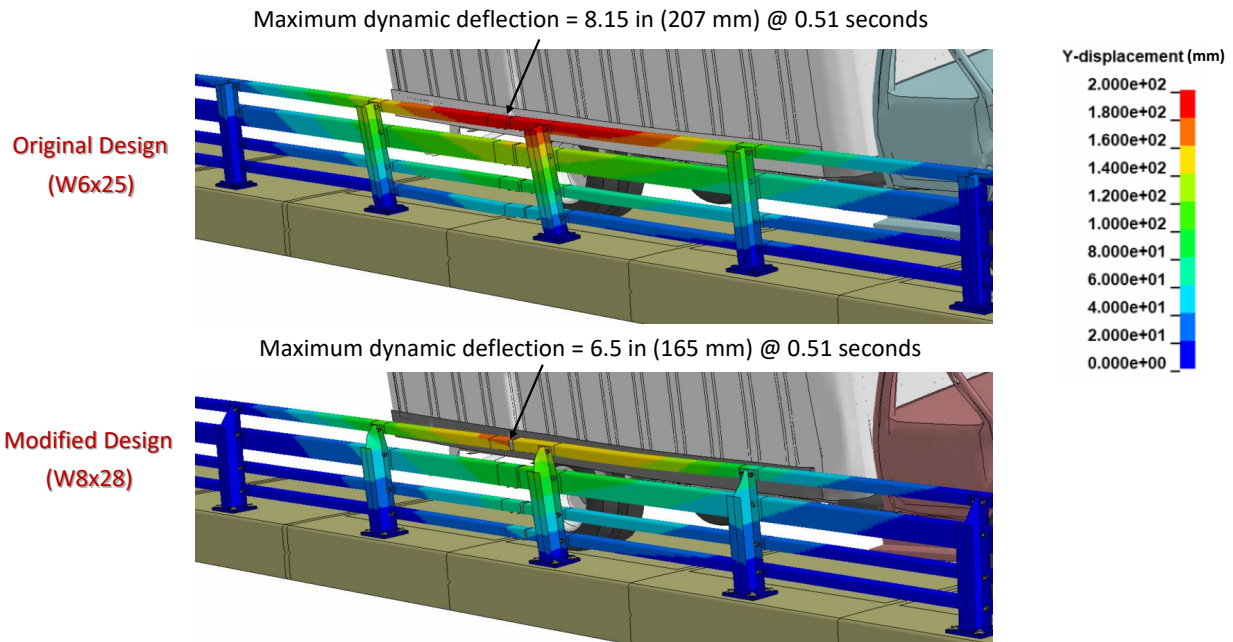


Figure 507. Contour plot of lateral displacement for the bridge rail from Test 4-12 at the time of maximum deflection for the original and modified design cases.

Figure 508 shows contours of true effective plastic strains on the bridge rail post and baseplate for the two analysis cases at Post 7. The post flanges buckled near the welded

connection to the baseplate, and the front-center edge of the baseplate was deflected upward. The damage to the post and base plate was reduced significantly for the modified design with W8x28 Posts. The vertical dynamic deflection of the base plate was reduced 8% (i.e., 1.01 vs. 1.11 inches), and the permanent deflection was reduced 21% (i.e., 0.65 vs. 0.82 inches). The effective plastic strain at the base of the post was reduced 34% from 0.33 to 0.22.

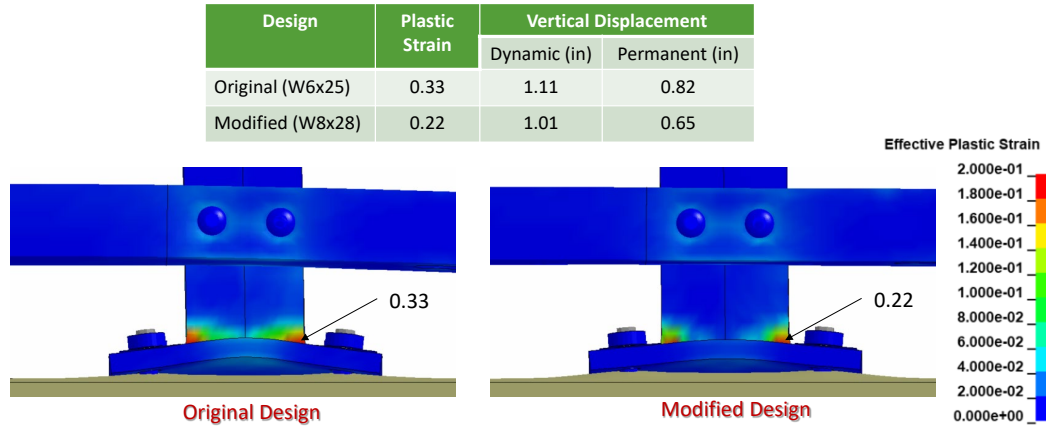


Figure 508. Contours of effective plastic strain on the bridge rail posts and baseplates for the original and modified design cases.

Figure 509 and Figure 510 show contours of 1st principal strain with contours cut off at strains of 0.1 for peak dynamic and permanent strains, respectively. Both the original and modified design cases resulted in notable concrete damage at the critical post; however, the damage was increased for the modified design. The maximum dynamic strain in the concrete was 11.5% higher for the modified design (e.g., increase from 0.079 to 0.099); while the maximum permanent strain in the concrete increased 5.5% from 0.054 to 0.057. The strain values for the modified design indicated significant crack opening in concrete at front anchor bolts at Post 7.

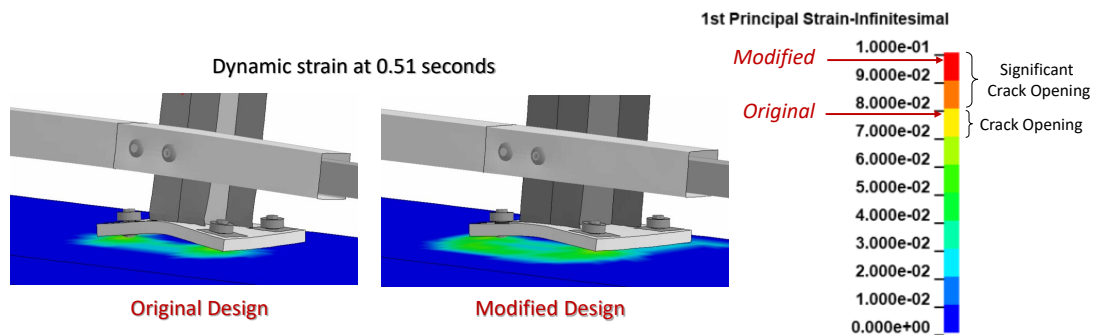


Figure 509. Contours of 1st principal strains for concrete at the critical post for the original and modified design cases at time of peak dynamic strain.

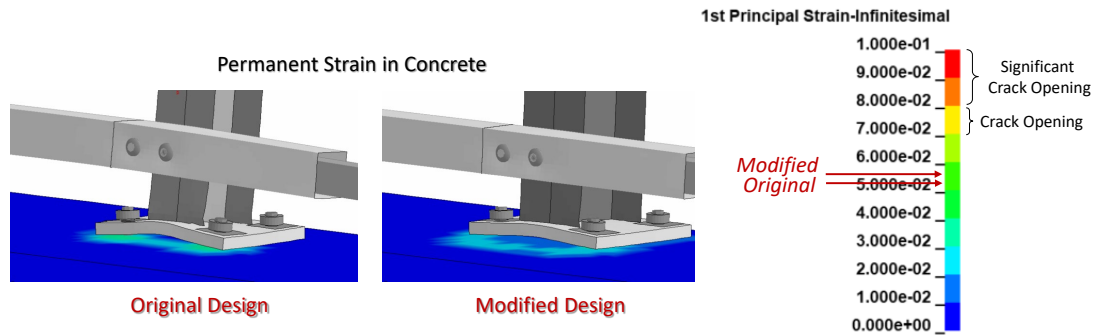


Figure 510. Contours of 1st principal strains for concrete at the critical post for the original and modified design cases (permanent strains).

15.3.2 Conclusions and Recommendations

The FEA results for the modified NETC 4-bar bridge rail system with W8x28 posts indicated that the system would meet *MASH* TL4 performance criteria. The barrier adequately contained and redirected the 10000S vehicle (single unit truck) with moderate damage to the bridge rail. Vehicle stability for the modified design was slightly improved compared to original design. The maximum roll angle at the c.g. of the SUT was 17.6 degrees, compared with 21.3 degrees for the original design. The maximum pitch angle was 2.8 degrees, compared with 3.5 degrees for the original design. The damage to the barrier for the modified design compared to original design included:

- Increased damage to concrete curb around the front anchor bolts (probable large cracks).
- Reduced plastic deformation of posts and base plates.
- Reduced maximum dynamic barrier deflection (6.5” vs. of 8.2”).

Based on the results of this analysis, it is recommended that the deck and anchorage should be strengthened at the post locations, such as increasing the reinforcement in the concrete. Test 4-10 and Test 4-11 simulations were not performed for the modified design; however, in addition to the stronger post, it is also recommended that the second rail from the bottom be strengthened to minimize pocketing for the small car (e.g., HSS 5x4x5/16). Although the snag at the splice did not adversely affect the performance of the system, it is also recommended that the splice design be revised to minimize the amount of internal gap-space between the surfaces of the splice tubes and the main rails to alleviate potential snags for both passenger and commercial vehicle impacts.

16 SUMMARY OF DESIGN EVALUATIONS

As stated in Section 1 of this report, the objectives of this project were to: (1) review existing NETC bridge rail designs and assess performance aspects to determine preliminary *MASH* compliance/equivalency, (2) review current standard details and specifications for NETC style bridge rails and transitions used by MaineDOT, NHDOT, RIDOT and VTrans to identify differences in material specifications and dimensional details and (3) evaluate the crash performance of the NETC bridge rail and approach guardrail transition (AGT) designs using finite element analysis (FEA) computer simulation.

16.1 Summary of *MASH* LRFD Strength and Rail-Geometric Calculations

Existing NETC bridge rail designs were initially reviewed to determine preliminary *MASH* equivalency based on strength and geometry of the railing according to AASHTO *LRFD Bridge Design Specifications* (BDS) and *MASH* loading. The results of that assessment indicated that the height of all systems met minimum height requirements for their specific *MASH* level (e.g., TL3 for the 2-bar and TL4 for all others). Regarding *post set back distance*, *max vertical openings*, and *contact width*, the 2-bar and 3-bar systems meet the preferred geometric criteria when the curb height is 9 inches (e.g., NETC and MaineDOT) but not when the curb height is 7 inches (e.g., NHDOT, RIDOT and VTrans). For the 7-inch curb option the *ratio of rail contact width to height* does not meet preferred criteria but does fall within the range of other systems that have met NCHRP Report 230, NCHRP Report 350 and *MASH* full-scale crash test performance. [AASHTO12; Dobrovolny17] For *MASH* equivalency assessments, however, the criteria established in NCHRP Project 22-07 (395) required that the designs meet preferred values. [Dobrovolny17] The 4-bar systems also do not meet the preferred criteria for the *ratio of contact width to barrier height* but, like the 2-bar and 3-bar systems, fall within the range of other systems that have been successfully crash tested regarding that metric. It should be noted that these geometric relationships have not yet been established for *MASH* test cases but are still commonly applied to bridge rail design. For example, the *MASH* equivalency assessment criteria established in NCHRP Project 22-07 (395) required that bridge rail designs meet preferred rail geometric criteria as currently defined in the AASHTO LRFD BDS in order to be grandfathered to *MASH*. [Dobrovolny17]

The strength of each of the NETC railing designs was evaluated using LRFD calculations with an equivalent *MASH* transverse load of 71 kips and 80 kips for *MASH* TL3 and TL4, respectively, based on work performed by TTI researchers (see Table 8 and Table 9). [Dobrovolny17] Based on the assessment, it was determined that the NETC 2-bar and 3-bar designs would likely meet *MASH* TL3 and TL4 strength requirements, respectively. All sidewalk-mounted 4-bar designs were considered marginal regarding strength criteria; the Maine and Rhode Island designs (with 5,000 psi concrete) just met strength requirements, while the strength of the New Hampshire design (with 4,000 psi concrete) was just under the *MASH* TL4 design criteria. Since formal strength criteria for bridge rails have not yet been established for *MASH*, these results are considered as preliminary estimates regarding *MASH* performance.

16.2 Comparison of Design Detail Specifications Summary

A critical review of the NETC style bridge rail and transition design specifications used by the NETC pooled fund states was conducted. This effort was performed for two purposes: (1) to identify differences in material specifications and dimensional details to determine if the designs could be harmonized and (2) to determine the least conservative design(s) for further evaluation using FEA crash simulation of *MASH* testing. For example, if the crash simulations showed that the least conservative design met *MASH* criteria, then the more conservative designs could be assumed to meet those criteria as well. The results of that effort were presented in Section 3.5 and the recommended design details for the *MASH* evaluations were presented in Section 4.1. Final design recommendations for a standardized design and/or for improved performance will be presented later in Section 17.1.

16.3 Summary of FEA Model Validation

Baseline FEA models for both the NETC 4-bar bridge rail and the 2-bar transition were developed and validated based on full scale crash tests performed under NCHRP Report 350 Test 4-12 and Test 3-21, respectively. These models included design details consistent with the tested systems. The validation included both qualitative and quantitative assessments. The qualitative assessments included comparing sequential snapshots of the test and simulation to verify vehicle kinematic response, as well as, the sequence and timing of key phenomenological events. The quantitative assessment was performed according to the procedures specified in NCHRP [Web-Document 179](#) (W179).^[Ray11] These procedures included: (1) verifying that the analysis solution was stable and obeying basic laws of physics, (2) point-by-point comparison of the acceleration and angular-rate time-history data from the FEA and test, which were collected from accelerometers and rate gyros placed on-board the vehicle, using the RSVVP software, and (3) comparison of crash-specific phenomena from the event related to structural adequacy, occupant risk and vehicle trajectory.

16.3.1 NETC 4-Bar Bridge Rail Model Validation

For validation of the NETC 4-bar bridge rail model, there were issues regarding missing test data which were noted in Sections 6.2.1 and 6.2.2. In particular, the physical properties of the test vehicle were not included in the test report but were visibly different from that of the FEA model. Also, quantitative comparison of the time-history data could not be performed, since the test data was not available. In general, however, the results of the analysis demonstrated that the finite element model replicated the basic phenomenological behavior of the system under Report 350 Test 4-12 impact conditions. There was good agreement between the tests and the simulations with respect to event timing, overall kinematics of the vehicle, barrier damage and deflections. One exception involved the rear bumper snagging on the bridge rail resulting in higher longitudinal deceleration of the vehicle than what occurred in the FEA. The model was, however, considered adequately “valid” and was used as a baseline model for developing and evaluating *MASH* impact conditions for the NETC bridge rails. More details on the validation of the NETC 4-bar bridge rail model is provided in Section 6.2.

16.3.2 NETC 2-Bar Transition Model Validation

For the validation of the 2-bar transition, the results of the analyses demonstrated that the finite element model replicated the basic phenomenological behavior of the system for Report 350 Test 3-21 impact conditions. There was also good agreement between the tests and the simulations with respect to event timing, overall kinematics of the vehicle, barrier damage and deflections. Quantitative comparison of the time-history data indicated that the finite element model sufficiently replicated the results of the baseline crash tests according to W179. Thus, the model was considered valid and was used as a baseline model for evaluation of *MASH* impact performance on this and similar NETC transition designs. More details on the validation of the 2-bar transition model is provided in Section 7.4.

16.3.3 Possible Accuracy Issues

16.3.3.1 Material Yield Strength Accuracy

Yield properties used for tubular railings, posts and baseplates corresponded to minimum values. For example, although the material characterization for the posts and baseplates were based on tensile tests performed on coupons extracted from W6x25 posts which resulted in yield strength of 51 ksi, actual yield strength for the post material varies considerably in field installations. The purpose of using the lower yield strength for posts and rails was to be conservative in evaluations of barrier deflections; however, an increase in post strength results in greater loading being transferred to the anchor bolts and the bridge deck.

Table 110 shows a summary of mill certification reports for bridge rail posts used in three MaineDOT projects, where the yield strength for the posts was as high as 71 ksi and the average yield strength was 59 ksi. Similarly, the mill certification reports for the tubular rail sections for these three projects is shown in Table 111, where the yield strength was as high as 84 kips and the average yield strength was 67.1 kips, compared to minimum required strengths of 45.7 kips for Grade B and 50 ksi for Grade C. The FEA simulations used a yield strength of 50 ksi for the tubular rails.

Table 110. Properties extracted from material certification reports for bridge rail posts in three MaineDOT projects.

Material Type	Supplier	Date	Yield Strength		Tensile Strength		% Elongation	
			Published Minimum	Tested Value	Published Minimum	Tested Value	Published Minimum	Tested Value
ASTM A709-15	NUCOR, AL	Jan-19	50	56.00	65	79.00	19	39
				56.00		79.00		39
				56.70		81.00		37
				56.70		81.00		37
ASTM A709-17	GERDAU, GA	Nov-18	50	54.50	65	76.50	19	23
				57.80		78.60		23
ASTM A709 Gr. 50	NUCOR, SC	Oct-17	50	59.90	65	71.20	19	30
				60.20		71.40		31
				68.00		73.00		28
ASTM A709 Gr. 50	SSAB, MN	Sep-18	50	63.00	65	72.00	19	32
				71.00		75.00		29
				65.00		74.00		34
				65.00		74.00		34
Multigrade (ASTM A572 Gr. 50)	NUCOR, NY	Jun-18	50	52.80	65	77.30	19	25
				53.40		76.00		25
Multigrade (ASTM A572 Gr. 50)	NUCOR, NY	Sep-18	50	56.10	65	76.80	19	25
				56.10		77.40		23
Multigrade (ASTM A572 Gr. 50)	NUCOR, NY	Sep-18	50	56.60	65	77.20	19	22
				54.90		77.10		23
		Max		71.00		81.00		39
		Min	50	52.80	65	71.20	19	22
		Avg		58.59		76.31		29

Table 111. Properties extracted from material certification reports for A500 Grade B&C tubular rail sections in three MaineDOT projects.

Material Type	Supplier	Date	Yield Strength		Tensile Strength		% Elongation		
			Published Minimum	Tested Value	Published Minimum	Tested Value	Published Minimum	Tested Value	
ASTM A500-13 Gr. B&C	Atlas Tube, IL	Feb-18		66.32		76.10		32	
				66.32		76.10		32	
				66.32		76.10		32	
		Dec-16		83.80		92.65		30	
				68.51		79.10		30	
				68.51		79.10		30	
ASTM A500-18 Gr. B&C	Atlas Tube, IL	Mar-19		71.28		80.48		33	
				71.28		80.48		33	
				58.93		75.27		28	
				58.93		75.27		28	
				45.70	58.93	58.00	75.27	23	28
				68.51		79.10		30	
ASTM A500-13 Gr. B&C	Atlas Tube, IL	Dec-16		68.51		79.10		30	
				68.51		79.10		30	
ASTM A500-13 Gr. B&C	Atlas Tube, IL	Apr-18		62.80		74.83		32	
				67.10		81.23		31	
ASTM A500-13 Gr. B&C	Atlas Tube, IL	Aug-17		65.29		81.29		32	
				67.24		82.61		30	
ASTM A500-13 Gr. B&C	Atlas Tube, IL	May-18		65.95		75.99		30	
				65.95		75.99		30	
ASTM A500-13 Gr. B&C	Atlas Tube, IL	Jun-17		69.34		82.36		27	
				69.34		82.36		27	
		Max		83.80		92.65		33	
		Min	45.70	58.93	58.00	74.83	23	27	
		Avg		67.10		79.09		30	

16.3.3.2 Concrete and Anchor Bolt Model Accuracy

The model for the concrete curb/deck was developed based on the results of a recent study performed by the research team in which the material model was validated against pendulum impact tests on reinforced concrete columns where the columns were subjected to lateral impact forces. The results of that study showed very good correlation of model results to the full-scale tests on the columns for all the lateral impact cases. [Ray18a; Ray18b] This model has since been used in the validation of an FEA model of the Oregon 3-Tube bridge rail, in which the model accurately predicted failure of the front anchor bolts and subsequent *push-out failure* of the concrete curb. [Plaxico16] Test data, however, was not available to the research team for validation of anchor pryout damage in the concrete model, which was the primary concrete damage mode for the NETC bridge rail in the MASH test simulations.

16.3.3.3 Post-in-Soil Model Accuracy

The post and soil models were validated based on single-post impact tests with no side-slope. The NETC transition designs include several posts that are spaced very closely together (e.g., 18.75” on centers) in which there will be overlap of the soil influenced by adjacent posts; and, also, include a 2:1 side-slope starting just behind the posts. The soil was modeled using the continuum-soil method with appropriate soil geometry to account for both the soil interaction between neighboring posts and soil slope; however, the degree to which the model accurately captures this behavior has not been validated.

16.3.3.4 Tire Model Response for Small Car

The tire model for this vehicle is very simplistic and does not have enough detail to accurately simulate tire compression, debanding and/or deflation. Past use of this model has resulted in adequate response for most applications but with overly stiff tire response during post impact trajectory. In this study, it was noted that the trajectory of the small car when traversing the sidewalk may have been exaggerated by the overly stiff tire response during rebound off the sidewalk. In which case, the vehicle likely impacted at a higher point on the barrier than would be expected.

16.4 Summary of the *MASH* Evaluations of NETC Bridge Rail and Transition Designs

Detailed finite element analysis models were developed for the NETC bridge rail and transition designs based on the validated models developed in Section 6 and Section 7, respectively. LS-DYNA was then used to simulate impact conditions for *MASH* TL3 or TL4 as appropriate for each hardware system. The crash performance evaluations were based on structural capacity, occupant risk measures, and vehicle stability during impact and redirection according to the recommended procedures and criteria contained in *MASH*. The systems included in the evaluation are listed below along with the target test level for each system:

- Bridge Rail Systems:
 - NETC curb-mounted 2-bar rail (TL3)
 - NETC curb-mounted 3-bar rail (TL4)
 - NETC sidewalk-mounted 4-bar rail (TL4)
- Bridge Rail Transitions:
 - NETC Style 2-bar rail to thrie beam (TL3) (NH DOT steel rail transition)
 - NETC Style 3-bar rail to thrie beam (TL4) (NH DOT steel rail transition)
 - Concrete transition barrier to thrie beam (TL4) (Maine DOT standard detail)

These basic designs are used by several New England states with slight variations in design details, such as spacing between tube rails and curb height. For each case, the baseline model was updated to include specific material and dimensional recommendations as defined in Section 4 to corresponded to the least conservative design options.

Some additional supplemental analyses were also performed which involved selective design improvements for the 3-bar and 4-bar bridge rail systems as deemed appropriate by the project panel and NETC advisory committee, as well as, additional analyses for the 3-bar transition with increased post spacing at the expansion splice connection between the transition system and bridge rail. These evaluations included:

- Select Bridge Rail Modifications
 - Modified NETC curb-mounted 3-bar bridge rail with stronger lower rail
 - Modified NETC sidewalk-mounted 4-bar bridge rail with W8x28 posts
- Select Transition Modifications
 - Modified 3-bar transition with 5.5-ft spacing at first bridge rail post

An overall summary of analysis cases that were conducted and the results of those evaluations are provided in Table 112. The following sections provide a summary and discussion of the results for each system design.

16.4.1 NETC 2-Bar Bridge Rail (TL3)

In a previous study, the NETC 2-bar bridge rail system was successfully full-scale crash tested according to the 1989 AASHTO *Guide Specifications for Bridge Railings* (GSBR) for performance level 2 (PL2) and R350 TL4. [Mak98] The eligibility letter for this system is [B-50](#) which can be found on the FHWA website.

Based on the results of the FEA analysis in the current study, the barrier also meets all structural and occupant risk criteria in *MASH* for Test Level 3. The system was evaluated for *MASH* Test 3-10 and Test 3-11. The critical impact point for both tests corresponded to the *MASH* recommendations for rigid barriers (i.e., 3.6' and 4.3', respectively, upstream from the critical post). The barrier successfully contained and redirected both the small car and pickup with minimal to moderate damage to the system. There were no detached elements from the barrier that showed potential for penetrating the occupant compartment or presenting undue hazard to other traffic. The vehicles remained upright and very stable throughout impact and redirection. The occupant risk metrics were within recommended limits specified in *MASH*. Since the FEA models used the least conservative design options (see Table 51 in Section 4.1) in the *MASH* crash test simulations, then it is assumed that the more conservative design options also meet *MASH* crash performance criteria.

The primary concern for this system, which applies to the analysis results of all the NETC bridge rail designs, is that maximum occupant ridedown acceleration (ORA) values are very sensitive to time of occupant impact with the interior of the vehicle for Test 3-10. Once the occupant is in contact with the interior, the ORA calculations assume that the occupant experiences the same accelerations as the vehicle, which are measured at the vehicle center of gravity. The peak longitudinal and lateral accelerations for Test 3-10 (e.g., the small car test) exceeded 25 G, and the vehicle occupant contacted the interior of the vehicle during the tail end of this acceleration pulse (refer to Figures 366 and 367). Further, the unloading side of the longitudinal acceleration pulse was very steep, thus the ridedown accelerations for the occupant would increase significantly if the flail space of the occupant compartment were slightly reduced allowing the occupant to contact the interior a few milliseconds sooner. The general shape of the acceleration pulse was consistent with other Test 3-10 cases on rigid barriers; however, the peak values for longitudinal accelerations generally range between 15 G - 20 G while lateral accelerations will often approach 30 G [Sheikh16]. It appeared that the acceleration magnitudes were exacerbated in this case by the deflection of the lower rail, which created a "pocket" just upstream of the critical post location. Incorporating design modifications to mitigate pocket-deflection should reduce acceleration magnitudes, particularly for longitudinal accelerations. A design modification was incorporated for the NETC-3 bar system, and those results are summarized in a following section (see Section 16.4.3).

16.4.2 NETC 3-Bar Bridge Rail (TL4)

This system has not been full-scale tested but was deemed NCHRP Report 350 TL4 complaint based on the NETC 4-bar test results, acknowledging that the 9-inch reinforced curb serves as a replacement for the lower rail of the system. The eligibility letter for the 3-bar design is [B-242](#) which can be obtained from the FHWA website.

Based on the results of the FEA analysis performed in this study, the barrier meets all structural and occupant risk criteria in *MASH* for Test Level 4. This system was evaluated for *MASH* Test 4-10, Test 4-11 and Test 4-12. The critical impact point for each of the three tests corresponded to the *MASH* recommendations for rigid barriers (i.e., 3.6 ft, 4.3 ft and 5 ft, respectively, upstream from critical post). The evaluation for Test 4-12 included two analysis cases, one in which the cargo-bed height was 47.5 inches and another where the cargo-bed height was 50 inches. These two cases represent a lower and upper bound for the cargo-bed height of various SUT vehicles used in recent tests.

The barrier successfully contained and redirected the vehicle in all three *MASH* tests for all evaluation cases. The occupant risk metrics were within critical limits specified in *MASH*. There were no detached elements from the barrier that showed potential for penetrating the occupant compartment or presenting undue hazard to other traffic. For Tests 4-10 and 4-11 analyses, the vehicles remained upright and very stable throughout impact and redirection. For the Test 4-12 analysis, the vehicle remained upright and stable for Case 1 (cargo-bed height = 47.5 inches) but rolled over onto its side for Case 2 (cargo-bed height = 50 inches). *MASH* states that it is preferred that the vehicle remain upright during the crash test, but it is not required. Since the FEA models used the least conservative design options in these crash simulations (see Table 51), then it is assumed that the more conservative design options also meet *MASH* crash performance criteria.

The damages to the bridge rail were minimal for Test 4-10, moderate for Test 4-11, and moderate to extensive for Test 4-12. The barrier damage in Test 4-12 was caused primarily by impact of the rear tandem wheel set and rear of cargo bed against the bridge rail. The damages included plastic deformation of bridge rail posts and baseplates with high stress concentrations at the welds on the outside edges of the front flange. The analysis indicated only slight potential for concrete damage around the front anchor bolts. The maximum dynamic and permanent deflections of the railing were 8.1 inches and 6.6 inches, respectively, for Test 4-12.

Recent full-scale tests on the TxDOT Type C2P bridge railing, which has similar geometric characteristics and strength as the NETC 3-bar system, showed similar results. In that test, the barrier contained and redirected the single unit truck, but the barrier sustained substantial damage during the backslap of the truck with the barrier. Refer to the conclusions in Section 9.4 for more discussion.

16.4.3 Modified NETC 3-Bar Bridge Rail with HSS 5x4x5/16 Lower Rail

As mentioned in the summary of for the NETC 2-bar bridge rail, the peak longitudinal acceleration for Test 4-10 on the NETC bridge rails exceeded 25 G. The analyses showed that the mid-span deflections for the rails for the 2-bar and 3-bar systems lead to pocketing, particularly for Test 4-10 in which the forces from the small car were largely concentrated on the lower HSS 4 x 4 x ¼" rail.

The NETC 3-bar bridge rail model was modified to include a larger HSS section for the lower rail to: (1) increase stiffness and lower deflection and (2) increase rail dimension in vertical direction to provide additional contact width at the lower portion of the bridge railing to reduce potential for wheel-snap on the posts.

The increased strength for the lower rail showed slightly improved performance compared to the original design. The deflection of the lower rail was reduced by 30% to 42%, and the peak longitudinal acceleration was reduced by 9.3% to 13.5%. There was a slight wheel

snag at the splice for both the modified and original designs, which likely affected peak acceleration magnitudes. The OIV values were essentially unchanged; while the ORA-x was slightly reduced, and the ORA-y was slightly increased. All occupant risk metrics, however, were well within critical limits specified in *MASH*. The barrier successfully contained and redirected the small car with minimal damage to the system.

For this system, it is recommended that the HSS 5x4x5/16 be used for the lower rail; however, the overall improvement may not be significant enough to warrant changing the design. It is further recommended that the splice design be revised to minimize the amount of internal gap-space between the surfaces of the splice tube and the main rails, since the lateral movement within the splice appears to be a key factor in causing the excessive deflection of the rail as well as wheel snag at the splice.

16.4.4 NETC 4-Bar Bridge Rail (TL4)

In a previous study, the NETC 4-bar bridge rail system was successfully full-scale crash tested according to NCHRP Report 350 for Test Level 4. The eligibility letter for this system is also [B-50](#) which can be obtained from the FHWA website.

Based on the results of the FEA analysis presented herein, the NETC 4-bar bridge rail was also determined to meet all structural and occupant risk criteria in *MASH* for Test Level 4. This system was evaluated for *MASH* Test 4-10, Test 4-11 and Test 4-12. The critical impact point for each of the three tests corresponded to the *MASH* recommendations for rigid barriers (i.e., 3.6 ft, 4.3 ft and 5 ft, respectively, upstream from the critical post).

The barrier successfully contained and redirected the vehicle in all three *MASH* tests and all evaluation cases. The occupant risk metrics were within critical limits specified in *MASH*. There were no detached elements from the barrier that showed potential for penetrating the occupant compartment or presenting undue hazard to other traffic. The vehicles remained upright and very stable throughout impact and redirection, with relatively low angular displacements for all test cases. Since the FEA models used the least conservative design options (see Table 51) in the *MASH* crash test simulations, then it is assumed that the more conservative design options also meet *MASH* crash performance criteria.

The damages to the bridge rail were relatively low for Test 4-10. The trajectory of the small car was affected by the tire rebound after it impacted and traversed the sidewalk during this test case. The tire model was very simplistic and did not have enough detail to accurately simulate tire compression, debanding and/or tire deflation. It is assumed, however, that in a full-scale test the vehicle would likely impact much lower on the bridge rail, in which case the barrier damage and vehicle response would be similar to that for the NETC 3-bar bridge rail. For Test 4-11 the barrier experienced moderate plastic deformations of the posts, rails and baseplates. Test 4-12 resulted in more extensive damage, primarily resulting from impact of the rear tandem wheel set and the rear section of cargo bed against the bridge rail. These damages included plastic deformation of posts and baseplates with high stress concentrations at the welds on the outside edges of the front flange. There was also damage to the concrete curb at the critical post that indicated potential cracks around the front anchor bolts and/or anchor bolt pryout damage. The maximum dynamic and permanent deflections of the railing were 8.15 inches and 5.8 inches, respectively, for Test 4-12.

16.4.5 Modified NETC 4-Bar Bridge Rail with W8x28 Posts

The evaluation of the baseline 4-bar bridge rail, which was summarized in Section 16.4.4 above, showed that the 4-bar bridge rail resulted in more severe damage to the post, base plate and curb than the 2-bar and 3-bar designs. The bridge rail post was changed from the W6x25 to a W8x28 to determine if the stronger post would improve crash performance for Test 4-12. For the analysis, the position of the front face of the barrier was not changed nor the curb/deck size. Therefore, the resulting distance from the anchor bolts on the backside of the posts to the back edge of the deck was reduced from 7.625" to 6", which reduces concrete strength.

The CIP for the Test 4-12 analysis was 5 feet upstream of the critical post. The FEA results for the modified NETC 4-bar bridge rail system with W8x28 posts indicated that the system would meet *MASH* TL4 performance criteria. The barrier adequately contained and redirected the 10000S vehicle (single unit truck) with moderate damage to the bridge rail. Vehicle stability for the modified design was slightly improved compared to original design. The maximum roll angle at the c.g. of the SUT was 17.6 degrees, compared with 21.3 degrees for the original design. The maximum pitch angle was 2.8 degrees, compared with 3.5 degrees for the original design.

The impact forces on the barrier were only slightly higher for the modified design with stiffer W8x28 post. For example, the longitudinal forces were 17.6 kips vs. 14.4 kips, and the lateral forces were 126 kips vs. 110 kips. The higher lateral force for the modified design is expected with the increased stiffness of the W8x28 posts. The higher longitudinal force, however, was due to the lower rail on the outside edge of the cargo-box snagging on top of the rail splice for the modified design. The damage to the barrier for the modified design compared to original design included:

- Increased damage to curb around the front anchor bolts (probable large cracks).
- Reduced plastic deformation of posts and base plates.
- Reduced maximum dynamic barrier deflection (6.5" vs. of 8.2").

Based on the results of this analysis, it is recommended that the deck and anchorage should be strengthened at the post locations, such as increasing the reinforcement in the concrete. Test 4-10 and Test 4-11 simulations were not performed for the modified design; however, with the use of the stronger post, it is also recommended that the second rail from the bottom be strengthened as well to minimize pocketing for the small car (e.g., HSS 5x4x5/16). Although the snag at the splice did not adversely affect the performance of the system, it is also recommended that the splice design be revised to minimize the amount of internal gap-space between the surfaces of the splice tube and the main rails to alleviate potential snags with both passenger and commercial style vehicles.

16.4.6 NETC 2-Bar Transition (TL3)

In a previous study, the NHDOT 2-bar rail to thrie-beam AGT was successfully crash-tested according to NCHRP Report 350 Test 3-21. [Alberson06] The eligibility letter for this system is [B-146](#) which can be obtained from the FHWA website.

Based on the results of the FEA analysis herein, the NETC 2-bar transition was determined to meet all structural and occupant risk criteria in *MASH* for Test Level 3. This system was evaluated for *MASH* Test 3-20 and Test 3-21. The critical impact point (CIP) for Test 3-20 was determined to be 6.5 feet upstream from Post 5 of the transition, and the CIP for

Test 3-21 was determined to be 9 feet upstream from the end of the tube rails in the transition section. The CIP for both cases was determined using FEA with respect to maximizing the potential for vehicle snag on either the first post of the tube-rail section of the transition or on the end of the transition tube rails, as well as, on maximizing OIV and ORA metrics. A total of five impact points ranging from 5 ft to 7 ft were evaluated for Test 3-20; and a total of eight impact points ranging from 6 ft to 9.5 ft were evaluated for Test 3-21.

The 2-bar transition successfully contained and redirected the vehicle for all impact cases evaluated, and the occupant risk metrics were within critical limits specified in *MASH*. There were no detached elements from the barrier that showed potential for penetrating the occupant compartment or presenting undue hazard to other traffic. The vehicles remained upright and very stable throughout impact and redirection with relatively low angular displacements for all test cases.

The damages to the transition were minimal for Test 3-20. The maximum dynamic and permanent deflections were 6.3 inches and 5.2 inches, respectively, and occurred at the lower corrugation of the thrie-beam at the point where the nested thrie-beam connects to the thrie-beam end shoe. The damages to the transition for Test 3-21 were moderate. The vehicle was in contact with the barrier for approximately 15.9 ft, and the maximum dynamic and permanent deflections were 11.8 inches and 10.4 inches, respectively.

An additional analysis case was evaluated for the 2-bar transition that involved impact from the opposing traffic direction and was focused on possible wheel snag against the lower edge of the thrie-beam terminal connector and the 3/8-inch thick connector plate, as illustrated in Figure 511. The results of that analysis were not included in this report, but the general conclusion was that the tire would directly contact the lower edge of the thrie-beam during the crash simulation, but it did not result in significant snagging for this particular impact case. However, to further mitigate potential snags, it is recommended that an additional deflector plate could be installed at this point and fastened to the lower section of the thrie-beam terminal connector and connection plate via a bolt through the bottom hole.

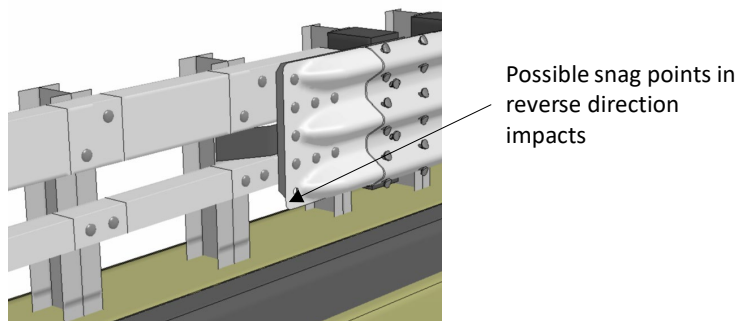


Figure 511. Possible snag point in reverse-direction impacts.

16.4.7 NETC 3-Bar Transition (TL4)

This system has not been full-scale tested; however, based on the results of the evaluation performed in this study, the NETC 3-bar transition meets all structural and occupant risk criteria in *MASH* for Test Level 4. This system was evaluated for *MASH* Test 4-20, Test 4-21 and Test 4-22. The critical impact point (CIP) for Test 4-20 and Test 4-21 was determined using the same procedure used for the 2-bar transition cases. The critical impact point for Test 4-22 was determined using FEA to maximize the potential for snag at the connection between the

transition and bridge rail. A total of six impact points ranging from 3.6 ft to 6 ft upstream of the critical impact point were evaluated for Test 4-20; a total of ten impact points ranging from 5.7 ft to 11.7 ft were evaluated for Test 4-21; and a total of five impact points ranging from 5 ft to 9 ft were evaluated for Test 4-22.

The CIP for Test 4-20 was determined to be 5.5 feet upstream of Post 5 of the transition. For Test 4-21 two CIPs were determined, including 6.2 feet upstream of the critical snag point at the end of the tube-rail section of the transition (e.g., considering overall results of pocketing, peak accelerations, and impact severity at the time when the vehicle approached the snag point) and 9.2 feet upstream of the critical snag point (e.g., based solely on maximum pocketing). Since the CIP at 9 feet was evaluated for the 2-bar case which resulted in good crash performance, the CIP at 6.2 feet was selected for further evaluation for the 3-bar transition system. Note that the 2-bar and 3-bar transition designs are equivalent regarding the section of the system extending from the attachment point of the guardrail to the attachment point of the transition tube rails. The CIP for Test 4-22 was determined to be 9 feet upstream of the bridge rail splice to maximize potential for vehicle snag on the end of the bridge rail and to also maximize potential for vehicle roll angle and contact between cargo-box and bridge rail posts.

The 3-bar transition successfully contained and redirected the vehicle for all impact cases evaluated, and the occupant risk metrics were within critical limits specified in *MASH*. The ORA values for Test 4-20 were highly dependent on time of occupant impact; however, the peak accelerations were below critical limits throughout the acceleration-time history. There were no detached elements from the barrier that showed potential for penetrating the occupant compartment or presenting undue hazard to other traffic. For the small car and pickup tests, the vehicles remained upright and very stable throughout impact and redirection, with relatively low angular displacements. The roll and pitch angles for the single unit truck test were relatively high. For Test 4-22 the final vehicle stability could not be determined at termination of the analysis at 1.5 seconds of the crash simulation. It is possible that the vehicle would have rolled onto its side had the analysis continued; however, *MASH* states that it is preferred that the vehicle remain upright, but it is not required.

The damages to the 3-bar transition were minimal for Test 3-20. The maximum dynamic and permanent deflections were 5.8 inches and 4.7 inches, respectively, and occurred at the lower corrugation of the thrie-beam at the point where the nested thrie-beam connects to the thrie-beam end shoe. The damages to the transition for Test 3-21 were moderate. The vehicle was in contact with the barrier for approximately 15.6 ft, and the maximum dynamic and permanent deflections were 7.95 inches and 6.8 inches, respectively. The damage to the transition for Test 4-22 was also moderate. The vehicle was in contact with the barrier from the point of contact until the truck cargo-box slid off the end of the bridge rail at 0.55 seconds. The maximum dynamic and permanent deflections for Test 4-22 were 4.29 inches and 2.8 inches, respectively. The greatest damage was to the bridge rail posts which resulted from the cargo-box extending over the top of the rail and snagging the tops of the posts. It is recommended that the tops of the transition and bridge rail posts be tapered down toward the field side of the post to avoid contact with the truck bed and mitigate this type of damage. The maximum working width prior to exiting the barrier was 3.9 ft resulting from the top of the cargo box extending over the bridge rail.

16.4.8 NETC 3-Bar Transition with 5.5-ft Post Spacing at First Bridge Rail Post (TL4)

The evaluations of the NETC 3-bar transition system summarized in Section 16.4.7 above included the current maximum post spacing specified between the last post of the transition and the first post of the bridge rail (i.e., 3 ft). However, there are many field installation cases in which it is difficult to meet this specification, such as at strip joints, compression seals, finger joints and modular joints. Supplemental analyses of the NETC 3-bar transition were performed to evaluate increasing the maximum post spacing to 5.5 feet.

For these analyses the 3-bar system design was modified by (1) extending the bridge rail tubes and deck to attain desired post spacing of 5.5-ft between first post of bridge rail and last post of transition, (2) tapering the tops of the W6x25 posts, and (3) widening the expansion splice gap from 0.75 inch to 2 inches. For Test 4-20, an additional analysis case was performed in which an HSS 5x4x5/16 tube section was used for the lower rail.

With the increased span between the transition and bridge rail posts, the expansion splice was considered to be more critical for passenger vehicles than the original design case. As such, for Tests 4-20 and 4-21, the critical impact point was determined using FEA with respect to maximum potential for wheel snag on the first post of the bridge rail and on the splice connection.

For Test 4-20, ten impact point locations ranging from 3.6 feet to 8 feet upstream from the first post on the bridge rail were evaluated. The analyses indicated that impact at 4.0 feet upstream of the bridge rail post resulted in the greatest chance for wheel snag on the post; while impact at 8.0 feet upstream of the post resulted in the greatest chance for snag on the expansion splice. In all cases, however, there was no contact with the post and only minimal snagging on the splice, due to the location of the splice on the downstream side of the transition post. The supplemental analysis with the HSS 5x4x5/16 lower rail resulted in improved crash performance including lower deflections and lower occupant risk metrics, as shown in Table 112; however, both design cases were shown to meet *MASH* performance criteria for the 5.5-ft post spacing.

For Test 4-21, five impact locations were evaluated ranging from 5 feet to 9 feet upstream of the first bridge rail post. None of the impact cases resulted in significant potential for wheel contact with the post; however, impact at 6.0 feet upstream of the critical post (i.e., 2-ft upstream of expansion splice) resulted in the highest potential for snag on the expansion splice. This impact case also corresponded to the highest peak longitudinal acceleration and the highest resultant acceleration. The fender snagged on the splice in this case, but the snag did not significantly affect overall crash performance, and the system met *MASH* criteria for all cases.

For Test 4-22, three impact cases were evaluated which involved two expansion splice gaps (i.e., $\frac{3}{4}$ -inch and 2-inch) and two different post designs (i.e., original and tapered posts). The critical impact point for all cases was 9 feet upstream of the expansion splice, which was adopted from the evaluation of the original design. In each case the bottom of the cargo-box snagged on the expansion splice but did not result in excessive forces of adverse performance of the system. The longitudinal impact force on the barrier increased approximately 19 percent due to the increase in post spacing with the non-tapered posts (43.8 vs. 36.9 kips); but was slightly reduced for the tapered posts (34.1 vs. 36.9 kips). The lateral force was reduced with the increase in post spacing, while the resultant force was higher for all increased post spacing cases with the highest resultant force occurring for Case 1 with the non-tapered posts (96.2 vs. 84 kips). The maximum lateral deflection occurred at the expansion splice in all cases. The lateral deflection was higher for 5.5-ft post spacing compared to the baseline 3-ft post spacing (i.e., 6"

vs. 4.3”). The highest deflection occurred for the 5.5-ft spacing with non-tapered posts. The plastic deformations of the transition components were very similar to the baseline case and was low to moderate. The plastic deformations of the bridge rail for the non-tapered posts was significant due to the bottom of the cargo-box snagging on the tops of the posts, while the deformations for the tapered post cases were minimal.

The FEA simulations of an increased post spacing of 5.5 feet for the NETC 3-bar transition was shown to meet *MASH* TL4 performance criteria. The increased spacing generally resulted in increased rail deflections, increased longitudinal forces and accelerations and reduced lateral forces and accelerations. However, tapering the tops of the posts notably reduced longitudinal forces for Test 4-22 by mitigating snag on the backs of the post.

The 2-inch wide expansion splice joint did not result in notable snag in the FEA, but the research team believes the potential for such a snag exists – particularly for reverse-direction impact scenarios (not evaluated). Previous analysis and full-scale tests on a similar system with 3¾-inch splice gap resulted in significant snag for the pickup test.[*Buth99b*] It is therefore recommended that the splice designs be revised to minimize the amount of internal gap-space between the outside surface of the splice tube and the internal surface of the main rails.

It is also recommended that the lower rail for the bridge rail, and consequently the lower rail of the transition, be changed to the HSS 5x4x5/16. The larger rail resulted in a 25 percent decrease in rail deflection for the small car test compared to the baseline analysis with HSS4x4x1/4, and a 17.9 percent decrease in peak longitudinal acceleration.

16.4.9 Concrete Transition Barrier to Thrie Beam (TL4)

This system has not been full-scale tested; however, based on the results of the evaluation performed in this study, it was determined that the concrete transition to thrie-beam system did not meet safety criteria in *MASH* for Test Level 3 or 4. However, only the sidewalk case was evaluated since it provided the greatest opportunity for snags on the concrete buttress. It is expected that the curb-mounted transition would have better crash performance, particularly for Test 3-20 and Test 3-21, since the curb would better shield the nose of the buttress from contact and snag against the vehicles’ tires.

This system was evaluated for *MASH* Test 4-20, Test 4-21 and Test 4-22. The critical impact point for all cases were designed to maximize potential for snag on the end of the concrete buttress. For Test 4-20 a total of five impact points ranging from 4 ft to 6 ft upstream of the nose of the concrete buttress were evaluated; a total of five impact points ranging from 5.5 ft to 7.5 ft were evaluated for Test 4-21; and a total of four impact points ranging from 9 ft to 12 ft were evaluated for Test 4-22.

The CIP for Test 4-20 was determined to be 5.5 feet upstream from the nose of the buttress. The longitudinal ORA was relatively high for impact points ranging from 5 to 6 feet; however, impact at 5.5 feet resulted in ORA values exceeding *MASH* criteria, while impact at 6.0 feet resulted in longitudinal ORA near critical limits. For Test 4-21 it was determined that impact at 7.0 ft upstream of the buttress provided the greatest potential for pocketing, and impact at 6.5 ft provided the highest ORA values. Thus, the CIP was selected as the midpoint between those two cases at 6.75 ft upstream of the buttress. The CIP for Test 4-22 was determined to be 12 feet upstream of the buttress to maximize potential for vehicle snag on the end of the buttress and to also to maximize potential for vehicle roll angle and contact between cargo-box and bridge rail posts.

The concrete transition to thrie-beam system contained and redirected the vehicle in all impact cases evaluated; however, containment was marginal for Test 4-22. The OIV values were within critical limits for all cases. The ORA values were above recommended limits, but below critical limits for Test 4-21. The longitudinal ORA for Test 4-20, however, exceeded *MASH* limit criteria. There were no detached elements from the barrier that showed potential for penetrating the occupant compartment or presenting undue hazard to other traffic. For the small car and pickup tests, the vehicles remained upright and very stable throughout impact and redirection, with relatively low angular displacements. For test 4-22 the roll and pitch angles were relatively low through 1.34 seconds of the impact event; however, given the final orientation, speed and roll rate of the vehicle, it was likely that the truck would have eventually rolled over onto its side. As previously stated, it is preferred that the SUT vehicle remain upright, but it is not a requirement of *MASH*.

The damage to the transition were moderate to significant for Test 3-20, but within expectations. Damage included kinking of the thrie-beam, lateral deflection of several posts and corresponding soil displacement at those posts. The maximum dynamic and permanent deflections were 6.7 inches and 5.7 inches, respectively, which occurred at the lower corrugation of the thrie-beam at the upstream edge of the blockout at Post 2. The damage to the transition for Test 3-21 were also moderate to significant but considered typical for this type of system. The vehicle was in contact with the barrier for approximately 10.2 ft, and the maximum dynamic and permanent deflections were 8.3 inches and 7.2 inches, respectively, which also occurred on the lower corrugation of the thrie-beam at the upstream end of the blockout at Post 2. The damage to the transition for Test 4-22 was significant with maximum dynamic deflection of 17 inches at the top of Post 2. Several of the transition posts near the buttress were deformed. The bridge rail was also damaged, due to the bottom of the cargo box snagging on the tops of the posts. The most significant damage to the bridge rail was to the downstream end post, in which the rail mounting bolts sheared off, and the post bent along the longitudinal direction of the rail.

Table 112. Summary of analysis cases conducted and the results of the evaluations.

System Type	System	MASH Test No.	Impact Conditions			RESULTS										
			Speed (mph)	Angle (deg)	CIP (ft)	Structural Adequacy		Occupant Risk Metrics						Vehicle Stability		Overall Result
						Contain	Max. Disp. (in)	OCI		OIV _x (ft/s)	OIV _y (ft/s)	ORA _x (g)	ORA _y (g)	Roll (deg)	Pitch (deg)	
								Location								
Bridge Rail	NETC 2-Bar	Test 3-10	62	25	3.6	Pass	3.6	Wheel Well/ Toe Pan	3.3	26.2	33.1	5.5 ⁽¹⁾	6.4	7	5.4	Pass
		Test 3-11	62	25	4.3	Pass	2.7	Wheel Well/ Toe Pan	2.8	20.7	26.9	4.6	15.4 ⁽²⁾	9	10.1	Pass
	NETC 3-Bar	Test 4-10	62	25	3.6	Pass	3.4	Wheel Well/ Toe Pan	2.8	25.6	32.5	6.7 ⁽¹⁾	6	7.3	5.2	Pass
		Test 4-11	62	25	4.3	Pass	4.2	Wheel Well/ Toe Pan	3.3	22	26.6	4.7	15.4 ⁽²⁾	9.9	7.5	Pass
		Test 4-12 ⁽³⁾	56	15	5	Pass	7.6	Wheel Well/ Toe Pan	1	2	14.8	7	5.3	20.8	7.8	Pass
		Test 4-12 ⁽⁴⁾	56	15	5	Pass	8.1	Wheel Well / lower edge of door	3.3	3	14.1	5.7	5.9	90*	6.9	Pass
	Mod 3-Bar [†]	Test 4-10	62	25	3.6	Pass	2.3	-	-	24.3	32.5	3.5 ⁽¹⁾	7.7	-	-	Pass
	NETC 4-Bar	Test 4-10	62	25	3.6	Pass	2.8	Wheel Well/ Toe Pan	3.4	24	31.5	7.1 ⁽¹⁾	10.3	10.9	6.5	Pass
		Test 4-11	62	25	4.3	Pass	5.4	Wheel Well/ Toe Pan	2.2	17.7	26.6	13.8	18 ⁽²⁾	7.2	8.3	Pass
		Test 4-12 ⁽³⁾	56	15	5	Pass	8.2	Wheel Well/ Toe Pan	1	3.9	16.7	4.3	6.7	18.8	5.6	Pass
Mod 4-Bar [‡]	Test 4-12 ⁽³⁾	56	15	5	Pass	8.2	Not Evaluated	1	3.9	16.7	4.3	6.7	18.8	5.6	Pass	
AGT	2-Bar (Tube Rails)	Test 3-20	62	25	6.5	Pass	6.3	Wheel well / Toe Pan	1.4	25.3	28.2	7.9 ⁽¹⁾	4.8	6.7	3.6	Pass
		Test 3-21	62	25	9	Pass	11.8	negligible	-	17.4	23.3	4.8	17.2 ⁽²⁾	9.3	5.5	Pass
	3-Bar (Tube Rails)	Test 4-20	62	25	5.5	Pass	5.8	Wheel Well/ Toe Pan	1	24.3	25.9	4.2 ⁽¹⁾	7.4	6.2	3.9	Pass
		Test 4-21	62	25	5.5	Pass	8	negligible	-	17.7	24.6	5.2	15.1 ⁽²⁾	8.1	3.7	Pass
		Test 4-22	56	15	9	Pass	7.6	Wheel Well/ Toe Pan	1	2.3	14.8	8.9	5.5	90*	11.9	Pass**
	4-Bar (Concrete Butress)	Test 4-20	62	25	5.5	Pass	6.9	Wheel Well/ Toe Pan	3.4	29.2	32.8	26	7.9 ⁽²⁾	5.4	6.8	Fail
		Test 4-21	62	25	6.5	Pass	8.3	Wheel Well/ Toe Pan	1	21	28.2	9.4	17.3	15.4	9.6	Pass
		Test 4-22	56	15	12	Pass	17.0	Wheel Well/ Toe Pan	5.5	8.9	14.4	13.9	8.7	8.7	12	Pass***
	3-Bar (Tube Rails) w/ 5.5-ft Post Space	Test 4-20 [§]	62	25	4	Pass	3.25	-	-	25.3	33.1	4.9	2.9 ⁽²⁾	-	-	Pass
		Test 4-20 ^{§§}	62	25	4	Pass	2.65	-	-	23.6	32.8	3.7	7.9 ⁽²⁾	4.4	5.1	Pass
		Test 4-21 [§]	62	25	6	Pass	-	-	-	22.6	27.9	5.8	≈18-19	-	-	Pass
		Test 4-22 [£]	56	15	9	Pass	5.4	-	-	-	-	-	-	-	-	Pass**

* The vehicle was still upright when the analysis was terminated, but 90-degree roll was expected.

** Resulted in significant snagging on and damage to bridge rail posts.

*** The analysis showed that the barrier contained and redirected the 10,000S vehicle, but with significant damage to the transition and bridge rail elements.

⁽¹⁾ Maximum ORA occurred on tail-end of a major acceleration pulse. Would have been higher if OIV had occurred slightly sooner.

⁽²⁾ Vehicle model tends to over-predict lateral accelerations associated with "tail-slap".

⁽³⁾ Cargo-box Bed Height = 47.5".

⁽⁴⁾ Cargo-box Bed Height = 50".

[†] NETC 3-bar with HSS 5x4x5/16 lower rail

[‡] NETC 4-bar with W8x28 posts

[§] 3-bar AGT with original components

^{§§} 3-bar AGT with HSS5x4x5/16 lower rail

[£] 3-bar AGT with 2-inch splice gap and top of posts tapered

17 CONCLUSIONS AND RECOMMENDATIONS

17.1 NETC Bridge Rail Designs

Based on the results of the study, several aspects of the designs were identified that could be modified to improve crash performance. Those design aspects are discussed below, followed by final conclusions and recommendations for each bridge rail design.

17.1.1 Conclusions regarding Critical Design Aspects

17.1.1.1 Anchor Embedment Depth

These conclusions relate to the 3-bar and 4-bar designs. The anchor embedment depth was determined to be the critical weakness based on LRFD strength calculations for the curb-mounted 3-bar system, while both anchor embedment and plastic strength of posts governed for the sidewalk-mounted 4-bar system. The LRFD strength calculations, as well as, the FEA simulations showed that the anchor rods have reserve strength but there was not enough embedment to fully utilize it. Unfortunately, because some States are starting to use more integral concrete wearing surfaces and bare decks, the depth of the curb/deck is very restricted; therefore, in many cases, it will not be possible to increase embedment depth for the anchors, but it should be considered when applicable.

17.1.1.2 Concrete strength

These conclusions relate to the 3-bar and 4-bar designs. Increasing the strength of the concrete from 4,000 psi to 5,000 psi would be an alternative means for increasing the overall strength of the anchors; however, recent studies have shown that the higher cement content leads to more shrinkage and cracking of concrete.[Safiuddin18] MaineDOT, which currently specifies 5,000 psi concrete for bridge curb/deck, is currently considering changing their specification to 4,000 psi for this reason.

17.1.1.3 Curb/Deck Reinforcement

These conclusions relate to the 3-bar and 4-bar designs. When embedment depth and concrete strength cannot be increased, another option may be to increase the steel reinforcement by adding additional longitudinal steel nearer to (but above) the anchor plates. For example, Figure 512 shows a comparison of the curb reinforcing in the current NETC designs to that of the MassDOT S3-TL4 design, which includes the second row of longitudinal steel.

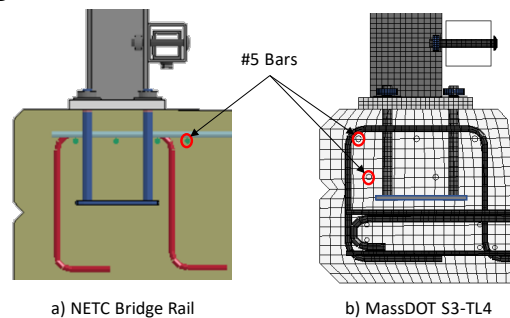


Figure 512. Comparison of longitudinal steel for a) the NETC and b) MassDOT's S3-TL4 bridge rail designs.

17.1.1.4 Post Size and Post Spacing

These conclusions relate to the 3-bar and 4-bar designs. After anchorage, the strength of the bridge rail posts was the governing factor regarding overall strength of the bridge rail system. One option would be to increase the size of the posts, as was shown in Section 15.3. Changing from the W6x25 to the W8x28 post results in a 44 percent increase in plastic strength for the post. However, the change in post size did not notably improve the potential for pocketing, even with an increase in the rail size, due primarily to the relatively large lateral movement within the splice. Another option would be to decrease post spacing, which would serve to improve strength in several areas. The decreased span for the railing would increase the stiffness of the rails (e.g., reduce pocketing) and better distribute impact forces among adjacent posts, thereby reducing forces on individual posts and anchorage. Preliminary LRFD calculations indicate that reducing the post spacing from 8 feet to 6.5 feet would result in meeting *MASH* strength requirements for the 4-bar system (calculations not shown).

17.1.1.5 Baseplate

These conclusions relate to the 3-bar and 4-bar designs. Although the LRFD calculations did not consider strength of the baseplates, the FEA analysis and previous NCHRP Report 350 testing showed that the baseplates experience significant deformations for Test Level 4. The deformation of the baseplate likely reduces forces on the anchors, but it also reduces the overall strength of the system. The FEA simulations also indicated that the deformation mode of the baseplate resulted in stress concentrations in the weld between the post and baseplate at the outside edges of the front post flange (refer to Figures 159 and 277).

17.1.1.6 Tubular Rails

These conclusions relate to all NETC bridge rail designs. The *MASH* equivalency evaluations showed that the NETC 2-bar and 3-bar systems met the preferred rail geometric criteria and strength requirements for *MASH*, but the sidewalk-mounted NETC 4-bar system was considered marginal for both conditions. FEA simulations showed that the mid-span deflections for the rails for the 2-bar and 3-bar systems lead to pocketing, particularly for Test 4-10 in which the forces from the small car were largely concentrated on the lower HSS 4 x 4 x ¼" rail (refer to Figure 123). Although the mill spec reports from recent MaineDOT projects which were presented earlier are not statistically reliable (i.e., not enough data points), they do indicate that material properties for HSS rail sections are often much stronger than the minimum specifications that were used in the FEA; thus, pocketing in full-scale crash tests or field installations would likely be less than what was shown in the FEA results.

Nevertheless, changing the sizes of the longitudinal rails to increase standoff distance from the post, as well as, to increase stiffness could greatly improve performance (possibly) without altering other design aspects of systems. Similar to the reduced post spacing option above, the stiffer tubes would reduce pocketing, better distribute forces among adjacent posts (e.g., reduce forces on posts and anchors), as well as provide additional standoff distance from the post (e.g., reduce potential for snagging).

Table 113 shows a comparison of strength and weight for two tubular rail options compared to the original NETC 4-bar design; the table also includes overall barrier strength for each option with all other design aspects remaining the same. In both options the tubular rails provide a 5-inch standoff distance between the face of the rail and the post. Option 1 uses HSS 5 x 5 x ¼ in place of the HSS 4 x 4 x ¼ rails and uses HSS 7 x 5 x ¼ in place of the HSS 8 x 4 x

5/16. This option results in a 13.4 percent increase in overall system strength and meets geometric and strength requirements for *MASH TL4*. It also results in an increase in total weight of 9.85 percent for the tubular rails, which would translate to a similar increase in cost for those components.

Option 2 uses HSS 5 x 5 x 3/16 in place of the HSS 4 x 4 x 1/4 rails and uses HSS 7 x 5 x 1/4 in place of the HSS 8 x 4 x 5/16. This option results in a 5.7 percent increase in overall system strength which meets both rail-geometric requirements and LRFD strength calculations for *MASH TL4*. It also results in a decrease in total steel weight for the tubular rails of 8.4 percent, which would translate to a similar decrease in cost for those components. Although Option 2 would increase the overall strength at less cost, it is recommended that additional evaluations be carried out to ensure that local buckling (crushing) of the tube walls does not occur during vehicle impact against the thinner rails.

Table 113. Comparison of strength and weight for tubular rail options for the New Hampshire 4-bar system (all other design aspects remaining the same).

Design Options		Rail 1 (lower)	Rail 2	Rail 3	Rail 4	Total Rail Weights (lbs/ft)	Weight Increase %	System Strength (kips)	Strength Increase %
Current Design	Size	4 x 4 x 1/4	4 x 4 x 1/4	8 x 4 x 5/16	4 x 4 x 1/4	59.97	-	75.9	-
	Z _p (in ³)	4.97	4.97	10.5	4.97				
	W (#/ft)	12.21	12.21	23.34	12.21				
Option 1	Size	5 x 5 x 1/4	5 x 5 x 1/4	7 x 5 x 1/4	5 x 5 x 1/4	65.88	9.85%	86.1	13.44%
	Z _p (in ³)	8.07	8.07	10.4	8.07				
	% increase	62.4%	62.4%	-1.0%	62.4%				
	W (#/ft)	15.62	15.62	19.02	15.62				
	% Increase	27.9%	27.9%	-18.5%	27.9%				
Option 2	Size	5 x 5 x 3/16	5 x 5 x 3/16	7 x 5 x 1/4	5 x 5 x 3/16	54.93	-8.40%	80.2	5.67%
	Z _p (in ³)	6.29	6.29	10.4	6.29				
	% increase	26.6%	26.6%	-1.0%	26.6%				
	W (#/ft)	11.97	11.97	19.02	11.97				
	% Increase	-2.0%	-2.0%	-18.5%	-2.0%				

17.1.1.7 Splice Design

These conclusions relate to all NETC bridge rail designs. The splice bars used in the full-scale crash tests of the NETC 4-bar bridge rail were fabricated from welded plates (refer to Table 2 for dimensions), in which the clearance of the splice bar inside the main rail tubes was 1/16” on all sides or 1/8” total. Refer to the drawings in the crash test report for construction details. [Kimbal99]

The current splice design used in the NETC bridge rails includes an HSS 7” x 3” x 3/8” inserted into the larger main rail tube (i.e., HSS 8 x 4 x 5/16), and an HSS 3” x 3” x 5/16” splice bar inserted into the smaller main-rail tubes (i.e., HSS 4 x 4 x 1/4”). The splice bars are connected to the main rails using four cap screws (see drawings in the Appendices). The dimensions of the splice bars result in an internal gap between the surfaces of the splice bar and main rail of 3/8 inch inside the larger rail splice; and an internal gap of 1/2 inch inside the smaller rail splice. The FEA simulations for these designs showed that the wheel rims did snag on the splice in the impact simulations, although the snag did not result in excessive vehicle decelerations or damages. Further, in an earlier study by Plaxico et al. and on previous full-scale testing by Buth et al. on similar expansion splice details, severe snagging did occur on the ends of the rail tubes at the expansion splice.[Plaxico16; Buth99b] The solution in those cases was to reduce the length of the splice gap opening from 3¾ inches to 7/8 inch.

As stated throughout this report, it is recommended that the current design be revised to reduce the internal gaps between the outside surfaces of the splice tube and the inside surfaces of the main rail to match that of the tested design, as much as feasibly possible. This could be accomplished by either adopting the tested design directly or by welding bushing-plates onto the sides of the splice bars to close the gaps in the lateral direction, noting that the gaps on the top and bottom of the splice are less important to crash performance (except possibly for Test 4-12).

17.1.1.8 Post Taper (at top of post)

These conclusions relate primarily to the 3-bar and 4-bar designs, although they may be considered for the 2-bar system as well. The FEA crash simulations for the NETC transition designs showed that during impacts with the single unit truck the bottom of the cargo-bed would extend over the top of the railing and snag on the tops of the bridge rail posts. Some bridge rail designs that include a taper on the top of the posts have been shown to mitigate the potential for this type of snag.[*Plaxico19b*] In the supplemental analyses in Section 15.2.4, the tapered post concept was included for the analysis of the 3-bar transition with 5.5 ft post spacing, in which the snag between the cargo-bed and posts was successfully mitigated. It is recommended that a similar taper be used for all NETC designs.

17.1.2 Conclusions and Recommendations on Final Design

The following conclusions regarding the crash performance of the existing NETC bridge rail designs are based on the *MASH* equivalency evaluations and the FEA crash simulations results from this study, as well as, the apparent in-service performance of field installations of these systems. The NETC bridge rail designs have been in service for more than 20 years, and, based on discussions with the State DOTs, there have been no known instances of serious injuries resulting from vehicle crashes with these system during that time.

It is therefore the opinion of the research team that all existing NETC 2-bar bridge rail designs used among the various New England states, and which include design aspects equal to or more conservative than those presented in Table 51 in Section 4.1, meet *MASH* TL3 performance criteria. Likewise, the research team also considers all existing NETC 3-bar designs, with designs aspects equal to or more conservative than those presented in Table 51, to meet *MASH* TL4 crash performance criteria. These systems meet LRFD strength requirements for their respective test levels, and the FEA results indicated successful crash performance under *MASH* crash testing conditions and criteria. Both the 2-bar and 3-bar designs also meet all preferred rail geometrics criteria when a 9-inch curb reveal is used. The 2-bar and 3-bar designs using a 7-inch curb reveal do not meet the preferred criteria for rail geometrics regarding *ratio of rail contact width to height*, but they fall within the range of other systems with similar rail geometrics that have been successfully crash tested.[*Dobrovolny17*]

The FEA results also indicated that the NETC sidewalk-mounted 4-bar design meets *MASH* TL4 crash performance, albeit with considerable damage to the bridge rail during *MASH* Test 4-12 simulations. It is highly recommended that the NETC 4-bar design be revised to meet *MASH* equivalency (i.e., rail geometric and strength criteria) or, alternatively, that further evaluation of this system be conducted to verify crash performance (e.g., conduct in-service performance evaluation and/or full-scale testing).

Based on the conclusions of critical design aspects discussed above, the research team provides some recommended design enhancement options for each of the NETC bridge rail

designs in the following sections. The conclusions and recommendations for the NETC bridge rails are also summarized in Tables 114 through Table 116..

17.1.2.1 NETC 2-Bar Bridge Rail

The NETC 2-bar bridge rail meets *MASH* TL3 performance criteria and no design changes are required. The following optional “general” design enhancements are provided by the research team to further improve crash performance for this system under *MASH* impact conditions.

- Increase size and strength of lower rail to HSS 5x4x5/16 to: (1) meet preferred ratio of rail contact area to height requirements and (2) reduce pocketing for the small car.
- Improve splice design by reducing internal gaps to mitigate snag with impacting vehicles.
- Taper top of posts to mitigate snag with over-hanging vehicles.

17.1.2.2 NETC Curb-Mounted 3-Bar and Sidewalk-Mounted 4-Bar Bridge Rails

The NETC 3-bar and 4-bar bridge rail meets *MASH* TL4 performance criteria and no design changes are required. The following recommended “general” design enhancements are provided by the research team to further improve crash performance for this system under *MASH* impact conditions. The first revision listed for each option is the primary revision for improving crash performance, while the subsequent revisions are intended to compliment or further improve performance for that option.

Option 1:

- Reduce post spacing (e.g., 8 ft to 6.5 ft) to meet LRFD strength requirements.
- Revise splice design by reducing internal gaps.
- Taper top of posts to mitigate snag when vehicles over-hang the top of the rail.

Option 2:

- Change size of all rails to meet preferred rail-geometric criteria and to improve strength.
- Increase curb reinforcement by adding additional longitudinal steel above the anchor plates and/or increase anchor-bolt embedment.
- Revise splice design by reducing internal gaps.
- Taper top of posts.
- Increase baseplate thickness and welds.

Option 3:

- Increase post size (e.g., W8x28) to meet LRFD strength requirements.
- Increase curb reinforcement by adding additional longitudinal steel above the anchor plates and/or increase anchor-bolt embedment.
- Improve splice design by reducing internal gaps.
- Taper top of posts to mitigate snag with over-hanging vehicles.
- Use an HSS 5x4x5/16 for the lower rail for the 3-bar system and for the 2nd rail from the bottom for the 4-bar system to reduce pocketing for small car.

17.2 NETC Transition Designs

The conclusions and recommendations for the approach guardrail transitions are presented below and are summarized in Tables 117 through 119. As with the bridge rail cases, redesign of the transition systems was not the focus this study; however, general design enhancement recommendations are presented for each of the transition designs.

The NETC 2-bar transition met *MASH* TL3 performance criteria based on the FEA crash simulations. The recommended design changes for the 2-bar system include: (1) an additional deflector plate at the lower edge of the three-beam terminal connector and (2) revising the expansion splice at the connection to the bridge rail to minimize internal gap space.

The NETC 3-bar transition met *MASH* TL4 performance criteria based on the FEA crash simulations. The performance of both the 2-bar and 3-bar systems was very good for the small car and pickup tests. The modifications suggested for this systems are: (1) to taper the tops of the transition and bridge rail posts down and toward the field side to avoid contact with the front-lower edge and bottom of the cargo-box during impacts with single unit trucks and (2) to revise the expansion splice to minimize internal gaps.

The concrete transition to three-beam did not meet *MASH* TL3 performance criteria, based on the FEA crash simulations. There are some basic modifications that could be made to the buttress design to improve performance, which include tapering the face of the buttress as described in Rosenbaugh et. al (refer to Figure 35).[Rosenbaugh18] However, when applicable (e.g., when space is available) it is recommended that the NETC 3-bar or 4-bar transition designs be used in lieu of the concrete transition to three-beam system.

Table 114. Summary of conclusions and recommendations for the NETC 2-Bar bridge rail.

MASH Test Case	FEA Results: MASH Criteria	FEA Results: System Damage	LRFD Calcs. for MASH Equivalency	Recommendations
Test 3-10 <u>Small Car</u>	<ul style="list-style-type: none"> • Structural Adequacy – PASS • Occupant Risk – PASS <ul style="list-style-type: none"> • Preferred < OIV < critical • ORA within preferred limits but sensitive to time of occupant impact. • Vehicle Stability – PASS 	<ul style="list-style-type: none"> • Minimal damage to system • Dynamic deflection = 3.6" • Some plastic deformation of post, and moderate plastic deformations of the lower rail and baseplate. • No detached elements from barrier that would present hazard. 	<ul style="list-style-type: none"> • Meets minimum height • 9" curb reveal meets all preferred rail-face geometrics criteria. • 7" curb reveal does <u>not</u> meet all preferred rail-face geometrics criteria but falls within the range of other systems that have been successfully crash tested. 	<ul style="list-style-type: none"> • <u>Meets MASH TL3</u> • <u>No design changes required.</u> <p>Recommendations for improving overall crash performance:</p> <ul style="list-style-type: none"> ○ Increase size and strength of lower rail to an HSS 5x4x5/16 to: (1) meet <i>contact area/rail height</i> requirements and (2) reduce pocketing. ○ Revise splice design to reduce internal gaps. ○ Taper top of posts
Test 3-11 <u>Pickup</u>	<ul style="list-style-type: none"> • Structural Adequacy – PASS • Occupant Risk – PASS <ul style="list-style-type: none"> • OIV within preferred limits • Preferred < ORA < critical • Vehicle Stability – PASS 	<ul style="list-style-type: none"> • Minimal to moderate damage to system. • Dynamic deflection = 2.7" • Moderate plastic deformations of the posts, both rails and baseplates. • Potential concrete curb damage at one post. • No detached elements from barrier that would present hazard. 	<ul style="list-style-type: none"> • Meets LRFD minimum lateral strength criterion of 71 kip. 	

Table 115. Summary of conclusions and recommendations for the NETC 3-bar bridge rail.

MASH Test Case	FEA Results: MASH Criteria	FEA Results: System Damage	LRFD Calcs. for MASH Equivalency	Recommendations
Test 4-10 <u>Small Car</u>	<ul style="list-style-type: none"> • Structural Adequacy – PASS • Occupant Risk – PASS <ul style="list-style-type: none"> • <i>preferred < OIV < critical</i> • ORA within preferred limits but <i>sensitive to time of occupant impact.</i> • Vehicle Stability – PASS 	<ul style="list-style-type: none"> • Minimal damage to system • Dynamic deflection = 3.4" • Some plastic deformation of post, and moderate plastic deformations of the lower rail and baseplate. • No detached elements from barrier that would present hazard. 	<ul style="list-style-type: none"> • Meets minimum height • 9" curb reveal meets all preferred rail-face geometrics criteria. • 7" curb reveal does <u>not</u> meet all preferred rail-face geometrics criteria but falls within the range of other systems that have been successfully crash tested. • Meets LRFD minimum lateral strength criterion of 80 kip. 	<ul style="list-style-type: none"> • <u>Meets MASH TL4</u> • <u>No design changes required.</u> <p>Recommendations for improving overall crash performance:</p> <p><u>Option 1:</u></p> <ul style="list-style-type: none"> ○ Reduce post spacing to meet LRFD strength requirements (e.g., 8 ft to 6.5 ft) ○ Taper top of posts. ○ Revise splice design by reducing internal gaps.
Test 4-11 <u>Pickup</u>	<ul style="list-style-type: none"> • Structural Adequacy – PASS • Occupant Risk – PASS <ul style="list-style-type: none"> • OIV within preferred limits • <i>Preferred < ORA < critical</i> • Vehicle Stability – PASS 	<ul style="list-style-type: none"> • Moderate damage to system. • Dynamic deflection = 4.2" • Moderate plastic deformations of the posts, rails and baseplates. • No detached elements from barrier that would present hazard. 	<ul style="list-style-type: none"> • Meets LRFD minimum lateral strength criterion of 80 kip. 	<p><u>Option 2:</u></p> <ul style="list-style-type: none"> ○ Change size of all rails to meet preferred rail-geometric criteria and to improve strength. ○ Increase curb reinforcement by adding additional longitudinal steel above the anchor plates and/or increase anchor-bolt embedment. ○ Revise splice design to reduce internal gaps. ○ Taper top of posts. ○ Increase baseplate thickness and welds.
Test 4-12 <u>SUT</u> Case 1: 47.5" Bed Case 2: 50" Bed	<ul style="list-style-type: none"> • Structural Adequacy – PASS • Occupant Risk – N.A. • Vehicle Stability <ul style="list-style-type: none"> • Case 1 – PASS • Case 2 – FAIL (<i>It is preferred that the vehicle remain upright but not required.</i>) 	<ul style="list-style-type: none"> • Moderate to extensive damage to system. • Dynamic deflection: <ul style="list-style-type: none"> • Case 1 = 7.6" • Case 2 = 8.1" • High plastic deformations of the posts, rails and baseplates. • The analysis resulted in notable concrete damage at two posts., corresponding to potential cracks around the front anchor bolts and/or anchor pullout. • No detached elements from barrier that would present hazard. 		<p><u>Option 3:</u></p> <ul style="list-style-type: none"> ○ Increase post size (e.g., W8x28) to meet LRFD strength requirements. ○ Increase curb reinforcement by adding additional longitudinal steel above the anchor plates and/or increase anchor-bolt embedment. ○ Improve splice design by reducing internal gaps. ○ Taper top of posts to mitigate snag with over-hanging vehicles. ○ Use an HSS 5x4x5/16 for the lower rail

Table 116. Summary of conclusions and recommendations for the NETC 4-bar sidewalk-mounted bridge rail.

MASH Test Case	FEA Results: MASH Criteria	FEA Results: System Damage	LRFD Calcs. for MASH Equivalency	Conclusions and Recommendations
Test 4-10 <u>Small Car</u>	<ul style="list-style-type: none"> • Structural Adequacy – PASS • Occupant Risk – PASS <ul style="list-style-type: none"> • <i>preferred < OIV < critical</i> • ORA within preferred limits but <i>sensitive to time of occupant impact.</i> • Vehicle Stability – PASS 	<ul style="list-style-type: none"> • Low levels of damage to system • Dynamic deflection = 2.8" • Low plastic deformation of post, rails and baseplates. • No detached elements from barrier that would present hazard. 	<ul style="list-style-type: none"> • Meets minimum height • Does <u>not</u> meet all preferred rail-face geometrics criteria but falls within the range of other systems that have been successfully crash tested. • Does <u>not</u> meet LRFD minimum lateral strength criterion of 80 kip. 	<ul style="list-style-type: none"> • <u>Meets MASH TL4, albeit with considerable damage to system.</u> • <u>Design changes are recommended for this design, unless additional evaluations are conducted.</u> <p>Recommendations for improving overall crash performance:</p> <p><u>Option 1:</u></p> <ul style="list-style-type: none"> ○ Reduce post spacing to meet LRFD strength requirements (e.g., 8 ft to 6.5 ft) ○ Taper top of posts. ○ Revise splice design by reducing internal gaps. <p><u>Option 2:</u></p> <ul style="list-style-type: none"> ○ Change size of all rails to meet preferred rail-geometric criteria and to improve strength. ○ Increase curb reinforcement by adding additional longitudinal steel above the anchor plates and/or increase anchor-bolt embedment. ○ Revise splice design to reduce internal gaps. ○ Taper top of posts. ○ Increase baseplate thickness and welds. <p><u>Option 3:</u></p> <ul style="list-style-type: none"> ○ Increase post size (e.g., W8x28) to meet LRFD strength requirements. ○ Increase curb reinforcement by adding additional longitudinal steel above the anchor plates and/or increase anchor-bolt embedment. ○ Revise splice design by reducing internal gaps. ○ Taper top of posts to mitigate snag with over-hanging vehicles. ○ Use an HSS 5x4x5/16 for the 2nd to bottom rail.
Test 4-11 <u>Pickup</u>	<ul style="list-style-type: none"> • Structural Adequacy – PASS • Occupant Risk – PASS <ul style="list-style-type: none"> • OIV within preferred limits • <i>Preferred < ORA < critical</i> • Vehicle Stability – PASS 	<ul style="list-style-type: none"> • Moderate damage to system. • Dynamic deflection = 5.4" • Moderate plastic deformations of the posts, rails and baseplates. • Snag damage at splice. • No detached elements from barrier that would present hazard. 		
Test 4-12 <u>SUT</u> 47.5" Bed	<ul style="list-style-type: none"> • Structural Adequacy – PASS • Occupant Risk – N.A. • Vehicle Stability – PASS 	<ul style="list-style-type: none"> • Moderate to extensive damage to system. • Dynamic deflection = 8.2" • Moderate plastic deformations of the rails. • High plastic deformations of posts and baseplates. • The analysis resulted in notable concrete damage at the critical post, corresponding to potential cracks around the front anchor bolts and/or anchor pullout. • No detached elements from barrier that would present hazard. 		

Table 117. Summary of conclusions and recommendations for the NETC 2-Bar transition.

2-Bar Transition (TL3)			
MASH Test Case	FEA Results: MASH Criteria	FEA Results: System Damage	Recommendations
Test 3-20 <u>Small Car</u>	<ul style="list-style-type: none"> • Structural Adequacy – PASS • Occupant Risk – PASS <ul style="list-style-type: none"> • OIV within preferred limits • ORA within preferred limits • Vehicle Stability – PASS 	<ul style="list-style-type: none"> • Minimal damage to system • Dynamic deflection = 6.3" • No detached elements from barrier that would present hazard. 	<ul style="list-style-type: none"> • <u>Meets MASH TL3</u> • <u>No design changes required.</u> <p>Recommendations for improving overall crash performance:</p> <ul style="list-style-type: none"> ○ An additional deflector plate at the lower edge of the thrie-beam terminal connector. ○ Revise expansion splice to reduce internal gaps.
Test 3-21 <u>Pickup</u>	<ul style="list-style-type: none"> • Structural Adequacy – PASS • Occupant Risk – PASS <ul style="list-style-type: none"> • OIV within preferred limits • <i>Preferred < ORA < critical</i> • Vehicle Stability – PASS 	<ul style="list-style-type: none"> • Moderate damage to system. • Dynamic deflection = 11.8" • No detached elements from barrier that would present hazard. 	

Table 118. Summary of conclusions and recommendations for the NETC 3-bar transition.

MASH Test Case	FEA Results: MASH Criteria	FEA Results: System Damage	Recommendations
Test 4-20 <u>Small Car</u>	<ul style="list-style-type: none"> • Structural Adequacy – PASS • Occupant Risk – PASS <ul style="list-style-type: none"> • OIV within preferred limits • ORA within preferred limits • Vehicle Stability – PASS 	<ul style="list-style-type: none"> • Minimal damage to system • Dynamic deflection = 5.8” • No detached elements from barrier that would present hazard. 	<ul style="list-style-type: none"> • <u>Meets MASH TL4</u> • <u>No design changes required.</u> <p>Recommendations for improving overall crash performance:</p> <ul style="list-style-type: none"> ○ Taper top of posts to mitigate snag with over-hanging vehicles. ○ Revise expansion splice to reduce internal gaps.
Test 4-21 <u>Pickup</u>	<ul style="list-style-type: none"> • Structural Adequacy – PASS • Occupant Risk – PASS <ul style="list-style-type: none"> • OIV within preferred limits • <i>ORA at preferred limits (e.g., ORAy = 15.1G)</i> • Vehicle Stability – PASS 	<ul style="list-style-type: none"> • Moderate damage to system. • Dynamic deflection = 8” • No detached elements from barrier that would present hazard. 	
Test 4-22 <u>SUT</u> 47.5” Bed	<ul style="list-style-type: none"> • Structural Adequacy – PASS • Occupant Risk – N.A. • Vehicle Stability – Possible roll onto side (It is preferred that the vehicle remain upright but not required.) 	<ul style="list-style-type: none"> • Minimal damage to transition system, but moderate damage to bridge rail. • Dynamic deflection = 4.3” • Plastic deformations on the tops of Post 1 of transition and all three bridge rail posts – caused by overhang of cargo-bed. • No detached elements from barrier that would present hazard. 	

Table 119. Summary of conclusions and recommendations for the *Concrete-to-Thrie-Beam* transition

MASH Test Case	FEA Results: MASH Criteria	FEA Results: System Damage	Recommendations
Test 4-20 <u>Small Car</u>	<ul style="list-style-type: none"> • Structural Adequacy – PASS • Occupant Risk – FAIL <ul style="list-style-type: none"> • OIV within preferred limit • ORA exceeded critical limit • Vehicle Stability – PASS 	<ul style="list-style-type: none"> • Moderate to significant damage to system. • Notable pocketing and sharp kink in terminal connector at edge of buttress. • Dynamic deflection = 6.7" • No detached elements from barrier that would present hazard 	<ul style="list-style-type: none"> • <u>Does Not Meet MASH TL4</u> • Use 3-Bar Transition when applicable. <p>Recommended design changes to reduce snag on buttress</p> <ul style="list-style-type: none"> ○ Taper face of buttress (e.g., MwRSF design or MassDOT design).
Test 4-21 <u>Pickup</u>	<ul style="list-style-type: none"> • Structural Adequacy – PASS • Occupant Risk – PASS <ul style="list-style-type: none"> • OIV within preferred limits • Preferred < ORA < critical • Vehicle Stability – PASS 	<ul style="list-style-type: none"> • Moderate to significant damage to system. • Notable pocketing and sharp kink in terminal connector at edge of buttress. • Dynamic deflection = 8.3" • No detached elements from barrier that would present hazard. 	
Test 4-22 <u>SUT</u> 47.5" Bed	<ul style="list-style-type: none"> • Structural Adequacy – Marginal • Occupant Risk – N.A. • Vehicle Stability – Probable Fail <i>(It is preferred that the vehicle remain upright but not required.)</i> 	<ul style="list-style-type: none"> • Significant damage to transition system. • Dynamic deflection = 17" • Bridge rail posts were also damaged due to overhang of cargo-bed. • No detached elements from barrier that would present hazard. 	

18 REFERENCES

- AASHTO12 AASHTO, “AASHTO LRFD Bridge Design Specification,” 6th Edition, American Association of State Highway and Transportation Officials, Washington, D.C., 2012.
- AASHTO16 Technical Committee for Roadside Safety, “Manual for Assessing Safety Hardware,” American Association of State Highway and Transportation Officials, Washington, D.C., 2016.
- Alberson06 Alberson, D.C., C.E. Buth, W.L. Menges, and R.R. Haug, “NCHRP Report 350 Testing and Evaluation of NETC Bridge Rail Transitions,” Report No. NETCR 53, New England Transportation Consortium, University of Connecticut, Storrs, CT (2006).
- Bligh11 Bligh, R.P. and W.L. Menges, “*MASH* Test 3-11 on the Texas T101 Bridge Rail,” Report 9-1002-1, Texas Transportation Institute, College Station, Texas (2010).
- Bullard 02 Bullard, D.L., W.F. Williams, W.L. Menges and R.R. Haug, *Design and Evaluation of the TXDOT F411 and T77 Aesthetic Bridge Rails*,” Report 4288-1, The Texas Transportation Institute, College Station, Texas, 2002.
- Bullard 08 Bullard, D.L., R.P. Bligh, and W.L. Menges. *Appendix A: MASH-08 TL4 Testing and Evaluation of the New Jersey Safety Shape Bridge Rail*. NCHRP Project 22-14, College Station, Texas, 2008.
- Buth99a Buth, C.E., W.L. Menges, and W.F. Williams, “Testing and Evaluation of the Massachusetts Type S3-TL4 Bridge Railing,” Report No. FHWA-RD-00-023, Texas Transportation Institute, College Station, TX, (1999).
- Buth99b Buth, C.E., W.L. Menges, and W.F. Williams, “Testing and Evaluation of the New York Two-Rail Curbless and Four-Rail Curbless Bridge Railing and the Box-Beam Transition,” Report No. 404531-F, for the Federal Highway Administration, Performed by the Texas Transportation Institute, College Station, TX (1999).
- Dobrovolny17 Silvestri-Dobrovolny, Chiara, N. Schulz, S. Moran, T. Skinner, R. Bligh, and W. Williams, “*MASH* Equivalency of NCHRP Report 350-Approved Bridge Railings,” Final Report, NCHRP Project No. 20-07 / Task 395, TTI Project No. 607141, Texas Transportation Institute, College Station, TX (2017).
- Epperson99 Epperson, B., R. Bligh, and H. Ross, Test Risk Assessment Program (TRAP) Version 2.0: User’s Manual, Texas Transportation Institute, College Station, TX (1999).
- FHWA12 Griffith, M.S., “Eligibility Letter B-231” https://safety.fhwa.dot.gov/roadway_dept/countermeasures/reduce_crash_severity/barriers/pdf/b231.pdf, accessed on 8/29/2019, Federal Highway Administration, Washington, D.C., (2012).
- FHWA14 Griffith, M.S., “Eligibility Letter B-236” https://safety.fhwa.dot.gov/roadway_dept/countermeasures/reduce_crash_severity/barriers/pdf/b236.pdf, accessed on 8/29/2019, Federal Highway Administration, Washington, D.C., (2014).

- Kimball99 Kimball, C.E. and J.B. Mayer, “Full-Scale Crash Evaluation of the NETC 4-Bar Sidewalk-Mounted Steel Bridge Railing,” Final Report Number 18-8518 (NETCR14), Southwest Research Institute, San Antonio, TX (1999).
- LSDYNA15 “LSDYNA User’s Manual,” Volumes I & II, Livermore Software Technology Corporation (LSTC), Livermore, CA (2015).
- Mak98 Mak, K.K
- Marzougui08 Marzougui, D. and S. Kan, “Advanced Crash Analyses to Improve Safety & Security”, FHWA Contract DTFH61-09-D-00001, National Crash Analysis Center, George Washington University, VA (2008).
- Marzougui10 Marzougui, D., M. Zink, A. Zaouk, C.D. Kan, and N. Dedewi, “Development and Validation of a Vehicle Suspension Finite Element Model for Use in Crash Simulations,” *International Journal of Crashworthiness*, 9:6, 565-576, DOI: 10.1533/ijcr.2004.0311 (2010).
- NCHRP12-90
- Plaxico06 Plaxico, C.A., J.C. Kennedy and C.R. Miele, “Development of an *NCHRP Report 350* TL3 New Jersey Shape 50-inch Portable Concrete Barrier,” Final Report No. FHWA/OH-2006/16, Ohio Department of Transportation, Columbus, OH (June 2006).
- Plaxico07 Plaxico, C.A., Kennedy, J.C., and Miele, C.R., “Evaluation and Redesign of a Culvert Guardrail and Transition System,” Technical Report, Ohio Department of Transportation, 2007.
- Plaxico15 Plaxico, C.A., M.H. Ray, C.E. Carrigan, T.O. Johnson, and A. Ray, “Criteria for Restoration of Longitudinal Barriers, Phase II,” Final Report, NCHRP Project 22-28, National Academy of Sciences, Washington D.C. (2015).
- Plaxico16 Plaxico, C.A. and T.O. Johnson, “Report 350 TL4 Evaluation of the Proposed Three-Rail Barrier, Final Report, Performed for HNTB New York Engineering Consultant, Prepared by Roadsafe LLC, Canton, ME (2016).
- Plaxico18 Plaxico, C.A. and M.H. Ray, “Evaluation of Transition System for *MASH* Test Level 4,” In Proceeding of the MassDOT Innovation and Mobility Exchange Conference, Paper Session 3B, Worcester, Massachusetts, April 2018.
- Plaxico19 Plaxico, C.A. and M.H. Ray, “*MASH* TL4 Evaluation of MassDOT’s Curb-Mounted and Sidewalk-Mounted Highway Guardrail Approach Transition Using Finite Element Analysis,” Technical Report prepared for the Massachusetts DOT, Prepared by Roadsafe LLC, Canton, Maine (2019).
- Plaxico19b Plaxico, C.A. and M.H. Ray, “*MASH* TL4 Evaluation of MassDOT’s Curb-Mounted and Sidewalk-Mounted S3-TL4 Bridge Railing Using Finite Element Analysis,” Technical Report No. TR 19-0429-GEA, Prepared for Gill Engineering Associates and the Massachusetts DOT, Prepared by Roadsafe LLC, Canton, Maine (2019).
- Polivka06 Polivka, K.A., D.L. Sicking, B.W. Bielenberg, R.K. Faller, J.R. Rohde, and J.D. Reid. *Performance Evaluation of the Permanent New Jersey Safety Shape Barrier – Update to NCHRP 350 Test No. 4-12 (2214NJ-2)*. Report No. TRP-03-178-06. Midwest Roadside Safety Facility, Lincoln, Nebraska, 2006.

- Ray11 Ray, M.H., Mongiardini, M., Plaxico, C.A. and Anghileri, M., “Recommended Procedures for Verification and Validation of Computer Simulations used for Roadside Safety Applications,” National Cooperative Highway Research Program Report No. 179, National Academy of Sciences, Washington, D.C., 2011.
- Ray18a Ray, M.H., C.E. Carrigan, and C.A. Plaxico, “Guidelines for Shielding Bridge Piers,” Final Report, Project 12-90 (Appendix D), National Cooperative Highway Research Program, National Academy of Science (April 2018).
- Ray18b Ray, M.H., C.E. Carrigan, and C.A. Plaxico, “Guidelines for Shielding Bridge Piers,” NCHRP Research Report 892, National Cooperative Highway Research Program, National Academy of Science (April 2018).
- Rosenbaugh18 Rosenbaugh, S.K., J.D. Schmidt, and R.K. Faller, “Development of a Standardized Buttress for Approach Guardrail Transitions,” Paper No. 18-05386, in proceedings of Transportation Research Board Annual Meeting, Washington D.C., (2018).
- Rosenbaugh19 Rosenbaugh, S.K., W.G. Fallet, J.D. Schmidt, R.W. Bielenberg and R.K. Faller, “34-Inch Tall Thrie Beam Transition to Concrete Buttress,” Technical Report No. TRP-03-367-19, Midwest Roadside Safety Facility, Lincoln, Nebraska (2019).
- Ross93 Ross, H.E., D.L. Sicking, and H.S. Perrara, “Recommended Procedures for the Safety Performance Evaluation of Highway Appurtenances,” *National Cooperative Highway Research Program Report No. 350*, Transportation Research Board, Washington, D.C. (1993).
- Sheikh11 Sheikh, N.M., R.P. Bligh, and W.L. Menges. Determination of Minimum Height and Lateral Design Load for *MASH* Test Level 4 Bridge Rails. Report No. 9-1002-5. Texas A&M Transportation Institute, College Station, Texas, 2011.
- Sheihk16 Sheihk, N.M., W.L. Menges and D.L. Kuhn, “*MASH* TL-5 Testing and Evaluation of the TBTA Steel Bridge Rail, Test Report No. 603911-1, Texas A&M Transportation Institute, College Station, Texas, 2016.
- Williams17a Williams, W.F., W.L. Menges and D.L. Kukn, “*MASH* TL4 Evaluation of the Pulaski Skyway Bridge Parapet,” Test Report No. 607451-1-3, Texas Transportation Institute, College Station, TX (Feb. 2017).
- Williams17b Williams, W.F., W.L. Menges and D.L. Kukn, “*MASH* TL4 Evaluation of the TxDOT Type C2P Bridge Rail,” Test Report No. 9-1002-15-2, Texas Transportation Institute, College Station, TX (Feb. 2017).
- Winkelbauer14 Winkelbauer, B.J., S.K. Rosenbaugh, R.W. Bielenberg, J.G. Putjenter, K.A. Lechtenberg, R.K. Faller, and J.D. Reid, “Dynamic Evaluation of MGS Stiffness Transition with Curb,” MwRSF Research Report No. TRP-03-291-14, Midwest Roadside Safety Facility, Lincoln, Nebraska (2014).
- Wright97 Wright, A. and M.H. Ray, “Characterizing Roadside Hardware Materials for LSDYNA3D Simulations,” *Report No. FHWA-RD-96-108*, Federal Highway Administration (Feb 1997).
- TTI98 TTI, “Test Risk Assessment Program (TRAP) Version 1.01: User’s Manual,” Texas Transportation Institute, College Station, TX, 1998.

- Safiuddin18 Safiuddin, Md., A. Kaish, C.O. Woon, and S.N. Raman, "Early-Age Cracking in Concrete: Causes, Consequences, Remedial Measures, and Recommendations," *Journal of Applied Sciences*, Volume 8, Issue 10, doi:10.3390 (2018).
- Zaouk96 Zaouk, A.K., N.E. Bedewi, C.D. Kan, and D. Marzougui, "Validation of a Non-Linear Finite Element Vehicle Model Using Multiple Impact Data," *The American Society of Mechanical Engineers* (1996).